

Lecture Notes in Mechanical Engineering

Akhmetova Irina
Pietro Zunino *Editors*


Proceedings of the International Symposium on Sustainable Energy and Power Engineering 2021

SUSE 2021

 Springer


Lecture Notes in Mechanical Engineering

Series Editors

Francisco Cavas-Martínez , Departamento de Estructuras, Construcción y Expresión Gráfica Universidad Politécnica de Cartagena, Cartagena, Murcia, Spain

Fakher Chaari, National School of Engineers, University of Sfax, Sfax, Tunisia

Francesca di Mare, Institute of Energy Technology, Ruhr-Universität Bochum, Bochum, Nordrhein-Westfalen, Germany

Francesco Gherardini , Dipartimento di Ingegneria “Enzo Ferrari”, Università di Modena e Reggio Emilia, Modena, Italy

Mohamed Haddar, National School of Engineers of Sfax (ENIS), Sfax, Tunisia

Vitalii Ivanov, Department of Manufacturing Engineering, Machines and Tools, Sumy State University, Sumy, Ukraine

Young W. Kwon, Department of Manufacturing Engineering and Aerospace Engineering, Graduate School of Engineering and Applied Science, Monterey, CA, USA

Justyna Trojanowska, Poznan University of Technology, Poznan, Poland

Lecture Notes in Mechanical Engineering (LNME) publishes the latest developments in Mechanical Engineering—quickly, informally and with high quality. Original research reported in proceedings and post-proceedings represents the core of LNME. Volumes published in LNME embrace all aspects, subfields and new challenges of mechanical engineering. Topics in the series include:

- Engineering Design
- Machinery and Machine Elements
- Mechanical Structures and Stress Analysis
- Automotive Engineering
- Engine Technology
- Aerospace Technology and Astronautics
- Nanotechnology and Microengineering
- Control, Robotics, Mechatronics
- MEMS
- Theoretical and Applied Mechanics
- Dynamical Systems, Control
- Fluid Mechanics
- Engineering Thermodynamics, Heat and Mass Transfer
- Manufacturing
- Precision Engineering, Instrumentation, Measurement
- Materials Engineering
- Tribology and Surface Technology

To submit a proposal or request further information, please contact the Springer Editor of your location:

China: Ms. Ella Zhang at ella.zhang@springer.com

India: Priya Vyas at priya.vyas@springer.com

Rest of Asia, Australia, New Zealand: Swati Meherishi at swati.meherishi@springer.com

All other countries: Dr. Leontina Di Cecco at Leontina.dicecco@springer.com

To submit a proposal for a monograph, please check our Springer Tracts in Mechanical Engineering at <https://link.springer.com/bookseries/11693> or contact Leontina.dicecco@springer.com

Indexed by SCOPUS. All books published in the series are submitted for consideration in Web of Science.

More information about this series at <https://link.springer.com/bookseries/11236>

Akhmetova Irina · Pietro Zunino
Editors

Proceedings
of the International
Symposium on Sustainable
Energy and Power
Engineering 2021

SUSE 2021

 Springer

Editors

Akhmetova Irina
Kazan State Power Engineering University
Kazan, Tatarstan Republic, Russia

Pietro Zunino
DIME
University of Genoa
Genova, Italy

ISSN 2195-4356

ISSN 2195-4364 (electronic)

Lecture Notes in Mechanical Engineering

ISBN 978-981-16-9375-5

ISBN 978-981-16-9376-2 (eBook)

<https://doi.org/10.1007/978-981-16-9376-2>

© The Editor(s) (if applicable) and The Author(s), under exclusive license to Springer Nature Singapore Pte Ltd. 2022

This work is subject to copyright. All rights are solely and exclusively licensed by the Publisher, whether the whole or part of the material is concerned, specifically the rights of translation, reprinting, reuse of illustrations, recitation, broadcasting, reproduction on microfilms or in any other physical way, and transmission or information storage and retrieval, electronic adaptation, computer software, or by similar or dissimilar methodology now known or hereafter developed.

The use of general descriptive names, registered names, trademarks, service marks, etc. in this publication does not imply, even in the absence of a specific statement, that such names are exempt from the relevant protective laws and regulations and therefore free for general use.

The publisher, the authors and the editors are safe to assume that the advice and information in this book are believed to be true and accurate at the date of publication. Neither the publisher nor the authors or the editors give a warranty, expressed or implied, with respect to the material contained herein or for any errors or omissions that may have been made. The publisher remains neutral with regard to jurisdictional claims in published maps and institutional affiliations.

This Springer imprint is published by the registered company Springer Nature Singapore Pte Ltd. The registered company address is: 152 Beach Road, #21-01/04 Gateway East, Singapore 189721, Singapore

Contents

Research of the Combined-Cycle Cogeneration Plant's Behaviour According to the Temperature Chart	1
D. A. Treshchev, M. A. Treshcheva, D. L. Kolbantseva, and A. A. Kalyutik	
Determination of Friction Coefficients as Well as Heat and Mass Transfer Coefficients in Film-Type Countercurrent Apparatuses with Intensifiers	17
A. G. Laptev and E. A. Lapteva	
Pressurized Heat Recovery Steam Generator Design for CCGT with Gas Turbine GT-25PA and Steam Turbine T-100	27
Konstantin A. Pleshanov, Kirill Sterkhov, Dmitry A. Khokhlov, and Mikhail N. Zaichenko	
Selection of the Appropriate Intelligence Level of Regulators of Thermal Power Plants Technological Processes	39
Edik Arakelyan, Sergey Mezin, Fedor Pashchenko, and Anatoly Kosoy	
Study of the Causes of the Gas Imbalance in High Capacity Steam Boilers	49
V. A. Pozdeev, E. A. Kravetc, K. E. Zhilin, D. O. Andreichuk, and D. V. Loginov	
Continuous Steelmaking Unit of Bubbling Type	63
Konstantin Strogonov, Lyubov Kornilova, Alexey Popov, and Alexander Zdarov	

Determination of the Conductor Sag According to the Period of Own Harmonic Oscillations, Taking into Account the Difference in Heights of the Suspension Points	73
Danil Aleksandrovich Yaroslavsky, Van Vu Nguyen, Marat Ferdinandovich Sadykov, Mikhail Petrovich Goryachev, and Dmitry Alekseevich Ivanov	
An Approach to Determining the Integrated Reliability of Technical Systems at the Development Stage	83
Ruslan Litvinenko, Aver Auhadeev, Azat Khusnutdinov, Irina Antipanova, and Leylya Kisneeva	
The Reconstruction Experience of the 60-KCS Condenser for Deaeration Intensification	95
Artem Vodeniktov and Nataliya Chichirova	
Construction of a Predictive Model of a Steam Generator Experimental Stand Based on the Organic Rankine Cycle	103
V. O. Miloserdov, M. O. Korlyakova, and D. A. Gorelov	
The Method of Calculating the Dew-Point Temperature of Stack Gases in the Compound Firing of Gases and Fuel Oil in the Boiler Furnace	111
Simeon Livshits, Natalia Yudina, Ruslan Lebedev, Tatiana Mantserova, and Alsu Galiakhmetova	
Usage of Woodworking Processing Industry Waste as a Fuel	121
Anastasia Pavlova, Semen Livshits, Natalia Yudina, Tatyana Dunaeva, and Aigel Sabirzyanova	
Mathematical Simulation of Electrodynamical and Thermal Processes in Electrical Process Plants	131
Sergei Trigorly, Andrey Yakovlev, Svetlana Kalganova, Anton Sivak, and Yulia Kadykova	
For Calculation of Perforated Hearth Burner Equipment to the Bubble-Type Furnaces	143
Konstantin Strogonov, Alexey Popov, Alexander Zdarov, and Lyubov Kornilova	
Issues of Using Digital Twins of Gas Turbine Units at Their Facilities ...	153
Vitalii L. Blinov, Sergey V. Bogdanets, and Ilya S. Zubkov	
Technical Condition Assessment of the Gas Turbine Units with Free Power Turbine	161
Vitalii L. Blinov, Oleg V. Komarov, Yuriy M. Brodov, and Ilya S. Zubkov	

Fault Isolation in Digital Instruments and Devices Used in Power-Engineering Systems	169
Pavel Pavlov, Valery Butakov, Azat Khusnutdinov, Aida Abdullina, Eve Snezhinskay, and Ivan CHerepenkin	
Study of the Orifice Inserts Influence on the Multisection Vacuum Condenser Operation Under Uneven Heating Conditions	179
A. Yu. Kartuesova, A. V. Ptakhin, and V. S. Krylov	
Joint Use of Distributed Ledger Technology and Centralized Software for Storing Power Equipment Reliability Data	189
M. M. Sultanov, I. A. Boldyrev, A. A. Smirnov, Yu. A. Gorban, and V. A. Yurov	
Methods for Improving the Efficiency and Reliability of Power Systems Equipment in the Context of Digitalization	195
Makhsud Sultanov, Ilia Boldyrev, and Yuliya Gorban	
Mathematical Simulation of the Flux of the Solar Radiation Coming to the Collector	207
Valentina Khoreva, Sergey Elistratov, Nadezhda Vorogushina, and Ivan Sadkin	
On the Importance of Applying RCM Technology to Passive Components of Russian NPPs	217
A. A. Arzhaev, A. I. Arzhaev, V. O. Makhanev, M. I. Antonov, N. M. Emelianova, A. V. Emelianov, A. A. Kalyutik, Yu. E. Karyakin, K. A. Arzhaev, I. N. Denisov, V. P. Derij, and M. A. Podlatov	
Change in Rheological Properties of M100 Fuel Oil After Ultrasonic Treatment	231
Rustem Kamalov	
Heat Transfer During Fuel Oil Flow in Storage Tanks and Heaters of the Reserve Facility of TPP	241
Rustem Kamalov	
Methodological Approaches to Building the Scenarios of Inflows into Reservoirs When Modeling Long-Term Regimes of Hydroelectric Power Plants	253
Viacheslav M. Nikitin, Nikolay V. Abasov, Tamara V. Bereznykh, and Evgeny N. Osipchuk	
Numerical Study of the Fluid Flow in a Passive Tangential Vortex Tube	263
Simeon Livshits, Natalia Yudina, Ruslan Lebedev, Svetlana Enikeeva, and Evgeny Panamarenka	

Assessment of the Possibility of NO_x Reduction in Smoke Gases of Steam Boilers DE-6.5/14 by Recirculation of Combustion Products	273
Eduard Korolev, Roman Lipantiev, Enza Barieva, Aleksey Eskin, and Elena Serazeeva	
Improvement of the Environmental Friendliness and Energy Efficiency of the Municipal Heating Network Through the Use of Coal-Water Slurry Fuel (on the Example of the City of Leninsk-Kuznetsky)	281
Vasily Murko, Oksana Chernikova, Aleksey Yur'ev, Valery Chaplygin, and Vladimir Vinograd	
Numerical Modeling of the Influence of the Atmospheric Meteorological State on the Efficiency of the Functioning of Solar Thermal and Power Plants	289
Nikolai Moskalenko, Azat Akhmetshin, Yana Safiullina, Ibragim Dodov, and Maryana Khamidullina	
Scientific and Technical Basis for Using External Heat Supply to a Turbine Unit in the Classic Brighton Cycle	305
Mikhail Laptev, Viktor Barskov, Viktor Rassokhin, Anton Kurnukhin, and Gong Boven	
Information-Measuring System for Monitoring Process Water in Power System Heat Supply Structures	319
Rimma Zaripova, Ilgizar Gaisin, Marina Tyurina, Olga Rocheva, and Elena Kubyshkina	
Development of a Method and Means for Saving Natural Non-Renewable Resources in the Operation of Electric Drives of Borehole Pumps of Water Supply Systems Operating in Hard Natural Conditions	329
George Palkin, Ivan Suvorov, Sergei Kakaurov, Roman Gorbunov, and Roman Dolgih	
Verification of Computer Flow Simulation in Confuser and Diffuser Channels	343
Ivan Komarov, Sergey Osipov, Andrey Vegera, Darya Kharlamova, and Aleksey Zonov	
Efficiency of Peat Combustion in a Low Capacity Boiler: Analysis of Peat Reserves in the Arkhangelsk Region and Efficiency of Its Energy Use	353
Victor Lyubov, Anatoly Popov, Evgeniya Popova, and Alexander Chernov	

General Methods for Loss Prediction in Axial Turbine Blade Cascades	369
A. A. Ukhlin, V. I. Brezgin, M. Yu. Stepanov, and G. R. Lotnik	
The Technique for Estimation of Thermal Power Equipment Remaining Life Based on Service Life Index	379
Makhsud Sultanov, Ilia Boldyrev, Valentina Lunenko, Pavel Menshikov, and Kirill Evseev	
Multichannel Majority System for Detection and Prevention of Emergency Modes of Gas Pumping Unit Filters	391
Marina Tyurina, Alexander Porunov, Alexander Nikitin, Rimma Zaripova, and Gulia Khamatgaleeva	
Study of the Properties of Fuel Gas in Gas Turbine Plants Depending on Its Composition	403
George Marin, Boris Osipov, and Dima Mendelev	

About the Editors

Akhmetova Irina is a Doctor of Technical Sciences, Associate Professor and Vice-rector for scientific work at the Kazan State Power Engineering University (Russia). Her total work experience is over 18 years, and the number of publications is over 90. Her interests include not only economics, but also an energy sector, heat and gas supply issues.

Pietro Zunino is a Full Professor at the University of Genova, Italy and a Visiting Professor at the Peter the Great St. Petersburg Polytechnic University, Russia and Harbin Engineering University, China. His experience includes positions such as principal investigator in many research projects related to aero-thermodynamics of turbomachinery for the European Commission and with industrial companies, etc. He is authored over 150 international scientific papers on aero-thermodynamics of turbomachinery for power generation and aeronautical propulsion.

Research of the Combined-Cycle Cogeneration Plant's Behaviour According to the Temperature Chart



D. A. Treshchev, M. A. Treshcheva, D. L. Kolbantseva, and A. A. Kalyutik

1 Introduction

Cogeneration is the most efficient way of using fuel heat, so expanding the use of cogeneration in Russia can be one of the most important elements in forming coherent energy policy [1–7].

According to industry reports (Table 1), currently about 46–48% of the total heat supply in district heating systems comes from thermal power plants (TPP) that is comparable with heat supply from large heat boiler stations (52–53%).

Thermal power plants comprise 67% of the installed capacity structure of Russian power plants. At the same time, 78% of them operate on the basis of steam-power plants. However, over the last 20 years, the share of combined cycle plants (CCPs) has dramatically increased, reaching 16% by the moment.

According to the energy strategy of the Russian Federation for the period until 2035, in 2018 the actual specific reference fuel consumption (SRFC) for electricity supply at cogeneration sources with installed capacity of 25 MW or more was 309.8 goe/kWh (which is 26.2 goe/kWh lower than in 2008). Further SRFC decrease, planned by the «Energy Strategy», can be achieved mainly through further large-scale implementation of combined cycle power plants (CCPPs) in upgrading and construction of old and new TPPs [8–10].

Determining the optimum value of the heat load connected to the CCP (otherwise the share of the system heat load covered by the plant) and justification of the value of the extraction factor are the most crucial aspects in the design and operation of highly efficient CCPs for cogeneration needs. These tasks are directly related for CCPs, as well as for the more common in the domestic power industry steam turbine plants (STPs).

D. A. Treshchev · M. A. Treshcheva · D. L. Kolbantseva (✉) · A. A. Kalyutik
Peter the Great St. Petersburg Polytechnic University, St. Petersburg, Russian Federation
e-mail: kolbantseva.dl@edu.spbstu.ru

Table 1 Structure of heat supply by type of energy units

Heat supply source	Years				
	2014	2015	2016	2017	2018
Heat generation in district heating systems, mln. Gigacalories (Gcal)	1240.2	1194.8	1269.1	1262.6	1286.1
Power plants, mln. Gcal, including:	598	567	591.8	591.6	599.5
TPPs, mln. Gcal	594.6	563.7	588.4	588.2	596.2
Atomic power stations, mln. Gcal	3.4	3.3	3.4	3.4	3.3
Heating boilers plants with a load of 20 Gcal/h and more, mln. Gcal	639.1	625.2	674.5	668.5	684.1
Other heat sources, mln. Gcal	3.1	2.6	2.8	2.5	2.5

In Russia, the STPs' development is focused on increasing the initial steam parameters and correspondingly increasing the extraction factor— α of TPP (α_{TPP}) (from 0.5 to 0.65). Given the climatic characteristics of the Russian climate, the use of the 150/70 temperature schedule caused the need for peak heat sources (hot water boilers (HWB)) at TPPs.

The first CCCP in the Russian Federation (Severo-Zapadnaya TPP, St. Petersburg) was designed with the operating capability at the extraction factor equal to 1. The use of high- and low-pressure loops steam in the peak heaters of heating-system water, provided by the thermal scheme of this CCCP, allowed to exclude the use of hot-water boilers [11, 12].

Determining the optimum extraction factor, depending on the conditions of TPP design, according to the scientific works of L.S. Khrilev, I.A. Smirnov, G.B. Leventhal, L.A. Melentyev, is possible in two main ways, providing different results:

1. Determination of the optimal version of coverage the given heat load of the power system;
2. Determination of the optimal value of the heat load connected to a given power plant.

Russian power systems tend to have a significant heat load and a relatively low value of electric capacity. For example, the determination of the optimal value of the connected heat load to the existing plant is the most relevant task for areas with an established structure of energy consumption. Setting a higher value of the extraction factor, we increase the operation time of the unit with condensing pass, and thus worsen its technical and economic parameters, but at the same time reduce the operating period, and therefore the fuel consumption of hot-water boilers, and vice versa.

A number of scientific schools were studying this question for TPPs. L. S. Khrilev, I. A. Smirnov, G. B. Leventhal, L. A. Melentyev, E. Y. Sokolov, A. I. Andryushchenko, and R. Z. Aminov formed the basis for the research, but no similar research for CCCPs has been conducted so far.

Table 2 GTE-160 parameters of the ISO standard conditions

Parameter	Value
Air temperature, °C	15
Electric capacity, MW	155.3
Coefficient of performance, %	34.12
Flue gas temperature from GTU, °C	537
Flue gas flow rate, kg/s	509

The purpose of this work is to study the optimal value of the heat load connected to the CCCP.

The object of the study is a CCCP on the basis of GTE-160 (two-boiler single-turbine unit). The process flow diagram of the double-loop CCCP includes two heating-system water heaters, and two water-water heat exchangers (WWHEs).

The steam turbine operates on variable pressure parameters. The temperature of the heating-system water is regulated after the top heating-system heater during CCCP operation according to the temperature chart. The temperature is regulated by changing the pressure in the draw-off sections. Range of pressure change in the top draw-off section is limited by the strength and reliability of the steam turbine compartments. For modern steam turbines it is 0.05–0.2 MPa. To unify the flow ranges this parameter is accepted the same for steam turbine units in the CCP for further studies.

Characteristics of the CCCP during its operation according to the temperature chart were obtained for the 450 MW CCP unit (PGU-450), based on the gas turbine system (GTU) GTE-160. Table 2 shows the values of the main design parameters of CCP, reduced to normal conditions according to ISO requirements at the lower heat value of natural gas 50 MJ/kg.

The calculations assumed an open heat supply system. The temperature chart is 150/70. Central ratio governing by the combined load of heating and hot water supply is accepted. Basic parameters of outdoor temperatures and heating period duration were determined according to the standards for St. Petersburg.

Since the potential heat supply of a heating power plant never coincides with the heat consumption schedule, the CCCP unit could be integrated into the heating system in various ways, depending on the time the hot-water boilers are in use during the heating period.

1—an option appropriate for the maximum heat load of the TPP (the base part of the heat load is supplied by the CCCP, the variable part by the peak water-heating boilers (PHWB) switched on at the very beginning of the heating period);

2—an option corresponding to the minimum heat load of the TPP (the sliding grid closes at -24 °C; the steam turbine runs with condensation pass for most part of the heating period, whereas PWHB does not operate);

3—several options relevant to the intermediate heat loads of the TPP (the sliding grid is closed at different heating period temperatures).

The main criterion used in the optimization calculations for STP in terms of the planned economy is the relative fuel savings compared to separate generation.

This parameter can also be used in current economic conditions for optimization calculations of the CCCP units since it is directly linked to the incremental economic effect of the cogeneration plant as well as to its parameters and structure [13].

Thus, the efficiency of the CCCP method of operation in the heat system (or the optimum value of the extraction factor) can be assessed by analyzing the increase in relative fuel savings compared to separate generation, depending on the connected heat load level.

In Eq. (1) for the incremental integral economic effect of combined generation compared to separate generation (ΔNPV), the sum ΔC_t represents the fuel savings compared to separate generation [13],

$$\Delta NPV = \sum_{t=0}^T \frac{\Delta A_t}{(1 + E_n)^t} + \sum_{t=0}^T \frac{\Delta C_t}{(1 + E_n)^t} + \sum_{t=0}^T \frac{\Delta E_t}{(1 + E_n)^t}, \quad (1)$$

where

ΔA_t —additional cash flow from the combined generation in the respective year t ;

ΔC_t —savings in capital investment compared to separate generation;

ΔE_t —savings in annual operating expenses due to increased efficiency compared to separate generation.

Assuming equal amounts of electricity and heat generation in the combined and separate cycles, the total additional cash inflow from combined generation ΔA_t equals 0, so the maximum integral effect of the CCCP will correspond to the maximum reduction of the total discounted costs (2),

$$\sum_{t=0}^T \frac{\Delta C_t}{(1 + E_n)^t} + \sum_{t=0}^T \frac{\Delta E_t}{(1 + E_n)^t} \rightarrow \max. \quad (2)$$

Equation (2) tends to the maximum when each of the components individually tends to the maximum,

$$\sum_{t=0}^T \frac{\Delta C_t}{(1 + E_n)^t} \rightarrow \max; \quad \sum_{t=0}^T \frac{\Delta E_t}{(1 + E_n)^t} \rightarrow \max. \quad (3)$$

Capital investment change compared to separate generation for the CCCP can be summarized as follows:

$$\Delta C = C_{sep} - C_{com} = (C_{CPP} + C_{HWB}) - (C_{CCCP} + C_{PHWB}), \quad (4)$$

where

C_{sep} —the capital investment in separate generation unit;

C_{com} —the capital investment in combined generation unit;
 C_{CPP} —capital investment in condensing power plant (CPP) (separate generation);
 C_{HWB} —capital investment in hot water boilers (separate generation);
 C_{CCCP} —capital investment in the CCCP (combined generation);
 C_{PHWB} —capital investment in PHWB (combined generation).

The capital costs of the power plant depend on the equipment and its unit output, determined by the connected/actual heat and electricity load of the consumer. These costs can be expressed in the following way (5–8):

$$C_{\text{CPP}} = k_{\text{CPP}} \times N_e, \quad (5)$$

$$C_{\text{HWB}} = k_{\text{HWB}} \times Q_C^{\text{inst}}, \quad (6)$$

$$C_{\text{CCCP}} = k_{\text{CCCP}}^{\text{CCCP}} \times N_e + k_{\text{CP}} \times Q_{\text{CCCP}}^{\text{inst}}, \quad (7)$$

$$C_{\text{PHWB}} = k_{\text{HWB}} \times Q_{\text{PHWB}}^{\text{inst}} = k_{\text{HWB}} \times (Q_C^{\text{inst}} - Q_{\text{CCCP}}^{\text{inst}}), \quad (8)$$

where

k_{CPP} , k_{HWB} , $k_{\text{CCCP}}^{\text{CCCP}}$, k_{CP} —specific capital investments in the substituting CPP, substituting hot water boilers, CPP based on CCCP equipment, and cogeneration plant, respectively;

Q_C^{inst} —the installed heating capacity of the consumer in the separate and combined cycle;

$Q_{\text{CCCP}}^{\text{inst}}$, $Q_{\text{PHWB}}^{\text{inst}}$ —the installed heating capacity of the steam tapping and of CCCP and PHWB, accordingly;

N_e —installed electric capacity in separate and combined cycle.

Since in this case, the CPP can be replaced by a condensing CCP based on the same GTU used in the CCCP, and the heat supply under the separate cycle can be carried out from the hot water boiler with the same efficiency as in the PHWB, Eq. (4) will be as follows:

$$\Delta C = (k_{\text{HWB}} - k_{\text{CP}}) \times Q_{\text{CCCP}}^{\text{inst}}. \quad (9)$$

Savings of annual operating costs as compared to separate generation (ΔE) are mainly formed at the expense of the fuel component; therefore, Eq. (10) is relevant:

$$\begin{aligned}
 \Delta E &\approx \Delta Q_f \times P_f = (Q_f^{\text{sep}} - Q_f^{\text{com}}) \times P_f \\
 &= [(Q_f^{\text{CPP}} + Q_f^{\text{HWB}}) - (Q_f^{\text{CCCP}} + Q_f^{\text{PHWB}})] \times P_f, \quad (10)
 \end{aligned}$$

where

ΔQ_f —fuel savings compared to separate generation, toe;
 P_f —price of fuel equivalent, rubles/toe;
 Q_f^{sep} —fuel-consumption rate during separate generation, toe;
 Q_f^{com} —fuel-consumption rate during combined generation, toe;
 Q_f^{CPP} —fuel-consumption rate by CPP (separate generation), toe;
 Q_f^{HWPB} —fuel-consumption rate of hot water boilers (separate generation), toe;
 Q_f^{CCCP} —fuel-consumption rate of CCCP (combined generation), toe;
 Q_f^{PHWPB} —fuel-consumption rate of PHWPB (combined generation), toe.

Then Eq. (2) can be transformed as follows (11):

$$\sum_{t=0}^T [(k_{\text{HWPB}} - k_{\text{CP}}) \times Q_{\text{PHWPB}}^{\text{inst}}] + \sum_{t=0}^T [(Q_f^{\text{CPP}} + Q_f^{\text{HWPB}} - Q_f^{\text{CCCP}} - Q_f^{\text{PHWPB}}) \times P_f] \rightarrow \max. \quad (11)$$

If the capital costs are incurred for the period $T = 1$ year, and the calculation period of annual costs is $T = 30$ years, Eq. (11) can be transformed as follows:

$$(k_{\text{HWPB}} - k_{\text{CP}}) \times Q_{\text{PHWPB}}^{\text{inst}} + (Q_f^{\text{CPP}} + Q_f^{\text{HWPB}} - Q_f^{\text{CCCP}} - Q_f^{\text{PHWPB}}) \times P_f \times T \rightarrow \max. \quad (12)$$

We can switch to relative values independent of the power level of generating equipment of TPP and extend the results of the study to all thermal systems with different loads by dividing both terms in Eq. (12) by the following expression $(Q_f^{\text{CPP}} + Q_f^{\text{HWPB}})$. Thus, we get the Eq. (13) to determine the specific integral economic effect of replacing the combustion of a ton of fuel equivalent at separate generation for combined heat and electricity generation (mln. rub./toe.):

$$\delta \text{NPV} = \frac{(k_{\text{HWPB}} - k_{\text{CP}}) \times Q_{\text{CCCP}}}{Q_f^{\text{CPP}} + Q_f^{\text{HWPB}}} + \left[\frac{Q_f^{\text{CPP}} + Q_f^{\text{HWPB}} - Q_f^{\text{CCCP}} - Q_f^{\text{PHWPB}}}{Q_f^{\text{CPP}} + Q_f^{\text{HWPB}}} \right] \times P_f \times T. \quad (13)$$

Then, according to (12), $\delta \text{NPV} \rightarrow \max$ or:

$$\frac{(k_{\text{HWPB}} - k_{\text{CP}}) \times Q_{\text{CCCP}}}{Q_f^{\text{CPP}} + Q_f^{\text{HWPB}}} + \left[\frac{Q_f^{\text{CPP}} + Q_f^{\text{HWPB}} - Q_f^{\text{CCCP}}}{Q_f^{\text{CPP}} + Q_f^{\text{HWPB}}} - \frac{Q_f^{\text{PHWPB}}}{Q_f^{\text{CPP}} + Q_f^{\text{HWPB}}} \right] \times P_f \times T \rightarrow \max. \quad (14)$$

In Eq. (14), the expression in square brackets represents the relative fuel savings at the TPP compared to separate generation (ΔQ_f), and the first component of the expression in square brackets represents the relative fuel savings of the CCCP compared to separate generation.

According to (3), the maximum of (14) is reached when each of the summands in the equation tends to the maximum. If specific capital investments for construction of a hot water boiler plant and cogeneration plant are comparable, the specific integral economic effect ΔNPV will have the maximum value when:

$$\overline{\Delta Q_f} \times P_f \times T \rightarrow \max. \tag{15}$$

The expression for determining the relative fuel savings compared to separate generation can be presented as follows (16):

$$\overline{\Delta Q_f} = 1 - \frac{\frac{\eta_{CPP}}{\eta_{fhu}} \times \left(1 + \frac{1}{y}\right)}{1 + \frac{1}{y} \times \frac{\eta_{CPP}}{\eta_{HWB}}} - \frac{\frac{Q_C}{\eta_{HWB}} - \frac{Q_{CCCP}}{\eta_{HWB}}}{\frac{W_e}{\eta_{CPP}} + \frac{Q_C}{\eta_{HWB}}}, \tag{16}$$

or

$$\overline{\Delta Q_f} = 1 - \frac{\frac{\eta_{CPP}}{\eta_{fhu}} \times \left(1 + \frac{1}{y}\right) \times \alpha_{TPP}}{\alpha_{TPP} + \frac{1}{y} \times \frac{\eta_{CPP}}{\eta_{HWB}}} - \frac{1 - \alpha_{TPP}}{1 + y \times \alpha_{TPP} \times \frac{\eta_{HWB}}{\eta_{CPP}}}, \tag{17}$$

where

- η_{fhu} —coefficient of fuel heat utilization;
- η_{HWB} —efficiency of the replacing hot water boiler plant;
- η_{CPP} —efficiency of the replacing CPP;
- α_{TPP} —extraction factor;
- y —specific power generation on thermal consumption;
- Q_C —total heat supply to the consumer in the separate and combined cycle;
- Q_{CCCP}, Q_{PHWB} —heat supply from CCCP and PHWB draw-offs, respectively;
- W_e —power generation in separate and combined cycle.

Thus, taking into account (15), expression (13) transforms into (18):

$$\left[1 - \frac{\frac{\eta_{CPP}}{\eta_{fhu}} \times \left(1 + \frac{1}{y}\right) \times \alpha_{TPP}}{\alpha_{TPP} + \frac{1}{y} \times \frac{\eta_{CPP}}{\eta_{HWB}}} - \frac{1 - \alpha_{TPP}}{1 + y \times \alpha_{TPP} \times \frac{\eta_{HWB}}{\eta_{CPP}}} \right] \times P_f \times T \rightarrow \max. \tag{18}$$

Expression (18) allows us to determine the optimal value of the connected heat load of the CCCP.

We applied the simulation method of the CCCP operation modes as the research method of the considered power unit operation. Modeling of the basic heat balance diagram was carried out using the software product “United Cycle”, which provides simulation and calculation of steady-state modes of operation of thermal power plants and systems.

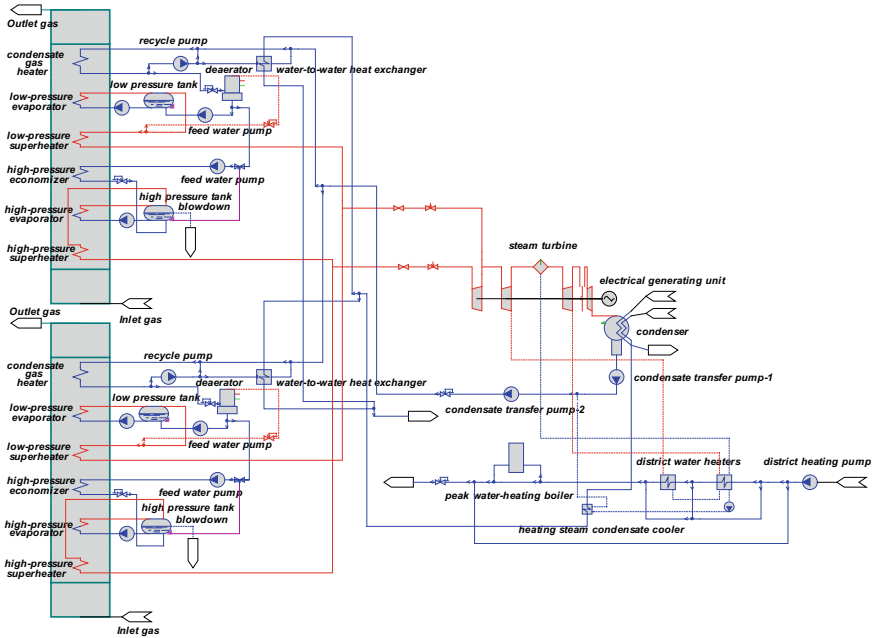


Fig. 1 Basic diagram of a double-loop combined-cycle CCCP, simulated in the CAD “United Cycle”

Figure 1 shows the design model of a CCCP unit based on GTE-160, simulated in the CAD “United Cycle”, including two vertical heat recovery steam generators (HRSGs) of two pressures and stationary heat recovery steam turbine, designed to work in the binary combined-cycle unit PGU-450, consisting of two GTUs type GTE-160, as well as peak water heating boilers.

The scheme parameterization is based on the warranted performance of the cogeneration unit, as well as on the thermal balance of the HRSG heating surfaces. The operation mode for nominal parameters under the factory characteristics of the equipment was simulated to check the adequacy of the model construction.

Adequacy test of the created mathematical model in relation to the real TPP, functioning on the basis of GTE-160 (Pravoberezhnaya TPP-5 public joint-stock company “TGK-1”) was carried out by method of stage-by-stage analysis of mode parameters, calculated with CAD “United Cycle”, and factory parameters of the combined cycle unit (HRSG and cogeneration unit). We compared the model for winter mode operation at the outside air temperature of $-24\text{ }^{\circ}\text{C}$. Table 3 provides the calculated characteristics of the model for this mode.

The study assumes the following:

- The assumed temperature diagram of the heating-system is 150/70, and the flow rate of heating-system water is constant and equal to 5000 t/h;

Table 3 Calculated parameters of the nominal mode of operation of the power plant unit simulated by CAD “United Cycle”

Parameter	Measurement unit	Value
<i>Gas turbine unit GTE-160</i>		
Outside air temperature	°C	−24
Outside air pressure	kPa	0.1013
Gas temperature at GTU outlet	°C	530.9
Gas flow rate at GTU outlet	t/h	1861.3
GTU capacity	MW	165.5
GTU efficiency	%	34.07
<i>Heat recovery steam generator (HRSG)</i>		
High pressure steam flow rate	t/h	221.65
Temperature of high-pressure steam at the outlet of HRSG	°C	508
High-pressure steam pressure	kg/cm ²	72.74
Temperature drop at the hot end of the low-pressure loop	°C	22.09
Pinch point of the low-pressure loop	°C	9.94
Low-pressure steam flow rate	t/h	52.14
Temperature of low-pressure steam at the outlet of the HRSG	°C	218.19
Low-pressure steam pressure	kg/cm ²	6.18
Temperature drop at the hot end of the low-pressure loop	°C	17.35
Pinch point of the low-pressure loop	°C	12.84
Water temperature at the inlet of HRSG	°C	64.93
Flue gas temperature	°C	106.47
<i>Steam turbine</i>		
High-pressure steam flow rate	t/h	443.31
Temperature of high-pressure steam at the outlet of HRSG	°C	507.19
Low-pressure steam flow rate	t/h	104.27
Temperature of low-pressure steam at the outlet of HRSG	°C	217.71
Calculated pressure in the condenser	kg/cm ²	0.02
Heating-system water flow rate	t/h	5460
Heating-system water temperature at the inlet to the district water heaters	°C	67
Heating-system water temperature at the outlet of the district water heaters	°C	117.26
Net electrical power	MW	96.73

- The water temperature at the inlet to the HRSG is maintained at 65 °C with the use of recirculation pumps;
- The reduced pressure in the condenser is 3 kPa in all calculated modes;
- WWHEs are switched off;
- The cooling water temperature at the condenser inlet during the considered heating period is constant and is 5 °C;
- No blowdown water losses in high- and low-pressure drum-type boilers.

The relative value of the deviation of the calculated parameters from the control parameters is less than 4%. Deviations are related to the simplification of the design model of the cogeneration unit, the non-simulation of turbine blowing and glands, and the assumptions that have been made.

2 Results

Figure 2 shows variants of integrating the CCCP into the heating system.

Line 1 indicates the change in the available heat load of the CCCP over the heating period.

Line 2 identifies the change in the TPP heat load, at the maximum connected heat load of 1354.94 MW—option 1. In this case, the sliding grid is closed completely at the beginning of the heating period, and the heat load is regulated entirely by the hot-water boilers, operating for the whole heating period. In this variant of integrating the CCCP into the heating system, the extraction factor is about 0.24.

Line 3 indicates the change in TPP heat load when the connected heat load corresponds to the minimum possible heat load. Here, the heat supply capacity is regulated by changing position of the sliding grid. The CCCP operates with condensing pass during the whole heating period. Peak water heating boilers are switched off. The extraction factor for this variant of CCCP integration into the heat system equals 1.

Lines 4–8 characterize the heating loads of the TPP, corresponding to the intermediate values of the extraction factor.

Figure 2 can be represented as the function of the plant total heat load on the number of hours of outside air temperatures during the year for the heating period for St. Petersburg, shown in Fig. 3.

Integral parameters of the considered variants of CCCP operation in the heating system during the heating period are shown in Table 4.

The relative fuel savings compared to separate generation for different values of the extraction factor were determined based on Eq. (17), and the calculated characteristics is presented in Table 4. The efficiency value of the substituting hot water boiler plant was assumed to be 93%, and the efficiency value of the substituting CPP—40%. Figure 4 shows a diagram of the dependence of the relative fuel savings in compared with the separate generation on the value of the extraction factor. According to Fig. 4, the relative fuel savings compared to the separate generation have a distinct maximum at $\alpha_{\text{TPP}} \approx 0.49$.

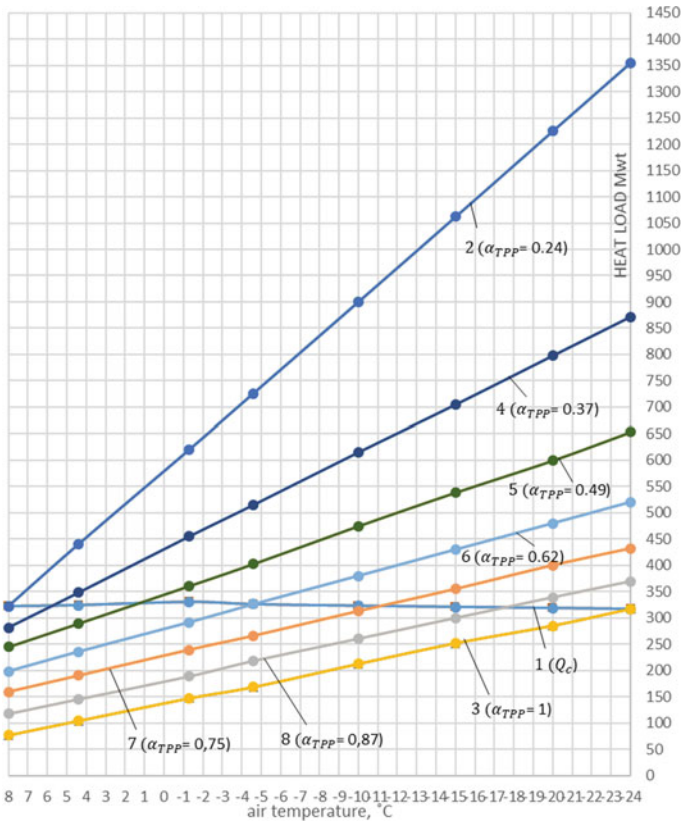


Fig. 2 Ways of integrating the CCCP into the thermal system: 1—available heat load of CCPP; 2—maximum connected heat load to CCPP; 3—minimum connected heat load to CCPP; 4—extraction factor of CCCP included in the heat system $\alpha_{\text{ТПР}} = 0.37$; 5—extraction factor of CCCP included in the heat system $\alpha_{\text{ТПР}} = 0.49$; 6—extraction factor of CCCP included in the heat system $\alpha_{\text{ТПР}} = 0.62$; 7—extraction factor of CCCP included in the heat system $\alpha_{\text{ТПР}} = 0.75$; 8—extraction factor of CCCP included in the heat system $\alpha_{\text{ТПР}} = 0.87$

Excluding construction and installation costs, the unit cost of hot water boilers (according to data currently being realized at Avtovskaya TPP-15 of public joint-stock company «TGK-1» in St. Petersburg) is 1.3 million rubles per Gcal of installed capacity. With similar cost of piping connection for heating-system water, the specific capital costs of steam heat exchangers of similar capacity in the calculations are based on a different ratio between the specific costs of a water heating boiler plant ($k_{\text{HВВ}}$) and steam heat exchangers ($k_{\text{СР}}$): $\frac{k_{\text{HВВ}}}{k_{\text{СР}}} = 0.5; 1; 2; 4; 8; 10$.

The increase of specific integral economic effect δNPV for different values of the extraction factor at different ratio of specific cost of HWB and steam heat exchangers, calculated by Eq. (18), is shown in Fig. 5.

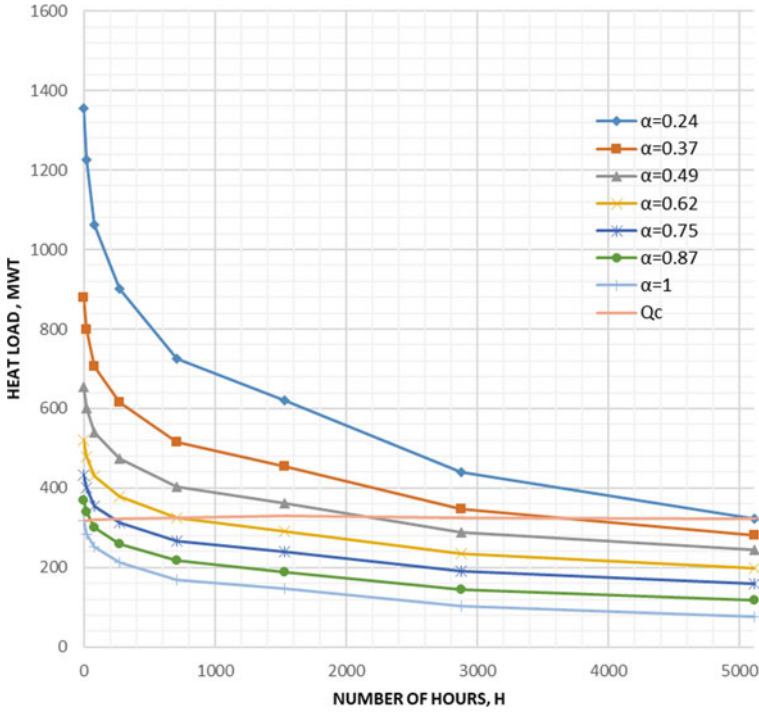


Fig. 3 Dependence of the plant total heat load on the number of hours of outside air temperatures during the year for the heating period of St. Petersburg (Rossander's diagram)

Figure 5 shows that regardless of the value of capital costs, the maximum specific integral economic effect δNPV is achieved at $\alpha_{TPP} \approx 0.49$. The maximum relative fuel saving compared to separate generation is achieved at this value.

3 Discussion

The selection of the optimal mix of equipment is a key issue for the construction of new, high-efficiency power plants. It affects not only the initial capital investment, but also the expected operating costs (fuel costs form the largest part of them). Determination of the optimal extraction factor, as in the design of thermal power plants designed not only for electric power supply but also for heat supply of the consumer, is an important aspect of this issue and requires a comprehensive analysis.

Whereas for CCCPs, regarded as traditional for the Russian energy sector, this task was solved, but we do not have a unified approach to solving this issue for CCCPs.

Table 4 Operating parameters of CCCP operation during the heating period with different connected heat loads

Parameters	Value ($Q_{\text{fuel}} = 50 \frac{\text{MJ}}{\text{kg}}$, $\eta_{\text{CCP}} = 40\%$, $\eta_{\text{HWB}} = 93\%$)						
	0.24	0.37	0.49	0.62	0.75	0.87	1.00
Extraction factor α_{TPP}	0.24	0.37	0.49	0.62	0.75	0.87	1.00
Total heat supply to consumers from CCCP, thousand Gcal	2369.0	1786.1	1448.0	1171.3	953.0	748.9	559.2
Heat supply from CCCP, thousand Gcal	1427.2	1388.3	1300.0	1136.6	945.3	747.7	559.2
Heat supply from hot water boilers, thousand Gcal	941.9	397.7	148.0	34.8	7.7	1.2	0.0
Total fuel consumption, t	438,949	389,916	367,415	357,209	354,767	354,186	354,077
Fuel consumption for the CCCP, t	354,077	354,077	354,077	354,077	354,077	354,077	354,077
Fuel consumption for hot water boilers, t	84,872	35,839	13,339	3133	691	109	0
Electricity generation, thousand MW*h	2139	2146	2164	2199	2243	2288	2316
Fuel heat utilization coefficient, (η_{fhu}), %	77.26	76.50	74.77	71.61	67.97	64.23	60.33
Specific electric power generation at thermal consumption, γ , MW/MW	1.29	1.33	1.43	1.66	2.04	2.63	3.56
Relative fuel savings compared to separate generation, ΔQ	0.266	0.288	0.293	0.287	0.275	0.261	0.242

Under the conditions of a planned economy for a TPP based on a steam turbines unit the problem of finding the optimal extraction factor was solved by using the rate of relative fuel savings compared to the separate production of electricity and heat. In the conditions of the formed market economy, the selection and final justification of technical solutions relies primarily on investment analysis with an assessment of the profitability, cost-effectiveness, and payback period of the project [14–16].

NPV is one of the main factors that characterize the investment prospects of a project. As shown by earlier studies [13], it is possible to correlate an increase in NPV using combined generation and the relative fuel savings compared to separate generation. This fact nowadays allows us to use the latter parameter, among other things, to optimize the coefficient of thermal efficiency of CCCP.

This article proposes an approach to optimizing the coefficient of thermal efficiency of CCCP, based on the basic elements of the method traditional for the Russian energy sector, which is quite applicable with a slight adaptation to modern economic conditions.

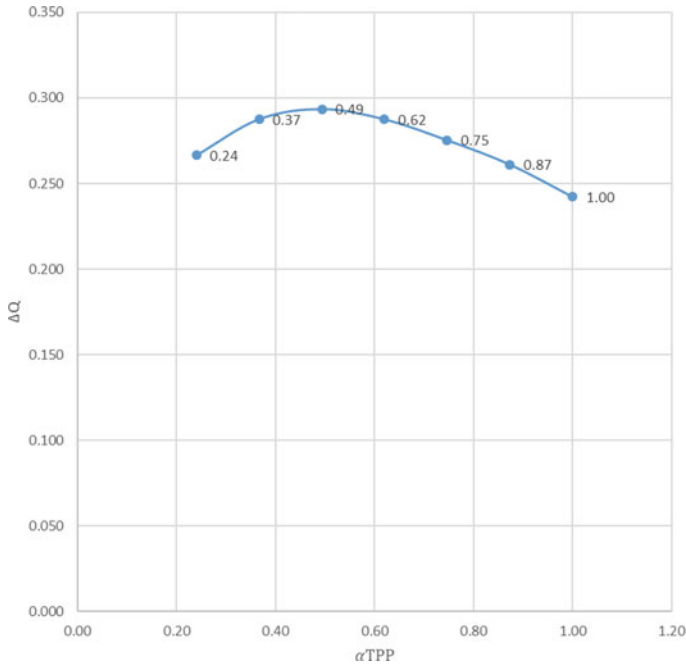


Fig. 4 Increase in relative fuel savings compared to separate generation for different values of the extraction factor

This method can be used to analyze and optimize the mix of CCCP equipment regardless of the geographic area, type of power system, energy resources cost, market conditions, and the characteristics of the used equipment.

In a competitive market environment absolute quantitative performance of power generating companies are less important than the relative indicators, qualitatively characterizing the degree of use of available resources. Thus, the use of the relative fuel savings, as a criterion of optimality, will allow in the future to form the most balanced, efficient energy systems, as well as create all conditions necessary to maximize profits of energy companies while optimizing the prices for electricity and heat and ensuring a reliable and uninterrupted power supply to the consumer.

4 Conclusion

1. In the current economic conditions, the relative fuel savings rate compared to separate generation can be used as an optimization criterion for solving the problem of selecting and justifying the thermal efficiency coefficient for CCCP.
2. For CCCP based on GTE-160 (two-boiler single-turbine unit) the value of the optimal extraction factor determined by the relative fuel economy rate,

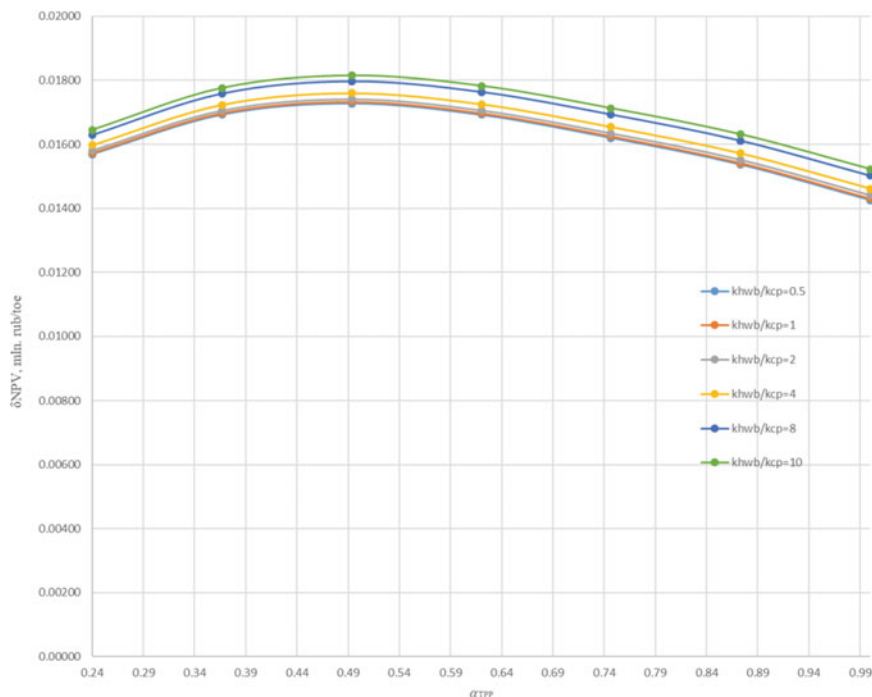


Fig. 5 Increase of specific integral economic effect δNPV for different values of the extraction factor at different ratio of the specific cost of hot water boilers and steam heat exchangers

compared to separate generation equals 0.49 under the climatic conditions of St. Petersburg.

- For a similar CCCP, the value of the optimal extraction factor, determined from the condition of maximizing the specific integral economic effect, is also 0.49. It should be noted that the ratio of specific capital investments in hot-water boilers and heat-exchange equipment of the CCCP has no significant impact on the obtained result.

References

- Makarov, A.A., Veselov, F.V., Makarova, A.S., Novikova, T.V., Pankrushina, T.G.: Strategic prospects of electric power industry in Russia. *Therm. Power Eng.* **11**, 40–52 (2017)
- Makarov, A.A., Mitrova, T.A., Veselov, F.V., Galkina, A.A., Kulagin, V.A.: Prospects for electric power industry in the context of world energy markets transformation. *Therm. Power Eng.* **10**, 5–16 (2017)
- Abdulrahman, A., Pericles, P., Nawaf, A.-M.: Energetic and exergetic analysis of combined cycle power plant: part-1 operation and performance. *Energies* **8**, 14118–14135 (2015)

4. Lorencin, I., Anđelić, N., Mrzljak, V., CarGenetic, Z.: Algorithm approach to design of multi-layer perceptron for combined cycle power plant electrical power output estimation. *Energies* **12**, 4352 (2019)
5. Keshavarzian, S., Gardumi, F., Rocco, M.V., Colombo, E.: Off-design modeling of natural gas combined cycle power plants: an order reduction by means of thermoeconomic input-output analysis. *Entropy* **18**, 71 (2016)
6. Toscano, C.F., Martín-del-Campo, C., Moeller-Chavez, G., de los Santos, G.L., François, J.-L., Fernandez, D.R.: Life cycle assessment of a combined-cycle gas turbine with a focus on the chemicals used in water conditioning. *Sustainability* **11**, 2912 (2019)
7. Olkhovskii, G.G.: Combined cycle plants: yesterday, today, and tomorrow (review). *Therm. Eng.* **63**(7), 488–494 (2016)
8. Tuznikova, E.M., Novikova, O.V., Tuznikov, M.A.: Technical and economic assessment of the selection of cogeneration technology to provide district heating. In: *Week of Science SPbPU, Materials of the Scientific Conference with International Participation*, 3 vols., pp. 728–73. Institute of Industrial Management, Economics and Trade (2019)
9. Bugaeva, T.M., Novikova, O.V.: Modern methods of planning the urban energy system. Power engineering. In: *Proceedings of Higher Educational Institutions and Energy Associations of the CIS*, vol. 62, no. 4, pp. 377–387 (2019)
10. Kabanov, M.S., Novikova, O.V.: Reducing the energy intensity of WDM by optimizing the heat supply system of a metropolis. In: *Effective Energy—2014, Proceedings of the All-Russian Scientific and Practical Conference*, pp. 427–438 (2015)
11. Kostyuk, R.I., Piskovatskov, I.N., Chugin, A.V., Kotsyuk, N.N., Radin, Yu.A., Berezinets, P.A.: Some features of operation modes of the main power unit PGU-45. *Teploenergetika* **9**, 6–11 (2002)
12. Radin, Yu.A., Lyubtsov, A.A., Makarov, O.N.: Basic performance indicators of the PGU-450T stream-gas unit during operation in the district heating and electric power mode. *Power Technol. Eng.* **46**(1), 70–74 (2012)
13. Kalyutik, A.A., Treshchev, D.A., Treshcheva, M.A.: Using the parameter of relative fuel savings to optimize the parameters of cogeneration CCGT. *Mater. Sci. Power Eng.* **26**(4), 51–63 (2020)
14. Balyinin, I.V.: Assessing the effectiveness of investment projects: rules, indicators and procedure for their calculation. *Econ. Anal.: Theory Pract.* **6**(453), 26–41 (2016)
15. Nikolenko, T.Y., Tarasova, E.V.: Balanced indicator system and tools for assessing the effectiveness of innovation projects. *Scientific and technical news of St. Petersburg State Polytechnic University, Economic Sciences* **6**, pp. 228–235 (2016)
16. Lisin, E., Rogalyov, N., Okley, P.: Development of a model for assessing the impact of power system production capacity structure on regional energy security. *Terra Economicus* **17**(2), 96–111 (2019)

Determination of Friction Coefficients as Well as Heat and Mass Transfer Coefficients in Film-Type Countercurrent Apparatuses with Intensifiers



A. G. Laptev and E. A. Lapteva

1 Introduction

Intensification of heat and mass transfer processes represents an important direction for the development of fundamental and applied science in chemical engineering as well as power engineering.

The Russian Federation has adopted a strategy for the development of the Russian chemical and petrochemical complex for the period up to 2030. In this regard, both the design of new highly efficient heat and mass transfer apparatuses and the modernization of those operating in industry are of great current interest. A wide class of such apparatuses is of the film type, mainly with countercurrent phases [1–4]. Despite extensive studies of film-type apparatuses in the second half of the last century, the design and calculation methods are constantly being improved [5–8]. Most of the work in this area is of an empirical nature and associated with numerous studies of hydrodynamics and heat and mass transfer on experimental walls or with the use of numerical methods. For practical calculations of film-type apparatuses, it seems expedient to use approximate modeling methods, which, with minimal expenditure of material resources and time, allow obtaining reliable results with acceptable accuracy. These methods include methods of linearization of differential transport equations, one-parameter integral methods in the theory of the boundary layer, film-type model, penetration model and a model of the diffusion boundary layer, conservative properties of the turbulent boundary layer, dissipative models, etc.

The purpose of the present work is to develop a dissipative mathematical model of the transfer of momentum, heat, and mass of components in the turbulent regime of gas motion in film-type apparatuses with intensifiers, which allows performing calculations using the hydraulic resistance of contact devices.

A. G. Laptev (✉) · E. A. Lapteva
Kazan State Power Engineering University, Kazan, Russia

2 Statement of the Problem

When flows move in channels with intensifiers (wire inserts, protrusions, dimples, etc.), the turbulent regime begins earlier than with smooth walls. For example, in channels with discretely rough walls, turbulization begins already at Reynolds numbers $Re > 200\text{--}500$, depending on the shape and height of the protrusions [1–3]. Almost always, the movement of gases in film-type apparatuses occurs at $Re > 500\text{--}1000$; therefore, only the turbulent regime in packings of various shapes at countercurrent with a liquid film is considered below.

Further, the processes of transfer of momentum, mass, and heat in the gas phase of film-type apparatuses with intensifiers are considered. Such apparatuses include cooling towers, gas cooling and water heating scrubbers, absorption and distillation columns with structured and random packings [9–12]. To intensify the transfer phenomena, annular and helical knurls, wire inserts, corrugations, notches, etc. are used [7–10], as well as roughness on the surface of contact devices [11–17].

In the present work, mathematical modeling is carried out and calculated dependences are obtained for the shear stress at the gas–liquid film interface as well as for the average heat and mass transfer coefficients connected with the hydraulic resistance of contact devices with transfer intensifiers. The regime of weak interaction of the gas with the film is considered. To achieve this goal, the model of the turbulent boundary layer in a local one-dimensional setting, as well as the properties of conservatism of the form of the mathematical description to perturbations, established by S. S. Kutateladze, A. I. Leontyev, etc., are used [18]. In the presence of perturbations caused by intensifiers, the form of the mathematical description does not change, but is taken into account parametrically.

3 Heat and Mass Transfer Coefficients

To determine the coefficients of heat and mass transfer, we use the expression obtained earlier by the authors of [15] based on the three-layer model of the turbulent boundary layer

$$\alpha_g = \frac{\rho_g c_p u_*}{Pr_g^{0.67} (R_1 + 2.5 \ln R_\delta)}, \quad (1)$$

$$\beta_g = u_* \left[Sc_g^{0.67} (R_1 + 2.5 \ln R_\delta) \right]^{-1}, \quad (2)$$

where u_* is the dynamic velocity, m/s; ρ is the density of the medium, kg/m^3 ; c_p is the specific heat of the medium at constant pressure, J/kg K; Pr_g is the Prandtl number; Sc_g is the Schmidt number; R_1 is the dimensionless thickness of the viscous

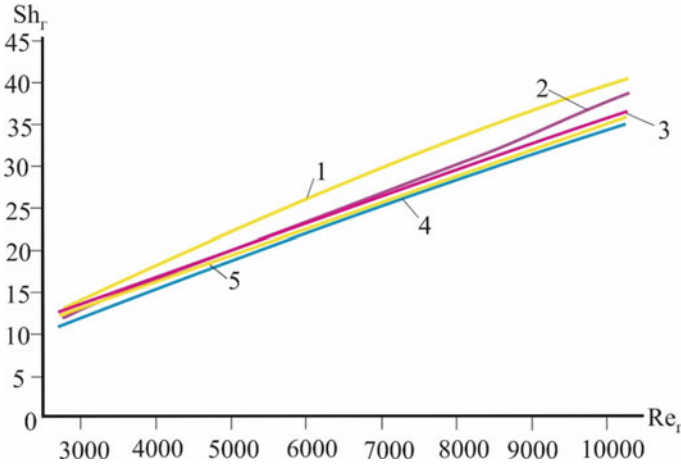


Fig. 1 Results of calculations of the number Sh_g : 1—calculation via the formula of hydrodynamic analogy [20]; 2—calculation via formula (2); 3—calculation via the Sherwood formula [19]; 4—calculation via the Barnett formula [19]; 5—calculation via the Prandtl formula [20]. (air–water, $Sc_g = 0.7$)

sublayer; $R_\delta = u_*\delta/\nu_g$ is the dimensionless thickness of the boundary layer; δ is the thickness of the boundary layer, m; ν_g is the kinematic viscosity, m^2/s .

According to the model of Deissler and Van Driest, $R_1 = 5.31$ for surfaces without intensifiers.

To determine the average value of the dynamic velocity in the gas phase in a conditionally smooth channel with a falling film at $ku_*/\nu < 60$, one can use an expression obtained from the equation of the balance of forces $u_* = (w_g + u_l)\sqrt{\xi_{irr}/8}$, where w_g is the average gas velocity, m/s; u_l is the average velocity of the falling film, m/s; ξ_{irr} is the coefficient of hydraulic resistance of the irrigated channel; k is the height of the intensifiers protrusions, m.

Calculations of the Sherwood number via formula (2) are in satisfactory agreement (Fig. 1) with the calculated and experimental data [19, 20] for smooth irrigated pipes with countercurrent phases at $3000 < Re < 10^5$, where $Re_g = (w_g + u_l)d_{eq}/\nu_g$ is the Reynolds number for the irrigated pipe; $d_{eq} = (d - 2\delta_l)$ is the equivalent diameter, m; δ_l is the film thickness, m; d is the pipe diameter, m.

4 Mathematical Model of Friction

On the surfaces of film-type contact devices with intensifiers, waves with different wave characteristics are formed, depending on the liquid flow rate (irrigation density) and the design features of the phases contact surface. At $ku_*/\nu > 60$, the regime of a gas flow around the film with a significant effect of roughness (protrusions,

knurls, wire inserts, etc.) on the wave characteristics of the film as well as on the hydraulic resistance of the contact devices occurs. In this case, the shear stress will be affected not only by friction at the interface but also by the form resistance of the wave surface of the film, and the above expression for the calculation will give an error. Under such conditions, to determine the average shear stress and, accordingly, the dynamic velocity, we use the approach using the average velocity of dissipated kinetic energy in the boundary layer. In a one-dimensional formulation, the rate of energy dissipation due to viscosity has the form [21]

$$\varepsilon = \frac{de}{dy} = \tau \frac{du}{dy}, \quad (3)$$

where $e = u\tau$ is the energy flux density, Pa s; du/dy is the velocity gradient, s^{-1} ; y is the transverse coordinate in the boundary layer, m; ε is the energy dissipation, $kg/(m s^3)$.

In expression (3), we write down the velocity gradient from the local momentum flux

$$\tau = -\rho_g(\nu + \nu_T)_g \frac{du}{dy}, \quad (4)$$

where ν , $\nu_T(y)$ are the kinematic coefficients of molecular and turbulent viscosity, m^2/s ; ρ_g is the gas density, kg/m^3 .

From expressions (3) and (4), we obtain

$$\varepsilon = \frac{\tau^2}{\rho_g(\nu + \nu_T(y))_g}. \quad (5)$$

Hence, the average value of the rate of dissipated energy in the boundary layer in the gas will take the form

$$\varepsilon = \frac{1}{\delta} \int_0^\delta \frac{\tau^2 dy}{\rho_g(\nu + \nu_T(y))_g}. \quad (6)$$

When integrating (6), we used the Deissler function of turbulent viscosity

$$\frac{\nu_T(y)}{\nu} = K_D(\chi y^+)^2 \frac{d}{dy} \left(\frac{u}{u_*} \right), \quad (7)$$

where $y^+ = u_* y / \nu_g$ is the dimensionless coordinate in the boundary layer; $\chi = 0.4$ is the turbulence constant; K_D is the damping factor, which is determined via the formula

$$K_D = \left[1 - \exp(-0.0092\chi^2 - (y^+)^2)^{0.5} \right]^2.$$

As a result of numerical integration of (6) with $v_T(y)$ from (7), the average value of the rate of dissipated energy in the turbulent boundary layer is obtained as follows:

$$\bar{\varepsilon} = \frac{\tau_w^2 (R_1 + 2.5R_\delta)}{\rho_g \nu_g R_\delta}, \quad (8)$$

where τ_w is the shear stress at the interface, Pa; $R_1 = 5.31$ is for smooth plate.

From expression (8), the shear stress and dynamic velocity $u_* = \sqrt{\tau_w/\rho_g}$ can be written in the form

$$\tau_w = \left(\frac{\bar{\varepsilon} \rho_g \nu_g R_\delta}{R_1 + 2.5 \ln R_\delta} \right)^{0.5}, \quad (9)$$

$$u_* = \left(\frac{\bar{\varepsilon} \delta}{\rho_g (R_1 + 2.5 \ln R_\delta)} \right)^{1/3}. \quad (10)$$

We write the average value of the rate of dissipation of energy $\bar{\varepsilon}$ in the gas phase through the hydraulic resistance of the contact devices

$$\bar{\varepsilon} = \frac{\Delta P G}{\rho_g V_g}, \quad (11)$$

where ΔP is the pressure drop, Pa; G is the mass flow rate, kg/s; V_g is the volume of the boundary layer in the gas phase, m^3 .

The volume of the boundary layer $V_g = \delta a_v \psi_o H S$, where ψ_o is the coefficient of contact between the surfaces of the packing elements; H is the packing height, m; S is the cross-sectional area of the apparatus, m^2 . At $\psi_o = 1$, the elements are not in contact with each other and the volume of the boundary layer is maximum for the given conditions. From the above expressions, we obtain

$$\bar{\varepsilon} = \frac{\Delta P w_g \varepsilon_{\text{free}}}{\delta a_v \psi_o H}, \quad (12)$$

where w_g is the gas velocity in the packed bed, m; $w_g = G/(\rho_g \varepsilon_{\text{free}} S)$; $\varepsilon_{\text{free}}$ is the specific free volume, m^3/m^3 ; a_v is the specific surface area of contact devices, m^2/m^3 .

The pressure drop across the packing is found using the Darcy-Weisbach expression

$$\Delta P = \xi_{\text{irr}} \frac{H}{d_{\text{eq}}} \frac{\rho_g w_g^2}{2}, \quad (13)$$

where $d_{eq} = 4\varepsilon_{free}/a_v$ is the equivalent diameter of the packing element, m.

As a result, from (10)–(13) we have

$$u_* = w_g \left(\frac{\xi_{irr}}{8\psi_o(R_1 + 2.5 \ln R_\delta)} \right)^{1/3}, \quad (14)$$

where the values of R_1 and R_δ for random packings and structured packings with intensifiers are calculated via the expressions [20]

$$R_1 = 5.31 \frac{w_g \sqrt{0.04/\text{Re}_g^{0.25}}}{u_*}, \quad R_\delta = 6.49(\text{Re}_g \xi_{irr})^{0.25}, \quad (15)$$

where $\text{Re}_g = w_g d_{eq}/v_g$ is the Reynolds number; ξ_{irr} is the resistance coefficient of irrigated packing.

The resistance coefficient is determined experimentally for each packing design.

5 Results of Calculations

Figures 2, 3, 4, 5 and 6 show results of calculating the coefficients of heat and mass transfer via formulas (1), (2) with a dynamic velocity from (14).

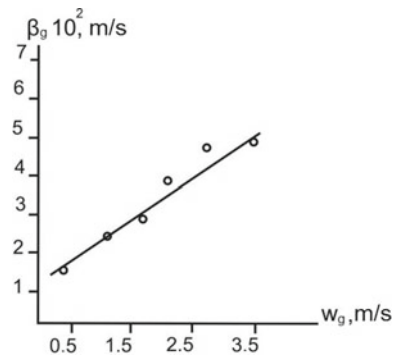
In Fig. 2, calculation results and experimental data on mass transfer are shown for a structured coiled packing made of metal strips with notches [22], $a_v = 480 \text{ m}^2/\text{m}^3$.

In Fig. 3, data are presented for various structured and random packings, summarized in the monograph [19]. In Fig. 4, data are presented for tubular structured packing made of polyethylene net [20], which is used in cooling towers.

Figure 5 shows dependences on the volumetric coefficients of mass transfer for the above-considered polyethylene packing in cooling towers.

Volumetric coefficients are written as

Fig. 2 Dependence of the mass transfer coefficient in the gas phase on the gas velocity at an irrigation density of $10 \text{ (m}^3/\text{m}^2 \text{ h)}$, $d_{eq} = 0.0079 \text{ m}$. \circ —experiment [22]; line—calculation via formula (2). Coiled metal packing with notches



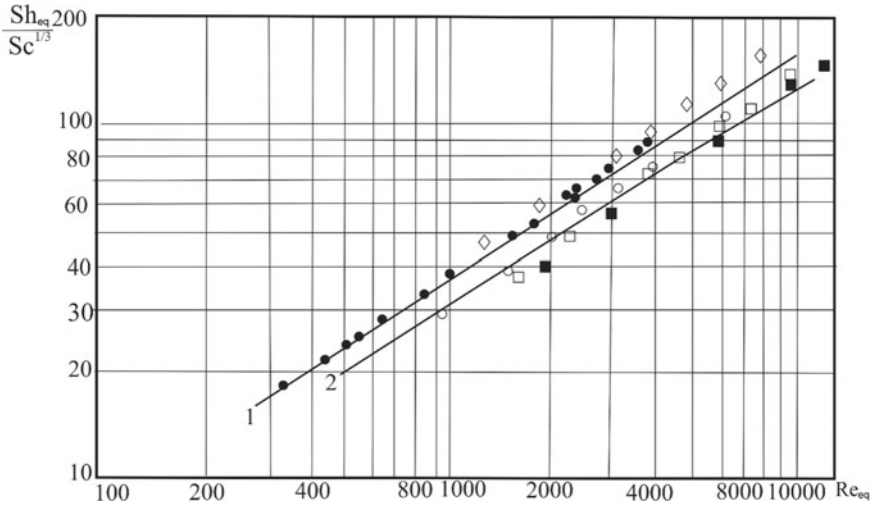


Fig. 3 Dimensionless group for mass transfer in the gas phase during the sublimation of naphthalene and evaporation of water from the surface of various packings. Dots—experimental data [19]: ●—Raschig rings 25 mm; ◇—Raschig rings 50 mm; ■—Raschig rings 50 mm, orderly laying; ○—Raschig rings 80 mm, orderly laying; □—100 mm, orderly laying (Gildenblat data). 1—calculation for random packings via formula (2); 2—calculation for structured packings via formula (2)

Fig. 4 Dependence of the mass transfer coefficient on the gas velocity for a mesh packing in a cooling tower. Irrigation density is $7.61 \text{ m}^3/(\text{m}^2 \text{ h})$, specific surface $a_v \approx 140 \text{ m}^2/\text{m}^3$, $d_{eq} = 0.026 \text{ m}$; 1—experiment [20]; 2—calculation via expression (2)

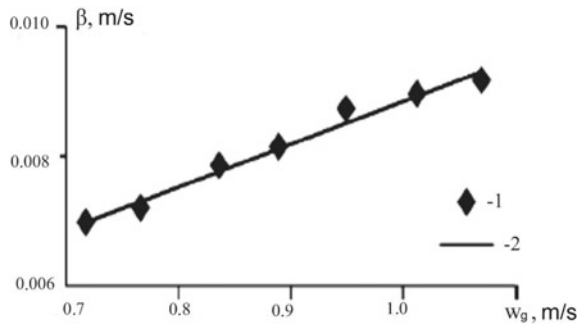


Fig. 5 Dependence of the volumetric coefficient of mass transfer on the air velocity: 1, 2—calculation via (16). 1—water consumption is $4.9 \text{ m}^3/(\text{m}^2 \text{ h})$; 2—water consumption is $7.0 \text{ m}^3/(\text{m}^2 \text{ h})$

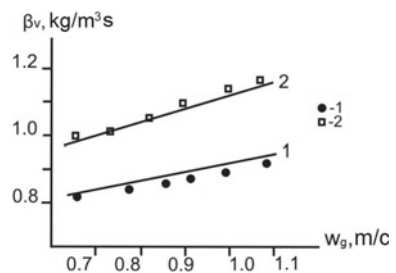
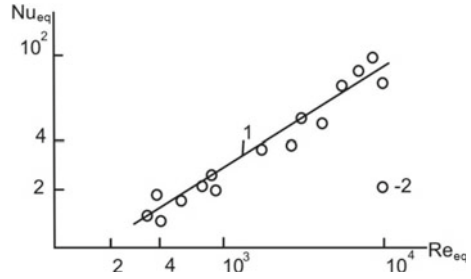


Fig. 6 Heat transfer in the layers of packing elements: 1—calculation via Eq. (1); 2—experimental data of Blinichev and Komleva [23]



$$\beta v = \beta_g \rho_g a_v \psi_w, \quad (16)$$

where ψ_w is the coefficient of wettability of the packing surface [19].

Calculated and experimental data on heat transfer in random packings having elements in the form of cylinders and parallelepipeds.

Satisfactory agreement of the results of calculations of transfer coefficients with experimental data [19, 20, 22] shows the adequacy of the developed mathematical model for film-type contact devices of various designs with intensifiers.

6 Conclusion

The main task in the development of pre-design solutions for industrial apparatuses in various industries and power engineering is to determine the efficiency of the processes. For this, numerical, analytical, approximate, and experimental methods are used. In order to reduce material and time costs, it seems expedient to determine the efficiency of heat and mass transfer processes using only data on the hydraulic resistance of contact devices, and the parameters of a mathematical model using the pressure drop and momentum balance in the boundary layer. In this work, this approach was applied on the example of film-type contact devices with transfer intensifiers.

References

1. Korovin, P.I., Lagutkin, M.G., Korovina, N.A., Pushnov, A.S.: Investigation of heat and mass transfer characteristics of structured packing. In: Collection of Scientific Papers Based on the Materials of the IV International Scientific and Practical Conference, pp. 88–92 (2019)
2. Bagomedov, M.G.-G., Pushnov, A.S., Berengarten, M.G.: Effect of packing type on hydraulic resistance of contact devices. Chem. Pet. Eng. **55**(5–6), 379–383 (2019)
3. Sister, V.G., Pushnov, A.S., Pirogova, O.V., Karpenko, A.S.: Modern methods of intensifying the processes of heat and mass transfer in contact with a packing. Theor. Found. Chem. Eng. **53**(3), 141–145 (2019)

4. Sister, V.G., Pushnov, A.S., Pirogova, O.V., Karpenko, A.S.: Advanced techniques for intensification of processes of heat and mass transfer in contact devices containing packings. *Khimicheskii Tekhnologii* **19**(4), 173–177 (2018)
5. Pushnov, A.S., Bagomedov, M.G.G., Berengarten, M.G.: Influence of geometric characteristics of contact devices on hydrodynamics and efficiency of heat and mass transfer processes. *Khimicheskaya Promyshlennost'* **95**(3), 124–133 (2018)
6. Sokolov, A.S., Pushnov, A.S., Shapovalov, M.V.: Hydrodynamic characteristics of mini-ring truncated-cone packing. *Chem. Pet. Eng.* **53**(1–2), 26–29 (2017)
7. Tikhonov, I.S., Folov, A.S., Voinov, N.A.: Films with helical roughness. In: Loginova, Yu.Yu. (ed.) *Young Scientists in Solving Urgent Problems of Science, Collection of Materials of the All-Russian Scientific-Practical Conference of Students, Graduate Students and Young Scientists*, pp. 194–196 (2017)
8. Voinov, N.A., Zemtsov, D.A., Zhukova, O.P.: Investigation of thermal distillation in a tower with small mass transfer on the stages. *Teor. Osn. Khim. Tekhnol.* **51**(2), 174–181 (2017)
9. Voinov, N.A., Zemtsov, D.A., Zhukova, O.P.: Study of thermal rectification in a column with low mass transfer on the steps. *Theor. Found. Chem. Eng.* **51**(2), 191–198 (2017)
10. Volodin, O., Pecherkin, N., Pavlenko, A., Zubkov, N.: Surface microstructures for boiling and evaporation enhancement in falling films of low-viscosity fluids. *Int. J. Heat Mass Transf.* **155**, 119722 (2020)
11. Pavlenko, A.N., Pecherkin, N.I., Zhukov V.E., Nazarov, A.D., Meski, G., Houghton, P. Effect of the angle of rotation of structured packing layers on separation efficiency in distillation column. In: *Journal of Physics: Conference Series, 5th International Workshop on Heat/Mass Transfer Advances for Energy Conservation and Pollution Control, IWHT 2019*, p. 012036 (2019)
12. Pavlenko, A.N., Kuznetsov, D.V., Volodin, O.A., Zubkov, N.N.: Heat transfer and dynamics of transient processes at liquid film flowing on smooth and modified surfaces. In: *Journal of Physics: Conference Series, 5th International Workshop on Heat/Mass Transfer Advances for Energy Conservation and Pollution Control, IWHT 2019*, p. 012052 (2019)
13. Pavlenko, A.N., Zhukov, V.E., Pecherkin, N.I., Nazarov, A.D., Slesareva, E.Y., Li, X., Sui, H.: Efficiency of mixture separation in distillation columns with structured packings under different ways of dynamically controlled irrigation. *J. Eng. Thermophys.* **28**(3), 313–323 (2019)
14. Sokolov, A.S., Pushnov, A.S., Shapovalov, M.V.: Hydrodynamic characteristics of mini-ring truncated-cone packing. *Chem. Pet. Eng.* **53**(1–2), 26–29 (2017)
15. Laptsev, A.G., Basharov, M.M.: Mathematical model and calculation of heat transfer coefficients of rough turbulent-flow-carrying channels. *J. Eng. Phys. Thermophys.* **88**(3), 681–687 (2015)
16. Karpenko, A.S., Pushnov, A.S., Berengarten, M.G.: Testing of a structured honeycomb packing for the implementation of heat and mass transfer processes in column apparatus in chemical technology. In: *The collection Energy-Efficient Environmentally Friendly Technologies and Equipment, Collection of Scientific Papers of the International Scientific and Technical Symposium “The Second International Kosygin Readings, Timed to Coincide with the 100th Anniversary of the Kosygin Russian State University” at the International Kosygin Forum-2019 “Modern Problems of Engineering Sciences”*, pp. 68–72 (2019)
17. Karpenko, A.S., Berengarten, M.G., Yudina, L.A., Pushnov, A.S.: Hydraulic and heat and mass transfer tests of honeycomb packing. *Vestnik Permskogo Natsional'nogo Issledovatel'skogo Politekhnikheskogo Universita. Khimicheskaya Tekhnologiya i Biotekhnologiya* **2**, 92–103 (2019)
18. Kutateladze, S.S.: *Fundamentals of Heat Transfer Theory*, pp. 416. Atomizdat, Moscow (1979)
19. Ramm, V.M.: *Absorption of Gases*, pp. 655. Khimiya, Moscow (1976)
20. Laptsev, A.G., Basharov, M.M., Laptseva, E.A., Farakhov, T.M., Laptsev, A.G. (eds.): *Models of interphase transport and calculation of process efficiency. In: Part 2: Heat and Mass Transfer Processes*, pp. 565. Center for Innovative Technology, Kazan (2020)
21. Landau, L.D., Lifshitz, E.M.: *Hydrodynamics*, 5th edn, pp. 736. Fizmatlit, Moscow (2003)

22. Dyakonov, S.G., Elizarov, V.V., Elizarov, V.I.: Theoretical Foundations for the Design of Industrial Apparatus of Chemical Engineering Based on Coupled Physical and Mathematical Modeling: Federal Education Agency, Kazan Technological University. Kazan State Technological University Press, Kazan (2009)
23. Blinichev, V.I.: Study of the coefficients of resistance and heat transfer of the packed bed. *Izvestiya Vuzov, Khimiya i Khimicheskaya Tekhnologiya* **30**(8), 1790–1800 (1987)

Pressurized Heat Recovery Steam Generator Design for CCGT with Gas Turbine GT-25PA and Steam Turbine T-100



Konstantin A. Pleshanov, Kirill Sterkhov, Dmitry A. Khokhlov, and Mikhail N. Zaichenko

1 Introduction

There is a problem with existing steam-power unit reconstruction in Russia. The proposed solution of this problem is using the Pressurized Heat Recovery Steam Generator (PHRSG) in Gas Turbine Combined Cycle (CCGT) [1–3]. It will save a part of equipment—a steam turbine and regeneration system and it will save the costs. This technology will maximize the electrical efficiency of energy unit and give the electrical capacity growth. Finally, yet importantly, it meets the requirements of the Russian energy development program.

One of the ways of solving this problem is usage of pressurized heat exchangers. They are divided in two directions: steam generators for nuclear power plants (NPP) and pressurized boilers. The NPP steam generators were used gas coolant with high temperature (400–650 °C) and pressure (up to 55 bar). The flue gas pressure in pressurized boilers (pressurized steam generators—PSG) is less than 7 bar, but its temperature is higher comparing steam generators.

The technology of gas pressurized boilers is not new. It comes in the late 19th—early twentieth centuries. The first units [4] has low efficiency from 3 to 14% with a maximum coolant pressure of up to 4 bar and low reliability. Their technical and economic characteristics were limited by the level of used technologies: compression equipment, fitting (not welding) of tubes, low quality of construction materials. Similar installations were used mainly as ship power unit.

The technological capabilities improvement in the middle of the twentieth century gave a new opportunity to use the positive features of the pressurized coolant. There are the heat transfer intensification and the lower hydraulic resistance in new power plants: CCGT with PHRSG [4] and nuclear power plants with gas coolant [5, 6].

K. A. Pleshanov (✉) · K. Sterkhov · D. A. Khokhlov · M. N. Zaichenko
Energy Units Simulation and Design Department, National Research University “MPEI”, 111250
Moscow, Russia

There were also transport and process modifications of such installations and binary CCGTs with nuclear fuel usage [4].

The CCGT with PHRSG projects were limited by the level of used technologies. Thus, the operating experience of gas-cooled reactors (Magneox and AGR) has shown that the reactivity of CO₂ increases significantly at high temperatures [5–8]. Providing reliable operation, the outlet CO₂ temperature in operating reactors was reduced from 675–650 to 600 °C [5, 6, 8]. The steel with 9% of chromium content was required because of corrosion resistance demands. The other limitation for this technology development is difficulties with helium coolant application in NPP.

The key problem for CCGT with PHRSG development in thermal power engineering was lack of high-power gas turbines with high-temperature combustion products at the combustion chamber exhaust.

The development of new power equipment has several stages. In the first stage, a computational study and justification of technical and economic characteristics are carried out. This has been done successfully in previous studies [1, 2]. At the second stage of research, a study of the PHRSG thermal scheme and its individual elements was carried out [3]. The current stage of development involves design characteristics determination and design project development.

The main goal of the current stage project is to design the construction of the PHRSG. The tasks are materials selection, binding to the manufacturing technology, and scientific substantiation of the main technical solutions.

2 Power Plants Operating Under Pressure of Flue Gas

Significant experience in research and development of flue gas pressurized power plants has been accumulated. It includes boilers under low pressure of flue gas (less than 2 bar), common water-tube and fire-tube boilers [9–14], and plants with a pressure of combustion products from 4 to 20 bar used in different industries: circulating fluidized-bed (CFB) boilers [15–17], NPP steam generators [8, 18–21] and PHRSG for CCGT [4, 13, 22–24]. It can be divided in two categories: plants with a reactor and a cooler (PHRSG for CCGT, CFB boilers) and plants with only gas cooling (NPP steam generators).

Technical solutions of these plants have important features for high efficiency and reliability. The typical features of such plant reactors are as follows:

- furnace and burners must provide efficient, reliable, and environmentally friendly combustion;
- furnace has radiant membrane gas-tight water-cooled steel panels.

There are several typical features for cooling part of such plants:

- crossflow of heat-transfer tubes;
- finned tubes with external fins;

- air or water cooling of vessel or heat resistant alloys usage instead of thermal insulation;
- forced circulation for low-pressure and once-through tube system for high-pressure or supercritical boilers;
- several units in case of big capacity;
- polyhedral or cylindrical shape of vessel;
- rising direction of steam-water mixture flow.

It could have been possible to use not only existing PHRSG and fossil-fuel PSG design experience but also PSG for NPP groundwork for new type of PHRSG development. It can be made by analyzing the construction and operation characteristics of energy units for NPP (Table 1) and TPP (Table 2).

Table 1 describes the generalized data for different NPP units: Magnox—Berkeley, Bradwell, Hunterston A, Hinkley Point A, Trawsfynydd, Dungeness A, Sizewell A, Oldbury, Wulfa, Calder Hall [5, 24]. AGR—Dungeness B, Hinkley Point B, Hunterston B, Hartepool, Heysam, Torness [5–8, 19]. Project of Helical-coil steam generator for Next Generation Nuclear Plant (NGNP) was given in [21].

Table 1 Main characteristics of pressurized steam generators for nuclear power plant

Characteristic	Name		
	Magnox	AGR	NGNP
Inlet gas temperature, °C	340–415	600–650	750
Inlet gas pressure, bar	8–26	40	70
Vessel cooling	Not used	Not used	Not used
Vessel material	MnCrMoV/Ducol	Austenitic stainless steel 316	No data
Vessel thickness, mm	30–60	60–90	No data
Superheater material	No data	Austenitic stainless steel 316	Inconel 617/ Incoloy 800
Units amount	4–8	12	1
Superheater outlet steam temperature, °C	390	541	540
Superheater outlet steam pressure, bar	94	173	182
Steam flow rate, kg/s	No data	525	250
Type	Circulating/Once-through	Once-through	Once-through
Coolant	CO ₂	CO ₂	He

Table 2 Main characteristics of pressurized steam generators for fossil-fuel thermal power plant

Characteristic	Name			
	PHRSG-45	PHRSG-120	PHRSG-450	PHRSG-450
Furnace exhaust combustion products temperature, °C	1720	1700	1580	1780
Combustion products pressure, bar	3.7	4.8	6.5	6.5
Vessel cooling	Combustion air			
Units amount	1	1	2	2
Superheater outlet steam temperature, °C	440	540	570	538
Superheater outlet steam pressure, bar	39	98	137.2	241
Steam flow rate, kg/s	12.5	33.3	125	250
Type	Forced circulation	Forced circulation	Forced circulation	Once-through

Modern steam generators for NPP consist of one vessel [5, 6, 8]. PSG for TPP commonly consist of vessel with two shells. The internal dividing shell has cylindrical shape in furnace part and prismatic shape in convective part.

There is a conical transition between furnace part and the convective part from one shape to another. The internal shell contains heat exchange surfaces and provide combustion products flow. The external shell has cylindrical shape. It bears main weight and pressure stress. Combustion air flows between the internal dividing shell and the external shell. This technical solution provides the vessel cooling. It makes possible to use less expensive materials and to reduce both shells wall thickness [4, 22].

First PSG for NPP with gas coolant were used vessel with two shells also. New material development provided its reliable work with high temperature coolant and interaction with CO₂. It has given a possibility to remove the internal dividing shell from construction of vessel [8]. The simple access to tubes and headers was provided, but it also has increased the quantity of tube passes in vessel. Tubes were combined into groups of 3–4 tubes [5, 24] to reduce the amount of temperature compensators. All headers were located inside the vessel in once-through PSG [5–8, 19]. It has reduced the amount of passes in vessel considerable [8].

Finned tubes were used in first generation of Magnox reactors for NPP. Later the finning technology have become simpler and cheaper. New fin shapes appeared. This provided spreading of finning technology for different types of another heat exchangers. One linear meter of helically-finned tube with solid or serrated fins gives

a heat transfer surface in 10–15 times greater than bare tube. Specific quantity of metal for bare tube (21.6 kg/m^2) is 5 times greater than for finned tube (4.86 kg/m^2).

SG for NPP with helium coolant have broken the $650 \text{ }^\circ\text{C}$ barrier for the outlet temperature of CO_2 coolant. It has given a possibility to increase the reactor outlet parameters up to $730\text{--}950 \text{ }^\circ\text{C}$ with He pressure from 11 to 49 bar (less pressure corresponds greater temperature) [19]. The experimental UHTREX reactor showed that it is possible to obtain the reactor outlet coolant (helium) temperature up to $1320 \text{ }^\circ\text{C}$ [8, 25]. The increase of coolant temperature above the $1000 \text{ }^\circ\text{C}$ demands the nickel alloys application. Further SG for NPP development was limited by only technical and economic conditions.

The NNGP project has partially used the same design solutions as in previous generations. There are no insulation and vessel without cooling. To reduce the temperature and vessel wall thickness, helium in NNGP is located inside the tubes, and water is on the outside.

The vessel material in the NPP SG was chosen as the superheater material. It satisfied the highest operating temperature (Table 1). The vessel thickness was calculated for the coolant total internal pressure and temperature difference.

Due to the air cooling of the PSG vessel, it was possible to make it from carbon steel. Steel E1756 ($12\text{Cr}11\text{W}2\text{MoV}$) was used for primary superheater. Steel E1351 ($10\text{Cr}2\text{MoVNb}$) was used for secondary superheater. The estimated superheater metal temperature has not exceeded $630 \text{ }^\circ\text{C}$.

3 PHRSG for CCGT with GT-25PA Gas Turbine

The design analysis of pressurized steam generators constructions has shown its typical technical solutions. This led to next design decisions for developing plant:

1. Vessel will be consisted of the internal dividing shell and external cylindrical shell. Shells will be cooled by exhaust flue gas after tail surface. This provides the less expensive steel usage and the shells wall thickness decrease.
2. The standard spacing for tubes will be used. It allows tubes finning.
3. The PHRSG heat transfer surfaces will be made of helically-finned tubes with serrated fins. It will reduce its capital cost.
4. The heat transfer surface headers will be located between two vessel shells. It will decrease the quantity of vessel passes and improve the PHRSG repairability.
5. PHRSG will be manufactured from standardized elements and separate blocks. These blocks will be shop-assembled.

The operational parameters choice, methodic description, and ways of thermal calculations were described in [1–3]. Key calculations were carried out with Boiler Designer [26–29] and Ansys [30–32] software. These programs have shown reliable results, and they are widely used in energy research and development sector.

The designed energy unit parameters are shown in Table 3. This plant works with

Table 3 Main characteristics of one PHRSG

Characteristic	Power unit
Inlet flue gas temperature, °C	787.6
Inlet flue gas pressure, bar	4.5
Inlet flue gas mass flow, kg/s	155
Vessel cooling	PHRSG exhaust combustion products
Vessel material	Steel 20
Vessel thick, mm	15
Units number	4
Superheater steam outlet temperature, °C	560
Superheater steam outlet pressure, bar	138
Superheated steam mass flow, kg/s	36.7
Exhaust flue gas temperature, °C	274

T-100 steam turbine. It consists of 4 units. Each unit consists of two GT-25PA gas turbines and one PHRSG. Total superheated steam mass flow equals 146.8 kg/s.

Main PHRSG construction characteristics are shown in Table 4. The results of its thermal calculation are shown in Table 5.

The construction of PHRSG is shown in Fig. 1. Flue gas comes to PHRSG and passes surfaces. The surfaces are located inside the internal dividing shell. This shell has quadratic shape with side length of 3.1 m. The flue gas passes superheater 2, superheater 1, evaporator, and economizer. After economizer the flue gas comes to annular gap between two vessel shells: internal and external. Flue gas leaves the PHRSG after cooling the internal shell.

Materials and tubes were taken from standard assortment. These materials are produced by Russian industry (Chelyabinsk Pipe Plant; Pervouralsk Pipe Plant, etc.). High-alloy steels for superheaters will be produced by special order. Tube spacing and fins parameters were taken according to HRSG manufacturing experience by JSC «Machine-Building Factory of Podolsk» (JSC «ZiO»).

The economizer and the superheater are made of counterflow scheme. The evaporator is designed with parallel flow scheme. This was made to increase the operation reliability.

The inlet part of PHRSG is made of 08Cr17H13Mo2Ti (factory code—EI756, analogue of 316H) alloy steel. Alloy steel EI914 (08Cr18H10Ti or 08Cr18Ni10Ti) is used for the internal dividing shell in the region with temperature less than 700 °C (after superheater 1). This shell is made of carbon steel 20 after evaporator.

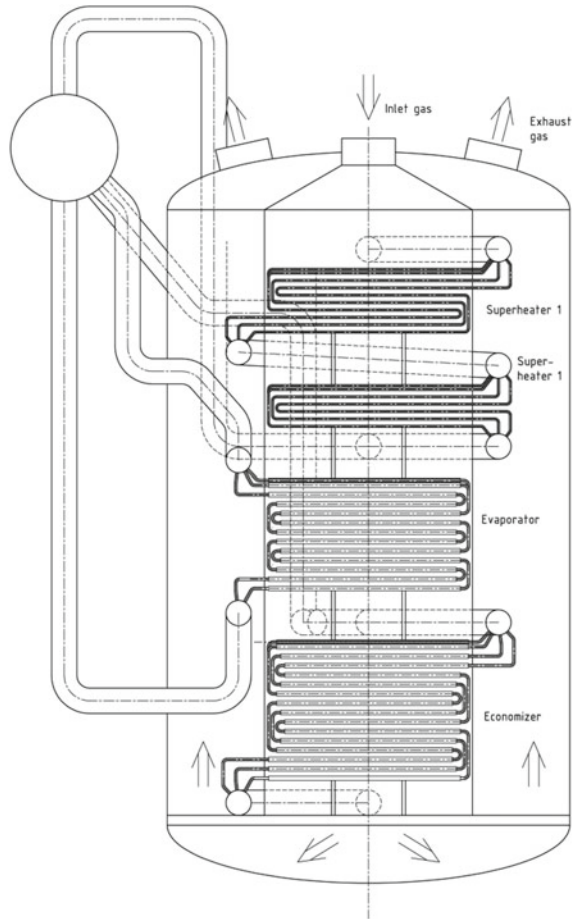
Table 4 Main heat-transfer surfaces characteristics

Characteristic	Heat surface			
	Super-heater 2	Super-heater 1	Evapo-rator	Econo-mizer
Material	EI756	12Cr1MoV	Steel 20	
Heat surface, m ²	259.3	259.3	2853.8	4566.1
External tube diameter, mm	32	32	38	38
Tube wall thickness, mm	5	5	4	4
Number of parallel tubes	104	104	760	76
In-line spacing, mm	60	60	80	80
Longitudinal spacing, mm	55	55	70	70
Number of tube rows	18	12	24	30
Heat surface height, mm	935	605	1610	2030
Gas flow cross-sectional area in last row, m ²	4.45	4.45	4.27	4.27
Medium flow cross-section area in tubes, m ²	0.118	0.118	0.107	0.161
Fin height, mm	–	–	15	15
Fin thickness, mm	–	–	1	1
Fin spacing, mm	–	–	4.1	4.1
Tube mass, kg	8532	8532	7852	12.6
Fin mass, kg	–	–	8026	12.8
Total mass, kg	8532	8532	15.9	25.4

Table 5 The PHRSG thermal calculation results for CCGT with GT-25PA gas turbine and T-100 steam turbine

Characteristic	Heat surface			
	Super-heater 2	Super-heater 1	Evapo-rator	Econo-mizer
Gas velocity, m/s	18.86	17.28	15.01	11.83
Heat capacity, MW	15.6	17.0	40.0	19.3
Inlet gas temperature, °C	788	704	612	387
Exhaust gas temperature, °C	704	612	387	274
Water/steam velocity, m/s	20.24	13.52	2.34	0.95
Water/steam enthalpy difference, kJ/kg	425.78	471.5	59.78	516.55
Inlet water/steam temperature, °C	417	339	338	232
Exhaust water/steam temperature, °C	560	428	339	330
Overall heat transfer coefficient, W/m ² ·°C	232	231	108	91
Temperature difference, °C	259	283	130	46

Fig. 1 PHRSG longitudinal section



4 Further Investigations

Further design development consists of natural circulation calculating and technical solutions substantiating for evaporator reliable operation. It could have been possible to organize natural circulation or multiplied forced circulation. Recent developments have shown that natural circulation can be used in horizontal tube evaporators [10, 28, 33].

The calculating of internal dividing shell wall temperature gives information about choosing less expensive materials for its production.

The water/steam enthalpy increase in PHRSG is much larger than in common energy boilers [26, 34]. However, there is no furnace in the PHRSG, and its construction is simpler. The flue gas density and flue gas flow steadiness are much higher. According to initial estimates, it is possible to simplify the design of heat exchange

surfaces. The final decision can be made only after thermal and hydraulic calculation of the heat transfer tubes in surfaces.

5 Conclusion

1. The analysis results of the SG for NPP with a gas coolant and old constructions of PHRSG made it possible to use its experience and technical solutions in the design of new PHRSG.
2. Cooling the vessel by flue gas allows the use of carbon steel. It reduces the use of expensive austenitic alloy steel.
3. The development and manufacturing of PHRSG can be carried out by enterprises of the power engineering industry in Russia.

Acknowledgements This work was supported by the Russian Science Foundation (project No. 18-79-10264 «Investigation of heat transfer characteristics in the flow of high-pressure combustion products and its state in the output stages of a gas turbine for the reasoning of the performance capabilities of a perspective installation with a high-pressurized heat recovery steam generator and useful application of water vapor condensation heat»).

References

1. Sterkhov, K.V., Khokhlov, D.A., Pleshanov, K.A., Zaichenko, M.N.: High-pressurized heat recovery steam generator for combined cycle gas turbine plant. In: Proceedings of the 1st IEEE 2019 International Youth Conference on Radio Electronics, Electrical and Power Engineering, REEPE 2019, 14–15 March (2019). <https://doi.org/10.1109/REEPE.2019.8708764>
2. Khokhlov, D.A., Zaichenko, M.N., Sterkhov, K.V., Pleshanov, K.A.: Computational model for high-pressurized heat recovery steam generator heat transfer study. In: 2020 5th International Conference on Information Technologies in Engineering Education, Inforino 2020—Proceedings April (2020). <https://doi.org/10.1109/Inforino48376.2020.9111734>
3. Khokhlov, D.A., Zaichenko, M.N., Sterkhov, K.V., Pleshanov K.A.: Thermal scheme development for combined cycle power plant with high-pressurized heat recovery steam generator. In: Proceedings of the 1st IEEE 2019 International Youth Conference on Radio Electronics, Electrical and Power Engineering, REEPE 2020, 12–14 March, pp. 1–5 (2020). <https://doi.org/10.1109/REEPE49198.2020.9059132>
4. Kanaev, A.A., Korneev, M.I.: Combined cycle gas turbine. Design and calculations. Mashinostroeniye, L. (1974). (in Russian)
5. Modern power station practice, 3rd edn. In: D.J. Litter et al. (eds.) Nuclear Power Generation, vol. J. Pergamon Press (1992)
6. Nonbol, E.: Description of the advanced gas cooled type of reactors (AGR). Graphic Service (1996)
7. Cameron, P.J., Walters, J.: The design and construction of boilers for advanced gas-cooled reactors in the United Kingdom. In: Nuclear Technology, pp. 151–162 (1981). <https://doi.org/10.13182/NT81-A32838>
8. Melese, G., Katz, R.: Thermal and Flow Design of Helium-Cooled Reactors. American nuclear society (1984)

9. Roslyakov, P.V., Pleshanov, K.A., Supranov, V.M., Zaichenko, M.N., Lonkin, I.L., Sterkhov, K.V., Grisha, B.G.: Development of a computer model of a fire-tube hot water boiler, its verification and use in the design process. In: 2018 4th International Conference on Information Technologies in Engineering Education, Inforino 2018—Proceedings 4, 8581782 (2018). <https://doi.org/10.1109/INFORINO.2018.8581782>
10. Pleshanov, K.A., Sterkhov, K.V., Roslyakov, P.V.: Stability of natural circulation in a vertical boiler-utilizer loop with horizontal evaporator pipes during startup. *Power Technol. Eng.* **50**(4), 407–412 (2016). <https://doi.org/10.1007/s10749-016-0722-7>
11. Gopalakrishnan, S., Makesh, M.: Design and analysis of fire tube boiler with heat flow analysis. *Int. J. Sci. Technol. Res.* **8**(7), 50–52 (2019)
12. Terebilov, S.V., Mikhailov, A.G., Slobodina, E.N.: Fire-tube boiler heat exchange surfaces fouling formation. *J. Phys.: Conf. Ser.* **1210**(1), 012139. In: 12th International Scientific and Technical Conference on Applied Mechanics and Systems Dynamics, AMSD 2018, Omsk, Russian Federation, 13–15 Nov 2018, 147986, pp. 1–5. <https://doi.org/10.1088/1742-6596/1210/1/012139>
13. Meyklar, M.V.: TKZ modern boilers. *Energy, M.* (1978). (in Russian)
14. Forster, M., Hannes, K., Telöken, R.: Combined cycle power plant with pressurized coal combustion (PPCC): state of development and perspectives. *VGB PowerTech* **81**(9), 30–35 (2001)
15. Lee, J.M.: Developments in fluidized bed conversion during 2011–2016. In: IEA-FBC TCP (2017)
16. Chalupnik, R.W., Krautz, H.J., Wirtz, M., Stuhlmüller, F.: Applied research for a new generation of lignite-fired combined cycle power plants using circulating pressurized fluidized bed combustion. In: Proceedings of the 16th International Conference on Fluidized Bed Combustion, May 13–16, Reno, NV (2001)
17. Robertson, A., Horazak, D., Newby, R., Goldstein H.: Pressurized fluidized bed combustion second-generation system research and development. In: Technical Progress Report for Phase 3 October 1, 2001 through September 2002. Foster Wheeler Development Corporation (2002)
18. Dean, D.W., Johns, J.G.: Structural integrity issues in high temperature nuclear plant: experience from operation of the UK advanced gas cooled reactor fleet. SMiRT-23 Manchester, United Kingdom—August 10–14, 2015 Division II, Paper ID 459
19. Technology of steam generators for gas-cooled reactors. In: Proceedings of a Specialists Meeting Organized by the International Atomic Energy Agency and held in Winterthur, Switzerland, 9–12 March 1987
20. EU Stress Test Heysham 2. EDF Energy plc. Registered in England and Wales. Registered No. 2366852. Registered Office: 40 Grosvenor Place, Victoria, London, SW1X 7EN
21. Hoffer, N.V., Sabharwall, P., Anderson, N.A.: Modeling a Helical-coil Steam Generator in RELAP5-3D for the Next Generation Nuclear Plant. Idaho National Laboratory Next Generation Nuclear Plant Project Idaho Falls, Idaho 83415
22. Arsen'ev, L.V., Tyryshkin, V.G., CCGT, L.: Mashynostroenye, 1982. (in Russian)
23. Pühr-Westerheide, H.: Kraftwerke mit Kohledruckvergasung—VGB Kraft werkstechn, 1974, 54, N 8, pp. 532–536
24. Rassohin, N.G.: Steam generators for the nuclear power stations. M.: Energoatomizdat, 1987. (in Russian)
25. Xinhe, Q., Xiaoyong, Y., Jie, W., Gang, Z.: Combined cycle schemes coupled with a very high temperature gas-cooled reactor. *Prog. Nucl. Energy* **108**, 1–10 (2018). <https://doi.org/10.1016/j.pnucene.2018.05.001>
26. Tugov, A.N., Supranov, V.M., Izyumov, M.A., Somova, E.V., Vereshchetin, V.A.: Substantiating the possibility of firing fuel oil as backup fuel in the P-50R coal-fired boiler at the Kashira state district power plan. *Therm. Eng.* **67**(11), 805–812 (2020). <https://doi.org/10.1134/S0040601520110105>
27. Tugov, A.N., Supranov, V.M., Izyumov, M.A., Vereshchetin, V.A., Usman, Y.M., Natal'in, A.S.: Experience of implementation of in-furnace methods of decreasing NO_x in E-320-13.8-560GM boilers: problems and ways for their solution. *Therm. Eng.* **64**(12), 884–890 (2017). <https://doi.org/10.1134/S0040601517120096>

28. Pleshanov, K.A., Sterkhov, K.V., Khokhlov, D.A., Zaichenko, M.N.: Development for vertical heat recovery steam generators with natural circulation. *Euroheat and Power (English Edition)* **16**(1), 12–17 (2019)
29. Moelling, D., Malloy, J., Graham, M., Taylor, M., Fabricius, A.: Design factors for avoiding FAC erosion in HRSG low pressure evaporators. In: *Proceedings of the ASME 2013 Power Conference POWER2013 July 29–August 1, 2013, Boston, Massachusetts, USA*
30. Prokhorov, V.B., Chernov, S.L., Kirichkov, V.S., Fomenko, N.E.: Developing and modelling the invert boiler furnace for A-USC steam parameters. *J. Phys.: Conf. Ser.* **1565**(1), 28 July 2020, Номер статьи 0120531 11th All-Russian Scientific Conference with International Participation on Thermophysics and Power Engineering in Academic Centers, TPEAC 2019; St. Petersburg; Russian Federation; 21 October 2019 to 23 October 2019; Code 162006. <https://doi.org/10.1088/1742-6596/1565/1/012053>
31. Dvoinishnikov, V.A., Khokhlov, D.A.: Numerical investigation of a pulverized-coal startup vortex burner. *Therm. Eng. (English translation of Teploenergetika)* **60**(6), 390–396 (2013). <https://doi.org/10.1134/S0040601513060037>
32. Bermúdez, C.A., Porteiro, J., Varela, L.G., Chapela, S., Patiño, D.: Three-dimensional CFD simulation of a large-scale grate-fired biomass furnace. *Fuel Process. Technol.* **198**(Feb 2020), Article number 106219. <https://doi.org/10.1016/j.fuproc.2019.106219>
33. Pleshanov, K.A., Khlyst, E.G., Zaichenko, M.N., Sterkhov, K.V.: Design of a natural circulation circuit for 85 MW steam boiler. *Therm. Sci.* **21**(3), 1503–1513 (2017). <https://doi.org/10.2298/TSCI161005320P>
34. Roslyakov, P.V., Attikas, R., Zaichenko, M.N., Pleshanov, K.A., Ionkin I.L.: Studying the possibility of separate and joint combustion of Estonian shales and oil shale retort gas at thermal power plants. *Therm. Eng.* **62**(10), 691–702 (2015). <https://doi.org/10.1134/S0040601515100080>

Selection of the Appropriate Intelligence Level of Regulators of Thermal Power Plants Technological Processes



Edik Arakelyan, Sergey Mezin, Fedor Pashchenko, and Anatoly Kosoy

1 Introduction

One of the most actual problems of modern power engineering is a significant increase in the production of heat and electricity. This problem cannot be solved without improving the efficiency of automated control systems (ACS), most of which are built today with the use of modern program and technical complexes (PTC). This can be achieved by increasing the level of ACS intelligence of thermal and nuclear power plants (TPP and NPP). This problem has been solved for many years using, among others, a hierarchical approach [1].

The creation of a large-scale intelligent automated process control system that works on the principle of decentralized processing, collection, and application of information for the entire TPP in the future is possible, but very time-consuming and expensive. As a result, for automated control systems of thermal power plants built on a hierarchical basis, it is advisable to divide the entire control system into hierarchical levels with interconnected blocks and to evaluate the degree of intelligence of the entire automated control system as the sum of all intelligent systems involved in the technological process.

This work aims to develop methodological provisions for assessing the level of intelligence of the TPP process control system at various hierarchical levels, and the automated control system as a whole is one of the subtasks in this hierarchical approach, aimed at finding and theoretically justifying new, innovative methods of optimal control [2–4].

E. Arakelyan (✉) · S. Mezin · A. Kosoy
ACS HP Department, NRU “MPEI”, 111250 Moscow, Russia
e-mail: edik_arakelyan@inbox.ru

F. Pashchenko
V.A. Trapeznikov Institute of Control Sciences of Russian Academy of Sciences, 117997
Moscow, Russia

2 Principles of Design an Intelligent Automated Control System (IACS)

Each separate block with interconnected processes of regulation and control can be built on the basis of artificial neural networks. As a training material, one can use long-term data recorded in the database of the archive of the control object and to test and evaluate the adequacy of the training results of the neural network, use the designed mathematical model. A large amount of archived data serving as a training sample will significantly improve the quality of the management process.

In the hierarchy of control systems, which is man–machine systems, the functions of the human-operator in process control system upper (for the TPP—plant level) are the most responsible and least automated functions of the control and the crucial link, while ACS lower level are determined by the functions of control and redundancy. From the point of view of intellectualization, this level of control is characterized by the possibility of completely excluding the human-operator from the control loop, leaving behind him; in some cases, the functions of monitoring the operation of software and hardware and redundancy. For the most critical technological processes, it is recommended to install as many intelligent sensors and actuators as possible. As for other, less critical areas, the replacement of all technical means of the field level with intelligent ones will lead to high costs; in addition, they also have their own shortcomings and in some processes their use is impractical. It is expected that this level will be carried out such tasks as diagnosis, treatment by instrumentation and automation means of information in real time, as well as the verification of signals and efficiency of the equipment.

For an intelligent control system (IACS), the executive level is important—various local automatic control systems that optimize, in the most developed systems, the operation of the object according to local criteria. Control objects are elements of complex systems that are integrated by means of an IACS into unified organizational systems that ensure the operation of the system as a whole in an optimal mode according to economic or technological criteria.

3 Level of Regulators

As for the level of regulators, it is proposed to develop algorithms for diagnostics, self-tuning, especially in the modes of shutdown and unloading the power unit. In addition, it is necessary to provide the possibility of automatic adjustment of regulators depending on the optimum parameters for critical processes—be sure to inform the operator. It is also expected to use a particularly popular and widely promising technology—artificial intelligence (AI). The task of the controller is to coordinate the control object and the external environment. The external environment consists of objects (or entities) that have a disturbing influence on the object of control. When synthesizing the reacting part of the controller, the properties of the control

object and the quality requirements for transients arising from external influences are taken into account, and continuous adjustment of the virtual model is required according to the “gray box” principle [5]. An intelligent system (IS) can consist of many components that have elements of AI. In the limit, each technical solution or software algorithm of the IS can be considered as an intelligent tool that has its own reacting and closing parts. The purpose of the latter is to ensure sustainable development not only for this tool individually but also for the entire system as a whole in relation to changes in the external and internal environment. One of the central problems in the development of complex AI systems is the problem of matching the reacting and closing parts of individual intelligent components. The solution to this problem is complicated by the fact that the closing parts of the system components can be created using different AI technologies. Therefore, in order to coordinate the reacting parts of these components, it is necessary to reduce the solutions obtained using different technologies to a single basis. Neural network methods and tools can be chosen as such a basis, since they can be used to simulate learning the rules of fuzzy logic, as well as to include genetic algorithms in their composition [6–9]. The increase in the quality and efficiency of the regulators is not only due to the use of neural networks that increase the accuracy of the analysis of the parameters of the control object, and, consequently, contribute to the improvement of its mathematical model, but also due to the established relationship between all the regulators. This principle of operation is a fundamental link in increasing the intelligence of an automated system at the level of regulators. An intelligent controller with a two-circuit structure consisting of two links of intellectual adaptation—the priory model of the object and the module of intellectual correction (Fig. 1) can

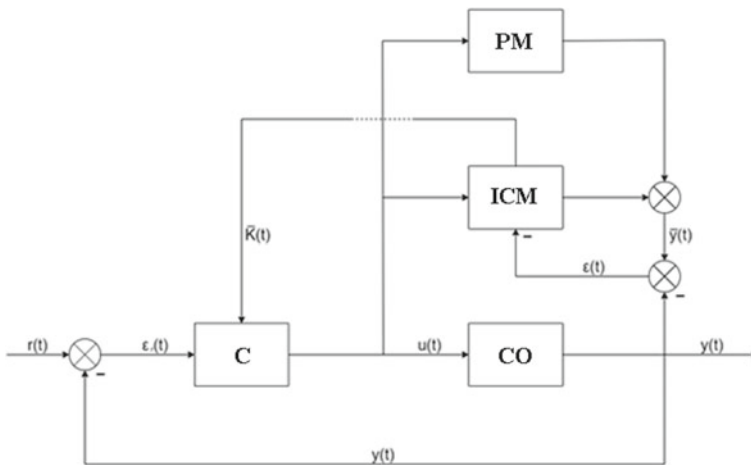


Fig. 1 Functional diagram of a two-circuit intelligent controller. C—controller; CO—control object; ICM—intelligent correction module; PM—a priori model of the process; $r(t)$ —task; $u(t)$ —control action; $y(t)$ —actual output value; $\bar{y}(t)$ —estimate of the output value; $\varepsilon(t)$ —simulation error; $\varepsilon_r(t)$ —error in real work; $\bar{K}(t)$ —correction coefficients

contribute to solving the problem of intellectualization at the local level. This will allow you to narrow down the optimization task and ensure that the system works in real time.

With this approach, an autonomous trained neural network, a static expert system or an adaptive (as far as possible) mathematical model can act as an a priori model of an object. The intelligent correction module must adapt the system online and ensure maximum identification of the processes occurring in the control object.

The choice of the optimal structure and further adjustment of the parameters of intelligent controllers, in contrast to the classic ones, are non-trivial tasks that place increased requirements on the qualification and experience of the designer. The intelligent controller must be structurally prepared for the learning process and the accumulation of experience. Training and adjustment of knowledge accompanies such a controller throughout its life cycle: training on simulator models at the design stage, training under the supervision of a human expert at the setup stage, and self-adjustment of knowledge during operation. Self-adjustment is limited to predefined corridors of expected natural changes in the parameters of the control object. Intelligent regulators are superior to classical regulators over time (simulation cycles), since their intelligence lies in the ability to improve over time, that is, to learn. Intelligent controllers, with all the theoretical advantages, have not yet received a well-deserved distribution in automated control systems for heat and power equipment [10–13]. The problem of initial setup, with the availability, simplicity, and triviality of the initial setup of classical PID controllers, makes it difficult to implement these controllers on real control objects. To configure the intelligent controller, a significant array of archived data on the behavior of the control object and/or a library module containing a preliminary mathematical model of this object for subsequent adjustment of the weight coefficients is required. The ready-made library module allows you, for typical control objects in the heat and power industry, to immediately turn on the intelligent ACS in self-learning mode. In the course of real-time operation, the neural network independently corrects the node coefficients in predefined ranges to achieve the highest quality of system control. To develop such a library module, when developing an intelligent controller that meets the above requirements, simulation modeling methods were used. The Python programming language was used for rapid prototyping. To describe the control objects, we used elementary links written to the system using recurrent expressions. To configure the classical PID controller, a modified method of the genetic algorithm was used. In it, for each population, the starting points were also the starting points for the opening of the simplex. And already the results of the work of the set of simplexes were processed by evolutionary methods [2, 8]. The use of numerical methods made it possible to search for the parameters of PID controllers, optimizing both the task channel and the channel for dealing with external disturbances.

Initially, numerical methods sought the optimal parameters of the PID controller to minimize the sum of the integral criteria of the two processes: control and regulation. And then, in the structure of the neural network controller, the obtained parameters of the PID controllers are an intermediate layer and are considered suboptimal values. And the learning error is the difference from zero of the sum of the integral criteria

of the obtained processes. It is clear that the zero integral criterion is impossible, but this sets the direction of training the neural network.

The resulting system not only sends its controller parameters to the simulation model, expecting it to respond to the quality of regulation with these settings [10, 11] but also forms its own simulation model in the intermediate layer, the parameters of which it corrects, learning from the responses from our initial simulation model.

At this stage of parameter optimization, the neural network module is already capable of further training on more complex tasks. We can set further conditions and restrictions, complicating and bringing our model closer to the real object, and the neural network controller will no longer compete with PID controllers configured for elementary models but will try to return to its records for the quality of regulation in new unfamiliar and complicated conditions.

4 Methodological Approach of Evaluating the Economic Efficiency of Control Systems Intellectualization

The economic efficiency of control system intellectualization is determined by comparing the costs of its creation and implementation with the economic effect obtained from its operation. Experience shows that with proper choice of means and setting targets ACS always effective and will be much more efficient intelligent control systems. However, it is very difficult to find a monetary expression of the economic effect. The difficulty lies in the fact that today there are no methods for determining the volume, collecting and processing information, as well as there is no modern concept and algorithms for calculating them, not to mention the automation of this process [14]. At the same time, it should be borne in mind that the qualitative effect of the development and implementation of the IACS is very large due to changes in the working conditions of TPP personnel. At present, it is difficult to conduct a reliable comparative analysis of labor costs when working on relay technology and microprocessor technology, as well as to make the necessary calculations for their direct expression in monetary form.

Until recently, the increase in the cost of control and control systems in the energy sector significantly outstripped the increase in their economic efficiency due to the development and adaptation of functional algorithms at various levels. At present, the level of automation for newly constructed power units has somewhat stabilized due to the typification of technical specifications for the development of technological algorithms for automated process control systems in the PTC of block-type power plants. And now, despite the relative complexity of solving the problem and, at first glance, the relatively low efficiency of implementation, it would be timely to return to these developments.

When intellectualizing the automated control system, an important problem is to determine the feasibility of developing and implementing each intelligent algorithm. The methodological provisions of the technical feasibility of increasing the level

of intelligence of the hierarchical levels of the automated control system and the automated control system as a whole, given in [3], provide such an opportunity on the basis of expert assessments. This report examines the methodological approaches to such an assessment from the point of view of technical and economic efficiency. To simplify the approaches, it is assumed that there is a project of a traditional automated control system based on PTC and changes in technical and economic indicators are considered during the development, implementation and operation of a certain intelligent algorithm.

Consider a methodological approach based on the example of developing an intelligent controller designed in accordance with the above principles.

It is clear that the degree of efficiency of the intelligent controller can be determined by two main criteria: intelligence and reliability. Intelligence, in turn, is determined by the capabilities of the system for performing logical tasks of a high degree of complexity, developed on the basis of optimized object control algorithms. Based on this provision, it can be argued that the degree of efficiency of the regulator is directly dependent on the quality and accuracy of the automatic control of the technological process, while excluding the intervention of operational personnel in the operation of the system and in the control process itself. The reliability indicator of the system determines the ability to ensure the survivability and safety of technical and software control tools.

The degree of effectiveness of the developed intelligent system should be based on the difference in quantitative estimates of the cost and profit parts of the project, calculated in relation to the “basic” version of the automated control system.

Based on this, as a criterion for the feasibility of implementing an intelligent control system, we take the maximum difference between the specified values in the version of the traditional system and the system with intelligent control ΔS_{IS} , i.e.,

$$\Delta S_{IS} = [P_{IS}(\tau) - C_{IS}(\tau)] - [P_{TR}(\tau) - C_{TR}(\tau)] \rightarrow \max, \quad (1)$$

where $P_{TR}(\tau)$, $P_{IS}(\tau)$ —the profit for the considered time due to the operation of the control system in the traditional and intelligent design; $C_{TR}(\tau)$, $C_{IS}(\tau)$ —the total cost of implementing and operating the control system, respectively, in the traditional and intelligent design.

Assuming that the profitable and costly parts for a traditional regulatory system are constant values, the maximum of function (1) will correspond to the maximum of the value

$$\Delta \bar{S}_{IS} = [P_{IS}(\tau) - C_{IS}(\tau)] \rightarrow \max. \quad (2)$$

The cost part for a certain period of time (for example, during the life cycle), depending on the quality of the regulation of $C(\tau)$, is determined from the ratio

$$C(\tau) = C_D + \tau \Delta C_M, \quad (3)$$

where C_D — a set of one-time costs associated with the development, design, installation, and commissioning of additional equipment at the development and implementation of software systems intelligent controller; ΔC_M —the annual additional resource costs of hardware and software of intelligent controller maintenance (service and repair provisions, cost of electricity, etc.); τ —the duration of the reporting period (number of years).

It should be borne in mind that the main resource costs for remote process control (control quality indicator) depend on individual performance, physical, and psychological state of the human-operator, leading the technological process when other ergonomic factors, including not standard, whereas in the presence of intelligent control these costs are of a continuing nature or completely absent.

The additional costs associated with ensuring the reliability of the developed intelligent system ΔC_R depend on the volume of use of the tasks set W_{VT} and the technical condition of the equipment during the commissioning and operation of the technical and software tools of the intelligent system W_{TC} :

$$\Delta C_R = f(W_{VT}, W_{TC}). \quad (4)$$

The initial data for the determination ΔC_R is the necessary and sufficient package of technological functions of the system that solves the issues of calculation and control tasks in accordance with the terms of reference, including the following indicators:

- technical condition of hardware (statistical data on technical equipment failures);
- the technical state of the software (statistical data on software failures).

If we assume that the coefficients of trouble-free operation of technical and software tools are constant over time, then the value ΔC_R can be estimated by an approximate expression:

$$\Delta C_R = [(1 - \mu_{VT})\tau_{YVT}y_{VT} + (1 - \mu_{TC})\tau_{YTC}y_{TC}]\tau, \quad (5)$$

where μ_{VT} , μ_{TC} —the coefficients of trouble-free operation of software and hardware, respectively; τ_{YVT} , τ_{YTC} —the annual number of hours of operation of software and hardware; y_{VT} , y_{TC} —the average hourly damage from an emergency shutdown of software and hardware, respectively.

Thus, the total costs for the development, implementation and operation of a control system based on an intelligent controller can be estimated by the expression:

$$C_{IS}(\tau) = C_D + \tau \Delta C_M + \Delta C_R. \quad (6)$$

The quantitative assessment of the profitable part of the project $P_{IS}(\tau)$ should be determined by the technical and economic indicators of the regulated object. In general, the increase in profit due to the introduction of an intelligent system can be represented in the form of three components:

- by improving the quality of process control— ΔC_{QC} ;
- by increasing the efficiency of the operation of the regulated object— ΔC_{EO} ;
- by increasing the reliability of the control system and the control object— ΔC_R .

$$C_{IS}(\tau) = (\Delta C_{QC} + \Delta C_{EO} + \Delta C_R)\tau. \quad (7)$$

5 Discussion and Conclusions

The first component in (7) is typical for controllers that support adjustable parameters within the acceptable range (the steam temperature, steam pressure, temperature flue gas, etc.) To assess its value is assumed that the regulation of this parameter is the traditional controller, as the practice of operation, the inevitable deviations within range, including due to changes in the dynamic properties of the object and timely bring the controller settings to the changed characteristics of the object. As shown above, the intelligent controller is able to adjust the settings independently and thus minimize the loss of heat (fuel) due to deviations in the parameters.

The second component in (7) is characteristic of regulators that ensure the optimality of the parameters or process in the control object (extreme regulators, pressure in the condenser, etc.). It is known that in the traditional design, extreme regulators have a number of disadvantages (the duration of step-by-step algorithms, the search for the optimum, a significant error in the result, etc.), which is due to their not very widespread implementation in practice. Intelligent regulators, having the ability to quickly analyze retrospective information based on neural network technologies and analyze the current situation, are able to find the optimal solution at the pace of the process. In some cases, the implementation of extreme regulators is complicated by the fuzzy nature and uncertainty of the initial information (for example, the choice of the optimal pressure in the condenser at low loads).

The third component is typical for the regulation of parameters, the deviation of which from the permissible values leads to an emergency shutdown of individual units or the power unit as a whole. In this case, it seems that the role of the intelligent controller, in addition to ensuring the quality of regulation, should also be to exclude both false positives and non-actuation of protections when the regulated parameter exceeds the permissible values.

As mentioned above, it is difficult to assess the appropriate (optimal) level of intelligence in the absence of reliable source data, but nevertheless, the estimated calculations carried out according to the above method on the basis of expert assessments of the source data showed that the appropriate level of intelligence of regulators is in the range of 0.7–0.85, depending on the purpose of the regulator.

Acknowledgements The study is being conducted with the support of the Russian science Foundation, grant № 19-19-00601.

References

1. Belenko, V.A., Grekhov, L.L., Svidersky, A.G.: Automation of domestic power units: development trends, problems, prospects. *Therm. Eng.* **10**, 3–12 (2012)
2. Sabanin, V.R., Smirnov, N.I., Repin, A.I.: Automatic control systems based on neural network technologies. In: Proceedings of the International Scientific Conference Control-2003, pp. 45–5. Publishing House of the Moscow Power Engineering Institute, Moscow (2003)
3. Arakelyan, E.K., Andryushin, A.V., Pashchenko, F.F., Mezin, S.V., Kosoy, A.A.: Methodological provisions of the assessment of the increase degree in the intelligence of TPP ACS TP on the basis of modern PTC. *Procedia Comput. Sci.* **170**, 941–946 (2020)
4. Makarov, I.M.: Conceptual bases of the organization of intellectual control of complex dynamic objects: new methods of control of complex systems, pp. 19–31. Nauka, Moscow (2004)
5. Ibragimov, I.M.: The use of artificial intelligence systems in the operation of energy facilities. In: Scientific and Technical Journal Reliability and Safety of Power Engineering, pp. 51–55. NPO Energobezopasnost, Moscow (2008)
6. Sabanin, V.R., Smirnov, N.I., Repin, A.I.: Modified genetic algorithm for optimization and control problems. *Exponenta Pro, Math. Appl.* **3–4**, 78–85 (2004)
7. Sarangapani, J.: Neural network control of nonlinear discrete time systems, p. 602. CRS Press, Missouri, USA (2006)
8. Sabanin, V.R., Smirnov, N.I., Repin, A.I.: Universal program for optimizing multi-extreme problems “Optim-MGA”. Certificate of official registration of computer programs, no. 2004610862 (2004)
9. Zakharov, V.N., Ulyanov, S.V.: Fuzzy models of intelligent industrial regulators and control systems: evolution and principles of construction. *Izvestiya Russ. Acad. Sci.: Tech. Cybern.* **4**, 189–205 (1993)
10. Rossiter, J.A.: Model-Based Predictive Control (2017). ISBN: 978131527261. <https://doi.org/10.1201/9781315272610>
11. Laurier, Zh.L.: Neural networks. In: Artificial Intelligence Systems, p. 568 (1991)
12. Omidvar, O., Elliott, D.L. (eds.): Neural Systems for Control, p. 358. Academic Press, New York (1997)
13. Zmeu, K.V., Markov, N.A., Shepitko, I.A., Notkin, B.S.: Model-free predictive inverse neurofeedback with regenerated reference transient. *Intell. Syst.* **3**, 109–117 (2009)
14. Pashchenko, F.F., Pikina, G.A.: Fundamentals of modeling of energy objects, p. 464. Fizmatlit, Moscow (2011)

Study of the Causes of the Gas Imbalance in High Capacity Steam Boilers



V. A. Pozdeev, E. A. Kravets, K. E. Zhilin, D. O. Andreichuk,
and D. V. Loginov

1 Introduction

On steam boilers of high productivity, such a phenomenon as stratification of temperature is observed. This phenomenon lies in the different temperature of the steam in a certain stage of the superheater, depending on the location of the pipe elements of the heating surfaces along the width of the boiler.

The difference in gas temperatures across the width of the boiler can reach 70–100 °C. Constructive measures like steam transfer along the sides of the boiler, as well as the inclusion of desuperheaters in the tract of the superheater do not fully cope with the stratification of temperature. This leads to overheating of steam and metal in separate packages and steam bypass tubes of the superheater and may cause their premature damage. If there is a stratification of temperature of 10 °C in one bypass pipe system, their resource can differ by up to 1.5–2 times.

For example, equipment service life of steam pipelines bends $\text{Ø}133 \times 16$ mm made of steel 12Kh1MF at a steam temperature of 560 °C and a pressure of 14 MPa in accordance with [1] is 75 thousand hours. The equipment service life of the same bends at a steam temperature of 550 °C, and the same pressure is 150 thousand hours. The same picture is observed with the resource of the heating surface coils. In [2] it is noted that the service life of the superheater coils when overheated by 10 °C is reduced by about 2 times.

With an increase of boiler power the stratification of temperature goes up due to the growth of its overall dimensions and, as a result, a significant change in the velocity field and temperatures of flue gases. This circumstance has a substantial impact on the reliability of boilers, since it is not possible to organize temperature control of all steam bypass pipes and coils of the boiler superheater. And if the damage to the

V. A. Pozdeev (✉) · E. A. Kravets · K. E. Zhilin · D. O. Andreichuk · D. V. Loginov
Federal State Budgetary Educational Institution of Higher Education, Petrozavodsk State
University, Petrozavodsk, Russia

coils leads to the shutdown of the boiler to turn them off, damage to the steam bypass pipes can lead to an accident with serious consequences.

The muffled coils burn out over time forming gas corridors in the superheater bundles with increased velocities and flow rates of exhaust gases. This, in turn, leads to overheating of entire coils and their premature failure [2]. The process of damage to the coils takes on an avalanche character.

Thereby, the study of the reasons for the stratification of temperature is of interest from the point of view of ensuring reliable and safe operation of boilers.

Stratification of temperature occurs due to gas and steam imbalances [3]. Steam imbalance is well understood, while the reasons for the gas imbalance have not yet been thoroughly clarified. As a rule, disturbances in the fuel supply system, different performance of burners, uneven operation of burners or nozzles across the width of the furnace are named as causes of gas imbalance [3]. However, even if these devices are in good condition and the operating parameters of the boilers are complied with, gas imbalance and stratification of temperature are observed [4, 5].

To find out the reasons for the gas imbalance, two types of boilers—BKZ-420-140 NGM4 and TGMP-314, for which there is information on the damageability of the superheater elements and on the value of the stratification of temperature, were examined.

In the research of the JSC “VTI” specialists it is suggested that one of the reasons for the gas imbalance is the stratification of the combustion products flow in terms of density in the rotating chamber in front of the convective superheater [2]. This phenomenon leads to an inhomogeneous temperature field at the entrance to the convective superheater, overheating of the coils in the zones of maximum temperatures and their premature damage [6, 7].

Figure 1 shows a diagram of the damage to the high-pressure convective superheater coils of the of the TGMP-314 boiler [2]. In [2] it was noted that if the temperature field and combustion products velocity were uniform over the width of the boiler, amount of damage to the coils would be approximately the same.

On boilers BKZ-420-140 NGM4 (Fig. 2), according to the test results, the stratification of temperature along the boiler sides in front of stage I desuperheaters (Fig. 3) can reach 34 °C. During the testing of the head boilers of this type value of the stratification of temperature did not exceed 10–15 °C [8].

When regulating the steam temperature in the stage I desuperheater the operating personnel are forced to increase the condensate flow rate for injection along the “A” line relative to the condensate flow rate along the “B” line. Opening percentage of the temperature regulator along the “A” line is 100%, and the temperature regulator along the “B” line is 48%.

On boilers of this type the first stage desuperheaters are installed in the cut between the first and second superheater stages. The desuperheater of the second stage is installed in the cut between the extreme and middle packs of the third stage of the superheater. The value of the stratification of temperature was determined from the difference in steam temperatures at the exit from the first stage of the superheater on the left and right (line A, line B) and on the difference in steam temperatures at the exit from the extreme packets of the third stage of the superheater.

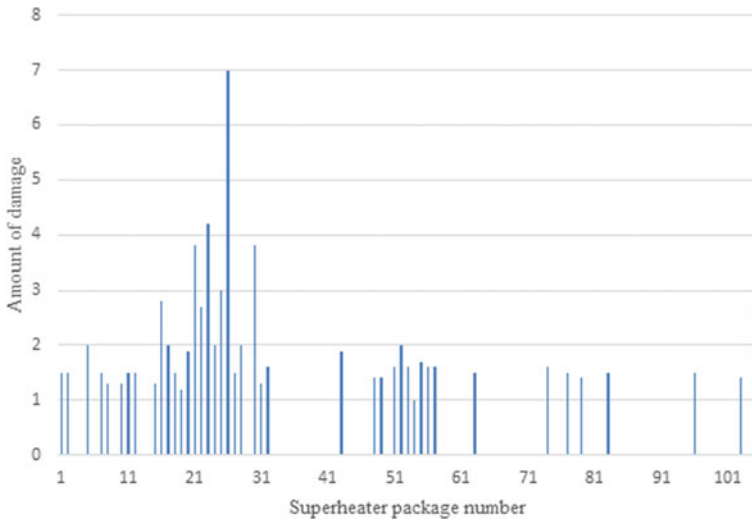
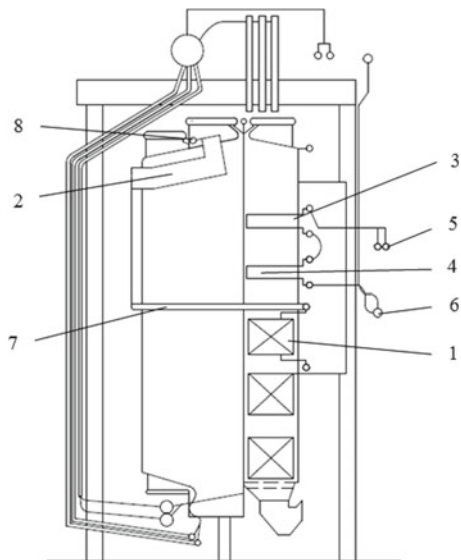


Fig. 1 Damageability diagram of high-pressure convective superheater coils of the of the TGMP-314 boiler [2]

Fig. 2 Scheme of BKZ-420-140 NGM4 boiler:
 1—stage I of the superheater, 2—screen superheater, 3—stage III of the superheater, 4—stage IV of the superheater, 5—stage II desuperheater, 6—steam collection chamber, 7—stage I desuperheater, 8—upper collector of the screen superheater



Despite the operation of the stage I desuperheaters and the equalization of the steam temperature on the sides of the boiler and mixing of the steam flows in the upper collector of the screen superheater (item 8 in Fig. 2), the stratification of temperature at the outlet from the packs on the stage III superheater edge up to the II

Fig. 3 Scheme of stage I superheater of BKZ-420-140 NGM4 boiler: 1—desuperheater headers, 2—coils of the I stage of the superheater, 3—steam bypass pipes to the screen superheater, 4—outlet chambers of the I stage of the superheater

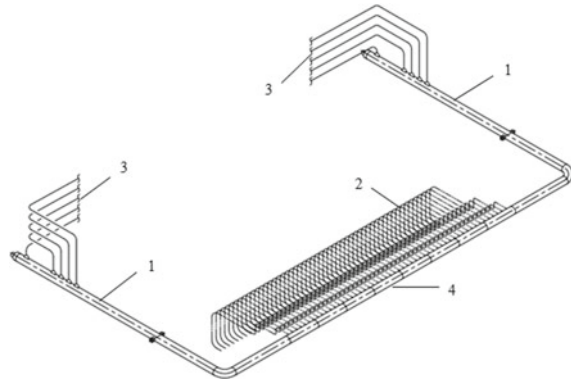
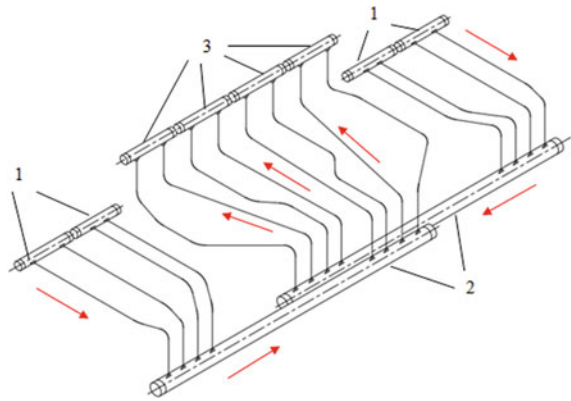


Fig. 4 Scheme of stage II superheater of BKZ-420-140 NGM4 boiler: 1—outlet chambers of the packs on the stage III superheater edge, 2—headers of the desuperheater of the II stage, 3—inlet chambers of the middle packs of the III stage of the superheater



stage desuperheaters (Fig. 4) again reaches 34 °C. In Fig. 4 arrows show the direction of steam movement.

The results of temperature measurements are presented in Table 1. Temperature measurements at the control points were carried out at the nominal boiler output after overhaul.

The same picture in terms of stratification of temperature is observed on neighbouring boilers of the same type, which indicates their design features that cause this phenomenon. In order to find out the reasons for the stratification of temperature a survey of the superheater path, the furnace, the convection shaft, as well as the gas-air path of the boilers was carried out. The operating modes of burners on all boilers were analysed.

According to the results of the survey of the boilers no defects, deformations, deviations from the design and their standard operating modes were revealed. In this regard, an assumption about the influence of gas imbalance on the occurrence of stratification of temperature was made. Thus, the determination of the gas imbalance causes will allow developing a set of measures for identifying it and reducing the value of the stratification of temperature.

Table 1 Measurement results of the temperature of steam along the superheater tract of the BKZ-420-140 NGM4 boiler

Parameter name	Superheated steam temperature value, °C	
	Line A	Line B
Superheated steam temperature before the stage I desuperheater at the outlet of the stage I superheater	433	400
Superheated steam temperature after stage I desuperheater	386	386
Superheated steam temperature after the screen superheater	425	425
Superheated steam temperature at the outlet from the packs on the stage III superheater edge up to the stage II desuperheater	487	453

The solution to this problem is complicated by the fact that direct measurement of the velocity field of combustion rates in a convective shaft is not possible. And the measurement of the temperature field of the exhaust gases passing through a convective superheater is contradictory [2]. In this regard, the work used the methods of mathematical modelling of the combustion products flow in the boiler BKZ-420-140 NGM4 gas flues.

2 Materials and Methods

During the inspection of the BKZ-420-140 NGM4 boiler it was assumed that the most probable reason of the gas distortion is the structural imperfection of the unit for combining gas flues and the exhaust blower suction line. As a result, vortices and low-pressure zones increasing aerodynamic resistance and reducing the flow of exhaust gases through one of the gas flues appear in this unit. The boiler gas flue scheme is shown in Fig. 5.

In accordance with the design of the boiler it is supposed to work under pressure. The exhaust gases are removed from the boiler through two gas flues 1 and passing through two regenerative air heaters (RAH-A and RAH-B), are combined in unit 3 into one flow. In this case, the symmetry of both flows is not violated and the equal flow rates of exhaust gases for both gas flues are ensured. Then the combined flow is directed to the chimney. Part of the exhaust gases is returned to the boiler by gas recirculation fans 2.

In fact, the operation of boilers under pressure is not possible for a number of reasons. In this regard, the boilers work in a mode with a balanced traction using an exhaust blower 5. The suction line of the exhaust blower is cut into the gas flue immediately after the unit for combining flows 3. After the suction line of the exhaust blower, a shut-off stoplog 4 is installed in the gas flue, designed to exclude overflows of exhaust gases during boiler operation with exhaust blower.

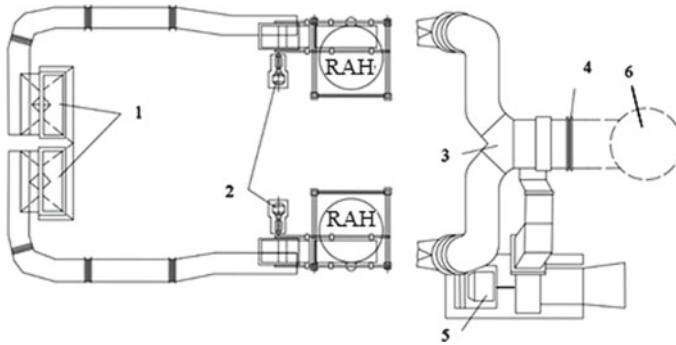


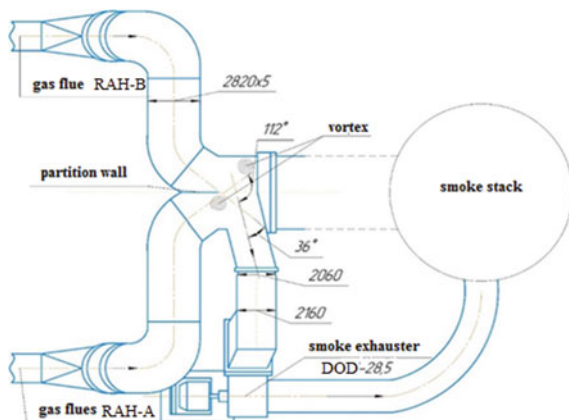
Fig. 5 BKZ-420-140NGM4 boiler flue gas scheme, view from above: 1—gas flues going out of the boiler, 2—gas recirculation fans, 3—gas flue union unit, 4—shut-off stoplog, 5—exhaust blower, 6—chimney

Presumably, due to the one-sided insertion of the suction line of the exhaust blower into the general gas flue immediately after unit 3 the symmetry of the flows along the gas flues is violated. This, in turn, leads to an increase in the aerodynamic resistance of one of the gas flues and a reduction of the consumption of gases leaving through it. The difference in gas flow rates in the gas flues can lead to a shift of the exhaust gas front in the convection shaft towards the gas flue with a higher flow rate. Thus, a gas imbalance occurs, which is the cause of the stratification of temperature of the superheated steam along the width of the boiler.

In order to confirm the proposed hypothesis it was decided to perform mathematical modelling of the unit for combining gas flows using the results of static pressure measurements in gas flues. Static pressure measurements were taken through sampling points mounted on straight sections of the gas flues after the boiler at a distance necessary to stabilize the flow.

The design scheme of the unit for combining flows is shown in Fig. 6. This figure

Fig. 6 The design scheme for mathematical modelling of BKZ-420-140 NGM4 boiler unit for combining flows



also shows the expected zones with reduced pressure, which are formed as a result of intense vortex formation. Mathematical modelling was carried out in the SolidWorks software package.

The results of mathematical modelling are presented in Figs. 7 and 8. These figures show that low pressure zones appear in the flow combining unit, which increase the aerodynamic resistance of the gas flue “B”. This, in turn, reduces the flow rate of exhaust gases through the gas flue “B” and leads to the displacement of the front of the exhaust gases in the convection shaft of the boiler towards the gas flue “A”.

Fig. 7 Visualization of the exhaust gas flow in the flow combining unit, flow rate: 1—gas flues from RAH-B, 2—gas flues from RAH-A

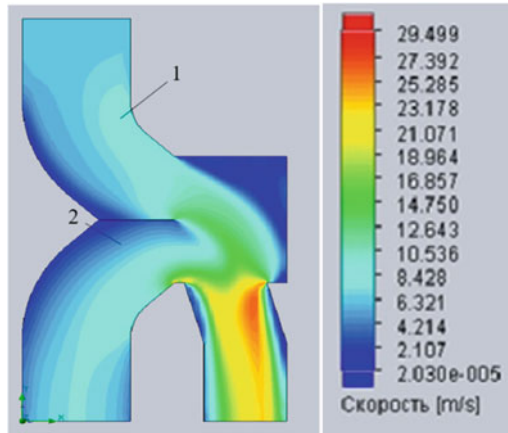
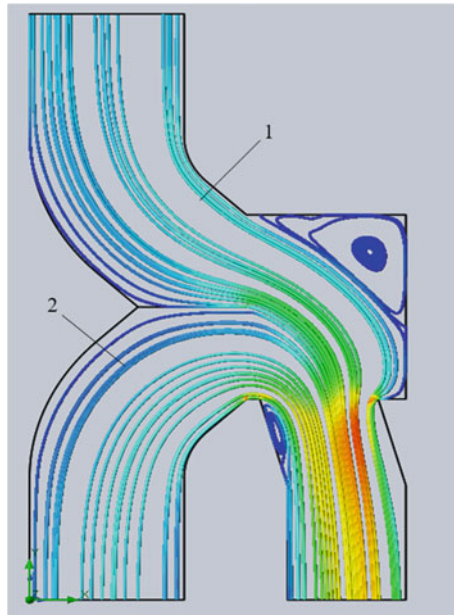


Fig. 8 Visualization of the exhaust gas flow in the flow combining unit, current lines: 1—gas flues from RAH-B, 2—gas flues from RAH-A



According to the results of calculations at the rated load of the boiler, the difference in flow rates for gas flues is 30%.

In this way, gas imbalance and stratification of temperature occur. During testing the head boilers of this type the value of the stratification of temperature was two times lower, since the boilers operated under pressure and the symmetry of the gas flows along the gas flues “A” and “B” was not violated in the combining unit.

Due to the fact that the operation of the boilers under pressure is not expected in the future and the re-routing of the gas flues is not possible, in order to equalize the flow rates on the sides of the boiler it was proposed to mount aerodynamic cowls in the form of vertical guide ribs in the flow combining unit, and also to remove the ledge in docking point of the exhaust blower suction gas flue with the unit for combining flows. The design diagram of the proposed design of the unit for combining flows is shown in Fig. 9.

Based on the results of mathematical modelling it was found that the minimum difference in gas flow rates for gas flues “A” and “B” is formed at an outlet angle of the central ridge installation of 90° and is 4%.

Visualization of simulation results is shown in Fig. 10.

The calculation results show that in the case of the implementation of the proposed measures for the installation of aerodynamic fairings the flow rates of exhaust gases along the gas flues will be equalized and, as a result, the gas imbalance along the width of the boiler and the stratification of temperature will be eliminated.

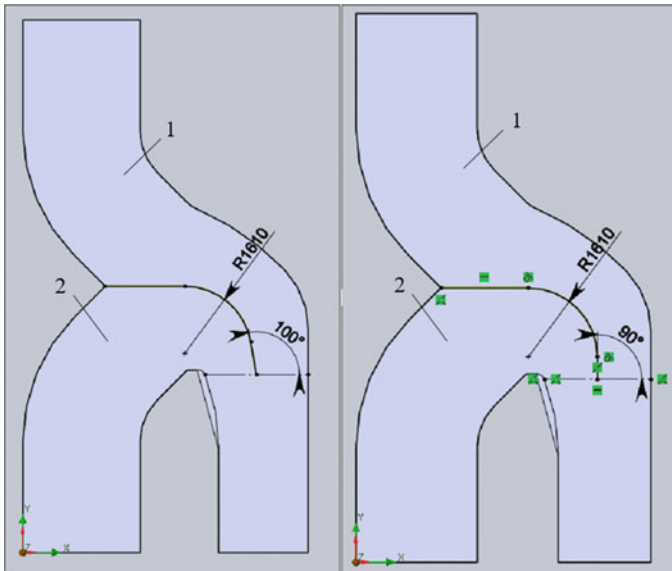
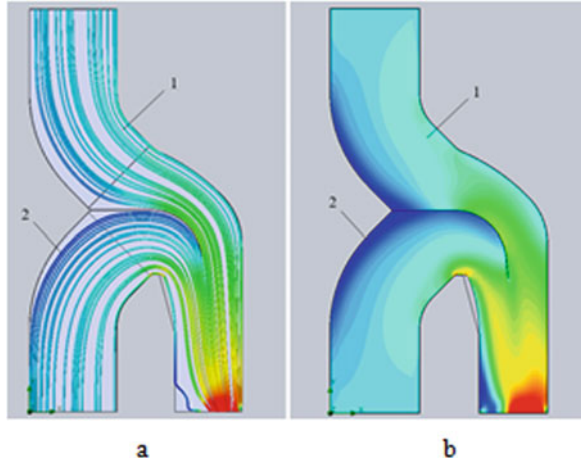


Fig. 9 The design scheme for flow combining unit with aerodynamic cowls: 1—gas flues from RAH-B, 2—gas flues from RAH-A

Fig. 10 Visualization of the exhaust gas flow in the flow combining unit: **a**—current lines, **b**—flow rate 1—gas flues from RAH-B, 2—gas flues from RAH-A



Regarding the TGMP-314 boiler it was also suggested that the cause of the gas imbalance is the difference in the flow rates of the exhaust gases along the boiler flue gas flues. To check this hypothesis an analysis of the gas path of this boiler was carried out, and also the experience of some stations in the reconstruction of gas flues was studied.

The TGMP-314 boiler is equipped with two DOD-31,5GM exhaust blowers connected in parallel into the gas path and removing the combustion products through two gas flues. Behind the exhaust blowers there is an integration of gas flues combined into a general gas flue, which enters the chimney. A diagram of the gas flues of two TGMP-314 TEC-23 Mosenergo boilers is shown in Fig. 11 [9].

Efficiency adjustment of the exhaust blowers is controlled by a two-stage rotary guide machine. The efficiency of the exhaust blower depends on the installation angle of the guide blades (Fig. 12). The transfer of the displacement force to the

Fig. 11 TGMP-314 boiler gas flues diagram: 1—boilers TGMP-314, 2—exhaust blowers of the boilers, 3—peak hot water boilers, 4—chimney

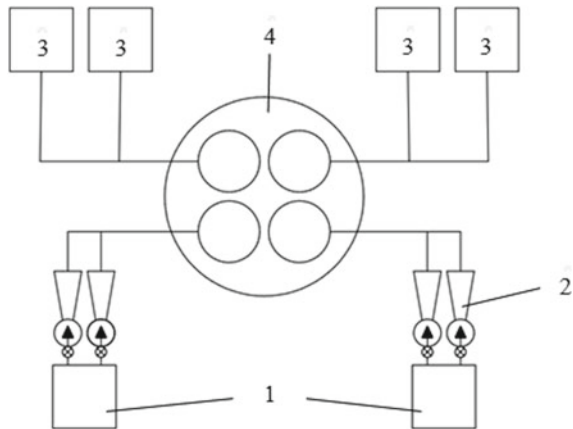
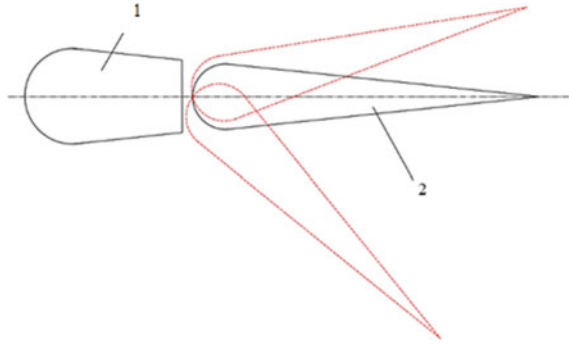


Fig. 12 Exhaust blower guide blade diagram:
1—guide blade nose,
2—guide blade flap



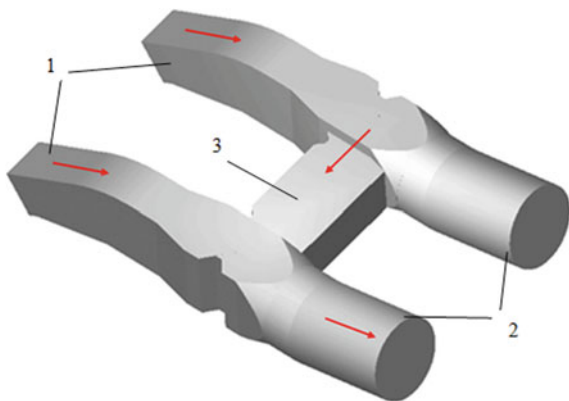
blades from the drive mechanism (ESM—electric single-turn mechanism) is carried out through a traction and rocking system. In this case, synchronization of the blades deflection at the same angle must be ensured.

The authors of the article have repeatedly had to deal with cases when, due to deformation of rods, rockers, platforms for ESM during operation, the installation angles of the guide blades changed relative to the position indicator on the panel device, and also the synchronism of the blades opening at the same angle disappeared. For these reasons, the efficiency of the exhaust blower changes. Since the TGM-314 boiler is equipped with two exhaust blowers, a change in the efficiency of one of them in comparison with the value set by the boiler operator can lead to gas imbalance.

Another possible reason of gas imbalance in boilers with two exhaust blowers, including the TGM-314 boiler, may be long-term operation of the boiler with only one exhaust blower through a jumper connecting the gas exhaust flues (Fig. 13).

In this case, by two additional turns 90° the aerodynamic resistance of the gas flue, the exhaust blower of which does not work, is significantly increased. A picture of gas imbalance will be the same as described above for the BKZ-420-140 NGM4 boiler. In this regard, it is necessary to limit the long-term operation of boilers equipped with two exhaust blowers through a jumper for one exhaust blower.

Fig. 13 Scheme of boiler operation for one exhaust blower: 1—gas flues from the boiler, 2—gas flues to the exhaust blowers, 3—jumper between the gas flues



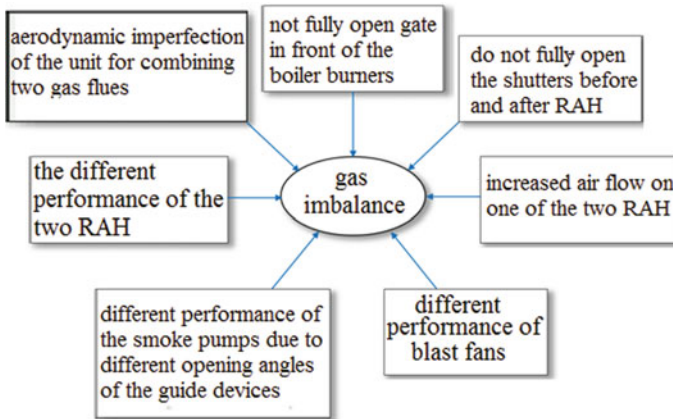


Fig. 14 Causes of gas imbalance in steam boilers

In addition to the above, there are a number of other reasons that can cause gas imbalance in boilers. An overall set of reasons is presented in Fig. 14. Figure 14 shows that there is a significant number of reasons causing gas imbalance and stratification of temperature in steam boilers.

Each of these reasons can have an effect both individually and in combination with other reasons. The effect of the complex impact of these reasons can multiply the gas imbalance and stratification of temperature. The only way to prevent gas imbalance is its timely detection using specialized control devices.

Ultimately, gas imbalance is caused by two reasons:

- different amounts of air entering the boiler on the sides of the boiler;
- different exhaust gas flow rates on the sides of the boiler.

Therefore, by installing control devices for air flow and exhaust gas flow on the sides of the boiler it is possible to diagnose the appearance of gas imbalance. In this case, there is no need to install exactly flow meters. It is enough to measure the flow rate of the working medium, since the cross-sectional area of the air ducts and gas ducts on the sides of the boiler is the same.

It is necessary to install sensors in the control cross-sections of the gas ducts and air ducts that measure the velocity head and output their readings to the boiler control panel. In case of difference in flow rate the boiler operator will be able to correct the situation by loading or unloading the appropriate exhaust blower or blower fan, thereby preventing the occurrence of gas imbalance and stratification of temperature.

As a result of this measure implementation premature exhaustion of the heating surfaces resource and the boiler as a whole will be prevented.

3 Conclusion

In this work a study of the gas imbalance causes is carried out using the example of the BKZ-420-140 NGM4 and TGMP-314 boilers, for which there is design documentation and statistical information on the damageability of heating surface elements.

In the course of the work analysis of the design gas-air ducts features of both boilers was completed and the main factors influencing the occurrence of gas imbalance were identified.

It has been established that one of the reasons for the gas imbalance is aerodynamic imperfection of the unit for combining two gas flues on the BKZ-420-140 NGM4 boiler. In the SolidWorks software mathematical modelling of the exhaust gases flow in the combining gas flows unit has been performed. Based on the results of the mathematical modelling it was found that the difference in the flow rates of exhaust gases on the sides of the boiler at rated load reaches 30%. A new design of the unit for combining exhaust gas flows is proposed. Repeated mathematical modelling confirmed the efficiency of the proposed measures. After reconstruction of the unit for combining gas flues the difference in the flow rates of exhaust gases on the sides of the boiler will be reduced to 4%.

The dependence of the TGMP-314 boiler gas imbalance presence on the technical condition of the exhaust blowers, which affects their performance, is assumed. It is recommended to limit long-term operation of boilers equipped with two exhaust blowers linked through a jumper for one exhaust blower.

For the purpose of the timely detection of gas imbalance a diagnostic system, that detects the fact of its occurrence by the difference in exhaust gases on the sides of the boiler and by the difference in the flow rates of air entering the burners, has been proposed.

References

1. WD 10-577-03 Standard instructions for metal control and prolongation of the service life of the main elements of boilers, turbines and pipelines of thermal power plants. Moscow: STC Industrial Safety (2004)
2. Bogachev, V.A., Taran, O.Y.: The effect of thermal unevenness on the temperature and reliability of metal convective superheaters. *Electr Stations* **2** (2002)
3. Baranov, P.A.: Prevention of accidents of steam boilers. Moscow: Energoatomizdat (1991)
4. Zainudin, A.F., Hasini, H., Fadhil, S.S.A.: CFD analysis of temperature imbalance in superheater/reheater region of tangentially coal-fired boiler. In: 4th International Conference on Mechanical Engineering Research (ICMER2017). IOP Conf. Series: Mater. Sci. Eng. (2017)
5. Fadhil, S.S.A., Hasini, H., Jaafar, M.N.M.: CFD analysis of temperature imbalance in full scale tangentially fired coal boiler. *Appl. Mech. Mater.* **V.564** (2014)
6. Bogachev, V.A., Pshechenkova, T.P., Shumovskaya, M.A.: The results of the examination of the superheaters of the TGMP-314 type boiler of the Kashirskaya GRES power units using a magnetic ferritometer. *Heat Power Eng.* **7** (2016)

7. Bogachev, V.A., Pshechenkova, T.P.: Investigation of the dependence of the resource characteristics of convective superheaters on the number of damaged coils. *Electr Stations* **12** (2016)
8. Shchetkin, V.S.: Testing and adjustment of the superheater of the head gas-tight boiler BKZ-420-140NGM on fuel oil. *Electr Stations* **3** (1980)
9. Zroychikov, N.A., Moskvina, A.G., Arkhipov, A.M., Prokhorov, V.B., Komissarov, Y.M., Kirichkov, V.S.: Reduction of aerodynamic drag of the gas path of the TGMP-314 TPP-23 boilers of Mosenergo OJSC. Conf.: Improving the reliability and efficiency of operation of power plants and energy systems. **1** (2010)

Continuous Steelmaking Unit of Bubbling Type



Konstantin Strogonov, Lyubov Kornilova, Alexey Popov,
and Alexander Zdarov

1 Introduction

The current technologies of mass, large-capacity steel production involve the use of a blast furnace process. The blast furnace process is optimal from a heat-engineering point of view, since it is continuous and implements a countercurrent flow pattern of the heated material and the exhaust gases. However, it also has disadvantages, of which mainly is the need to use the expensive coke. At the same time, the process of coke production significantly affects the environment, polluting it with emissions. After the melting process, liquid cast iron is usually sent to steelmaking shops, which use either an oxygen converter or electric arc steelmaking furnaces. The previously widespread open-hearth process of processing cast iron into steel has not actually been used recently.

The disadvantages of the blast furnace process cause the world's interest in technologies outside the blast furnace production of cast iron and steel, for example, the Midrex and Romelt processes operating both in Russia and abroad.

The first (Midrex) is a device for producing sponge iron by reducing ore in a mine furnace with gas obtained by the catalytic conversion of natural gas CO_2 and water vapor of grate gas. The use of natural gas makes it possible to reduce the temperature of direct reduction of iron in this method to 780–900 °C, while the mentioned blast furnace melting process takes place at a temperature of more than 1500 °C [1].

The second (Romelt) is a unit that uses a liquid-phase metal production process. The peculiarity of this device is the use of a slag bath, bubbled by an oxygen blast (the process of interest to us; in the source [2] it is noted that the bubbling of the melt significantly increases the speed of melting, chemical reactions and also improves the uniformity of the molten material), as a reaction zone for the iron reduction, as well as the process being one-staged [3].

K. Strogonov · L. Kornilova (✉) · A. Popov · A. Zdarov
NRU MPEI, Moscow 111250, Russian Federation

2 Relevance of the Development

Based on the analysis of literary sources, it was found that the use of natural gas in smelting processes is being actively studied at the moment. It was noted that the use of hydrogen in the composition of the fuel has a number of advantages, such as high-energy intensity and a small ecological footprint from the use of the gas in chemical reactions [4]. The use of carbon in the composition of the fuel contributes to the active carburization of the melt. The use of gas with a carbon content will allow it to replace the actively used coal in production. The use of gaseous fuel will save on fuel transportation by using existing gas pipelines for this process [5]. Foreign research also studied the process of bubbling the melt with natural gas through small-diameter holes and noted that this process needs further study in practice [6]. The processes of steel degassing were also considered in the sources [7, 8], where it was noted that a decrease in pressure above the melt has a positive effect on the homogenization and strength of the final metal structure.

Thus, this development is aimed at updating the research of both domestic and foreign scientists. The need for new methods of iron processing served as an incentive for the development of the unit discussed below; the public interest in the use of the widespread natural gas (in our case, methane) formed the basis of the proposed steel production process. The scientific group of the Department of Energy of High Temperature at NRU MPEI analyzed, applied, and developed the ideas of their predecessors, who were looking for the most energy-efficient method of steel production.

Thus, one can judge the relevance of the development considered below.

3 Proposed Method

The developed method (Fig. 1) is aimed at direct continuous production of steel from iron ore charge by redox reactions of incoming materials by CHM (carbon and hydrogen mixture of 75% C + 25% (H₂ + A)) and oxygen blast. The method is supposed to be implemented by a three-stage unit equipped with a device for heating the incoming charge and a degasser.

The unit design is shown below and includes a lined multi-stage case, the first stage of which has a hole for the flow of molten iron ore and lime, withdrawal of hot gas for heating the furnace 1, a perforated wall for oxygen and protective gas 2, a perforated wall for the flow of natural gas 3, a tap hole to pump out the slag 4, a device for preheating the charge 5, and water-cooled fences of the unit 6. On the second stage of the unit, there are holes for liquid scrap supply 7, a perforated hearth for oxygen and protective gas supply 8, and steelmaking slag tap hole 9. In the third stage of the unit, there is a perforated wall for argon flow 10, an opening for deoxidizers, slag-forming and alloying materials flow 11, a hole for the withdrawal of inert gas after steel processing 12, electrodes for heating metal 13, an opening to

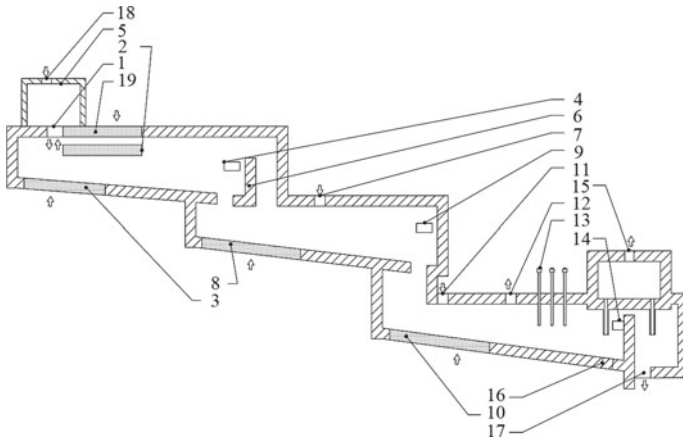


Fig. 1 Drawing of the unit under development

pump out the slag at the slag refining site 14, a degasser 15, made with the technical hole for the exhaust gases to create vacuum, bottom holes for the metal and slag flow during unit shutdown 16, and a hole for steel flow for further processing 17. In addition, on the first stage of the unit, there are also holes for feeding the charge into the device for heating it 18, and a perforated wall for supplying oxygen 19 (elements 2 and 19 form an exhaust gases afterburning system).

The unit works as follows: through the hole 1, the charge heated in 5 to 600–700 °C is fed (in turn, it enters the heating device through the hole 18). Next, the material is purged with the carbon and hydrogen mixture coming out of the perforated fence 3 at a speed that allows the CH₄ gas not to disintegrate into components within the lining. The bubbling liquid forms a zone of direct reduction, which is subsequently divided due to the difference in the densities of the metal and the slag melt into a zone of iron-carbon alloy and slag—the latter, in turn, is removed through the tap hole 4. The remaining alloy then enters the second stage of the structure through the water-cooled enclosure of the unit 6, where it is blown by oxygen coming out of the perforated wall 8, oxidized, and scrap is added to the alloy through a hole in the housing 7—an oxidative refining zone is formed. The mixture is also separated due to the difference in densities into steel and steelmaking slag (drained through tap hole 9), after that, the product enters the third stage. There, the steel is purged with argon supplied through the perforated hole 10, deoxidizers, slag-forming, and alloying materials are also supplied through the opening 11 under which a deoxidation zone is formed; inert gases are removed through the hole 12. 13—a metal heating node (it is necessary to compensate for heat losses), after which the alloy enters the degassing area, in the zone of which there is the opening 14 for pumping out residual slag. The operation of the degasser 15, made with a technical hole for the removal of gases, occurs during the air discharge—the alloy is drawn into the structure, where, under the action of the degasser [9], excess gas molecules are removed from it through its technical hole and after the process of degassing the finished product is sent for

casting or for finishing to special grades of steel through the hole 17. The proposed unit also has bottom holes for the release of metal and slag in case the unit stops 16. To achieve maximum energy efficiency of the unit and reduce the amount of volatile substances, the exhaust gases are after-burned with oxygen supplied through the perforated walls 2 and 19.

The use of a carbon and hydrogen mixture (CHM) [10]—a two-phase mixture of solid carbon and hydrogen gas—is due to its greater energy efficiency: this significantly reduces the energy cost of heating. In addition to the heat of the chemical reactions of redox processes, the purge of the melt with CHM provides a uniform heat exchange inside the melt due to the formation of convective flows inside the entire basin. Supplying room temperature mixture (about 20 °C) through a perforated fence at the bottom of the structure, we get H₂ and C at the exit from it, which are formed when methane is heated from the heat of the reactor. This helps to reduce heat losses through the walls of the structure—this heat is spent on heating the supplied fuel; the resulting skull also acts as a heat insulator [11]. Bubbling of the melt promotes additional mixing of the metal.

The conversion of methane to CHM occurs in three phases [11]:

- The rapture of the carbohydrate-hydrogen bond, formation of a single-phase mixture of two gases.
- Recombination of atomic carbon into molecular carbon, condensation of super-cooled carbon gas into soot particles.
- Formation of a heterophase mixture: soot particles evenly distributed in the volume of molecular hydrogen—hot CHM.

The time interval [12] from the formation of carbon gas to its condensation into soot particles (induction time) is 0.27–1.27 ms. This time is sufficient to organize the produce and use of the CHM.

The features of the unit we are developing also include the process continuity, the presence of a degasser, and a device for preheating the charge. The degasser (low-pressure chamber) provides degassing of the melt, which has a favorable effect on the quality of the resulting alloy, and the initial heating of the charge with gases leaving the furnace allows us to spend less fuel on melting the supplied material.

4 Calculating of Perforation Dimensions

One of the features of this unit is not only the fuel used (CHM) but also the mechanism of its supply to the furnace, so it is important to calculate the unit parameters of the hearth, namely the dimensions of its perforation.

It was assumed that the heat costs for producing cast iron are the same as in a blast furnace [13]:

$$Q = 20 * 10^6 \text{ [J/kg]}$$

or based on the fact that the consumption of the resulting cast iron is 1 million tons per year

$$Q = 20 * 10^6 * 10^9 = 2 * 10^{16} \text{ [J/year]} \quad (1)$$

According to Monograph [11], the consumption of natural gas for the reduction of 1 kg of iron is

$$V_{\text{CHM}} = 0.189 \text{ [m}^3\text{/kg]}$$

Heat of combustion of natural gas is as follows:

$$Q_{\text{NG}} = 3.6 * 10^7 \text{ [J/m}^3\text{]}$$

Chemical heat of the gas per 1 kg of reduced iron is

$$Q_{\text{C.NG}} = V_{\text{CHM}} * Q_{\text{NG}} = 6.815 * 10^6 \text{ [J/kg]} \quad (2)$$

Amount of chemical heat of the gas per second to form a given capacity is

$$Q_{\text{reduct}} = (Q_{\text{C.NG}} * 10^9) / (365 * 24 * 60 * 60) = 2.161 * 10^9 \text{ W} \quad (3)$$

Taking into account the chemical heat of the fuel combustion, the value of the required volume of gas is

$$V = Q / Q_{\text{NG}} = 5.556 * 10^{16} \text{ [m}^3\text{/year]} \quad (4)$$

Then the gas consumption in the perforation to produce 1 million tons per year of cast iron is

$$G = V / (365 * 24 * 60 * 60) = 17.617 \text{ [m}^2\text{/s]} \quad (5)$$

According to the sources [11, 14], the diameter of the holes and the gas supply velocity are [14]

$$d = 0.004 \text{ [m]}$$

$$w = 10 \text{ [m/s]}$$

Such values are due to the conditions of CHM formation without soot deposition on the surface of the channels and eliminate clogging of the perforation. Thus, it is possible to calculate the flow rate of natural gas through one hole:

$$S_{\text{circle}} = \pi * (d/2)^2 = 1.257 * 10^{-5} \text{ [m}^2\text{]} \quad (6)$$

$$G_1 = S_{\text{circle}} * w = 1.257 * 10^{-4} \text{ [m}^3/\text{s]} \quad (7)$$

Let's set the gas temperatures at the inlet/outlet and the wall:

$$\begin{aligned} t_1 &= 20 \text{ [}^\circ\text{C]} \\ t_2 &= 999 \text{ [}^\circ\text{C]} \\ t_w &= 999 \text{ [}^\circ\text{C]} \end{aligned}$$

The temperature of 999 °C is due to the condition of the CHM formation start. During the passage of the perforated hearth, the gas temperature and its properties change, so for approximate calculations, we can take the average gas temperature, which is the determining temperature in these calculations:

$$t_g = (t_1 + t_2)/2 = 509.5 \text{ [}^\circ\text{C]} \quad (8)$$

The following thermophysical characteristics of methane are assumed for this temperature [15–18]:

$$\begin{aligned} \text{Dynamic viscosity : } \mu &= 2286.715 \text{ [Pa/s]} \\ \text{Kinematic viscosity : } \nu &= 92.909 * 10^{-6} \text{ [m}^2/\text{s]} \\ \text{Prandtl number : Pr} &= 0.726 \\ \text{Coefficient of thermal expansion : } \beta &= 3.678 * 10^{-3} \\ \text{Coefficient of thermal conductivity : } \lambda &= 124.2 * 10^{-3} \text{ [W/(m * K)]} \\ \text{Thermal capacity : } C_p &= 3984.206 \text{ [J/(kg * K)]} \end{aligned}$$

Let's determine the gas flow mode in the perforation channel [19]:

$$\text{Re} = (4 * G_1)/(\pi * d * \mu) = 1.749 * 10^3 \text{---laminar flow} \quad (9)$$

$$\text{Ra} = [g * \beta * (t_w - t_g) * d^3 * \text{Pr}]/\nu^2 = 95.068 \text{---viscous flow} \quad (10)$$

Then the Nusselt number for the conditions under consideration according to the source [19] is

$$\text{Nu} = 4.36 \quad (11)$$

Then the heat transfer coefficient is

$$\alpha = (\text{Nu} * \lambda)/d = 135.377 \text{ [W/m}^2 * \text{K]} \quad (12)$$

These values allow us to calculate the heat flow density:

$$q = \alpha * (t_w - t_1) = 1.326 * 10^5 \text{ [W/m}^2\text{]} \quad (13)$$

Amount of physical heat introduced by the gas through one perforation hole per second is

$$Q_1 = G_1 * C_p * (t_2 - t_1) = 490.156 \text{ [W]} \quad (14)$$

Heat transfer surface area is

$$F = Q_1/q = 3.698 * 10^{-3} \text{ [m}^2\text{]} \quad (15)$$

Accordingly, the perforation thickness is obtained as

$$l = F/(\pi * d) = 0.294 \text{ [m]} \quad (16)$$

Total amount of chemical heat introduced through each hole per year is

$$Q_{c.h.1} = G_1 * Q_{NG} * (365 * 24 * 60 * 60) = 1.546 * 10^{11} \text{ [J/year]} \quad (17)$$

Amount of physical heat input through each hole per year is

$$Q_{p.h.1} = Q_1 * (365 * 24 * 60 * 60) = 1.546 * 10^{10} \text{ [J/year]} \quad (18)$$

That is, the total amount of heat input through one hole is

$$Q_2 = (Q_{c.h.1} + Q_{p.h.1}) = 1.581 * 10^{11} \text{ [J/year]} \quad (19)$$

Let's calculate the number of perforation holes:

$$n = Q/Q_2 = 1.265 * 10^5 \quad (20)$$

For the initial calculation, we will set the step $s = 0.006$ m and calculate the area occupied by the holes:

$$S_{\text{hole}} = n * [(3)^{1/3} * (d + s)^2]/4 = 5.477 \text{ [m}^2\text{]} \quad (21)$$

That is, by setting the length $L = 5$ m, we get the perforation width $B = 1.095$ m.

The estimated dimensions of the perforated fence are as follows: $5 \times 1.095 \times 0.294$ m.

The number of perforation holes depends on both the heat capacity of the entire perforation and the heat capacity derived from one hole (adjustable by velocity of gas)—graphs of the dependences under consideration are shown below.

The dependence of the number of holes in the perforation on the total value of the thermal power, with other constants, is linear—this follows from formula (12), by which we determine the number of holes in the perforation. Therefore, without

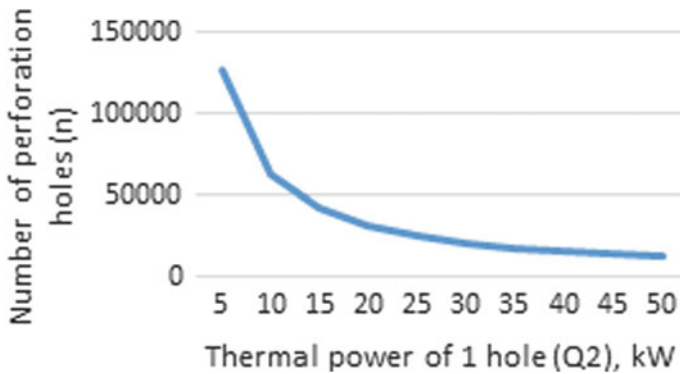


Fig. 2 Graph of the dependence of the number of perforation holes on the thermal power of one hole

changing the diameter of the holes, the gas supply rate, the heating temperature, and other characteristics of the fuel supply process, we increase the dimensions of the perforation in proportion to the required (real) heat consumed per kg of iron ore charge.

The dependence of the number of perforation holes on the thermal power of one hole is a hyperbolic dependence. From the formulas presented above, it can be seen that the thermal power obtained from a single perforation hole is a value that depends on a number of factors: gas supply speed, wall-to-gas temperature pressure, gas temperature difference along the perforation length, fuel consumption, and so on. To obtain the dependence graph presented below, the gas supply speed was changed in the range from 10 to 100 m/s.

Based on the graph shown in Fig. 2, it can be assumed that the most suitable speed to find the optimal value between the size of the hearth and the thermal load [6] on it is the point corresponding to the speed of 10–20 m/s. However, in this situation, it is also necessary to take into account the transition of the gas supply process to a turbulent mode, which causes the need to increase the length of the perforation channel and generally changes the above calculation.

5 Conclusion

Mass production of steel necessitates the creation of effective steelmaking processes. The method of steel production proposed in this article is relevant and has a number of advantages in comparison with the most common technologies for producing cast iron and steel. The main advantages include direct reduction of iron, continuity, use of energy-efficient fuel (CHM), lower fuel consumption—use of exhaust gases to heat the incoming charge, and presence of a degasser.

The calculation of the perforated hearth of the furnace, carried out in this article, allowed us to draw preliminary conclusions about the dimensions of the perforation of the reduction zone for the unit, the annual capacity of which is 1 million tons of melt. Thus, at a gas supply speed of 10 m/s, a perforation hole diameter of 4 mm, gas inlet and outlet temperature of 20 °C and 999 °C, respectively, it is obtained that the area of the perforated hearth is 5.475 m², and the thickness of the perforated hearth is 0.294 m.

The work was carried out within the “Breakthrough technologies of energy-efficient structures of bubbling furnaces” project with the support of the grant of the National Research University “Moscow Power Engineering Institute” for the implementation of research programs “Energy”, “Electronics, Radio Engineering and IT” and “Industry 4.0 Technologies for industry and robotics” in 2020–2022.

References

1. Baldauf-Sommerbauer, G., Lux, S., Siebenhofer, M.: Sustainable iron production from mineral iron carbonate and hydrogen. *G. C.* **23** (2016)
2. Pioro, L.S., Pioro, I.L., Kostyuk, T.O., Soroka, B.S.: Industrial Application of Submerged Combustion Melts. *F. P., Kyiv-80, Ukraine*, 240 p
3. Romenets, V.A., Valavin, V.C., Usachev, A.B., Karabasov, Y.S., Balasanov, A.V., Vandariyev, S.V., Verein, V.G., Galkin, V.I., Zaitsev, A.K., Levin, M.Ya., Rekhersak, V.E., Pokhvisnev, Yu.V., Stomakhin, A.Ya., Chaikin, B.S., Yatsenko-Zhuk, A.D.: Process Romelt. In: V.A. (ed.). M.: MISIS P. h. “O. & M.”, p. 400 (2005)
4. Sapountz, F.M., Gracia, J.M., Weststrat, C.J., Fredricso, H.O.A.: Electrocatalysts for the generation of hydrogen, oxygen and synthesis gas. *P. E. & C. S.* **58**, 1–35 (2017)
5. Michael, A., Kinnon, M., Brower, J., Samuelsen, S.: The role of natural gas and its infrastructure in mitigating greenhouse gas emission, improving regional air quality, and renewable resource integration. *P.E. & C. S.* **64**, 62–92 (2018)
6. Roger, F., Carreau, J.-L., Hobbes, P., Allou, A., Beauchamp, F.: Structure of strongly underexpanded gas jets submerged in liquids. *N. E. & D.* **273**, 119–130 (2014)
7. Mattox, D.M.: Ch. 3—The «Good» Vacuum (Low Pressure). In: *Processing Environment, Handbook of Physical Vapor Deposition (PVD) Pressing (Second Edition)*, pp. 73–14. William A. Publication (2010)
8. Zhu, B., Chattopadhyay, K.: Optimization of sampling location in the ladle during RH vacuum refining process. *Vac.* **152**, 30–39 (2018)
9. Pivtsaev, V.V., Enders, V.V., Gulyaev, M.P.: Comparative efficiency of steel degassing during vacuuming at RH and VD units. In: *Collection of S. W. of spec. of the Belarus, M. P.*, p. 360. *Tekhnologiya, Minsk* (2006)
10. Tesner, P.A.: Formation of carbon from the hydrocarbon gas phase. M., “Chemistry” (1972)
11. Neshporenko, E.G., Kartavtsev, S.V.: Questions of energy resource saving in the extraction of iron from ores: monograph, p. 153. GOU VPO “MSTU”, Magnitogorsk (2007)
12. Kartavtsev, S.V.: Intensive energy saving and technical progress of ferrous metallurgy: monograph, p. 311. GOU VPO “MSTU”, Magnitogorsk (2008)
13. Isaev, V.A.: Assessment of the energy intensity of the production of cast iron and steel. *Electrician* **6**, 15–18 (2008)
14. Dzhigiris, D.D., Makhova, M.F.: Basics of the Production of Basalt Fibers and Products, p. 412. *Teplotenergetik, Moscow* (2002)
15. Electronic resource. <http://thermalinfo.ru/svoystva-gazov/gazy-raznye/dinamicheskaya-vyazkost-gazov-i-parov>

16. Electronic resource. <http://thermalinfo.ru/svoystva-gazov/organicheskie-gazy/svoystva-gazov-metanovogo-ryada>
17. Electronic resource. [https://www.fxyz.ru/spravochnye_dannye/termodinamicheskie_svoystva_veshchestv/koefficient_ob"emnogo_rasshireniya_gazov/](https://www.fxyz.ru/spravochnye_dannye/termodinamicheskie_svoystva_veshchestv/koefficient_ob)
18. Electronic resource. <http://thermalinfo.ru/svoystva-gazov/gazy-raznye/teploprovodnost-gazov>
19. Tsvetkov, F.F., Kerimov, R.V., Velichko, V.I.: Task Book on Heat and Mass Transfer. MPEI P. H, Moscow (2008)

Determination of the Conductor Sag According to the Period of Own Harmonic Oscillations, Taking into Account the Difference in Heights of the Suspension Points



Danil Aleksandrovich Yaroslavsky, Van Vu Nguyen,
Marat Ferdinantovich Sadykov, Mikhail Petrovich Goryachev,
and Dmitry Alekseevich Ivanov

1 Introduction

Electricity is delivered to consumers via overhead power transmission lines (OTL). In this regard, there is an acute problem of monitoring the state of OTL in order to ensure a reliable power supply to consumers [1]. Recently, work has been actively carried out on the creation of intelligent OTL, which will be more efficient and safe [2]. However, any system for monitoring the state of OTL elements is based on methods and approaches to receiving and interpreting input data.

There are many approaches to assessing the technical condition of OTL: the study of the conductor heating temperature in order to increase its carrying capacity for the most effective use of existing OTL instead of building new ones [3–5]; use of unmanned aerial vehicles in order to estimate the geometric parameters of OTLs (use of video cameras or laser scanners), as well as control of insulators and conductor connections (video recording in the ultraviolet and infrared ranges) [6]; control of ice-rime deposits on the OTL conductors by the method of echolocation (inputting a signal into the conductor and analyzing its reflected value, which determines the wall thickness of the ice-rime deposits) [7]; determination of the conductor sag to assess the mechanical loads acting on it [8, 9].

In this article, we propose the method for determining the sag of the conductor, since it allows one to describe its geometry, and, therefore, determine the mechanical loads it experiences. This may be relevant when the OTL is exposed to external factors, for example, ice-rime deposits [10, 11]. To control the sag of the conductor, the following methods can be used: optical (a source and receiver of optical radiation are used, the shift of one of which determines the change in the conductor sag value)

D. A. Yaroslavsky · V. V. Nguyen · M. F. Sadykov · M. P. Goryachev (✉) · D. A. Ivanov
Kazan State Power Engineering University, Kazan, Russia

[12–14]; inclinometric (the angle of inclination of the conductor is determined, which is then used to calculate the mechanical loads experienced by the conductor) [9, 15].

Previously, our team developed methods where the mechanical loads experienced by OTL were determined using such parameters as the angle of inclination of the OTL conductor [8, 16] and the angle of its rotation [8, 17, 18]. At present for the first time, a method has been developed for determining the conductor sag by the period of its oscillations [19, 20]. This technique is also applicable for the case when the points of the conductor suspension are at different heights [19].

This article describes a method for determining the sag of a conductor by the period of its oscillations, and theoretical estimations are compared with the data of a model experiment. Comparison of the calculated values of the oscillation period of the conductor with the experimental ones should be carried out at different sags and heights of one of the points of the conductor suspension.

2 Brief Theory of the Method for Determining the Conductor Sag at Different Heights of Its Suspension Points

A conductor in the span of an OTL is considered as an absolutely rigid isotropic construction. This construction has one rotational degree of freedom relative to the axis passing through the suspension points of the OTL conductors, which are at different heights (Fig. 1).

The geometry of the conductor in the OTL span can be determined using the equations of the parabolic sag of a flexible thread [21]:

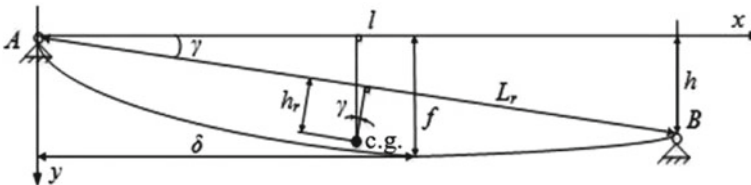


Fig. 1 Model of OTL conductor, fixed at the points of its suspension at different heights and representing a physical pendulum, with the designation of the main geometric parameters: L_r —the minimum distance between the suspension points, m; l —the OTL span length, m; f is the vertical distance between the highest point of the suspension and the lowest point of the conductor in the OTL span, m; h is the difference in the heights of the points of the OTL conductor suspension, m; h_r is the distance from the center of gravity (c.g.) of the OTL conductor to the segment with the ends at the points of suspension of the conductor A and B , m; δ is the distance from the suspension point A to the projection of the lower point of the conductor on the x -axis, m; γ is the angle between the segment AB and the x -axis

$$y = \frac{1}{a} \left(\delta x - \frac{x^2}{2} \right), \quad y' = \frac{\delta - x}{a}, \quad \delta = \frac{l}{2} + \frac{h}{l} a, \quad (1)$$

where a is the coefficient of the parabola, x is the coordinate of the conductor section and the origin is at point A .

The minimum distance from a straight line passing through the suspension points of the conductor to the center of swinging of the OTL conductor is determined as follows:

$$L_k = \frac{l^2(l^4 + 56a^2l^2) + 28a^2h^2}{14a(l^4 + 40a^2l^2 + 20a^2h^2)}. \quad (2)$$

The distance from the axis of rotation to the center of oscillation can be found from the oscillation period T :

$$L_k = \frac{gT^2}{4\pi^2}. \quad (3)$$

Joint consideration of Eqs. (2) and (3) allows finding the coefficient of the parabola a .

We can calculate the parameter f from the equations of the parabolic sag of a flexible thread (1), substituting the value δ instead of x and using the coefficient of the parabola a :

$$f = \frac{\delta^2}{2a}. \quad (4)$$

The vertical distance from the lowest point of the curve to the straight line passing through the points of suspension of the OTL conductor, according to [22], is the sag of the conductor. This distance can be found using the following expression:

$$f_p = f - \delta tg\gamma = f - \delta \frac{h}{l}. \quad (5)$$

Thus, to determine the sag of a conductor for OTL spans with suspension points located at different heights, additional data is required, such as the difference in heights of the points of suspension of the OTL conductor, the length of the OTL span and an acute angle between the horizontal straight line and the straight line passing through the points of the OTL conductor suspension (Fig. 1).

This data is difficult to obtain experimentally, which complicates the calculation of the conductor sag arrow.

In this regard, this work considers the possibility of applying the formula for determining the sag of a conductor, where only the period of own harmonic oscillations of the OTL conductor is used as input data [20, 23]:

$$f_p = \frac{5gT^2}{16\pi^2} \approx 0.31T^2. \quad (6)$$

3 Technique for Measuring Own Harmonic Vibration Period of a Conductor when Changing its Sag and the Height of One of the Points of the Conductor Suspension

The stand for measuring the own harmonic vibrations of a conductor when changing its sag and the height of one of the conductor suspension points includes a span of 5.368 m (horizontal distance between the conductor suspension points) with a conductor; flexible bearings at the conductor attachment points (in this case, the conductor at point B is attached so that the parameter h is 0, 0.25, 0.503, 0.753 and 1.003 m); laser level for easy measurement of the heights of the suspension points and the lower point of the conductor sag; a ruler for measuring vertical distances (the difference in the heights of the points of the conductor suspension and its sag).

The period T is determined as follows: (1) the conductor is retracted to the side and released, 40 full oscillations of the conductor are counted (the conductor returns to its original extreme position in which it was at the initial moment); (2) the time is measured during which these 40 complete oscillations of the conductor occurred; (3) the period of the conductor oscillation is determined as the arithmetic mean. Oscillations were observed visually.

To measure distances, for example, a sag, a ruler 1000 mm long is used (the minimum length measurement step is 0.5 mm). To increase the accuracy of measuring the sag, a BOSCH PCL 20 SET laser level is used, using which the horizontal and vertical laser beams are projected onto the wall. The use of a laser level allows one to project the position of the suspension point B and the lower point of the conductor onto a ruler. This allows the parameters h , f and δ to be determined. The conductor sag arrow in the experiment is determined in accordance with expression (5).

The description of the experimental setup at $h = 250$ mm is shown in Fig. 2.

4 Comparison of the Results of Calculating the Conductor Own Oscillations Period with the Available Experimental Data

A series of experiments is carried out at $h = 0 \div 1.003$ m. The oscillation period is determined in accordance with Formula (6) based on the data on the conductor sag:

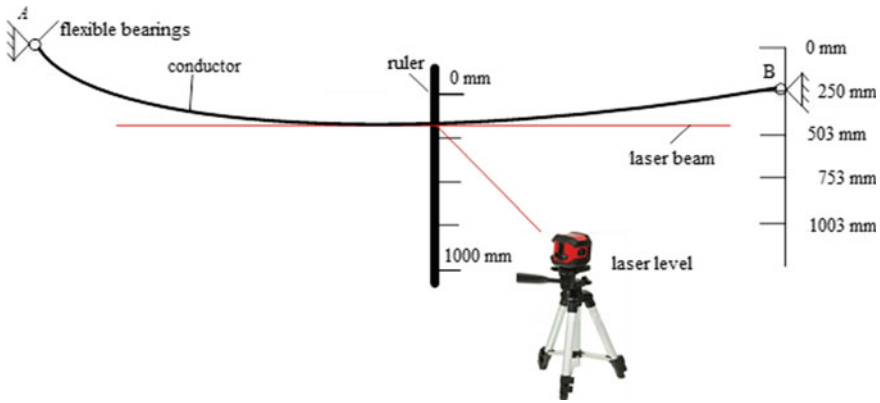


Fig. 2 Experimental setup with $h = 250$ mm

$$T = \sqrt{\frac{16\pi^2 f_p}{5g}}. \tag{7}$$

The error in calculating the period of own harmonic oscillations of a conductor at various sags is determined by the following formula:

$$\delta_T = [(T_{\text{exp}} - T_{\text{calc}})/T_{\text{exp}}] \cdot 100\%, \tag{8}$$

where T_{exp} is the oscillation period of the conductor, determined experimentally at a certain sag f_{exp} , estimated experimentally; T_{calc} is the oscillation period of the conductor, calculated by Formula (7) with the current sag f_{exp} , estimated experimentally.

Conductor’s own harmonic oscillation period on its sag at the difference in height between the suspension points $h = 0$ m dependence is considered in this article [23].

The dependences of the period of own harmonic oscillations of the conductor on its sag at a difference in heights between the suspension points $h = 0.25$ m and $h = 0.503$ m are shown in Fig. 3. The experimental values of the conductor sag (f_{exp} , m) are plotted along the abscissa axis, and the periods of the conductor’s own harmonic oscillations (T_{calc} are the periods calculated by Formula (7) for the values of f_{exp} ; $T_{0.25\text{exp}}$ and $T_{0.503\text{exp}}$ are the periods measured experimentally at $h = 0.25$ m and $h = 0.503$ m, respectively).

The sag of the conductor at $h = 0.25$ m varies from 0.1 to 0.553 m. The period of own harmonic oscillations of the conductor in this case changes from 0.578 to 1.331 s. The error in calculating the period of own harmonic oscillations of a conductor at different sags at $h = 0.25$ m lies in the range from 0.01 to 1.34%. At $h = 0.503$ m, the sag of the conductor changes from 0.106 to 0.667 m. The period of own harmonic oscillations of the conductor in this case changes from 0.592 to 1.456 s; the error in

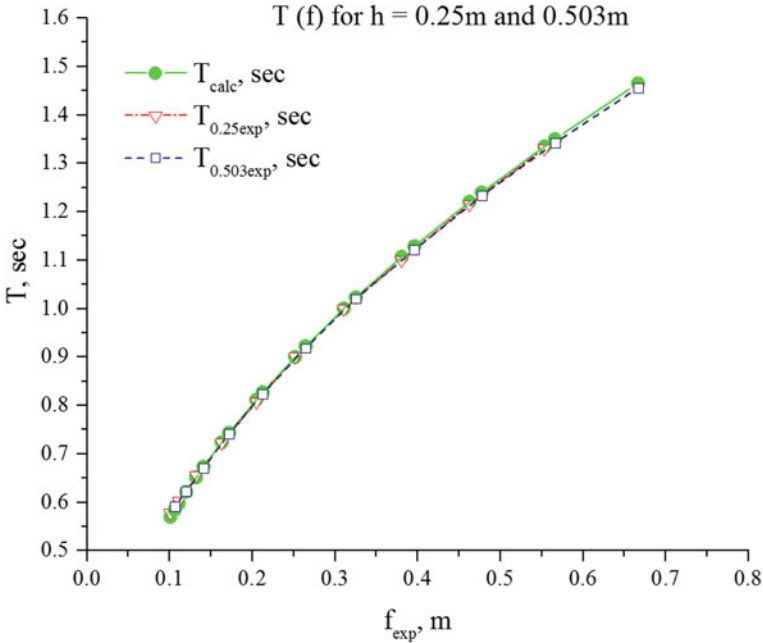


Fig. 3 Dependences of the period of own harmonic oscillations of the conductor on its sag at $h = 0.25$ m and $h = 0.503$ m

calculating the period of oscillations of a conductor with different sags is from 0.17 to 1.26%.

The dependences of the period of own harmonic oscillations of the conductor on its sag at $T_{1.003exp}$, and the difference in heights between the suspension points $h = 0.753$ m and $h = 1.003$ m are shown in Fig. 4. The experimental values of the conductor sag (f_{exp} , m) are plotted along the abscissa axis, and the conductor's own harmonic oscillation period values are plotted along the ordinate axis (T_{calc} —periods calculated by Formula (7) for f_{exp} values; $T_{0.753exp}$ —periods obtained experimentally at $h = 0.753$ m; $T_{1.003exp}$ —periods obtained experimentally at $h = 1.003$ m).

The sag of the conductor at $h = 0.753$ m during the experiment changes from 0.102 to 0.757 m. The period of own harmonic oscillations of the conductor in this case changes from 0.579 to 1.546 s. The error in calculating the period of the conductor oscillations at various sags at $h = 0.753$ m is from 0.04 to 1.16%. At $h = 1.003$ m, the sag of the conductor during the experiment changes from 0.080 to 0.705 m. The period of own harmonic oscillations of the conductor in this case changes from 0.495 to 1.503 s. The error in calculating the period of oscillations of a conductor at different sags at $h = 1.003$ m lies in the range from 0.06 to 2.67%.

The dependences of the period of own harmonic oscillations of the conductor on its sag, obtained by the proposed theoretical model, indicate that expression (6) for determining the sag of the conductor by the period of its own harmonic oscillations

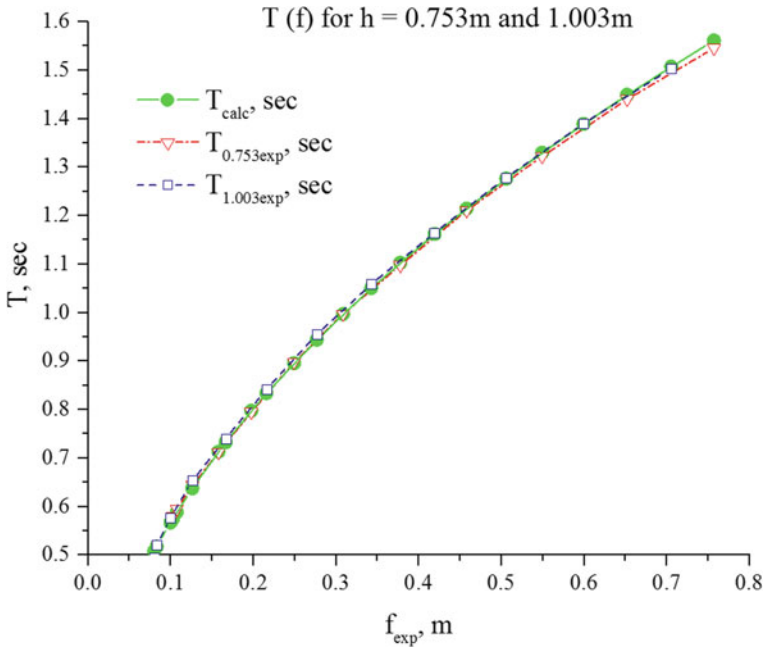


Fig. 4 Dependences of the period of own harmonic oscillations of the conductor on its sag at $h = 0.753 \text{ m}$ and $h = 1.003 \text{ m}$

makes it possible to reliably estimate the boom of the conductor sag even if there is a difference in heights between the points of the conductor suspension.

5 Conclusion

In this work, the possibility of using the method for determining the sag of a conductor by the period of its own harmonic oscillations at the nonzero difference in heights between the points of the conductor suspension is experimentally confirmed. A mathematical model is proposed that describes well the experimental dependences of the period of oscillations of the conductor on its sag. The error of the model for determining the oscillation period of the conductor, depending on its sag, does not exceed 2.735% when a span length does not exceed 5.368 m, a difference in the heights of the suspension points ranges from 0 to 1.003 m and a change in the sag varies from 0.080 to 0.757 m.

In the future, the method for determining the sag of a conductor by the period of its own harmonic oscillations can be implemented on the basis of existing and newly developed systems for monitoring the state of OTL [24].

Acknowledgements The research work was carried out under the financial support of the Ministry of Science and Higher Education within the scope of the state Research and Development task no. 075-03-2022-151 of 14.01.2022 “Distributed automated systems of monitoring and diagnostics for technical condition of overhead power lines and substations based on broadband data transmission technology through power lines and the industrial Internet of Things”.

References

1. Szopa, K., Iwaniec, M., Iwaniec, J.: Identification of technical condition of the overhead power line supporting structure. *Eksploatacja i Niezawodnosc*, **21**(1), 115–124 (2019)
2. Solyonyj, S.V., Shishlakov, V.F., Solenaya, O.Y., Kuzmenko, V.P., Kvas, E.S., Rysin, A.V.: Robotic power line maintenance systems. *IOP Conference Series: Materials Science and Engineering* **734**(1) (2020)
3. Gołaś, A., Ciesielka, W., Szopa, K., Zydroń, P., Kot, A., Bączorek, W., Benesz, M., Moskwa, S.: Analysis of the possibilities to improve the reliability of a 15 kV overhead line exposed to catastrophic icing in Poland. *Eksploatacja i Niezawodnosc* **21**(2), 282–288 (2019)
4. Rahman, M., Atchison, F., Cecchi, V.: Temperature-dependent system level analysis of electric power transmission systems: A review. *Electr. Power Syst. Res.* **193** (2021)
5. Popova, Y., Voitov, O., Semenova, L.: An algorithm to calculate feasible operating conditions of electrical network, given overhead conductor temperature and sag constraints. *E3S Web of Conferences*, **58** (2018)
6. Gheisari, M., Esmaili, B.: Applications and requirements of unmanned aerial systems (UASs) for construction safety. *Saf. Sci.* **118**, 230–240 (2019)
7. Minullin, R.G., Piskovatskiy, Y.V., Kasimov, V.A.: In: *Proceedings—2020 International Conference on Industrial Engineering, Applications and Manufacturing*, vol. 2020. ICIEAM (2020)
8. Yaroslavsky, D.A., Ivanov, D.A., Nguyen, V.: *Proceedings—2020 International Conference on Industrial Engineering, Applications and Manufacturing*, vol. 2020. ICIEAM (2020)
9. Fedotov, A., Vagapov, G., Grackova, L.: In: *Proceedings of the 10th International Scientific Symposium on Electrical Power Engineering*, pp. 284–288. ELEKTROENERGETIKA 2019 (2019)
10. Makarov, V.G., Fedotov, A.I., Basyrov, R.Sh., Vagapov, G.V.: Modeling of an overhead power transmission line in the Matlab/Simulink package. *Bull. Kazan Technol. Univ.* **20**(13), 93–96 (2017)
11. Levchenko, I.I., Satsuk, E.I., Shovkoplyas, S.S.: In: *Proceedings—2019 International Russian Automation Conference. RusAutoCon 2019* (2019)
12. Guo, J., Li, J., Rong, C., Dong, Z., Guan, W., Zheng, Y., Tan, L.: In: *Proceedings of 2019 IEEE 3rd International Electrical and Energy Conference*, pp. 314–319. CIEEC 2019 (2019)
13. Shilin, A., Shilin, A., Demytyev, S.: In: *Proceedings—2018 International Conference on Industrial Engineering, Applications and Manufacturing. ICIEAM 2018* (2018)
14. Wydra, M., Kisala, P., Harasim, D., Kacejko, P.: Overhead transmission line sag estimation using a simple optomechanical system with chirped fiber bragg gratings. part 1: Preliminary measurements. *Sens. (Switzerland)* **18**(1) (2018)
15. Golinelli, E., Bartalesi, D., Ogliaari, G.M., Perini, U.: In: *AEIT International Annual Conference. AEIT* (2019)
16. Sacerdotianu, D., Nicola, M., Nicola, C., Lazarescu, F.: In: *International Conference on Applied and Theoretical Electricity. ICATE 2018—Proceedings* (2018)
17. Yaroslavsky, D.A., Goryachev, M.P., Sadykov, M.F., Konov, A.B., Ivanov, D.A., Yambaeva, T.G.: *Proceedings of higher educational institutions. Energy Probl.* **19**, 89–97 (2017)

18. Goryachev, M.P., Sadykov, M.F., Yaroslavskiy, D.A.: Method for control the mechanical parameters of overhead power lines based on improved inclinometry. *Power Eng. Res. Equip. Technol.* **21**(3), 160–171 (2019)
19. Sadykov, M.F., Yaroslavsky, D.A., Ivanov, D.A., Tyurin, V.A., Galiyeva, T.G., Goryachev, M.P.: Inclinometric method for determining the mechanical state of an overhead power transmission line. *E3S Web of Conferences*, **124** (2019)
20. Yaroslavsky, D.A., Nguyen, V., Sadykov, M.F., Goryachev, M.P., Ivanov, D.A., Galieva, T.G., Vassunova, Y., Tyurin, A.N.: Studying the model of free harmonic oscillations of overhead power lines. *Int. J. Emerg. Trends Eng. Res.* **8**(6) (2020)
21. Yaroslavsky, D., Nguyen, V.V., Sadykov, M., Goryachev, M., Ivanov, D., Andreev, N.: In: *E3S Web of Conferences*, vol. 220 (2020)
22. Merkin, D.: Introduction to the mechanics of a flexible thread. M.: Sci. Main editors of physical and mathematical literature, vol. 240 (1980)
23. Overhead power transmission lines with a voltage higher than 1 kV // M, JSC “VNIIE”. PUE. ed. 7-e. Chapter 2.5-2003.
24. Sadykov, M.F., Yaroslavsky, D.A., Ivanov, D.A., Goryachev, M.P., Savelyev, O.G., Chugunov, Yu.S., Toropchin, Yu.V.: Implementation of an automated monitoring system for ice formation in the distribution networks of PJSC TATNEFT. *Oil Ind.* **7**, 53–55 (2020)

An Approach to Determining the Integrated Reliability of Technical Systems at the Development Stage



Ruslan Litvinenko, Aver Auhadeev, Azat Khusnutdinov, Irina Antipanova, and Leylya Kisneevea

1 Introduction

When setting the requirements for the reliability of an engineering object at the stage of development of basic specifications and terms of reference, the nomenclature and values of reliability measures (RM) are determined and agreed upon between the customer and the designer. The components of the targeted RMs are selected from among the measures regulated by international standards IEC 62347:2006 and in accordance with IEC 60300-3-15:2009. The number of targeted RMs should be minimal in order to reduce the cost of verification, confirmation and evaluation of RMs available during manufacture and operation. At the same time, these RMs should be sufficient and fully describe the reliability of the engineering object at all stages of the life cycle. For comprehensive engineering systems, complex RMs or a specific single characteristic of reliability and maintainability, as well as their combinations, are used. If the engineering object during operation can be stored or shipped, then it is also necessary to set the preservation factors and the durability factors, if the criteria for reaching the limit state are determined for the engineering object. The numerical values of RMs are found by calculation, trial or computational and experimental methods using reference statistical data on the reliability of equivalents (prototypes) of the engineering object being designed, as well as operation and test data obtained from component suppliers. The engineering object being designed meets the requirements for reliability, subject to compliance with the applicable requirements of all RMs [1, 2].

At the design stage, the reliability requirements are possible to update with an appropriate feasibility study in the course of considering possible options for the engineering object followed by calculation of their reliability; selection of a schematic and design version of the structure that meets the customer's requirements in terms

R. Litvinenko (✉) · A. Auhadeev · A. Khusnutdinov · I. Antipanova · L. Kisneevea
Kazan State Power Engineering University, Kazan, Russia

of the set of RMs and costs; clarification of the values of RMs of the engineering object.

The analysis of international standard IEC 60300-3-15:2009 makes it possible to conclude that for comprehensive engineering systems, if they are recoverable, provided that requirements for durability and preservation are defined for them, the total number of single and complex RMs is within 5–7 units. In the situation where the engineering system is unique, consisting of promising, unparalleled components, it is sufficient that all the RMs set comply with the requirements described in the specification. In practice, the designed or upgraded engineering system includes, however, in part or in whole, existing components for which statistical data on reliability are known. Therefore, at the design stage, there may be several possible schematic and design options for building such systems that meet the specified reliability requirements. A balanced approach to the issue of choosing a particular system design comes into importance, which is a solution to the multicriteria challenge of comparative assessment of reliability levels, as one of the technical requirements for the design engineering of options. Similar to the requirements for reliability, the specification indicates the requirements, characteristics, norms, indicators and other parameters that determine the purpose, performance of the products being designed. Therefore, the designer shall choose such a version of the engineering system that would satisfy all technical requirements (requirements for operation, stability, electromagnetic compatibility, etc.), including the reliability requirements described in the specification. Various schematic and design versions of the engineering system have different quantitative RMs, which do not allow unambiguously giving preference to one or another engineering solution. At the same time, the difference between RMs can vary from insignificant to significant, and the superiority of one option of the engineering solution over another is possible only in certain measures from those specified in the reliability requirements.

Thus, the relevance of the study is due to the objective need for developing such a reliability measure R that would characterize the entire set of basic reliability properties of the engineering system, if all the individual measures described in the specification meet the reliability requirements [3]. As IEC 62347:2006 provides exact definitions and the list of complex measures, the authors suggest calling this measure as the Integrated Reliability Measure (IRM).

Note that the authors do not set out to develop an approach for assessing the IRM of the engineering system; the purpose of the proposed methodology is to determine generalized indicators for several schematic and design options that synthesize individual RM into a single one. At the next stage of assessing the technical level of alternatives for the system being designed, taking into account all the requirements of the specification, the numerical value of reliability will be represented by one single indicator—IRM, and not a set of single and complex RMs.

2 Materials and Methods. Methodology for Determining the IRM Based on the Analytic Hierarchy Process

Generally, the Analytic Hierarchy Process (AHP) is a mathematical apparatus of the systematic approach to decision-making technology based on calculations and the use of the method of pairwise comparisons, which makes it possible to find such an option (alternative) that best suits the essence of the challenge and the requirements to its solution. This process was developed by Thomas L. Saaty in the 1970s and is actively used in addressing various multicriteria problems (analysis of possible scenarios, ranking, resource allocation, risk management, etc.). In addition, AHP has become widespread in the practical solution of problems of comparative analysis of the technical level of alternatives for engineering objects being designed [4–6].

The solution to the problem by means of AHP consists of the following steps:

1. Setting the goal, main criteria (performance indicators) and alternatives.
2. Decomposition of the problem into a hierarchical structure: a tree from the goal through criteria to alternatives.
3. Building matrices of pairwise comparisons of criteria by purpose and alternatives by criteria.
4. Checking the consistency of experts' judgments (criterion of the quality of the experts' performance).
5. Application of the mathematical apparatus for the analysis of the resulting matrices.
6. Determination of local priorities of criteria and global priorities of alternatives.
7. Selection of the dominant alternative.

A more detailed description of the content of these AHP steps is widely presented in various sources [7–9].

The AHP has the following advantages:

- takes various factors and multiple goals into account;
- regards the possible effect of the interaction of factors;
- simplicity of mathematical calculations;
- for pairwise comparisons, a scale of relative importance is used, which streamlines and simplifies the procedure for setting expert assessments;
- is able to assign ranks to alternative options (numerical indicators reflecting the significance or importance of an object).

The latter provision is recommended to be used for building the quantitative value of the IRM for alternative options of the engineering system, where the corresponding RMs will act as criteria [10]. It is suggested using the calculated values of global (composite) priorities as the IRM. Note that the IRM is determined for specific structural and schematic options for constructing the system being designed and the adequate quantitative values of the RM. Modification of any of these provisions will result in a re-determination of the IRM.

As a disadvantage of the AHP, it can be noted that.

- the number of measures should not exceed 7 ± 2 , since human consciousness is not capable of simultaneous perception and processing of more than the specified number of information units [11, 12];
- the AHP allows for finding the ranks of the selected alternatives, but does not have internal means of interpreting these ranks;
- despite checking the consistency of the judgments of experts, expert assessments are subjective.

The performance and adequacy of the proposed approach to the AHP-based determination of IRM for the subsequent assessment of the technical level of design and schematic versions of the engineering system being designed will be then specifically exemplified.

3 Results. AHP-Based Calculation of the IRM for a Multi-motor Drive

For the multi-motor drive (MMD) used in electric transport, the customer described the following reliability requirements in the specification:

- gamma-percentile time to failure (*GPTF*)—minimum 7500 h;
- mean time between failures (*MTBF*)—minimum 12,000 h;
- average overhaul life (*AOL*)—minimum 5 years;
- availability factor (*AF*)—minimum 0.99;
- mean lifetime till discarding (*MLTD*)—minimum 20 years.

The designer proposed three possible options for MMD with pre-calculated values of the measures shown in Table 1.

Using the AHP, it is required to calculate the IRM R_1 , R_2 and R_3 for alternative options of the MMD for the subsequent comprehensive analysis of the compliance of all technical requirements with the system being designed.

Decomposition of the problem into a hierarchy. The decomposition of the IRM calculation problem is shown in Fig. 1. In the most elementary form, the hierarchy consists of a top (conditionally, there is a common goal—generating the IRM), from which there are intermediate levels, consisting of 5 criteria (reliability measures) that

Table 1 Reliability measures for MMD versions

	Reliability measures				
	<i>GPTF</i> , kilohours	<i>MTBF</i> , kilohours	<i>AOL</i> , years	<i>AF</i>	<i>MLTD</i> , years
Alternative 1	7.6	12.5	7	0.998	22
Alternative 2	8	13.5	6.5	0.999	24
Alternative 3	5.2	14	5	0.994	25

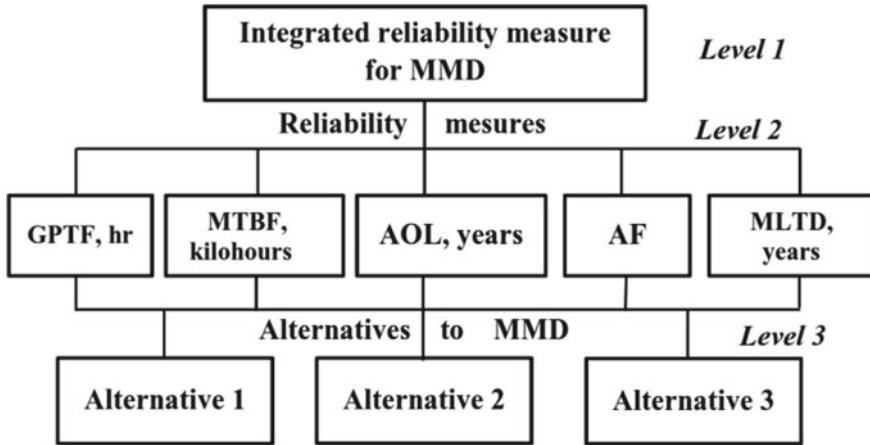


Fig. 1 Decomposition of the IRM calculation problem for the MMD options

clarify the goal, to the lower level, consisting of 3 alternative options of the MMD. This hierarchy is called dominant.

Building matrices of pairwise judgments. When using AI, the problem to be solved was presented hierarchically; therefore, the matrix of comparing the importance of the second-level RM is made available relative to the overall goal (level 1). Similar matrices are also built for pairwise comparisons of each alternative MMD in relation to the elements of level 2. For subjective paired comparisons, Thomas L. Saaty developed a numerical scale of relative importance [8, 12], according to which experts determine the weight of functions (measures) that describe the system being designed.

To build a pairwise judgment matrix for level 2 A_1 with the dimension $k \times k$, where $k = 5$ is the number of specified RMs, a table is drawn up in k rows and columns, in which the headers of the columns and rows refer to the measures used in generating the IRM and described in the specification. Actions begin with the indicator located in the heading of row 1 (gamma-percentile time to failure *GPTF*), while a question arises how much this measure is more important than the measures referred to in the column heading, respectively, the mean time between failures *MTBF* and then the rest of the measures. When comparing the measure with itself, the ratio is equal to one. If the compared measure is more important than the RM from the column heading, then an integer from the relative importance scale [13] is used, otherwise, the reciprocal. Thus, in turn, the importance of all RMs is compared with each other and all elements of the matrix A_1 of pairwise comparisons for level 2 (RM level) are determined (Table 2).

The compilation of matrices $A_{2j}, (j = \overline{1, k})$ for level 3 (the level of alternatives) is greatly simplified, since the RM values are expressed quantitatively, not qualitatively. Elements of matrices $A_{2j}, (j = \overline{1, k})$ are generated by dividing the RM values of the corresponding alternative options of the MMD for each measure j (matrices

Table 2 Matrix A_1 of pairwise comparisons for level 2

Measures	$GPTF, j = 1$	$MTBF, j = 2$	$AOL, j = 3$	$AF, j = 4$	$MLTD, j = 5$
$GPTF$	1	3	4	1	5
$MTBF$	1/3	1	4	2	3
AOL	1/4	1/4	1	1/5	3
AF	1	1/2	5	1	6
$MLTD$	1/5	1/3	1/3	1/6	1

Note $j = \overline{1, k}$ is the serial number of the reliability measure

$A_{21}, A_{22}, A_{23}, A_{24}$ and A_{25}). Table 3 lists matrices A_{2j} of pairwise comparisons for level 3.

Thus, actions of this stage resulted in a matrix A_1 of pairwise comparisons for the RM level and a matrix $A_{21} \dots A_{25}$ for the level of alternatives to the MMD.

Determination of local priorities and consistency of expert opinions for level 2. For the matrix A_1 of pairwise comparisons of the measure level, a set of local priorities is determined, which describe the relative influence of the set of top elements on the bottom element of the hierarchy. This identifies the weight of each individual component of the matrix. In view of this, it is necessary to calculate the eigenvector $\overline{A} = [x_1 \dots x_k]^T$ of the matrix A_1 , the components of which are the characterization of the priority vector by the rows of the matrix x_i , determined by the formula

$$x_i = \frac{\overline{a}_i}{\sum_{i=1}^k \overline{a}_i},$$

where $\overline{a}_i = \sqrt[k]{\prod_{i=1}^k a_i}$ is the geometric mean of the elements of the i th row of the matrix $A_1, i = \overline{1, k}$.

For solving the given problem, the eigenvector \overline{A} of the matrix A_1 received the following values:

$$\overline{A} = \begin{bmatrix} x_1 \\ x_2 \\ x_3 \\ x_4 \\ x_5 \end{bmatrix} = \begin{bmatrix} 0.3573 \\ 0.2388 \\ 0.0817 \\ 0.2708 \\ 0.0514 \end{bmatrix},$$

where x_1 is the characteristic of priority of the $GPTF$; x_2 — $MTBF$; x_3 — AOL ; x_4 — AF ; x_5 — $MLTD$.

The vector of local priorities (eigenvectors of the matrix A_1) $\lambda_{\max} = [\lambda_{\max 1} \dots \lambda_{\max k}]$ is calculated by reducing the value x_i to a normalized form formula:

Table 3 Matrices of pairwise comparisons for the level of alternatives to the MMD

<i>Matrix A₂₁ of pairwise comparisons for the measure GPTF, j = 1</i>			
	Alternative 1	Alternative 2	Alternative 3
Alternative 1	1	7.6/8 = 0.95	7.6/8.2 = 0.9268
Alternative 2	8/7.6 = 1.0526	1	8/8.2 = 0.9756
Alternative 3	8.2/7.6 = 1.0789	8.2/8 = 1.025	1

<i>Matrix A₂₂ of pairwise comparisons for the measure MTBF, j = 2</i>			
	Alternative 1	Alternative 2	Alternative 3
Alternative 1	1	12.5/13.5 = 0.9259	12.5/14 = 0.8929
Alternative 2	13.5/12.5 = 1.08	1	13.5/14 = 0.9643
Alternative 3	14/12.5 = 1.12	14/13.5 = 1.037	1

<i>Matrix A₂₃ of pairwise comparisons for the measure AOL, j = 3</i>			
	Alternative 1	Alternative 2	Alternative 3
Alternative 1	1	7/6.5 = 1.0769	7/5 = 1.4
Alternative 2	6.5/7 = 0.9586	1	6.5/5 = 1.3
Alternative 3	5/7 = 0.7143	5/6.5 = 0.7692	1

<i>Matrix A₂₄ of pairwise comparisons for the measure AF, j = 4</i>			
	Alternative 1	Alternative 2	Alternative 3
Alternative 1	1	0.998/0.999 = 0.999	0.998/0.994 = 1.004
Alternative 2	0.999/0.998 = 1.001	1	0.999/0.994 = 1.005
Alternative 3	0.994/0.998 = 0.996	0.994/0.999 = 0.995	1

<i>Matrix A₂₅ of pairwise comparisons for the measure MLTD, j = 5</i>			
	Alternative 1	Alternative 2	Alternative 3
Alternative 1	1	22/24 = 0.999	22/25 = 1.004
Alternative 2	24/22 = 1.001	1	24/25 = 1.005
Alternative 3	25/22 = 0.996	25/24 = 0.995	1

$$\lambda_{\max i} = x_i \cdot \sum_{j=1}^k a_{ij},$$

where $\lambda_{\max i}$ are the eigenvalues of the Perron vector [12, p. 15]; a_{ij} is the value of the element of matrix A_1 in the i th row of the j th column, $j = \overline{1, k}$.

Using the described procedure, the local priorities $\lambda_{\max i}$ will be determined for level 2 (level of measures). For solving the problem of generating the IRM for the alternative MMDs, the vector of local priorities is represented by the following values:

$$\lambda_{\max} = \begin{bmatrix} 0.9945 \\ 1.2139 \\ 1.171 \\ 1.1825 \\ 0.9252 \end{bmatrix}.$$

The sum of all the elements of the resulting vector of local priorities λ_{\max} is 5.4871, called Perron’s eigenvalue, and it is denoted by the letter Λ [12, p. 16]. If the matrix is absolutely consistent, the condition $\Lambda = k$ is met.

After determining local priorities $\lambda_{\max i}$ and the value Λ , the procedure for assessing the consistency of expert opinions will be applied when generating the matrix of pairwise comparisons A_1 for level 2, since the generalized opinion of the group of experts is not devoid of subjectivity, because of using a qualitative rating scale. For this, the AHP provides for the use of the consistency index (μ), which gives information on how much the numerical and ordinal consistency is disturbed. If the consistency is significantly disturbed, then it is recommended to search for additional information and revise the judgments of experts in the second round of the examination.

The consistency index will be calculated by the formula

$$\mu = \frac{\Lambda - k}{k - 1} = \frac{5.4871 - 5}{4} = 0.1218.$$

The value μ will be compared with the value of random consistency (μ_{rand}), which would be obtained with a random set of quantitative judgments from the scale $\frac{1}{9}, \frac{1}{8}, \frac{1}{7}, \dots, 1, 2, \dots, 9$, but provided that an inversely symmetric matrix was created. The source [6] provides a table that allows determining the average consistency μ_{rand} for random matrices of various orders. For solving the given problem for $k = 5$, the value $\mu_{\text{rand}} = 1.12$. To compare the values μ and μ_{rand} , the consistency ratio (CR) will be found by the formula

$$\text{CR} = \frac{\mu}{\mu_{\text{rand}}} \cdot 100\% = 10.9\%.$$

The CR must be 10% or less to be acceptable. In some cases, 20% is possible, but not more. If CR exceeds 20%, it is necessary to conduct a second round of examination and clarify the elements of the matrix of pairwise comparisons A_1 for level 2 [12, 14].

Since $CR = 10.9\%$, it is possible to conclude about the admissible consistency of the matrix of pairwise comparisons A_1 for level 2 of the problem of generating the IRM for alternative MMDs.

Determination of local priorities for level 3. Further, in a similar way, local priorities are determined for level 3 (the level of alternative MMDs); the calculation results are listed in Table 3. It should be noted that if the measures of alternatives are given in the form of numerical values, then it is not necessary to determine μ , since $\mu = 0$, and therefore $\mu_{rand} = 0$. Hence, no determination of μ_{rand} was made for level 3.

Determination of global priorities. To generate the IRM of alternatives, priorities are synthesized starting from the level of measures. Local priorities are multiplied by the priority of the corresponding RM at a higher level and are summed up for each element in accordance with the criterion driven by this element (each element of level 2 is multiplied by 1, i.e. by the weight of the single goal of the highest level). This gives the composite or global priority of that element, which is then used as a criterion for weighing the local priorities of the elements below it. As mentioned above, it is proposed to accept the value of the global priority as the IRM for alternatives.

The results summarized in Table 4 will be presented in the form of a 5×3 matrix A_3 , where the columns will correspond to the values of the vector of level 2 RM priorities, and the rows will correspond to the alternative MMDs.

Thus, for each measure the priority matrix A_3 will take the following form:

$$\begin{aligned}
 A_3 &= \begin{bmatrix} x_1^{(GPTF)} & x_1^{(MTBF)} & x_1^{(AOL)} & x_1^{(AF)} & x_1^{(MLTD)} \\ x_2^{(GPTF)} & x_2^{(MTBF)} & x_2^{(AOL)} & x_2^{(AF)} & x_2^{(MLTD)} \\ x_3^{(GPTF)} & x_3^{(MTBF)} & x_3^{(AOL)} & x_3^{(AF)} & x_3^{(MLTD)} \end{bmatrix} \\
 &= \begin{bmatrix} 0.3193 & 0.3337 & 0.3784 & 0.3125 & 0.3099 \\ 0.3361 & 0.334 & 0.3514 & 0.3375 & 0.338 \\ 0.3445 & 0.3323 & 0.2703 & 0.35 & 0.3521 \end{bmatrix}.
 \end{aligned}$$

The vector of global priorities will be determined by the formula

$$\bar{W} = A_3 \cdot \bar{A} = \begin{bmatrix} x_1^{(GPTF)} & x_1^{(MTBF)} & x_1^{(AOL)} & x_1^{(AF)} & x_1^{(MLTD)} \\ x_2^{(GPTF)} & x_2^{(MTBF)} & x_2^{(AOL)} & x_2^{(AF)} & x_2^{(MLTD)} \\ x_3^{(GPTF)} & x_3^{(MTBF)} & x_3^{(AOL)} & x_3^{(AF)} & x_3^{(MLTD)} \end{bmatrix} \cdot \begin{bmatrix} x_1 \\ x_2 \\ x_3 \\ x_4 \\ x_5 \end{bmatrix} = \begin{bmatrix} W_1 \\ W_2 \\ W_3 \end{bmatrix},$$

where W_1, W_2, W_3 are the global priorities of the corresponding alternative MMDs.

Substituting the numerical values obtained for A_3 and \bar{A} will result in the following values of global (eigen) priorities:

Table 4 Determination of local priorities for level 3 (the level of alternatives)

Alternatives to MMD	Alternative 1	Alternative 2	Alternative 3	Values of vector of priorities x_i	Vector of local priorities $\lambda_{\max i}$
<i>For specified failure-free service hours GPTF</i>					
Alternative 1	1	0.95	0.9268	0.3193	0.9999
Alternative 2	1.0526	1	0.9756	0.3361	0.9999
Alternative 3	1.0789	1,025	1	0.3445	0.9999
Definition Λ_1					3
<i>For mean time between failures MTBF</i>					
Alternative 1	1	0.9259	0.8929	0.3337	1.001
Alternative 2	1.08	1	0.9643	0.334	1
Alternative 3	1.12	1.037	1	0.3323	0.9999
Definition Λ_2					3
<i>For specified overhaul life AOL</i>					
Alternative 1	1	1.0769	1.4	0.3784	1.0001
Alternative 2	0.9586	1	1.3	0.3514	1.0001
Alternative 3	0.7143	0.7692	1	0.2703	1.0001
Definition Λ_3					3.0003
<i>For availability factor AF</i>					
Alternative 1	1	0.999	1.004	0.3125	1
Alternative 2	1.001	1	1.005	0.3375	1
Alternative 3	0.996	0.995	1	0.35	1
Definition Λ_4					3
<i>For specified life MLTD</i>					
Alternative 1	1	0.999	1.004	0.3099	1.0001
Alternative 2	1.001	1	1.005	0.338	0.9999
Alternative 3	0.996	0.995	1	0.3521	1
Definition Λ_5					3

$$\bar{W} = \begin{bmatrix} 0.3193 & 0.3337 & 0.3784 & 0.3125 & 0.3099 \\ 0.3361 & 0.334 & 0.3514 & 0.3375 & 0.338 \\ 0.3445 & 0.3323 & 0.2703 & 0.35 & 0.3521 \end{bmatrix} \times \begin{bmatrix} 0.3573 \\ 0.2388 \\ 0.0817 \\ 0.2708 \\ 0.0514 \end{bmatrix} = \begin{bmatrix} 0.3268 \\ 0.3372 \\ 0.3363 \end{bmatrix}.$$

The sum of global priorities must be equal to one.

Equating the calculated values of global priorities W_1, W_2, W_3 to the measures R_1, R_2 and R_3 will yield the numerical values of the IRM of the corresponding alternatives to MMD, characterizing the set of single and complex RMs. Because of solving the given problem, the highest IRM corresponds to the alternative 2 to MMD, as $R_2 = 0.3372 > 0.3363 > 0.3268$. These measures, which are a generalized (unified) RM, can be then used along with other technical and economic requirements to the MMD for the subsequent selection of the most preferable schematic and the design version of the multi-motor drive being designed.

4 Discussion

The analysis of the calculation results has shown the adequacy and correctness of the proposed approach, and its suitability for use for further analysis of the IRM of alternatives of the sophisticated engineering systems being designed. The practical effect of determining the IRM by the analytic hierarchy process can be further developed because of the integration of the expert system used at the stage of constructing the matrix of pairwise judgments for the level of reliability measures, and artificial neural network technologies. The ability of neural networks to learn on multiple qualitative and quantitative examples with unknown regularities between input and output data will further allow the developed neuro-expert system to automate the process of determining the weight of specified reliability measures [15, 16]. Also, the use of neural network technologies in determining the IRM will make it possible to increase the number of individual analyzed RMs in connection with the ability to process a large amount of information.

5 Conclusion

Thus, the approach to determining the IRM of engineering systems at the design stage, synthesizing up to 5–7 individual measures that describe various properties of reliability, makes it possible to give a comprehensive assessment and, based on this, to rank options of schematic and design solutions. The proposed mechanism for determining the IRM for the alternatives of the engineering system being designed is a convenient tool for scientific research at the stage of basic specifications and terms of reference. The use of the AHP for this purpose facilitates a deep analysis of a large volume of expert and statistical information about the specified reliability criteria, taking into account the weight characteristics of the analyzed measures. The integral measure to determine the level of reliability is useful to get a formalized result, which is expressed through the corresponding value of the vector of global priorities and enables to quantitatively assess the superiority of one alternative over another.

References

1. Auhadeev, A., Litvinenko, R., Fandeev. Research of reliability of urban electric transport system, V.: E3S Web Conf. **124**(05078) (2019)
2. Georgievskaya, E. Metodicheskie printsipy otsenki nadezhnosti oborudovaniya na rannikh stadiyakh proektirovaniya: *Novoe v Rossiiskoi elektroenergetike* **11**, 25–26 (2018)
3. Litvinenko, R., Aukhadeev, A., Zalyalov, R.. Podkhod k issledovaniyu nadezhnosti elektrotransportnoi sistemy goroda, kak slozhnoi tekhnicheskoi sistemy: *Mir transporta I tekhnologicheskikh mashin* **3**(58), 108–114 (2017)
4. Pavlov, P., Litvinenko, R., Mubarachin, M. A technique for selecting a rational variant of a multifunctional aircraft system: *Russ. Aeronaut.* **51**(2), 198–201 (2008)
5. Li, J., Yang, Y., Saaty, T. Cultural ranking of countries using the analytic hierarchy process methodology: *Adv. Intell. Syst. Comput.* **1074**, 949–963 (2020)
6. Saaty, T. The analytic hierarchy and analytic network processes for the measurement of intangible criteria and for decision-making: *Int. Ser. Oper. Res. Manag. Sci.* **233**, 363–419 (2016)
7. Saaty, T. Relative Measurement and its Generalization in Decision Making: Why Pairwise Comparisons are Central in Mathematics for the Measurement of Intangible Factors - The Analytic Hierarchy: *RACSAM* **102**(2), 251–318 (2008)
8. Bykova, T. Metod analiza ierarkhii, kak instrument resheniya prakticheskikh zadach mnogokriterial'noi optimizatsii: *Matematicheskoe modelirovanie, komp'yuternyi i naturnyi eksperiment v estestvennykh naukakh* **1**, 48–62 (2019)
9. Grivachev, A., Avdeev, V., Varganov, V. Modifitsirovannyi metod analiza ierarkhii dlya otsenki nazemnykh robototekhnicheskikh kompleksov: *Ekstremal'naya robototekhnika* **1**, 409–416 (2018)
10. Voronkov, I. Vektor global'nykh prioritetov metoda analiza ierarkhii kak otноситel'nyi pokazatel' urovnya nadezhnosti potentsial'nykh uchastnikov investitsionno-stroitel'nykh proektov: *Vestnik BGTU im. V.G. Shukhova* **11**, 137–145 (2018)
11. Saaty, T. Seven is the magic number in nature: *Proc. Am. Phil. Soc.* **160**(4), 335–360 (2016)
12. Saati, T. Ob izmerenii neosyazaemogo. Podkhod k otноситel'nym izmereniyam na osnove glavnogo sobstvennogo vektora matritsy parnykh sravnenii: *Cloud Sci.* **1**(2), 5–39 (2015)
13. Slavnov, K. Osobennosti modifikatsii metoda analiza ierarkhii T.Saati dlya otsenki sistem kontrolya konfidentsial'noi informatsii: *Okhrana, bezopasnost', svyaz'* **1–2**, 119–125 (2017)
14. Finogenko, I., D'yakovich, M. Metod analiza ierarkhii i postroenie integral'nykh pokazatelei slozhnykh system: *Vestnik Tambovskogo universiteta, Seriya: estestvennye i tekhnicheskie nauki* **1–6**(22), 1335–1340 (2017)
15. Dolinina, O. Metod generatsii testov dlya otladki baz znaniy ekspertnykh system: *Programm-naya inzheneriya* **5**, 40–47 (2011)
16. Pyatakovich, V., Vasilenko, A. Teoreticheskie polozheniya sinteza obuchayushchei vyborki neiro-ekspertnoi sistemy klassifikatsii morskikh tekhnicheskikh ob'ektov: *Tekhnicheskie nauki: problemi i resheniya*, 10–19 (2017)

The Reconstruction Experience of the 60-KCS Condenser for Deaeration Intensification



Artem Vodeniktov and Nataliya Chichirova

1 Introduction

The modern regenerative surface condensers usually guarantee a low concentration of dissolved oxygen in the steam turbine feed water. However, the old steam turbines with the unsatisfactory conditions of the vacuum system and the high level of the air leakages cannot provide the required quality of the condensate. This problem is typical for the cogeneration turbines that usually work with a low steam flow rate into the condenser during the heating period. Reducing the steam flow rate into the condenser leads to the deterioration of the condensate deaeration conditions and increasing the dissolved oxygen concentration [1].

The efficiency of the steam turbine and the fuel consumption do not depend on the value of the dissolved oxygen concentration, but the long-time work of the steam turbine feedwater system with high dissolved oxygen concentration increases the risk of the failures of the main and auxiliary equipment of the power plant unit. The condenser efficiency is considered in [2–6] via formulas and equations. In [7–10], the results of the experimental studies are presented. The threat of financial losses from unscheduled downtime leads the power plant personnel to look for ways to ensure the proper deaeration of the condensate inside the steam turbine condenser over the entire load range.

Nowadays, there are no innovative deaerating devices for steam surface condensers. Modern deaerating hot well constructions are based on the concepts proposed in the 60s of the last century. The ability of the condenser to remove the dissolved oxygen is determined at the design stage. In the first half of the twentieth century, non-regenerative condensers were used. They usually had the tube bundles with high hydraulic resistance on the steam side without regenerative

A. Vodeniktov (✉) · N. Chichirova
Department of Thermoelectric Plants, Kazan State Power Engineering University, Kazan, Russia

passages for good contact between the steam and the condensate. Using the regenerative condensers allowed to increase the contact area and time between the condensate draining from the pipes and the steam. This led to a decrease in the supercooling of the condensate and, as a result, to a decrease in the dissolved oxygen concentration. Also, the rational tube pattern allows for increasing the efficiency of the steam turbine condenser [11, 12]. Thus, according to [12], the replacement of the base tube pattern with the optimized tube pattern allowed to reduce the shell-side pressure drop.

Other studies are dedicated to the investigation of the operational condition of the steam surface condensers [13–15]. In the work [16], a CFD-based estimation method was employed to study the effect of the thermal resistance of fouling on the power output of a condensing turbine unit. This work contains the dynamics of pipe fouling and a recommendation for the tube-cleaning period.

The next step in improving the deaeration capacity was the use of the deaerating hot wells. In the designs of the condensers for the Soviet and foreign turbines, this solution has been used for more than 60 years. Depending on the flow path of the condensate and the heating fluid, deaeration devices of the condensers are classified by film type, nozzle type, jet type (when water moves in steam), and bubbling type (when steam moves in the water). Similar devices are used on K-500-60/1500 HTGZ (Fig. 1), K-300-240 LMZ, and T-175/210-130 UTZ, and many other turbines [1]. As the experience of operation has shown, these devices allow maintaining the required concentration of the dissolved oxygen in the main condensate at the most operating regimes of the steam turbine.

The regime analysis of the surface condenser was considered in the work [17]. The results show a negative correlation between dissolved oxygen concentration in the

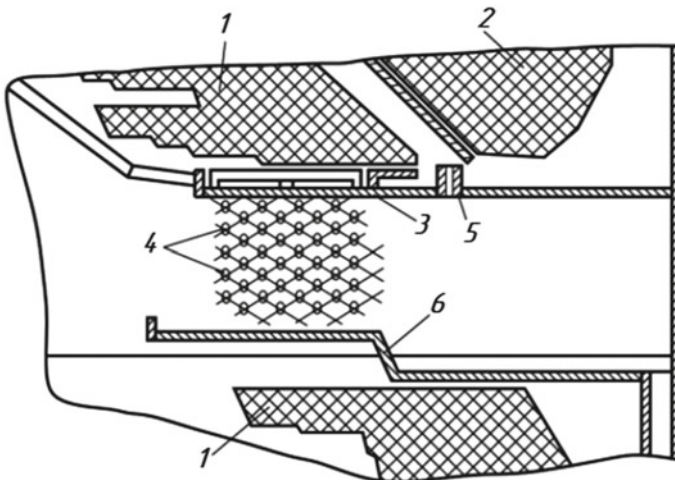


Fig. 1 Deaerating device of the K-22550 HTGZ surface condenser. 1—tube bundle, 2—air cooler, 3—water distributing sheet, 4—uncooled tubes, 5—non-condensable vent, 6—water collecting sheet

feedwater and the cooling water temperature. The surge of the concentration of the dissolved oxygen was found in the water temperature of about 11 °C. However, for the most numerous cogeneration turbines, PT-60-130/13 LMZ and T-100/110-130 UTZ, deaeration devices of condensers are not widely used. This fact encourages the power station personnel to develop unique deaerating devices and use such solutions as the external deaerating hot well.

2 Description of the Steam Turbine PT-60-130/13 LMZ

The modernization of the steam turbine with the deaerating hot well was carried out on the PT-60-130/13 turbine of the Naberezhnye Chelninskaya TPP equipped with a 60-KCS condenser. The layout of the low-pressure feedwater system of the turbine unit is typical—it includes six low-pressure surface-type heaters and the heat exchangers of the main ejectors (A and B) (Fig. 2).

The considered low-pressure feedwater system has the cascade drain of the steam condensate from heaters. Depending on the working regimes, it can be directed into the condenser or, via the pumps, can be returned into the feedwater system after the second surface heater.

The 60-KCS condenser has a transverse arrangement. It is made of a two-way, single block; the cooling surface area is 3000 m². The nominal steam flow rate into the condenser is 160 t/h [18]. As the exploitation of similar turbines shows, with an increase of the steam flow into the condenser, an improvement in the deaeration process is observed. However, the results of the deaerating tests for these turbines model are still not presented.

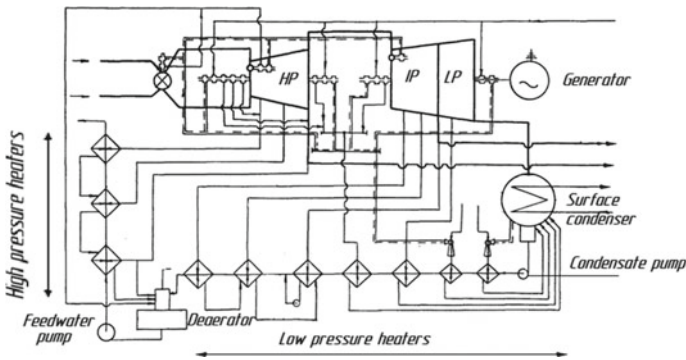


Fig. 2 Layout of steam turbine PT-60-130/13

2.1 Description of the Deaerating Hot Well

The described turbine is equipped with a deaerating hot well. This work was a part of the investment program in 2009. The external deaerating hot well was developed and installed by the Ecotech company. This hot well is designed to remove the dissolved oxygen from the steam turbine feedwater to protect the feedwater system from corrosion. The typical regime, when the high concentration of dissolved oxygen can be found, corresponds to the heating regime with a high steam flow rate to the district water heaters and the low steam flow rate into the condenser.

The design of the considered deaerating hot well is based on the two-stage condensate deaeration scheme, which includes first processing on a buried bubbling device, and then processing on a bubbling sheet in a thin layer. The long period of operation of the deaerating hot well has confirmed the high reliability of the two-stage deaeration scheme, which provides a low dissolved oxygen concentration in the condensate with its overcooling and variable turbine operating modes. The scheme of the hot well is shown in Fig. 3.

The specific steam flow rate for the deaeration in the external deaerating hot well is about 0.1 t/h. The vapor flow rate does not exceed 1 t/h, which does not impose significant restrictions on the power generation of the turbine unit.

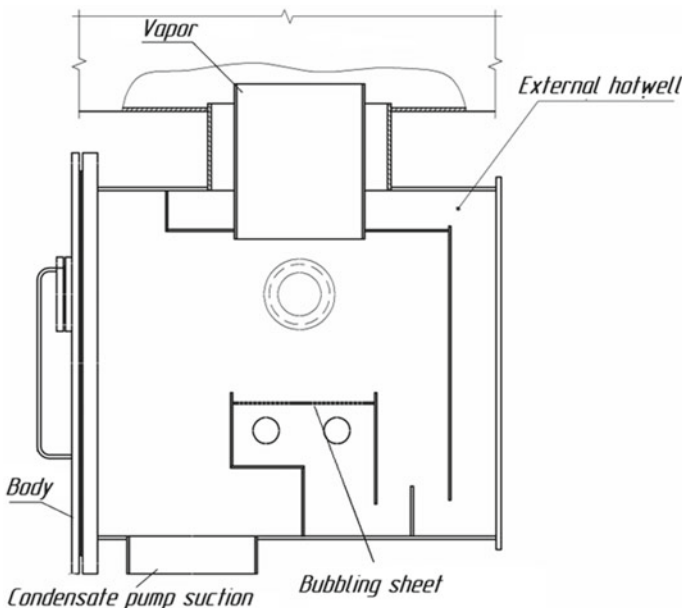


Fig. 3 Drawing of the external deaerating hot well

3 Thermal Test Description and Results

There is no special thermal test code for the external deaerating device. The usual working regime of the steam turbine was used for the estimation of the external deaerating hot well efficiency. Turbine electric load was 56 MWt, and the initial dissolved oxygen concentration was 27 mcg/l. The next steps were included:

- 11:00. The oxygen concentration was measured with the heating fluid valve fully closed;
- 11:30. The heating fluid flow rate was 5 t/h. Slow decreasing of the oxygen concentration has begun;
- 12:05. The heating fluid flow rate was 5.5 t/h. The dissolved oxygen concentration value of 15 mcg/l was reached;
- 12:30. At the end of the thermal test, the dissolved oxygen concentration value of 8 mcg/l was reached.

The graph of changes in the oxygen concentration and condensate temperature during the test period is shown in Fig. 4.

The above results indicate the device’s operability and its effectiveness as a vacuum deaerator. An increase in the condensate temperature was followed by a decrease in the concentration of the dissolved oxygen. The necessary dissolved oxygen concentration (20 mcg/l) was reached after about 50 min from the experiment started. The results of thermal tests of the external deaerating hot well show that its operation is most effective at low steam flow into the condenser. This recommendation is confirmed by the experience of the operation and deaeration tests of the

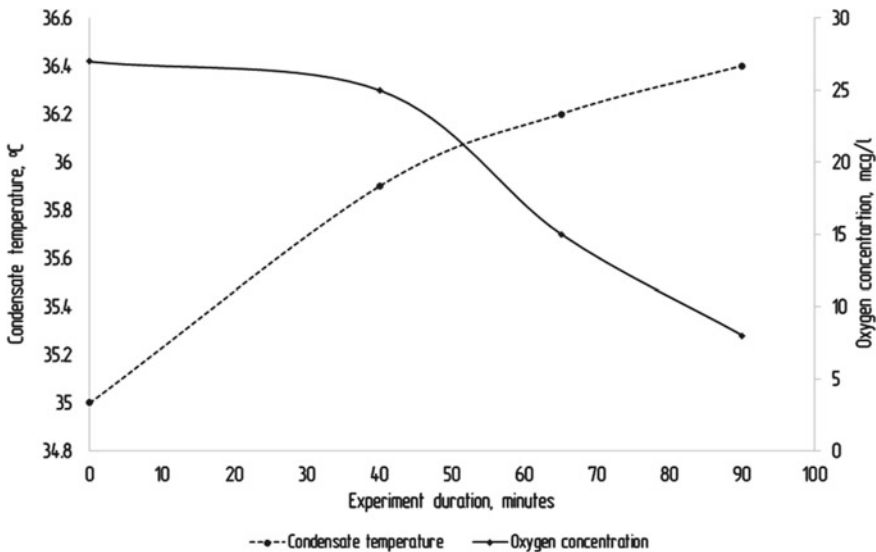


Fig. 4 The dynamics of oxygen concentration and condensate temperature changes

condensing turbines. Thus, according to [19], with an increase in the steam flow to the condenser, the amount of dissolved oxygen in the main condensate will decrease. For most condensers, the quality of the main condensate deteriorates with a steam load of 50% or less of the nominal value.

4 Conclusions

1. The design of the external deaerating hot well made by the “Ecotech” company allows achieving the concentration of the dissolved oxygen below the values established by the rules of technical operation.
2. This design, despite its simplicity and efficiency, has some disadvantages. The bulkiness of the device, which leads to an increase in the volume of the vacuum system, creates a potential danger of increasing the amount of air suction into the vacuum system.
3. It is recommended to turn on the hot well in the modes with a small flow rate of the steam into the condenser. This mode is typical for the operation of a heat-generating turbine according to a heat load schedule with a closed diaphragm, which, together with the high flow rate of the makeup water into the condenser, makes it difficult to obtain high-quality condensate in the steam turbine condenser.

References

1. Oliker, I.I., Permjakov, V.A.: *Termicheskaja deajeracija vody na teplovyh jelektrostantsijah. Jenergija, Leningrad (1971)* (in Russian)
2. Pattanayak, L., Padhi, B.N., Kodamasingh, B.: Thermal performance assessment of steam surface condenser. *Case Stud. Therm. Eng.* **14**, 100484 (2019)
3. Laskowski, R., Smyk, A., Rusowicz, A., Grzebielec, A.: A useful formulas to describe the performance of a steam condenser in off-design conditions. *Energy* (2020)
4. Strušnik, D., Mar, M., Golob, M., Hribernik, A., Živić, M., Avesec, J.: Energy efficiency analysis of steam ejector and electric vacuum pump for a turbine condenser air extraction system based on supervised machine learning modelling. *Appl. Energy* **173**, 386–405 (2016)
5. Medica-Viola, V., Pavković, B., Mrzljak, V.: Numerical model for on-condition monitoring of condenser in coal-fired power plants. *Int. J. Heat Mass Transf.* **117**, 912–923 (2018)
6. Mirzabeygi, P., Zhang, C.: Multi-objective optimization of a steam surface condenser using the territorial particle swarm technique. *ASME J. Energy Resour. Technol.* **138**(5), 052001 (2016)
7. Rusowicz, A., Laskowski, R., Grzebielec, A.: The numerical and experimental study of two passes power plant condenser. *Therm. Sci.* **21**, 353–362 (2017)
8. Ahmadi, G.R., Toghraie, D.: Energy and exergy analysis of Montazeri steam power plant in Iran. *Renew. Sustain. Energy Rev.* **56**, 454–463 (2016)
9. Prabu, S.S., Manichandra, M., Reddy, G.B.P., Vamshi, D.R., Bramham, P.V.: Experimental study on performance of steam condenser in 600MW Singareni thermal power plant. *Int. J. Mech. Eng. Technol.* **9**, 1095–1106 (2018)

10. Wei, W., Deliang, Z., Jizhen, L., Yuguang, N., Can, C.: Feasibility analysis of changing turbine load in power plants using continuous condenser pressure adjustment. *Energy* **64**, 533–540 (2014)
11. Laskowski, R., Smyk, A., Rusowicz, A., Grzebielec, A.: Determining the optimum inner diameter of condenser tubes based on thermodynamic objective functions and an economic analysis. *Entropy* **18**(12), 444 (2016)
12. Gap Park, Y., Youl Yoon, S., Min Seo, Y., Yeong Ha, M., Min Park, Y., Soo Koo, B.: A study on the optimal arrangement of tube bundle for the performance enhancement of a steam turbine surface condenser. *Appl. Therm. Eng.* **114681** (2019)
13. Anozie, A.N., Odejebi, O.J.: The search for optimum condenser cooling water flow rate in a thermal power plant. *Appl. Therm. Eng.* **31**, 4083–4090 (2011)
14. Akpan, P.U., Fuls, W.F.: Application and limits of a constant effectiveness model for predicting the pressure of steam condensers at off-design loads and cooling fluid temperatures. *Appl. Therm. Eng.* **158**, 113779 (2019)
15. Laskowski, R.: Relations for steam power plant condenser performance in off-design conditions in the function of inlet parameters and those relevant in reference conditions. *Appl. Therm. Eng.* **103**, 528–536 (2016)
16. Alabrudzinski, S., Markowski, M., Trafczynski, M., Urbaniec, K.: The influence of fouling build-up in condenser tubes on power generated by a condensing turbine. *Chem. Eng. Trans.* **52**, 1225–1230 (2016)
17. Vodeniktov, A.D., Chichirova, N.D.: Influence of the temperature of the cooling water on the deaeration capacity in the KCS-200-2 condenser. *Trans. Academenergo* **4**(61) (2020)
18. RD 34.30.705, Tipovaja jenergeticheskaja harakteristika turboagregata PT-60–90/13 (VPT-50–2) LMZ. Moscow, SPO Sojuztehjenergo, 35 (1978) (in Russian)
19. Shklover, G.G., Mil'man, O.O.: Issledovanie i raschet kondensacionnyh ustrojstv parovyh turbin. Jenergoatomizdat, Moscow (1985) (in Russian)

Construction of a Predictive Model of a Steam Generator Experimental Stand Based on the Organic Rankine Cycle



V. O. Miloserdov, M. O. Korlyakova, and D. A. Gorelov

1 Introduction

Nowadays, the generation of electrical energy is carried out by using steam turbines, the working fluid in which is water vapor. The advantage of this type of working fluid is its availability and cheapness. In order for water vapor to become an effective working fluid (WF), it should have a high temperature, which is combined only with high pressure. It creates its own chain of problems—it is necessary to have high-temperature steam generators, high-performance capacitors, high-performance pumps, and so on [1]. An alternative to the steam-water Rankine cycle for heat recovery stands are installations based on the organic Rankine cycle, using low-boiling organic working bodies (OWB).

However, the behavior of the stands, using OWBs, differs significantly from the classical steam-water cycle [2]. Moreover, the supplied heat flow is very changeable, as it is determined by the operating mode of the main equipment. All these facts require the development of a control system that could adapt to significant disturbances and operate under conditions of uncertainty about the parameters of the control object, which implies the inclusion of intelligent controllers in the system. A necessary step is to build predictive models of control objects.

Modern modeling methods allow us to build digital equivalents of complex technical systems based on the use of example-based learning technologies [3, 4]. It is a class of models that allow to form a description of an object's behavior and predict how it will react to certain types of impacts. Moreover, when building a model of adequate complexity, one can get a high-quality prediction not only in the area where

V. O. Miloserdov (✉) · D. A. Gorelov
Scientific Production Company Turbocon, Komsomolskaia rosha st. 43, Kaluga 248010, Russia

M. O. Korlyakova
Bauman Moscow State Technical University (Kaluga Branch), Bazhenova st. 2, Kaluga 248000, Russia

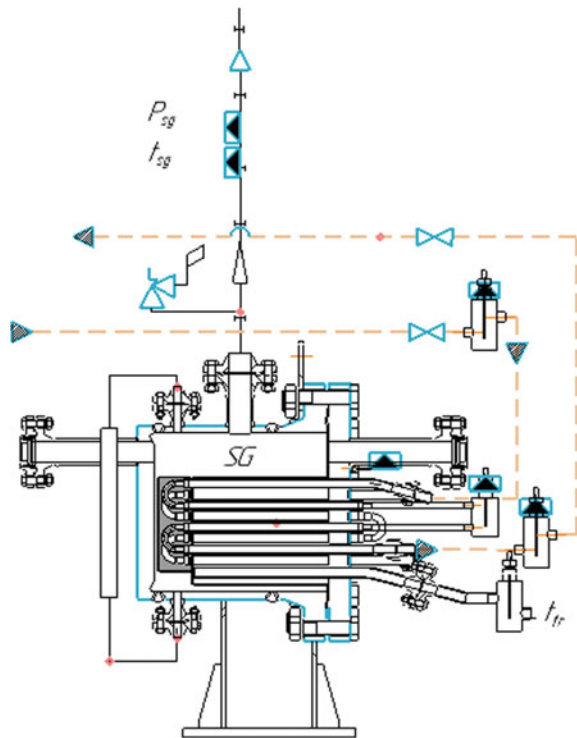
the training took place but also outside of it [5, 6]. Among all the models trained, neural network systems can be distinguished as a type of algorithms with the widest range of capabilities [3]. Let us consider the formation of a neural network model of a steam generator with a compact superheater.

2 Materials and Methods

The schematic diagram of the experimental stand is shown in Fig. 1. The working fluid in the stand is freon R-113 and high-pressure water is used as the heating medium.

The work of the stand is organized according to the principle of the organic Rankine cycle [7]. Freon enters the steam generator in the liquid phase and is heated and evaporated by the heat released from the high-pressure water. At the exit of the steam generator, the freon enters the condenser and enters the steam generator again. In the condenser, the phase state of the freon changes due to the supply of cooling water. At the inlet of the steam generator, an auxiliary electric heater is installed, designed for additional heating of freon at the inlet [8–10].

Fig. 1 Schematic diagram of the steam generator



3 Results and Discussions

Modeling aims to predict the target parameter—the temperature t_{sg} and the pressure p_{sg} at the outlet of the steam generator after a period of time t_h with known current information about the object parameters measured during the time t_c . During the time interval t_c , several sets of information are measured directly on the stand [11].

The original sampling rate was 0.33 Hz. However, the data analysis showed that the sampling frequency of the measurements has a fairly significant spread (0.24 s) within one measured parameter, and between the parameters the average discrepancy is 0.6 s, and the maximum reaches 6.8 s. That is why in the process of data preprocessing, resampling with a frequency of 1 Hz with interpolation was performed by polynomials $P(n)$ at $n = 2$.

The prediction problem can be solved as a regression problem, when a certain set of input data $X_{inp}(t_0 - t_c : t_0)$, obtained during the period from $t_0 - t_c$ to t_0 , is associated with a certain value of the target features $y(t_0 + t_h)$, which were obtained at the time $t_0 + t_h$.

The second version of the problem statement is the time series prediction, when the input information of the model contains $X = \langle y(t_0 - t_c : t_0), X_{inp}(t_0 - t_c : t_0) \rangle$ where $y(t_0 - t_c : t_0)$ is an endogenous feature of the series, $X_{inp}(t_0 - t_c : t_0)$ is exogenous factors, and the output information $y(t_0 + t_h)$ is considered as a regression not only of the internal parameters of the system but also of the states of the output parameter measured in time [12].

In our case, the prediction model was tested in a regression form. Thus, each training example is constructed as a vectored representation of the data from $X_{inp}(t_0 - t_c : t_0)$ and the vector $y(t_0 + t_h)$, the output parameters at the time $t_0 + t_h$. The total number of measured input parameters is 12, and the amount t_c determines how much data will be involved in solving the regression problem. In the modeling process, you need to fix t_h and t_c , defining them by the rule $t_c = 2t_h$, as it is assumed that when solving the prediction problem, the amount of information about the history should not be less than the length of the forecast horizon. To train the models, 5 cycles of experiments were provided under different operating conditions

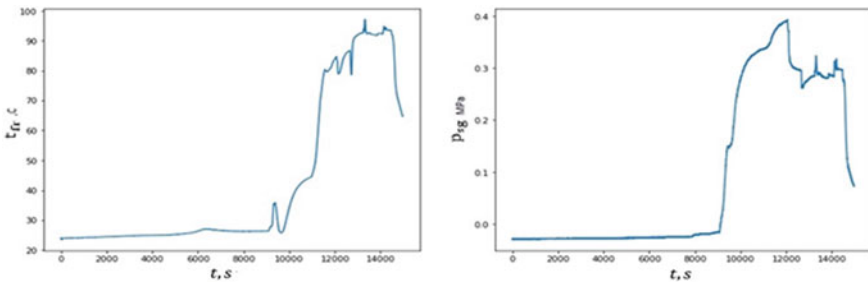


Fig. 2 Changing the output parameters of the steam generator in one of the operating modes

Table 1 Values of the parameter t_{fr}

Mode	Max (°C)	Min (°C)	Mean (°C)	Std (°C)
Mode 1: training	52.56	24.19	27.94	5.80
Mode 2: training	72.19	64.72	67.70	2.10
Mode 3: training	22.71	18.98	21.29	0.96
Mode 4: test	97.57	89.89	95.03	1.47
Mode 5: test	78.53	21.31	53.98	25.92

of the stand. An example of one of the modes is shown in Fig. 2 for the parameter t_{fr} and the output parameter p_{sg} .

All modes differ significantly from each other and form a spectrum of examples for the test and training according to the following rule: the first three experiments are used for training, and the last two are used for tests. This corresponds to the methods of generating data for time models, where the examples for training the test are separated in time. In our case, it is necessary to separate the data, because the purpose of the modeling predicts the response of the object in the ranges of parameters unknown at the time of training. An example of the values of the parameter t_{fr} for all experiments is shown in Table 1.

It is obvious that the parameter ranges in Modes 4 and 5 (test) are significantly different from those on which we train.

When building neural network models for processes that take place over time, several different approaches can be used [13]. We will focus on the main models, which include regression models based on fully connected networks (FC), convolutional regression models (CNN), and models based on recurrent blocks (RNN).

Preliminary modeling for FC, RNN, and CNN networks has shown that they provide the quality of target parameter estimation at the level of the following indicators.

The RNN model is considered the most promising one and the neural network parameters are evaluated in terms of the number of nodes of the LSTM layer and neurons of the fully connected layer [14]. The modeling results are shown in Fig. 3, where it can be seen that the number of LSTM nodes has the strongest influence on the error level. Thus, the final configuration of the model was selected (see Table 2), and the model errors were 11 and 4% in signal strength for p_{sg} and t_{sg} , respectively.

The operation of the final model for mode 4 is shown in Fig. 4. Thus, the use of neural network models allows us to predict the behavior of a steam generator with a compact superheater not only in the area where the examples were presented but also in modes that go beyond the boundaries of training.

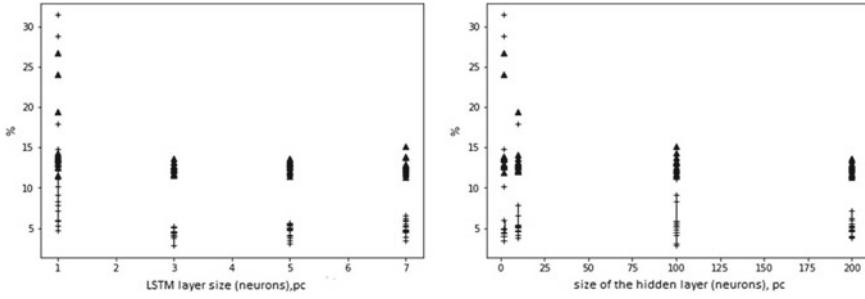


Fig. 3 Training results of RNN networks for predicting p_{sg} and t_{sg} on the interval $t_h = 5s$

Table 2 Training results

Network architecture	R ^{2a} p_{sg} (MPa)	R ^{2a} t_{sg} (°C)	MAPE ^b p_{sg} (%)	MAPE ^b t_{sg} (%)
FC: (100(linear), 10(logistic), 2(linear) neurons)	0.87	0.87	12.92	7.13
CNN: (Conv1D(10, 3), Conv1D(10, 3), MaxPool, Conv1D(10, 3), Conv1D(10, 3), MaxPool, 10(logistic neurons), 2(linear neurons))	0.92	0.91	11.53	9.00
RNN: (LSTM (10), 10(logistic neurons), 2(linear neurons))	0.88	0.88	12.2	7.10
Final model: RNN: (LSTM (5), 100(logistic neurons), 2(linear neurons))	0.88	0.99	11.48	4.17

^aRegression determination coefficient

^bAverage percentage absolute error

4 Conclusion

As a result of the tests, measurements of the main thermodynamic parameters of the steam generator operation were obtained, which were used to create a neural network model in the class of recurrent systems [15].

Training the model on a limited set of examples allowed us to predict with an error of 10–11% in areas that were not included in the training, which allows us to count on the use of neural network models as digital counterparts of the steam generator.

As part of the next stage of predictive model modeling, it is planned to consider the solution of the problem in the form of time series analysis.

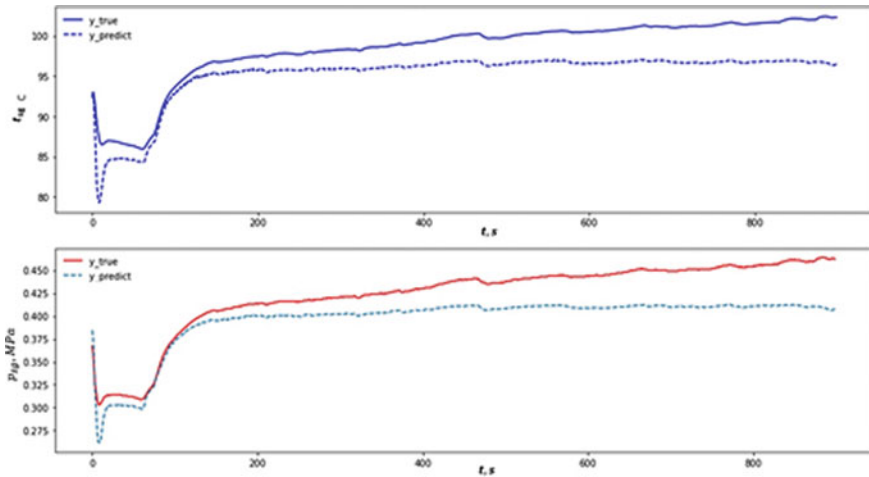


Fig. 4 Operation of the predictive model in mode 4

References

1. Mago, P.J., Chamra, L.M., Srinivasan, K., Somayaji, C.: An examination of regenerative organic Rankine cycles using dry fluids. *Appl. Therm. Eng.* **28**, 998–1007 (2008)
2. Saleh, B., Koglbauer, G., Wendland, M., Fischer, J.: Working fluids for low-temperature organic Rankine cycles. *Energy* **32**, 1210–1221 (2007)
3. Rasheed, A., San, O., Kvamsdal, T.: Digital Twin: Values, Challenges and Enablers. <https://arxiv.org/pdf/1910.01719.pdf>
4. Ritto, T.G., Rochinha, F.A.: Digital twin, physics-based model, and machine learning applied to damage detection in structures. <https://arxiv.org/pdf/2005.14360.pdf>
5. Kiryukhin, A.V., Loshkareva, E.A., Kondratev, A.V., Korljakova, M.O., Miloserdov, V.O.: Comparative analysis of the possibility to reduce vibration transmission through a pipeline compensator by suppressing dynamic forces and pressure pulsations by active methods. *J. Phys. Conf. Ser.* **1565**(1), 012089 (2020). <https://doi.org/10.1088/1742-6596/1565/1/012089>
6. Kiryukhin, A.V., Milman, O.O., Sereshkin, L.N., Korljakova, M.O., Miloserdov, V.O.: Physical features of fluid and structure interaction inside power unit pipeline vibration-isolating expansion joints. *J. Phys. Conf. Ser.* **1565**(1), 012088 (2020). <https://doi.org/10.1088/1742-6596/1565/1/012088>
7. Milman, O.O., Ananyev, P.A., Korljakova, M.O., Miloserdov, V.O.: Experimental studies of non-stationary thermo-hydraulic processes at freon R113 boiling. *J. Phys. Conf. Ser.* **1382**(1), (2019). <https://doi.org/10.1088/1742-6596/1382/1/012114>
8. Milman, O.O., Kondratev, A.V., Ptakhin, A.V., Korlyakova, M.O.: Experimental studies on the distribution of air flows in air cooled steam condensers. *Therm. Eng.* **66**(12), 936–943 (2019). <https://doi.org/10.1134/S0040363619120051>
9. Milman, O.O., Krylov, V.S., Ptakhin, A.V., Kondratev, A.V., Yankov, G.G.: High-efficiency condenser of steam from a steam-gas mixture. *Therm. Eng.* **64**(12), 874–883 (2017). <https://doi.org/10.1134/S0040601517120072>
10. Milman, O.O., Kartuesova, A.Y., Yankov, G.G., Ptakhin, A.V., Krylov, V.S., Korlyakova, M.O.: Investigation of parallel operation of vacuum condenser sections with nonuniform cooling. *Therm. Eng.* **66**(2), 77–83 (2019). <https://doi.org/10.1134/S0040601519020022>
11. Lei, Y., Hu, J., Ding, J.: A hybrid model based on deep LSTM for predicting high-dimensional chaotic systems. <https://arxiv.org/abs/2002.00799v1>. Last accessed 20 Feb 2020

12. Brynza, A.A., Korlyakova, M.O.: Approach to forecasting behaviour of dynamic system beyond borders of education. In: Neuroinformatics, Studies in Computational Intelligence, vol. 856. Springer, Cham (2019). https://doi.org/10.1007/978-3-030-30425-6_43
13. Husam Fayiz, A.M.: Adaptive neural network algorithm for power control in nuclear power plants. J. Phys. Conf. Ser. **781**(1)
14. Brynza, A.A., Korlyakova, M.O.: Estimation of the complexity of the classification task based on the analysis of variational autoencoders. In: Neuroinformatics, Studies in Computational Intelligence, vol. 925. Springer, Cham (2020). https://doi.org/10.1007/978-3-030-60577-3_51
15. Feurer, M., Klein, A., Eggenberger, K., Springenberg, J., Blum, M., Hutter, F.: Efficient and Robust Automated Machine Learning (2015). <https://papers.nips.cc/paper/5872-efficient-and-robust-automated-machine-learning.pdf>

The Method of Calculating the Dew-Point Temperature of Stack Gases in the Compound Firing of Gases and Fuel Oil in the Boiler Furnace



Simeon Livshits, Natalia Yudina, Ruslan Lebedev, Tatiana Mantserova, and Alsu Galiakhmetova

1 Introduction

The issue of ensuring reliable and economical operation of thermal power plants is one of the issues of relevance for Russian energy. This issue is of particular importance in the modern state of Russian thermal power engineering due to the exhaustion of the design resource of the main standard equipment, the expansion of the use of non-design or non-ignited fuels, the need for the development of energy, and environmental saving technologies for fuel use.

In many power plants, especially during peak loads, contrary to technological regulations, it is necessary to simultaneously burn several types of fuels (coal with fuel oil, coal with gas, gas with fuel oil). This practice is justified not only by the presence of a fuel imbalance at the enterprise but also by an attempt to solve the problem of stabilizing the burner flare. Nowadays, there are no methods for a comprehensive assessment of the impact of such parameters on the efficiency of boilers: dew-point temperature of exhaust gases, a specific concentration of NO_x and SO_x when organizing the combined combustion of gas and fuel oil in steam boiler furnaces.

S. Livshits (✉) · N. Yudina
Kazan State Power Engineering University, Krasnoselskaya st., 51, 420066 Kazan, Russia

R. Lebedev
Gazprom VNIIGAZ LLC, Moscow, Russia

T. Mantserova
Belarusian National Technical University, Independence Avenue 65, Minsk, Belarus

A. Galiakhmetova
Kazan Innovative University Named After V.G. Timiryasov (IEML), Moskovskaya st., 42, 420111 Kazan, Russia

2 Literature Review

Unfortunately, the question of finding the dew-point temperature of the exhaust gases when burning together various types of fuels is not sufficiently covered in the literature. Although this temperature has a decisive effect on the efficiency of the steam boiler, a decrease in the temperature of the exhaust gases by 12–16 °C leads to an increase in the efficiency of the boiler by about 1%.

Sulfuric acid generated by the combustion of high sulfur fuels (fuel oil, and some coals) is one of the significant reasons for the decrease in the reliability and economy of boilers. Therefore, it is important to accurately determine the dew-point temperature of the exhaust gases. Numerous theoretical studies carried out by various scientific groups [1–7] cover in sufficient detail the issue of the production of sulfurous anhydride when burning separate fuels, and empirical dependencies are given for them. Also, for particular cases, graphical dependencies of SO₃ generation were obtained when burning various types of fuels, depending on excess air, load, flare temperature, boiler grade, etc. In addition, work was carried out to determine the temperature of the sulfate dew point of the exhaust gases, but when burning only certain fuels, such as coal, gas, and fuel oil.

The practical implementation of mixed combustion of gas and fuel oil has set another important task for researchers to estimate the value of specific emissions (or concentrations) of NO_x in the joint combustion of fuels (gas and fuel oil). The started developments in this area in the 70s–80s of the last century led to the creation of methodological guidelines [8], however, by the time they were approved, it was not possible to collect sufficient information on NO_x emissions for the joint combustion of fuels. It was decided to use the principle of additivity but, with respect to the task of mixed combustion, it showed large discrepancies with experimental data up to 25–30%. Subsequently developed by the group of authors method of calculation of emissions of nitrogen oxides [9], taking into account the duration of combustion products stay in the zone of active combustion, made it possible to correlate experimental and calculated data.

Work [10] shows a reduction of NO_x concentration level by 30–50% during gas combustion together with fuel oil (relative to the level of the highest concentration of nitrogen oxides realized during combustion of fuel oil alone), which is confirmed in practice.

3 Materials and Methods

With mixed combustion of gas and fuel oil, an additional effect is achieved by a more complete filling of the volume of the combustion chamber with a luminous flare, which causes a noticeable change in the flare temperature in the active combustion zone. The gas burns at the start of the flare at a higher rate than fuel oil. This causes

the active combustion zone to “stretch” and further reduces the maximum temperature in the flare core. The reduction of NO_x in the combined combustion of gas and fuel oil requires additional analysis. It is possible to study in-depth the theory of the processes of power units passing in combustion chambers when organizing joint combustion of gas and fuel oil, possibly during numerical experiments using modern computational complexes and applied programs that allow modeling various conditions, while creating a complete and objective picture of the process.

The complex solution of problems: reducing the concentration of NO_x and finding the dew-point temperature of the stack gases, and as a consequence of this, the optimal alignment of the combustion mode and finding the corridor of the optimal permissible temperatures at which the stack gases will have the lowest possible temperature (at which the formation of sulfuric acid can’t yet begin and the associated low-temperature corrosion of the tail heating surfaces), and a minimum concentration of nitrogen oxide, will increase both the efficiency and improve the environmental picture of the process as a whole.

To solve this problem, the work proposes a method for calculating the dew-point temperature of exhaust gases during mixed combustion in various proportions of gas and fuel oil in boiler furnaces. Calculations were carried out on the example of the Ulyanovsk CHP-2. Tests were carried out on boilers of type TPE-429; during the tests, gas analyzers of type TESTO-33 were used.

Below is a summary table of the measurements (Fig. 1).

The developed technique is as follows:

The true steam consumption of the steam generator is determined by the formula [1]:

$$D_t^b = D_n \sqrt{\frac{V_n}{V_p}}, \tag{1}$$

D_n —steam consumption as indicated by the steam meter, t/h; V_a —actual specific volume of superheated steam; V_c —specific volume of the steam parameters at calibration (calibration temperature t_n^{calib} and calibration pressure P_n^{calib} according to the instrument passport).

Next, the heat load of the boiler unit is determined:

$$Q_b^{br} = [D_a^b(i_n - i_{fw}) + G_{bw}(i_{bw} - i_{fw})] \times 10^{-3} \text{ MW}, \tag{2}$$

heat content of superheated steam, kJ/kg (determined from the table depending on the parameters of superheated steam, i.e. superheated steam pressure P_n and superheated steam temperature t_s); i_{fw} —heat content of feedwater, kJ/kg, (we find from tables for parameters of feedwater, $P_{fw}t_{fw}$ —pressure and temperature of feedwater obtained as a result of measurements); i_{bw} , kJ/kg—the heat content of the blowdown water, is also determined depending on the parameters of the blowdown water: pressure and temperature determined, respectively, as a result of measurements by instruments;

№	Name	Unit	Experience number				
			1	2	3	4	5
1	Station boiler type	-	TPE-429 2A	TPE-429 1B	TPE-429 1A	TPE-429 1A	TPE-429 1A
2	Superheated steam pressure	atm	132	131	132	140	140
3	Superheated steam temperature	°C	555	555	555	555	555
4	Superheated steam consumption	t/hr	395	375	275	320	382
5	Feedwater flow	t/hr	400	375	275	320	380
6	Air temperature in front of the blower fan	°C	18	23	32	32	28
7	Air temperature before RAH	°C	90-96	55	40	36	43
8	The stack gases before RAH	°C	168-185	159	126	132	165
9	The stack gases before the exhauster	°C	170	180	140	150	195
10	Excess air in the operating section	-	1,063	1,037	1,065	1,037	1,057
11	Gas flow to the boiler	m ³ /hr		18000	19000	19000	10500
12	Flue oil to the boiler	kg/hr	30200	11000	3500	7500	19500
13	The number of burners operating on fuel oil	-	8	3	1	2	5
14	The number of burners operating on gas	-	0	5	7	6	3
15	Oxygen in the flue gas	%	1,3	0,8	1,55	0,8	1,2
16	The dew-point temperature of the stack gases	°C	157,5	113,0	102,4	105,8	136

Fig. 1 The summary table of experimental data

G_{bw} —blowdown water consumption, t/h (determined empirically), D_t^b —true steam consumption.

The adjusted fuel consumption is calculated [2] as

$$B_f = \frac{\left(\frac{Q_b^{br}}{\eta_b} - B_g Q_{ng}^c \right)}{Q_{nf}^c} \text{ kg/h,} \quad (3)$$

where η_b —boiler efficiency determined by mode cards; Q_{ng}^c —specific heat of combustion of the natural gas, kJ/m^3 , according to the Ulyanovsk TPP-2 laboratory; Q_{ng}^c —specific heat of combustion of the fuel oil, kJ/kg , laboratory analysis data.

The proportion of the gas in the mixture with the fuel oil in terms of heat release is determined according to the ratio:

$$d_g = \frac{B_g Q_{ng}^c}{B_g Q_{ng}^c + B_f Q_{ng}^c} = \frac{B_g Q_{ng}^c}{Q_b^{br}} \eta_b, \quad (4)$$

where d_g —the proportion of the gas by the heat release; B_g —the natural gas consumption.

The specific volumes of air, the flue gases, and water vapor in the flue gases are found from

$$V_g = V_{gg}^0 \left(\frac{B_g V_{gg}^g}{B_g V_{gg}^g + B_f V_{gf}^0} \right) + V_{gf}^0 \left(1 - \frac{B_g V_{gg}^g}{B_g V_{gg}^g + B_f V_{gf}^0} \right) + 1.016(\alpha - 1) \left[V_{wg}^0 \frac{B_g V_{wg}^0}{B_g V_{wg}^0 + B_f V_{wf}^0} + V_{wf}^0 \left(1 - \frac{B_g V_{wg}^0}{B_g V_{wg}^0 + B_f V_{wf}^0} \right) \right], \text{ m}^3/\text{kg} \quad (5)$$

where V_{gg}^g —the specific volume of the flue gases during combustion of 1 m^3 of the natural gas; V_{gf}^0 —the specific volume of the flue gases during combustion of 1 kg of the fuel oil; V_{wg}^0 —the specific volume of air required for combustion of 1 m^3 of the natural gas m^3/m^3 ; V_{wf}^0 —the specific volume of air required for combustion of 1 kg of the fuel oil, m^3/kg .

Excess air α in the operating section behind the regenerative air heater (RAH) is determined [3, 4] as

$$\alpha = \alpha_p + \Delta\alpha \sqrt{\frac{D_{sn}}{D_{st}}}, \quad (6)$$

where α_p —leaked-in air along the exhaust duct; $\Delta\alpha \sqrt{\frac{D_{sn}}{D_{st}}}$ —leaked-in air in RAH.

According to operational regulation (OR) and normative calculation for RAH $\Delta\alpha = 0.25$, and for tubular-air heater (TAH) value $\Delta\alpha = 0.1$; in turn, the leaked-in air along the exhaust duct can be calculated from the ratio:

$$\alpha_p = \frac{20.96 - O_2 \frac{B_g K_g + B_f K_f}{B_g + B_f}}{20.96 - O_2}, \quad (7)$$

where K_g, K_f —coefficients, respectively, for gas $K_g = 0.05$, for the fuel oil $K_f = 0.1$; O_2 —excess oxygen concentration in the operating section.

The weighted average volume of the water vapor by fuel mass during combustion of mixed fuel is determined from the ratio:

$$V_{H_2O} = V_{H_2O_g}^0 \left(\frac{B_g V_{H_2O_g}^0}{B_g V_{H_2O_g}^0 + B_f V_{H_2O_f}^0} \right) + V_{H_2O_f}^0 \left(1 - \frac{B_g V_{H_2O_g}^0}{B_g V_{H_2O_g}^0 + B_f V_{H_2O_f}^0} \right) + 0.0161(\alpha - 1) \left[V_{wg}^0 \frac{B_g V_{wg}^0}{B_g V_{wg}^0 + B_f V_{wf}^0} + V_{wf}^0 \left(1 - \frac{B_g V_{wg}^0}{B_g V_{wg}^0 + B_f V_{wf}^0} \right) \right] \quad (8)$$

where $V_{H_2O_g}^0$ —the specific volume of the water vapor in the flue gases, m^3/m^3 ; $V_{H_2O_f}^0$ —the specific volume of the water vapor in the flue gases when burning the fuel oil, m^3/kg .

The determination of the condensation temperature of the water vapor of the flue gases is carried out according to the formula obtained from an approximate dependence of the form:

$\ln P = \frac{A+Bt}{C+t}$, where the value of the coefficients A, B, C was obtained as a result of approximation in the temperature range which determines the smallest error for our case ($0 < t < 100$ °C)

$$t_b = \frac{244.838 * \ln P_s + 1252.593}{12.677 - \ln P_s}, \quad (9)$$

$P_s = P_g r_{H_2O_g} = \frac{V_{H_2O}}{V_g} P_g$ —the saturation pressure of water vapor of flue gases (for boilers with balanced draft); P_g —absolute flue gas pressure taking into account the flue gas rarefaction behind the air heater.

The formula for determining the temperature of sulfuric acid dew point in the flue gases has the form [3, 4]:

$$t_p^s = t_b + 250\sqrt{S^r O_2}, \quad (10)$$

where $S^r = \frac{\bar{S}^c}{\bar{Q}_n^c}$ —reduced sulfur content of fuel, \bar{Q}_n^c —weighted average by the calorific value of the fuel calorific value, which is directly proportional to the coefficient K_g^Q , $\bar{S}^c = S^c \frac{B_f}{B_g + B_f}$ —weighted average content of sulfur by fuel mass, and S^c —sulfur content in the fuel oil.

$$\bar{Q}_n^c = \bar{Q}_{ng}^c K_g^Q + \bar{Q}_{nf}^c (1 - K_g^Q), \quad (11)$$

where

$$K_g^Q = \frac{\overline{Q}_{ng}^c B_g}{\overline{Q}_{ng}^c B_g + \overline{Q}_{ng}^c B_f}. \tag{12}$$

4 Results

Comparative analysis of the results obtained when carrying out numerical studies of the dew-point temperature (Fig. 2) and the data obtained from the readings of the devices (Fig. 1) gives the right to speak about the suitability of the proposed method for calculation. The discrepancy between the calculated values and the experimental data is insignificant, despite the fact that the calculations were carried out at different loads and with different quantitative ratios of fuels in the total mixture.

The results of calculations using this technique are listed in Fig. 2.

For the first time, a general view of the curve was obtained that characterizes the change in the dew-point temperature, from the gas fraction by heat release (Fig. 3).

Value	Experience number				
	1	2	3	4	5
Sulfur content in fuel oil, $S^c, \%$ (laboratory data)	2.5	2.5	2.31	2.31	2.4
Weighted average content of sulfur by fuel mass, $\bar{s}^c, \%$	2.5	0.746	0.2112	0,4815	1.3
Coefficient, K_g^Q	1	0.579	0.8535	0.6892	0.331
Weighted average by the calorific value of the fuel calorific value, $\overline{Q}_n^c, \text{kJ/kg}$	38887.39	44806.94	47608.91	46024.01	42290.93
Reduced sulfur content of fuel, S^r	6.433×10^{-2}	1.666×10^{-2}	4.4393×10^{-3}	1.047×10^{-2}	3.076×10^{-2}
Excess oxygen concentration in the O_2 operating section (as indicated by the device)	1.3	0.8	1.55	0.8	1.2
Sulfuric acid dew-point temperature in flue gases, t_c^s	154.1	113.2	101.9	105.12	135.32

Fig. 2 The summary table of the results of calculations

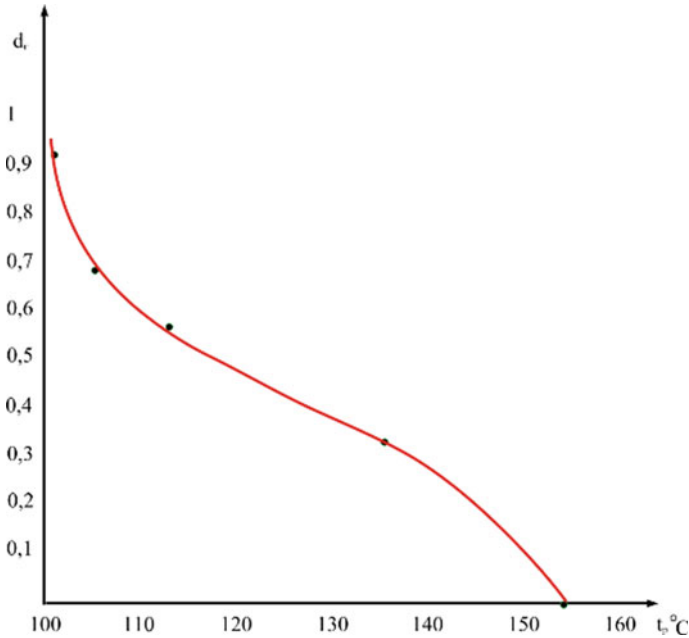


Fig. 3 General view of the curve describing the change in the dew-point temperature from the gas fraction by heat release

5 Conclusions

Analysis of the proposed method will help to study in more detail the effect of co-combustion of gaseous and liquid fuels on harmful emissions, and develop recommendations to ensure the combustion process with co-combustion.

References

1. Instructions and guidelines for carrying out express operational tests of boiler units. CCNIT (1974)
2. Lipov, Y., Samoilov, O.: Layout and thermal calculation of a steam boiler. Energoatomizdat (1988)
3. Yureniev, V., Lebedev, P.: Thermal engineering reference. Energy M **2**(2) (1976)
4. Khzmalen, D.: Theory of furnace processes. Energoatomizdat (1990)
5. Methodological guidelines for drawing up a report for electric power plants RD 34.08.5552-95. Service of best practices OGRES, Moscow (1995)
6. Ashurov, S.: Determination of the excess air ratio when burning natural gas together with other types of fuel. Ind. Heat Power Eng. **5** (1987)
7. Reznikov, N., Lipov, Y.: Boiler Plants of Power Plants **3** (1990)
8. Guidelines for calculating emissions of nitrogen oxides with flue gases from boilers, RD 34.02.304-88. ATEI (1989)

9. Kotler, V.R.: Emissions of nitrogen oxides during co-combustion of coal with gas or fuel oil. *Heat Power Eng.* **5** (1996)
10. Fatkullin, R., Pakhomov, A., Arslanov, R., Valiev, A.: Reducing nitrogen oxide emissions at PK-41 boilers by rational organization of co-firing of gas and fuel oil. *Heat Power Eng.* **12** (1998)
11. Yörük, C.R., Meriste, T., Sener, S., Kuusik, R., Trikkel, A.: Thermogravimetric analysis and process simulation of oxy-fuel combustion of blended fuels including oil shale, semicoke, and biomass. *Int. J. Energy Res.* **42** (2018)
12. Sun, B., Guo, P., Zhang, W.: Research on prediction of dew point pressure of condensate gas reservoir based on gwo-lssvm and ace models. *Fresenius Environ. Bull.* **29**(12) (2021)
13. Xu, M.-X., Wu, H.-B., Wu, Y.-C., Ouyang, H.-D., Lu, Q.: Design and evaluation of a novel system for the flue gas compression and purification from the oxy-fuel combustion process. *Appl. Energy* **285** (2021)
14. Burgass, R., Chapoy, A., Filho, V.D.O.C.: Development of a new method for measurement of the water dew/frost point of gas. *Fluid Phase Equilib.* **530** (2021)
15. Seebold, J.G., Chevron: Quantifying the products of incomplete combustion from petroleum, petrochemical & chemical sector gas-fired process heaters & industrial boilers. *Ind. Combust.* **15** (2015)
16. Novikova, O.V., Erastov, A.E., Livshits, S.A.: Features of evaluating the efficiency indicators of the electric power enterprise. *E3S Web Conf.* **124** (2019)

Usage of Woodworking Processing Industry Waste as a Fuel



Anastasia Pavlova, Semen Livshits, Natalia Yudina, Tatyana Dunaeva, and Aigel Sabirzyanova

1 Introduction

One of the production development perspective directions is the processing of manufacture and municipal solid waste and second usage of resources. Nowadays, effective waste application is necessary for decreasing their harmful impact on the environment [1, 2].

Among the waste management area problems in Russia, there is an imperfection of the current waste management system in the legal, informational, and organizational spheres, poor cooperative relations development by the type of «industrial symbiosis» between the industrial enterprises (when one manufacture's wastes become raw material for another one), and poor highly efficient waste utilization industries development. Also, the ecological condition of the country is damaged a lot as a consequence of continuing legislation violations in the waste handling field: often, only landfill, not proper, disposal and decontamination occurs [3].

These problems require immediate government agencies', organizations', and enterprises' interference.

The purpose of this scientific work is to substantiate a waste applying economical expediency on enterprises.

The sub-targets of the work are to justify a woodworking industry waste processing and applying as a fuel efficiency, and to justify a waste processing efficiency in an enterprise's own division.

A. Pavlova · S. Livshits (✉) · N. Yudina · T. Dunaeva · A. Sabirzyanova
Kazan State Power Engineering University, Institute of Digital Technologies and Economics,
Kazan, Russia

© The Author(s), under exclusive license to Springer Nature Singapore Pte Ltd. 2022
A. Irina and P. Zunino (eds.), *Proceedings of the International Symposium on Sustainable Energy and Power Engineering 2021*, Lecture Notes in Mechanical Engineering,
https://doi.org/10.1007/978-981-16-9376-2_12

2 Methods

Decrease and rational industrial waste usage are the waste management priority directions, which are encouraged by the state. According to the Federal Law of June 24, 1998, N 89-FZ «On industrial and consumer waste», there is a scientific substantiated combination of a society's ecological and economic interests, comprehensive raw materials resources processing for the purposes of waste amount decrease, and usage of activity regulation economic methods in the waste management area for the purposes of waste amount decrease and their involvement in economic turnover among the main principles of the state policy in waste management field [4].

One of the ways of applying wastes is to obtain energy from them.

Most of the woodworking factories give from 25 to 40% of waste materials which are not used after the production cycle.

Woodworking industry leavings are divided into 4 categories.

The first category includes slabs, tailings, and backing boards. Slab is the first board obtained in the process of cutting logs into boards. It can be only half sawn or not sawn at all.

The second category includes lump and longitudinal cuts, end faces, dry logs' pieces, wood details' scraps, and plywood sheets' ridges.

Finished material scraps are referred to as the third category. Among them are fiberboard, plywood, veneer, chipboard, and other materials made from primary or secondary timber products. Often, this type of remains is left after building renovation or restoration.

The fourth category consists of shavings, wood dust, sawdust, and bark. These wastes serve as the materials for wood plates.

Moreover, all wastes are divided into reusable (they include large pieces, for example, slabs or lump cuts; this type of raw is easy to process and use for creating appropriate materials), and cull lumber (this type includes smaller fraction; for cull lumber processing, certain conditions and equipment are needed, so these materials are less in demand because their processing is more expensive) [5, 6].

The first category of waste may be applied for massive or bulky item producing like boards, parquet, pallets, box packaging, and also for small component part production in the furniture industry. Lump waste may be applied as a raw material for pulp-and-paper production manufacturing at the industrial enterprises of this direction. Wood chip is used as a filter at the treatment facilities [7].

A potential way to use wood industry scraps is to produce materials for heating such as fuel briquettes and fuel pellets.

Fuel briquette is a preparation form of different woodworking processing industry waste, peat, agricultural industry waste, and other materials for applying as a fuel; pressed waste of woodworking processing industry (sawdust, wood chips, etc.), agricultural industry (straw, husk, corn, etc.), peat, and charcoal.

The fuel briquette producing technology consists in the waste (as waste may serve sunflower, buckwheat husk, etc.) and finely milled wood waste (sawdust) pressing at a high-pressure process. Producing process may also assume raw material heating

for obtaining the final product; however, it may not be needed. Completed fuel briquettes contain no binding agents in their structure except for lignin, a natural substance contained in plant cells [8].

Fuel briquettes are used at thermal power plants, steamships, industrial furnaces, railway transport, and low-capacity boilers. Also, they are demanded by the population for small square dwelling heating.

Fuel pellets are pressed under high-pressure natural raw materials of plant origin in the standard size cylindrical granule form [8].

As the raw materials for their production serve bark, sawdust, wood chips, other logging wood waste, agricultural waste (sunflower husk, straw, substandard flax, etc.), as well as organic packaging materials, cardboard packaging, etc.

Pellet producing process consists of 3 stages. The first stage is splitting. The point of this stage is in raw material milling to flour condition. The second stage is drying (the mass resulted must be thoroughly dried). The third stage is granulation. To compress the processed material into standard-size pellets, the special equipment—granulator—is needed. It heats the source material, therefore crushed particles of the material tightly glue together. The polymer lignin, which is contained in plant cells, performs here as the binding agent, as well as it does in fuel briquette producing, so no other chemical binders are required in the production process. The function of the granulator also comprises shaping the pellets.

Pellet producing process is technologically more complicated than the fuel briquette producing process: it requires high-quality raw materials and thorough pre-processing because it may affect the product's quality, its transportation, and storage options hereinafter [9, 10].

In terms of calorific value, fuel briquettes and fuel pellets quantitatively exceed the values of unprocessed woodworking waste.

The comparison of different fuel types calorific value is performed in Table 1. Consequently, fuel briquette or fuel pellet application as a fuel is physically more effective than just burning raw, unprocessed leavings that emerge during wood processing.

On the Alabuga Special Economic Zone (Tatarstan, Russia), the Kastamonu Integrated Wood Industry factory is situated. This factory is specialized in the production of MDFs, chipboards, laminate floorings, door skins, and glossy panels [11, 12]. The enterprise has its own power supply system: two gas turbine units and energy blocks operating on the wood waste of the production. On the factory territory, a waste processing complex is planned to be built. The capacity of this complex is supposed to be about 30,000 tons per year.

Building this complex has advantages for both the factory itself and the country as well.

According to the regional normative act, the Territorial scheme in the waste management sphere of the Republic of Tatarstan, 9053.4 tons of industrial waste emerged on the enterprise in 2017. If during the wood processing only 60% of all waste becomes raw materials and 40% becomes waste (among them 14% is slabs, 12% is sawdust, 9% is trimmings and small pieces, and the rest are bark and end face cuts), then about 3168.690 tons of the enterprise wastes are the first category wastes

Table 1 Comparison of the calorific value of different fuel types

Fuel type	Measurement unit	Specific combustion heat			Equivalent		
		kcal	kW	MJ	Natural gas (m ³)	Diesel fuel (l)	Fuel oil (l)
Natural gas	1 m ³	8000	9.30	33.50	–	0.777	0.825
Wood chips	1 kg	2610	3.00	10.93	0.326	0.253	0.269
Sawdust	1 kg	2000	2.30	8.37	0.250	0.194	0.206
Wood charcoal	1 kg	6510	7.50	27.26	0.814	0.632	0.671
Dried wood (<i>W</i> = 20%)	1 kg	3400	3.90	14.24	0.425	0.330	0.351
Fuel briquettes	1 kg	4600–4900	5.35–5.70	19.26–20.52	0.575–0.613	0.447–0.476	0.474–0.505
Fuel pellets	1 kg	3465–4320	4.00–5.00	14.51–18.09	0.433–0.540	0.336–0.419	0.357–0.445

(slabs), 2716.020 tons is sawdust, 2037.015 tons are trimmings and small pieces, and 1131.675 tons are bark and end face cuts.

The amount of energy obtained due to waste burning may be calculated by Eq. (1):

$$Q = m \cdot q, \quad (1)$$

where

Q fuel energy (kW);
 m mass of the fuel (kg);
 q specific combustion heat (kW/kg) [13].

The equivalent amount of natural gas required to obtain the same amount of combustion heat is calculated by Eq. (2):

$$\rho \cdot q = \frac{Q}{V}, \quad (2)$$

where

ρ fuel density;
 V fuel volume.

In this calculation, the natural gas amount was assumed to equal about 0.7614 kg/m³ ($\rho \approx 0.7614$ kg/m³); 1 m³ of natural gas specific combustion heat was introduced in Table 1.

To calculate the cost-saving due to waste incineration instead of natural gas burning, Eq. (3) is used:

$$C = P_{ng} \cdot V, \quad (3)$$

where

C cost of natural gas required to obtain energy;
 P_{ng} 1 m³ of natural gas cost.

Therefore, if all these wastes obtained during a year use as a fuel in the factory energy blocks, waste combustion produce 28,110,807 kW of energy. At the cost of natural gas equal 6.00781 rubles for 1 m³ (the natural gas cost for legal entities and businesses in the Republic of Tatarstan, for which annual gas consumption limit amounts from 10 to 100 million m³), the enterprise cost saving due to production waste using as a fuel will amount 18,371,198.27 rubles (Table 2, in the energy obtained from trimming, small pieces, bark and end face cuts combustion calculating the wood chips specific combustion heat is assumed).

If we suppose that in the new waste processing complex fuel pellets will be produced and wholesale price will be 5000 rubles per ton, then fuel pellet production from this enterprise wastes only will earn revenue equal to more than 45 million rubles per year (Eq. 4):

Table 2 Energy retrieving by incineration of waste

Waste structure	Specific combustion heat q (kW/kg)	Waste amount (fuel mass) m (kg)	Amount of energy obtained Q (kW)	Equivalent amount of natural gas V (m ³)	Waste type instead of natural gas combustion cost-saving C , thousands of rubles
First category wood processing wastes	3.9	3,168,690	12,357,891	1,328,805.48	8076.23
Sawdust	2.3	2,716,020	6,246,846	671,703.87	4082.49
Trimming, small pieces, bark and end face cuts	3.0	3,168,690	9,506,070	1,022,158.07	6212.48
Total	–	9,053,400	28,110,807	3,022,667.42	18,371.20

$$I = P_{\text{pell.}} \cdot m, \quad (4)$$

where

I revenue;

$P_{\text{pell.}}$ sale price for 1 ton of pellets;

m mass of waste obtained at the enterprise [14].

Not only this enterprise waste processing but also other waste processing (which are obtained beyond the enterprise) will contribute to quick payback and profitability of the complex (its productivity planned to be equal to 30,000 tons per year). Also, at the use of own produced pellets by the factory itself, the amount of energy received may be greater than the amount of energy gained by unprocessed waste combustion, since the calorific power of pellets is greater than the dried wood, sawdust, or wood chip calorific power. The amount obtained, which is calculated as the product of pellet specific combustion heat (in this calculation by Eq. (1), it is supposed to be equal to 4.5 kW/kg) and the waste amount of the enterprise (9053.4 tons), is equal 40,740,300 kW that is equivalent to 4,380,677.42 m³ of natural gas (the calculation is proceeded by Eq. (2)).

Also, we may suppose that at the new waste processing plant, not only wood-working processing waste will be handled, but, for example, polyethylene, plastic, paper, cardboard wastes too.

3 Results

In 2017, the Kastamonu company sent more than 350 tons of waste for processing to external specialized organizations, gained due to it extra profit equal to more than 2.5 million rubles [11]. Therefore, we consider two versions: to send wastes for processing into external organizations, or to realize processing in the own enterprise department. The cost-effectiveness of each of the two versions is compared in Fig. 1.

In the calculation, the profit is defined by Eq. (5):

$$Pr = I - Cost, \tag{5}$$

where

Pr profit;
 Cost cost.

The new object building payback period is defined by Eq. (6):

$$T_{pp} = \frac{TIC}{NCF}, \tag{6}$$

where

T_{pp} payback period;
 TIC total investment costs;
 NCF net cash flow per planning interval.

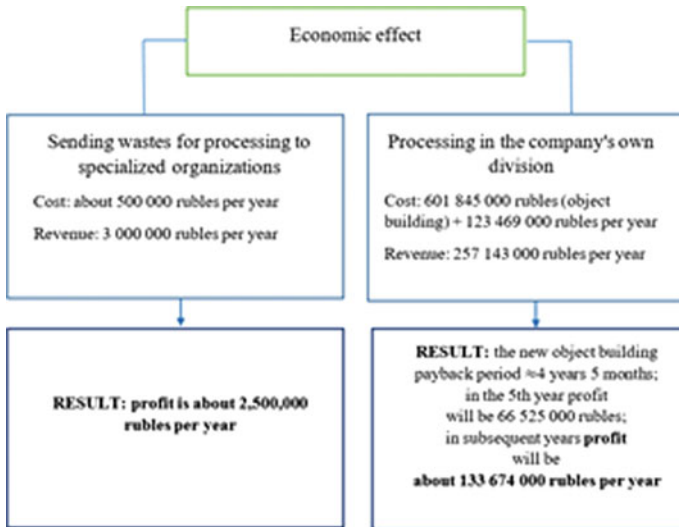


Fig. 1 The economic effect comparison

Therefore, from the scheme performed in Fig. 1, we can see that the waste processing complex building will be paid for itself in less than 5 years. Processing realizing in volumes supposed by the capacity of the complex will start to make a profit in a larger size than just sending wastes into external organizations. Thus, this project realizing is economically effective.

4 Discussion

Based on all of the above, we may make a conclusion that the implementation of effective waste applying undertakings favorably affects not only a country's ecologic conditions, but the economic stability of enterprises too because the waste removal, obtaining of extra energy, and revenue source items are solved. Enterprises should not neglect the waste issue because effective applying of processing technologies may favorably impact a company's financial results [15].

References

1. Hatipoglu, E., Muhanna, S., Al Efidr, B.: Renewables and the future of geopolitics: revisiting main concepts of international relations from the lens of renewables. *RuJE* **6**, 358 (2020)
2. Mikheeva, N.N.: Economic dynamics of Russian regions: crises and ways to restore growth. *Reg. Res. Russ.* **10**, 2 (2020)
3. Barinova, V.A., Zemtsov, S.P.: Inclusive growth and regional sustainability of Russia. *Reg. Res. Russ.* **10**, 10 (2020)
4. Grigoryev, L.M.: Energy transition and game changers. *RuJE* **6**, 339 (2020)
5. Borges, E.R., Carvalho, F.A., Dexter, K.G., Bueno, M.L., Pontara, V.: The evolutionary diversity of urban forests depends on their land-use history. *UECO* **23**, 631 (2020)
6. Shi, J., Peng, J., Cai, L., Huang, Q., Shi, S.Q.: Fabrication of densified wood via synergy of chemical pretreatment, hot-pressing and post mechanical fixation. *J. Wood Sci.* **66**, 5 (2020)
7. Bortoluz, J., Bonetto, L.R., Da Silva Crespo, J., Giovanela, M., Ferrarini, F.: Use of low-cost natural waste from the furniture industry for the removal of methylene blue by adsorption: isotherms, kinetics and thermodynamics. *Cell* **27**, 6445 (2020)
8. Hong, L., He, Q., Ju, Z., Zhang, H., Lu, X., Brosse, N.: Effect of vacuum hot pressing on the bonding quality and heat transfer performance of plywood. *HolzAlsRoh-UndWerkstoff* **78**, 441 (2020)
9. Gordeev, A.S.: *Energy Management in Agriculture*, vol. 75. Saint-Petersburg (2018)
10. Sani, F.R., Enayati, A.A.: J. Reduced use of urea-formaldehyde resin and press time due to the use of melamine resin-impregnated paper waste in MDF. *Indian Acad. Wood Sci.* **17**, 100 (2020)
11. The official website of the Kastamonu Integrated Wood Industry LLC. <http://kastamonu.ru/ru/news/kastamonu-has-put-into-operation-the-second-gas-turbine-installation-as-part-of-the-plant-s-thermal-power-station>. Last accessed 05 Oct 2020
12. Gurkov, I.B.: Location of Russian enterprises of foreign corporations opened in 2012–201. *Reg. Res. Russ.* **10**, 29 (2020)
13. Ferronato, N., Torretta, V., GorrityPortillo, M.A., GuisbertLizarazu, E.G.: Application of a life cycle assessment for assessing municipal solid waste management systems in Bolivia in an international cooperative framework. *Waste Manag. Res.* **38**, 98 (2020)

14. Magrini, C., D'Addato, F., Bonoli, A.: Municipal solid waste prevention: a review of market-based instruments in six European Union countries. *Waste Manag. Res.* **38**, 3 (2020)
15. Gordeev, R.V.: *For. Policy Econ.* **119**, 102286 (2020)

Mathematical Simulation of Electrodynamical and Thermal Processes in Electrical Process Plants



Sergei Trigorly, Andrey Yakovlev, Svetlana Kalganova, Anton Sivak,
and Yulia Kadykova

1 Introduction

Electrical process plants are widely used in various industries. The electrical energy consumed by these plants is about 25% of the total consumption [1]. Induction and microwave plants, which can increase the productivity and quality of products, are used in various technological processes. The use of electromagnetic waves of various frequencies to heat materials is common in these processes.

Induction heating is widely used in various technological processes [2–7] for heat treatment and melting of conductive materials. The advantage of induction heating is the ability to achieve high temperatures and the required uniformity in the heated material.

Along with induction heating, electrical technology uses microwave heating, which is used to intensify the heat treatment of various dielectric materials [8–12]. In comparison with conventional methods for heating dielectric materials, microwave heat treatment provides fast volumetric heating of dielectrics, high efficiency of conversion of the electromagnetic field into thermal energy, and improved product quality.

In addition, a non-thermal effect on the physical and mechanical properties of polymeric materials was identified during microwave exposure, which contributes to an increase in operational parameters.

An urgent task is to develop energy-efficient induction and microwave plants that meet the increased requirements for the quality of products. In addition, electrical process plants such as high-tech power consumers can be classified as objects, the control of which should be organized on the basis of digital twins along with the distributed generation system in the power industry. Therefore, the development of

S. Trigorly · A. Yakovlev (✉) · S. Kalganova · A. Sivak · Y. Kadykova
Yuri Gagarin State Technical University of Saratov, Saratov, Russia
e-mail: red.and2012@yander.ru

mathematical models of electrical process plants and systems is an urgent problem [13].

The purpose of the work is a mathematical simulation of electrodynamic and thermal processes during copper melting in an induction crucible furnace and in a microwave plant for thermal modification of composite materials.

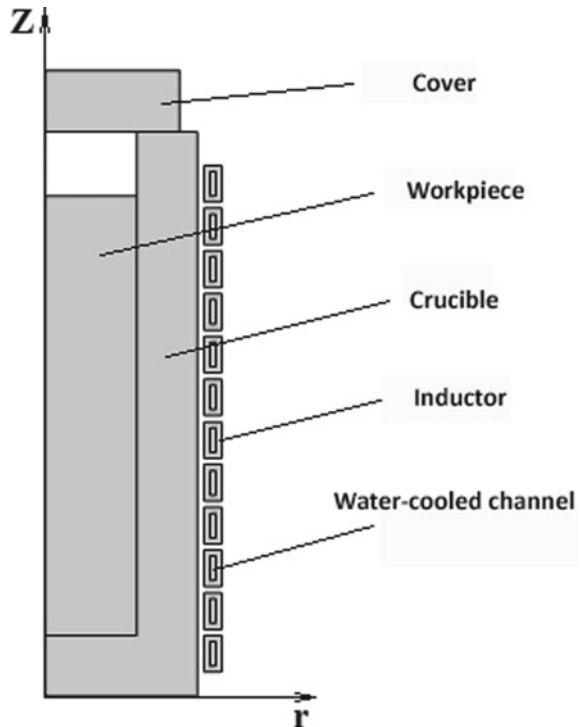
2 Description of the Mathematical Model

2.1 Mathematical Model of Induction Heating

This paper considers the mathematical simulation of technological processes in an induction plant for melting copper. The induction plant contains the following main components: a water-cooled inductor made of a rectangular copper tube; a graphite crucible with a heated workpiece, which is placed inside the inductor (Fig. 1).

For mathematical simulation of the processes in the crucible furnace during induction melting, the equations of electrodynamics and thermal conductivity are used [2]. The electrodynamic process in the induction plant is described by differential

Fig. 1 Simplified geometric model of the induction crucible furnace



equations:

$$(j\omega\sigma - \omega^2\varepsilon_0\varepsilon_r)A + \nabla \times (\mu_0^{-1}\mu_r^{-1}B) = J_e, \quad (1)$$

$$B = \nabla \times A, \quad (2)$$

where A —vector of magnetic potential; B —vector of magnetic induction; ω —circular frequency; σ —electrical conductivity; $\varepsilon_0, \varepsilon_r$ —vacuum dielectric constant and relative dielectric constant of the medium; μ_0, μ_r —magnetic permeability of vacuum and relative magnetic permeability of the medium; J_e —current density vector [7, 8].

The heat conduction equation has the following form [14]:

$$\rho C_p \frac{\partial T}{\partial t} = \nabla \cdot (\lambda \nabla T) + q_v, \quad (3)$$

where ρ, C_p —density, the specific heat capacity of the material of the corresponding medium; q_v —specific power of the heat sources due to the induction heating of the workpiece by the induced currents; λ —coefficient of thermal conductivity.

The water flow cooling the inductor is turbulent. In this case, the process of cooling the inductor can be approximately described by the following Eq. (2):

$$Q_{\text{ohl}} = \frac{v\rho C(T_b - T_{\text{ust}})}{V}, \quad (4)$$

where v —speed of water flow inside the inductor channel; ρ —density of water; T_b —temperature at the initial moment of time; T_{ust} —steady-state temperature at a certain point in time; C —specific heat capacity of water.

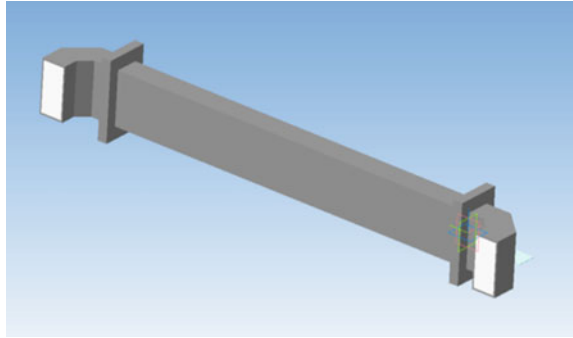
2.2 Mathematical Model of Dielectric Microwave Heating

Mathematical simulation of the conveyor-type microwave electrical process plant based on a traveling wave chamber for the modification of polymer composite materials was carried out. The microwave plant is designed to improve the physical and technical properties of the processed materials (Fig. 2).

The waveguide with a cross section of 45 mm × 90 mm, which contains a transporting belt, was selected. A 3 kW water-cooled magnetron operating at a frequency of 2450 MHz was used as a microwave power source.

For mathematical simulation of microwave thermal modification of polymer composite materials (PCM), a system of interrelated equations of thermal conductivity (3) and electrodynamics [15] was used:

Fig. 2 The geometry of the microwave working chamber based on the waveguide



$$\nabla \times (\mu_r^{-1} \nabla \times \mathbf{E}) - k_0^2 \left(\varepsilon_r' - \frac{j\sigma}{\omega\varepsilon_0} \right) \mathbf{E} = 0$$

$$q_v = 0,5\omega\varepsilon_0\varepsilon_r'' \cdot |\mathbf{E}|^2 \quad (5)$$

where \mathbf{E} —vector of the electric field strength, q_v —specific power of heat sources due to dielectric losses, μ_r —relative magnetic permeability, $k_0 = \omega\sqrt{\varepsilon_0\mu_0}$ —wave number, ε_r' —relative dielectric constant (real part), $\sigma = \omega\varepsilon_0\varepsilon_r''$ —electrical conductivity, $\omega = 2\pi f$ —circular frequency, ε_0 —electric constant, ε_r'' —effective loss factor (imaginary part of the dielectric constant), and f —frequency of the electromagnetic field.

The mathematical simulation was carried out using the COMSOL Multiphysics software product. This software product allows solving interrelated differential equations of electrodynamics and thermal conductivity, which characterize technological processes in both induction and microwave heating of materials [15].

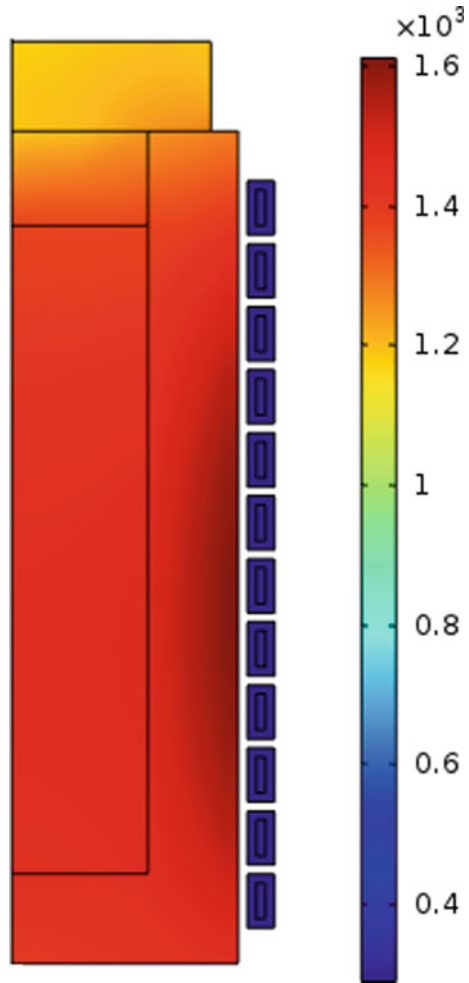
3 Results

3.1 The Results of Modeling Copper Melting Processes in the Crucible Induction Plant

The results of mathematical simulation of the processes of heating and melting copper in the crucible induction plant are considered. Figures 3, 4, and 5 show, respectively, the temperature field in the longitudinal section of the induction plant, in the volume of the plant, and the boundary of the phase transition during melting of copper at the time 3600 s.

Figure 6 shows a graph of temperature changes in time in the center of the copper workpiece until 7200 s. The results of studying the influence of various graphite grades, from which the crucible is made, on the heating rate of the copper workpiece are shown in Fig. 7.

Fig. 3 Temperature distribution in the copper workpiece during 3600 s

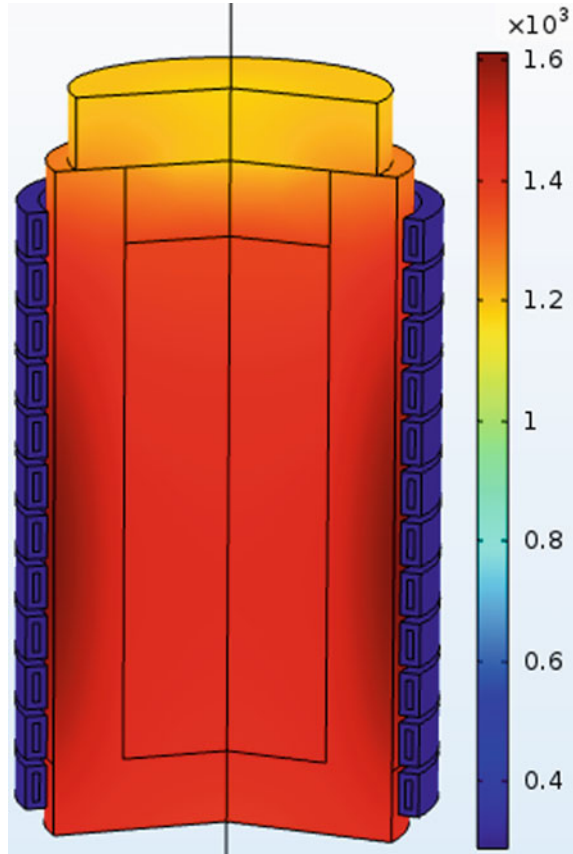


By analyzing the above dependences (Fig. 7), it is possible to select a material for the manufacture of the crucible with higher electrical conductivity and faster heating in order to increase the energy efficiency of the copper melting process.

It was found that the phase transformation of copper from the solid phase to the melt occurs in the time range from 3600 to 4000 s. In this case, the copper workpiece reaches a temperature of 1300–1400 K, which corresponds to the real experiment.

Application of the methodology for simulating melting processes in crucible induction furnaces using the COMSOL Multiphysics software package allows developing energy-efficient plants of this type.

Fig. 4 Temperature distribution in the copper workpiece during 3600 s



3.2 Results of Simulation of PCM Microwave Heat Treatment

As a result of mathematical simulation in COMSOL Multiphysics, the distribution of temperature fields in the processed polymer composite material was obtained (Fig. 8).

The distribution of the temperature field in the cross section of the material for different times is shown in Fig. 9.

As was previously found in the works of the authors [10], the modifying effect on the PCM is due to the magnitude of the intensity of the microwave electromagnetic field. In this regard, when simulating the technological process, it is necessary to determine the distribution of the microwave electric field strength. The result of this simulation is the distribution of the electric field strength in the microwave working chamber (Fig. 9) and in the processed material (Fig. 10).

Figures 10 and 11 show that when passing through the dielectric, the distribution pattern of the electric field strength changes. In particular, the distance between the

1- Boundary of the phase transition

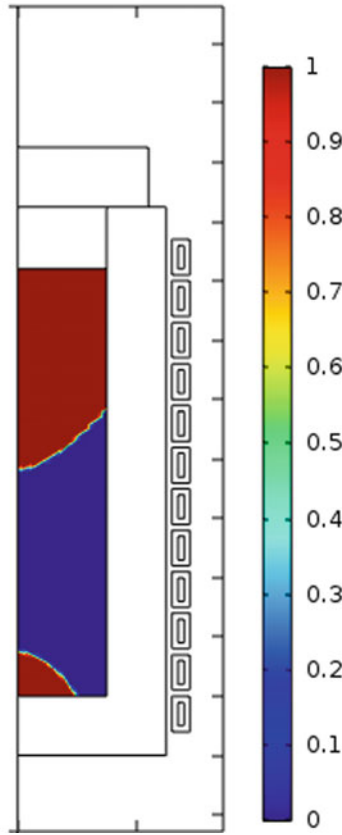


Fig. 5 Phase transition at 3600 s

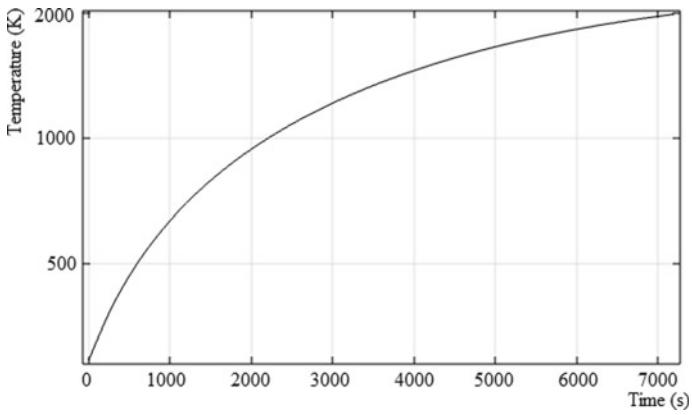


Fig. 6 A graph of temperature changes in time in the center of the copper workpiece during 7200 s

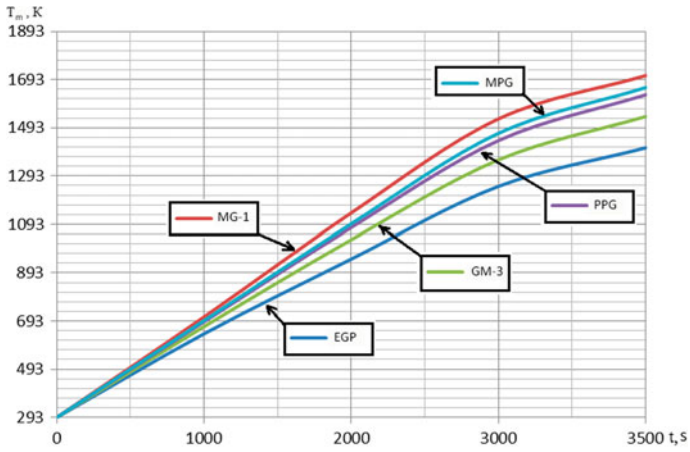


Fig. 7 Influence of graphite grade on induction heating

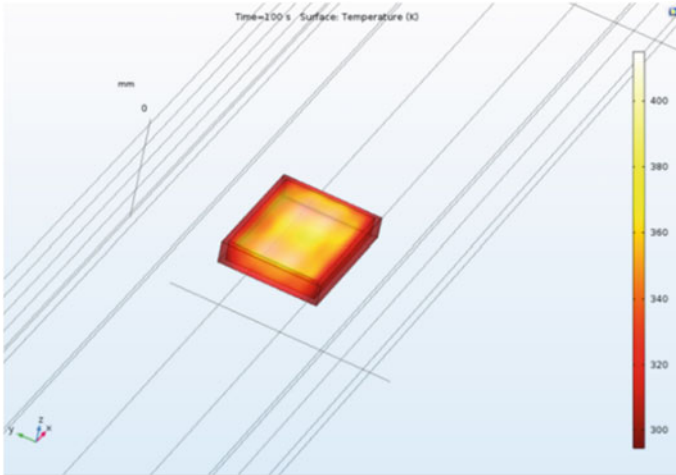


Fig. 8 Distribution of the temperature field in the material

maxima and minima of the electric field strength changes. These features must be taken into account when carrying out a non-thermal modification of PCM.

4 Conclusion

Based on the mathematical simulation, it has been established that the most energy-efficient graphite grade for the induction crucible furnace for melting copper is MG-1.

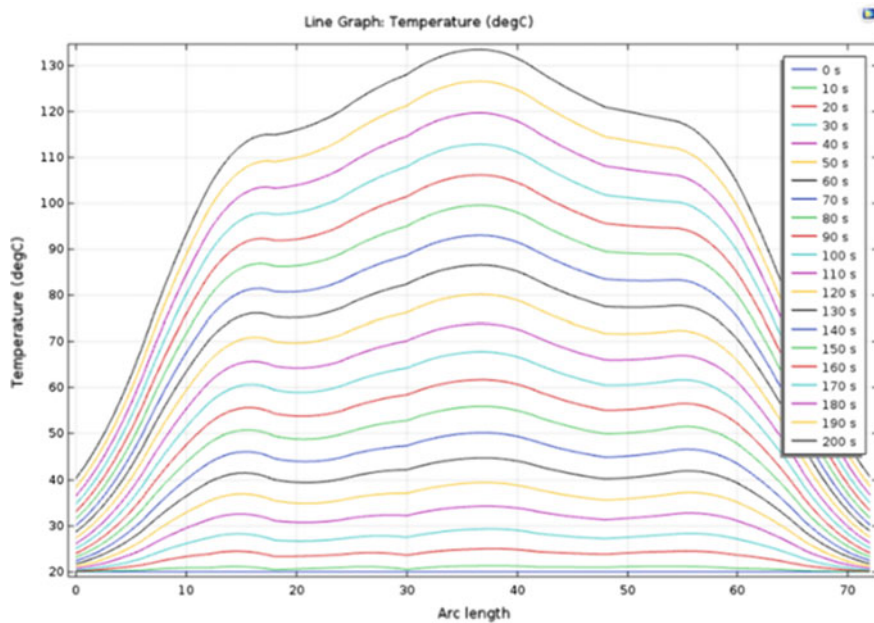


Fig. 9 Distribution of the temperature field in the material

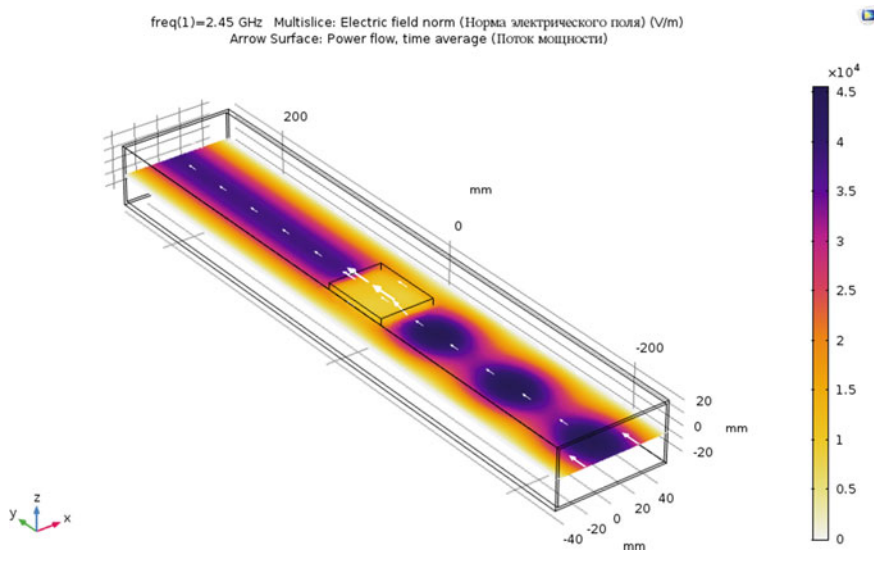


Fig. 10 Electric field distribution in the microwave chamber with dielectric

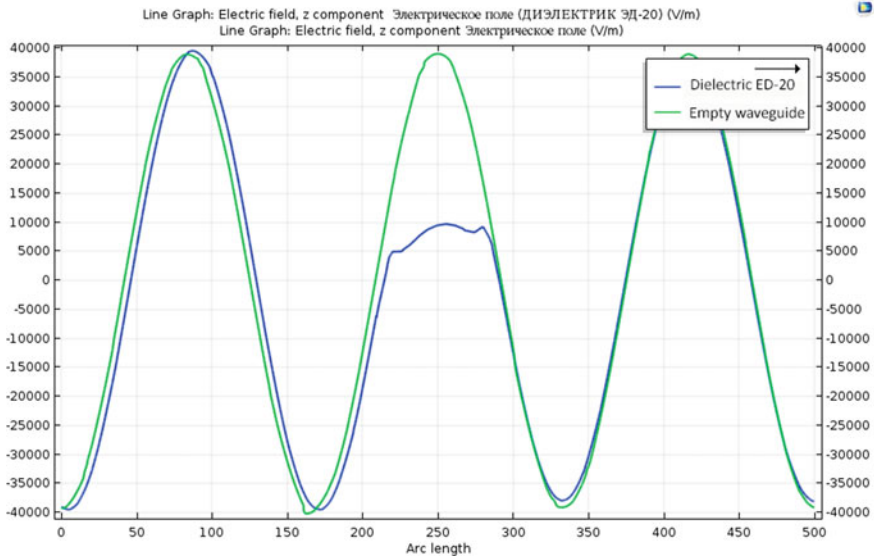


Fig. 11 Electric field strength distribution in the dielectric along the z coordinate

In this case, the rate of heating and melting of copper increases by 7.5% in comparison with similar graphite crucibles of other brands.

When designing process microwave chambers of a rectangular type with a traveling wave for the modification of various materials, it is advisable to carry out numerical simulation of thermal and electric fields in the material. This allows predicting changes in the distribution of temperature and electric fields depending on the properties of polymer composite materials and to select the best parameters of microwave exposure.

References

1. Arkhangelskiy, Yu.S.: Microwave electrothermy. SSTU **408** (1998)
2. Bhat, A.A., Agarwal, S., Sujish, D., Muralidharan, B., Reddy, B.P., Padmakumar, G., Rajan, K.K.: Thermal Analysis of Induction Furnace. Fast Reactor Technology Group, Chemistry Group. Indira Gandhi Centre for Atomic Research, Kalpakkam (2017)
3. Demidovich, V.B., Chmilenko, F.V., Rastvorova, I.I.: Utilization of induction heating in the line of continuous castingcontinuous rolling of steel. *Acta Tech.* **60**(2), 107–118 (2015)
4. Ptitsyna, E.V., Kuvaldin, A.B., Ptitsyn, D.V.: The influence of mixed load with complex waveform current supply on the electrical energy quality. *IOP Conf. Ser. Earth Environ. Sci.* **378** (2019)
5. Demidovich, V.B., Chmilenko, F.V., Andrushkevich, V.V., Rastvorova, I.I.: 3D-Simulation of electromagnetic and temperature fields in the continuous induction heaters. In: Proceedings of the 6th International Conference on Coupled Problems in Science and Engineering Coupled Problems, pp. 976–984 (2015)

6. Kuvaldin, A.B., Fedin, M.A., Polyakov, O.A.: Studying the parameters of an electromagnetic field in a discrete medium. *Bull. Russ. Acad. Sci. Phys.* **84**(2), 122–124 (2020)
7. Ptitsyna, E., Kuvaldin, A., Ptitsyn, D.: The effective modes of infrared radiators and heating systems. *E3S Web Conf.* **140** (2019)
8. Chen, L., Huang, Z., Wang, K., Li, W., Wang, S.: Simulation and validation of radio frequency heating with conveyor movement. *J. Electromagn. Waves Appl.* 473–491 (2015)
9. Zlobina, I., Bekrenev, N.: Microwave electromagnetic field influence on the stability of reinforced carbon plastics with built-in lightning protective coating during dynamic loads action. *Mater. Sci. Forum* 992 MSF, 427–433 (2020)
10. Vasinkina, E., Kalganova, S., Alekseev, V., Kadykova, Yu., Arzamastsev, S.: Dolzhikova Influence of microwave electromagnetic field on the structure of polymers. *J. Phys. Conf. Ser.* **1124**(7), 071018 (2018). <https://doi.org/10.1088/1742-6596/1124/7/071018>
11. Perovskite, R.B., Nuernberg, M.R.: Morelli microwave assisted synthesis and sintering. *Mater. Res. São Carlos* **18**(1), 85–91 (2015)
12. Nuhiji, B., et al.: Simulation of carbon fibre composites in an industrial microwave. *Mater. Today Proc.* (2020)
13. Kovalyov, S.P.: Information architecture of the power system digital twin. *Syst. Means Inf.* **30**(1), 66–81 (2020)
14. Isachenko, V.P., Osipova, V.A., Sukomel, A.S.: Heat transfer. *Energy (Moscow)*, 472 (1968)
15. Kalganova, S., Trigorly, S., Zakharov, V.: Computer simulation of microwave heat treatment of dielectrics. In: 2018 IV International Conference on Information Technologies in Engineering Education (INFORI), MPEI, pp. 1–5. Moscow (2018)

For Calculation of Perforated Hearth Burner Equipment to the Bubble-Type Furnaces



Konstantin Strogonov, Alexey Popov, Alexander Zdarov,
and Lyubov Kornilova

1 Introduction

The relevance of energy and resource conservation issues is determined by the need to reduce production costs, increase the competitiveness of enterprises and increase their profits. A significant energy-saving effect is possible with a decrease in the most significant cost items of production; from the point of view of the energy approach, attention should be paid to the most energy-consuming industries, such as smelting processes among high-temperature ones. So in ferrous metallurgy, metals are melted at temperatures above 1600 °C; the energy consumption of steel reaches 28.073 GJ/t [1], and the energy intensity of the product (for example, a steel pipe) is 43.443 GJ/t. In glass production, the energy consumption of products reaches 14.651 GJ/t [2]; for continuous basalt fiber, this figure can reach 57.63 GJ/t [3]. Most of the energy costs are associated with melting processes, which are usually organized in bath-type aggregates with a luminous torch; meanwhile, the most effective is the organization of submerged combustion, and its varieties: dispersed blowing of melts [4]. An important issue in organizing dispersed blowing of melts is the issue of the capacity of single burners.

2 Description of the Submersible Combustion Process

According to the principle of operation, submersible combustion devices are characterized by bubbling processes occurring between combustion products and solutions. Combustion products, passing through the liquid, break up into gas bubbles, which form a large interface when floating up.

K. Strogonov (✉) · A. Popov · A. Zdarov · L. Kornilova
NRU MPEI, Moscow 111250, Russian Federation

It is characteristic that at equilibrium temperature, gas bubbles leave solutions with a temperature 1–2 °C higher than the melt temperature, therefore, with direct contact of combustion products with a liquid, heat and mass transfer processes proceed with a sharp decrease in heat loss. The utilization rate of the heat of combustion of the fuel is 95–96% [5].

The relevance of the development of energy-efficient burner equipment is also determined by a wide range of applications, as in the article [6] the authors presented a variant of using a submersible torch for waste disposal. A submersible burner was developed to remove nitrates and nitrite ions from the waste solution. In the 90s of the last century, JSC “Teploproekt” developed and created a submerged hot water boiler with a capacity of 800 kW for heating premises with an area of more than 5000 m².

The results of a three-year successful pilot operation of the above-mentioned CIT at Komasa LLC (the successor of Teploproekt JSC) confirmed its reliability with an efficiency of 97% at an exhaust gas temperature of less than 50 °C. At the same time, the content of nitrogen oxides and carbon oxides in exhaust gases was at a level that did not meet modern achievements [7].

An important advantage of submersible combustion devices is the combination in one device of the functions of several devices at once; this is a generator of thermal energy and a stimulator of movement, mixing of liquid [8, 9].

The high temperature of bubbling combustion inside the melt leads to the formation of a complex gas–liquid structure and a relatively large heat transfer surface. This situation significantly increases the heat exchange between the combustion products and the processed material, and leads to the formation of a complex gas–liquid structure, a relatively large heat transfer surface. The authors of [10] note that intensive mixing of the melt has several advantages:

- the rate of melting increases;
- the rate of chemical reaction increases;
- the homogeneity of the molten material is improved.

A description of the technology of submersible combustion in molten basalt is presented in the article [11]. In the 1990s, melting installations were developed at the Gas Institute of the National Academy of Sciences of Ukraine, in which submerged combustion was realized.

Based on the peculiarities of submerged combustion, burners must meet the following conditions [12]:

- stable combustion at the point of injection of the fuel–air mixture in order to avoid the formation of cold channels and explosive combustion;
- fast fuel combustion due to constant, reliable and fast mixture supply;
- long service life, reliability and ease of maintenance.

Studies carried out in the sources [13, 14] prove that it is necessary to take into account also the nature of the formation of gas bubbles, the size and their changes in the process of interaction with the melt. These parameters are of interest because

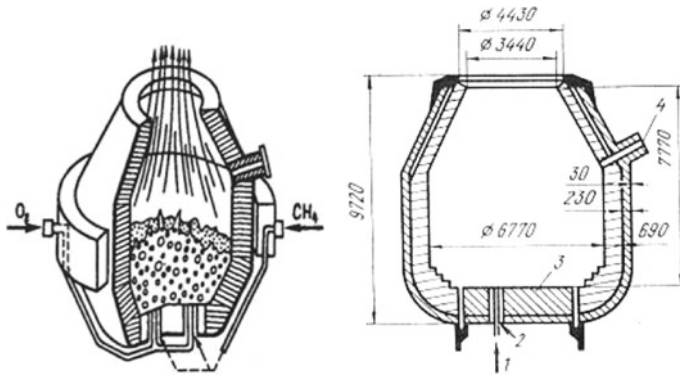


Fig. 1 Construction of a 250-ton bottom-blown converter: 1—oxygen; 2—carbon gas; 3—bottom; 4—outlet hole

they affect the convection inside the melting furnace and the interface between the melt and the charge layer.

Melt bubbling has long found its application in steelmaking. It is implemented in converter steelmaking. Flame heating of melts in an open-hearth furnace is performed from the surface. However, due to the low thermal conductivity of the slag, such heating is ineffective, especially if the melt is poorly mixed. In open-hearth furnaces during the melting and finishing periods, when the bath is covered with a significant slag layer, the thermal efficiency does not exceed 25%.

For comparison, in converter smelting, the diagram of the furnace is shown in Fig. 1; the total duration of melting in 100–350 t converters is 40–50 min [15]. The use of bubbling can significantly increase furnace productivity and significantly reduce fuel consumption.

The schematic and general view of the bottom-blown converter is shown in Fig. 1.

To protect the masonry of the converter bottom from high temperatures, the lance is made in the form of two coaxial tubes. Oxygen is supplied through the central one, and some natural gas is supplied along the peripheral. Such lances are usually installed 16–22, the diameter of the oxygen nozzle ranges from 28 to 50 mm, the gap for fuel supply depends on the type of fuel and is 0.5–2 mm. A large number of smaller tuyeres provide better mixing of the bath and a smoother melting process [16].

The paper provides a link to the results of a study of the functioning of various types of burners submerged into the melt. It has been found that premixed gas-oxygen burners are not suitable for submersible fuel combustion. The same conclusion was made regarding gas-oxygen burners with preliminary combustion of gas in the chamber and subsequent release of high-temperature combustion products.

3 Calculation of Submersible Burner Parameters

The use of a perforated enclosure for the purpose of returning (regenerating) heat back to the reactor is discussed in the monograph [17]; the general view of the perforation is shown in Fig. 2. In this work, the installation of the burners is shown in Fig. 3.

In the lining of the hearth of furnace 1, there is a perforation in which the burners are installed. The burners consist of two concentric tubes. An oxidizer is supplied through pipe 3, and natural gas is supplied through pipe 2, which is heated from

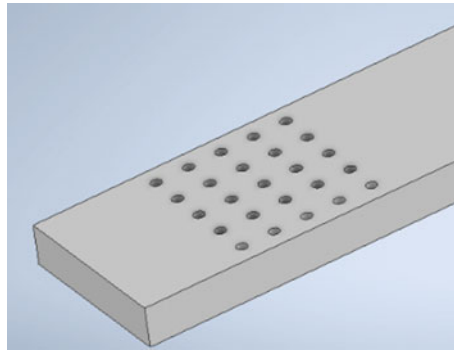


Fig. 2 Sketch of the perforation in the oven enclosure

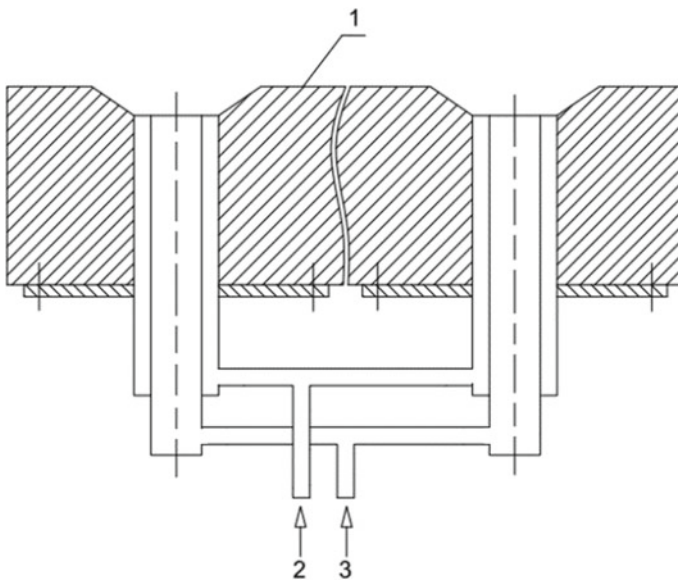


Fig. 3 Scheme of the lance

the walls and at the outlet as a result of thermal decomposition and with constant temperature control [18] and maintaining the outlet gas temperature at 1000 °C. Under the influence of high temperatures of about 1000 °C, hydrocarbons entering through the gap between the inner and outer pipes decompose, absorbing heat [19], and a soot-hydrogen mixture is formed:



Combustion of the outgoing components occurs at some distance from the burner.

The gas outflow velocity is investigated in the range from 1 m/s, as is implemented in the oxygen-converter production with bottom blowing [4], to 10 m/s, as suggested in the source [20]. Oxidizer velocity is calculated but is limited to 1–300 m/s.

In accordance with practical experience in the use of blowing basalt melt with a gas-air mixture [21] and converters with bottom blowing [15], holes with a diameter of more than 4 mm can be filled with melt after shutting off the gas supply; therefore, in the calculations, the diameter of the inner pipe for supplying the oxidizer is taken as 4 mm, and for the supply of gaseous fuel, the gap between the inner and outer pipes is considered in the range from 0.5 to 4 mm.

The outer diameter of the branch pipe for the oxidizer, which takes into account the thickness of the metal separating the oxidizer from the gaseous fuel, is calculated by the formula:

$$d_{ok.outer} = d_{ok.inside} + 2 * s = 6 * 10^{-3}, [m] \quad (2)$$

where $d_{ok.inside} = 0.004$ —diameter of the inner part of the burner for oxidizer, m;
 $s = 0.001$ —wall thickness of the inner and outer pipes, m.

Burner inner diameter for fuel:

$$d_{gas.inside} = d_{ok.outer} + 2 * z, [m] \quad (3)$$

where $z = 0.0005/0.004$ —gap between inner and outer pipes, m.

The outer diameter of one burner is considered from 9 to 16 mm, as shown in Fig. 4 and is calculated by the formula:

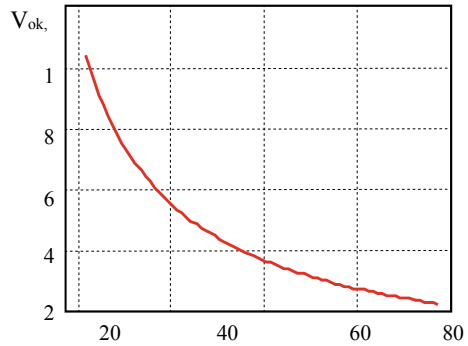
$$d_{outer} = (d_{gas.inside} + 2 * s) * 1000, [mm] \quad (4)$$

The area of the outer circumference along the oxidizer required to calculate the throughput of the oxidizer is calculated by the formula:

$$S_{ok.inside} = (\pi * d_{ok.inside}^2)/4 = 1.257 * 10^{-5}, [m^2] \quad (5)$$

The fuel gap area required to determine the gaseous fuel throughput depends on the gap z and ranges from $1.021 * 10^{-5}$ to $1.257 * 10^{-4}$ m².

Fig. 4 Graph of the dependence of the specific yield of the oxidizer on the oxygen content



Fuel consumption is calculated by multiplying the feed rate of gaseous fuel in the range from 1 to 10 m/s by the cross-sectional area in the obtained range and is from $1.021 \cdot 10^{-5}$ to $1.257 \cdot 10^{-3}$ m³/s.

According to calculations, the material balance of fuel combustion is determined by the heat of combustion of the fuel, MJ/m³:

$$Q_{n.fuel} = (Q_{CH_4} * CH_4 + Q_{C_2H_4} * C_2H_4 + Q_{C_3H_8} * C_3H_8 + Q_{C_4H_{10}} * C_4H_{10} + Q_{C_5H_{12}} * C_5H_{12}) / 100 = 35.753, \text{ [MJ/m}^3\text{]} \quad (6)$$

where Q_{CmHn} —net calorific value of gas components, MJ/m³; CmHn—gas fuel composition, %.

The specific theoretical consumption of oxygen introduced by the oxidizer m³/m³ of fuel is calculated by the formula:

$$V_{O_2} = V_C + 0.25 * V_H - 0.5 * V_O = 1.992, \text{ [m]} \quad (7)$$

where $V_C = 0.998$ —specific volume of carbon in gas fuel, m³/m³ fuel; $V_H = 3.979$ —specific volume of hydrogen in gas fuel, m³/m³ fuel; $V_O = 1.992$ —specific volume of oxygen in gas fuel, m³/m³ fuel.

Specific oxidant consumption, m³/m³ fuel:

$$V_{ok}(K_{O_2}) = \alpha * (V_{O_2} / K_{O_2}) = 1.992, \text{ [m]} \quad (8)$$

where α —coefficient providing complete combustion of fuel, adopted 1.1; $K_{O_2} = 0.21/0.98$ —proportion of oxygen content in oxidizer.

With an oxygen content of 21% in the oxidizer, the specific oxidizer consumption is 10.436 m³/m³ fuel; with 98% oxygen in the oxidizer, the specific oxidant consumption is 2.236 m³/m³ fuel. Graph showing how the specific consumption of the oxidant changes from the amount contained in the oxidant oxygen is shown in Fig. 5.

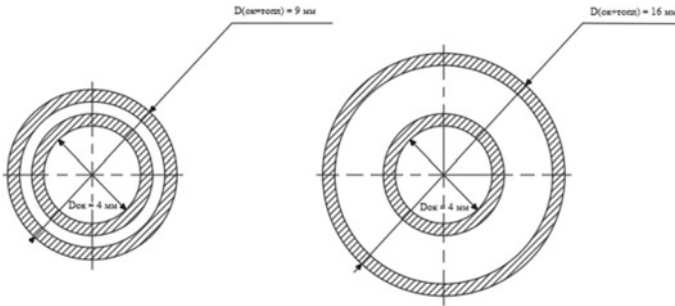


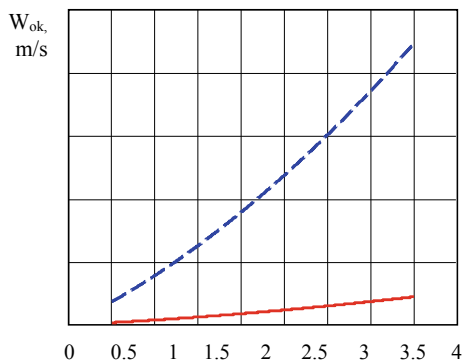
Fig. 5 Minimum and maximum sizes of burners

The obtained values are presented in Fig. 5; the graph indicates that the oxidizer with the highest oxygen content must be used to calculate the heat output of a single burner.

The speed of the supplied oxidant largely depends on the speed of the fuel supply and the gap, which is from 0.5 to 4 mm, and through which the gaseous fuel is supplied. The set of all options for the conditions under consideration is between the lines shown in Fig. 6. So for the variant with a gap of 0.5 mm and a gaseous fuel feed rate of 1 m/s, the oxidizer feed rate (98% O₂) is 1.817 m/s; for the burner version with a 4 mm fuel gap, the oxidizer feed rate is 22.364 m/s. The top line shown in Fig. 6 characterizes the dependence of the change in the oxygen supply rate on the gaseous fuel supply cross section at a gaseous fuel velocity of 10 m/s and ranges from 18.170 m/s for a gap of 0.5 mm to 223.635 m/s for a gap of 4 mm.

The design power of a single burner is from 0.365 kW for the variant with a fuel feed rate of 1 m/s through a gap of 0.5 mm to 44.929 kW for a variant with a fuel feed rate of 10 m/s through a gap of 4 mm.

Fig. 6 The speed of the oxidizer, depending on the section and speed for gaseous fuel



4 Conclusion

The proposed design of burners for a perforated hearth consists of coaxially arranged tubes that exclude mixing of the oxidizer and fuel; the outer diameter of a single burner varies from 9 to 16 mm, while the cross-sectional diameter of the oxidizer is 4 mm, and the gap for supplying gaseous fuel varies from 0.5 mm to 4 mm.

With a constant diameter of the oxidizer nozzle and a change in the gap for supplying gaseous fuel in the range from 0.5 mm to 4 mm, and in the range of rates of supply of gaseous fuel from 1 m/s to 10 m/s, the feed rate of the oxidizer, with an oxygen content of 98%, changes nonlinearly from 1.817 m/s to 223.635 m/s, and the burner power can vary from 0.365 kW for the option with a fuel feed rate of 1 m/s through a gap of 0.5 mm to 44.929 kW for a version with a fuel feed rate of 10 m/s through a gap in 4 mm.

The results of the studies carried out make it possible to select the required parameters of a single burner for the formation of perforated sub-smelting units, depending on the required power.

Acknowledgements The work was carried out within the framework of the project “Breakthrough technologies for energy-efficient designs of bubbling-type melting furnaces” with the support of a grant from NRU “MPEI” for the implementation of research programs “Energy”, “Electronics, Radio Engineering and IT” and “Industry 4.0 Technologies for Industry and Robotics” during 2020–2022.

References

1. Zhuravlev, Yu.P., Nikiforov, G.V., Zaslavets, B.I., Oleinikov, V.K.: Complex solutions to the problems of energy saving at metallurgical enterprises. *Chief Power Eng.* **3**, 48–53 (2011)
2. Danilov, N.I.: Fundamentals of energy saving: textbook. In: Danilov, N.I., Shchelokov, Ya.M. (eds.) N.I. Danilov. Ekaterinburg: GOU VPO USTU-UPI, 564 p (2006)
3. https://otherreferats.allbest.ru/manufacture/00148273_0.html#text
4. Klyuchnikov, A.D., Kuzmin, V.N., Popov, S.K.: Heat Transfer and Thermal Modes in Industrial Furnaces: Textbook for Universities, 176p. Energoatomizdat (1990)
5. Alabovskiy, A.N., Udima, P.G.: Submersible Combustion Devices. Publishing house of MPEI, 256p (1994)
6. Mattus, A.J.: Submergible torch for treating waste solutions and method there of. *Environ. Int.* **22**, 11 (1996) Oak Ridge, TN, United States Assigned to Martin Marietta Energy Systems Inc
7. Gurov, V.I.: Efficient heat supply of buildings based on submerged combustion of fuel. In: Gurov, V.I., Kurmosov, V.V., Shestakov, K.N. (eds.) Conversion in Mechanical Engineering, no. 5, pp. 77–78 (2001)
8. Tovazhnyansky, L.L.: Thermal power engineering of submerged combustion in solving problems of heat supply and ecology of Ukraine. In: Tovazhnyansky, L.L., Pertsev, L.P., Shaporev, V.P. et al. (eds.) Integrated Technologies and Energy Saving, no. 3, pp. 3–12 (2004)
9. Alabovskiy, A.N.: Submersible combustion apparatuses. In: Alabovskiy, A.N., Udyma, P.G. (eds.) 256p, MPEI, Moscow (1994)
10. Pioro, L.S., Pioro, I.L., Kostyuk, T.O., Soroka, B.S.: Industrial Application of Submerged Combustion Melters, 240pp. Fact Publishers, Kyiv-80, Ukraine

11. Pioro, I.L., Pioro, L.S., Rue, D., Khinkis, M.: Advanced melting technologies with submerged combustion. In: 73rd Conference on Glass Problems, Cincinnati, OH, USA, October 1–3, Paper # 101657, 21p (2012)
12. Glass Melting Technology: A Technical and Economic Assessment. Glass Manufacturing Industry Council, the US Department of Energy-Office of Industrial Technologies. Westerville, 292p (2004)
13. Guillen, D.P., Cambareri, J., Abboud Igor, A.W., Bolotnov, A.: Numerical comparison of bubbling in a waste glass melter. *Ann. Nucl. Ene.* **113**, 380–392 (2018)
14. Bai, L., Baker, D.R., Rivers, M.: Experimental study of bubble growth in Stromboli basalt melts at 1 atm. *Earth Planet. Sci. Lett.* **267**, 533–547 (2008)
15. Voskoboinikov, V.G., Kudrin, V.A., Yakushev, A.M.: *General Metallurgy*, 5th ed. Textbook for Universities, Revised and add. Metallurgy (1998)
16. Krivandin, V.A., Egorov, A.V.: *Thermal Work and Design of Furnaces in Ferrous Metallurgy*, 462p. Textbook for Universities, Metallurgy (1989)
17. Neshporenko, E.G., Kartavtsev, S.V.: *Issues of Energy Saving in the Extraction of Iron from Ores: Monograph*, 153p. GOU VPO “MSTU”, Magnitogorsk (2007)
18. Ulanovskiy, A., Taake, M., Belenkiy, A., Bursin, A., Chibizova, S.: Using an autonomous automated system from Phoenix TM for monitoring the temperature field of heated metal in metallurgical furnaces. *Ferrous Met.* **9**, pp. 56–60 (2019)
19. <http://metal-archive.ru/konverternye-processy/554-shema-kislorodno-konverternogo-processa-s-donnoy-produvkoy.html>
20. Kartavtsev, S.V.: *Intensive Energy Saving and Technical Progress of Ferrous Metallurgy: Monograph*, 311p. GOU VPO “MSTU”, Magnitogorsk (2008)
21. Dzhigiris, D.D., Polevoy, P.P., Polevoy, R.P.: Bathroom furnace for melting the main rocks. *Buil. Mater.* # 9 (1974)

Issues of Using Digital Twins of Gas Turbine Units at Their Facilities



Vitalii L. Blinov, Sergey V. Bogdanets, and Ilya S. Zubkov

1 Introduction

The digital technologies development such as numerical modeling, the Internet of Things, Big Data, Cloud computing, and Augmented/Virtual Reality provide a modern process of industry digitalization [1–8]. The digital transformation of industry affects all stages of the product life cycle: from development and production to operation and disposal. The result of digital technologies applying to a product at various stages of the life cycle is an aggregated entity—a Digital Twin (DT).

At the first stage of development, the digital twin concept was proposed by Michael Greaves in 2003 in accordance with his “white paper” [9–11]. The digital twin was defined in three dimensions: a physical object, a digital analog, and the connection of these two parts together [12, 13]. At the same time, the formation of this concept is implemented in the field of PLM and assumes that the interaction of virtual and real spaces occurs at all stages of the product life cycle (four main stages: Conceive, Design, Realize, and Service). In general, a digital twin is a virtual model of a product that is constantly corrected and reliably predicts its behavior throughout the entire life cycle. Due to the novelty of the concept, the universality of the term, and the lack of generally accepted terminology, its discrepancy arises. Various companies from various fields have their own vision of this issue.

This paper discusses the vision of this issue by some companies. The main goals and tasks that the digital twin of a gas turbine unit (GTU) should solve from the point of operating organization view are formulated.

Gas turbine units are one of the most common power generating machines. Implementation of digital twins of such complex technical objects as gas turbine units is not an easy task.

V. L. Blinov (✉) · S. V. Bogdanets · I. S. Zubkov
Department of Turbines and Engines, UrFU, Yekaterinburg, Russia
e-mail: v.l.blinov@urfu.ru

2 Materials. DT Concepts

According to the work of the authors from NTI SPbPU [14], the main goal of a digital twin is to reduce money and time costs for the design and production of a high-tech competitive product. The digital twin in this understanding is based primarily on the use of high-precision three-dimensional physical modeling programs.

According to researchers from NASA [15–18], a digital twin is an integrated multi-disciplinary, multi-scale, and probabilistic simulation of an aggregate or system that uses the most accurate physical models, sensors, history, etc., to show the corresponding physical object. Based on the information collected from sensors of real objects, a digital twin must create a long-term forecast of the unit or system resource. By predicting the system response, the digital twin should prevent modes that have never existed. In addition, according to NASA, a digital twin should have the ability to reduce damage and degradation of technical parameters by connecting self-recovery mechanisms or using recommendatory changes in the unit operating mode.

The goal of the Siemens digital twin [19] is to gain a deeper understanding and predict the performance characteristics of a product. In this case, a digital twin is necessary throughout the entire product life cycle in order to model, predict, and optimize the product and its manufacturing system until resources investing to the physical prototype of the product. The company distinguishes the digital twin of product, production, and operation.

In the concept of a digital twin, researchers at ANSYS [20, 21] put three basic ideas. First, a digital twin must have a real working prototype. Second, there must be a complete correspondence of a digital twin to its physical counterpart. Third, there must be a set of sensors for measuring physical quantities and the possibility of their further transfer to a digital twin. This task can be performed by the industrial Internet of Things and multiphysics simulation.

According to General Electric [22], a digital twin is a unique representation of individual products, systems, or processes in order to achieve improved business results. The main components of a digital twin are a product model, an analytical part, and a database. GE digital twin classification is based on facility or system scale. The digital twin of the product component, product, and system and the digital twin of the process are distinguished.

3 Results. DT of GTU

Based on the various technologies development directions analysis of digital twins of enterprises engaged in the design, manufacture, maintenance, and operation of gas turbine units, the following definition of DT GTU was formulated.

The digital twin of the GTU is a virtual model (copy) of the GTU, which is continuously updated and adjusted based on the results of full-scale and numerical experiments and reliably predicts their behavior throughout the entire life cycle,

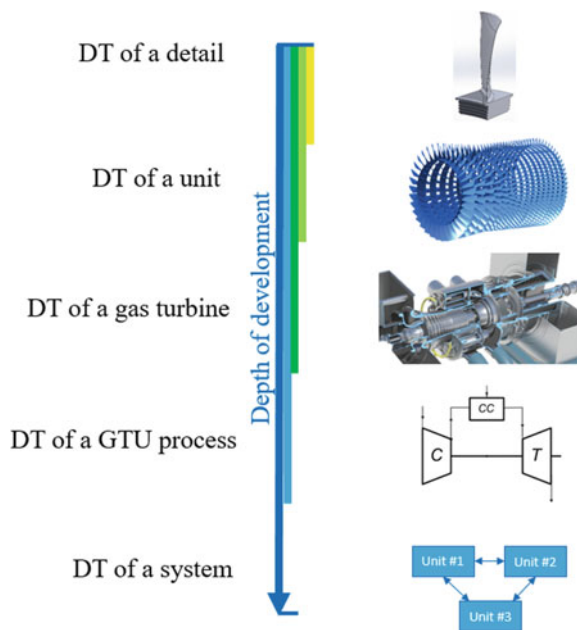
aimed at reducing time, money, and management costs at various stages of the life cycle.

From the operation point of view, this definition can be transformed into the following. The digital twin of the GTU at the operational stage is a virtual model (copy) of the GTU, which is continuously updated and adjusted based on the results of full-scale or numerical experiments and reliably predicts its behavior in various operating modes, aimed at increasing the efficiency and reliability of operation of the physical prototype and the system where it is set.

With regard to gas turbine equipment, it is very important to implement the design, storage, and interrelation between various digital information about the engine, its components, and main and auxiliary systems at all stages of the life cycle. This is particularly about newly developed GTU prototypes. In this case, a digital twin is created for each physical engine at the time of production and becomes its exact digital copy, going through all stages of the physical engine life cycle and changing along with the engine upgrade or modification, and at the end of its service life, it can be decommissioned along with it. Full digitization of already working (old) equipment, especially with a large operating time, can be difficult and not fully feasible (no need). For such units, it makes sense to create digital twins not of the entire facility, but only of its individual components and systems, relying primarily on operating experience and the needs for modernization of the existing park [23–25].

Thus, the following structure of the DT GTU at the operation facility can be distinguished, the implementation depth of which in each specific case will depend on the actual needs (Fig. 1).

Fig. 1 DT GTU structure in operation



Many note that a digital twin must evolve throughout the life cycle of its physical prototype. It follows that the division of DT into types/goals/tasks, etc., existing today from different companies, manufacturers, experts, scientific groups, etc., is nothing more than their vision and description of a separate stage in the existence of DT. It is necessary to distinguish (summarize) all previously formulated definitions of DT and build them from the DT development point of view. So, it is obvious that DT appears before its physical prototype (in some definitions, it is a prototype of a digital twin), and separate DT elements can be developed at the stage of the product idea creating (assessing the need to create a product, the effect of its implementation, etc.), then together with the production and testing of a real physical object, further filling and development of DT occur, similarly at the operation, repair, and maintenance; modernization; and decommissioning stages. At each subsequent step and life cycle stage, the DT continuously develops, filling it with new functions, setting new goals and objectives, developing a data exchange environment, etc., as well as developing data on the digital twin existence for understanding the DT theory. In comparison with the physical prototype, its DT can continue to evolve after the physical object disposal. Therefore, the DT life cycle can be much wider than its prototype. In addition, it is assumed that a digital twin may appear already at a certain stage in the prototype life cycle, for example, for old equipment or long-running systems. In this case, DT does not necessarily repeat the development path described earlier, but can be formed, starting with the modeling of specific units or processes, which are now more of interest (for example, the technical condition assessment of old equipment by means of processing and analysis of operating parameters in the real time).

This vision of DT allows to give a generalized definition of its concept and operate not with DT types, but with the stage of DT appearance and the direction of its development. This allows you to consider DT of different companies, regardless of their goals (whether it is equipment manufacturing, expert analysis, or equipment operation) and types of activities, to evaluate and compare DTs among themselves, etc. (to form the cost of DT depending on the depth of its development). The diagram is shown in Fig. 2.

4 Discussion. Targets and Goals of GTU DT

An important requirement in the gas turbine digital twin concept is that it should be a dynamic and constantly updated representation of a real physical unit (or its part, process, etc.). The static model of real space is not a digital twin. Therefore, the GTU digital twin should not be limited to collecting data obtained at the stage of their development and manufacture.

In operation, DT continuously receives data from the measuring equipment from the GTU. The mathematical description of the processes occurring in the elements of a GTU during operation can be a source of a large number of additional data. In this case, each mode of unit operation is supplemented with this data after appropriate

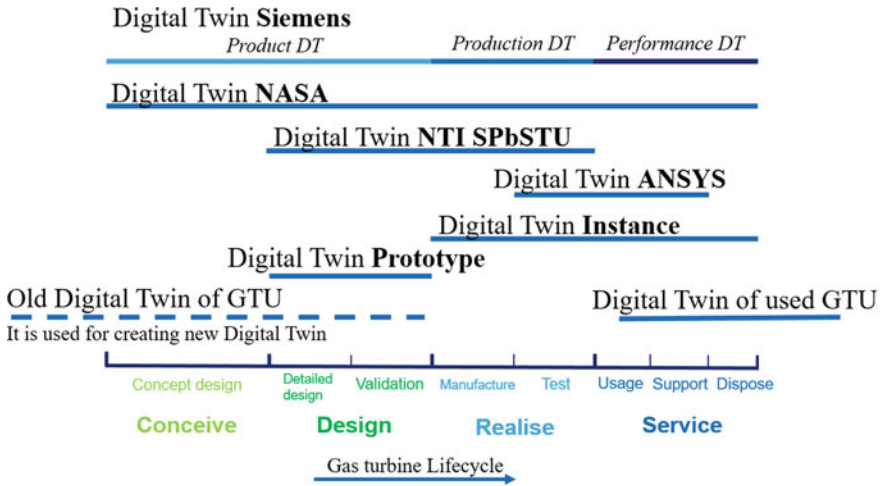


Fig. 2 Product life cycle and digital twins

calculations. It should be kept in mind that the GTU operating modes for solving a number of tasks should be filtered.

Another source of data can be the results of numerical modeling of the processes occurring in the GTU elements. Referring to both fluid dynamic and structural characteristics of parts and units. Today, there is an active digital technologies development and a constant growth in the numerical modeling use at all stages of the gas turbine engine life cycle, from the stage of research activity and design to the stages of full-scale testing and operation. An important issue in this case is the verification of numerical models. In addition, the process numerical model can become a part of the digital twin, when data from the GTU operation is fed into the model, and the model outputs the results of calculations. For example, in real time, it is possible to simulate the change in the stress–strain state of the turbine blades at different operating modes or to analyze the stall phenomena that occur in their flow paths, which is especially important for compressors. Analysis of the obtained data will allow reasonable decision-making on the operation and maintenance of the GTU. Thus, the main purpose of using the GTU digital twin at the operational stage can be to increase the efficiency and reliability of equipment operation due to the possibility of predicting its operation.

The main tasks that can be solved on the basis of digital twins technology are as follows: increasing the reliability of the GTU and increasing its resource by increasing the operating time with timely maintenance as per condition (as opposed to maintenance based on operating time); predicting and preventing damage to GTU elements and units; reducing the number of emergency shutdowns in operation; increasing the efficiency of the GTU using individual recommendations for operating modes; increasing the level of service in operation by ensuring and timely delivery of the necessary spare parts to reduce the downtime of the GTU for repair; formation of

directions for equipment modernization due to the development of technical solutions in the virtual space.

For the successful implementation of this technology at GTU facilities, a number of issues need to be solved. First, the underdevelopment of the data transmission system in the GTU/CAD/CAE system. To solve it, it is necessary to create a single digital platform that combines design data, numerical calculations, and tests. This will allow to establish reliable contact between various departments of the enterprise and reduce the number of errors in data transmission. Second, the limited bandwidth of information systems can become a problem. If the use of digital twins involves handling huge volumes of structured and unstructured data (Big Data), then for their successful transmission and processing, it is necessary to create high-bandwidth data transmission highways, as well as various cloud storage and transmission schemes. Third, to carry out a large number of calculations and fill digital models, large computing power is required. This is solved by the creation of high-power computing clusters, both on the basis of enterprises and corporations and on the basis of the country's leading institutions. It will be necessary to modify the existing data management systems, make more extensive use of the industrial Internet of things (IIoT), and, of course, not to forget about the security of data transmission. There is a need to create unified approaches and methods for digital twin use.

In connection with the above, the question of the development depth of digital twins is raised. This is especially true for equipment that is already in operation (in comparison with newly designed and manufactured equipment).

5 Conclusion

This paper analyzes the concept of a digital twin of various industrial companies. The main goals and objectives of the GTU digital twin are described, and its general structure and concept are determined. The digital twin technology is the logical result of digitalization in the industry. The use of DT GTU in operation will improve the efficiency and reliability of the units.

References

1. Gartner Identifies Five Emerging Technology Trends That Will Blur the Lines Between Human and Machine (2018). <https://www.gartner.com/en/newsroom/press-releases/2018-08-20-gartner-identifies-five-emerging-technology-trends-that-will-blur-the-lines-between-human-and-machine>
2. Prokhorov, A., Konik, L.: Digital Transformation. Analysis, Trends, World Experience, p. 368. OOO "Alliance Print" (2019)
3. Prokhorov, A., Lysachev, M., Borovkov, A. (scientific editor professor): Digital Twin. Analysis, Trends, World Experience, 1st edn., revised and enlarged, p. 401. OOO "Alliance Print" (2020)
4. Qinglin, Q., et al.: J. Manuf. Syst. <https://doi.org/10.1016/j.jmsy.2019.10.001>

5. Nikolaev, S., et al. (eds.): In: PLM 2018, IFIP AICT, vol. 540, pp. 193–203 (2018). https://doi.org/10.1007/978-3-030-01614-2_18
6. Tahan, M., et al.: Appl. Energy **198**, 122–144 (2017). <https://doi.org/10.1016/j.apenergy.2017.04.048>
7. Dawes, B., et al.: Digital Geometry to Support a Gas Turbine Digital Twin. <http://arc.aiaa.org>. <https://doi.org/10.2514/6.2019-1715>
8. Moroz, L., et al.: Application of Digital Twin for Gas Turbine Off-Design Performance and Operation Analyses. <http://arc.aiaa.org>. <https://doi.org/10.2514/6.2019-3913>
9. Grieves, M.: Digital twin: manufacturing excellence through virtual factory replication. Whitepaper (2014)
10. Grieves, M.: Origins of the Digital Twin Concept. Digital Twin: Mitigating Unpredictable, Undesirable Emergent Behavior in Complex Systems (Excerpt), https://www.researchgate.net/publication/307509727_Origins_of_the_Digital_Twin_Concept. Last accessed 2020/11/25
11. Grieves, M.: Digital Twin: Mitigating Unpredictable, Undesirable Emergent Behavior in Complex Systems (Excerpt). https://www.researchgate.net/publication/307509727_Origins_of_the_Digital_Twin_Concept
12. Tao, F., Zhang, M.: Digital Twin Driven Smart Manufacturing
13. Tao, F., Liu, A., Hu, T., Nee, A.Y.C.: Digital Twin Driven Smart Design
14. Borovkov, A.I., Gamzikova, A.A., Kukushkin, K.V., Ryabov, Yu.A.: Digital Twins in the High-Tech Industry. Brief report, 62p. SPb. Politech-Press (2019)
15. Glaessgen, E., Stargel, D.: The digital twin paradigm for future NASA and U.S. air force vehicles. In: 53rd Structures, Structural Dynamics and Materials Conference (2012). <https://ntrs.nasa.gov/archive/nasa/casi.ntrs.nasa.gov/20120008178.pdf>. Last accessed 2020/11/25
17. Shafto, M., Conroy, M., Doyle, R., Glaessgen, E., Kemp, C., LeMoigne, J., et al.: Draft Modeling, Simulation, Information Technology & Processing Roadmap. National Aeronautics and Space Administration (2010)
18. Tuegel, E.J., Ingraffea, A.R., Eason, T.G., Spottswood, S.M.: Reengineering aircraft structural life prediction using a digital twin. Int. J. Aerosp. Eng. (2011). <https://doi.org/10.1155/2011/154798>
19. DigitalTwin. <https://www.plm.automation.siemens.com/global/en/our-story/glossary/digital-twin/24465>. Last accessed 2020/11/25
20. Brook, P.A.: Digital twins based on the simulation of multiphysics processes. http://www.rem-mag.ru/upload_data/files/2019-0102/ANSYS.pdf. Last accessed 2020/11/25
21. Creating a Digital Twin for a Pump. <https://www.ansys.com/en-in/about-ansys/advantage-magazine/volume-xi-issue-1-2017/creating-a-digital-twin-for-a-pump>
22. What is a digital twin? https://www.ge.com/digital/applications/digital-twin?source=post_page
23. Komarov, O.V., Blinov, V.L., Shemyakinsky, A.S.: Thermal and gas-dynamic calculations of gas turbine units: a study guide, p. 164. Ural Publishing House University, Yekaterinburg (2018)
24. Blinov, V.L., Komarov, O.V., Zaslavskiy, E.A.: Estimation of the driven gas turbine unit technical performance using the standard measuring systems, vol. 178, p. 01044. In: E3S Web of Conferences (2020)
25. Murmanskii, I.B., Aronson, K.E., Blinov, V.L., Zhelonkin, N.V., Murmanskyy, B.E.: Digital diagnostic complex for power turbine units equipment. In: IOP Conf. Ser.: Mater. Sci. Eng. **643**, 012109 (2019)

Technical Condition Assessment of the Gas Turbine Units with Free Power Turbine



Vitalii L. Blinov, Oleg V. Komarov, Yuriy M. Brodov, and Ilya S. Zubkov

1 Introduction

In accordance with the development strategy of the Russian gas industry, one of the tasks is to reduce the cost of gas transition. Thus, up to 5–8% of the gas pumped through main gas pipelines (MGP) is used as fuel gas for the operation of mechanical drive gas turbine units (GTU) [1]. The fulfillment of this task is impossible without the implementation of a system aimed to ensure the most energy efficient and reliable operation of the gas-compressor units (GCU)—the main equipment of compressor stations (CS). Such a system, in particular, provides monitoring of the GTU technical condition (TC) [2].

Assessment of the gas turbine's technical condition, as well as any equipment, is of particular importance for optimal utilization, timely maintenance, increased MTBF, and overall service life.

Today, the gas transmission system has many diagnostic systems and devices intended to diagnose the condition of the GTU in real time. Most of them are aimed to identify dangerous phenomena and prevent emergency situations, as well as eliminate the risk for service personnel's life and health. These diagnostic methods include measuring the temperatures of lubricating and cooling liquids, elements of the hot gas path, anti-surge protection of compressors, and vibration measuring. In this case, any deviation of one of the parameters from the permissible deviation limits may mean the imminent emergency.

Nevertheless, there are not so many systems and algorithms aimed specifically at online monitoring of the efficiency and efficiency degradation rate of this equipment during the life cycle. In some cases, it is not possible to determine, for example, how much the maintenance has affected efficiency increasing. Real-time TC monitoring

V. L. Blinov (✉) · O. V. Komarov · Y. M. Brodov · I. S. Zubkov
Department of Turbines and Engines, UrFU, Yekaterinburg, Russia
e-mail: v.l.blinov@urfu.ru

can be used for remote monitoring of the GTU technical condition and early planning of repair operations.

In the modern gas transmission industry, the most widespread ones are two-shaft and multi-shaft GTU with a dedicated power turbine, unlike power GTUs, which are often used as single-shaft plants.

2 Materials and Methods

When assessing the GTU technical condition, it makes sense to consider and analyze both integral and local parameters of the TC (Table 1). Tracking the degradation of these parameters will make it possible to assess and predict the GTU technical condition with the prediction of probable malfunctions of separate units and a GTU as a whole [3, 4].

Integral parameters are those that characterize the operation of the GTU as a whole. For example, effective and available power, effective efficiency, technical condition coefficients for power, efficiency and fuel gas consumption, etc.

Table 1 Classification of integral and local parameters of the GTU technical condition

Parameter name	Classification
Technical condition coefficient for GTU power	Integral
Technical condition coefficient for GTU efficiency	Integral
Technical condition coefficient for GTU fuel gas consumption	Integral
Actual reduced power of GTU at nominal mode	Integral
Actual effective efficiency of GTU at nominal mode	Integral
Actual reduced fuel gas consumption of GTU at nominal mode	Integral
Reduced temperature of combustion products in the turbine (at any point of measurement)	Local
Temperature imbalance of combustion products after the last GTU turbine	Local
Air pressure behind the GTU axial compressor	Local
Polytropic efficiency of GTU axial compressor	Local
The efficiency of separate GTU units (calculated according to the measured parameters, the possibility of use depends on the type of gas turbine and the number of measured parameters; the efficiency values can be calculated approximately using mathematical models of GTU elements and used as auxiliary criteria of the technical condition)	Local
Reduced rotor speeds	Local
Vibration displacement and vibration velocity	Local
Local parameters (parameters measured for monitoring and control of separate GTU systems, for example, anti-icing, lubrication system, etc. The scope of measurements and recommendations for their control are provided by the GTU manufacturer)	Local

Local parameters are the TC parameters of separate GTU units (axial compressor, combustion chamber, gas turbine, bearings, etc.), as well as elements of these units (for example, a blade row). To assess the technical condition of separate units, the power generated or consumed by them, polytropic and adiabatic efficiency, qualitative and quantitative changes in the key parameters of these units operation under various conditions, and other factors are also used. In general, local parameters affect the integral ones.

Today, the technical condition coefficients (TCC) are most often used as the criteria for evaluating TC in operation. Based on the TCC data of the entire GCU fleet, a rational choice of load distribution of compressor yards, CS, and MGP in general is made. In addition, this criterion is used to control the quality of the unit repair. The TCC of a GTU can be determined by the power of the unit, its efficiency, and fuel gas consumption. For example, to estimate the TCC by power, it is required to establish the reduced available power, which a GTU develops in the actual technical condition, and refer it to the nominal (rated) power. The reduced available power is understood as the effective power, which is developed by a GTU, which has the actual condition, under standard station conditions when the nominal value of any parameter is reached.

The most widely used method for determining the power of a GTU is by the power consumed by a centrifugal gas compressor (CGC). For this, the head pressure developed by the CGC is determined by the “enthalpy” method or by the polytropic Schultz method [5] using measurements of the temperature and pressure of the compressed gas at the inlet and outlet of the CGC, as well as by the known gas composition. The critical influence in this case is the accuracy of temperature measurement. Another problem of this method is the accuracy of determining the process gas flow rate. The absence of individual measuring units for the GCU leads to the necessity to determine the CGC performance by other methods: by the pressure drop across various kinds of constriction device (a confuser or a suction chamber), or indirectly by the CGC characteristics. The first approach is associated with determining the exact confuser coefficient: such devices require individual calibration due to technological deviations in geometry, pressure taps installation locations, and differences in the piping of gas compressors, and such calibration in the absence of a more accurate flow meter in the unit is an impossible task. To improve the measurement accuracy, various flow meters are used, for example, an ultrasonic flow meter, but this requires specialized tests using expensive equipment. The application of the CGC gas-dynamic characteristics to determine the gas flow rate in most cases shows significant divergences in the data obtained from the actual values. This is due to the fact that when obtaining factory characteristics, the air is used as a working fluid, and then the obtained characteristics are recalculated from air to gas. In addition, inaccuracies can be caused by restrictions on the number of tests with a large range of characteristics, the lack of the CGC piping influence consideration.

In the last quarter of the twentieth century, Gazprom VNIIGAZ carried out the work to summarize the results of heat engineering tests of gas pumping units operated at CS. The authors [6] have made an explication of the generalized characteristics,

based on new aggregates. However, using this method, the particular gas turbine power determination accuracy may be unsatisfactory.

Other methods for calculating the power of a GTU do not use data on CGC operation. One of these methods assesses the available power and TCC from the shift in the GTU characteristics [7]. This method requires the presence of factory characteristics or characteristics obtained during acceptance tests carried out before the GTU is put into operation to check their compliance with the requirements of state standards and technical documentation. But, as a rule, a GCU manufacturer does not provide such characteristics in sufficient volume.

Moreover, GTU power can be determined from the heat balance compiled for the control volume [8]. This method is difficult to implement in operational conditions, it requires additional measurements, and its application for each GTU is almost impossible.

The methods described above are based on the thermo gas-dynamic parameters of the GCU operation. A different approach is implemented when determining power using a torque meter (TM). This approach has not found wide application, since it requires the use of expensive equipment, which, moreover, must be periodically sent to the factory for calibration.

Another trend is based on using parameters of a power turbine to determine the efficient power of a GTU. In the current paper, the authors present some results of this method application.

3 Results and Discussion

The perspective method for determining the effective power of a GTU is the approach described by the authors in articles [9, 10]. The feature of this approach is the use of standard measurements of the GTU operation parameters. It was a common knowledge that the effective power of a GTU is the power developed by a power turbine (PT). In the described work, the PT power is determined from the heat drop and the gas flow rate. In this case, gas-dynamic functions are used to calculate the gas flow rate.

This technique has been tested on several types of gas turbine units. Nowadays, more than 500 units of the studied types are in operation. The implementation procedure is currently in process. For this, verification of the design models was carried out on the basis of field tests of several units. The work was carried out on several units, representing different types and different powers: 10, 12, 16, 25, and 30 MW, as well as different purposes of engines: stationary, aero-, and marine derivative. For example, Figs. 1 and 2 show the test results of 30 and 10 MW GTU, respectively.

Figure 1 shows the experimental dependences for two GTU-30. Trend lines were plotted from the measured points and then parameters for the nominal exhaust temperature were determined. The coincidence of the power values determined by the proposed method [9, 10] and by VNIIGAZ [5] lies within 2% for both GTUs. Power

Fig. 1 Test data for GTU-30

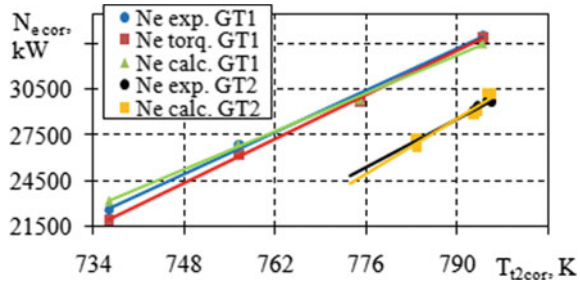
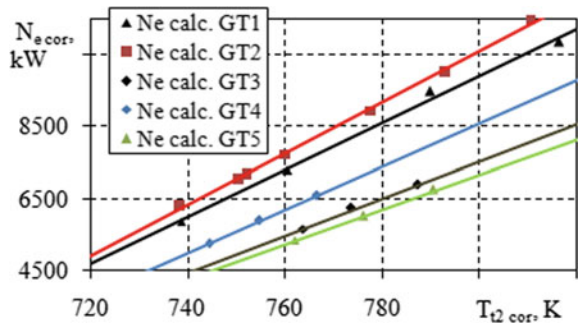


Fig. 2 Test data for GTU-10



was also determined for the GT1 using a torque meter (Ne torq.) [11]. R.M.S. deviation Ne torq. of powers determined by thermo gas-dynamic parameters does not exceed 2.5%. The deviation of the gas turbine power by several methods at once can be used as a reliability criterion of the data obtained in the gas turbine diagnostic systems, as well as the calibration of one approach relative to another.

Figure 2 presents statistical information for five units of GTU-10. All points were calculated according to the presented method [9, 10] based only on standard measurements with calibrated measuring instruments. The obtained values of the GTU power were also checked using the methodology [5] based on the test results. The lines shown on the chart are trends for their group of points. As can be seen, these engines have different technical conditions. This is mainly due to the fact that each of them has a different operating time after repair. Figure 2 shows that the shift of the trend line can be judged on the degradation of the technical condition of a particular unit. At the same time, it is not necessary to determine the exact value of the GTU power, and the main thing is to track its quantitative change (for example, in %). In addition, it is not necessary to start tracking from the “ideal” GTU condition. This feature can be used in diagnostic systems for assessing and predicting the GTU technical condition degradation [12–15].

The described technique for assessing technical condition can be used to quantify the effectiveness of repair and restoration measures based on normally measured parameters. It means that a GTU can be tested before and after maintenance

(compressor washing, restoration of radial clearances, etc.), and the results can be used to note the effect of the event.

4 Conclusion

The paper analyzes various methods for assessing the technical condition of gas turbine units with a free power turbine and considers the main indicators of the GTU technical condition. The method for assessing the coefficient of GTU technical condition by power and efficiency has been implemented, which has shown good convergence with experimental data obtained using measurements of the power consumed by a centrifugal compressor. For each type of GTU with a separate power turbine, it is theoretically possible to implement the principle of monitoring the technical condition in real time using normally measured parameters. The considered method can be used to quantitatively assess the effectiveness of repair measures, which is extremely important for a large gas transmission system operating more than a thousand gas pumping units. Tracking the degradation of technical condition indicators will allow us to assess and predict the technical condition of the GTU with the prediction of probable malfunctions of separate units and GTU as a whole.

References

1. Revzin, B.S.: Gas-Pumping Units with a Gas-Turbine Drive (transl.). UGTU-UPI, Ekaterinburg (2002)
2. Shaikhutdinov, A.Z., Zhdanov, S.F., Salnikov, S.Y.: Scientific and Technical Policy of Gazprom in the Field of Gas Pumping Equipment, pp. 11–16. Consumers-Manufacturers of Compressors and Compressor Equipment (2010)
3. Murmanskii, I.B., Aronson, K.E., Blinov, V.L., Zhelonkin, N.V., Murmanskii, B.E.: Digital diagnostic complex for power turbine units equipment. IOP Conf. Ser.: Mater. Sci. Eng. **643**, 012109 (2019)
4. Burnes, D., Kurz, R.: Performance degradation effects in modern industrial gas turbines. In: Proceedings of Zurich Global Power and Propulsion Forum (2018)
5. Shchurovsky, V.A., Sinitsyn, Y.N., Korneev, V.I., Cheremin, A.V., Stepanov, G.S.: Methodical instructions for carrying out heat engineering and gas-dynamic calculations when testing gas turbine gas-pumping units. VNIIGAZ, PR 51-31323949-43-99, 26p. Moscow (1999)
6. Krotov, S.I., Martynov, A.I.: Application of generalized characteristics of gas turbine units in determining the technical condition coefficients. Territory Oilgaz **2**, 44–55 (2012). <http://neftegas.info/tng/vypusk-2-2012-g/>
7. Vanchin, A.G.: An express method for assessing the available power of a gas turbine unit and the technical condition coefficient for power based on the regularities of the shift in the characteristics of a gas turbine unit when its technical condition changes. Electron. Sci. J. “Oil Gas Bus.” **5**, 287–292 (2012). <http://www.ogbus.ru>
8. Gas turbines, Test methods, Acceptance tests, ISO/DIS 2314 (2007)
9. Blinov, V.L., Komarov, O.V., Zaslavskiy, E.A.: Estimation of the driven gas turbine unit technical performance using the standard measuring systems. In: E3S Web of Conferences, vol. 178, p. 01044 (2020)

10. Komarov, O.V., Blinov, V.L., Sedunin, V.A., Skorochoodov, A.V.: Parametrical diagnostics of gas turbine performance on site at gas pumping plants based on standard measurements. In: Proceedings of ASME Turbo Expo, GT2014-25392 (2014)
11. Millingen, R.D. van, Eng, C., Millingenp, J.D. van: Phase shift torquemeters for gas turbine development and monitoring. In: International Gas Turbine and Aeroengine Congress and Exposition. Orlando (1991)
12. Kurz, R., Brun, K.: Degradation in gas turbine systems. *J. Eng. Gas Turbines Power* **123**, 70–77 (2001)
13. Botros, K.K., Golshan, H., Rogers, D.: Effects of Engine Wash Frequency on GT Degradation in Natural Gas Compressor Stations. ASME Turbo Expo (2013)
14. Ahsan, S., Lemma, T.A.: Remaining useful life prediction of gas turbine engine using autoregressive model. In: MATEC Web of Conferences, vol. 131, p. 04014 (2017)
15. Loboda, I., Miró Zárata, L.A., Yepifanov, S., Maravilla Herrera, C., Pérez Ruiz, J.L.: Estimation of gas turbine unmeasured variables for an online monitoring system. *Int. J. Turbo Jet Eng.* **37**(4), 413–428 (2020)

Fault Isolation in Digital Instruments and Devices Used in Power-Engineering Systems



Pavel Pavlov, Valery Butakov, Azat Khusnutdinov, Aida Abdullina, Eve Snezhinskay, and Ivan Cherepenkin

1 Introduction

Modern power-engineering systems (PES) refer to sophisticated engineering systems (SES) and consist of a variety of sub-systems (SS) for various purposes and modes of operation, including digital controls, monitoring, and testing.

Test gears (TG) are the most important and sophisticated tools used in the control and test system (CTS) at power-engineering sites. These sub-systems shall meet the applicable reliability requirements [1, 2].

They are primarily designed for detection, search, and isolation of failures that may occur in the control and test system.

Test gears may fail while in service. For prevention of failures followed by correction actions, there are a few approaches:

- Preventing the occurrence of failures.
- Improving the maintainability.
- Ensuring the resistance of the hardware to failures (fault tolerance).

The first approach does not completely exclude the occurrence of failures at this stage of the development of science and technology. The introduction of the second approach hinders the performance of the sub-system, and the non-availability of backup components (units) will disrupt it. The third approach relates to fault tolerance, which is understood as the capacity of test gears to continue their performance with a probability not lower than a given one in the event of internal malfunctions (failures). The fault tolerance is based on the processes of testing and making a multi-alternative decision on the condition of the test gears following the results of its self-testing [3].

P. Pavlov · V. Butakov · A. Khusnutdinov (✉) · A. Abdullina · E. Snezhinskay · I. Cherepenkin
Kazan State Power Engineering University, Kazan, Russia

In modern power-engineering systems, the fault tolerance of their test gears is not fully used as this is not provided for by the existing self-testing philosophy and applicable operating manuals (OM). However, not all the malfunctions cause the failure of test gears to perform, since some of them cause only the loss of a part of their inherent functions. Therefore, the third approach is the most promising one, specifically toward test gears used in current power-engineering systems.

Thus, the need to ensure the fault tolerance of test gears by means of the automated detection and isolation of failures is an actual scientific challenge that requires to design test gears with a flexible self-testing algorithm, which can vary depending on the type of failure and the operating conditions of the sun-system. Such a self-testing algorithm should take into account the functional configuration of test gears and the ability to assess the influence of failure in their various functional parts on the result of the performance verification and determine the feasibility of the entire system to continue its performance [4].

2 Analysis of Purposes and Functions Performed by Test Gears and Features of Its Functional Configuration

Test gears together with the control and test system, auxiliary equipment, and other components and systems used in the power-engineering system ensure the performance of a number of primary and secondary purposes and functions. Distinguishing between the concepts of the purpose and the functions of the sub-system comes hereinafter [5].

The purpose refers to a set of operations that enable the achievement of one of its final goals.

The function means a set of operations that enable the achievement of one of the goals within this purpose. At the same time, test gears perform their individual functions off-line.

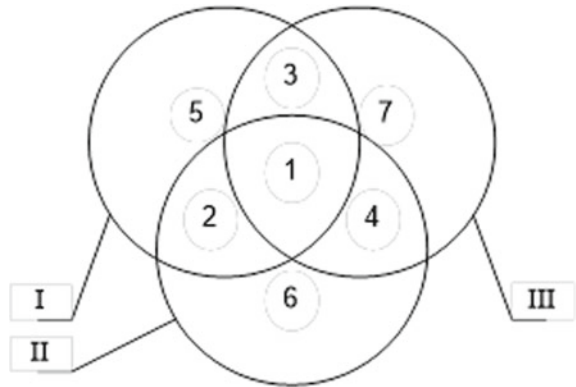
Analyzing the functions performed by test gears identifies their key purposes:

1. Testing and setting up the control and test equipment for its intended use.
2. Testing the availability of the control and test equipment.
3. Testing the performance of the control and test equipment.

Each purpose performed by test gears is implemented by a certain set of hardware, i.e. verification and setup of control and test system for its intended purpose require test and setup equipment (TSE). The performance test equipment (PTE) is used for testing the performance. The availability test equipment (ATE) is used for testing the availability. The combination of TSE, PTE, and ATE with self-testing components represents the entire test gear.

In terms of the design, the test gears do not always coincide with their functional purpose, i.e. components of a functional device can be mounted in different units or parts [6, 7].

Fig. 1 Model of the test gear configuration in the form of three overlapping functional parts



At the same time, some of these general operations to be performed at the setup stage are not mandatory with regard to ensuring the performance of key purposes of the control and test system.

Making these operations possible rides on the need for providing safety in setting up the operation of a definitely healthy control and test system. Each test and control operation is possible by using some test gear components [8]. Therefore, the coincidence of operations at testing healthy condition and correct performance and setting up the auxiliaries and control and test equipment determines the possibility of using some of the test gears for addressing all the three purposes.

Thus, the test gear configuration model, from the point of view of performing the above purposes and taking into account the coincidence of some of the operations to make these purposes happen, can be represented as a set of three overlapping functional parts of a test gear, as shown in Fig. 1 (I—TSE; II—ATE; III—PTE).

This representation of the test gear configuration gives its splitting, in general, into seven subsets (1-A&P SU, 2-A&SU, 3-P&SU, 4-A&P, 5-SU, 6-AT, and 7-PT). In Fig. 1, each point a_i inside the circles displays a certain component of the test gear $[a_i^{1-7} \in A(TG)]$, where

- segment 6 represents a set of test gear components used only in testing the availability of the control and test system $[a_i^6 \in A(AT)]$;
- segment 5 represents a set of components that are applicable only in testing and setting up the control and test system for its intended purpose $[a_i^5 \in A(SU)]$;
- segment 7 represents a set of test gear components necessary only for testing the performance of the control and test system $[a_i^7 \in A(PT)]$;
- segment 2 represents a set of test gear components, which are used both in testing the availability and in setting up the control and test system for its intended purpose $[a_i^2 \in A(A\&SU)]$;
- segment 3 represents a set of test gear components that are applicable in testing the performance and setup of the control and test system for its intended purpose $[a_i^3 \in A(P\&SU)]$;

- segment 4 represents a set of components necessary for testing the availability and performance of the control and test system [$a_i^4 \in A(A\&P)$];
- segment 1 represents a set of components that are applicable in all three purposes of test gears [$a_i^1 \in A(A\&P\ SU)$].

The consistency between those test gear parts can be quite varied depending on how the components of the test and setup equipment are used in testing auxiliaries and control and test system and how the procedures of availability and testing as well as setting up the control and test system for its intended purpose synchronize.

3 Analysis and Selection of Performance Indicators for Self-Testing of Test Gears

Given the importance of the functions and purposes of test gears, they are subject to increased requirements for the availability and reliability of the results of testing the condition of the control and test system. Actions taken to meet these requirements are carried out both at the design and production stage of test gears, and while in service [9, 10].

The main way to ensure high methodological accuracy of test gears (high tool accuracy of test gears used in the existing control and test systems can be achieved through the accuracy of the readings during their periodic calibration) through detection of latent failures is the self-testing (ST) of test gears.

Self-testing of test gears is the determination of the type of condition of test gears using self-testing tools (STT) and/or special procedures.

The existing self-testing function of test gears in sophisticated control and test systems discharges a two-alternative assessment of test gear condition, i.e. in multi-dimensional space, there are two condition vector regions that correspond to two classes of availability of test gears—healthy or unhealthy. Further, the base equipment (BE) means that part of control and test equipment is used in testing and setting it up for its intended use [11, 12].

The availability of only two alternative solutions based on the results of self-testing increases its negative aspects in relation to the probability of successful operation of the power-engineering system with healthy base equipment (BE).

Such a conclusion can be drawn from considering the equation for the probability of successful setup (P_{SSU}) of power-engineering system, which in general can be represented as

$$P_{SSU} = P_{AO} \cdot P_{(\tau)}, \quad (1)$$

where P_{AO} is the probability of successful setup of the control and test equipment (base equipment + test gears), i.e. its admission to operation according to the results of testing base equipment and self-testing test gears;

$P_{(\tau)}$ is the conditional probability of failure-free operation of the base equipment and test gears that successfully completed the setup stage, during the performance.

Or

$$P_{SSU} = P(F) \cdot P(H/F) \cdot R(F) \cdot R(H/F), \tag{2}$$

where $P(F)$, $R(F)$ is the probability of obtaining the result “fit” for testing the base equipment and control and test equipment, respectively;

$P(H/F)$ is the conditional probability of the state of health of base equipment recognized as fit according to the output of test gears;

$R(H/F)$ is the conditional probability of the state of health of test gears according to the results of self-testing, provided that the result is “fit”.

Given the possibility of representing test gears as a set of functional parts (test gears = setup + test), the following equations can be written for these probabilities as:

$$P(F) = P_{NF}^T \cdot P_{NF}^{TE} \cdot P_{\tau}^T \cdot P_{\tau}^{TE} \cdot (1 - P_{FR}^{BE}); \tag{3}$$

$$P(F) = P_{NF}^{TG} \cdot P_{NF}^{STT} \cdot P_{\tau}^{TG} \cdot P_{\tau}^{STT} \cdot (1 - P_{FR}^{TG}); \tag{4}$$

$$P(H/F) = P_{NF}^{UT} \cdot (1 - P_{UF}^{BE}); \tag{5}$$

$$R(H/F) = P_{NF}^{UT} \cdot (1 - P_{UF}^{TG}); \tag{6}$$

where

- P_{NF}^T, P_{NF}^{UT} is the a priori probability of non-failure in the tested and untested parts of base equipment;
- P_{NF}^{TG}, P_{NF}^{TE} is a priori probability of non-failure in test gears and test equipment;
- R_{NF}^{STT} is a priori probability of non-failure in self-testing tools (STT);
- $P_{\tau}^T, P_{\tau}^{TE}, P_{\tau}^{TG}, P_{\tau}^{STT}$ is the probability of non-failures during the test period in the tested part of base equipment, test equipment, test gears, and self-testing tools, respectively;
- P_{FR}^{BE}, P_{FR}^{TG} is the probability of false rejection of base equipment and test gears, respectively;
- P_{UF}^{BE}, P_{UF}^{TG} is the probability of undetected failure of base equipment and test gears, respectively.

Taking (3), (4), (5), and (6) into account, Eq. (2) becomes

$$P_{SUU} = P_{NF}^{BE} \cdot P_{\tau}^T \cdot P_{NF}^{TE} \cdot P_{\tau}^{TE} \cdot P_{NF}^{TG} \cdot R_{NF}^{STT} \cdot P_{\tau}^{TG} \cdot R_{\tau}^{STT} \times (1 - P_{FR}^{BE}) \cdot (1 - P_{UF}^{BE}) \cdot (1 - P_{FR}^{TG}) \cdot (1 - P_{UF}^{TG}). \tag{7}$$

Factor $R_{NF}^{SST} \cdot P_{\tau}^{TG} \cdot R_{\tau}^{SST} \cdot (1 - P_{FR}^{TG}) \cdot (1 - P_{UF}^{TG})$ in (7) directly describes the drawback of the self-testing function of test gears, and the factor $P_{\tau}^T \cdot P_{NF}^{TE} \cdot P_{\tau}^{TE} \cdot (1 - P_{FR}^{BE}) \cdot (1 - P_{UF}^{BE})$ describes drawbacks of base equipment test.

The occurrence of failures in base equipment and test gears caused by testing and self-testing is described by probabilities $P_{\tau}^T, P_{\tau}^{TE}, P_{\tau}^{TG}, R_{\tau}^{SST}$.

The possibility of failures in the test gears and self-testing tools by the time of verification commencement, which makes it impossible to get the result “fit”, is described by probabilities $P_{NF}^{TE}, P_{NF}^{TG}, R_{NF}^{SST}$.

If the self-testing of test gears and the testing of base equipment is not performed, then Eq. (7) becomes

$$P_{SSU} = P_{NF}^{BE} \cdot P_{NF}^{TE}, \quad (8)$$

that is, the probability of successful operation will be determined only by the a priori reliability of base equipment and test equipment.

A comparison of Eqs. (7) and (8) shows that self-testing with a two-alternative assessment of test gear condition, in relation to a single control and test system, results in a decrease in the probability of successful setup of the entire power-engineering system.

Since the discussed sophisticated engineering system is designed to meet specific goals, failures that occur in various functional parts do not always cause the inability to perform all its key functions. At the same time, it goes into a state, in which it is able to perform specific tasks, i.e. to function with different levels of quality.

As a criterion for evaluating the efficiency of setting up control and test system, it is advisable to use the probability of completing the task (P_{TP}). This indicator is applicable if the change in the system performance characteristics causes not a complete, but only a partial decrease in its performance [3, 13, 14].

Then, in general terms, from the standpoint of testing and self-testing operations, this indicator can be represented as

$$P_{TP} = P_{SSU} = P_{AO} \cdot P_{(\tau)}. \quad (9)$$

Analyzing the Eqs. (1), (2), (7), (8), and (9) shows that conducting self-testing:

on the one hand, it reduces the probability P_{TP} by reducing P_{AO} (false rejection and occurrence of failures due to testing and self-testing);

on the other hand, it increases P_{TP} due to the increase in $P(\tau)$ (detection of latent failures of the control and test system).

It is a matter of fact that there is an optimal self-testing of test gears, the results of which will determine the optimal scope of test gears to test base equipment if the following conditions have been fulfilled:

$$P_{TP} \geq P_{TP}^R, \quad (10)$$

here P_{TP}^R is the required value of the probability of completing the purpose set forth in the performance specification at the design stage of a power-engineering system.

Based on the goals of testing and self-testing, the probability of completing the task of the power-engineering system means a posteriori probability of non-failures in the control and test equipment necessary and sufficient for the successful operation of the power-engineering system. Applying Bayes' theorem [15] yields the following equation for P_{TP} :

$$P_{TP} = P(H/F) = \frac{P(H) \cdot P(F/H)}{P(F)}, \tag{11}$$

where

- $P(H)$ is the absolute probability of non-failure in the control and test equipment;
- $P(F/H)$ is the conditional probability of getting a result “fit” for the control and test system, provided that the healthy equipment is subject to inspection;
- $P(F)$ is the probability of getting the result “fit” when testing the control and test system.

Taking the total probability formula into consideration, Eq. (11) will become

$$P(H/F) = \frac{P(H) \cdot P(F/H)}{P(H) \cdot P(F/H) + P(FL) \cdot P(F/FL)}, \tag{12}$$

where

- $P(FL)$ is the absolute probability of failure in the control and test equipment;
- $P(F/FL)$ is the conditional probability of getting the result “fit”, provided that the faulty control and test equipment is subjected to inspection.

The equations for the probabilities $P(H) \cdot P(F/H)$ and $P(FL) \cdot P(F/FL)$ can be written as follows:

$$P(H) \cdot P(F/H) = P_{NF}^{BE} \cdot P_{NF}^{TG} \cdot R_{NF}^{STT}; \tag{13}$$

$$P(FL) \cdot P(F/FL) = P_{NF}^T \cdot P_{NF}^{TE} \cdot R_{NF}^{STT} \cdot (1 - P_{NF}^{SE} \cdot P_{NF}^{UT}). \tag{14}$$

Substituting (13) and (14) in (12) yields

$$P(H/F) = \frac{1}{1 + \left(\frac{1 - P_{NF}^{SE} \cdot P_{NF}^{UT}}{P_{NF}^{SE} \cdot P_{NF}^{UT}} \right)}. \tag{15}$$

Terms of this equation describe only the influence of the fullness of self-testing of test gears on how the control and test system is set up, i.e. are part of the methodological reliability of testing.

Equation (15) yields that the probability $P(H/F)$ does not explicitly contain the characteristics of the self-testing tools of test gears, which makes it difficult to use self-testing in evaluating the efficiency of the existing self-testing strategy.

Therefore, to evaluate the efficiency of various options for self-testing tools, the probability of obtaining a result “fit” for self-testing in the process of getting test gears available, which has the following form:

$$\begin{aligned}
 P(F) &= P(H) \cdot P(H/F) + P(FL) \cdot P(F/FL) = \\
 &= P_{NF}^{BE} \cdot P_{NF}^{TG} \cdot R_{NF}^{STT} + P_{NF}^T \cdot P_{NF}^{TE} \cdot R_{NF}^{STT} \cdot (1 - P_{NF}^{SE} \cdot P_{NF}^{UT}) \\
 &= P_{NF}^T \cdot P_{NF}^{TE} \cdot R_{NF}^{STT}.
 \end{aligned} \tag{16}$$

The probability $P(F)$ will decrease with an increase in the number of output parameters that are covered by testing, the depth of troubleshooting test gears, as well as with a decrease in the reliability of self-testing tools of test gears.

Thus, the application of the above criteria enables evaluating the efficiency of strategies for applying self-testing of test gears, taking into account the completeness, depth, and reliability of the self-testing tools. Therefore, the challenge of optimizing the process of testing and self-testing of the control and test equipment is to meet the following conditions:

$$\begin{cases} P(H/F) \geq P_{TP}^R; \\ P(F) \rightarrow max. \end{cases} \tag{17}$$

This model of evaluating the efficiency of automated control systems is used in the case of testing facilities which failure can cause serious consequences dangerous to human life (12). Such facilities to be tested also include power-engineering systems.

4 Conclusion

The analysis of the purposes performed by test gears shows that test gears use a certain set of functions as a function of a specific purpose. Each function of test gears is implemented by a certain set of hardware, which partially overlaps with each other. As a result, the test gear configuration can be represented as a set of functional parts, each of which is necessary for a specific function or set of functions. This makes it possible to assess the influence of a particular failure, taking into account its belonging to a certain functional part, on the ability of test gears to perform as appropriate and, using a change in the algorithm of test gear functioning, to exclude inspections that cover damaged areas (components), i.e. to use the fault tolerance of the equipment [16, 17].

References

1. Korolev, N., Solovlev, S.: IOP Conf. Ser.: Mater. Sci. Eng. **177**(1), 012007 (2017)
2. Litvinenko, R., Aukhadееv, A., Zalyalov, R.: Mir transporta I tekhnologicheskikh mashin **3**(58), 108–114 (2017)
3. Zagirnyak, M., Melnykov, V., Kalinov, A.: Przegląd Elektrotechniczny **95**(1), 141–144 (2019)
4. Kashapov, N., Sabitov, L., Litvinenko, R., Auhadeev, A., Gatiyatov, I.: IOP Conf. Ser.: Mater. Sci. Eng. **570**(1), 012043 (2019)
5. Fandееv, V., Baymeeva, D., Safiullina, V.: E3S Web Conf. **216**, 01063 (2020)
6. Budkin, A., Soldatenko, S.: Kontrol' i diagnostika obshchej tekhniki 44–45 (1992)
7. Shprekher, D., Kolesnikov, E.: FarEastCon **2018**, 8602600 (2018)
8. Khusnutdinova, E., Pavlov, P., Fandееv, V., Khizbullin, R., Khusnutdinov, A., Cherepenkin, I.: IOP Conf. Ser.: Mater. Sci. Eng. **915**, 012032 (2020)
9. Tarasov, A.: Nadezhnost' **2**(37), 24–29 (2011)
10. Sabitov, L., Pavlov, P., Fandееv, V., Butakov, V., Khusnutdinov, A., Siyetinskaya, A.: IOP Conf. Ser.: Mater. Sci. Eng. **915**, 012047 (2020)
11. Truhanov, V., Sultanov, M., Kuhtik, M., Gorban, Yu.: Nadezhnost' i bezopasnost' energetiki **11**(3), 235–240 (2018)
12. Osadchij, E., et al.: Proektirovanie sistem diagnostiki (1984)
13. Voropaj, N., Fedotova, G.: Nadezhnost' i bezopasnost' energetiki **11**(4), 280–287 (2018)
14. Martynov, A., Nikiforova, D.: Nadezhnost' i bezopasnost' energetiki **4**, 50–54 (2009)
15. Kulikov, A., Osokin, V., Papkov, B.: Vestnik NGEI **1**(90), 123–136 (2018)
16. Papkov, B.: Issledovanie i obespechenie nadyozhnosti sistem energetiki **68**, 441–452 (2017)
17. Auhadeev, A., Idiyatullin, R., Kisneeва, L., Litvinenko, R.: IOP Conf. Ser.: Mater. Sci. Eng. **643**(1), 012028 (2019)

Study of the Orifice Inserts Influence on the Multisection Vacuum Condenser Operation Under Uneven Heating Conditions



A. Yu. Kartuesova, A. V. Ptakhin, and V. S. Krylov

1 Introduction

Any violation of the condensing unit normal operation, caused by one reason or another, manifests itself, first, in the exhaust steam pressure increase compared to its standard characteristic value for the given operating conditions [1]. Degradation of the condensing unit operation can be caused by various factors, analysis and comparison of which allows determining the true cause of the deterioration of the condensing unit efficiency and taking measures to restore normal operation. Vacuum condensers design for steam turbines is carried out under such calculation conditions, when all parts of the condenser are cooled equally, the consumption of cooling water (air—for air condensers) and air suction are also equal. Deviation of operation parameters from the design operation mode occurs for several reasons, one of which is dirtying of the heat exchange surface. For multisection air condensers with a large number of sections, the cause of uneven heat removal may be section fans malfunctioning [2–4].

Analysis of the condensing unit equipment failures that cause shutdowns of steam turbine units (STU) shows that up to 56% of such failures are caused by condensers; 23% of STU shutdown cases are associated with ejector failures; circulation and condensate pumps account for 10–11% of cases. It should be noted that almost every failure (up to 96%) of the ejector causes turbine shutdown.

The specific number of ejector failures per turbine per year is, depending on the type of turbine, from 0.036 to 0.098. Thus, the ejectors' reliability is of great importance for the stable operation of the STU condensing unit; the influence of ejectors is more significant than that of circulation or condensate pumps [5–7].

A. Yu. Kartuesova (✉) · A. V. Ptakhin · V. S. Krylov
CJSC Scientific-Production Implementation Enterprise “Turbocon”, st. Komsomolskaya Grove,
43, 248010 Kaluga, Russia
e-mail: turbocon@kaluga.ru

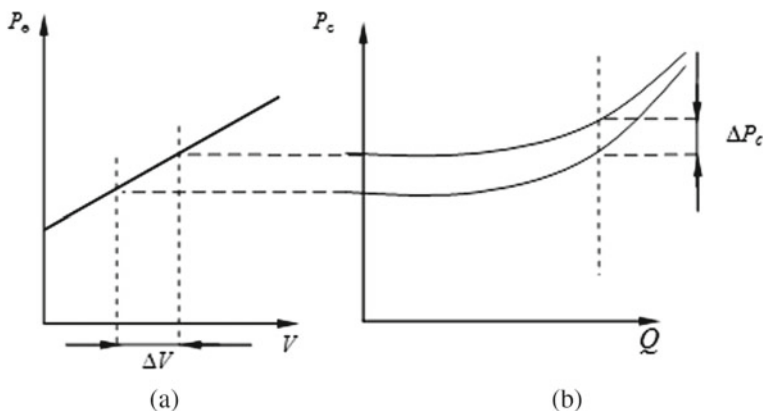


Fig. 1 Interaction of the air removal device with the condenser with the cooling water flow rate decrease in one of its parts: **a** the ejector characteristic (the dependence of the volumetric air flow rate on the pressure at the inlet to the ejector); **b** the condenser characteristic (the heat removal dependence on the condensation pressure)

One of the uneven cooling consequences is the additional volume of non-condensed steam at the condenser outlet, which then enters the ejector. This leads to the pressure increase at the ejector suction and, consequently, to the condenser characteristic shift into the higher-pressure zone with an increase in the condenser pressure, as shown in Fig. 1.

There is a close connection between the condenser operation and that of the air removal device (steam-jet/water-jet ejector or water-ring pump), which manifests itself in all condensing unit operating modes. Any change in the condenser operating mode causes a temperature change of the vapor-air mixture sucked from it and, consequently, a change in the suction side pressure of the air removal device and the pressure in the condenser.

The water-jet ejector characteristics differ significantly from the steam-jet ejector characteristics: firstly, for a water-jet ejector, the suction pressure depends on the working water temperature, and, secondly, the water-jet ejector operates with an almost constant volumetric efficiency only suctioning dry air [8–11].

The main advantages of a water-jet ejector over a steam-jet one are the following: design simplicity, the intermediate and end heat exchangers absence, the possibility of vacuum gaining regardless of the steam parameters and its consumption by the plant. But a water-jet ejector consumes significantly more water than the steam-jet one; the condensate loss in a water-jet ejector is also greater, as it is necessary to install a lift pump for its operation.

When orificing the steam–air mixture (SAM) at the condenser outlet, the steam mass proportion in the mixture decreases, the air flow remains constant, therefore, the pressure in front of the ejector will decrease, lowering the pressure in the condenser. Thus, if a low resistance orifice is placed at the outlet of each heat exchange module

of the condensing unit, then due to hydraulic losses in it, the flow of non-condensed steam into the ejector will decrease [12].

2 Materials and Methods

The purpose of the work was a computational and experimental study of the joint operation of the condenser and the gas removal device in the conditions of uneven heat removal and the development of technical solutions to improve the thermal efficiency.

Tasks:

- development and justification of a technical solution to improve the efficiency of the system for removing the steam–air mixture from the condenser based on the introduction of orifice inserts and the use of steam-jet ejectors;
- experimental study of the efficiency of using orifice inserts in the gas exhaust system of a steam–air mixture of vacuum condensers with volumetric gas exhaust devices with uneven cooling of the heat exchange surface and the presence of suction air in different zones;
- experimental determination of the value of the optimal steam diameter for the system under study;
- development of recommendations for calculating the optimal orifice diameter for multisection systems of vacuum condensers, including air-condensing installations with a large number of fans.

3 Results and Discussions

A method was developed to calculate the optimal orifice diameter for multisection condensers under a given uneven cooling. Figure 2 shows a diagram of an air-condensing unit (ACU) with n number of sections.

The change in steam velocity along the length of the pipe can be described by the formula

$$w = w_0[(1 - x)(1 - \bar{l}) + x] \quad (1)$$

Pressure loss considering the change in velocity along the length of the pipe during steam condensation:

$$\Delta p = \Delta p_0 \left(\frac{(1 - x)^2}{3} + x(1 - x) + x^2 \right) = \Delta p_0 C_x \quad (2)$$

Parameter C_x depends on the value of the flow rate mass steam content.

Then $\Delta p = K w_0^2 C_x$ —condensation pressure loss.

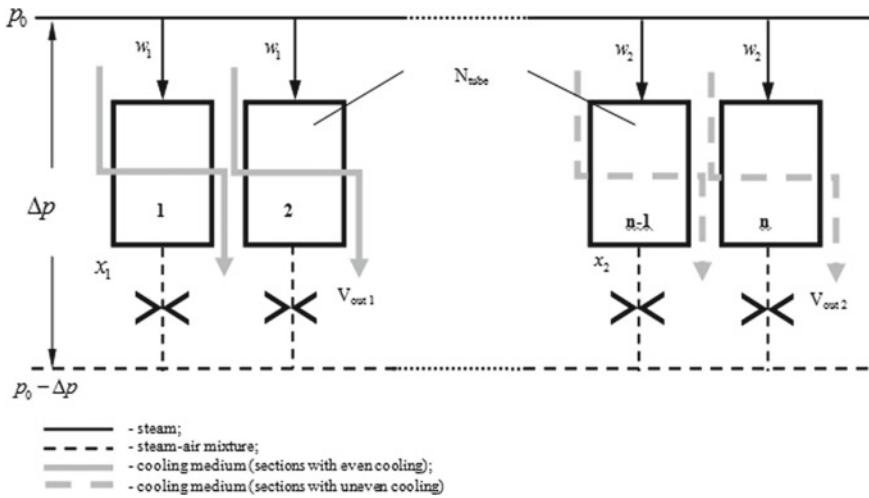


Fig. 2 ACU scheme with n number of sections

Let us specify the velocity, flow rate and pressure loss of steam for the air-conditioning unit with the number of sections n_0 in Fig. 2, where the parameters are set with indices 1 for sections with even cooling and with indices 2 for sections with uneven cooling.

$$K = \lambda \frac{l}{d} \frac{\rho}{2} L = \xi \frac{\rho}{2} n_t \left(\frac{d_t}{d_{or}} \right)^4 \quad (3)$$

For sections with even cooling $w_1; x_1$

$$\begin{aligned} \Delta p_t &= K w_1^2 C_{x1} \\ \Delta p_{or} &= L w_1^2 x_1^2 \\ \Delta p_{\Sigma 1} &= K w_1^2 C_{x1} + L w_1^2 x_1^2 = K w_1^2 \left(C_{x1} + \frac{L}{K} x_1^2 \right) \end{aligned} \quad (4)$$

For sections with uneven cooling $w_2; x_2$

$$\begin{aligned} \Delta p_t &= K w_2^2 C_{x2} \\ \Delta p_{or} &= L w_2^2 x_2^2 \\ \Delta p_{\Sigma 2} &= K w_2^2 C_{x2} + L w_2^2 x_2^2 = K w_2^2 \left(C_{x2} + \frac{L}{K} x_2^2 \right) \end{aligned} \quad (5)$$

$G_1 = \rho n_1 S_t w_1$ —team consumption through sections with even cooling, kg/s;

$G_2 = \rho n_2 S_t w_2$ —steam consumption through sections with uneven cooling, kg/s;

w_0 —steam velocity with even cooling of all sections, m/s.

$$w_1 = w_0 \frac{1}{\bar{n}_1 + \bar{n}_2 M}; \bar{n}_1 = \frac{n_1}{n_0}; \bar{n}_2 = \frac{n_2}{n_0};$$

$$w_2 = w_0 \frac{M}{\bar{n}_1 + \bar{n}_2 M} \quad (6)$$

$$M = \sqrt{\frac{C_{x1} + \frac{L}{K} x_1^2}{C_{x2} + \frac{L}{K} x_2^2}} \quad (7)$$

Changing the volumetric flow rate into the ejector

$$\Delta V = V_0(\bar{w}_1 \bar{n}_1 \bar{x}_1 + \bar{w}_2 \bar{n}_2 \bar{x}_2) - V_0$$

$$\frac{\Delta V}{V_0} = \bar{w}_1 \bar{n}_1 \bar{x}_1 + \bar{w}_2 \bar{n}_2 \bar{x}_2 - 1 \quad (8)$$

Change in ejector pressure

$$\Delta P_V = \frac{\Delta V}{V_0} (P_e - P_{e0}) \quad (9)$$

Additional orifice losses

$$\Delta P_{or} = L \frac{w_0^2 x_1^2}{(\bar{n}_1 + \bar{n}_2 M)^2} = L' \frac{\rho}{2} \frac{w_0^2 x_1^2}{(\bar{n}_1 + \bar{n}_2 M)^2} \quad (10)$$

$$L' = \xi n_t^2 \left(\frac{d_t}{d_{or}} \right)^4 \quad (11)$$

Additional pressure losses due to flow rate changes

$$\Delta P_t = K' \frac{\rho (w_1^2 - w_0^2)}{2} C_x = K' \frac{\rho w_0^2}{2} C_x \left[\left(\frac{w_1}{w_0} \right)^2 - 1 \right]$$

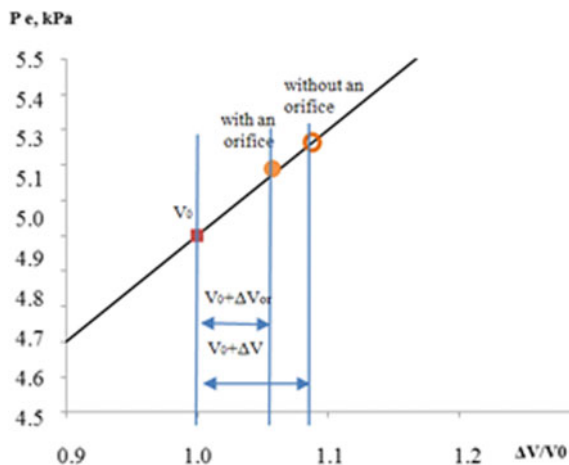
$$= K' \frac{\rho w_0^2}{2} C_x \left[\left(\frac{1}{\bar{n}_1 + \bar{n}_2 M} \right)^2 - 1 \right] \quad (12)$$

$$K' = z x \xi \frac{l}{d} \frac{\rho}{2} \quad (13)$$

where z is the number of passes in the heat exchange section.

An example of calculating ACU for the case when 1 of 10 sections is not cooled has been performed. The module for the air condenser section is three-way. Calculations are performed for a certain range of orifice values with hole diameters 0.025/0.2 m. The goal is to determine the minimum flow rate into the ejector and the minimum

Fig. 3 Dependence graph of $\Delta V/V_0 = f(P_e)$ with calculated points with an optimal orifice diameter and without an orifice



P_e . The optimal orifice diameter was 0.1 m. The calculation results showed a 35% decrease in steam flow into the ejector relative to the mode calculation without an orifice. Consequently, the pressure in the ejector and condenser decreases. Figure 3 shows graphically that the pressure at the ejector inlet shifts into the zone of lower values when the orifice is installed.

To study the orifices effect on the processes in the condenser and ejector under conditions of uneven cooling, an experimental test plant of the condenser model was created, described in [13, 14].

The model condenser consists of two parallel channels with a common steam supply. Each channel is a “tube in a tube”: steam moves from top to bottom in the internal tube; cooling water moves in the external one. The movement pattern is counterflow. Internal heat exchanger tube $\text{Ø}25 \times 2$ mm, external— $\text{Ø}32 \times 2$ mm. The length of the tubes was 2000 mm and the angle of installation was 45° .

The mass flow rate of steam G_s to the model condenser was about 14.4 kg/h; the pressure in the condenser was 8–20 kPa. The holes diameters of the installed orifices are 2.7; 3.5; 4.9 mm. For some modes, the air was supplied into the common steam header in front of the condensers through a rotameter. This was used to simulate the suction of air into the condenser. The mass flow rates of the supplied air ranged from 0 to 1.6% of the steam flow rate for the condenser.

The processing of test results was carried out through the following parameters:

- the available condenser temperature difference, which is determined from the equation

$$\Delta = t_s - t_{c.w. \text{ inlet}} \quad (14)$$

where t_s —condenser saturation temperature, $^\circ\text{C}$; $t_{c.w. \text{ inlet}}$ —cooling water temperature at the condenser inlet, $^\circ\text{C}$;

- the relative flow rate of cooling water into the first condenser channel

$$\bar{G}_{c.w.} = \frac{G_{c.w.1}}{G_{c.w.2}} \cdot 100\% \tag{15}$$

where $G_{c.w.1}$ —mass flow rate for the first channel cooling, kg/s; $G_{c.w.2}$ —mass flow rate for the second channel cooling, kg/s;

- the proportion of air in the steam was calculated as \bar{G}_{air}

$$\bar{G}_{air} = \frac{G_{air}}{G_s} \cdot 100\%, \tag{16}$$

where G_n —mass steam consumption per condenser, kg/s.

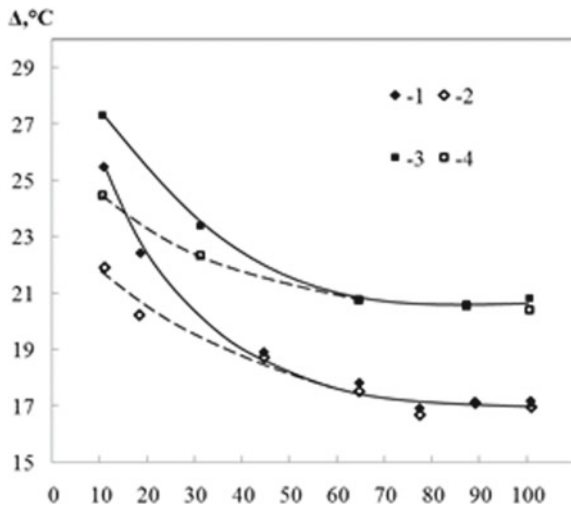
Figure 4 shows the dependence graphs of the available temperature difference of the condenser Δ on the relative flow rate of cooling water to the first channel. In these modes, uneven cooling of a condenser heat exchange surface part was simulated: the flow rate of cooling water into the first channel varied in the range of 10–100% relative to the flow rate in the second channel. In modes No. 3,4, the air was supplied into the steam.

With an increase in the unevenness of the condenser cooling, the available temperature difference increases, and the condenser operation deteriorates.

In the flow rates range for the first channel cooling from 100 to 50%, the growth is weak; with a further decrease in water consumption, Δ begins to increase.

The effect of Ø3.5 mm orifices is detected when the cooling water flow rate decreases from 50 to 10%. When orifices are installed and the water flow to the first channel is reduced, the available temperature drop in the condenser does not increase as much as in the modes without orifices, and with $\bar{G}_{c.w.} = 11\%$, the difference is 3.5 °C for modes No. 1 and 2 and 2.8 °C for modes No. 3 and 4.

Fig. 4 Dependence of the available condenser temperature difference from Δ on the relative cooling water flow rate into the first channel $\bar{G}_{c.w.}$ with orifices Ø3,5 mm: 1—mode No. 1 without orifices; 2—mode No. 2 with orifices; 3—mode No. 3 without orifices, with $\bar{G}_{air} = 1\%$; 4—mode No. 4 with orifices, with $\bar{G}_{air} = 1\%$



Tests were carried out to determine the optimal orifice size for this experimental condenser model. As it follows from the results [15], the optimum lies between d_{or} 3 and 4 mm.

The presence of the optimum orifice resistance is due to the following physical reasons:

- in the absence of an orifice, uneven cooling of the condenser leads to the ejector steaming and pressure increase in the condenser;
- with a large hydraulic resistance of the orifice, the condenser characteristic will shift to the higher pressures zone at given air suction.

Consequently, there is a certain optimum in the pressure drop at the orifice, which does not lead to a noticeable change in the air removal device characteristics, but does not give the ejector “steaming”.

4 Conclusion

The results obtained during this study implementation make a significant contribution to understanding the processes of condensing units' operation at off-design modes and the way to combat a decrease in thermal efficiency due to the resulting uneven cooling and local air suction. They can be used to

- assess the influence of unevenness factors on the condensing unit performance;
- increase condensers efficiency when deviating from the design conditions.

Acknowledgements This study was funded by the Russian Science Foundation (project no. 17-19-01604).

References

1. Operation guidelines for condensing units of steam turbines at power plants, MU 34-70-122-85
2. Fedorov, V.A., Milman, O.O.: Steam Turbine Condensers, p. 560. Publishing House of Bauman MSTU, (2013)
3. Milman, O.O., Anan'ev, P.A.: Dry coolers and air-condensing units (review). *Therm. Eng.* **63**(3), 157–167 (2016). <https://doi.org/10.1134/S0040363616030061>
4. Milman, O.O., Kalinin, A.Y., Loshkareva, E.A.: Evaluation of the efficiency of air-condensation installations. *Int. Sci. J. Altern. Energy Ecol.* **4**(144), 40–45 (2014)
5. Merkulov, V.A.: Research and development of ways to improve the efficiency and reliability of condensation devices for heating turbines. Ph.D. thesis. Ivanovo, 178 (2004)
6. Sharapov, V.I., Malikov, M.A.: Improvement of operating conditions of heat-exchange equipment in condensate and feed system of a heat station. *Trans. Academenergo* **3**, 37–55 (2012)
7. Brodov, Y.M., Aronson, K.E., Ryabchikov, A.Y., Nirenshteyn, M.A.: Current state and trends in the design and operation of water-cooled condensers of steam turbines for thermal and nuclear

- power stations (review). *Therm. Eng.* **66**(1), 16–26 (2019). <https://doi.org/10.1134/S0040363619010028>
8. Sokolov, E.Ya., Zinger, N.M.: *Inkjet Devices*, 3rd ed., Rev. p. 352. Energoatomizdat, Moscow (1989)
 9. Aronson, K.E., Ryabchikov, A.Y., Brodov, Y.M., Brezgin, D.V., Zhelonkin, N.V., Murmanskii, I.B.: Analysis of experimental characteristics of multistage steam-jet ejectors of steam turbines. *Therm. Eng.* **64**(2), 104–110 (2017). <https://doi.org/10.1134/S0040601517020021>
 10. Berman, L.D., Singer, N.M.: *Air pumps of condensing installations of steam turbines*. Gosenergoizdat (1962)
 11. Shklover, G.G., Milman, O.O.: *Research and Calculation of Condensation Devices for Steam Turbines*, p. 240. Energoatomizdat (1985)
 12. Kartuesova, A.Yu.: Methodology for calculating the distribution of steam flows in the section of an air-condensing unit under conditions of complete and deteriorated cooling. In: *Proceedings of the 6th International Scientific-Practical Conference: Modern Trends in the Development of Science and Technology*, p. 52. Belgorod, Part 2 (2015)
 13. Mil'Man, O.O., Isaev, S.A., Ptakhin, A.V., Kondrat'Ev, A.V., Kartuesova, A.Y., Krylov, V.S.: Influence of cooling medium flow character on the operation of heat exchangers with steam condensation inside tubes. *J. Eng. Phys. Thermophys.* **93**(5), 1115–1125 (2020)
 14. Milman, O.O.: Sectional condensing unit: Utility model patent, RU 185511 U1. Patent holders: CJSC Scientific-Production Implementation Enterprise “Turbocon”, no. 2018124027. Year of publication 5 p. (2018). Date of registration 2018/07/02. Date of publication 2018/12/07
 15. Milman, O.O., Kartuesova, A.Y., Yankov, G.G., Ptakhin, A.V., Krylov, V.S., Korlyakova, M.O.: Investigation of parallel operation of vacuum condenser sections with nonuniform cooling. *Therm. Eng.* **66**(2), 77–83 (2019). <https://doi.org/10.1134/S0040601519020022>

Joint Use of Distributed Ledger Technology and Centralized Software for Storing Power Equipment Reliability Data



M. M. Sultanov, I. A. Boldyrev, A. A. Smirnov, Yu. A. Gorban,
and V. A. Yurov

1 Introduction

Distributed ledger technologies, or blockchain, play an increasingly important role in the global energy sector. Though the amount raised in blockchain projects funds is hundreds of millions of dollars per year, there are few real examples of working tested systems [1, 2].

Many startups for the introduction of smart contracts in the energy sector are expanding in Germany. German pioneer companies Slock.it and RWE have launched two projects aimed at simplifying electric vehicles' charging system. Designing a simple billing model will eliminate the main barrier, which currently prevents mass adoption of the electric mobility concept [3].

With regard to the growing technological diversity of power distribution systems, methods and means of ensuring power equipment reliability and safety play an increasingly important role. A system for storing data on power equipment reliability indicators establishment enables optimizing the repair work volume and timing, as well as power equipment operating modes accurately choice.

The article introduces a developed software package for testing and researching algorithms for ensuring power equipment reliability and safety with the use of various data storage technologies.

M. M. Sultanov · I. A. Boldyrev (✉) · A. A. Smirnov · Yu. A. Gorban
The Research Laboratory of Digital Technologies, Volzhsky Branch of MPEI, Lenina St., 404110
Volzhsky, Russia
e-mail: boldyrev@vfmei.ru

V. A. Yurov
SocMediaMarketing LLC, Kosmonavtov St., 404110 Volzhsky, Russia

2 Distributed Ledgers for Storing Power Equipment State Data

Consider the system of stores information about power equipment technical condition, owners, life cycle, its reliability, and efficiency indicators. These data are a trade secret for energy companies. Even though the ledger is supposed to be closed, the data between participants who may be competitors will be open.

As a solution to this problem, the distributed ledger can be supplemented with a centralized data storage system with a strict differentiation of rights and roles.

In the suggested approach, the roles between a distributed ledger and a centralized data storage system are shared as follows:

- All the data about the reliability, measured parameters, and transactions with power equipment are published in a centralized data storage system.
- Data checksums (hashes) are published in an open distributed ledger and are signed with the participant's electronic digital signature (EDS).
- All the participants have equal and open access to data in the distributed ledger.
- Access to data in the centralized storage is carried out with the established access rights and user roles.
- Each participant who has access to the data in the centralized storage can verify its validity by calculating the checksum and comparing it with the entry in the distributed ledger.

3 A Data Block Design

The blockchain technology is based on the principle of data storage in a chain of blocks. Each block has the previous block checksum.

Figure 1 shows an information blocks scheme in the blockchain network.

The block in the network contains the following:

- block number—a numeric field defining the block number in the network;
- node—network participant address or a public key of this participant;

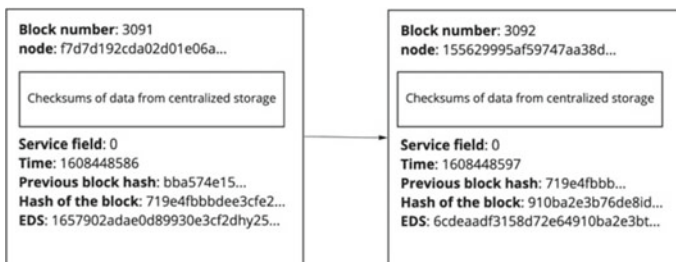


Fig. 1 General scheme of information system blocks

- data—data array with the checksums of the centralized storage data;
- service field—a field defining the block type. Zero value that it is a simple information block. Other values can be used for service blocks, for example, when voting;
- previous block hash—previous field checksum;
- time—the time when the block was created in the UnixTimestamp format. It is generated by the network participant;
- entire block hash—all block data checksum, including the hash of the previous block.

All of the objects have their owners and a universally unique identifier (UUID) label. Object owners can generate access keys (tokens) to their objects and give them to other users. The access key is a unique 128-bit identifier that is randomly generated.

All transmitted to the blockchain information must be linked with UUID tags from the centralized storage and divided by the provided in its transaction types.

All other information, including the type of equipment and its characteristics, is available in the centralized system to those participants who have an access key to it. They can compare the information from the centralized system with the information published in the blockchain.

4 Centralized Data Storage System

The system for collecting, storing, and processing data on the energy systems operating modes to ensure a high level of reliability is a software package designed for storing and processing data on the power equipment reliability and safety indicators.

The software is a set of modules implemented in separate docker containers, with each container running as an independent application. Containers have their own isolated environment and contain necessary for program performance functions.

Containers interact with each other by means of the HTTP protocol and the JSON data format on the local network, forming a network of microservices. Only the one with an application programming interface (API) has external access.

Different database management systems are used for efficient storage and different types of data processing.

The main software container automatically checks and distributes data between the DBMS and provides access to it through a single entry point (endpoint).

5 Software Structure

The software for collecting, storing, and processing data consists of the following:

- InFlux and ClickHouse—DBMS for storing time series. Influx can pre-group time series in a series of stored data, whereas ClickHouse shows the best execution time characteristics for all types of queries. Hence, data are duplicated in both systems. This approach enables redundancy in data storage, but reflects the advantages of both systems. DBMS data are well suited for horizontal scaling and designed specifically for working in clusters. They support such scaling technologies as sharding and replication [4, 5].
- Postgres DB—DBMS for storing relational data. PgBouncer-based cluster solutions help with horizontal scalability [6].
- GraphQL API—software implementing an interface for accessing data. GraphQL-based API makes it possible to solve the problem of fast access to the modified data structure [7–9].

6 System General Operating Principle

All data operations are implemented through an input point in the microservice architecture “Load Balancer”. The Nginx service serves as a load balancer. It distributes the load on the processing services. Php process managers are used as handlers.

After Nginx the data goes to the GraphQL handler implemented on the lighthouse library. It works with GraphQL models and requires only mutations and data retrieval requests descriptions.

Access rights to the system differentiation are carried out through the interaction of the secret key and object unique identifier. All of the entities are marked with secret keys associated with users and UUID tags [10].

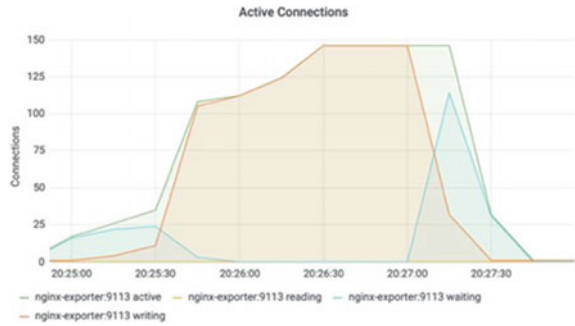
Thus, the right to receive, record, and mutate data is finely differentiated between the system participants. Requesting the API and depending on the user’s role, he can see the entities and the access type to them. Hence, it is possible to set access rights from the specific equipment metrics to full access to the system of one or more enterprises. All operations with the program interface must be performed with an access key.

Power equipment manufacturers can register their equipment brands and specific equipment units via the API. After the equipment has been registered, a pair of public and private keys is generated.

Manufacturers register a list of metrics that need to be recorded to ensure the equipment reliability and safety.

All of the metrics are described in the PostgreSQL-based storage, but their values are stored in ClickHouse and Flux.

Fig. 2 Load profile in the Grafana interface



7 The Method of Researching the Efficiency of the System and the Results

Being a part of this work, a blockchain laboratory has been created on the basis of the branch of the National Research University “Moscow Power Engineering” in Volzhsky town. It enables simulating the power system operation and testing centralized and decentralized approaches to data storage.

The lab consists of PCs linked together in a blockchain network, with each PC acting as a node in the network. The machines are equipped with the software, sending requests to the blockchain and centralized storage via the operator’s interface and launching containers, simulating measurements transmitting from power equipment.

A separate cluster is deployed in Kubernetes for API testing units. It creates a load on the centralized system. This cluster consists of 50 pods, generating write and read requests in different proportions.

An Exporter from Nginx, Prometheus, and Grafana is used to record the measurements.

Figure 2 shows the load profile displayed in the Grafana interface, resulting from the load pods distribution as 45 for writing and 5 for reading.

The service supports 125 write requests per second and 150 active read requests per second with this load. At the same time, the queue processing service manages to process all of the messages. Taking into account that the deferred message handler is able to smooth out load peaks and the Kubernetes service provides horizontal scaling, the number of requests processed by the system can be increased tenfold.

8 Conclusions

Decentralized information system based on a closed distributed ledger use enables all the energy market participants to exchange information about the power equipment state, its operating modes, and reliability indicators. Blockchain technology allows

increasing trust between market participants, since data integrity and validity are ensured by a consensus algorithm and encryption.

The developed software suite, consisting of a blockchain and a centralized system, allows the secure storage and collection of data on the reliability of energy equipment. As a result of the study, the developed system shows high characteristics of the speed of information collection and processing.

Acknowledgements The research is funded by Russian Federation public contract № FSWF-2020-0025 “Technique development and method analysis for ensuring power system object security and competitiveness based on the digital technologies”.

References

1. Mulligan, S.: Energy, blockchain, and the role of tokens (2018). <https://www.investinblockchain.com/energy-blockchain-tokens>
2. Metelitsa, C.: Four predictions for blockchain in energy in 2018 (2018). <https://www.greentechmedia.com/articles/read/four-predictions-for-blockchain-in-energy-in-2018#gs.zktEQwA>
3. Goranović, A., Meisel, M., Fotiadis, L., Wilker, S., Treytl, A., Sauter, T.: Blockchain applications in microgrids an overview of current projects and concepts. In: IECON 2017–43rd, Annual Conference of the IEEE Industrial Electronics Society, pp. 6153–6158 (2017)
4. Struckov, A., Yufa, S., Visheratin, A., Nasonov, D.: Evaluation of modern tools and techniques for storing time-series data. *Procedia Comput. Sci.* **156**, 19–28 (2019)
5. Gangadhar, S.: The real time environmental time series data analysis using influx DB. *IJASI* **1**(1) (2020)
6. Le, Q.H., Xie, J., Millington, D., Waniss, A.: Comparative performance analysis of PostgreSQL high availability database clusters through containment. *IJARCCCE* **4**(12) (2015)
7. Eizinger, T.: API Design in Distributed Systems: A Comparison Between GraphQL and REST (Doctoral dissertation, Master’s Thesis). University of Applied Sciences Technikum Wien-Degree Program Software Engineering, Austria (2017)
8. Brito, G., Valente, M.T.: REST versus GraphQL: A Controlled Experiment, pp. 81–91. IEEE, ICSCA (2020)
9. Seabra, M., Nazário, M.F., Pinto, G.: REST or GraphQL? A performance comparative study, pp. 123–132. In: SBCARS ‘19 (2019)
10. Cui, B., Xi, T.: Security analysis of openstack keystone. *IEEE IMIS* **6**(6), 283–288 (2015)

Methods for Improving the Efficiency and Reliability of Power Systems Equipment in the Context of Digitalization



Makhsud Sultanov, Iliia Boldyrev, and Yuliya Gorban

1 Introduction

The development of the energy sector in the Russian Federation is associated with the concept and state programs of upgrading technological mechanisms for managing the united energy system. The introduction of the national project “Digital Economy” in the concept of energy development until 2035 forms new approaches for energy companies to implement digital transformation programs.

According to the Ministry of Energy of the Russian Federation, there are a number of challenges and problems in the electrical and heat power supply sectors, which require certain legal regulation. It should be noted that the existing models of energy facilities management (operation, repair, reconstruction, etc.) in the conditions of digitalization are not efficient enough, some of them have already lost their significance, and the digital technologies introduced often relate only to the line of newly introduced new equipment. However, the current equipment of the country’s energy industry (more than 60%) operates with a service life of more than 25 years and can still be effectively used for the production and transmission of energy resources. A whole layer of problems of digital transformation of energy enterprises is highlighted: optimization of the processes of proactive management of existing energy facilities; introduction of modern algorithms for digital signal processing; introduction of wireless transmission of measurement information and control signals; and application of modern approaches to the construction of diagnostic systems for power equipment to improve reliability, efficiency, and safety.

The key features of management principles improvement in the energy sector are algorithm complexity increase and decentralization. Papers [1–4] present the direction development need. It should be noted that the results are highly fragmented. At

M. Sultanov · I. Boldyrev (✉) · Y. Gorban
Branch of National Research University “MPEI”, Volzhsky, Russian Federation
e-mail: boldyrev@vfmei.ru

the same time, technologies for processing large amounts of data, machine learning, and artificial intelligence lay the prospect of creating a unified approach to the implementation of such systems, including the development of DaaS services, which can fundamentally accelerate the development of systems and increase the reliability of results.

Modern system design requires applying complex algorithms for real-time monitoring a large number of energy system facilities, as well as developing an automated system for resource and service market for the participants. Papers [5–8] present decisions of such problems.

An urgent and economically feasible task is to develop a universal methodology for implementing methods and techniques for improving reliability and efficiency indicators at all energy facilities, taking into account the technical condition of power equipment in the context of digitalization.

2 Analysis of the Reliability Level and Power Equipment Failure Reasons

The problem of developing the algorithms for managing reliability and efficiency indicators requires determining the groups of operational parameters that have the greatest impact on the reliability indicators of the main and auxiliary equipment of energy generation, transmission, and distribution facilities.

Based on the data on the types and causes of equipment failures, data on the main and auxiliary equipment of power generation, transmission, and distribution facilities were obtained. The structure of power equipment failures is shown in Fig. 1.

For the turbines presented in Table 1, the reasons for failures over a 10-year period are considered on the basis of reports of investigations of technological failures and violations.

The generalized structure of failures of heat-generating turbines is shown in Fig. 2. It is revealed that the largest number of failures is accounted for by the turbine control system. As a result of the analysis, it is shown that in the vast majority of cases, malfunctions occur as a result of violations during the operation of equipment, installation defects after the end of current and major repairs, as well as physical and moral wear of units and components.

The analysis of the thermal and hydro power plant power equipment reliability, power plant and substation electrical equipment and groups of operational characteristics of overhead power line wires was performed. Based on the proposed classification of statistical data groups, the possibility of analyzing the reliability indicators of generating equipment is proved.

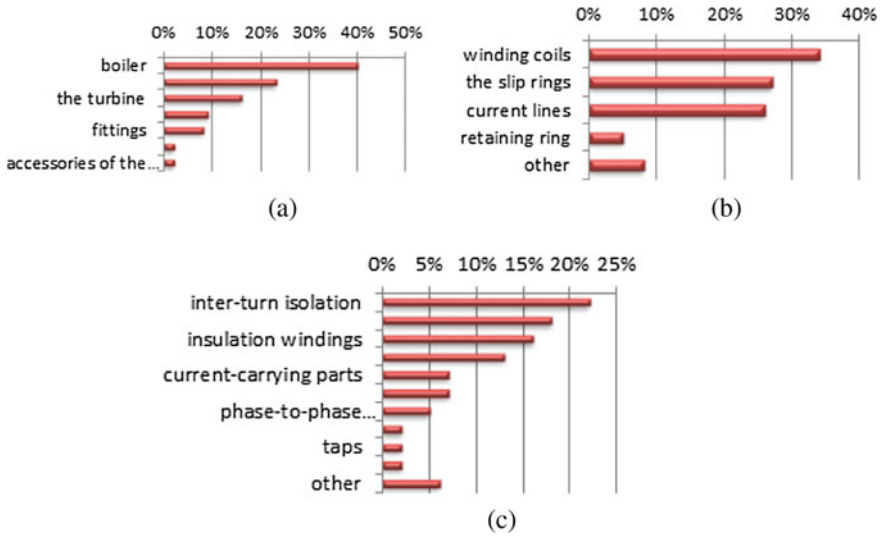


Fig. 1 Structure of power equipment failures by type (**a** heat and power equipment, **b** power generating equipment, and **c** power distribution equipment)

Table 1 Commissioning of steam turbine equipment

S. No.	Type (brand) of the turbine	Unit power, capacity, MW	Commissioning year
1	PT-65/75-130/13	65	2002
2	PT-65/75-130/13	65	1998
3	T-50-130	50	1967
4	T-100-130	100	1971
5	T-100-130	100	1972
6	PT-135-130	135	1974

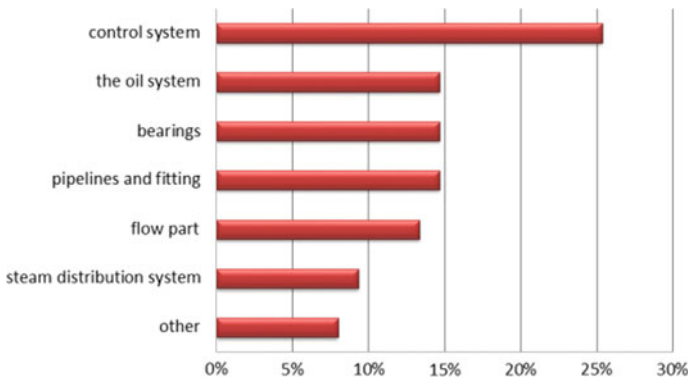


Fig. 2 Structure of heat-generating turbines of failures

3 The Mathematical Modeling of Power Equipment Reliability and Efficiency Characteristics

It should be noted that the implementation of algorithms for improving the efficiency, reliability, and safety of energy systems requires the construction of models of the processes occurring in the systems under study. The application of both the classical approach based on the construction of mathematical models of processes and the application of machine learning algorithms is considered.

A mathematical model for assessing the technical condition of boiler plants in terms of reliability and efficiency for use in monitoring and diagnostics systems of power equipment has been developed. An approach to the predictive evaluation of the performance of each element is developed in order to obtain a reliable and representative sample of failure statistics for assessing the reliability of boiler installations of thermal power plants. The analysis of statistical data shows that the reliability of the elements of the boiler unit directly depends on the temperature regime of the metal. About 40–50% of the emergency shutdown of the boiler unit occurs due to damage to the metal of the superheaters, about 35–40%—damage to the evaporative heating surfaces, and up to about 10%—failures in the operation of water economizers.

Theoretical analysis of the data showed (Fig. 3) that according to the statistics of failure of the main elements of the boiler equipment, superheaters and evaporative heating surfaces are the most damaged. Reliability, which primarily depends on the intensity of heat transfer characteristics of combustion and corrosion processes, leads to wear of the walls of the heat transfer surfaces.

One of the main criteria of assessment of the actual technical condition is proposed to use the current value of the average integral temperature of the gases at the exit from the zone of active combustion, which takes into account the important sensitive conditions and thermal characteristics of the firebox in the boiler.

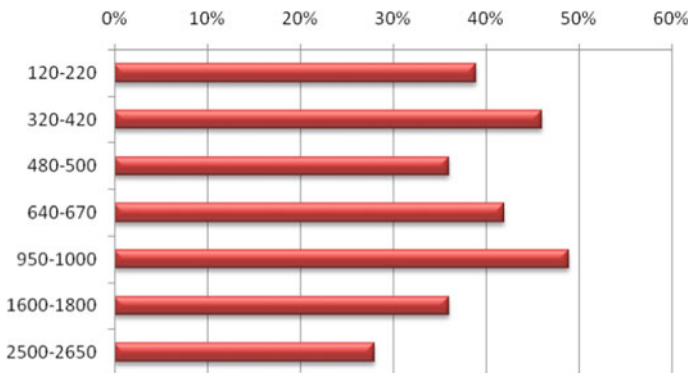


Fig. 3 Statistical data on failures due to damage to superheaters of boiler plants, depending on performance

The probability of reliable operation of the element in the range of changes in the operating temperatures is proposed to be determined by the expression:

$$P_i = 1 - \int_{T_{\min}}^{T_i} \frac{(T_i - T_{\min})}{(T_{\max} - T_{\min})} \cdot f(T) dt \tag{1}$$

where

- T_i is the average integral value of the gas temperature at the exit of the active burning zone;
- T_{\min} and T_{\max} are minimum and maximum values of the gas temperature at the exit from the zone of active combustion, respectively;
- $f(T)$ is the probability distribution function.

Special attention is also paid to the reliability of boiler drums and bends of non-heated pipes, while failures in the operation of which occur due to the appearance of residual deformation in the presence of a temperature difference in the metal of the pipe walls and heating surfaces. To determine the technical condition of the boiler equipment, technical diagnostics of its elements are carried out.

Another result obtained in the framework of the work is a method for assessing the influence of the mode parameters and power quality indicators on the reliability of power transformers.

To account for the influence of the higher harmonic components of the current on the daily reduction in the service life of the transformer coil insulation, the coefficient of influence of electricity quality indicators on the increase in the rate of relative wear of the coil insulation can be used:

$$k_v = V' / V = 4.22 \cdot 10^{-3} e^{5.468 \cdot k_i} \tag{2}$$

where V' is the relative wear rate of the coil insulation, taking into account the higher harmonic components of the current; k_i is the distortion coefficient of the shape of the current curve, determined by the expression:

$$k_i = \frac{\sqrt{\sum I_v^2}}{I_1} \tag{3}$$

where I_v is the current of the v th harmonic component; I_1 is the current of the main harmonic.

It is shown that taking into account the higher harmonics of the current in calculating the rate of relative wear of the coil insulation and the daily reduction in its service life will allow predicting the residual life of transformers and planning the timely withdrawal of equipment for repair according to the current state.

The implementation of approaches to increase the values of technical and economic indicators of generating systems is possible with the use of machine learning. A common approach to ranking the efficiency of generating facilities is

the use of technical and economic indicators (TEI). At the same time, the currently used methods of calculating and analyzing TEI do not provide the operator with visual information in an online mode about which initial parameters currently most strongly affect efficiency, as well as which parameters need to be affected first to improve performance.

Determining the degree of influence of the current values of technological parameters on the result of calculating the TEI of generating equipment allows you to create a list of parameters that you should pay attention to when managing the generating equipment of thermal power plants, informing the operator in real time.

The problem of assessing the degree of influence of the parameters of the generating system on its technical and economic indicators can be solved by using machine learning methods.

The following methods for assessing the effect of technological parameters on the TEP values were tested: linear regression model, random forest, and gradient boosting. The results obtained are comparable to the results obtained by the analytical method in [9].

The analysis of the obtained results allows us to draw conclusions about the possibility of applying the approaches studied in the work to analyze the influence of technological parameters on the efficiency of the process. The proposed approach allows to predict the value of the efficiency of the thermal energy facilities and to determine the most influencing parameters, which gives the possibility of creating a feedback loop in the calculation of technical and economic parameters and eliminates the need for the operator to adjust the control, thus adding properties and functions of an expert system.

4 Developing Highly Reliable High-Speed BDMS for Power Equipment Data Handling

The implementation of the developed models and algorithms for evaluating and improving reliability and efficiency indicators on the scale of the power system requires the implementation of a high-speed, highly reliable Database Management System (DBMS) that provides storage and processing of collected data on the state of energy facilities [10–13].

The paper proposes the software for centralized data storage, which can be used for the development and research of algorithms and methods for improving the reliability and safety of power equipment. A unique feature of the developed software is the control over the entire life cycle of the equipment, from production to decommissioning. Due to the fine separation of access rights to the system and the use of a flexible data access interface, users of the system can change their composition and structure, and these changes will be available in real time.

This system contains information about power producers, operators, and manufacturers of power equipment. This makes it possible to control the reliability and

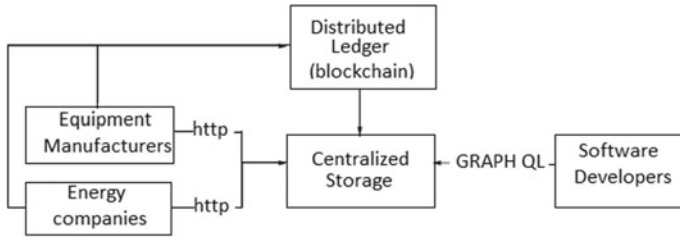


Fig. 4 Operating principle of the system for storing and processing data on reliability modes

quality of power equipment throughout its entire life cycle—from the moment of production to decommissioning.

The general scheme of the system is shown in Fig. 4.

The use of specialized DBMS for storing metrics allows you to monitor and adjust the operating modes of equipment in almost real time, and the use of the GraphQL query language allows energy companies to change the data structure based on their needs and software developers to get this data without waiting for changes in the software interface.

5 Development of the Decentralized Informational System Based on the Closed Distributed Registry

A decentralized information system based on a closed distributed registry is proposed, the use of which allows all participants in the energy market to exchange information about the state of power equipment, its operating modes, and reliability indicators. The blockchain technology allows to increase trust between the participants of the power equipment market, since the integrity and validity of the data are ensured by the consensus algorithm and encryption.

All information transmitted to the blockchain must be associated with UUID tags from the centralized storage and divided by the types of transactions provided in it. The block structure contains the following fields:

- Block number;
- Node;
- Data block;
- Service field;
- Time;
- The hash of the previous block;
- Hash of the entire block;
- Electronic digital signature.

The data block contains the following information:

1. **UUID**—the entity ID of the new piece of equipment from the centralized storage system.
2. **Hash**—the checksum of the data about this entity. Contains a snapshot of all the data transmitted to the centralized system, such as serial number, model, and characteristics.
3. **Type**—the field responsible for the type of transaction in the system. This field also defines the rules for the verification of a block in the system.

At the time of the release of new equipment, the manufacturer registers it in the distributed registry. At the same time, at this stage, all participants in the registry know only the fact of the released equipment. All other information, including the type of equipment and its characteristics, is available in the centralized system to participants who have an access key to it and can verify the information from the centralized system with the information published in the blockchain.

A decentralized network can exist indefinitely as long as it has members. The data written to the chain is protected and cannot be modified. The data is stored as long as there is at least one network member. But, since the use of a closed distributed registry implies that the data inside it will be open to all participants, it is proposed to store not the data itself, but their checksums. To ensure the separation of data access rights, it is necessary to apply centralized approaches to the storage of information. The developed data management algorithm allows us to use modern methods of reliability and efficiency of power equipment throughout the entire life cycle from production to decommissioning.

The proposed model of the information system for managing the power equipment of modern generating systems based on centralized and distributed registers allows you to use the advantages of each of the systems and minimize their disadvantages. This approach allows us to create a system that will be open and transparent to all participants in the power equipment market and, on the other hand, meet the requirements for security and trade secrets. Since a distributed registry uses a public key as node identifiers, and instead of direct data, its hash is stored, which cannot be used to restore data, but can be verified for its authenticity, the use of such a registry should be beneficial to all participants.

6 Development of the Decentralized Informational System Based on the Closed Distributed Registry

The implemented DBMS with a database of parameter values about the state of the equipment provides the ability to create software packages for monitoring the state and optimizing the operating modes of power equipment.

A software package has been developed for calculating the reliability and efficiency indicators of power equipment, taking into account the actual technical condition, which includes three calculation subsystems:

1. The power equipment diagnostic and parameter monitoring application allows monitoring the condition of power equipment, calculating the operating time and other reliability indicators [14];
2. The application for calculating the reliability indicators of power equipment allows you to manually or automatically monitor changes in the values of technological parameters and calculate the reliability indicators of power equipment [15];
3. The application for estimating the efficiency indicators of power equipment calculates the TEI values based on the values of the initial values of discrete and analog parameters loaded from the DBMS [16].

An algorithm for predicting the efficiency indicators of a thermal power plant for the production of heat and electric energy under the conditions of performing the schedule of electrical loads, taking into account the technical condition, for use in monitoring and diagnostics systems of generating equipment.

The application of a systematic approach to the construction of a system for collecting and managing data on the state of power equipment makes it possible to implement a comprehensive solution to the issues of efficiency, reliability, and safety management.

To ensure timely diagnosis failures and their elimination, as well as the definition of indicators of reliability of power generation equipment according to actual condition requires the collection, storage, and backup of data on failures of specific items of equipment in the first place, characterized by a high degree of failure, such as thermal stress of the heating surface and the elements under high pressure, rotary equipment, and spinning gears to create databases of multivariate data which allows for Park resources, inter-repair period, failure rate, the state of the metal, which can be used to develop predictive models that provide approaches to prolonging the operational state of the elements of power equipment and create digital energy systems for monitoring and diagnostics of the main equipment, allowing to implement the creation of a methodology for ensuring a high level of safety, reliability, and efficiency of equipment operation at existing power plants.

7 Conclusions

The results obtained in the framework of the study can be used for further research in such areas as:

- Developing algorithms of the implementation of repair activities of energy enterprises on the technical condition of power equipment, taking into account the data of monitoring and diagnostics systems;
- design of the automated system for estimation of the power equipment reliability and optimal technical condition;

- creation of databases of automated and information-measuring systems for determining the level of reliability of power equipment and conditions of optimal technical condition;
- development of a methodology for studying the reliability levels of power equipment based on data from power equipment monitoring and diagnostics systems;
- development of techniques for analyzing the technical condition, monitoring and diagnostics systems of power equipment, collecting, storing, and managing data on the technical condition of power equipment and a comprehensive assessment of the level of reliability of generating and power systems;
- development of a methodology for the digital transformation of energy enterprises in the framework of collecting, accounting, and storing data on the current and forecast technical condition of energy equipment.

Acknowledgements The research is funded by Russian Federation public contract № FSWF-2020-0025 “Technique development and method analysis for ensuring power system object security and competitiveness based on the digital technologies”.

References

1. Florkowski, M.: Classification of partial discharge images using deep convolutional neural networks. *Energies* **13**, 5496 (2020)
2. Topolsky, D., Topolskaya, I., Plaksina, Y.B.: Real-time diagnostics of an intelligent electrical drive proceedings, pp. 416–420. In: *RusAutoCon*, p. 9208170 (2020)
3. Lozanov, Y., Petleshkov, A., Tzvetkova, S.: Capabilities for diagnostics of pump system’s electrical equipment via frequency converters (Conference Paper). In: *21st International Symposium on Electrical Apparatus and Technologies, International Symposium on Electrical Apparatus and Technologies*, p. 916708021 (2020)
4. Lavrinovich, A.V., Mytnikov, A.V.: Diagnostics facility for effective control of winding condition of high voltage transformers. *Geo As. Eng.* **331**, 48–59 (2020)
5. Mudialba, P.J.: The impact of cloud technology on the automation of businesses. In: *Proceedings of the International Conference on Platform Technology and Service (PlatCon)* (2016). <https://doi.org/10.1109/PlatCon.2016.7456831>
6. Jurasz, J., Canales, F.A., Kies, A., Guezgouz, M., Beluco, A.: A review on the complementarity of renewable energy sources: concept, metrics, application and future research directions. *Sol. Energy* **195**, 703–724 (2020)
7. Farhadzade, E.M., Muradaliev, A.Z., Rafieva, T.K., Rustamova, A.A.: Dostovernost’ integral’nykh pokazateley effektivnosti raboty energoblokov TES. Nadezhnost’ i bezopasnost’ energetiki **12**(4), 252–259 (2019)
8. Farhadzade, E.M.: Sravnenie i ranzhirovanie paroturbinnnykh ustanovok energoblokov TES po effektivnosti raboty. *Tepoenergetika* **10**, 41–49 (2018)
9. Sultanov, M.M., Boldyrev, I.A., Gorban, Y.A.: Research of dynamic characteristics of signals for calculation of technical and economic indicators and increase in power efficiency of the equipment of thermal power plant. *IOP Conf. Ser.: Mater. Sci. Eng.* **552**, 012007 (2019)
10. Mullor, R., Mulero, J., Trottini, M.A.: Modelling approach to optimal imperfect maintenance of repairable equipment with multiple failure modes. *Comput. Ind. Eng.* **128**, 24–31 (2019)

11. Ma, Z., Ren, Y., Xiang, X., Turk, Z.: Data-driven decision-making for equipment maintenance. *Autom. Constr.* **112**, 103103 (2020)
12. Melchor-Hernández, C.L., Rivas-Dávalos, F., Maximov, S., Coria, V.H., Guardado, J.L.: A model for optimizing maintenance policy for power equipment. *Electr. Power Energy Syst.* **68**, 304–312 (2015)
13. Ivanitckii, M.S., Sultanov, M.M., Trukhanov, V.M.: Analysis of the influence of operating modes of heat generating plants on the energy and environmental safety of thermal power plants. In: *Proceedings of the 2nd 2020 International Youth Conference on Radio Electronics, Electrical and Power Engineering, REEPE 2020*, p. 9059205 (2020)
14. Sultanov, M.M., Boldyrev, I.A., Lunenko, V.S., Menshikov, P.D.: Program for monitoring parameters and diagnostics of power equipment, 2020667806 (2020)
15. Sultanov, M.M., Boldyrev, I.A., Lunenko, V.S., Menshikov, P.D.: Program for calculating reliability indicators of power equipment, 2020667679 (2020)
16. Sultanov, M.M., Boldyrev, I.A., Lunenko, V.S., Menshikov, P.D., Gorban, Yu.A.: Program for calculating the efficiency indicators of power equipment, 2020667357 (2020)

Mathematical Simulation of the Flux of the Solar Radiation Coming to the Collector



Valentina Khoreva, Sergey Elistratov, Nadezhda Vorogushina,
and Ivan Sadkin

1 Introduction

Solar energy resource maps are often used to determine the potential for solar power generation. These maps are created from satellite imagery and interpolation of data from ground-based weather stations, which are often very far from each other, and their data are not always accurate. The data on the maps are not always of high quality and of sufficient scale to be a reliable basis for making decisions on installing a solar collector. A mistake in choosing the location or angle of inclination of the solar collector can lead to a significant decrease in the energy of solar radiation incident on the collector.

In the course of work, several methods of calculating the power of solar radiation coming to the collector were studied and analyzed [1–12]; as a result, five methods were found to calculate the power of solar radiation falling on the surface of the solar collector. These calculation methods are not universal, since the final value of the solar radiation power in some methods does not depend on the installation height of the solar collector above sea level; the final height of the atmosphere is not taken into account; the calculation can be carried out only for zenith angles up to 75°; the dependence of the power of solar radiation falling on the Earth's surface on the collector installation height is linear, which has no physical justification. The task of this work is to create a universal scientifically based methodology for assessing the efficiency of using solar radiation.

V. Khoreva (✉) · S. Elistratov · N. Vorogushina · I. Sadkin
Department of Thermal Power Plants, Novosibirsk State Technical University, Prospect Karla
Marxa street, 630073 Novosibirsk, Russia

2 Materials and Methods

At the moment, a program has been created that calculates the power of solar radiation arriving at the collector as a dependence on the air density (not linearly changing depending on the collector installation altitude above sea level), the path of the Sun's rays through the atmosphere (not linearly changing at every moment of time) and the angle between the normal to the collector plane and the Sun. This calculation method is fundamentally new and scientifically grounded, since it is based on geometry, astronomy and physical laws.

The calculation program shows the maximum potential (exergy) of solar radiation in a given area (at a given geographic latitude and altitude) [13–15], calculates the value of the solar radiation power coming to the collector for any angle of inclination and azimuth of the solar collector and allows you to choose the optimal angle of inclination of the solar collector, taking into account the latitude, altitude and possible azimuths of the installation. At the moment, the program is written in the SMath Studio.

The absorption of light in the atmosphere depends on its density. The density of the atmosphere is calculated using the Mendeleev-Clapeyron Eq. (1):

$$\rho = \frac{P \cdot M}{R \cdot T} \quad (1)$$

At altitudes of 40 km and above, the density of the atmosphere can be neglected. For the accuracy of calculations, we take the significant height of the atmosphere $h_{\max} = 40,000$ m. We introduce the concept of the density coefficient. The density coefficient is calculated by the formula (2), where $\rho_0 = 1.225 \text{ kg/m}^3$ is the density of dry air at a temperature of 15 °C and a pressure of 101,330 Pa. For the equator with a collector installation height above sea level $h = 0$ m, $k_\rho = 1$. When $h = 40,000$ m, $k_\rho = 0$.

$$k_\rho = \frac{P \cdot M}{\rho_0 \cdot R \cdot T} \quad (2)$$

For the equator, when the Sun is at its zenith, the power of the solar radiation flux arriving at the plane perpendicular to the flow depends on the density coefficient k_ρ :

$$\frac{dI}{I} = -dk_\rho$$

Integrating the right and left sides of the equation and substituting the integration limits for the density factor from 0 to k_ρ and for the radiation power from I to I_0 , where $I_0 = 1362 \text{ W/m}^2$ [16], we get

$$I = I_0 \cdot e^{-k_\rho} \quad (3)$$

The maximum solar radiation flux at sea level at the equator is $I = 1050 \text{ W/m}^2$. Therefore, we add the correction factor to (3) $k_e = 0.26016$:

$$I = I_0 \cdot e^{-k_p \cdot k_e} \quad (4)$$

For the general case, it is necessary to take into account the path that the Sun's rays travel through the atmosphere.

$$L_{\text{rays}} = \sqrt{h_{\text{max}}^2 + 2R_{\text{Earth}}h_{\text{max}} + R_{\text{Earth}}^2 \sin^2 a} - R_{\text{Earth}} \cdot \sin a, \quad (5)$$

where $R_{\text{Earth}} = 6371 \text{ km}$ is the radius of the Earth;

a is the angle of the Sun's rise above the horizon.

Thus, taking into account (4) and (5), the intensity of direct solar radiation on a perpendicular surface is calculated by the formula (6):

$$I = I_0 \cdot e^{-k_p \cdot k_e \cdot \frac{L_{\text{rays}}}{h_{\text{max}}}} \quad (6)$$

The angle of the rise of the Sun above the horizon is a function of time and the width of the collector installation (7):

$$a = f(\varphi, t) \quad (7)$$

Instantaneous power is a function of the collector's height above sea level and the angle of the Sun's elevation above the horizon:

$$N = f[h, a(\varphi, t)] \quad (8)$$

Integrating the instantaneous power function (8) over a time interval from 0 to 24 h, we obtain the daily production of electrical energy:

$$Q_{\text{day}} = \int_0^{24} N[h, a(\varphi, t)] dt \quad (9)$$

Integrating the instantaneous power function (9) over a time interval from 0 to 365 days, we obtain the annual electric power generation:

$$Q_{\text{year}} = \int_0^{365} N[h, a(\varphi, t)] dt = \sum_{\text{day}=1}^{365} Q_{\text{day}} \quad (10)$$

The written program allows at any time to calculate the height of the Sun above the horizon and azimuth at any latitude, which can be used to control the system of collectors that track the Sun (Fig. 1).

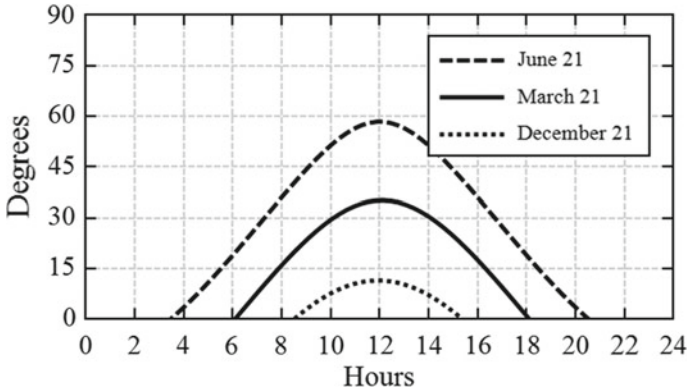


Fig. 1 Relationship between the height of the Sun above the horizon and time. For 55° north latitude

The written program allows us to calculate the relationship between the power of solar radiation and the angle of the Sun’s rise above the horizon at any height and for any angle of inclination of the collector (Figs. 2, 3).

Using the written program, you can calculate the power of solar radiation arriving at receivers with different tilt angles and compare them (Figs. 4, 5). The graphs are calculated for Kazan (55° north latitude, 60 m above sea level).

Using the written program, you can calculate the energy of solar radiation arriving at receivers with different tilt angles during the year and compare them (Figs. 6, 7).

Annual production of solar energy for Kazan, calculated according to (10): $Q_{\text{year}} = 2680 \text{ kW h/year m}^2$ (for the surface perpendicular to the solar radiation flux).

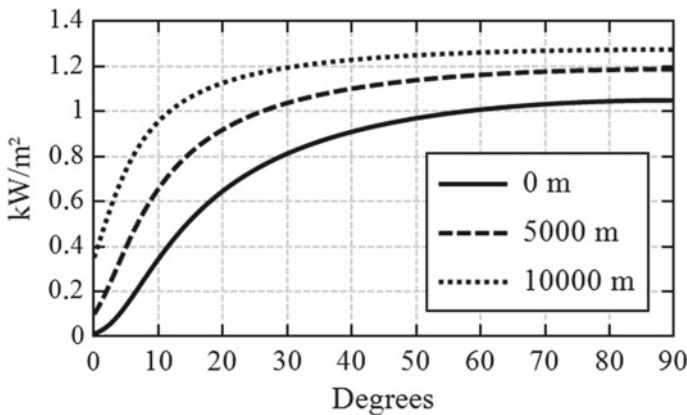


Fig. 2 Relationship between the specific power of radiation entering the surface perpendicular to the flow and the Sun’s height above the horizon

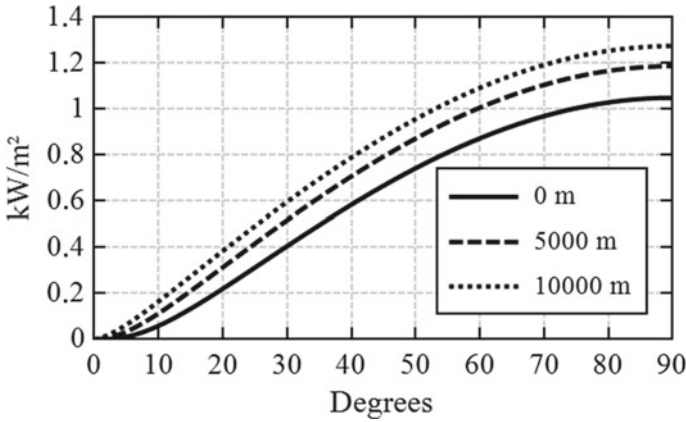


Fig. 3 Relationship between the specific power of radiation arriving at the horizontal surface and the height of the Sun above the horizon

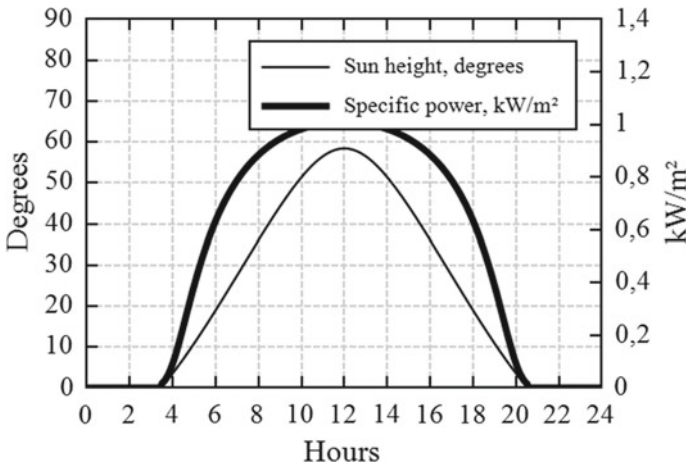


Fig. 4 Relationship between the height of the Sun above the horizon, specific power and time for the surface perpendicular to the flow (55° north latitude, 60 m above sea level, June 21)

Annual production of solar energy for Kazan, calculated according to (10): $Q_{year} = 1341 \text{ kW h/year m}^2$ (for a horizontal surface). The obtained calculations were compared with the data obtained by long-term measurements of solar radiation in a clear sky [17]. According to the results of long-term observations for Kazan:

$Q_{year} = 2676 \text{ kW h/year m}^2$ (for the surface perpendicular to the solar radiation flux);

$Q_{year} = 1253 \text{ kW h/year m}^2$ (for a horizontal surface).

In the laboratory of the International Training Center at the Novosibirsk State Technical University, a vacuum solar collector and a heat-insulated storage tank

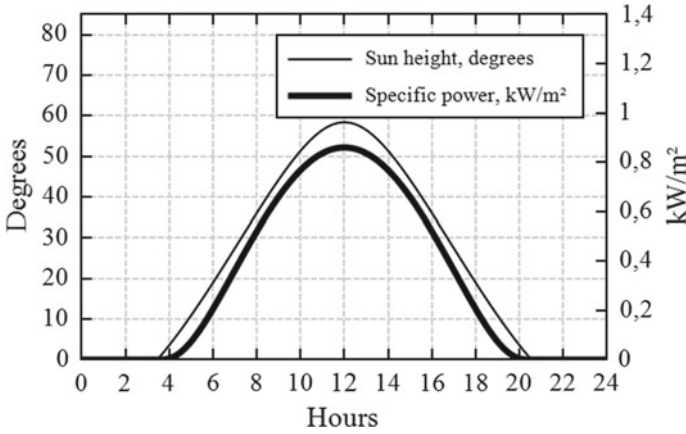


Fig. 5 Relationship between the height of the rise of the Sun above the horizon and specific power from time for horizontal collector surface (55° north latitude, 60 m above sea level, June 21)

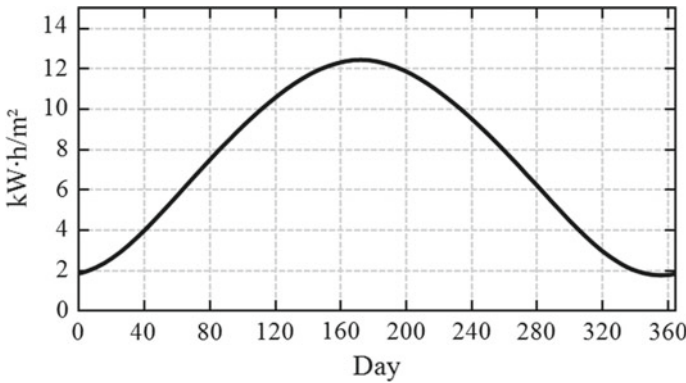


Fig. 6 Relationship between the energy of solar radiation arriving at the surface perpendicular to the flow and the day of the year (55° north latitude, 60 m above sea level)

with a volume of 950 L are installed. The collector and the tank supply hot water to the underfloor heating system and heating convectors. The vacuum manifold is installed on the southwest wall of the building and is tilted at an angle of 15 degrees, and azimuth of the collector is 135 degrees. The graph for this collector is shown in Fig. 8 Using the written program, you can calculate these graphs for any period of time.

Annual production of solar energy for the collector installed at the NSTU, calculated according to (10): $Q_{\text{year}} = 1390 \text{ kW h/year m}^2$.

With the help of the written program, you can calculate the most optimal installation angle of the solar collector at a known latitude, altitude and azimuth. Figure 9

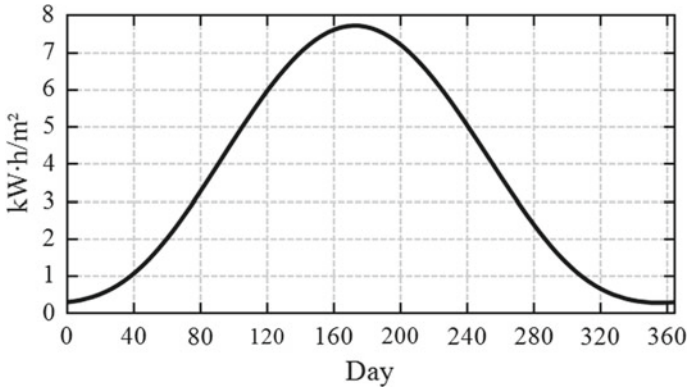


Fig. 7 Relationship between the energy of solar radiation arriving at the horizontal surface and the day of the year (55° north latitude, 60 m above sea level)

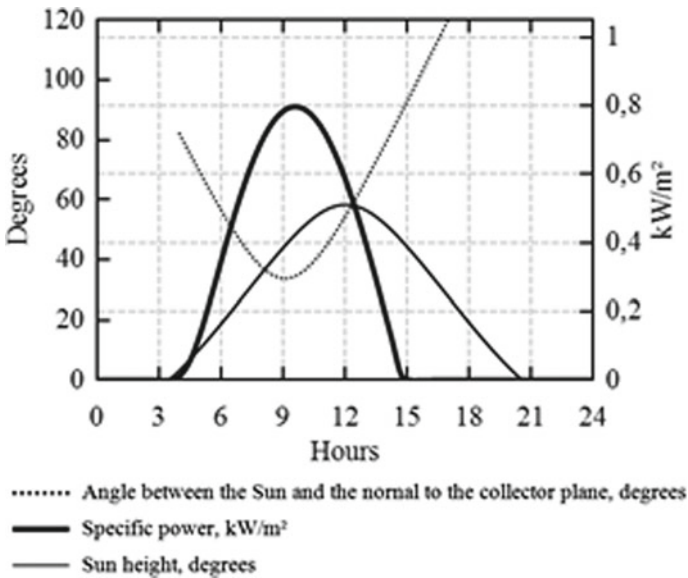


Fig. 8 Relationship between the specific power of solar radiation arriving at the collector installed in NSTU; the height of the rise of the Sun above the horizon; the angle between the Sun and the collector and hours (55° north latitude, 150 m above sea level, June 21)

shows a graph for the collector installed at the Novosibirsk State Technical University. The angle of inclination of the solar collector installed in NSTU is 15 degrees. Figure 9 shows that the power of solar radiation coming to the collector would be maximum if the collector was installed at an angle of 40–60 degrees.

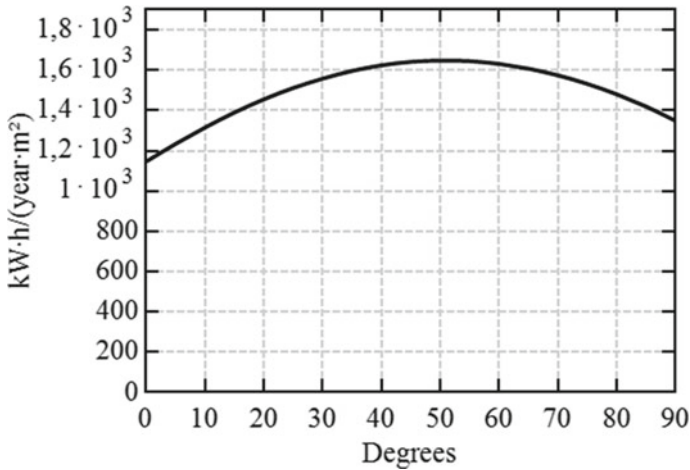


Fig. 9 Relationship between the energy of solar radiation supplied to 1 m² of the collector during the year and the collector tilt angle (55° north latitude, 150 m above sea level, 135 degrees azimuth)

3 Conclusion

The written program allows you to calculate the amount of solar radiation entering the solar collector installed at any angle to the solar radiation flux; evaluate the effectiveness of its installation in any region; calculate the power of the solar collector for any day or for a certain period of time and for any height above sea level; choose the optimal angle of installation of the collector. The obtained calculations coincide with the data of long-term observations.

Further work on the program is to ensure that the program calculates the optimal installation angle of the solar collector for a given region, taking into account the limitations of the installation angles when mounting on a specific object; calculate the most optimal period of use of the collector using meteorological data; based on the installation price of 1 m² of collector, choose the most optimal manufacturer.

References

1. Loan, S.C.: Sebarchievici: solar heating and cooling systems. In: TNQ Books and Journals 441. London (2017)
2. Stephenson, D.G.: Tables of solar altitude and azimuth. In: Intensity and Solar Heat Gain Tables. National Research Council of Canada, Ottawa, Technical Paper 31 (1967)
3. Laue, E.G.: The measurement of solar spectral irradiance at different terrestrial elevations. *Sol. Energy* **13**(1), 43–50 (1970)
4. Meinel, A.B., Meinel, M.P.: Wesley Pub. Co. Michigan, Applied solar energy 651 (1976)
5. Wolfe, P.R.: The solar generation. In: IEEE Press Wiley, vol. 369 (2018). ISBN: 9781119425588
6. Kapur, A.S.: A Practical Guide for Total Engineering of MW Capacity Solar PV Power Project, vol. 118. White Falcon Publishing (2016)

7. Wald, L.: Basics in solar radiation at Earth surface. In: Mines, I. (ed.), Paris Tech, PSL Research University, France. Sophia Antipolis, 57 (2018)
8. Raschety teplopostuplenij v zdanie ot pronikayushchej solnečnoj radiacii za otopitel'nyj period. Metodicheskoe posobie. Federal'noe avtonomnoe uchrezhdenie «Federal'nyj centr normirovaniya, standartizacii i sootvetstviya v stroitel'stve, Moskva, 111 (2017)
9. Doskenov, A.Kh., CHigak, A.S.: Modelirovanie processa postupleniya solnečnoj energii. Kurganskaya gosudarstvennaya sel'skohozyajstvennaya akademiya im. T.S. Mal'ceva. In: Materialy I Vserossijskoj nauchno-prakticheskoj konferencii «Prioritetnye napravleniya razvitiya energetiki v APK», pp. 124–129 (2017)
10. Bohren, K.F.: Atmospheric Optics. Pennsylvania State University, Department of Meteorology, p. 266 (2018)
11. Naranjo, J.D.: Crissiane Ancines. Comparative analysis of a passive system with an active water heating system by means of vacuum solar collectors glass tubes (2018). <https://doi.org/10.5380/reterm.v15i1.62154>
12. Julius, E.: Yellowhair. Field Guide to Solar Optics. Spie Press Book, 134 (2020). ISBN: 9781510636972
13. Gervits, E.S., Shishkin, A.G.: Eksergo-ekonomicheskij podhod k energeticheskoj effektivnosti. Moskva, Neft' i biznes 9, 42–47 (2017). ISSN 2218–4929
14. Neri, M., Luscietti, D.: Computing the exergy of solar radiation from real radiation data. J. Energy Resour. Technol. 139/6 (2017). <https://doi.org/10.1115/1.4036772>
15. Radwan, A., Katsura, T.: Development of a new vacuum-based photovoltaic/thermal collector, thermal and exergy analyses. Sustain. Energy Fuels 4/12 (2020). <https://doi.org/10.1039/D0SE01102A>
16. Kopp, G., Lean, J.: A new, lower value of total solar irradiance: evidence and climate significance. Geophys. Res. Lett. (2011). <https://doi.org/10.1029/2010GL045777>
17. Nauchno-prikladnoj spravocnik po klimatu SSSR. Seriya 3. Mnogoletnie dannye. Chasti 1–6. Vypusk 12. Tatarskaya ASSR, Ul'yanovskaya, Kujbyshevskaya, Penzenskaya, Orenburgskaya, Saratovskaya oblasti. Leningrad Gidrometeoizdat, p. 647 (1988)

On the Importance of Applying RCM Technology to Passive Components of Russian NPPs



A. A. Arzhaev, A. I. Arzhaev, V. O. Makhanev, M. I. Antonov,
N. M. Emelianova, A. V. Emelianov, A. A. Kalyutik, Yu. E. Karyakin,
K. A. Arzhaev, I. N. Denisov, V. P. Derij, and M. A. Podlatov

1 Introduction

“The overall direction in which the world energy sector is developing is already visible: influenced by the changes in the energy policy and the development of new technologies, the world is entering the 4th energy transition phase, characterized by the widespread use of renewable energy sources and displacement of fossil fuels. However, the pace of these changes and the speed of transition are associated with high uncertainty” as stated in [1]—Fig. 1a.

General energy “decarbonization” (Fig. 1b) seems to be ineffective without taking into account nuclear energy which is discussed in some aspects here below with respect to its optimization by application of Reliability Centered Maintenance (RCM) technology.

A. A. Arzhaev · A. I. Arzhaev (✉) · V. O. Makhanev
LLE “SPE “DIAPROK”, Moscow, Russia
e-mail: arjaev@dsc.msk.ru

M. I. Antonov · N. M. Emelianova · A. V. Emelianov · A. A. Kalyutik · Yu. E. Karyakin
Peter the Great St. Petersburg Polytechnic University, Sankt-Petersburg, Russia

K. A. Arzhaev · I. N. Denisov
ANO “International Nuclear Safety Center”, Moscow, Russia

V. P. Derij · M. A. Podlatov
JSC “Atomtechenergo”, Moscow, Russia

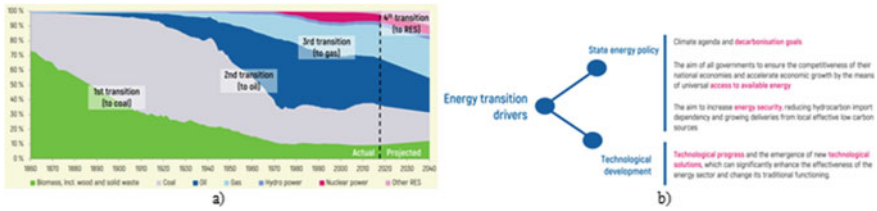


Fig. 1 Current energy transition policies and technologies: **a** structural changes in global total primary energy consumption by fuel type in 1860–2040 and the four energy transitions; **b** energy transition drivers

2 The Place of Nuclear Energy in Ensuring the Sustainability of the Russian Energy Sector

The concept of “sustainable energy” is very relevant for the Russian Federation, where nuclear power plants (NPPs) are an integral part of the overall energy supply [2], as shown in Fig. 2.

For technologically isolated power systems (Fig. 2), floating NPPs have already been introduced in Russian nuclear industry [3], and proposals have been developed for use of small modular reactors (SMR) on the shelf [4] and in the mining industry [5].

Taking into account the proposed transition from an open nuclear fuel cycle (ONFC) to a closed one (CNFC) with the use of NPPs with fast breeder reactors

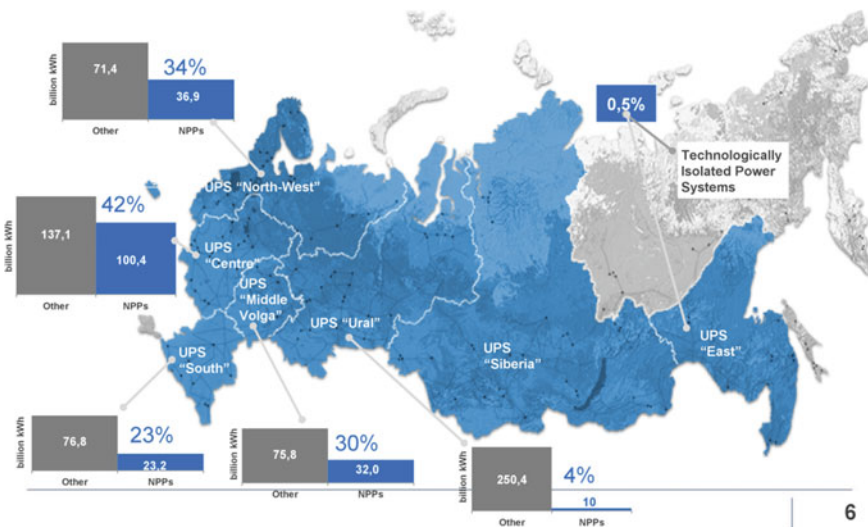


Fig. 2 NPP share in Russian electricity generation in 2018—18.4% (204.5 billion kWh); *Note* UPS—United Power System

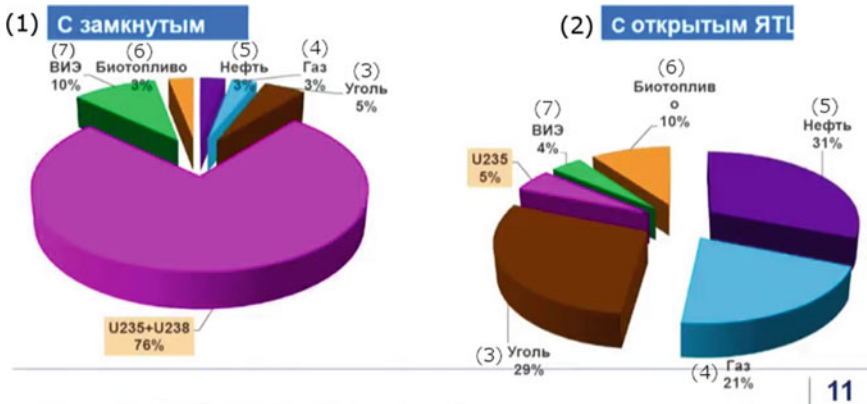


Fig. 3 Energy potential of various types of reserves of raw materials for energy generation in Russia: (1)—NPPs with CNFC; (2)—NPPs with ONFC; (3)—coal; (4)—gas; (5)—oil; (6)—biofuels; (7)—renewables

[5], additional opportunities open up for the use of Russian resources for the development of nuclear power plants based on CNFC (Fig. 3). Transition to CNFC could allow changing the raw material base of the nuclear power from a limited resource of U-235 (0.7% of natural uranium) to almost unlimited U-238 (99.3%).

International and domestic experts mainly consider NPPs as an integral part of “green” energy [6, 7] (Fig. 4).

By 2020, the contribution from “green” energy sources was equal to the contribution to the generation of coal-fired power plants [8].

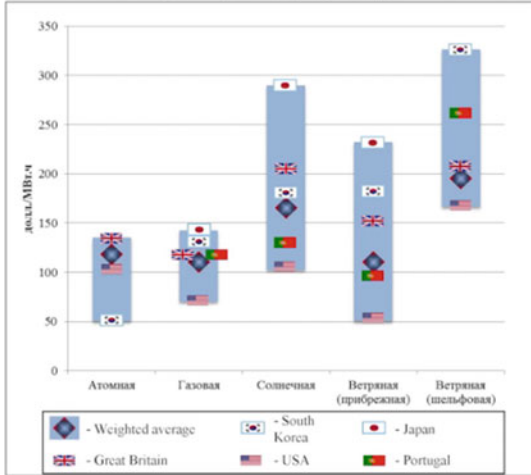
Nuclear power has a good potential to survive in the economic struggle with renewable energy sources (Fig. 4, [7]); however, there is the risk for RF nuclear power to become uncompetitive with energy produced by combined-cycle plants [9]: “The main barrier to the development of modern NPPs is the issue of competitiveness, which rests on the problem of safety. Attempts to solve the problem of safety by creating additional active safety systems have led to decrease in the competitiveness of nuclear power vs organic energy”.

To increase the share of nuclear power generation, the IAEA proposes a transition to the concept of long-term operation [6, 10], demonstrating that extending the service life of existing nuclear power plants significantly increases the availability of reliable low-carbon energy, helping to achieve climate goals and transition to clean energy by 2050.

3 Current Issues for Nuclear Power

The stability of generation at nuclear power plants is associated with ensuring safe operation, the problems of which are schematically reflected in Fig. 5, refined in

LCOE for new powerplants projects (commission date - 2020)



- Competitiveness of renewables very much depends on the region
- Several renewables projects are currently under development in Russia
- Combined cycle plants will continue to be the main competitor for nuclear, along with emerging renewable power

Sources: Projected Costs of Generating Electricity – 2015 Edition. International Energy Agency (IEA), Nuclear Energy Agency (NEA), 2015. ставка дисконтирования 10%

Fig. 4 Indicators of modern energy-generating technologies [7]

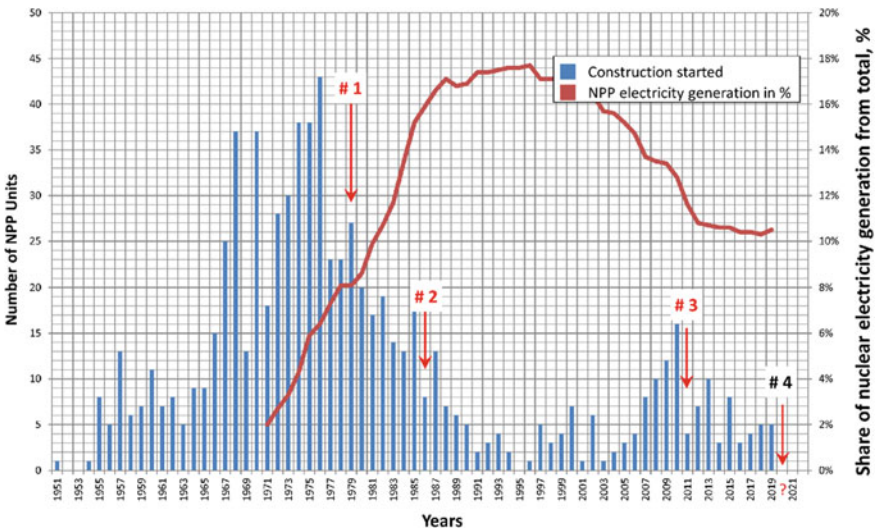


Fig. 5 Impact of accidents on the share of generation at NPPs (# 1—1979, NPP “Three-Mile Island” (USA): The construction of 38 NPP units, started before 1979, was canceled in the United States, and the construction of 4 new NPP units was started only in 2013 [15]; # 2—1986, Chernobyl NPP, Unit 4 (USSR) [16]; # 3—2011, Fukushima-1 NPP (Japan) [17]; # 4—2020, environmental disaster in Norilsk (Russia), as a warning for the NPPs of the Russian Federation [18])

Table 1 Changes in forecasts for the development

2009 ^a	2019 ^b /2020	2030	2040	2050	Forecast
13.8	14.6	13.8	–	7.1	Low (%)
	16.0	16.6	–	17.0	High (%)
–	10.4	8.2	6.4	5.7	Low (%)
		10.5	11.4	11.2	High (%)
	2657	3682	4933	5762	High (TWh)

Notes Impact of the accident at the Fukushima-1 NPP (Japan)

^abefore the accident: according to [19]; ^bafter the accident: according to [20]; the actual energy output indicators are shown in bold

comparison with the figure from [11].

Table 1 shows the change in the IAEA's forecasts for the development of nuclear power (optimistic-high; minimum-low), especially sharp for the “high” estimates after the accident at the Fukushima-1 NPP (Japan), which led to pollution of the world's oceans [12].

Given the above, it seems reasonable assessment of the global nuclear energy at the beginning of 2018, as “metastable” [13], which characterizes the possibility of a sharp curtailment of the world nuclear power in significant accidents at nuclear power plants (Fig. 5). Taking into account the plans for the construction of new NPPs in Russia [2] and a substantial number of orders for the construction of NPPs of Russian projects abroad [14], the nuclear power security issues acquire greater relevance to our country.

4 Ways to Optimize the Performance of NPPs in the Russian Federation

4.1 Proposals for Managing the Life of NPPs Based on RCM Technology

In 2013–2014, the possibilities of NPP life cycle management were considered to improve the efficiency of new NPP units by implementing an additional set of works at the design, start-up, adjustment works and commissioning stages [21–24]. After the introduction of new regulatory documents at the end of 2015, the proposed set of measures for the long-term operation of new NPP units was confirmed in the requirements of new federal rules and norms [25–28].

Based on the IAEA document [29], proposals were developed for the implementation of RCM technology on new NPP units, starting from the design stage [24] (Fig. 6).

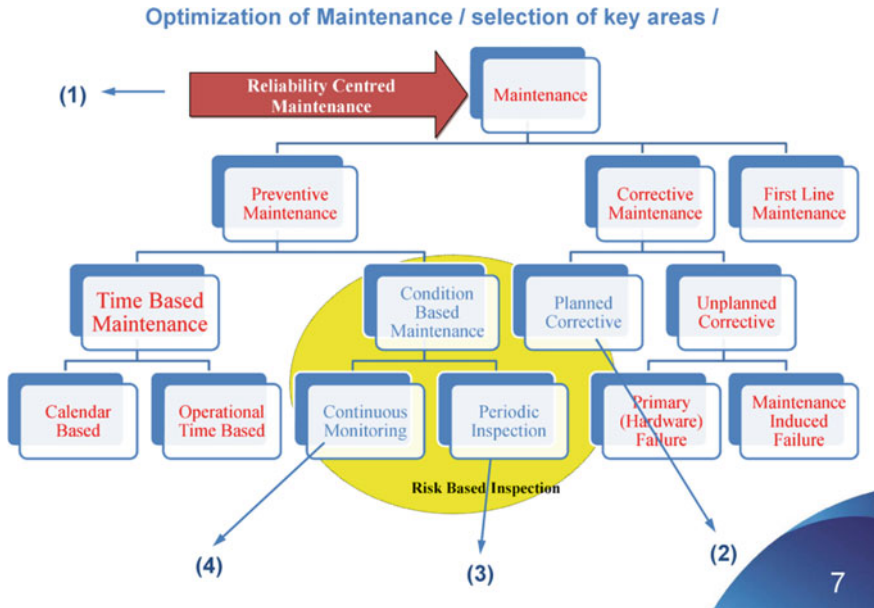


Fig. 6 Components of RCM technology for new NPP units

Items (1)–(4) in Fig. 6 include the measures proposed for thermal–mechanical equipment including piping (TME):

- (1) Ranking of systems and components according to the degree of criticality of a failure leading to a NPP unit shutdown, as the basis for application of maintenance and repair [29];
- (2) Development of a structural integrity justification for TME within the framework of the “leak before break” (LBB) [30] and “break exclusion” (BE) [31] methodology in order to prevent guillotine breaks, as well as through-wall defects;
- (3) Optimization of non-destructive testing (NDT):
 - Development of new NDT technologies to eliminate the time for inspection (typical for nuclear power plants of the “AES-2006” series»);
 - Implementation in the industry of a special center (independent of NDT service providers and utilities) for NDT tools and techniques qualification (to obtain indicators of crack-like defect detection probabilities, comparative assessments of time spendings on inspection, etc.) [32];
 - Development of NDT programs for NPP TME based on risk assessment;
 - Implementation of a system for monitoring changes in the properties and structure of TME metal during long-term operation [33];
- (4) Development of design standard solutions for monitoring and diagnostics systems for the NPP “pre-operation” and “operation” stages [34].

4.2 Features of RCM Technology Application at NPPs

RCM technology is used at NPPs mainly in the framework of active component maintenance [29, 35, 36]. However, in accordance with the existing standards [37, 38], the RCM technology is also applicable to passive NPP components, for example, to TME.

The last appendix in these standards contains guidelines for developing failure management policies for all structures or TME. Once these policies are established, a maintenance schedule is determined which will assure continued safe operation throughout the TME's life.

There are two failure management approaches for TME, safe-life and damage-tolerant TME:

1. Safe-life TME is designed to be free from failure during its operational life.
2. Damage-tolerant TME is designed to be resistant to the effects of damage during its operational life.

Safe-life TME is characterized by the following features:

- (1a) failure of one or more structural elements results in complete loss of function;
- (1b) rapid progression from potential to functional failure (e.g. crack propagation rate is too fast to allow inspection before failure).

Damage-tolerant TME is characterized by the following features:

- (2a) failure of part of the structure (for example, sub-critical crack or even a leak) does not result in complete loss of function;
- (2b) gradual progression from potential to functional failure (e.g. crack propagation rate allows for inspection before failure).

The group of "safe-life TME" according to criteria (1a) and (1b) can include TME, which failures are extremely undesirable: for example, VVER reactor pressure vessel [40] or metal structures of the RBMK-1000 reactor [14], both of which, in particular, are located in the zone of radiation exposure.

To the group of "damage-tolerant TME" according to criteria (2a) and (2b), it is necessary to refer, in the first place, primary circuit TME of NPP with VVER, main steam piping and feed water piping within the containment, and the main and auxiliary piping outside containment.

To the group of "damage-tolerant TME" at RBMK NPPs, it is necessary to refer, in the first place, TME of the multiple forced circulation circuit and the sections of the adjacent piping:

- steam piping;
- feed water piping;
- blowdown and cooldown piping;
- emergency reactor cooling ping.

The report [24] recommended the development of differentiated cost-effective approaches to ensure the structural integrity of the TME within the framework of RCM technology application (Figs. 6 and 7).

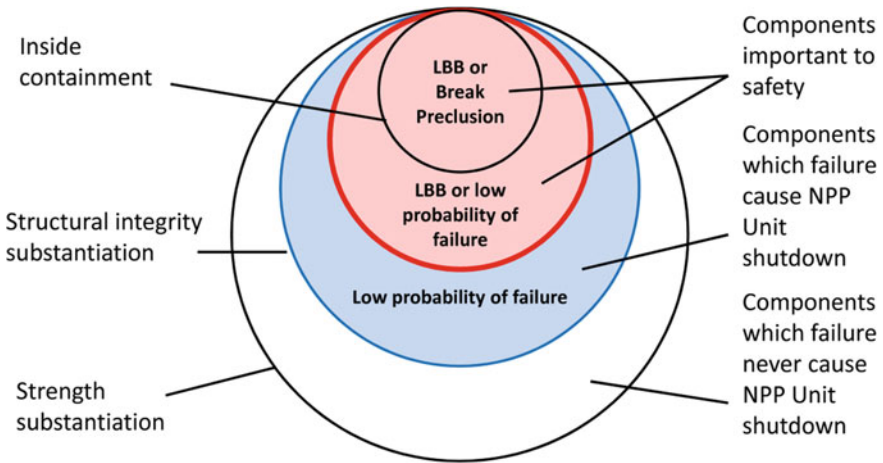


Fig. 7 Areas of application of the structural integrity concepts

4.3 Detailed Proposals for the Use of RCM Technology at Russian NPPs

The approaches described in paragraph 3.40 of the IAEA document [39] can be recommended for the most critical elements of the primary circuit TME as a basis for not considering the ruptures of these pipelines as postulated initiating events of design accidents:

- LBB [30];
- break preclusion;
- low probability of failure (or BE according to [31]).

The features of the listed methodological approaches are considered in [40, 41].

By 1995, Russia had developed a procedure for the calculation justification of LBB concept application to NPP piping, and in 1999, the document RD 95 10,547-99 was developed [30], which for a long time was used to justify the safe operation of new and existing NPPs in Russia [11] and units of Russian design NPPs abroad: Tianwan NPP (China), Bushehr NPP (Iran) and Kudankulam NPP (India).

4.4 Consideration of Aging Effects During RCM Technology Application at Russian NPPs

For pipelines and NPP equipment with potentially active damage mechanisms, the classical LBB concept [30] cannot be applied, as well as the Break Preclusion

Concept, according to [42]. This applies to the following damage mechanisms, known from the experience of operating existing NPP units:

- intergranular stress corrosion cracking in
 - welds of RBMK piping and headers DN (200 ÷ 300) mm made of steel grade 08Ch18N10T;
 - repair zones welded by austenitic materials in RBMK DN 800 mm pipelines with a transition layer made by electrodes EA-395 (in connection with primary circuit coolant);
 - DN 1100 mm welded joints connecting primary circuit headers to steam generator branches at VVER-440;
- delayed deformation and corrosion cracking:
 - DN 1200 mm welded joints connecting primary circuit headers to steam generator branches at VVER-1000;
- erosion and corrosion wear (E/C):
 - base metal and welded joints of steam pipelines, feed water and condensate piping and wet-steam piping at all NPP units;
 - sections of pipelines and valve housings of the RBMK DN800 at the inner surface without austenitic cladding.

Currently, paragraph 3.3.3 of NP-001-15 [25] requires the application of the LBB concept to the reactor coolant circuit (RCC). The national standard [43] on the application of the LBB concept to NPP pipelines, taking into account the requirements of regulatory documents [25–28], is currently in force for the RCC and other safety relevant pipelines of the Russian NPP.

Therefore, it is necessary to update the previously developed justifications for the application of the LBB concept to TME (previously according to [30]), taking into account actual requirements [25–28, 43] in order to incorporate aging effects [10] and eliminate the identified deficiencies in the application of the LBB concept [44]. One of the main ones is the deficit associated with the lack of NDT system qualification [45] in terms of confirming indicators of the probability of detecting crack-defects (Table 2).

The requirement to apply countermeasures if there are non-design damage mechanisms in the candidate pipeline reduces the integrity of the methodological approach of the LBB concept [43] in comparison with [42] and the basic RF document [30], accepted by all foreign customers of Russian-designed NPPs.

It is difficult to suggest effective long-term countermeasures to eliminate the susceptibility of TME to damage due to aging by the mechanism of E/C [52, 53]. Therefore, deficiencies of NDT for TME susceptible to E/C damages need to be fixed in the first place. For the designed NPP units, it is recommended to replace the material of the second circuit pipelines with a material having increased damage resistance against E/C.

Table 2 NDT system—comparison of requirements for qualification before and after 2015

Before 2015	After 2015–2016
Conformity assessment in the form of tests of NDT tools and procedures for NPPs belong to category “PRODUCTION” according to [46] (and later according to paragraph 3 of NP-071-18 [47]) and to the following documents:	Conformity assessment in the form of tests of NDT system (NDT tool and procedures, and personnel performing inspection) which do not belong to category “PRODUCTION” according to [46] (and according to paragraph 2 of NP-071-18 [47]) and to the following documents:
<ul style="list-style-type: none"> – PNAE G-7-010-89 [48] (paragraphs 1.4, 1.10); – Utility document 0487-2005 [49] (before 2015); – Utility document 1.1.2.25.0487-2015 [50] 	NP-084-15 [27]: <ul style="list-style-type: none"> – paragraphs 61-64: obligatory conformity assessment of NDT system performance reliability indicators confirmation by NDT system qualification (testing), obtaining indicators of the probability of detecting crack-defects and/or deviations from the geometric dimensions; NP-105-18 [51]: <ul style="list-style-type: none"> – paragraph 28: obligatory conformity assessment of specific NDT procedures

All the deficiencies in the application of the basic technologies used in the application of RCM technology since 2014 [24] and recommendations for eliminating already known deficiencies [44, 45] were presented in May 2019 at the conference of JSC OKB “Gidropress» and then at the technical seminar of the State Corporation “Rosatom”—“Design of pipelines in accordance with ASME BPVC and EN 13,480. The practice of applying the concept of ‘Leak-before-break’ at nuclear power plants of American and French design” [54].

Other TME of NPP unit, the failure of which during operation at capacity leads to the shutdown of the NPP unit and the generation losses of electricity, should also be attributed to the group of damage-tolerant TME.

For such structures, it is advisable to use the concept of low probability of failure [31, 40, 41], which does not require expensive leak detection systems or allows the use of their simplest variants (for example, sump water level monitoring), as well as performing of TME strength assessment according to the PNAE G-7-002-86 [55] based on TME material substantiation according to the requirements of paragraph 16 of NP-096-15 [28].

Leading design organizations have worked out the issues of ranking the TMO of new nuclear power plants by their impact on safety [56] and readiness [57].

The standards of design organization were developed and enacted [58, 59], which formally can be used to determine the significance of TME for safety classes [25] and readiness indications for aging management and application of RCM technology.

The implementation of the TME structural integrity concepts will be an important component of the justification of the safe operation conditions, as well as an effective

tool for ensuring high NPP readiness indicators based on the application of RCM technology.

5 Conclusion

Nuclear energy is an important sector of the sustainable energy of the Russian Federation.

Russian NPPs are large (1000–1200 MW) and medium (440 MW) power units, as well as SMR for technologically isolated power systems.

For passive components of NPPs, in particular TME, the RCM technology is applicable in accordance with the recommendations of the IAEA and international standards.

It's necessary to ensure that TME meets the requirements for “safe-life structures” (as is provided, for example, for the VVER reactor vessel by application of large margin of strength above the expected loads) and for “damage-tolerant TME”, based on the concepts of structural integrity (LBB, Break Preclusion, “low probability of failure”).

Disclaimer The presentation of material and details in maps used in this chapter does not imply the expression of any opinion whatsoever on the part of the Publisher or Author concerning the legal status of any country, area or territory or of its authorities, or concerning the delimitation of its borders. The depiction and use of boundaries, geographic names and related data shown on maps and included in lists, tables, documents, and databases in this chapter are not warranted to be error free nor do they necessarily imply official endorsement or acceptance by the Publisher or Author.

References

1. ERI RAS.: Moscow School of Management SKOLKOVO. Global and Russian energy outlook (2019). <https://clck.ru/TB5fi>
2. Asmolov, V.G.: Strategy of 2018. In: Proceedings of the 11th Conference “Safety Assurance of NPP with VVER” (2019). <https://clck.ru/TB4QS> (in Russian)
3. Goltsov, E.N., Kulikov, D.G., Pimenov, A.O., Rapnitskiy, V.A.: Shelf reactor for SMRs. In: Proceedings of the IV International Scientific and Technical Conference (2016). <https://clck.ru/TB5io> (in Russian)
4. Adamov, E.O.: Small nuclear power for power supply of mining facilities. In: Proceedings of the V National Mining Forum (2019). <https://clck.ru/TB5vh> (in Russian)
5. Adamov, E.O.: The second nuclear project “proryv”. In: Proceedings of the Intelligent platform “Knowledge. Technologies. The future” (2018). <https://clck.ru/TB85h> (in Russian)
6. IAEA.: STI/PUB/1911 (2020). <https://clck.ru/TB8Na>
7. Adamov, E.O.: Project “Proryv” (Breakthrough). Results achieved and further development of closed nuclear fuel cycle technologies. In: Proceedings of the VIII International Forum ATOMEXPO (2016). <https://clck.ru/TB8qX>
8. IEA.: Global Generation Shares from Coal and Low-Carbon Sources, 1971–2020 (last updated 30 April 2020). <https://clck.ru/TB9Vr>

9. Adamov, E.O.: The role of fast reactors in Russian nuclear power development strategy. In: Proceedings of 11th Conference "Safety Efficiency and Economics of Nuclear Power Industry" (2018). <https://clck.ru/TB9Zc> (in Russian)
10. SSG-48.: Safety Standards Series, IAEA (2018). <https://clck.ru/TB9cw>
11. NEI.: The Lingering Ghost of Chernobyl (9 July 2019). <https://clck.ru/TBBDU>
12. "Fukushima" Kills the Ocean Under the Silence of the World Community (2019). <https://clck.ru/TBBau> (in Russian)
13. Adamov, E.O.: In: Proceedings of at the Event "Day of Science" in the State Corporation "Rosatom" (6 February 2018). <https://clck.ru/TBBmW> (in Russian)
14. Rosatom.: Nuclear Power Plants Under Construction. <https://clck.ru/MzkCp>
15. IAEA.: Country Nuclear Power Profiles. United States of America (2019). <https://clck.ru/TBa4J>
16. NIKIET.: RBMK Channel Nuclear Power Reactor. Chapter 13 (2006). <https://clck.ru/TBBQm> (in Russian)
17. Narabayasi, T.: In: Proceedings of 8th Conference "Safety Efficiency and Economics of Nuclear Power Industry" (2012). <https://clck.ru/TBBUy> (in Russian)
18. Norilsk Disaster 2020: Oil Spill (2019). <https://clck.ru/TBBYh> (in Russian)
19. IAEA.: IAEA-RDS-1/30 (2010). <https://clck.ru/TBBha>
20. IAEA.: IAEA-RDS-1/40 (2020). <https://clck.ru/TBBhL>
21. Arzhaev, A.I., Makhanev, V.O., Podlatov, M.A., et al.: Up-to-date technologies of component technical condition inspection and diagnostics during NPP unit construction and commissioning (Paper Reference #1541). In: International Conference on Flow Accelerated Corrosion (2013)
22. Arzhaev, A.I., Derij, V.P., Dub, A.V., Makhanev, V.O., Podlatov, M.A., et al.: NDE Tools Selection for Components' State Characterization During NPP Unit Commissioning and Operation. In: JRC-NDE 2013 (2013). <https://clck.ru/TBMZC>
23. Arzhaev, A.I., Makhanev, V.O., Pavlovich, A.A., Podlatov M.A., et al.: Support of design service life of NPP equipment and pipelines in long-term operation conditions. In: Proceedings of 9th Conference "Safety Efficiency and Economics of Nuclear Power Industry" (2014). <https://clck.ru/TBJ3y> (in Russian)
24. Arzhaev, A.I., Butorin, S.L., Vostrikov, A.V., Derij, V.P.: About ensuring optimal technical and economic operational indicators of existing and new NPP power units (2014). In: IBA "INTERATOMENERGO" Meeting, Czech, Plzen (December 2014)
25. NP-001-15.: General Provisions For Nuclear Power Plant Safety Assurance. <https://clck.ru/TBDqi> (in Russian)
26. NP-089-15.: Rules for Design and Safe Operation of Equipment and Pipelines of Nuclear Power Installations. <https://clck.ru/TBDv5> (in Russian)
27. NP-084-15. Rules for Control of Base Metal, Welded Joints and Deposited Surfaces During Operation of Equipment, Pipelines and Other Components of Nuclear Power Plants. <https://clck.ru/TBDvd> (in Russian)
28. NP-096-15.: Requirements for Management of Service Life of Equipment and Pipelines of Nuclear Power Plants. General Provisions. <https://clck.ru/TBELW> (in Russian)
29. IAEA-TECDOC-1590.: IAEA (2008). <https://clck.ru/TBM8V> (in Russian)
30. RD 95 10547-99.: Guidance on the Application of the LBB Concept for NPP Piping. <https://clck.ru/TBDjc> (in Russian)
31. Application of "Break Exclusion" concept for pipelines and headers of DN 300 KMPC and safety important systems of NPP power units with RBMK-1000. Utility document 0513-2003 (2003) (in Russian)
32. Peter the Great St. Petersburg Polytechnic University. Letter to JSC OKB "Gidropress" NoOD-21-6-361 at 23.07.2014 (in Russian)
33. JCP "Leading Institute VNIPIET". Decision of the Joint Scientific and Technical Council Section "Nuclear power plants with thermal neutron reactors" (29 November 2013) (in Russian)
34. Arzhaev, A.I., Kozyrev, V.D.: Technical diagnosis as control element of NPP life cycle. In: Proceedings of 9th Conference "Safety Efficiency and Economics of Nuclear Power Industry" (2014). <https://clck.ru/TBJ3y> (in Russian)

35. Perez-Cerdan, A.B.: Scope setting process and ageing management review for LTO at Ringhals NPP. In: Fourth International Conference on Nuclear Power Plant Life Management (2017)
36. Chaban, O.G.: Justification of Reliability Centred Maintenance application in the design of foreign NPPs (October 2019) (in Russian)
37. EC 60300-3-11.: Dependability management—Part 3—11: Application Guide—Reliability Centered Maintenance. Edition 2.0 (June 2009)
38. Dependability in technics. Dependability management, Reliability centered maintenance. GOST R 27.606–2013. <https://clck.ru/TBHPL> (in Russian)
39. IAEA.: STI/PUB/1191. <https://clck.ru/TBHJs>
40. Schulz, H.: The Evolution of the Break Preclusion Concept for Nuclear Power Plants in Germany NUREG/CP-0155 (1995). <https://clck.ru/TBHKb>
41. European Safety Practices on the Application on the Leak Before Break (LBB) Concept. European Commission, EUR 18549 EN (2000). <https://clck.ru/TBH4j>
42. KTA Safety Standard. KTA 3206 (2014). <https://clck.ru/TBGQz>
43. Piping of nuclear power plants, “Leak before break” concept. GOST R 58328-18. <https://clck.ru/TBFTY> (in Russian)
44. Peter the Great St. Petersburg Polytechnic University, LLE “SPE “DIAPROK”. About weak points of LBB Concept application to reactor coolant circuit of old and new generation NPP Units. Scientific and technical report (2018) (in Russian)
45. Peter the Great St. Petersburg Polytechnic University, LLE “SPE “DIAPROK”. Proposals for the creation of a system for assessing the compliance of NDT systems for the condition of metal equipment and pipelines to ensure the safe operation of NPP. Scientific and technical report (2017) (in Russian)
46. Russian Federation Government decree, no. 544 (15 June 2016). <https://clck.ru/TBMEH> (in Russian)
47. NP-071-18.: Rules for Assessment of Compliance of Products, for Which Requirements Related to Safety in the Field of Atomic Energy Use as Well as Requirements for Processes of Its Designing (Including Surveys), Production, Construction, Installation, Adjustment, Operation, Storage, Shipment, Sale, Utilization and Final Disposal Are Established, <https://clck.ru/TBFHv> (in Russian)
48. PNAE G-7-010-89.: Equipment and Piping of Nuclear Power Installations. Weld Joints and Weld Overlays. Rules of inspection. <https://clck.ru/TBLF3>
49. Utility document 0487-2005.: Typical Requirements for the Order of Development of a Technical Task, Performing Tests, and Conditions of Use for the Means and Procedures of Operational Nondestructive Monitoring Performed on Objects Using Atomic Energy (2005) (in Russian)
50. Utility document 1.1.2.25.0487-2015.: Typical Requirements for the Order of Development of a Technical Task, Performing Tests, and Conditions of Use for the Means and Procedures of Operational Nondestructive Monitoring Performed on Objects Using Atomic Energy (2005). <https://clck.ru/TBMNf> (in Russian)
51. NP-105-18.: Rules for Control of Metal of Equipment and Pipelines of Nuclear Power Installations During Manufacture and Assembling. <https://clck.ru/TBEM9> (in Russian)
52. Arzhaev, A.I., Makhanev, V.O., Pavlovich, A.A., Podlatov, M.A., et al.: Ensuring safe operation of the nuclear power unit equipment and pipelines potentially susceptible to FAC. In: Proceedings of 9th Conference “Safety Efficiency and Economics of Nuclear Power Industry” (2014). <https://clck.ru/TBJ3y> (in Russian)
53. Arzhaev, A.I., Makhanev, V.O., Podlatov, M.A., Arzhaev, K.A., et al.: Complex management of FAC issues for operating and new NPP units (Paper Reference n°6L01). In: International Conference on Flow Accelerated Corrosion (2016)
54. Kalyutik, A.A., Arzhaev, A.I., Makhanev, V.O., et al.: Problematic issues of structural integrity ensuring for NPP piping and vessels. In: Proceedings of the 11th Conference “Safety Assurance of NPP with VVER” (2019). <https://clck.ru/TBJF5> and <https://clck.ru/TBJLS> (in Russian)
55. PNAE G-7-002-86.: Rules of Equipment and Pipelines Strength Calculation of Nuclear Power Plants. <https://clck.ru/TFWKM>

56. Ershov, G.A., Gurin, V.V., Nikolaev, F.V., Chaban, O.G., et al.: Methodology for justifying safety classes of systems and components of nuclear power plants. In: Proceedings of 11th Conference "Safety Efficiency and Economics of Nuclear Power Industry" (2018). <https://clck.ru/TBJeC> (in Russian)
57. Ershov, G.A., Gurin, V.V., Nikolaev, F.V., Chaban, O.G., et al.: Methodology for NPP readiness analysis. In: Proceedings of 11th Conference "Safety efficiency and Economics of Nuclear Power Industry" (2018). <https://clck.ru/TBJeC> (in Russian)
58. STO 8841271.058-2017.: Methods of Substantiation of Safety Classes of Systems and Elements of Nuclear Power Plants (2017) (in Russian)
59. STO 8841271.050-2017, Methods of NPP Readiness Analysis at the design stage (2017) (in Russian)
60. JSC Rosenergoatom, Floating Nuclear thermal power plants (PATES). <https://clck.ru/NMqhq> (in Russian)
61. Cacuci, D.G. (ed.): VVER-Type Reactors of Russian Design. Chapter 20 in Handbook of Nuclear Engineering, vol. 4

Change in Rheological Properties of M100 Fuel Oil After Ultrasonic Treatment



Rustem Kamalov

1 Introduction

Fuel oil obtained from high-viscosity oil is characterized by an increased content of paraffins, which worsens its low-temperature properties and creates some difficulties during transportation and storage. The main parameter that characterizes the possibility of transportation and combustion of fuel oil is viscosity. Reducing the viscosity allows to reduce the hydraulic resistance in the pipeline, and as a result, to reduce the cost of transportation and storage.

Methods for reducing viscosity include thermal heating and ultrasonic treatment of fuel oil. Thermal heating, used to control the rheological properties of fuel oil and other heavy oil products, is the most effective from both the technological and economic points of view [1, 2]. The literature notes the advantages of using circulating heating in fuel storage tanks and a small number of works on this topic, despite the widespread use of this method for improving rheological properties [3, 4]. However, heating of fuel oil is a rather laborious procedure, in connection with which one of the promising methods of processing fuel oil is ultrasonic treatment [5–21], which is aimed at changing the physical and chemical properties of fuel oil.

As a result of ultrasonic treatment of fuel oil, intermolecular bonds are ruptured, due to the occurrence of cavitation processes, and viscosity decreases. Ultrasonic treatment is able to effectively reduce the viscosity of heavy oil products for a long period of time, sufficient for their production, as well as for transportation over long distances.

During ultrasonic treatment on heavy oil products, thermal heating occurs. In this case, the presence of a synergistic effect is possible, which makes it possible to

R. Kamalov (✉)

Institute of Power Engineering and Advanced Technologies, FRC Kazan Scientific Center, Russian Academy of Sciences, Lobachevsky st., 2/31, 420111 Kazan, Russia

significantly reduce the viscosity and pour point of fuel oil, as well as increase the relaxation time of the structural and rheological parameters.

The study [22, 23] describes the effect of intense ultrasonic treatment on the rheological properties of heavy oil products, such as fuel oils M100 and M40. Relaxation of rheological properties was observed within 10 days after ultrasonic treatment. Authors found that ultrasonic treatment can reduce the viscosity of fuel oils for a sufficient time for transportation and spraying.

The purpose of this work was to experimentally determine the effectiveness of ultrasonic treatment of fuel oil, namely, the effect of acoustic exposure on its rheological properties.

2 Experimental Technique

To determine the rheological properties of fuel oil, SV-10 Sine Wave Vibro Viscometer (A&D, Japan) (Fig. 1) and RM 100 Rotating Viscometer (LAMY Rheology, France) (Fig. 2) were used together with VT-8 Thermostat (Laboratory Equipment Center, Russia) (Fig. 3). The viscometers are connected to a personal computer and equipped with compatible Visco RM software for RM 100 and RsVisco



Fig. 1 SV-10 sine wave vibro viscometer

Fig. 2 RM 100 rotating viscometer



ver. 1.07 V for SV-10. Ultrasonic device UZTA-0.2/22-OM series «Volna-T» (Center of Ultrasonic Technologies, Russia) was used as a source of ultrasonic exposure (Fig. 4).

During experimental studies, a modified method for determining the dynamic viscosity of heavy hydrocarbons was used, taking into account the critical parameters and molecular weight, depending on the structure of the object under study, temperature and pressure.

The initial temperature of fuel oil subjected to ultrasonic treatment is 25 °C. Immediately after ultrasonic treatment of the samples, experimental studies were carried out to determine the viscosity of fuel oil. To identify the repeatability of obtained results, two experiments were carried out on two fuel oil samples.



Fig. 3 VT-8 thermostat



Fig. 4 Ultrasonic device UZTA-0.2/22-OM series «Volna-T»

The experiment procedure includes the following steps:

- fuel oil is poured into the measuring cylinder of the viscometer;
- the measuring cylinder is thermostated for 10 min with simultaneous rotation of the cylindrical spindle;
- obtaining the values of the coefficient of dynamic viscosity with increasing shear rate;
- processing of experimental data.

Thus, dependences of dynamic viscosity coefficients of fuel oil on shear rate and temperature were obtained.

3 Results and Discussion

Figure 5 shows dependence of the dynamic viscosity of M100 fuel oil on temperature. To identify the repeatability of obtained results, two experiments were carried out on two samples of fuel oil. The relative error of the experiments performed was 1.8%.

For the most correct simulation of heating process of fuel oil, as well as for the correct operation of the equipment, it is necessary to know at what temperature the fuel oil is a pseudoplastic fluid, and at what temperature it becomes Newtonian.

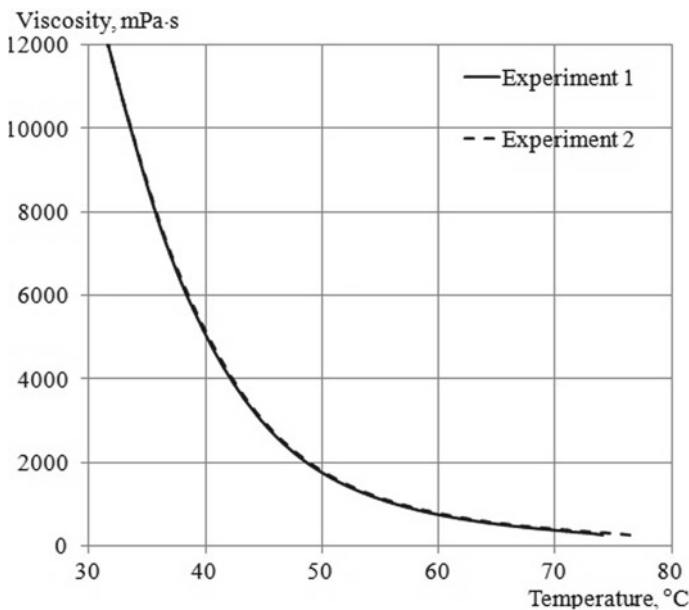


Fig. 5 Dependence of the dynamic viscosity of M100 fuel oil on temperature

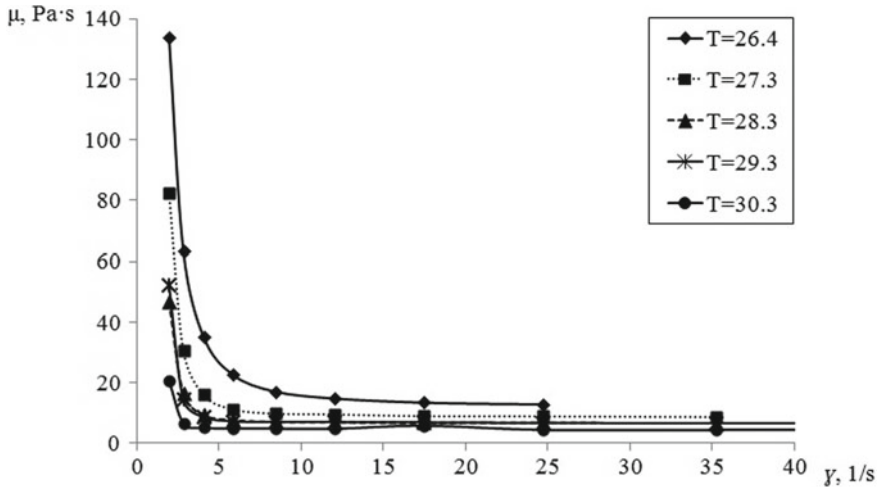


Fig. 6 Dependence of dynamic viscosity on shear rate

It has been experimentally established that in the temperature range of 26–30 °C fuel oil can be characterized as a non-Newtonian fluid [24]. Figure 6 shows the experimental data for measuring the dynamic viscosity of fuel oil depending on shear rate and approximating dependences.

The experimental data were approximated by the Ostwald–de Ville law:

$$\mu = K \cdot \gamma^{n-1} \quad (1)$$

where γ —the shear rate, K —the consistency coefficient, n —the flow index.

Figure 7 shows the obtained values of the flow index n from temperature [24]. At temperature below 31 °C, the value $n < 1$, thus fuel oil is a pseudoplastic fluid. At higher temperatures, M100 fuel oil becomes a Newtonian fluid.

Figure 8 shows the dependence of dynamic viscosity of M100 fuel oil on temperature after ultrasonic treatment. To identify the repeatability of obtained results, two experiments were also carried out on two samples of fuel oil. The relative error of the experiments performed was 1.3% at ultrasonic exposure equal to 1 min, 1.7%—at 1 min 30 s, and 1.6%—at 2 min.

Figure 9 shows the dependence of dynamic viscosity of M100 fuel oil on temperature with and without ultrasonic treatment. As can be seen from the diagram, the viscosity of fuel oil decreased after ultrasonic treatment. The decrease of viscosity is characteristic for all three experiments, which differ in the exposure time. Thus, with ultrasonic treatment on fuel oil equal to 1 min, we find that the maximum decrease in viscosity is 14.2%, the minimum is 5.6%, and the average value is 9%.

At the ultrasonic treatment on fuel oil equal to 1 min 30 s (Fig. 10), we find that

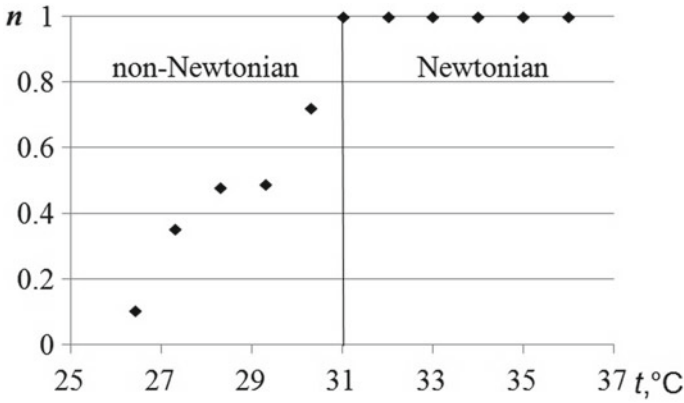


Fig. 7 Dependence of the flow index n on temperature

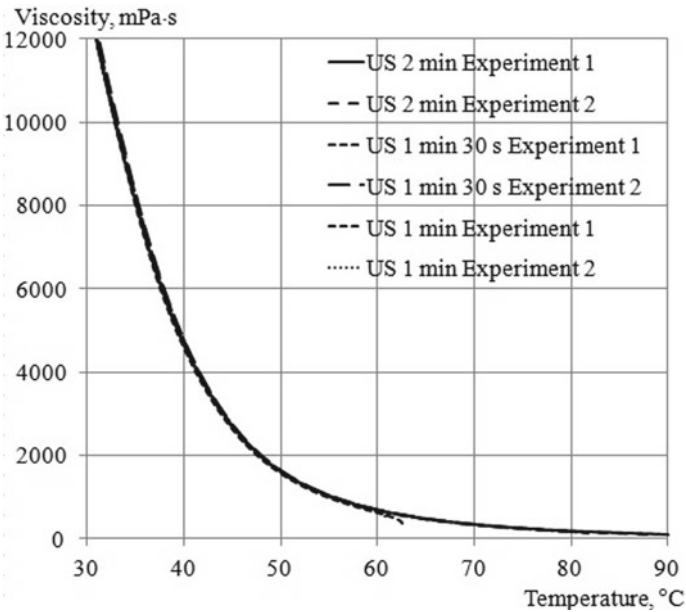


Fig. 8 Dependence of the dynamic viscosity of M100 fuel oil on temperature during ultrasonic treatment

the maximum decrease in viscosity is 6.6%, the minimum is 3.7%, and the average value is 5.2%.

Figure 11 shows the results of changes in the dynamic viscosity of fuel oil after ultrasonic treatment equal to 2 min. In this case, we find that the maximum decrease in viscosity is 7.5%, the minimum is 5.5%, and the average value is 6.4%.

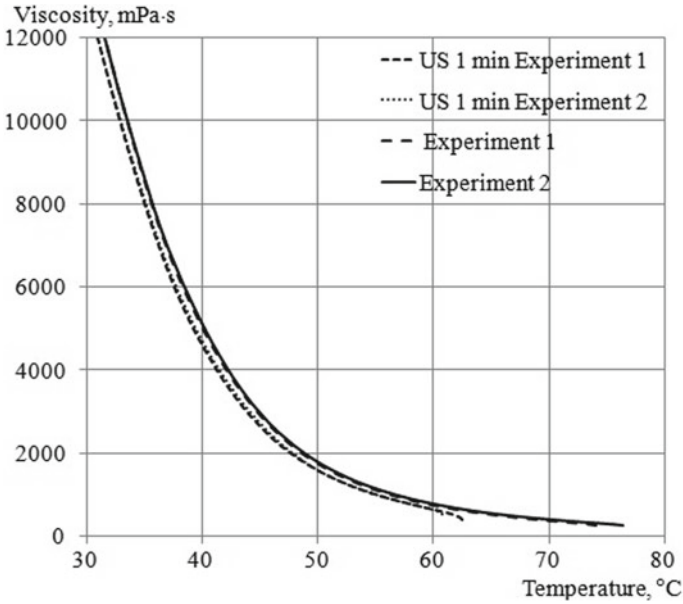


Fig. 9 Dependence of the dynamic viscosity of M100 fuel oil on temperature after ultrasonic treatment, equal to 1 min

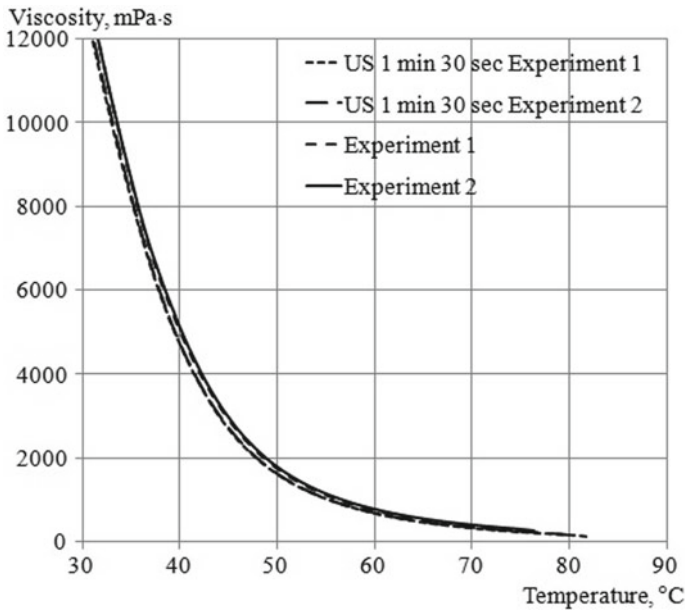


Fig. 10 Dependence of the dynamic viscosity of M100 fuel oil on temperature after ultrasonic treatment, equal to 1 min 30 s

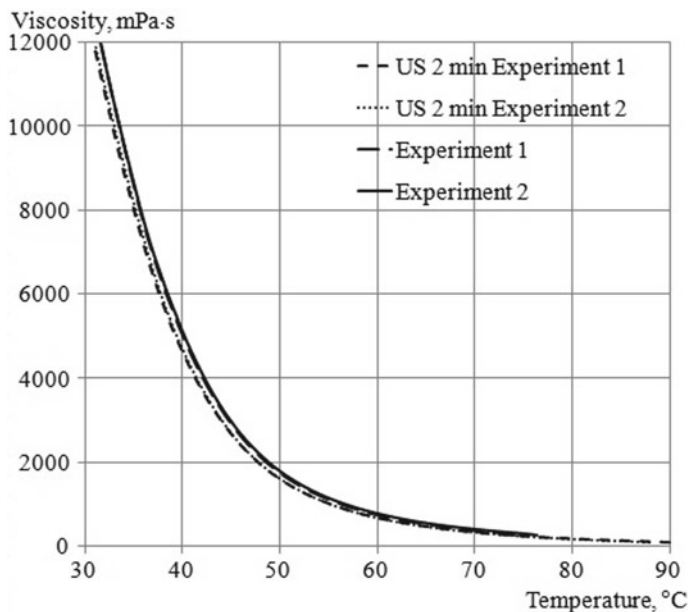


Fig. 11 Dependence of the dynamic viscosity of M100 fuel oil on temperature after ultrasonic treatment, equal to 2 min

4 Conclusions

As a result of experimental studies, it can be concluded that the ultrasonic exposure helps to reduce the viscosity of fuel oil. This means that ultrasonic treatment is able to effectively reduce the viscosity of heavy oil products for a period of time sufficient for their production, as well as for transporting heavy oil products and fuel oil over long distances. The temperature range at which fuel oil can be characterized as a pseudoplastic and Newtonian fluid has been experimentally determined. The experimental data on the measurement of the coefficient of dynamic viscosity of fuel oil depending on the shear rate were approximated by the Ostwald–de Ville law.

The part of the reported study was funded by RFBR (project number 20-08-00924) and RFBR and the government of Tatarstan Republic of Russian Federation (project number 18-48-160035). Dependence of the dynamic viscosity fuel oil on temperature was studied under financial support of the government assignment for FRC Kazan Scientific Center of Russian Academy of Sciences (project number FMEG-2021-0001).

References

1. Nazmeev, Yu.G.: Fuel Oil Facilities TPP. MPEI, Moscow (2002)
2. Nazmeev, Yu.G.: Heat Transfer and Hydrodynamics in Storage Systems for Liquid Organic Fuel and Petroleum Products. MPEI, Moscow (2005)
3. Kuznetsova, S.A., Maksimov, V.I.: MATEC Web Conf. **23**, 01047 (2015)
4. Zhao, J., Wei, L., Dong, H., Liu, F.: Case Stud. Therm. Eng. **7**, 109–119 (2016)
5. Volkova, G.I.: Petrol. Ref. Petrochem. **2**, 3–6 (2012)
6. Mullakaev, M.S.: Petrol. Ref. Petrochem. **11**, 23–28 (2011)
7. Ershov, M.A., Mullakaev, M.S., Baranov, D.A.: SSTU Bulletin **1**, 250–253 (2012)
8. Khmelev, V.N., Shalunov, A.V., Golykh, R.N., Khmelev, S.S., Sib, S.: Sci. Bull. **2**, 138–142 (2014)
9. Hamidi, H., Mohammadian, E., Junin, R., Rafati, R., et al.: Ultrasonics **54**, 655–662 (2014)
10. Qiang, H., Donghan, T., Laicheng, C., et al.: Oil Gas J. **115**, 46–49 (2017)
11. Li, J., Qi, D., Wang, Z.: Petrol. Sci. Tech. **37**, 61–67 (2019)
12. Dousta, A.M., Rahimia, M., Feyzib, M.: Chem. Eng. Process. **95**, 353–361 (2015)
13. Kent, J.A.: Riegel's Handbook of Industrial Chemistry. Springer, New York (2003)
14. David, S.J., Pujado, P.R.: Handbook of Petroleum Processing. Springer, New York (2006)
15. Heinemann, H., Spelght, J.G.: The Chemistry and Technology of Petroleum. Taylor and Frances Group, USA (2006)
16. Simanzhenkov, V., Idem, R.: Crude Oil Chemistry. Marcel Dekker, New York (2003)
17. David, J., Cheeke, N.: Fundamentals and Applications of Ultrasonic Waves. CRC Press, Canada (2002)
18. Saikia, B.K., Dutta, A.M., Saikia, L., Ahmed, S., Baruah, B.P.: Fuel Process. Technol. **123**, 107–113 (2014)
19. Prajapat, A.L., Gogate, P.R.: Chem. Eng. Process. Process Intensif. **88**, 1–9 (2015)
20. Ramisetty, K.A., Pandit, A.B., Gogate, P.R.: Chem. Eng. Process. Process Intensif. **88**, 70–77 (2015)
21. Mishra, K.P., Gogate, P.R.: Ultrason. Sonochem. **18**, 739–744 (2011)
22. Makarev, D.I., Rybyanets, A.N., Sukhorukov, V.L.: Indian J. Sci. Technol. **9**(29), 1–7 (2016)
23. Makarev, D.I., Rybyanets, A.N., Sukhorukov, V.L.: Indian J. Sci. Technol. **9**(42), 1–7 (2016)
24. Zdor, V.O., Vachagina, E.K., Kamalov, R.F., Karaeva, J.V.: Bulletin Technol. Univer. **9**(21), 66–68 (2018)

Heat Transfer During Fuel Oil Flow in Storage Tanks and Heaters of the Reserve Facility of TPP



Rustem Kamalov

1 Introduction

Fuel oil takes a significant role in Russia's fuel and energy balance. According to the energy strategy of Russia, crude production in 2020 is 512.68 million tons. About 30% of produced crude oil after refining is converted into fuel oil, the main consumer of which is boiler houses and power plants. Recently, there has been a tendency for the deterioration of fuel oil properties, which is associated with improper preparation for its combustion. The use of surface heaters significantly watering it, which leads to a decrease in combustion efficiency. During fuel oil storage, the amount of precipitation in containers increases, when operating boiler equipment, its efficiency decreases, and an increased amount of soot is emitted into the environment with flue gases.

In fuel oil facilities of boiler houses and thermal power plants, in which the method of fuel oil heating in tanks using coil or sectional heaters is still preserved, it is advisable to replace it with circulation heating [1–4]. The circulating heating method has many advantages. The costs for the reconstruction of the fuel oil facility are paid off in a short time due to the improvement of the quality of fuel preparation, its savings during combustion, increased reliability of operation, and cheaper cleaning and repair of tanks. Circulation heating of fuel oil in tanks is used to replenish heat losses to the environment, ensure fuel homogeneity and prevent sediment [5–9].

Most of the studies of heat transfer and hydrodynamics processes during circulation heating of fuel oil were carried out at the Federal Research Center of the KazSC RAS by a team of authors under the leadership of Associate member of RAS Yu. G. Nazmeev [10–17]. In these works, fuel heating systems are considered; the operation of each element of the system is analyzed. Algebraic methods for calculating heating processes in tanks have been developed. The most significant results for

R. Kamalov (✉)

Institute of Power Engineering and Advanced Technologies, FRC Kazan Scientific Center, Russian Academy of Sciences, Lobachevsky st., 2/31, 420111 Kazan, Russia

storage of liquid organic fuel and petroleum products in tanks and reserve facilities equipped with circulation heating systems are presented in the monograph [18]. This work presents mathematical models and results of numerical studies of thermal and hydrodynamic processes for flooded flat constrained and free jets of viscous liquid in filled storage tanks. In a two-dimensional formulation [19], numerical studies of heat transfer processes during circulation heating of fuel oil for a part of the reservoir in the bottom area were carried out. On the basis of three-dimensional numerical modeling of heat transfer in reservoirs, recommendations for energy saving in the system of circulating heating of fuel oil have been developed [20].

In [21], numerical studies of hydrodynamics and heat and mass transfer in small-volume liquid fuel storage tanks were carried out. Using the Navier–Stokes equations, the author proposed a mathematical model that describes processes of hydrodynamics and heat transfer in facility for circulating heating of heavy liquid fuel.

The complexity of the experiment for the study of circulating fuel heating explains the small base of experimental data on this topic. The main experimental data were obtained by Z. I. Geller in 1966–1969 [22–24], who conducted extensive research on free cooling and heating of heavy fuel oil on an industrial scale for tanks of various sizes.

A large number of works are also presented, aimed at studying the circulation mixing of various media in tanks [25–28]. In [29], the dependence of the mixing time on the angle of inclination of the nozzle for the tanks with the ratio of the height to the diameter of the apparatus is less than 1. The authors have also proposed a mathematical model of turbulence for jet mixing apparatus. The influence of the jet angle and the number of jets on the mixing time was considered in [30]. The performed 3D modeling showed that the jet injection angle is the most important parameter for determining the mixing time. In [31], different turbulence models were used to simulate jet-mixed reservoirs. It should be noted that the goal of most studies is to study the mixing process in tanks. In [32], the processes of heat transfer in a tank for storing fuel oil in the presence of a heat source at the lower boundary were modeled, taking into account the interaction with the environment. A comparative analysis of the dependences of the average volumetric temperatures in the reservoir on time, calculated using a simplified (balanced) method and obtained as a result of numerical modeling, is carried out. It should be noted the work [33], which presents a study of the circulation heating of oil in a tank with a floating cover. Currently, despite the widespread use of circulating fuel heating in storage tanks, as well as the need to improve this method of temperature control, this publication notes a small number of works on this topic.

The purpose of this work is to determine the influence of the operating modes of fuel oil heaters on the heat transfer process inside the storage tank, to determine the average volumetric temperature depending on heating time and the efficiency of fuel oil heaters with various heat exchange intensifiers.

2 Modeling of Heat Transfer at a Laminar Flowing of a Fuel Oil Jet

When formulating the mathematical model of heat transfer at the laminar flow of the fuel oil jet, the following assumptions are made [34, 35]:

- nonstationarity of heat transfer processes is determined by the time dependence of the fuel oil temperature in the storage tank;
- thermophysical properties of fuel oil—density ρ , heat capacity c_p , thermal conductivity λ , and kinematic viscosity of fuel oil ν depend on the temperature T ;
- volume force influencing on the flow process of the fuel oil jet from the nozzle has the form:

$$\vec{F} = \alpha g \rho (T - T_{\text{mazut}}), \quad (1)$$

where $\alpha = \frac{\rho_{20} - \rho_0}{\rho_0 (T_0 - 293)}$ —coefficient of volume expansion, 1/K; g —acceleration of gravity, m/s²; T_{mazut} —fuel oil temperature at the nozzle outlet, K;

- the flow of the fuel oil jet is laminar, rheological behavior of fuel oil is Newtonian.

The primary system of equations is based on the fundamental differential equation system of energy conservation and continuum mechanics—equations of motion and continuity.

Since the supply manifolds in the fuel oil storage tanks in most cases have closely spaced nozzles, the single jets flowing out of them can be replaced by a single plane jet flowing out of the plane-slot nozzle. Mathematically, this approximation allows reducing the three-dimensional formulation of the problem of heat transfer to the two-dimensional axisymmetric problem.

The geometric domain for determining the unknown variables of the problem for the fuel oil jet is shown in Fig. 1.

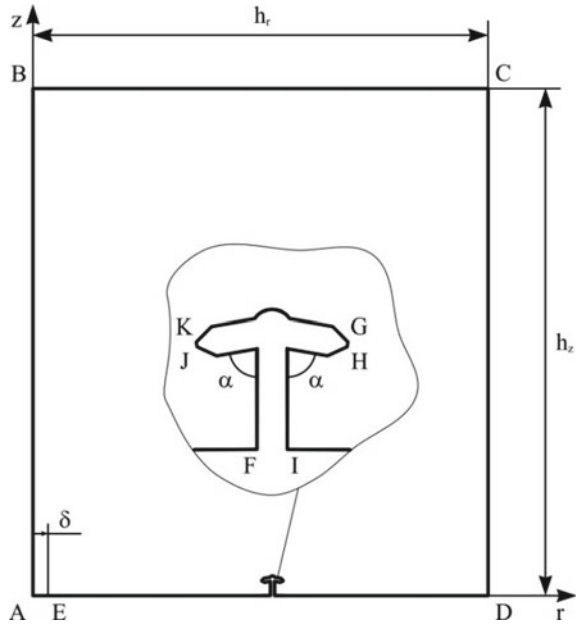
Because of the symmetry of the problem the flow is considered in the plane $ABCDE$ where r —the coordinates of points C and D , z —the coordinates of points B and C , δ —outlet of the AE tank, h_r —radius AD and BC of the studied area, h_z —height AB and DC of the studied area, α —inclination angle of the nozzle, GH and JK —output of jets of heated fuel oil.

The initial system of equations of motion and energy transfer describing the heat transfer process at flowing of a fuel oil jet in the general tensor formulation for the accepted assumptions has the form:

$$\rho c_p \frac{dT}{dt} = \text{div}(\lambda \text{grad}T), \quad (2)$$

$$\frac{d\vec{V}}{dt} = \frac{1}{\rho} \text{div}\mathbf{T} + \vec{F}, \quad (3)$$

Fig. 1 The geometric domain of fuel oil jet flow in the tank



$$\frac{\partial \rho}{\partial t} + \text{div} \vec{V} = 0, \tag{4}$$

where \vec{V} —velocity vector; T —stress tensor.

We write down the initial and boundary hydrodynamic and thermal conditions at flowing of fuel oil jet to close this system of equations.

The initial hydrodynamic condition has the form:

$$\vec{V}(t = 0) = \vec{V}_0. \tag{5}$$

The initial temperature condition has the form:

$$T(t = 0) = T_0. \tag{6}$$

The hydrodynamic boundary conditions:

- the velocity profile corresponding to the formed velocity profile of the Newtonian fluid in the circular pipe is specified at the inlet opening;
- at the outlet—condition of the fluid flow stabilization;
- the no-slip conditions of the fluid are specified at the solid and open boundaries of the tank.

Thermal boundary conditions:

- second-type boundary conditions—environmental heat losses—are specified at the solid and open boundaries;
- at the tank outlet we accept the predominance condition of the heat flow due to the convection compared to the heat flow due to the thermal conductivity in a direction perpendicular to the boundary;
- the temperature of the hot fuel oil fed to the tank is specified at the inlet.

The reliability of the mathematical model and the solution method was verified by comparison with the experiment results of the Z. I. Geller for circulatory heating of the cracking residues [36].

3 Mathematical Model of Heat Transfer Intensification in Fuel Oil Heaters

The formulation of the problem of stationary heat transfer during fuel oil flow in discretely rough channels was carried out at the following assumptions:

- fuel oil flow—stationary and laminar;
- the rheological behavior of fuel oil is characterized by the presence of viscous properties;
- thermophysical properties of fuel oil—density ρ , heat capacity c_p , thermal conductivity λ , and kinematic viscosity of fuel oil ν depend on the temperature T ;
- gravity forces enter the equations implicitly through the excess pressure.

The initial system of equations of motion and energy transfer describing the heat transfer process at flowing of a fuel oil in tube in the general tensor formulation for the accepted assumptions has the form:

$$\vec{v} \cdot \text{grad}T = a\Delta T + \frac{\Phi}{\rho c_p}, \quad (7)$$

$$\rho(\text{grad}\vec{v} \cdot \vec{v}) = -\text{grad}P + \text{div}\mathbf{T}^0, \quad (8)$$

$$\text{div}\vec{v} = 0, \quad (9)$$

where \vec{v} —velocity vector; a —coefficient thermal diffusivity; $\Phi = \mu(I_2)I_2$ —dissipative function; P —pressure; \mathbf{T}^0 —stress tensor deviator.

To close this system of equations, the initial and boundary hydrodynamic and thermal conditions are determined for the fuel oil flow in the pipe.

Hydrodynamic boundary conditions:

- at the inlet, a velocity profile is set that corresponds to the formed velocity profile of a Newtonian fluid in a round pipe;
- at the outlet—the condition for stabilizing the fluid flow;
- conditions of adhesion of liquid are set on solid boundaries of the pipe.

Thermal boundary conditions:

- at the inlet, the temperature of the fuel oil supplied to the fuel oil heater is set;
- first-type boundary conditions are set on solid boundaries;
- at the outlet, the condition of predominance of the heat flux due to convection in comparison with the heat flux due to thermal conductivity in the direction perpendicular to the boundary is accepted.

4 Results and Discussion

Numerical studies of heat transfer during circulation heating of M100 fuel oil were carried out for a vertical steel tank RVS-3000. The fuel oil in the tank is stored at the «cold» storage mode at $T_{\text{cold}} = 303$ K. Fuel oil flow rate was set $G = 8.33\text{--}16.67$ kg/s, which is 50–100% with a step of 10% of the performance of the PM-10-60 fuel oil heater. Fuel oil temperature at the fuel oil heater outlet $T_{\text{output}} = 303$ K.

Figures 2 and 3 show streamlines and thermal field during circulation heating of fuel oil in the tank at the nominal operating mode of the fuel oil heater. From the figures, it can be seen that the fuel oil movement and its heating occur throughout the entire volume of the tank.

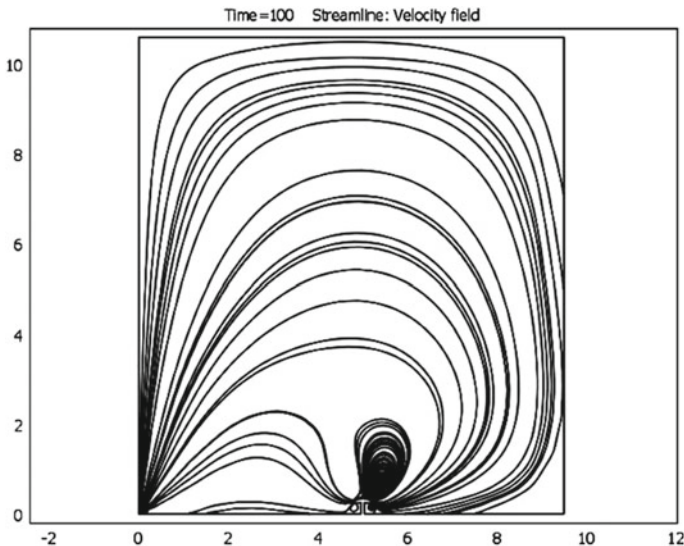


Fig. 2 Streamlines during circulation heating of fuel oil in the tank

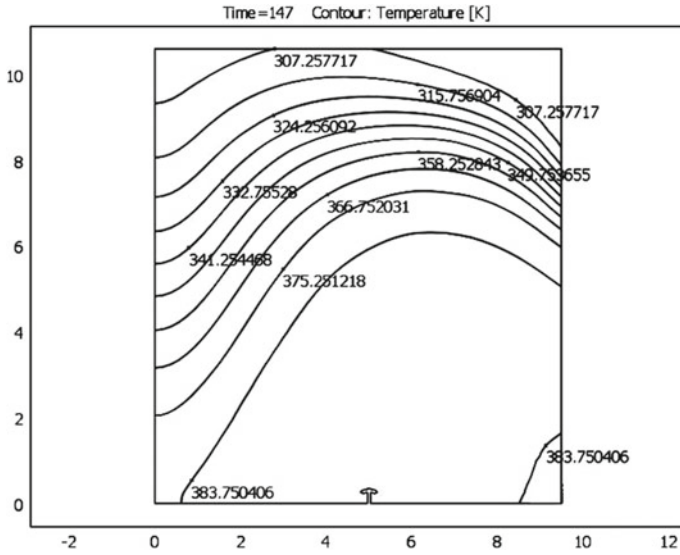
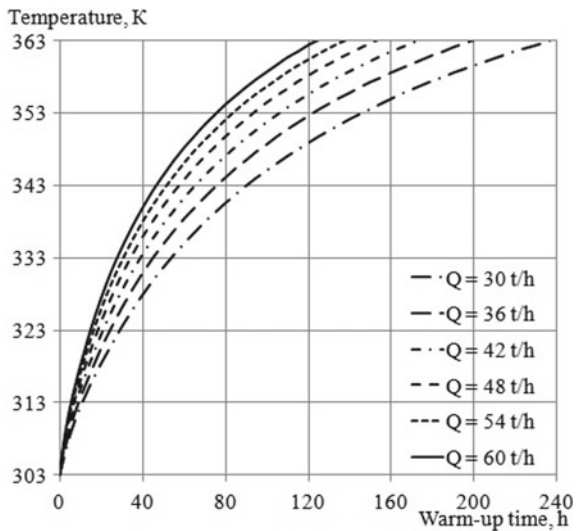


Fig. 3 Thermal field during circulation heating of fuel oil in the tank

Figure 4 shows the temperature and heating time of fuel oil in the tank, depending on the operating mode of the fuel oil heater. Comparison of the results shows that the slowest heating of fuel oil in the tank occurs when the fuel oil heater is operating at 50% of the nominal capacity, and fuel oil heating in the entire volume of the tank to 363 K occurs in 240 h. At the maximum capacity of fuel oil heater, transition time

Fig. 4 Temperature and heating time of fuel oil in the tank, depending on the operating mode of the fuel oil heater



from the «cold» storage mode to the «hot» storage mode is 125 h. Due to the fact that fuel oil temperature in the storage tanks of the reserve fuel oil facilities of TPP must be maintained at a level of 60–70 °C, the time for reaching this temperature of the entire tank in possible emergency situations is 27–55 h.

Numerical studies of intensification in the channels of the PM-10-60 fuel oil heater were carried out under the following conditions: the mass flow rate of liquid through one tube of the fuel oil heater is $Q = 0.174\text{--}1.042$ kg/s, which corresponds to the flow rate through the entire heater $Q = 10\text{--}60$ t/h with a step of 10 t/h, steam temperature on the wall $T_w = 473$ K (first-type boundary conditions), initial fuel oil temperature $T_0 = 303$ K. Geometrical dimensions of the channel: tube diameter $D = 0.038$ m, channel length $l = 10$ m, pitch ratio to diameter $S/D = 0.66$, the ratio of the width of the protrusion to the diameter $b/D = 0.2$, the ratio of the height of the protrusion to the diameter $h/D = 0.1$, the protrusions are in the form of spheres and triangles.

Figure 5 shows Nusselt numbers ratios for spherical and triangular heat transfer intensifiers in the tube of fuel oil heater. When comparing the discrete rough channel (DRC) and the smooth channel, it was found that in the channel under study the intensification of heat transfer is 1.463–2.228 times for spheres and 2.341–3.752 times for triangles.

Figure 6 shows ratios of hydraulic resistance coefficients. When comparing, it was found that the increase in hydraulic resistance due to the protrusions is 1.363–1.396 times for spheres and 1.365–1.402 times for triangles.

Figure 7 shows criterion ratios of thermohydrodynamic efficiency. The criterion of thermohydrodynamic efficiency in this case is 1.073–1.595 for spheres and 1.715–2.677 for triangles, which shows the efficiency of the investigated DRC at different fuel oil flow rates. It can be seen direct dependence of the flow rate on the criterion.

Fig. 5 Nusselt numbers ratios: 1—spheres; 2—triangles

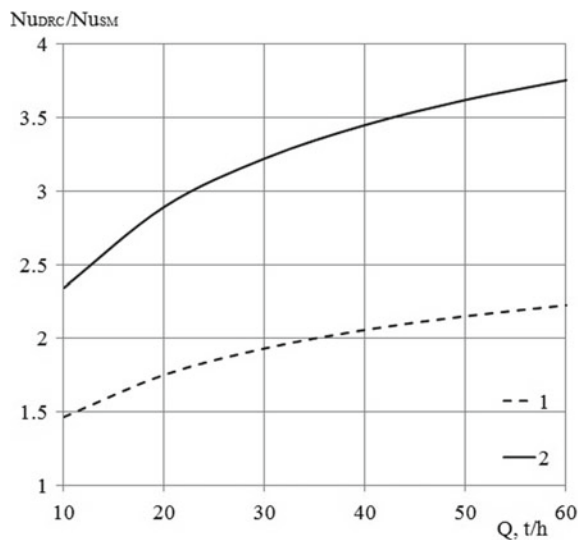


Fig. 6 Ratios of hydraulic resistance coefficients: 1—spheres; 2—triangles

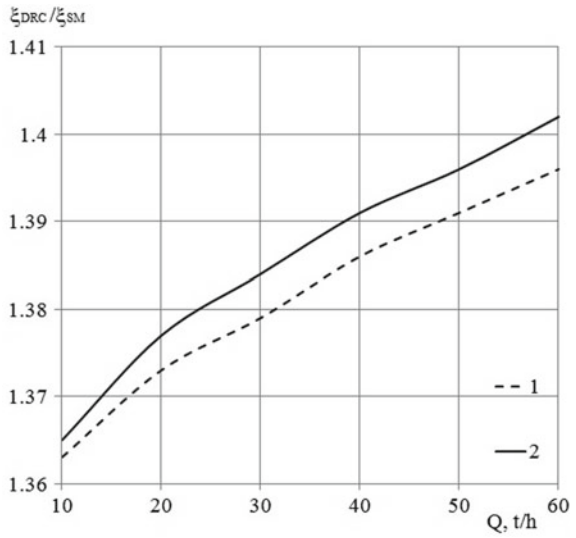
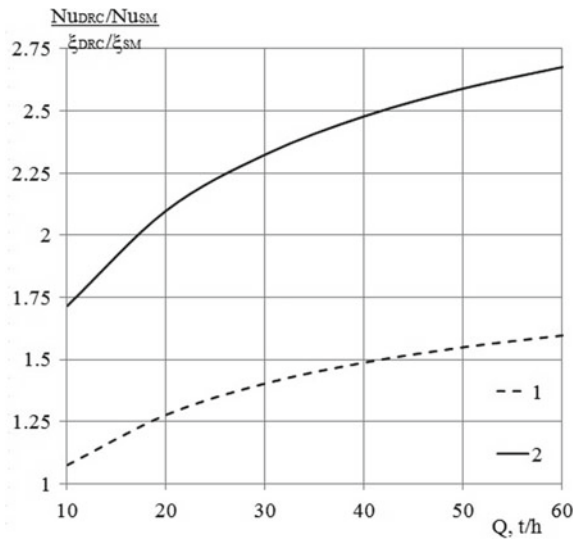


Fig. 7 Criterion ratios of thermohydrodynamic efficiency: 1—spheres; 2—triangles



5 Conclusions

Mathematical models are presented for the intensification of convective heat transfer during the laminar fuel oil flow in fuel oil heaters and circulation heating of fuel oil in storage tanks. Transition time from the «cold» storage mode to the «hot» storage mode for fuel oil tank was determined for supply hot fuel oil to the boilers. The

obtained results make it possible to estimate the heating time and optimal operating modes of fuel oil heaters during fuel oil heating in storage tanks.

The part of reported study was funded by RFBR (project number 20-08-00924) and RFBR and the government of Tatarstan Republic of Russian Federation (project number 18-48-160035). Temperature and heating time of fuel oil in the tank, depending on the operating mode of the fuel oil heater, was studied under financial support of the government assignment for FRC Kazan Scientific Center of Russian Academy of Sciences (project number FMEG-2021-0001).

References

1. Nazmeev, Y.G.: Fuel Oil Facilities TPP Moscow. MPEI (2002)
2. Rahimi, M., Parvareh, A.: *Comput. Chem. Eng.* **31**, 737–744 (2007)
3. Neyestanak, A.A.L., Asadi, G., Daneshmand, S.: *Rev. Roum. Chim.* **61**, 67–74 (2016)
4. Barekatain, H., Hashemabadi, S.H.: In: AIP Conference Proceedings vol. 1389, p. 123 (2011)
5. Butov, V.G., Nikulchikov, A.V., Nikulchikou, V.K., Solonenko, V.A., Yashchuk, A.A.: *Bulletin Tomsk Polytech. Univer. Geo Assets Eng.* **329**, 93–100 (2018)
6. Maleki, A., Hormozi, S.: *J. Non-Newton. Fluid* **252**, 19–27 (2018)
7. Ali, B.: *Sci. Papers Ser. A, Agron.* **60**, 449–454 (2017)
8. Bamberger, J.A., Enderlin, C.W.: *FEDSM* **2**, 10 (2016)
9. Bhattacharjee, P.K., Kennedy, S., Eshtiaghi, N., Parthasarathy, R.: *Chem. Eng. J.* **276**, 137–144 (2015)
10. Belov, I.A., Budilkin, V.V., Nazmeev, Yu.G.: *Izv. VUZov. Energy Problems* **1–2**, 60–67 (2003)
11. Shageev, M.F., Lopukhov, V.V., Salakheldin, B.: *Exposition Oil Gas* **4**, 52–53 (2009)
12. Shageev, M.F., Khairieva, E.M.: *Scientific problems of transport in Siberia and the Far East* **2**, 210–211 (2011)
13. Osipov, G.T.: *Izv. VUZov. Energy Problems* **5–6**, 70–76 (2003)
14. Ivanov, N.V.: *Izv. VUZov. Energy Problems* **1–2**, 148–150 (2003)
15. Kazaykin, K.F., Budilkin, V.V., Nazmeev, Yu.G.: *Izv. VUZov. Energy Problems* **7–8**, 19–24 (2003)
16. Nazmeev, Yu.G., Shamsutdinov, E.V., Kamalov, R.F.: *Izv. RAS. Energy* **2**, 52–60 (2006)
17. Shamsutdinov, E.V., Kamalov, R.F.: *Trans. Academenergo* **1**, 42–46 (2005)
18. Nazmeev, Yu.G.: *Heat Transfer and Hydrodynamics in Storage Systems for Liquid Organic Fuel and Petroleum Products*. MPEI, Moscow (2005)
19. Kamalov, R.F.: *Modelirovanie teploperenosa i razrabotka energoeffektivnykh teplotekhnologicheskikh skhem tsirkuljatsionnogo podogreva mazuta dlja rezervnykh mazutnikh khozjajstv TES [Simulation of heat transfer and development of energy-efficient heat technics of oil heating at TPP fuel storages]*. PhD Thesis, Kazan Scientific Center of Russian Academy of Sciences (2006)
20. Taktashev, R.N.: *Razrabotka rekomendatsij po energosberezheniju v sisteme tsirkuljatsionnogo podogreva mazuta na osnove chislenno modelirovania teploperenosa v rezervuarakh [Development of recommendations for energy savings the heating system based on numerical simulation of heat transfer in tanks]*. PhD Thesis, Moscow Power Engineering Institute (2008)
21. Varfolomeeva, O.N.: *Chislennoe modelirovanie gidrodinamiki i teploobmena v ustanovkakh dlja tsirkuljatsionnogo razogreva tzhazelogo zhidkogo topliva [Numerical simulation of hydrodynamics and heat transfer in heavy liquid fuel circulation heating installations]*. PhD Thesis, Izhevsk State Technical University (2003)
22. Geller, Z.I.: *Fuel Oil as Fuel*. Nedra, Moscow (1965)
23. Geller, Z.I., Ashikhmin, V.I., Vysota, K.P., Shevchenko, N.V.: *Therm. Eng.* **1**, 73–75 (1969)

24. Geller, Z.I., Ashikhmin, V.I.: *Power Technol. Eng.* **4**, 15–24 (1966)
25. Manjula, P., Kalaichelvi, P., Shanawaskhan, C., Dheenathayalan, K.: *Asia-Pac. J. Chem. Eng.* **5**, 544–551 (2010)
26. Bumrunghthaichaichan, E., Namkanisorn, A., Wattananusorn, S.: *J. Chin. Inst. Eng.* **41**(7), 612–621 (2018)
27. Jorakit, T., Phaiboonsilpa, N., Namkanisorn, A., Ponpo, P., Bumrunghthaichaichan, E., Wattananusorn, S.: In: *MATEC Web Conference*, vol. 192, p. 03019 (2018)
28. Bumrunghthaichaichan, E., Wattananusorn, S.: *J. Chin. Inst. Eng.* **42**(5), 428–437 (2019)
29. Grenville, R.K., Tilton, J.N.: *Chem. Eng. Res. Des.* **89**, 2501–2506 (2011)
30. Zughbi, H.D., Rakib, M.A.: *Chem. Eng. Sci.* **59**(4), 829–842 (2004)
31. Zughbi, H.D., Ahmad, I.: *Ind. Eng. Chem. Res.* **44**(4), 1052–1066 (2005)
32. Kuznetsova, S.A., Maksimov, V.I.: In: *MATEC Web Conference* vol. 23, p. 01047 (2015)
33. Zhao, J., Wei, L., Dong, H., Liu, F.: *Case Stud. Therm. Eng.* **7**, 109–119 (2016)
34. Kamalov, R.F., Zdor, V.O., Karaeva, Yu.V.: *Energy-Saf. Energy-Econ.* **1**, 16–22 (2019)
35. Kamalov, R.F., Zdor, V.O., Daminov, A.Z.: *Energy-Saf. Energy-Econ.* **4**, 33–37 (2019)
36. Zdor, V.O., Kamalov, R.F., Karaeva, Yu.V., Kadyrov, A.I.: *Trans. Academenergo* **1**, 42–49 (2018)

Methodological Approaches to Building the Scenarios of Inflows into Reservoirs When Modeling Long-Term Regimes of Hydroelectric Power Plants



Viacheslav M. Nikitin, Nikolay V. Abasov, Tamara V. Bereznykh, and Evgeny N. Osipchuk

1 Introduction

In energy and water management systems, the planning (regulation) of reservoir operation is usually limited to a period of 1–3 months. Such a planning horizon for the hydroelectric power plant is associated with the extreme complexity of long-term forecasting of water inflows into reservoirs and low reliability of forecasts even for an indicated period. Currently, the Hydrometeorological Center of Russia gives a probable (interval) inflow forecast for the coming month—at the end of the previous month and for 3 months—once a quarter. There are no forecasts for a more distant period. However, planning and forecasting in the electric power industry are made for the time horizon of up to one year or more. This is due to the need to plan long-term operating conditions and forecast the balance of electricity and capacity in the power system. This issue is especially relevant for power systems with a large share of hydroelectric power plants. Such power systems include the interconnected power system of Siberia, in which hydroelectric power plants account for about 50% of the total electricity generation.

The main feature of energy systems with a high share of hydroelectric power plants is the considerable dependence of electricity generation on a natural factor, i.e., natural fluctuations in water inflows into reservoirs. For example, the deviation in the power output of the Angara–Yenisei HPPs cascade from the long-term average values can reach up to 30% in some water years [1, 2]. This circumstance highly complicates the planning of electricity and heat output at thermal power plants

V. M. Nikitin (✉) · N. V. Abasov · T. V. Bereznykh · E. N. Osipchuk
Melentiev Energy Systems Institute of Siberian Branch of the Russian Academy of Sciences, 130 Lermontov St., Irkutsk 664033, Russia

V. M. Nikitin
Irkutsk Scientific Center of Siberian Branch of the Russian Academy of Sciences, 134 Lermontov St., Irkutsk 664033, Russia

(TPPs), the creation of fuel reserves, the planning of repairs of power equipment and electrical networks, and the solving of other problems. In addition, when regulating the regimes of HPPs many water management restrictions and environmental conditions are often required, for example, level regime regulation in Lake Baikal, which is the reservoir of the first stage of the Angara cascade (Irkutsk HPP) [3, 4].

In the absence of forecast indices of water inflows into reservoirs for more than three months, the long-term planning of operation and prospective energy balances, as a rule, relies on past period statistical data in the form of average long-term and monthly average indices. Such planning and forecasting provide acceptable results under normal conditions (close to the long-term average) but are not appropriate in other contexts, especially during extreme water periods [5–7].

Recent years have seen significant changes in global and regional climate and changes in the previously established trends, which makes it ineffective to use the average long-term and monthly average indices for forecasting [8–12]. It is therefore advisable to use new approaches to plan the long-term energy balances and operating conditions of power plants. In particular, one can use prognostic scenarios of water inflows into reservoirs for a period of up to 1 year and more, based on the data from global climate models and multivariate neural networks.

2 Materials and Methods

2.1 Global Climatic Models

Over the past two decades, significant progress has been made in the creation and use of global climate models for long-term forecasting of natural processes. They can also be used to make long-term assessments of water inflows into reservoirs for one year. One of the best-known models is the global climate model CFSv2 (Climate Forecast System version 2), developed by the international organization NCEP (National Centers for Environmental Prediction) [13–16]. This model is employed daily to update the prognostic ensembles of the state of the atmosphere and the ocean with a time interval from several hours to 9 months for the entire globe. The ensemble forecasting method used in global climate models allows making probabilistic estimates of the atmospheric state in the long term.

To increase the reliability of long-term projected estimates of water conditions and temperatures under current conditions, the Energy Systems Institute SB RAS has developed a long-term forecasting system GeoGIPSAR, which is used in energy and water management studies [17, 18]. The system includes various methods designed to analyze spatially distributed climatic data (Reanalyses, GPCC), which can serve as a basis for quickly calculating long-term estimates of precipitation, temperature, pressure, geopotential, and other indices on the territory of the river basins, and for periodically updating them (in a week, a decade, a month, a quarter, a season). To refine the prognostic estimates, one can also use the data from meteorological and

gauging stations, various geo- and heliographic indices, such as solar activity, lunar cycles, and others.

The estimates of the indices of individual predictive ensembles obtained from different sources can vary within wide limits, which complicates their direct use in practice. The method developed in the GeoGIPSAR system for processing a set of individual forecast ensembles makes it possible to form, through their aggregation (with different weights), the most probable spatial distributions of meteorological indices for given periods. For example, we can create climatic maps of absolute and relative indices for each month that show the boundaries of river catchment areas. For specific points and individual territories, there are tools developed to process the data on dynamics of changes in studied indices. The data obtained from the ensemble projections based on the global climate model and monitoring the data from global centers are used to determine the most probable characteristics of meteorological indices in the region under consideration and build the scenarios of inflows into the reservoirs of hydroelectric power plants in the form of ranges of probability distributions.

Figure 1 shows a schematic diagram of building long-term scenarios of water inflows into reservoirs of hydroelectric power plants and temperature conditions. Scenarios are based on the synthesis of two approaches (1) based on the projected estimates obtained by approximate and probabilistic methods, including neural network; (2) based on prognostic maps of meteo-hydrological indices, created through the processing of individual sets of prognostic ensembles, for example, averaged statistical indices over a selected time interval.

By regularly monitoring the ensembles of predictive data on the state of the atmosphere, converting, accumulating, and subsequently processing them, we create the most probable maps of the distribution of a selected index (surface temperatures,

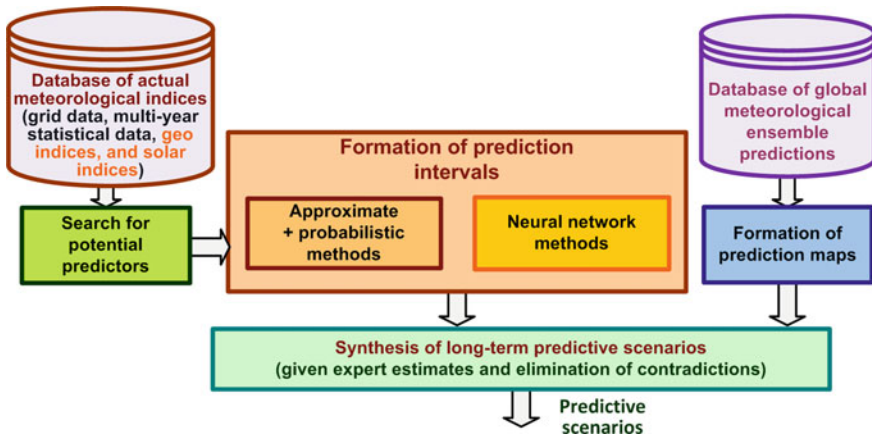


Fig. 1 Scheme of building long-term prognostic scenarios of water inflows into reservoirs of hydroelectric power plants and temperature conditions

precipitation rates, pressure, geopotential, etc.) with the assignment of various weight coefficients of their significance.

2.2 Multivariate Neural Network

In the GeoGIPSAR system, there is a multivariate neural network developed, first of all, to make the interval estimates of the index under study, for example, the net inflow of water into reservoirs for individual months or the temperature for specific points or a selected region. The use of the interval estimation method is associated with the inaccuracy of measurements of the actual inflow indices.

Figure 2 shows a neural network with an input layer (x_i), output layer (y_s), and with two hidden layers. The neurons of each layer include signal adders with different weighting coefficients ($w_{i,j}^{m,n}$) and sigmoid functions ($\phi_x^m(p)$) with varied parameter p . The coefficients are determined by the back-propagation method. For interval estimates according to a given algorithm, the interval of admissible values of the studied process is divided into k intervals. Then, instead of the value of the time series index, the number of the interval to which this value belongs is substituted.

Figure 3 shows a methodology for building interval projected estimates of the process under study. A set of potential predictors (Ω) affecting the projected estimates is determined from the global GeoGIPSAR database. Sets of internal parameters (Λ) and predictors are determined through the block for minimizing the error of deviations in prognostic and actual indices for a given verification sample. It is worth noting that once any parameter has changed complete training and verification cycle is performed.

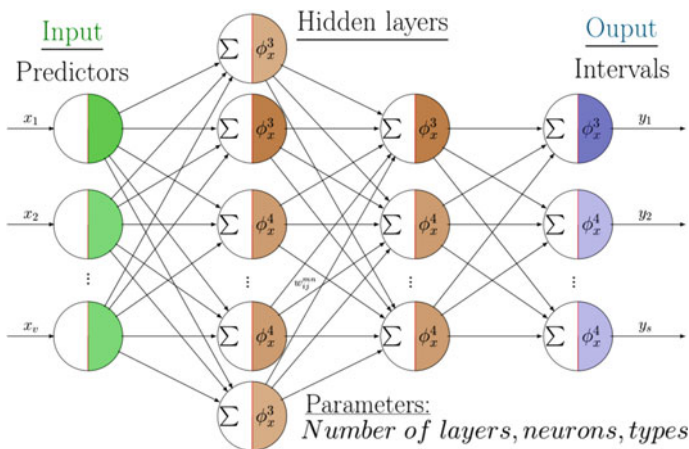


Fig. 2 An example of a core of a 2-layer multivariate neural network

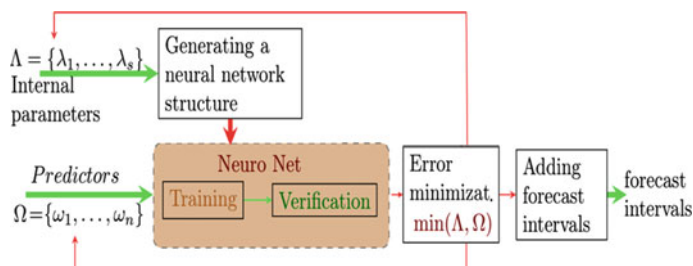


Fig. 3 Methodology for calculating interval projected estimates

Since the verification usually generates a significantly larger error compared to the training sample, the parameters of a multivariate neural network (MNN) are selected to satisfy the criterion of minimum verification error (for example, a deviation of no more than one interval from actual indices), and are then recorded in special storage. The developed MNN with the interval estimate method allows large-scale studies for various indices: water inflows into reservoirs of hydroelectric power plants, temperature conditions, and other stochastic natural processes.

3 Results and Discussion

A methodological approach that employs the data of global climate models and multivariate neural networks was used to build predictive scenarios of water inflows into Lake Baikal and reservoirs of the Angara–Yenisei cascade HPPs for the period from January 2021 to April 2022.

As an example, Fig. 4 shows the distributions of average temperatures in July and average daily deviations of precipitation rates in the catchment basins of Lake Baikal and the reservoirs of the Angara–Yenisei cascade HPPs in months 6–9 of 2021.

Temperature conditions are expected to be close to normal, while the increased precipitation is likely in the basin of the Selenga River, especially in its eastern tributaries (the Chikoi, Khilok, and Uda). Naturally, these are probabilistic indices as of the beginning of February 2021. In the case of significant disturbances (changes) in the atmosphere, the prognostic indices may also change, given the processing of new ensembles of the global CFSv2 model. The generated most probable predictive distributions of meteorological indices are used to determine the closest analogous years based on which (according to the available statistics of inflows) the predictive scenarios are synthesized for the future of up to 2 years with a time resolution of a month or a decade. For the period of over nine months, only neural networks and approximate long-term forecasting methods are employed.

Generally, the most probable scenario for the period under consideration is an increased water level in the Baikal and Angara basins and an average and low water level in the Yenisei basin.

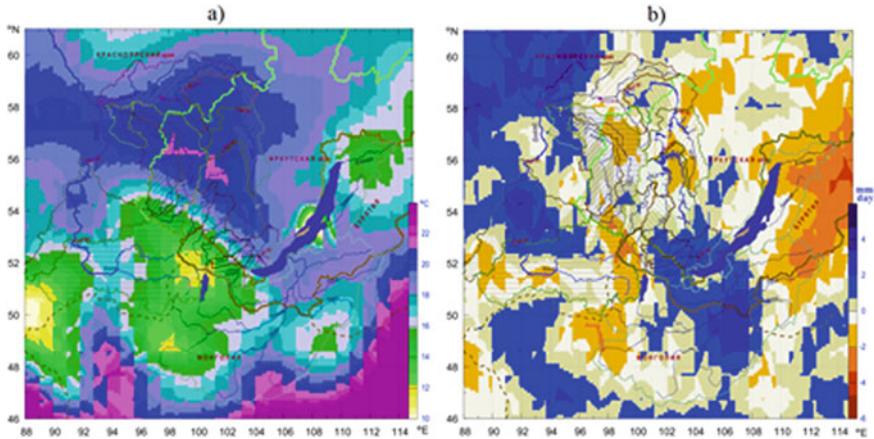


Fig. 4 An example of the distribution of predicted indices in the Lake Baikal, Angara River, and Yenisei River basins in the summer of 2021: **a** temperatures for July; **b** average daily precipitation rate deviations from the norm for months 6–9

Based on the predictive scenarios of water inflows into Lake Baikal and the reservoirs of the Angara–Yenisei cascade HPPs, and using the system of HPP control models developed by a research team of ESI SB RAS [19, 20], we obtained the estimates of projected electricity generation by individual hydroelectric power plants for the minimum, maximum and most probable inflow scenarios (Table 1).

The results of modeling the operation of the Angara–Yenisei cascade HPPs for 2021–2022 show that the electricity generation index can change significantly, depending on the inflow scenario. The range of fluctuations over the summer period can reach 11 200 million kWh, and in winter—9200 million kWh, which is comparable to the operation of one large HPP of the cascade. In the summer, there is also a risk of idle discharges in the Angara cascade under the maximum inflow scenario because the Bratsk reservoir is full, and there are large snow reserves accumulated in the basin during the winter. Therefore, planning the HPP operation should factor in the long-term most probable forecast scenarios of water availability.

4 Conclusion

A long-term forecasting system GeoGIPSAR was developed to increase the reliability of long-term projected estimates of water availability and temperatures to model long-term operating conditions of a cascade of HPPs. This system employs the data from various sources of information, including global climate models and multivariate neural networks. These tools help quickly obtain long-term estimates of precipitation, temperature, pressure, geopotential, and other indices on the territory

Table 1 Estimates of electricity generation by HPP of the Angara–Yenisei cascade (million kWh) for the minimum, maximum, and most probable inflow scenarios for the period from January 2021 to April 2022

HPP period	Inkutsk	Bratsk	Ust-Ilimsk	Boguchany	Sayano-Shushensk	Mainskaya	Krasnoyarsk	Angara–Yenisei cascade
January–April 2021	1402*	6695	6374	5297	6058	458	5463	31 745
	1479*	7079	6712	5578	6812	513	5644	33 814
	1428*	6826	6504	5395	6556	494	5474	32 677
Summer 2021 (May–October)	2134	11 572	10 707	9055	14 837	1033	11 955	61 292
	2261	13 922	12 662	10 615	17 991	1144	13 913	72 510
Winter 2021 (November–April 2022)	2196	12 953	11 847	9970	16 314	1094	12 692	67 065
	1983	11 791	10 853	9118	9412	695	8326	52 179
	2399	13 858	12 624	10 542	10 841	796	10 309	61 368
Total in 2021	2176	12 758	11 681	9737	10 177	750	9870	57 149
	4364	22 835	21 036	17 528	24 250	1725	20 303	112 039
	4613	26 161	23 837	19 764	28 176	1891	22 860	127 302
Total over the period	4453	24 582	22 505	18 694	26 229	1822	21 435	119 720
	5519	30 058	27 934	23 470	30 307	2186	25 744	145 216
	6139	34 859	31 998	26 735	35 644	2453	29 866	167 692
	5800	32 537	30 032	25 102	33 047	2338	28 036	156 891

*The first value in the column is calculated according to the minimum inflow scenario, the second—according to the maximum inflow, the third—according to the most probable inflow (highlighted in bold)

of the considered basins, and refine them periodically (in a week, decade, month, quarter, season).

Processing the data of predictive ensembles obtained by global climate models, other data and forecasting methods, as well as a multivariate neural network, enables us to build the scenarios of average monthly net inflows and dynamics of changes in operating conditions. It also allows us to estimate the amount of electricity generation by individual HPPs and the Angara–Yenisei cascade as a whole for up to one year or more.

The research was carried out under State Assignment Project (no. FWEU-2021-0003, reg. number AAAA-A21-121,012,090,014-5) of the Fundamental Research Program of Russian Federation 2021–2025.

References

1. Nikitin, V.M., Abasov, N.V., Bereznykh, T.V., Osipchuk, E.N.: The Angara–Yenisei HPP cascade under a changing climate. *Energy Policy* **4**, 62–71 (2017). (in Russian)
2. Osipchuk, E.N., Nikitin, V.M., Abasov, N.V.: Possibilities of enhancing the efficiency of the Angara cascade of hydroelectric power plants. *J. Phys. Conf. Series* **1652**, 012022 (2020). <https://doi.org/10.1088/1742-6596/1652/1/012022>
3. Nikitin, V.M., Abasov, N.V., Bychkov, I.V., et al.: Level regime of Lake Baikal: problems and contradictions. *Geogr. Nat. Resour.* **40**, 353–361 (2019). <https://doi.org/10.1134/S1875372819040073>
4. Abasov, N.V., Bolgov, M.V., Nikitin, V.M., et al.: Level regime regulation in Lake Baikal. *Water Resour.* **44**, 537–546 (2017). <https://doi.org/10.1134/S0097807817030022>
5. Klimenko, V.V., Mikushina, O.V., Volkov, D.M.: An improved quasi-rhythm method to forecast the annual side inflow to the reservoirs of the Volga–Kama Hydropower Plants Cascade. *Dokl. Earth Sc.* **476**, 1080–1083 (2017). <https://doi.org/10.1134/S1028334X17090148>
6. Bednaruk, S.E., Motovilov, Yu.G.: Information support technology for the reservoir cascade management. *Hydraulic Eng. Constr.* **7**, 22–35 (2017). (in Russian)
7. Demin, A.P.: Water management complex of Russia: concept, state of the art, and problems. *Water Resour.* **37**, 711–726 (2010). <https://doi.org/10.1134/S0097807810050118>
8. Vasiliev, Y.S. (ed.): Water and energy regimes of hydroelectric plants in the context of climate change. St. Petersburg Polytechnic University, **274** (2017) (in Russian)
9. Klimenko, V.V., Fedotova, E.V.: Russian Hydropower under the Global Climate Change. *Dokl. Phys.* **64**, 39–43 (2019). <https://doi.org/10.1134/S1028335819010051>
10. Bereznykh, T.V., Abasov, N.V.: The increasing role of long-term forecasting of natural factors in energy system management. *Int. J. Global Energy Issues* **20**(4), 353–363 (2003). <https://doi.org/10.1504/IJGEI.2003.004408>
11. Bereznykh, T.V., Marchenko, O.Y., Abasov, N.V., et al.: Changes in the summertime atmospheric circulation over East Asia and formation of long-lasting low-water periods within the Selenga river basin. *Geogr. Nat. Resour.* **33**, 223–229 (2012). <https://doi.org/10.1134/S1875372812030079>
12. Dias, V.S., Luz, M.P., Medero, G.M., Nascimento, D.T.F.: An overview of hydropower reservoirs in Brazil: current situation, future perspectives, and impacts of climate change. *Water* **10**, 592 (2018). <https://doi.org/10.3390/w10050592>
13. Saha, S., et al.: The NCEP climate forecast system version 2. *J. Climate* **27**, 2185–2208 (2014). <https://doi.org/10.1175/JCLI-D-12-00823.1>
14. Yuan, X., Wood, E.F., Luo, L., Pan, M.: A first look at climate forecast system version 2 (CFSv2) for hydrological seasonal prediction. *Geophys. Res. Lett.* **38**, 13 (2011). <https://doi.org/10.1029/2011GL047792>

15. Rai, A., Saha, S.K.: Evaluation of energy fluxes in the NCEP climate forecast system version 2.0 (CFSv2). *Clim Dyn.* **50**, 101–114 (2018). <https://doi.org/10.1007/s00382-017-3587-z>
16. Hourdin, F., Mauritsen, T., Gettelman, A., Golaz, J.C., Balaji, V., Duan, Q., Williamson, D.: The art and science of climate model tuning. *Bull. Am. Meteorol. Soc.* **98**(3), 589–602 (2017). <https://doi.org/10.1175/BAMS-D-15-00135.1>
17. Abasov, N.V., Berezhnyh, T.V., Reznikov, A.P.: Long-term forecast of environment-related factors of the energy industry in the information-forecasting system GIPSAR. In: Proceedings of the Russian Academy of Sciences, Power Engineering, vol. 6, pp. 22–30 (2000) (in Russian)
18. Abasov, N.V.: The GeoGIPSAR system of long-term forecasting and analysis of environment-related factors of the energy industry. In: Proceedings of the International Meeting of APN (MAIRS/NEESP/SIRS). Extreme manifestations of global climate change in North Asia, Enviromis-2012, pp. 63–66 (2012) (in Russian)
19. Abasov, N.V., Nikitin, V.M., Osipchuk, E.N.: A system of models to study long-term operation of hydropower plants in the Angara cascade. *Energy Syst. Res.* **2**(6), 5–18 (2019). <https://doi.org/10.25729/esr.2019.02.0001>
20. Nikitin, V.M., Abasov, N.V., Osipchuk, E.N.: Modeling of long-term operating regimes of hydro power plants as part of energy and water systems in the context of uncertainty. In: E3S Web of Conference ENERGY-21—Sustainable Development & Smart Management, vol. 209 (2020). <https://doi.org/10.1051/e3sconf/202020905014>

Numerical Study of the Fluid Flow in a Passive Tangential Vortex Tube



Simeon Livshits, Natalia Yudina, Ruslan Lebedev, Svetlana Enikeeva, and Evgeny Panamarenka

1 Introduction

Recently, there has been a clear trend towards the decentralization of heat supply networks. This process has covered almost all the technically developed countries of Europe and America, and every year it is becoming more and more noticeable in Russia. Thus, in recent years, the commissioning of boiler houses with a capacity of 100 Gcal/hour and above has been practically stopped, and autonomous heat supply systems are increasingly preferred. In addition to the existing and actively developing classical directions of autonomous heat supply systems, in the 90 s of the twentieth century, a promising direction of individual heat supply based on the use of vortex heat generators received a new round of development.

Currently, heat generators are used for heating and hot water supply to consumers (including as emergency or autonomous sources) in places where there are no centralized heat supply systems. Unlike traditional central heating systems, which are characterized by high material consumption and require significant space for equipment placement, fuel supply and the cost of transporting the final product to the consumer, autonomous systems designed on the basis of vortex heat generators do not require fuel storage and transportation costs, reduce heat loss to a minimum, are simple in design and do not require significant maintenance costs.

S. Livshits (✉) · N. Yudina
Kazan State Power Engineering University, Krasnoselskayast., 51, Kazan 420066, Russia

R. Lebedev
Gazprom VNIIGAZ LLC, Moscow, Russia

S. Enikeeva
Kazan National Research Technological University, Kazan, Russia

E. Panamarenka
Belarusian National Technical University, Independence Avenue 65, Minsk, Belarus

Since the appearance of the first static-acting vortex apparatuses, there has been an active debate about the nature of the occurrence of the effect, which has been defined in the literature as “mechanical activation” of the working flow [1–3].

Unfortunately, at the moment there is no proper scientific justification for the observed effect of “mechanical activation”. In this regard, there is an important task of detailed study of the physical and chemical nature of the interaction realized in heat generators of the cavitation-vortex type.

2 Literature Review

The analysis of works devoted to this problem allows us to distinguish two of the most frequently encountered opinions that characterize the physics of the process:

1. the presence of structural changes in the working fluid flow at the intermolecular level (due to the formation of hydrogen bonds between the liquid molecules, the process of forming associates occurs, accompanied by a change in temperature) [1];
2. When the liquid moves, energy is released due to the collapse of cavitation bubbles, which results in an increase in the flow temperature [2].

Proponents of the second hypothesis point out that the thermo kinetic process under consideration takes place in a state far from equilibrium. The energy supply in the nonequilibrium state is associated with the processes characteristic of dissipative structures [2].

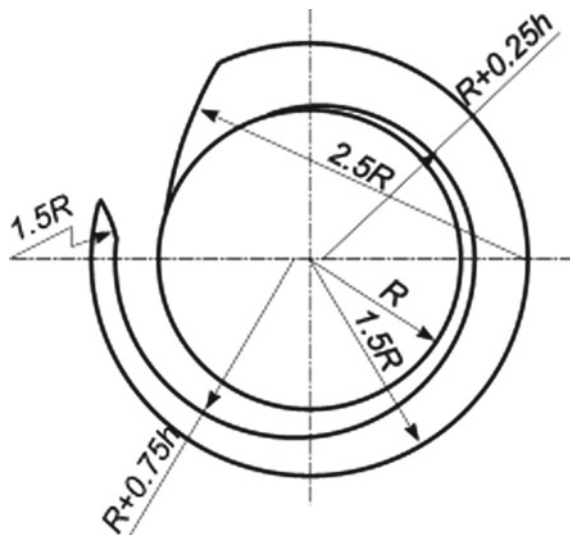
Cavitation—as a phenomenon has become the subject of numerous studies during the period when scientists were faced with such a complex and potentially dangerous phenomenon as the longitudinal oscillatory instability observed in high-flow fuel supply systems of launch vehicles, in turbine engines of civil and military aircraft [4, 5].

In vortex heat generators, cavitation, on the contrary, brings a positive effect, consisting in an increase in temperature [2], this indicates the need for its in-depth study. The complexity of the hydrodynamic conditions of the working flow can affect the distribution of the local areas of cavitation origin, so the numerical experiment allows not only to study in detail the processes accompanying cavitation, but also to identify the areas of its occurrence to find the optimal geometric parameters of the installation [6].

3 Materials and Methods

To date, the most rational and affordable method of studying physical processes is numerical modeling, implemented in specialized software packages. The choice of

Fig. 1 The scheme of the nozzle device according to Merkulov



this method is supported by the convenience of processing, analyzing, and presenting data (i.e., visualization) using computer graphics.

Modeling of three-dimensional fluid flow in a passive tangential vortex heat generator was carried out using the Flow Vision software package, based on the finite-volume method for solving hydrodynamic equations [6].

The first stage of the simulation was the creation of a computational domain for the constructed mathematical model.

As a reference model, a vortex tube with a nozzle inlet developed by A. P. Merkulov was adopted (Fig. 1).

This model combines high efficiency, simplicity, and low cost of manufacturing. However, despite all its advantages over the others, with a single fluid flow input, the vortex axis does not coincide with the axis of the working chamber in the nozzle section, which negatively affects the process of forming an axisymmetric vortex flow and the hydrodynamics of the vortex flow in the working chamber. An increase in the number of inputs should be accompanied by a decrease in the intensity of disturbances exerted on the swirling space of the water flow in the working chamber. The study and analysis of the most well-known high-precision twisting systems have shown that the centrifugal nozzle with four nozzle inputs has the lowest losses and the best effect of twisting the flow (Fig. 2).

In a centrifugal nozzle, a coolant is fed through tangential channels to the working chamber of the swirling device. The flow in it is twisted and is supplied to the nozzle. At the nozzle section, under the influence of internal hydro-mechanical forces, the membrane is crushed into small droplet-like fractions and enters the working area at a certain opening angle. Due to the centrifugal force, the flow is pressed against the walls and a region of reduced pressure is formed around the axis. When exiting the jet-twisting device, in order to avoid flow disruption, it is necessary to minimize

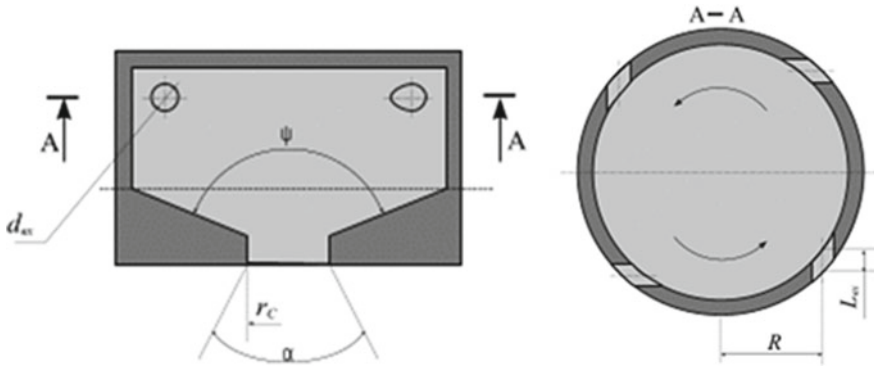


Fig. 2 Diagram of the centrifugal nozzle (R —twist shoulder; $d_v L_v$ —the diameter and length of the tangential channels; ψ —angle of the cone part; α —the angle of the stream output)

the length of the nozzle, and the diameter of the nozzle outlet should be as large as possible for each specific mode. Tangential channels can be circular or rectangular in cross-section.

Adapting the theory of the centrifugal nozzle [4] to the problem of designing the nozzle inlet of a passive tangential vortex heat generator, and taking the initial parameters of the water flow: the pressure before entering the nozzle channels $p = 0.7 \cdot 10^6$ Pa; initial temperature before entering the nozzle channels $t = 20$ °C; mass flow through the swirling device $G = 4005.2$ kg/h, According to the calculated data in the COMPASS 3D CAD, the three-dimensional space of the working flow was modeled for models with a nozzle input of the nozzle type (Fig. 3) and with a Merkulov nozzle inlet (Fig. 4).

The calculated area is the volume of the internal space of the vortex heat generator (see Figs. 3 and 4). The surface of the calculated area is a collection of flat polygons-facets. In the study of hydrodynamic characteristics, the interaction of flows in the

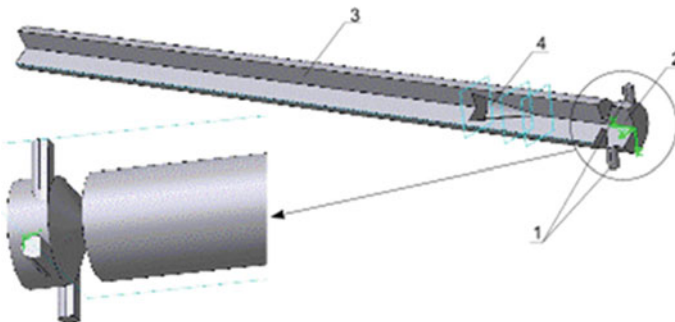


Fig. 3 A three-dimensional solid-state model with a flow input calculated by the author in the first modification; 1—tangential flow inputs; 2—a jet-twisting device; 3—a rectilinear cylindrical working chamber; 4—a brake cone-shaped device

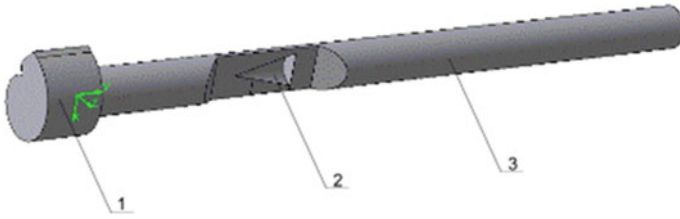


Fig. 4 Three-dimensional solid-state model of the internal space of a passive tangential vortex heat generator with a nozzle input by A. P. Merkulov. 1—Nozzle inlet according to A. P. Merkulov; 2—brake cone-shaped device; 3—straight cylindrical working chamber

area of the brake device location and at the exit from the swirling device is of particular interest.

The study of the influence of the geometry of the working area of the heat generator on the thermal efficiency of its operation was carried out with the same linear characteristics of the working chamber and the vortex twisting device [7, 8]. Only the area of the brake device location was changed at the initial section of the working chamber ($L = 200$ mm), in its middle part ($L = 400$ mm) and at the end of the working chamber ($L = 600$ mm) with the calculated length of the working space $L = 800$ mm.

The purpose of the calculation was to simulate the fluid motion in the calculated region to obtain the pressure and temperature field distributions at any point in the internal space of the vortex heat generator.

As a mathematical model for describing the motion, the “weakly compressible fluid” model was chosen, which allows us to model the flow at large Reynolds numbers and modes in which cavitation is possible [8]. For the numerical solution of the equations of the standard mathematical the turbulence model $\kappa - \varepsilon$ adopted a rectangular adapted locally ground grid.

The “weakly compressible fluid” model describes the motion of a viscous fluid at subsonic Mach numbers and various density changes, using the method of joint solution of the equations of motion, energy, and $\kappa - \varepsilon$ turbulence.

As the boundary conditions for the solution of the problem under consideration, the following are chosen:

the normal flow rate at the entrance to the channel model:

$$V|_0 = V|_n \tag{1}$$

$$P|_0 = \text{const} \tag{2}$$

the logarithmic law for the velocity profile in a turbulent boundary layer:

$$V \approx \sqrt{\frac{\sigma}{\rho}} \ln \frac{x}{C} \tag{3}$$

where C, σ —is the integration constants, ρ —flow density, x —the current coordinate;
The model is represented by the Eqs. (4), (6), (9) and (10).

Navier–Stokes equations

$$\frac{\partial \rho V}{\partial t} + \nabla(\rho V \otimes V) = -\nabla P + \nabla((\mu + \mu_t)(\nabla V + (\nabla V)^T)) + S \quad (4)$$

where V is the velocity; t is the temperature; P is the pressure; μ, μ_t are the dynamic and turbulent viscosity; S is the dimensionless parameter characterizing the source.

The energy equation

$$\frac{\partial(\rho h)}{\partial t} + \nabla(\rho V h) = \nabla\left(\left(\frac{\lambda}{C_p} + \frac{\mu_t}{Pr_t}\right)\nabla h\right) + Q \quad (5)$$

where h is the enthalpy, λ is the coefficient of thermal conductivity, C_p is the specific heat capacity, Q is the heat source, and Pr_t is the turbulent Prandtl number [11].

To determine the concentration of bubbles in the flow, the convective-diffusion transport equation is solved:

To determine the concentration of bubbles in the flow, the convective-diffusion transport equation is solved:

$$\frac{\partial(\rho C)}{\partial t} + \nabla(\rho V C) = \nabla\left(\left(\frac{\mu}{Sc} + \frac{\mu_t}{Sc_t}\right)\nabla C\right) \quad (6)$$

Sc_t —the turbulent Schmidt number.

In the accepted standard k - ε turbulence model, the turbulent viscosity μ_t is expressed in terms of the values k and ε as follows:

$$\mu_t = C_p \rho \frac{k^2}{\varepsilon} f_\mu \quad (7)$$

where k is the turbulent energy, ε is the rate of dissipation of the turbulent energy, $f_\mu = f_1 = 1$.

The equations for k and ε have the form:

$$\frac{\partial(\rho k)}{\partial t} + \nabla(\rho V k) = \nabla\left(\left(\mu + \frac{\mu_t}{\sigma_k}\right)\nabla k\right) + \mu_t G - \rho \varepsilon \quad (8)$$

$$\frac{\partial(\rho \varepsilon)}{\partial t} + \nabla(\rho V \varepsilon) = \nabla\left(\left(\mu + \frac{\mu_t}{\sigma_\varepsilon}\right)\nabla \varepsilon\right) + C_1 \frac{\varepsilon}{k} \mu_t G - C_2 f_1 \rho \frac{\varepsilon^2}{k} \quad (9)$$

where $\sigma_k = 1, \sigma_\varepsilon = 1.3, C_1 = 1.44, C_2 = 1.92$ —standard model constants k - ε turbulence.

$$G = D_{ij} \frac{\partial V_i}{\partial x_j} \tag{10}$$

$$D_{ij} = S_{ij} - \frac{2}{3} \left(\nabla \cdot V + \frac{\rho k}{\mu_t} \right) \delta_{ij} \tag{11}$$

$$S_{ij} = \frac{\partial V_i}{\partial x_j} + \frac{\partial V_j}{\partial x_i} \tag{12}$$

D —the doubled strain rate tensor.

4 Results

Figure 5 presents the results of a numerical experiment of the flow of a weakly compressible fluid for a passive tangential vortex heat generator with a nozzle input by A. P. Merkulov and with the flow input proposed in this article [12].

After entering the flow through the tangential channels into the working chamber [15] (Fig. 5a), there is a slight decrease in pressure, which may be a consequence of pressure losses, both in the tangential channels themselves, and as a result of the interaction of flows in the working chamber of the jet-twisting device [16]. After the flow enters the working chamber of the heat generator (due to the specific geometry of the channel and the complexity of the movement), there is a sharp drop in the flow pressure to the level of the saturation temperature, and it is in this region that the liquid–vapor phase transition occurs. Further movement of the flow is accompanied by an increase in pressure, which is caused by the presence of a braking device. As a result, the resulting vapor bubbles collapse [17]. The region from the input of the flow into the working chamber to the braking device, based on the theory set out in [2], should be called the cavitation region. The further pressure drop is obviously due to the process of re-forming the flow after the brake device and the presence of roughness.

As can be seen from the graph (Fig. 5a, b), cavitation is possible only when the brake device is located at a distance of $L = 200$ mm from the end wall of the swirl chamber. In the other two cases, when $L = 400$ and $L = 600$ mm, the pressure drop to the saturation state did not occur. The location of the brake device affects the flow characteristics in the area from the nozzle to the area of the brake device [18].

In the graph (Fig. 5b), after the flow enters through the Merkulov nozzle inlet in the swirling chamber, there is a slight decrease in pressure due to losses associated with both the interaction of the flows and the change in the velocity vector, and with hydraulic losses [19]. The further increase is due to the action of mass forces caused by the movement around the circle [20].

Figure 5b and d, shows a graph of visualization of the calculation data in each cell by temperature, for three variants of the location of the braking devices.

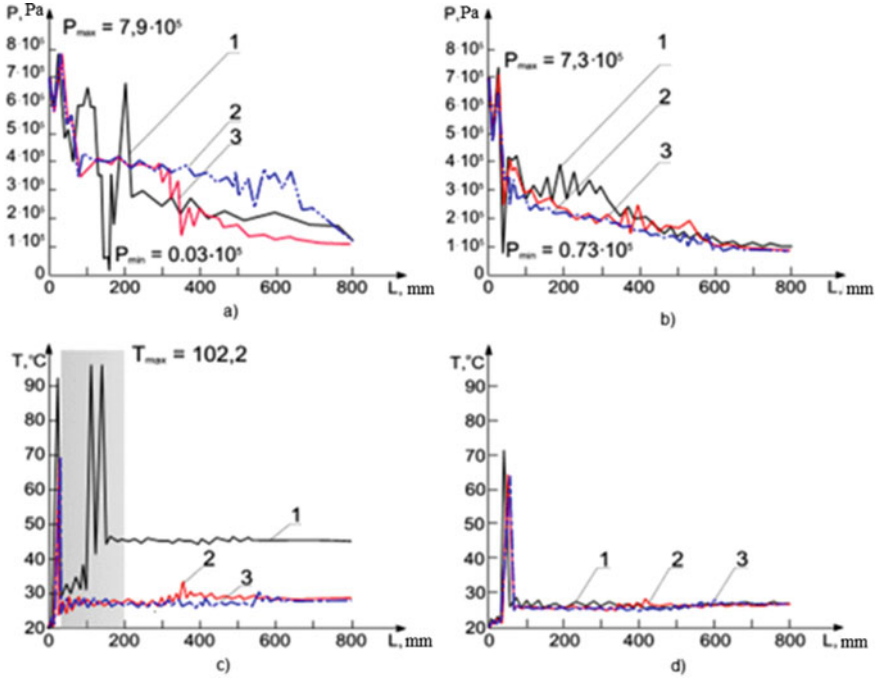


Fig. 5 The results of numerical experiment on the argument the total pressure (a) and (b), the argument of the temperature field (c) and (d): a, c with jet-twisting device type—“atomizer”, b, d with jet-twisting device according to the type of snail (A. P. Merkulov) [13]. 1—working flow pressure line for a model of a vortex generator with a braking device removed at a distance of 200 mm from the end wall of the swirling chamber; 2—working flow pressure line for a model of a vortex generator with a braking device removed at a distance of 400 mm from the end wall of the swirling chamber; 3—working flow pressure line for a model of a vortex generator with a braking device removed at a distance of 600 mm from the end wall of the swirling chamber [14]

In Fig. 5b, curve 1 has three maxima at the interval from 0 to 170 mm. Also, in the range from 0 to 170 mm, a minimum is observed at a temperature of 20 °C and a pressure of 3.5 kPa, which characterizes the evaporation process, as a result of which the flow temperature decreases on average by 3 ÷ 4 °C. The size of the area of possible cavitation has a huge impact on the percentage of the liquid being boiled. Therefore, the main task is to artificially increase the area of cavitation origin. Obviously, the further a braking device is located from the nozzle part of the swirler, the less effective halogenerator. This is due to the presence of reverse flow, which has a strong effect on the outgoing flow of the twisting device, leading to a decrease in heat generation [9]. The gradual increase in temperature behind the braking device is due to a decrease in turbulence pulsations and flow velocity in general, as a result of which the only source of heat—the dissipation of internal energy, due to a constant decrease in tangential stresses that directly depend on the main flow parameters, tends to zero, which is well illustrated by the graph in (Fig. 5b and d).

The nature of the temperature function in (Fig. 5d) is similar to the graph shown in (Fig. 5c), but there is no clearly defined cavitation region. The flow temperature increases by $5^{\circ} - 8^{\circ} \text{C}$, which indicates a low efficiency of the input type “A. P. Merkulov”, and the temperature increase is explained by the presence of viscous friction forces.

5 Conclusions

As a result of the numerical experiment for the proposed jet-twisting device, the distributions of velocities, pressure, heat flow, and liquid temperature at all points of the calculated space were obtained, which made it possible to evaluate the efficiency of the design of the alternative jet-twisting device and the vortex tube as a whole. The flow temperature increased by an average of 25°C .

References

1. Merkulov, A.: Vortex effect and its application in engineering. *Mashinostroenie* (1969)
2. Suslov, A., Ivanov, S., Murashkin, A., Chizhikov, Y.: Vortical apparatuses. *Mashinostroenie* (1985)
3. Merkulov, A.: Vortical effect and its application in engineering. *Kuibyshev, KuAI* (1988)
4. Adamov, V.: Burning of fuel oil in boiler furnaces (1989)
5. Serebryakov, R.: Heat generator with vortex cavitation of the working body. *Bulletin of Agrarian Science Don* 4 (2016)
6. Akhmetov, Y., Kalimullin, R., Tselishchev, V.: Numerical and physical modeling of a liquid flow in a vortex heat generator. *Bull. Ufa State Aviation Tech. Univ.* **4**, 39 (2010)
7. Piralishvili, S.: Vortex effect. Theory, experiment, numerical simulation. In: *Collection of Scientific Papers SWorld*, vol. 3, 3 (2013)
8. Gorbenko, V.: Numerical simulation of temperature fields of complex-shaped bodies on the principle of diaktics. *Bull. South Ural State University, Series: Energy* **20**, 92 (2007)
9. Iokova, I., Tarasevich, E.: Study of the possibility of application of a vortex heat generator in the heat supply systems of residential, industrial and public buildings. *Energy: News Higher Educ. Inst. Energy Assoc. CIS* **61**, 2 (2018)
10. Dutta, T., Sinhamahapatra, K.P., Bandyopadhyay, S.S.: Experimental and numerical investigation of energy separation in counterflow and uniflow vortex tubes | [Étude expérimentale et numérique de la séparation de l'énergie dans les tubes vortex à contre-courant et à courant parallèle]. *International Journal of Refrigeration* 123 (2021)
11. Wang, K., Xie, L., Ouyang, X., Wang, H., Han, T., et al.: Numerical simulation on the flow and temperature field of natural gas single circuit vortex tubes. *Natural Gas Industry* **40**(7) (2020)
12. Lagrandeur, J., Poncet, S., Sorin, M.: Review of predictive models for the design of counterflow vortex tubes working with perfect gas. *Int. J. Therm. Sci.* **142** (2019)
13. Rehman, A., Athar, M., Mansoor, T.: Mechanism of vortex motion. *ISH J. Hydraul. Eng.* **23**(2) (2017)
14. Novikova, O.V., Erastov, A.E., Livshits, S.A.: Features of evaluating the efficiency indicators of the electric power enterprise. In: *E3S Web of Conferences*, vol. 124 (2019)
15. He, L.-J., Wang, S.-X., Wu, X.-W., Sun, S.-Z.: Effect of nozzle structure on the performance of vortex tube. *Reneng Dongli Gongcheng/J. Eng. Therm. Energy Power* **35**(6) (2020)

16. You, Y., Seibold, F., Wang, S., Weigand, B., Gross, U.: URANS of turbulent flow and heat transfer in divergent swirl tubes using the $k-\omega$ SST turbulence model with curvature correction. *Int. J. Heat Mass Transfer* **159** (2020)
17. Pan, H., Pan, P.: Effect of hot-end tube diameter on flow field of vortex tube: a simulation study. **40**(7) (2020)
18. Wang, J., He, X., Li, J., Zou, S., Xu, H., et al.: Simulation of heat transfer enhancement and flow resistance characteristics of twisted slice tubes with openings. *Guocheng Gongcheng Xuebao/The Chinese J. Process Eng.* **20**(5) (2020)
19. Li, R., Hu, Z., Gao, Y.: Numerical simulation of energy separation in a vortex tube with different vane number rectifiers. In: *Proceedings of the 31st Chinese Control and Decision Conference, CCDC* (2019)
20. Shamsoddini, R., Abolpour, B.: A geometric model for a vortex tube based on numerical analysis to reduce the effect of nozzle number. *Int. J. Refrig.* **94** (2018)

Assessment of the Possibility of NO_x Reduction in Smoke Gases of Steam Boilers DE-6.5/14 by Recirculation of Combustion Products



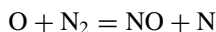
Eduard Korolev, Roman Lipantiev, Enza Barieva, Aleksey Eskin,
and Elena Serazeeva

1 Introduction

In recent years, the development of the fuel and energy complex of Russia has been rapidly increasing. In the developed Energy Strategy for the period up to 2035 for 2008–2020, a steady increase in energy consumption was noted, which amounted to 5.4% of the initial one, with an increase in the installed capacity of power plants by 11%. This is due to an increase in global demand for electrical energy from the electric transport sector, housing and communal services, the construction industry, as well as the expansion of existing and the formation of new energy-intensive industrial enterprises [1, 2].

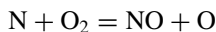
With an increase in the capacity and expansion scale of energy enterprises, their load on the environment also increases [3]. One of the significant factors of impact on the environment is gas emissions from enterprises, among which nitrogen oxides are the leading ones. These substances contribute to the formation of smog and acid precipitation and also cause inflammatory and asthmatic processes in the human body. Therefore, the development of a technological solution aimed at reducing the formation of nitrogen oxides in the process of fossil fuel combustion is an urgent problem for ecology and energy [4, 5].

As is known, a high-temperature mechanism for the oxidation of molecular nitrogen by atomic oxygen in the combustion zone was proposed by Ya. B. Zeldovich:

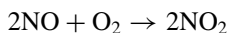


E. Korolev (✉) · A. Eskin
Kazan Federal University, Kazan, Russia

R. Lipantiev · E. Barieva · E. Serazeeva
Kazan State Power Engineering University, Kazan, Russia



Under normal conditions, nitric oxide combines with oxygen with the subsequent formation of dioxide:



The content of nitrogen dioxide in the exhaust gases of energetic enterprises depends primarily on the design features of burner arrangement and equipment, the schedule of heat loads, and the combustion mode. Therefore, the achievement of optimal results in the field of reducing the amount of nitrogen dioxide, as a rule, is carried out in two directions: improvement of the fuel combustion process and combustion products purification. The first area includes measures to reduce the combustion temperature, reduce the residence time of combustion products in the high-temperature area, and flue gas recirculation. Other equally effective methods are catalytic and non-catalytic reduction of nitrogen oxides. These methods are based on the injection of a reagent into the flue gas stream with the subsequent conversion of the substance under study into molecular nitrogen and water. At the same time, the most frequently used methods for reducing the concentration of nitrogen dioxides are recirculation of flue gases and the use of special burner arrangements given their high efficiency and low cost in comparison with other methods [6–8].

The introduction of a flue gas recirculation scheme for boilers TGM-84B, KVGM-180, TGME-464 made it possible to reduce emissions of nitrogen oxides by 40–60%. At the same time, the application of this method for reducing NO_x emissions has not been sufficiently studied on boilers of low steam capacity, such as DKVR-4/13 and DE-25/14GM. Therefore, the purpose of our study was to assess the possibility of using the flue gas recirculation method on DE-6.5/14 boilers [9–11].

2 Experimental Part, Results, and Discussion.

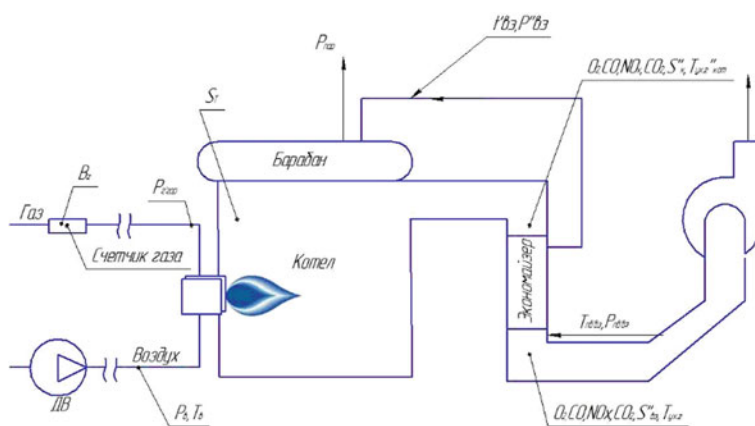
The studies were carried out at a gasified industrial heating boiler house, which is equipped with two DE-6.5/14 steam boilers and one water-heating boiler KVZH-4.0G. These boilers are equipped with GM-4.5 burner arrangements with a maximum heated capacity of 5.24 MW and gaseous fuel consumption by 510 m³/h. The main fuel is gas, and the reserve is M100 fuel oil. To determine the real amount of nitrogen oxides formed during the combustion of gaseous fuel, process flow tests were carried out during the operation of the boiler unit in the load range of 25–100% from the nominal steam capacity. The test results are shown in Table 1 (Fig. 1).

During the tests the following was found:

1. Steam consumption through the boiler was determined by the direct balance;
2. Gas consumption was determined using a standard general boiler gas consumption meter, type “Logic” LNG-761;

Table 1 Operating parameters of the boiler unit st. No. 1, obtained as a result of operational testing

Parameter	Loading			
	25%	50%	75%	100%
Steam production, t/h	1.71	3.48	4.84	6.06
Fuel consumption (gas $Q_n^r = 34.09$ MJ/kg), m ³ /h	154	278	380	473
Flue gas consumption, m ³ /s	1.34	2.54	3.82	4.89
NO _x concentration in flue gases, mg/m ³	181.3	199.8	215.9	224.4
Mass emission of NO _x , mg/h	243.2	507.9	825.4	1099.1
Steam pressure in the drum, kgf/cm ²	7.0	7.2	7.3	7.6
Burner gas pressure, kPa	2.0	8.0	15.0	25.0
Flue gas temperature outside the boiler, °C	230	255	308	325
Gross boiler unit efficiency, %	76.03	85.71	87.21	87.73

**Fig. 1** Scheme of points for measuring the parameters of the boiler unit DE-6.5/14

3. In the calculation of technical and economic indicators, the flue gas temperature values determined using a portable gas analyzer of the DAG-500 type were used;
4. The concentration of nitrogen oxides varied depending on the steam capacity and amounted to 181.3–224.4 mg/m³ for boiler st. No. 1.

After a series of experiments and data recording, it was proposed to use a simplified scheme with the supply of a part of the flue gases to the inlet air unit of the blower fan for the boiler station No. 1 DE-6.5/14. The implementation of these measures became possible when the unused $\text{Ø}108 \times 5$ pipelines were converted into a process pipeline for flue gas recirculation. Cutting-in into the gas duct was carried out between the economizer and the boiler. The control of flue gases amount was carried out by flue damper. The results of repeated process flow tests in the boiler unit st. No. 1 are shown in Table 2.

Table 2 Operating parameters of the boiler unit st. No. 1, obtained using flue gas recirculation

Parameter	Loading			
	25%	50%	75%	100%
Steam production, t/h	1.73	3.42	4.86	6.15
Fuel consumption (gas $Q_n^r = 34.09$ MJ/kg), m ³ /h	156	274	381	470
Flue gas consumption, m ³ /s	1.36	2.53	3.88	4.90
NO _x concentration in flue gases, mg/m ³	172.6	190.3	212.9	226.5
Mass emission of NO _x , mg/h	235.5	481.3	825.9	1109.8
Steam pressure in the drum, kgf/cm ²	6.9	7.1	7.3	7.7
Burner gas pressure, kPa	2.0	8.0	15.0	25.0
Flue gas temperature outside the boiler, °C	232	260	315	329
Gross boiler unit efficiency, %	75.93	85.47	87.34	89.59

It was found by the calculation method that due to a decrease in the excess air and an increase in its temperature in front of the burner arrangement to 40 °C, the efficiency of the boiler unit increased by an average of 0.4%. The results of measuring the concentration of nitrogen oxides at various operating modes of the boiler unit after using recirculation at 10% are shown in Fig. 2a. It can be seen that with the same heat output in modes at 25% and 50% load, the mass emission of nitrogen oxides after the use of recirculation decreases by 7.4 mg/h and 26.6 mg/h, respectively. At 75% loading, after recirculation was applied, the mass NO_x emissions remained virtually unchanged. With a further increase in fuel consumption, the indicator exceeded the

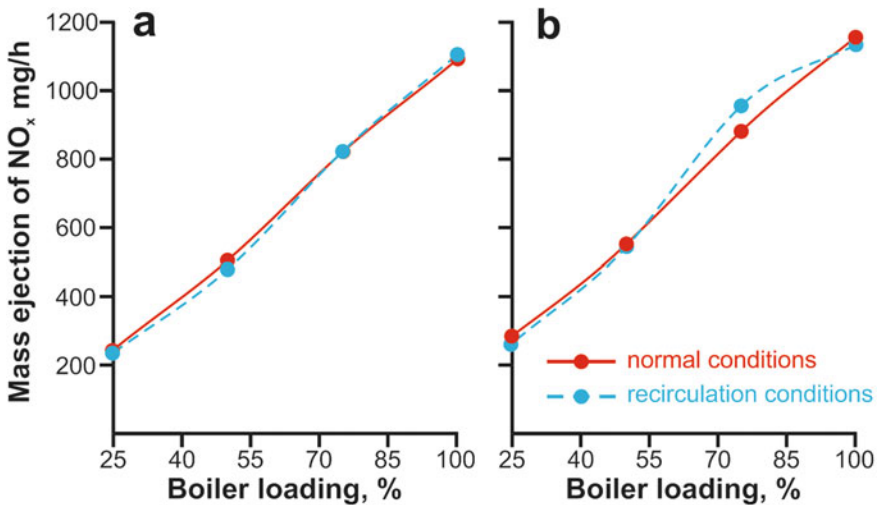


Fig. 2 Dependence of emitted nitrogen oxides amount of the boiler DE-6.5/14 loading: **a**—st. No.1; **b**—st. No. 3

nominal by 10.7 mg/h, which is explained by the insufficient blower discharge of the fan.

Successful experience in the implementation of these measures at the object under study allowed us to assume that the recirculation unit will be effective at the second identical boiler DE-6.5/14 on station No. 3. The results of process flow tests on the boiler unit st. No. 3 before and after the use of recirculation are given in Tables 3 and 4.

As can be seen from the results of Tables 3 and 4, operating parameters of boiler units on stations No. 1 and No. 3 differ significantly in some indicators. However, this does not prevent us from comparing the efficiency of using flue gas recirculation on this equipment. With the same heated capacity in modes at 25% and 50% load, the mass emission of nitrogen dioxide after recirculation decreased by 21.5 mg/h and 8.1 mg/h, respectively. At 75% load, after recirculation was applied, the mass NO_x emission value exceeded the nominal value by 8%, which indicates a malfunction in

Table 3 Operating parameters of the boiler unit st. No. 3, obtained as a result of operational testing

Parameter	Loading			
	25%	50%	75%	100%
Steam production, t/h	1.80	3.51	5.0	6.25
Fuel consumption (gas $Q_n^r = 34.09$ MJ/kg), m ³ /h	162	293	400	499
Flue gas consumption, m ³ /s	1.42	2.67	4.09	5.22
NO _x concentration in flue gases, mg/m ³	201.8	207.6	216.5	222.4
Mass emission of NO _x , mg/h	288.1	554.0	884.8	1160.7
Steam pressure in the drum, kgf/cm ²	6.6	7.0	7.3	7.8
Burner gas pressure, kPa	2.5	8.2	15.0	25.5
Flue gas temperature outside the boiler, °C	236	253	317	331
Gross boiler unit efficiency, %	76.08	82.03	85.59	85.76

Table 4 Operating parameters of the boiler unit st. No. 3, obtained using flue gas recirculation

Parameter	Loading			
	25%	50%	75%	100%
Steam production, t/h	1.79	3.55	4.95	6.20
Fuel consumption (gas $Q_n^r = 34.09$ MJ/kg), m ³ /h	160	295	402	496
Flue gas consumption, m ³ /s	1.40	2.70	4.06	5.16
NO _x concentration in flue gases, mg/m ³	189.8	202.0	236.5	220.9
Mass emission of NO _x , mg/h	266.6	545.9	959.8	1140.3
Steam pressure in the drum, kgf/cm ²	6.8	7.1	7.4	7.9
Burner gas pressure, kPa	2.5	8.2	15.0	25.5
Flue gas temperature outside the boiler, °C	234	256	310	328
Gross boiler unit efficiency, %	76.60	82.39	84.31	85.59

the boiler of station No. 3. With a further increase in fuel consumption, the indicator decreased compared to the nominal by 20.4 mg/h. The efficiency coefficient of boiler unit st. No. 3 at modes at 25% and 50% load increased by an average of 0.45%, however, at 75% load, the boiler unit worked worse than the nominal mode that gave an average by four indicators negative result in -0.13% . The results of measuring the concentration of nitrogen oxides at various operating modes on st. No. 3 boiler unit after using recirculation at 10% are shown in Fig. 2b.

Due to the complexity of the technological process of heat energy production and a sufficiently large number of factors affecting the effectiveness, it is not easy to determine a malfunction in the system. Therefore, to study the current situation, a conceptual model of the flue gas recirculation process was developed, shown in Fig. 3, which makes it possible to assess the degree of influence of qualitative factors and form a direction for further research.

The criterion for the optimality of this model is the NO_x concentration indicator in the flue gases, expressed using an objective function of the form [12, 13]:

$$Y = \max f(X, A, S, F) \tag{1}$$

while limiting the values of the variables X , P_y , and Q .

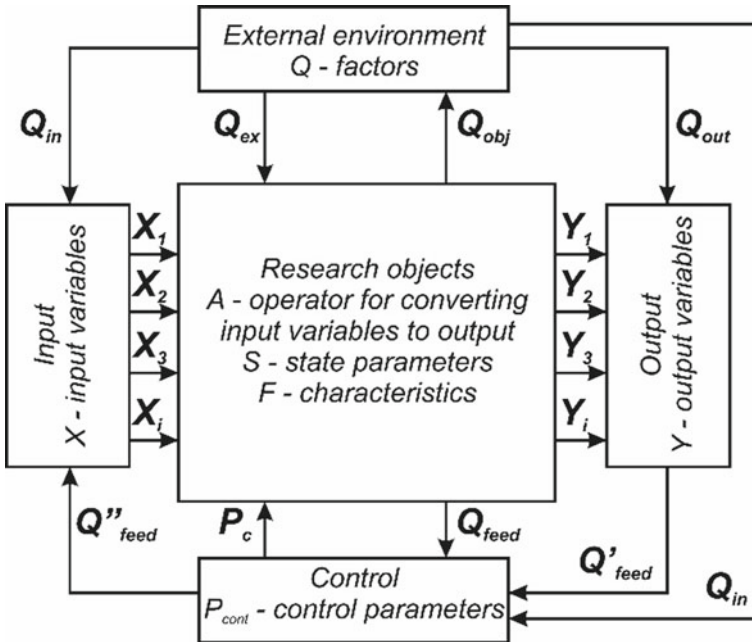


Fig. 3 Diagram of a conceptual model of a flue gas recirculation system

Table 5 The value of NO_x harmful emissions concentration when the load on the boiler changes from 25 to 100%

Object name	Load factor, %			
	25—A ₁	50—A ₂	75—A ₃	100—A ₄
Boiler station No. 1 meas. 1	181.3	199.8	215.9	224.4
Boiler station No. 1 meas. 2	172.6	190.3	212.9	226.5
Boiler station No. 3 meas. 1	201.8	207.6	216.5	222.4
Boiler station No. 3 meas. 2	189.8	202.0	236.5	220.9

In the course of the experiment, a change in the quantitative input variables X (gas and airflow rates, flue gas temperature, etc.) leads to changes in the output variables Y —the NO_x concentration.

Since the quantitative variables on boiler units st. No. 1 and No. 3 are practically equal, we needed to assess the impact degree on their value in the range of the load. Let the considered quantitative value X be influenced by the qualitative load factor A , which has four levels of values from 25 to 100%. For each level of factor A , the same measurement number of harmful emissions concentration X is carried out. The number of such measurements at each of the levels is $n = 4$. The measurement results are presented in the form of Table 5.

We believe that the aggregates of measurement data obey the law of normal probability distribution and to test the null hypothesis H_0 about the insignificant influence of factor A , we use the Fisher–Snedecor criterion [13, 14]:

$$F_{расч} = \frac{S_{факт}^2}{S_{осм}^2} = 15,02 \quad (2)$$

According to the Fisher distribution table for the significance level $\alpha = 0.05$ and degrees of freedom $k1 = k - 1 = 3$, $k2 = k(n - 1) = 12$, we find $F_{crit.}(0.05; k1; k2) = 3.49$. Thus $F_{crit.} < F_{calc.}$, which means that the load factor significantly affects the output concentration of nitrogen oxides and rejects the null hypothesis, which gives us the right to speak about the effectiveness of the proposed method of recirculation of flue gases on boilers DE-6.5/14 [9–11].

3 Summary

1. The process flow tests carried out in the industrial heating boiler house indicate that the use of the flue gas recirculation scheme on the DE-6.5/14 steam boiler is effective.
2. According to the results of the calculation, it was found that at the boiler at station No. 1 with the same heated capacity in modes at 25% and 50% load, the mass emission of nitrogen oxides after the use of recirculation decreases to

- 7.4 mg/h and 26.6 mg/h respectively. For boiler No. 3, these indicators changed and amounted to 21.5 mg/h and 8.1 mg/h at 25% and 50% load, respectively.
3. A conceptual model of the flue gas recirculation system has been built, based on which a qualitative factor influencing the quantitative indicators has been selected.
 4. An analysis of variance was used to assess the significance of the load factor on the output concentration of nitrogen oxides. It has been established that the change in the amount of discharged harmful impurities in each of the boiler operation modes does not occur randomly but as a result of the directional effect of the proposed flue gas recirculation method.

References

1. On the state and protection. Russian Federation State report (2020)
2. Russian Federation order, 1523-R (2020)
3. Korolev, E.A., Morozov, V.P., Eskin, A.A., Korolev, A.E., Barieva, E.R.: *SGEM* 19(4.1), 785–792 (2019)
4. Lipantiev, E.R.: *Izv. VUZov. Energy prob.* **5–6**, 144–148 (2017)
5. Gavrilov, A.F., Gorbanenko, A.D.: *Teploenergetika* **9**, 13 (2016)
6. Krivoruchenko, D.S., Telegina, N.S., Bokarev, D.A., Stakheev, A.Y.: *Kinet. Catal.* **56**(6), 729–734 (2015)
7. Soloviev, S.O., Kyriienko, P.I., Popovych, N.O., Larina, O.V.: *Sci. Innov.* **15**(1), 59–71 (2019)
8. Kryca, J., Piątek, M., Gancarczyk, A., Iwaniszyn, M., Kołodziej, A., Jodłowski, P., Łojewska, J.: *PrzemysłChemiczny* **94**(9), 1602–1604 (2015)
9. Ivanitskiy, M.S.: *Problems of energy* **7–8**, 16–23 (2016)
10. Vnukov, A.K., Alshevsky, V.N.: *Power Stations* **7**, 15 (2015)
11. Roslyakov, P.V., Ionkin, I.L., Pleshanov, K.A.: *Teploenergetika* **12**, 54–59 (2010)
12. Micel, A.A.: *Tomsk St. Un. of Cont. Sys. Radioelectronics* 113 (2016)
13. Khartov, A.A.: *Theory of Prob. App.* **63**(1), 57–71 (2018)
14. Kornienko, V.S.: *Volgogr. St. s.-kh. Acad.* (2010)
15. Girguis, M.S., Li, L., Breton, C., Gilliland, F., Habre, R., Lurmann, F., Wu, J., Stram, D.: *Air Quality. Atm. Health* **13**(6), 631–643 (2020)

Improvement of the Environmental Friendliness and Energy Efficiency of the Municipal Heating Network Through the Use of Coal-Water Slurry Fuel (on the Example of the City of Leninsk-Kuznetsky)



Vasily Murko, Oksana Chernikova, Aleksey Yur'ev, Valery Chaplygin, and Vladimir Vinograd

1 Introduction

One of the main strategic trends in the energy paradigm of the domestic and world economic systems is to ensure a significant reduction of anthropogenic impact on the environment while maintaining it in a state favorable for human life [1–4]. At the same time, the issues of environmental component of sustainable development in various industries and complexes have been in the focus of attention of Russian and foreign scientists for a long time. [5–12].

At the same time, from the economic point of view only the technologies of integrated processing and production of coal chemical products with high added value will be able to use effectively the energy value of coal and change its perception as a “dirty fuel” taking into account the growing share of renewable sources in the global energy balance and development of hydrogen energy, as well as infrastructural

V. Murko · V. Chaplygin

Department of Open-Pit Mining and Electromechanics, Siberian State Industrial University, Kemerovo Region, Kuzbass, 654007 Novokuznetsk, Russia

O. Chernikova (✉)

Department of Economics, Accounting and Finance, Siberian State Industrial University, Kemerovo Region, Kuzbass, 654007 Novokuznetsk, Russia

A. Yur'ev

Department of Metal Forming and Metal Science, Siberian State Industrial University, Kemerovo Region, Kuzbass, 654007 Novokuznetsk, Russia

V. Vinograd

LLC International Institute for the Implementation of Alternative Technologies, 220072 Minsk, Republic of Belarus

and logistical constraints on the development of the coal industry in the context of the pandemic.

At the moment of the adoption of the “Integrated program of socio-economic development of Leninsk-Kuznetsky urban district until 2025” (decision of the city Council of People’s Deputies No. 123 of December 23, 2010) the demand of population in heat energy was covered by 21 municipal and 2 departmental boiler houses, including 22 boiler houses that provided heating and hot water on the city territory. One municipal boiler house heated the residential area and organizations providing social services in Nikitinsky settlement. Heat supply in Leninsk-Kuznetsky was carried out by 5 boiler houses, 2 pumping stations, and 7 central heat supply stations, in which 44 heat exchangers were installed. In 7 boiler houses the processes of fuel supply and slag removal are fully mechanized, the rest of the boiler houses are equipped with furnaces with manual slag removal, 9 boiler houses are equipped with chemical water treatment plants. The physical deterioration of buildings in which city boilers are located is 62% (5 out of 21 boiler houses have 100% wear and tear). Physical equipment depreciation at boiler houses reaches 64%. Estimated heat consumption in the city of Leninsk-Kuznetsky is 750 thousand Gcal/year or approximately 150 Gcal/h.

At present, losses of heat energy during its production and transportation exceed 20% with the established standard losses of 12% due to the great depreciation of boiler equipment and heating networks. This condition of boiler equipment, in addition to low energy and economic efficiency, causes great harm to the environment and people. The similar state of heat supply facilities is typical for the city of Polysaevo.

In order to solve energy, economic and environmental problems of the heating network in Leninsk-Kuznetsk urban district, the authors propose a project for generating heat from Belovskaya Regional Power Station (RPS). It will make possible to refuse the idea of constructing new boiler houses instead of ineffective existing ones. The installed capacity of Belovskaya RPS is 1260 MW, and the thermal capacity is 229 Gcal/h.

Partial, combined with the main pulverized coal, combustion of coal-water slurry fuel (CWSF) in PK-40 boilers in the amount up to 25% (by heat value) is proposed as a part of the implementation of the project under consideration. Such technical solution will allow obtaining a significant economic effect and increasing the environmental safety of the RPS, but it will not affect the heat balance of boiler units and will not require their reconstruction.

This type of fuel has been sufficiently studied in domestic and world practice [13–17]. The first pilot plant for the CWSF preparation was constructed at Belovskaya RPS (Belovo, Kemerovo Region), where the pilot industrial coal pipeline “Belovo-Novosibirsk” was built (Fig. 1).

The years of project implementation are 1986–1997. During this time, more than 15 thousand tonnes of CWSF were prepared and burned in PK-40A boiler of Belovskaya RPS, and more than 350 thousand tonnes of CWSF were prepared and pumped through the pipeline and burned in TPE-214 boilers of Novosibirsk TPP-5.



Fig. 1 Coal pipeline “Belovo-Novosibirsk”, Belovo, Kemerovo Region, Russia

At that time, a boiler with a heating capacity of 670 tonnes of steam/h was completely transferred to the combustion of coal-water slurry fuel for the first time in the world. The hydraulic transport of coal-water slurry fuel was carried out over a distance of 262 km. A decrease in the content of nitrogen oxides NO_x in flue gases by 25–30% and a decrease in the concentration of other harmful substances during the combustion of CWSF to 15–70% were achieved.

The construction of coal pipelines is also not unusual. They are used in the USA, France, Canada, China, India (Table 1). In the American state of Ohio, earlier than in Russia, back in 1957, a coal pipeline with a throughput capacity of 1.2 million tonnes of coal per year and a length of 175 km was put into operation.

Table 1 The length and throughput capacity of coal pipelines in the world

Country	Length of a coal pipeline, km	Throughput capacity of a coal pipeline, th. tonnes
USA	20,000	250,000
France	7.2	330
Canada	1287	10,200
Poland	400	5000
China	No data available	30,000
India	2500	26,000

In the last decade, coal-water slurry fuel has become very popular. A number of projects have been implemented in Kazakhstan, Uzbekistan, Armenia, Austria, Ireland providing great opportunities for the export of manufactured products.

At present, it seems relevant to recommence the coal pipelines construction in Kuzbass. They are more economically profitable compared to rail transportation of coal, and the preparation and combustion of coal-water slurry fuel is more economically profitable compared to burning fuel oil in furnaces, especially taking into account the geographic location of the region, the continuous growth of tariffs for rail transportation and the volatility of oil prices.

2 Methods

Setting the goal and defining the tasks of scientific research, the authors used an empirical method for studying and analyzing the performance results of the heating network in the cities of Leninsk-Kuznetsky and Polysaev and assessing its impact on the economic and environmental aspects of society. A systematic approach was used for a comprehensive study of the research problem, based on the analysis of scientific literature given in the references. The statistical method with the analysis of actual data on emissions of harmful substances, the method of comparative analysis of the results of the impact of boiler houses and RPS on the environment were used in the process of studying the influence of power generating enterprises on the environment of the region.

3 Results

The conducted field studies during combustion of CWSF, prepared from filter cake of coal preparation plant in the experimental installation with a capacity of 500 kW, showed the following values of harmful emissions in flue gases: nitrogen oxides NO_x —not more than 190 mg/m^3 ; sulfur oxides SO_2 —not more than 20 mg/m^3 ; carbon monoxide CO —not more than 135 mg/m^3 ; dust—not more than 48 mg/m^3 ; polycyclic aromatic hydrocarbons (PAHs)—absent. In addition, the reduction of carbon dioxide emissions (CO_2) is up to 2 times compared to the layer combustion of run-of-mine coal (Figs. 2 and 3).

The CWSF economic efficiency is determined by 15–25% of savings in coal combustion; 20–35% of decrease in the cost of generating 1 Gcal/h of heat energy depending on the type of boiler; application of low-quality coals in the power industry with high efficiency and environmentally friendly combustion; a significant reduction in the expenses for utilization of ash and slag from the operation of boiler houses, since almost 70% of their volumes can be used, for example, in the production of building materials.



Fig. 2 The CWSF preparation block of experimental installation, Siberian State Industrial University, Russia

Belovskaya RPS burns approximately 4500 thousand tonnes of coal per year, while at a distance of 30–35 km from it there are coal preparation plants (Zarechnaya and mines n.a. Kirov and Komsomolets of JSC SUEK-Kuzbass) producing more than 1.5 million tonnes of filter cake. It is disposed in the dumps, erodes, produces dust, releases gases in the summer time, polluting the surrounding lands and groundwater and worsening the environmental situation in the area.

CWSF characteristics prepared from filter cake of the coal preparation plants of mines n.a. Kirov and Komsomolets are shown in Table 2.

At the same time, filter cake is a ready-made semi-finished product for producing coal-water slurry fuel with characteristics that allow its efficient co-firing in the coal-fired boiler units.



Fig. 3 The CWSF combustion block of experimental installation, Siberian State Industrial University, Russia

Table 2 CWSF characteristics prepared from filter cake of the coal preparation plants of mines n.a. Kirov and Komsomolets

Name, unit of measure	Indicator value
Particle size (mm)	0–0.200
Mass fraction of solid phase (%)	56.6–58.6
Ash content of the solid phase (%)	26.0–48.4
Effective viscosity at shear rate 81 s^{-1} (mPa s)	119–444
Low heat value MJ/kg (Kcal/kg)	8.24–12.72 (1967–3037)
Fuel consumption for production 1 MW (Gcal/h), t	0.361 (0.420)

In connection with the above, the project proposed by the authors includes the implementation of the following set of measures:

1. Creation of a specialized overhead transport technological line laid on overpasses and supports and consisting of
 - pipeline for CWSF hydrotransportation with a capacity of 1.5 million tonnes per year, which will allow CWSF, prepared from high-moisture coal sludge of coal preparation plants (CPP) of mines n.a. Kirov and Komsomolets (and, possibly, CPP of mine Zarechnaya), to be transported to Belovskaya RPS;
 - heating mains, consisting of direct and return pipelines, intended for provision consumers with heat, located along the route and preventing CWSF from freezing during its hydraulic transportation;
2. Development of a technological complex for the CWSF preparation based on slurry coal from the coal preparation plants of JSC SUEK Kuzbass with a capacity of 150 t/h (1200 thousand tonnes per year) with further CWSF transportation through the pipeline to Belovskaya RPS;
3. Installation of CWSF storage tanks and a pumping station at the industrial site of Belovskaya RPS equipping three operating boilers with burners (8 pcs.) with nozzles for CWSF supplying and burning in order to partially replace pulverized coal fuel. This system does not require modernization of the draft equipment and systems of ash and slag removal and gas cleaning. This ensures stable operation of the boilers in the nominal mode with a significant reduction in environmentally hazardous emissions in the gas combustion products;
4. Transition from the current heating network in the cities of Polysaev and Leninsk-Kuznetsky serviced by the local boiler houses (low-efficient, environmentally unsafe, with almost completely worn out equipment requiring major repairs) to the heat supply from Belovskaya RSP.

4 Discussion

According to the preliminary estimates, investment costs for the implementation of the proposed project will amount to 2.5–3.0 billion rubles. At the same time, its implementation will bring significant economic and environmental effects.

Estimated heat consumption in Leninsk-Kuznetsky is 750 thousand Gcal/year, or approximately 150 Gcal/h. To ensure the production of this amount of heat with an average efficiency of the operating city boiler houses at approximately 60%, it is necessary to burn about 300 thousand tonnes of coal with a lower combustion heat of 5 Gcal/t. Combustion of this amount of coal is a serious burden for the city environment characterized by the following indicators of emissions of harmful substances: SO₂—3250 t; CO—15,200 t; CO₂—about 600 thousand tonnes; NO₂—1390 thousand tonnes; solid dusty—12 thousand tonnes; about 120 thousand tonnes of ash and slag, etc.

The production of 1–1.5 million tonnes of CWSF per year with its delivery to Belovskaya RPS will ensure the possibility of utilization of sludges and cakes from the JSC SUEK coal preparation plants, while the company will receive additional annual profit from the sale of this waste in the amount of over 400 million rubles.

The combustion of more than 1 million tonnes of CWSF at Belovskaya RPS will reduce the amount of consumed coal by 73.2 t/h or 641 thousand tonnes per year in addition to the significant improvement in the environment. The cost of pulverized coal fuel at Belovskaya RPS is 1320 rub/t, the CWSF cost is 660 rub/t. The annual economic effect from the joint combustion of coal and water-coal slurry fuel in the boilers of Belovskaya RPS will amount to 186 million rubles.

Besides, Belovskaya RPS will sell heat in the amount of 750 thousand Gcal per year. Additional income from the sale of heat will amount to more than 500 million rubles per year even with a relatively low price of 1000 rub/Gcal.

The total economic effect from the implementation of the proposed project will amount to over 1.1 billion rubles per year.

At the same time, the integral economic effect for the cities of Polysaev and Leninsk-Kuznetsky will include saving of funds not spent on construction, modernization, and operation of boiler houses; profit from the sale of unburnt coal due to its replacement with coal-water slurry fuel; saving in the cost of the obtained heat unit in the heat networks.

References

1. Hussain, A., Arif, S.M.: *Renew. Sustain. Energy Rev.* **71** (2017)
2. Guo, P., Kong, J., Guo, Y., Liu, X.: *J. Cleaner Prod.* **215** (2019)
3. Xiangyan, Q., Di, W., Jia, W., Sai, C.: Resource curse, environmental regulation and transformation of coal-mining cities in China *Resources Policy*. In press, corrected proof (2019)
4. Chernikova, O., Zlatitskaya, Y., Klimashina, Y.: In: *IOP Conference Series: Earth and Environmental Science*, vol. 395 (2019)
5. Martins, V.W.B., Rampasso, I.S., Siltori, P.F.S., Cazeri, G.T., Leal, W.: *Filho J. Cleaner Prod.* **272** (2020)
6. Glushakova, O.V., Chernikova, O.P., Strelakova, S.A.: *Steel Transl.* **50**(5) (2020)
7. Chernikova, O.P., Strelakova, S.A., Zhdanova, N.G., Grinkevich, O.V.: *IOP Conf. Series Mater. Sci. Eng.* **976**(1) (2020)
8. Mealy, P., Teytelboym, A.: *Research Policy* (2020)
9. Hummels, H., Argyrou, A.: *J. Cleaner Prod.* (2020)
10. Du, Z., Lin, B.: *J. Cleaner Prod.* **176** (2018)
11. Schlör, H., Venghaus, S.: *J.-F. Nexus* **142** (2017)
12. Lin, B., Xu, M.: *J. Cleaner Prod.* **233** (2019)
13. Murko, V.I., Khyamyalyainen, V.A., Baranova, M.P.: *International Science and Technology Conference “EastConf”* (2019)
14. Oh, G., Ra, H.W., Yoon, S.M., Mun, T.Y., Yoon, S.J.: *J. Energy Inst.* **92** (2019)
15. Vershinina, K., Shabardin, D., Strizhak, P. *Powder Technol.* **3431** (2019)
16. Wang, R., Liu, J., Lv, Y., Ye, X.: *Appl. Thermal Eng.* **9925** (2016)
17. Hao, H., Liu, Z., Zhao, F., Du, J., Chen, Y.: *J. Cleaner Prod.* **14110** (2017)

Numerical Modeling of the Influence of the Atmospheric Meteorological State on the Efficiency of the Functioning of Solar Thermal and Power Plants



Nikolai Moskalenko, Azat Akhmetshin, Yana Safiullina, Ibragim Dodov, and Maryana Khamidullina

1 Introduction

Currently, boiler plants operating on fossil gas and solid fuels are widely used to generate thermal and electric energy. The cost of producing energy with their use is currently the cheapest. Considering the fact that the reserves of fossil fuels are limited, and the emissions of exhaust combustion products into the atmosphere are toxic to living organisms and have carcinogenic effects, and also affect anthropogenic climate changes. In recent decades, technologies have been developed for the use of alternative energy using wind installations, solar, thermal and power plants, and hydroelectric power plants.

The sun is an inexhaustible source of energy, but the energy of solar radiation (SR) arriving at the underlying surface has a large temporal variability (daily and seasonal) and depends on the location of the stations and the meteorological state of the atmosphere [1, 2]. In light of the above, to optimize the design of solar thermal power plants (STS) and solar power plants (SPP) requires knowledge of the dependences of the light energy of solar radiation arriving at the light-receiving surface of the boiler plant, depending on the meteorological state of the atmosphere at the location of the station and the time of the station [2, 3]. In this paper, we consider the obtaining of the initial data necessary for the development of structures of STS and SPP by the method of numerical simulation of incoming SR fluxes in the spectral region of their operation.

The SR inflows to the light-perceptible surface of the STS and SPP are determined taking into account the molecular absorption and scattering of SR by the atmosphere, scattering of radiation by aerosol and the overlap of the sky by a multi-tiered cloud cover, taking into account the downward SR flux reflected from the

N. Moskalenko · A. Akhmetshin (✉) · Y. Safiullina · I. Dodov · M. Khamidullina
Kazan State Power Engineering University, str. Krasnoselskaya 51, 420066 Kazan, Russia
e-mail: dr.akhmetshin@ieec.org

underlying surface. In this regard, it is required to simulate the optical characteristics (OC) of the gaseous components of the atmosphere, atmospheric aerosol, and clouds, which are discussed below.

2 Modeling of Molecular Absorption of SR by the Atmosphere

The main characteristic of SR absorption by the atmosphere is the spectral transmission function (STF). The STF is calculated by the two-parameter method of equivalent masses, which makes it possible to solve the problems of radiation heat transfer in structurally inhomogeneous media. STF for component i is determined from the relation [4].

$$\left(\frac{1}{\ln \tau_{\Delta vi}}\right)^2 = \left(\frac{1}{\ln \tau'_{\Delta vi}}\right)^2 + \left(\frac{1}{\ln \tau''_{\Delta vi}}\right)^2 + \frac{M}{\ln \tau_{\Delta vi}' \ln \tau''_{\Delta vi}} \quad (1)$$

where

$$\begin{aligned} |\ln \tau'_{\Delta vi}| &= \int_L k_{\Delta vi} F_1[L(T)] P_i(L) dL \\ |\ln \tau''_{\Delta vi}| &= \left[\int \beta_i P_i(L) P_p^{n_i/m_i}(L) F_2^{1/m_i} l(T) dL \right]^m \end{aligned} \quad (2)$$

where $n_i, m_i, k_{\Delta vi}, \beta_{\Delta vi}, M_i$ —are the empirical parameters of the STF by the spectrum of the wave number ν , L —optical path, P_i —pressure of the i component.

$$\tau_{\Delta v} = \exp \left[- \sum_i \ln \tau_{\Delta vi} \right] \quad (3)$$

$F_1(T), F_2(T)$ —temperature dependences $k_{\Delta vi}/k_{\Delta v0}, \beta_{\Delta vi}/\beta_{\Delta v0}$.
In relation (2) P_p —effective pressure

$$P_p = P_{N_2} + \sum_k B_{ik} P_k, \quad (4)$$

where B_{ik} —is the broadening factor of spectral lines for collisions of molecules i with molecule k . For oxygen $B(O_2) = 0.8$, $B(CO_2) = 1.4 \div 1.6$. For water vapor $B(H_2O) \in [6, 30]$ and depends significantly on temperature.

The parameter M determines the rate of transition of the STF from the weak absorption approximation to the strong absorption approximation. With overlapping spectral lines, the Bouguer law for the STF is fulfilled when $k_{\Delta v}(T) = \beta_{\Delta v}(T)$, $m = 1$, $n = 0$, $M = -1$. For bands with pressure-induced absorption and continuous

absorption of radiation by the wings of the spectral lines absorption (SLA) $m = n = 1, M = -1, k^{-n}, -\Delta\nu(T) = \beta - \Delta\nu$. For an arbitrary STF $m \in \{0, 1\}, n \in \{0, 1\}, M \in \{0, -1\}$.

For a multicomponent inhomogeneous medium

$$|\ln \tau'_{i\Delta\nu}| = \int_L \kappa_{i\Delta\nu}(T) \rho[L(T)] dL, \tag{5}$$

$$|\ln \tau''_{i\Delta\nu}| = \left\{ \int_L \beta_{i\Delta\nu}^{1/m_i}(T) \rho_i[L(T)] P_{ip}^{n_i/m_i}(L) dL \right\}^{m_i}, \tag{6}$$

$$|\ln \tau_{\Delta\nu}| = \sum_i |\ln \tau_{i\Delta\nu}[L(T)]|, \tag{7}$$

$$\tau_{\Delta\nu} = \exp \left[- \sum_i \ln \tau_{i\Delta\nu}[L(T)] \right]. \tag{8}$$

The parameterization of the STF is determined for gaseous optically active ingredients broadened with nitrogen. Taking into account the effect on the STF of the broadening of the SLA in collisions with molecules of other components is realized by introducing an effective pressure.

$$P_{ip} = P_{N_2} + \sum_k B_{ik}[L(T)] P_k(L), \tag{9}$$

where $B_{ik} = \alpha_{0i}(i - k)/\alpha_{0i}(i - N_2), \alpha_{0i}(i - k), \alpha_{0i}(i - N_2)$ —reduced to pressure $P = 1$ atm half-width of the lines for collisions of $(i - k)$ and $(i - N_2)$.

3 Modeling the OC of Atmospheric Aerosol

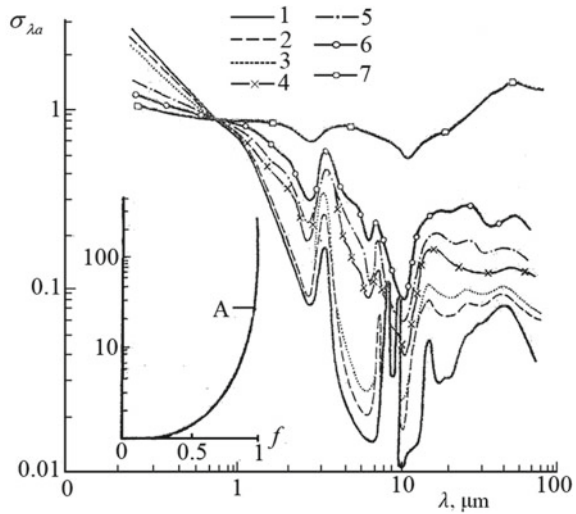
To model SR fluxes in a turbid atmosphere, it is necessary to know the spectral attenuation coefficients of SR by atmospheric aerosol $\sigma_{\lambda a}(z)$ of SR scattering $\sigma_{\lambda a}^s(z)$, SR absorption $\sigma_{\lambda a}^a(z)$, scattering indicatrix $f_{\lambda a}(z)$, where Z is the height above sea level, λ is the wavelength.

The aerosol has a multicomponent composition. Its OC depends on the relative humidity of the atmosphere. According to the chemical composition, the salt fraction of atmospheric aerosol, dust aerosol, sea aerosol, and soot ash from forest fires are distinguished.

Condensation growth of particles is an important factor determining its effect on the OC of the atmosphere. Figure 1 shows the spectral dependences of the attenuation coefficient, radiation, salt fraction of atmospheric aerosol [5].

Figure 2 shows the spectral dependences of the normalized attenuation coefficients $\sigma_{\lambda a}(a)$, absorption $\sigma_{\lambda a}^a(a)$, scattering $\sigma_{\lambda a}^s(a)$ at different relative humidity [6].

Fig. 1 Normalized spectra of attenuation coefficients $\sigma_{\lambda a}$ of salt fraction, atmospheric aerosol for various relative humidity f , %: 1—40; 2—80; 3—95; 4—99; 5—99.5; 6—99.8; 7—100. A—dependence of optical density on relative humidity f at a wavelength $\lambda = 0.55 \mu\text{m}$



The sea aerosol is represented by particles of SPP sea salt and the height of its turbulent transport over the sea area is much lower than over land [5]. When it is carried over the continents, one should expect the rise of sea salt particles due to an increase in the height of the turbulent heat transfer zone. Examples of modeling vertical profiles of the optical density of a multicomponent atmospheric aerosol are considered in [5–7].

Figure 3 shows the spectral dependences $\sigma_{\lambda a}$, $\sigma_{\lambda a}^a$, $\sigma_{\lambda a}^s$ for soot aerosol (fraction 4) of the electronic database at different relative humidity indicated in the figure.

The electronic database on the OC of atmospheric aerosol includes light scattering matrices for various fractions of atmospheric aerosol for the range of relative humidity $f \in (0, 1)$, which makes it possible to take into account its effect on the intensity of the scattered SR incident on the underlying surface. The diffuse SR reflected from the underlying surface is calculated from the landscape map [8] taking into account seasonal changes in the spectral albedo of the underlying surface.

Figure 4 shows the scattering indicatrix $f(\theta)$ by urban haze for wavelengths 0.3; 0.63; 1.08; 1.7 μm over Manchester (curve 1); Rennes (curve 2) and the White Sand subarid zone (curves 3,4) corresponding to the value of the real part of the refractive index complex $n = 1.5$ and 1.65.

Table 1 shows the coefficients of attenuation, radiation, scattering, and absorption of particles of sea salt (A) and continental dust (B) normalized to optical density. The microstructure of sea salt is described by the γ -distribution of I with parameters $a = 1$; $b = 7.5$; $c = 0.5$. Dust aerosol II has microstructures with γ -distribution parameters $a = 1$; $b = 9$; $c = 0.5$.

In works [1, 4, 5, 9, 10], a closed simulation of the OC of atmospheric aerosol has been developed. According to the modeling we have chosen, the aerosol is represented as a superposition of individual fractions. The microstructure $N(r)$ is given by the formula

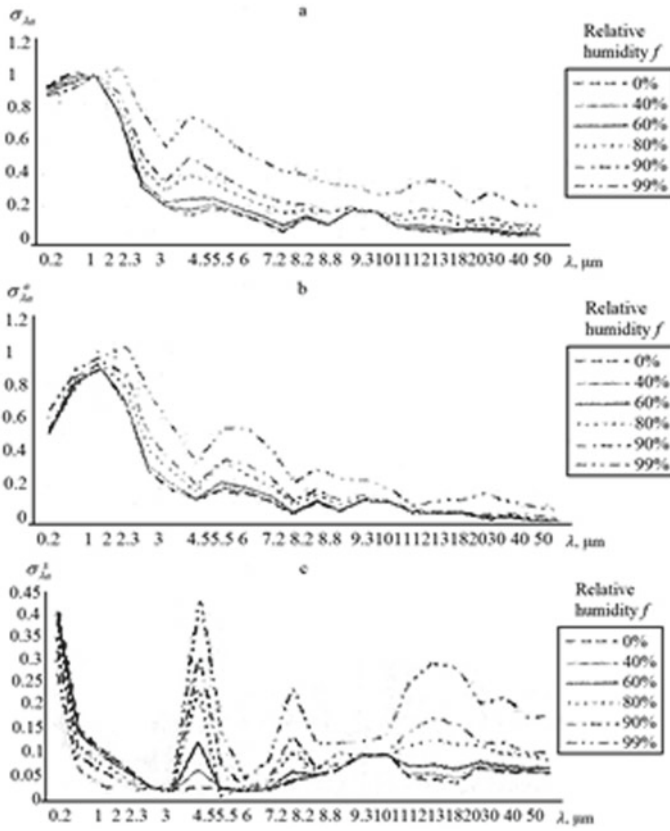


Fig. 2 Spectral dependence of normalized coefficients of attenuation $\sigma_{\lambda a}$ (a), absorption $\sigma_{\lambda a}^a$ (b), and scattering $\sigma_{\lambda a}^s$ (c) for dust aerosol at different relative humidity of the f

$$N(r) \sum_{i=1}^N N_i(r) = \sum_{i=1}^N A_i r_a^{a_i} \exp(-b_i r^{c_i}) \tag{10}$$

where A_i, a_i, b_i, c_i are the parameters of the i th fraction, N is the number of fractions.

Due to the fact that the most reliable information on the vertical structure of the aerosol was obtained by optical density, spectral attenuation, scattering, and absorption are normalized to optical density. Each aerosol fraction is specified by its own vertical profile, which makes it possible to simulate changes in the chemical composition, microstructure, and OC with height. The spectral coefficients of attenuation, scattering, absorption, scattering indicatrix are determined by the formulas [11].

$$\sigma_{\lambda a} = \sum_{i=1}^N B_i(z) \sigma_{i \lambda a}, \tag{11}$$

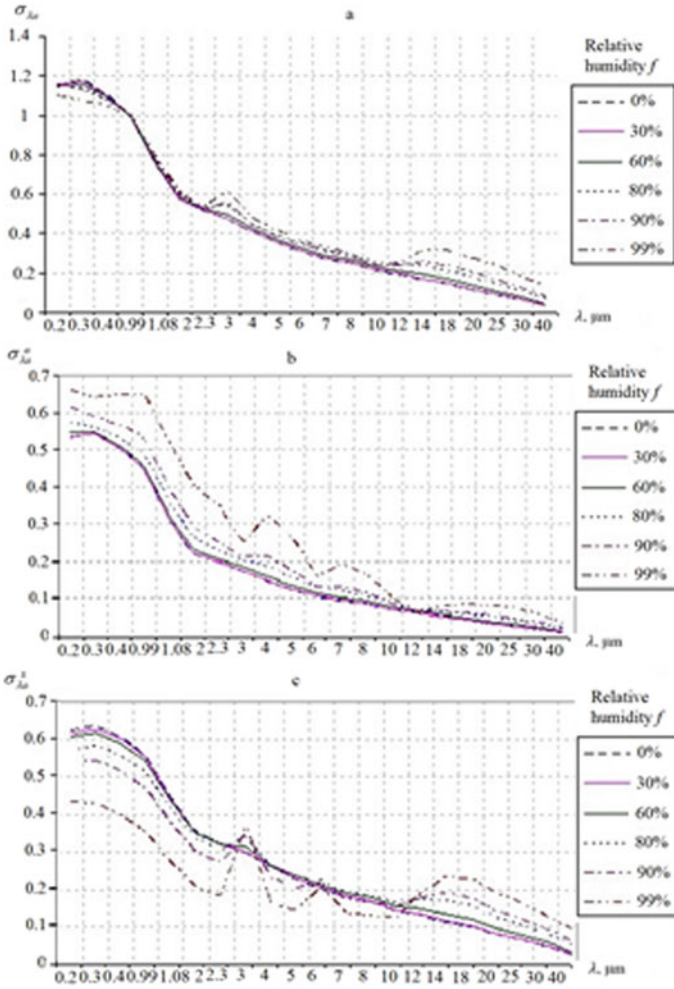


Fig. 3 Spectral dependence of normalized attenuation $\sigma_{\lambda a}^s$ (a), absorption $\sigma_{\lambda a}^a$ (b), and scattering $\sigma_{\lambda a}^i$ (c) coefficients for soot aerosol (fraction no. 4) at different relative humidity f

$$\sigma_{\lambda a}^s = \sum_{i=1}^N B_i(z) \sigma_{i \lambda a}^s, \tag{12}$$

$$\sigma_{\lambda a}^a = \sum_{i=1}^N B_i(z) \sigma_{i \lambda a}^a, \tag{13}$$

$$f(z, \theta) = \sum_{i=1}^N B_i(z) f_i / \sum_{i=1}^N B_i(z), \tag{14}$$

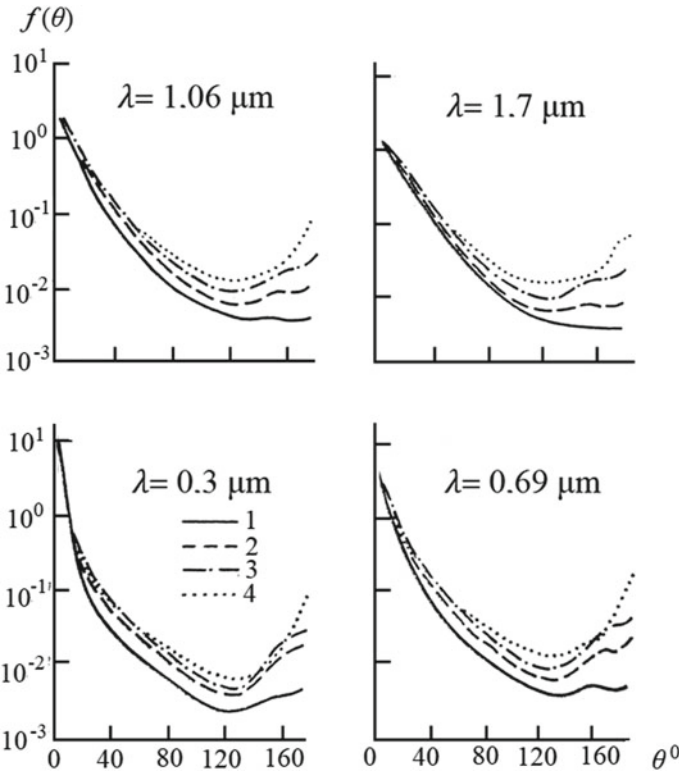


Fig. 4 Indicatrixes of radiation scattering by urban haze

where $B_i(z) = d\tau/dz$ —is the vertical cut of optical density, $\sigma_{i\lambda a}$, $\sigma_{i\lambda a}^a$, $\sigma_{i\lambda a}^s$, f_i —are the coefficients of attenuation, scattering, absorption, scattering indicatrix for the i th fraction of atmospheric aerosol.

The formation of models is carried out on a computer using the “aerosol block program” included in a single complex of the SR transfer program in the atmosphere.

4 Optical Cloud Models

Table 2 presents microstructure models for clouds of various shapes, recommended for calculating the optical characteristics of clouds. Allocated stratocumulus (Sc), altocumulus (Ac), stratocumulus (St), altostratus (As), nimbostratus (Ns), cumulonimbus (Cb), power-cumulus (Cu Cong), C.6, a microstructure that is described by distributions with parameters a, b, c , modal radius R_m . N , sm^{-3} —number of particles, in cubic centimeter; W , g/m^3 —moisture content of clouds. Cloud moisture W is defined as the mass of water per unit volume of atmospheric air [6, 12].

Table 1 Normalized to optical density coefficients of attenuation σ_a , scattering σ_a^s , and absorption σ_a^a of particles of sea salt (A) and continental dust (B)

I				II			
A				B			
μm	s_a	s_a^s	s_a^a	μm	s_a	s_a^s	s_a^a
0.55	1.000	0.946	0.054	0.55	1.000	0.855	0.145
1.00	1.149	1.074	0.075	1.00	0.729	0.481	0.248
2.00	1.024	0.803	0.221	2.00	0.324	0.248	0.076
2.50	0.888	0.820	0.068	3.00	0.140	0.109	0.031
2.70	0.801	0.587	0.214	4.50	0.145	0.119	0.026
3.00	1.147	0.667	0.480	6.00	0.064	0.020	0.044
3.50	0.708	0.687	0.021	6.50	0.058	0.013	0.045
4.00	0.623	0.577	0.046	7.20	0.143	0.086	0.057
4.50	0.465	0.401	0.064	8.20	0.074	0.008	0.066
6.00	0.351	0.286	0.073	8.50	0.112	0.032	0.080
6.50	0.284	0.173	0.111	8.70	0.137	0.051	0.086
7.20	0.123	0.039	0.084	9.00	0.227	0.120	0.107
7.90	0.111	0.064	0.047	9.50	0.224	0.111	0.113
8.20	0.262	0.062	0.200	10.00	0.210	0.104	0.106
8.50	0.721	0.397	0.324	11.00	0.133	0.064	0.069
8.70	0.740	0.386	0.354	12.00	0.107	0.077	0.030
9.00	0.636	0.296	0.340	13.00	0.075	0.020	0.055

Note (I) $a = 1, b = 7.5, c = 0.5$; (II) $a = 1, b = 9, c = 0.5$

Table 2 Distribution of cloud droplets by size

Cloud shape	a	b	c	r_m (μm)	N (sm^{-3})	A	W (g/m^3)
Stratocumulus (Sc)	5	0.576	1.19	5.33	10^2	2.82×10^{-1}	0.141
Alto cumulus (Ac)	2	0.0027	2.46	10.19	10^2	1.97×10^{-1}	0.796
Stratocumulus (St)	5	0.936	1.05	4.70	10^2	9.79×10^{-1}	0.114
Altostratus (As)	3	0.193	1.30	6.75	10^2	3.81×10^{-1}	0.379
Nimbostratus (Ns)	5	0.402	1.24	6.41	10^2	8.06×10^{-1}	0.235
Cumulonimbus (Cb)	1	0.0017	2.41	9.67	10^2	1.097	1.034
Power-cumulus (Cu Cong)	4	0.667	1.00	6.00	10^2	0.548	0.297
C.6	2	0.100	1.00	20.00	10^1	0.5×10^{-4}	0.025

$$W = \frac{3\pi}{4} \rho_{iw} \int_r r^3 n(r) dr_i \tag{15}$$

where ρ_w —is the density of water. Parameter A is determined by the ratio.

$$A = Ncb^{(a+1)c} / r \left(\frac{a+1}{c} \right) \tag{16}$$

We have developed an electronic database of light scattering matrices for the cloud models presented in Table 2 in the wavelength range 0.3–60 μm . Table 3 shows an example of a light scattering matrix for an Ns cloud for wavelengths $\lambda = 0.3 \mu\text{m}$.

Figure 5 shows the probabilities of overlapping the sky with clouds of various levels for the month of June.

In the interests of automated modeling, the OC cloud library has been prepared for eight modifications of the microstructure from Table 3 for discrete wavelengths in the spectral range of 0.3–60 μm . The data on the refractive index spectrum [13].

5 Calculations of the Efficiency of Thermal and Power Plants

For a cloudless atmosphere, the fluxes of downward radiation are determined from the SR flux at the outer boundary of the atmosphere, weakened by the atmosphere by gaseous components and aerosol. As an example, Fig. 6 shows the functions of the spectral transmission of the atmosphere depending on the zenith angle for the model of the average global atmosphere [7]. Illumination by scattered downstream SR is calculated in multi-stream approximation [1].

Calculation of fluxes of shortwave radiation $F_{s\uparrow}(z)$, $F_{s\downarrow}(z)$ is produced in the multithreaded approximation [1]. According to [1], having radiation fluxes in two mutually perpendicular directions for each of the listed radiation fluxes, it is possible to obtain fluxes in mutually perpendicular directions scattered by a system of two layers, taking into account the redistribution of radiation between the layers. The scheme of transformation of the incident flux can be represented in the form of an infinite series, which, using a matrix apparatus, can be folded and obtain relations in matrix form for fluxes scattered by a two-layer radiation system [1, 9].

$$\begin{bmatrix} I_1^\downarrow, I_2^\downarrow \end{bmatrix} = [x, y] \begin{bmatrix} i_1 & m_1 \\ m_3 & i_3 \end{bmatrix} \tag{17}$$

$$\begin{bmatrix} I_1^\uparrow, I_2^\uparrow \end{bmatrix} = [B_1, C_1] + [x, y] \begin{bmatrix} j_1 & k_1 \\ k_3 & j_3 \end{bmatrix} \begin{bmatrix} A_2 & D_2 \\ D_4 & A_4 \end{bmatrix} \tag{18}$$

$$[x, y] = \frac{1}{(1-a)(1-d) - bc} [A_1, D_1] \begin{bmatrix} 1-a & b \\ c & 1-d \end{bmatrix},$$

Table 3 Ns cloud scattering matrix. $\lambda = 0.3 \mu\text{m}$, $\sigma_a = 43.235 \text{ km}^{-1}$, $\tilde{\omega} = 0.99999$

Q	M_2		M_1		S_{21}		D_{21}	
0.0	0.1715	04	0.1715	04	0.1715	04	0.0	
0.5	0.5915	03	0.5916	03	0.5915	03	0.2378	01
1.0	0.6241	02	0.6235	02	0.6236	02	-0.7276	00
2.0	0.7139	01	0.7060	01	0.7093	01	-0.4210	-01
3.0	0.2667	01	0.2608	01	0.2633	01	-0.1932	-01
4.0	0.1437	01	0.1393	01	0.1412	01	-0.8196	-02
5.0	0.1025	01	0.9936	00	0.1007	01	-0.3444	-02
6.0	0.8176	00	0.7895	00	0.8013	00	-0.2972	-02
7.0	0.7176	00	0.6947	00	0.7041	00	-0.2170	-02
8.0	0.6425	00	0.6235	00	0.6311	00	-0.2542	-02
9.0	0.5925	00	0.5752	00	0.5921	00	-0.8558	-03
10.0	0.5546	00	0.5432	00	0.5472	00	-0.7680	-03
15.0	0.4222	00	0.4217	00	0.4204	00	0.1246	-03
20.0	0.3207	00	0.3302	00	0.3298	00	0.2898	-03
25.0	0.2409	00	0.2527	00	0.2451	00	0.3977	-03
30.0	0.1774	00	0.1904	00	0.1814	00	0.1211	-02
35.0	0.1271	00	0.1410	00	0.1311	00	0.1277	-02
40.0	0.8887	-01	0.1031	00	0.9309	-01	0.9668	-03
45.0	0.6146	-01	0.7531	-01	0.6509	-01	0.7655	-03
50.0	0.4216	-01	0.5254	-01	0.4443	-01	0.8022	-03
55.0	0.2848	-01	0.3626	-01	0.2948	-01	0.7830	-03
60.0	0.1890	-01	0.2417	-01	0.1892	-01	0.6088	-03
65.0	0.1219	-01	0.1551	-01	0.1147	-01	0.3966	-03
70.0	0.8011	-02	0.9376	-02	0.6446	-02	0.2904	-03
75.0	0.5457	-02	0.5465	-02	0.3367	-02	0.1730	-03
80.0	0.3980	-02	0.3067	-02	0.1513	-02	0.1016	-03
85.0	0.3079	-02	0.1731	-02	0.4860	-03	0.4739	-04
90.0	0.2579	-02	0.1083	-02	-0.5136	-04	0.4473	-04
95.0	0.2294	-02	0.8320	-03	-0.3000	-03	0.2883	-04
100.0	0.2160	-02	0.8619	-03	-0.3801	-03	0.4729	-04
105.0	0.2165	-02	0.1051	-02	-0.3019	-03	0.1225	-03
110.0	0.2368	-02	0.1336	-02	-0.1225	-03	0.2846	-03
115.0	0.2584	-02	0.1680	-02	0.8922	-04	0.6289	-05
120.0	0.6955	-02	0.1817	-02	0.1518	-02	0.7657	-03
122.0	0.7269	-02	0.1736	-02	0.1172	-02	0.1424	-02
124.0	0.6059	-02	0.1525	-02	0.4287	-03	0.1503	-02

(continued)

Table 3 (continued)

Q	M_2		M_1		S_{21}		D_{21}	
126.0	0.4404	-02	0.1325	-02	-0.2313	-03	0.1222	-02
128.0	0.3174	-02	0.1145	-02	-0.6448	-03	0.8619	-03
130.0	0.2383	-02	0.1029	-02	-0.8295	-03	0.6019	-03
132.0	0.2048	-02	0.1001	-02	-0.9295	-03	0.4691	-03
134.0	0.2022	-02	0.1110	-02	-0.8952	-03	0.5495	-03
136.0	0.4347	-02	0.1659	-02	-0.1003	-02	0.1549	-02
138.0	0.9342	-02	0.2563	-02	0.4246	-03	0.3656	-02
140.0	0.2982	-01	0.4493	-02	0.3501	-02	0.9053	-02
142.0	0.6133	-01	0.4246	-02	0.9205	-02	0.9095	-02
144.0	0.5279	-01	0.5065	-02	0.9478	-02	-0.5489	-02
146.0	0.1811	-01	0.1181	-01	0.4344	-02	-0.4135	-02
148.0	0.1914	-01	0.1119	-01	0.4986	-02	0.2610	-02
150.0	0.1900	-01	0.1050	-01	0.3901	-02	0.1289	-02
152.0	0.1614	-01	0.1086	-01	0.3166	-02	0.7275	-03
154.0	0.1382	-01	0.1124	-01	0.2560	-02	0.5816	-03
156.0	0.1206	-01	0.1134	-01	0.1849	-02	0.7596	-03
158.0	0.1010	-02	0.1107	-01	0.1259	-02	0.8780	-03
160.0	0.9973	-02	0.1097	-01	0.6966	-03	0.7384	-03
162.0	0.8952	-02	0.1089	-01	0.2258	-03	0.5622	-03
164.0	0.8336	-02	0.1072	-01	-0.2647	-03	0.6141	-03
166.0	0.7948	-02	0.1046	-01	-0.5535	-03	0.5512	-03
168.0	0.7376	-02	0.1065	-01	-0.9550	-03	0.4286	-03
170.0	0.7169	-02	0.1078	-01	-0.9224	-03	0.4250	-03
171.0	0.7055	-02	0.1071	-01	-0.1003	-02	0.3824	-03
175.0	0.7414	-02	0.1313	-01	-0.2798	-03	0.4110	-03
176.0	0.8037	-02	0.1495	-01	0.5700	-03	0.4699	-03
177.0	0.9158	-02	0.1774	-01	0.1527	-02	0.2709	-04
178.0	0.1124	-01	0.2467	-01	0.4765	-02	0.8958	-03
179.0	0.3633	-01	0.5023	-01	0.2404	-01	-0.2826	-03
180.0	0.4958	-01	0.4958	-01	-0.4958	-01	0.0	

$$\begin{bmatrix} a & b \\ c & d \end{bmatrix} = \begin{bmatrix} C_2 & B_2 \\ C_4 & B_4 \end{bmatrix} \begin{bmatrix} k_3 & j_1 \\ j_3 & k_1 \end{bmatrix} \tag{19}$$

where $[I_1^\downarrow, I_2^\downarrow]$ are downward and $[I_1^\uparrow, I_2^\uparrow]$ —ascending radiation fluxes in the first and in the second layers of the medium for angles $\theta_0, \theta_0' = \pi/2 - \theta_0$ at the zenith angle of the Sun θ_0, B_1, C_1 —reflected and A_1, D_1 —transmitted fluxes of radiation,

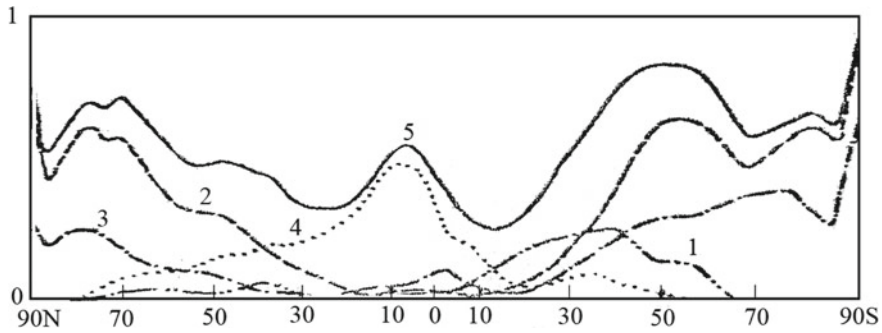


Fig. 5 Probability of overlapping the sky with clouds of various levels and types N—northern latitude; S—southern latitude; 1—cloudiness CL₃; 2—cloudiness CL₂; 3—cloudiness CL₄; 4—cloudiness CL₁; 5—the probability of covering the sky with all types of clouds

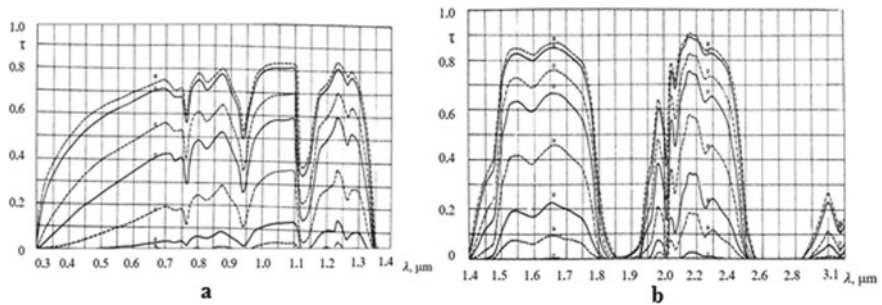


Fig. 6 Spectral transparency of the atmosphere in the spectral range of 0.3–3.1 μm at zenith viewing angles $\theta(z_1)$: 10—0°, 11—30°, 12—60°, 13—70°, 14—80°, 15—85°, 16—87°, 17—89°, 18—90°, 19—90°20'. **a** spectral region 0.3–1.04 μm ; **b** spectral region 1.4–3.1 μm

determined by the angles θ_0 and θ'_0 , scattered by the upper layer when the radiation is incident from above; B_2, C_2, A_2, D_2 —similarly, the streams of scattered radiation for radiation incidence from below, but at the zenith angle

$$\theta'_0 : i_1, j_1, k_1, m_1 : i_2, j_2, k_2, m_2 : i_3, j_3, k_3, m_3 : i_4, j_4, k_4, m_4$$

correspond to radiation fluxes for the second layer. Using relations (15–17), which represent an exact solution to the problem of radiation scattering by a system of two layers in the decomposition of the total flux into fluxes in two mutually perpendicular directions, an exact computational scheme of the reflected and transmitted fluxes for a multilayer atmosphere inhomogeneous in height is constructed and implemented. For this, for each inhomogeneous layer, heterogeneous in height of the atmosphere, scattered fluxes are calculated for the four directions of incidence of the study described above. Further, using formulas (16–17), we find the scattered fluxes for a system of two layers with the same four directions of incidence. The obtained solution for a

two-layer atmosphere is used to obtain a solution in a three-layer atmosphere using the same relationships (15–17). The procedure for connecting the following layers is carried out until a complete search of the atmospheric layers. In the presence of an underlying surface with an albedo q , the albedo of the “underlying surface—atmosphere” system, depending on the zenith angle of the sun θ_0 , is determined by the ratio:

$$q^*(\theta_0) \left[I_1^\uparrow(\theta_0) + I_2^\uparrow(\theta_0) \right] + \left[I_1^\downarrow(\theta_0) + I_2^\downarrow(\theta_0) \right] \frac{Tq}{1 - Rq} \tag{20}$$

where $I_1^\uparrow(\theta_0)$, $I_2^\uparrow(\theta_0)$ —are radiation fluxes at the upper boundary of the atmosphere; $I_1^\downarrow(\theta_0)$, $I_2^\downarrow(\theta_0)$ —radiation fluxes at the level of the underlying surface; T is the transfer function of the atmosphere for the diffuse radiation of the underlying surface; R is the albedo of the atmosphere when viewed from below.

For the downward SR, the spectral flux onto the light-receiving surface is determined by the ratio

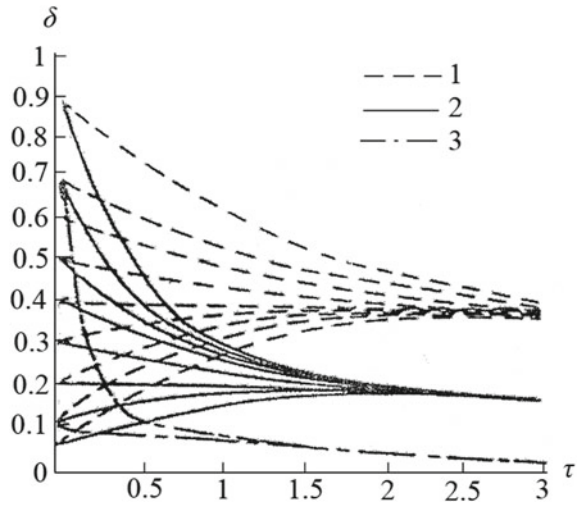
$$J^\uparrow(\theta_0) = J_1^\downarrow(\theta_0) + J_2^\downarrow(\theta_0) + \left(J_1^\downarrow(\theta_0) + J_2^\downarrow(\theta_0) \right) qR \tag{21}$$

where R is the spectral albedo of the atmosphere for the diffusely reflected downward SR, scattered into the back hemisphere, q is the spectral albedo of the underlying surface. To determine the albedo integral over the spectrum, monochromatic fluxes (19, 20) are integrated according to the operational calculation scheme taking into account the spectral weight of the solar radiation in the integral flux. Taking into account the absorption of radiation by the one-parameter or two-parameter equivalent mass method described above.

Figure 7 shows the dependence of the albedo δ of the “underlying surface—atmospheric aerosol layer” system on the optical thickness τ of the aerosol cloud for the models of the average global, industrial and soot aerosols at various values of the underlying surface albedo. For the model of the average global atmospheric aerosol 1, the probability of quantum survival $\tilde{\omega} = 0.9$ was obtained. For tropospheric aerosol model 2 over Western Europe $\tilde{\omega} = 0.75$. For industrial carbon black aerosol, $\tilde{\omega} = 0.6$ [5]. The considered curves in Fig. 6 make it possible to assess the effect of atmospheric aerosol on the albedo of the system depending on the albedo of the underlying surface, on the optical properties of the aerosol, and on the optical thickness of the aerosol cloud [5, 14, 15]. If δ is greater than 0.37, then the aerosol always decreases the albedo of the “underlying surface—atmosphere” system. In the atmospheric aerosol model over Western Europe (industrial areas $\tilde{\omega} = 0.75$), at $\delta \geq 0.2$, the albedo of the system always decreases. In model 3 (soot sol), the albedo of the system decreases at $\delta \geq 0.06$. Atmospheric aerosol of any type reduces the albedo of the “cloudy-aerosol cloud”, “snow-covered surface— aerosol cloud” systems.

Atmospheric influences (clouds, fog, dust, humidity, etc.) not only change the SR flux falling on the heat-sensing surface of the STS and SPP, but also change the ratio between direct and scattered radiation. The maximum thermal perception of SR is

Fig. 7 Dependence of the albedo δ of the underlying surface—atmospheric aerosol layer system on the optical thickness t of the aerosol cloud for the models of the average global atmospheric aerosol (1), industrial aerosol (2), and strong absorbing aerosol (3) at various albedo values of the underlying surface [5, 16]



achieved in installations with automated orientation of the mirror system to the solar disk.

The method of numerical modeling developed in this work makes it possible to assess the degree of influence of the meteorological state of the atmosphere (clear, cloudy, cloudy, anthropogenically disturbed) and calculate the efficiency of the STS and SPP functioning depending on their location and design solutions. The location of STS and SPP in places with high average annual illumination of the underlying surface (for example, Crimea, Orenburg, Astrakhan, Voronezh regions) is promising.

Next, we will consider the application of the method of numerical modeling for the STS, SPP. Figure 8 shows the spectral albedo of the atmosphere for SR

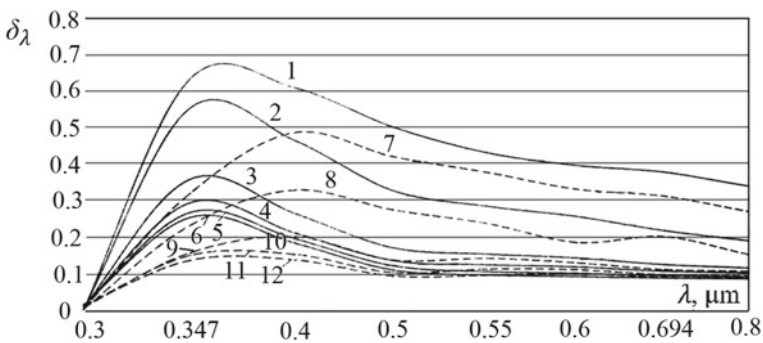


Fig. 8 Spectral albedo of the atmosphere for solar radiation when viewed from below for an undisturbed atmosphere (at zenith angles of sight 0:1—85; 2—75; 3—45; 4—15; 5—5; 6—0) and for an atmosphere with urban aerosol (at zenith angles of sight 0:7—85; 8—75; 9—45; 10—15; 11—5; 12—0) in the spectrum range 0.3–0, 8 μm

when observing the atmosphere from below for the unperturbed atmosphere and the atmosphere with urban haze.

6 Conclusion

The problem of numerical modeling of the influence of the meteorological state of the atmosphere on the functioning of STS and SPP is considered. The analyzed influence of humidity on the optical characteristics of atmospheric and anthropogenic aerosols. The multicomponent composition of the atmospheric aerosol is taken into account; each fraction of the atmospheric aerosol is set in the form of a vertical profile and its optical density, at a wavelength of $\lambda = 0.55 \mu\text{m}$ in accordance with the atmospheric humidity r . The spectral dependences of the attenuation, absorption and scattering coefficients and the scattering indicatrix are determined from the electronic database, according to OC normalized to the optical density, OC, specified for discrete lengths in the spectrum range of $0.2\text{--}50 \mu\text{m}$ in the range of relative humidity $r \in (0.100\%)$. The cloudiness of the atmosphere is assumed to be multi-level and is given in the form of probability, overlap of the sky, cloudiness of the lower, middle and upper levels. To simulate OC objects, an electronic database of light scattering matrices for clouds of various shapes, given by gamma distributions of their microstructure, is substituted. OC of mixed forms is formed by software for PECM. The molecular absorption SR is calculated by the parametric equivalent mass method.

The incoming SR is perceived by the light-receiving surfaces of the STS and SPP and is transmitted by the system of mirrors to the thermal receiving surface of the boiler plant for generating steam with subsequent conversion of the thermal energy of the steam into electrical energy in the steam turbine. SR fluxes are calculated by the layer stacking method in the multithreaded approximation [1], taking into account the molecular absorption of the study, scattered radiation of atmospheric aerosol, and multi-level clouds.

Based on the results of the simulation, the efficiency of the STS and SPP was revealed for various meteorological compositions of the atmosphere and the latitudinal belt of the earth (the geographical dislocation of the STS and SPP).

The developed semi-analytical method and software complex for calculating shortwave radiation are used to calculate the spectral and integral albedo of the system «Earth-atmospheres» for real models of a turbid atmosphere with simultaneous consideration of molecular scattering, molecular absorption and in the presence of multi-tiered clouds and taking into account the spectral albedo of the underlying surfaces.

Compared to the method of multiple SR scattering, the method of adding layers in the multithreaded approximation allows many times to reduce the computer time spent on calculating the SR fluxes arriving at the underlying surface and the SR flux to the light-receiving surfaces of the STS and SPP.

References

1. Kondratyev, K.Ya., Moskalenko, N.I., Fedorov, Yu.Ts., Kurt, D.V.: DAN SSSR **315**, 3 (1990)
2. Moskalenko, N.I., Akhmetshin, A.R., Safiullina, Ya.S.: In: E3S Web Conf., **216**, 01031 (2020)
3. Moskalenko, N.I., Khamidullina, M.S., Akhmetshin, A.R.: In: E3S Web Conf., **209**, 03019 (2020)
4. Moskalenko, N.I., Mirumyants, S.O., Loktev, N.F., Misbakhov, R.Sh.: Equilibrium and non-equilibrium radiation processes. High temperature mediums, Radiation heat exchange, Publishing house of KSPEU, Kazan, 264 (2014)
5. Kondratyev, K.Ya., Moskalenko, N.I., Pozdnyakov, D.V.: Atmospheric aerosol. Gidrometeoizdat, Leningrad, **224** (1983)
6. Moskalenko, N.I., Terzi, V.F., et al.: Tallinn **5**, 94–97 (1980)
7. Moskalenko, N.I., Mirumyants, S.O.: Atlas of spectral transparency along arbitrarily oriented paths of the atmosphere CSRI information, p. 494. Moscow (1979)
8. Kondratyev, K.Ya., Donchenko, V.K.: Global Problems, vol. 1. St. Peterburg, p. 1032 (1992)
9. Kondrat'ev, K.Ya., Moskalenko, N.I., Fedorov, Yu.N., Yakupova, F.S.: DAN SSSR **299**, 2 (1998)
10. Moskalenko, N.I., Dodov, I.R., Khamidullina, M.S.: J. Phys. Conf. Ser., **1683**, 022080 (2020).
11. Kondratyev, K.Ya., Moskalenko, N.I., Yakupovka, F.S.: In: Proc. St. Geog. Soc. **489**, 32–50 (1982)
12. Feigelson, E.M., Krasnokutskaya, L.D.: Streams of solar radiation and clouds. Gidrometeoizdat, Leningrad, 157 (1978)
13. Hale, G.M., Querry, M.R.: Appl. Opt. **12**(3), 555–563 (1973)
14. Moskalenko, N.I., Dodov, I.R., Akhmetshin, A.R.: J. Phys.: Conf. Ser. **1683**(4), 042071 (2020)
15. Tampieri, F., Fomasi, C.: Tellus **28**, 1584–1593 (1976)
16. Deirmendjian, D.J.: Appl. Met. **14**, 1584–1593 (1975)

Scientific and Technical Basis for Using External Heat Supply to a Turbine Unit in the Classic Brighton Cycle



Mikhail Laptev, Viktor Barskov, Viktor Rassokhin, Anton Kurnukhin, and Gong Boven

1 Introduction

Now, there is a tendency in Russia to increase the number of low-power power plants. This trend is due to the strategy of long-term development of power engineering until 2030, where the goal is to eliminate the backlog of generating capacities (Fig. 1), as well as to make a smooth transition from a centralized power supply system to a distributed one with the least economic losses [1]. Microturbines on biomass, microturbines on hydrocarbon fuel, solar power units (SPU), and other renewable energy sources (RES) are the potential sources of distributed energy. In the next few years, there will be a need to invest in thermal power plants that were put into operation 40–50 years ago. The microturbine units (MTU) (low-power power plants) are the best option for investment [2]. Such installations have a more developed manufacturing scheme and are also more mobile in contrast to machines running on renewable energy sources, which in turn helps to solve the problem of developing hard-to-reach areas of the far North and Siberia. The transition to microturbine units requires the lowest economic costs, so this product can be implemented at the existing turbine-building enterprises.

Microturbine is a new type of gas turbine unit (GTU), operating in the field of cogeneration type. Now, these machines are used to solve applied problems of energy generation. Structurally, microturbines do not differ from power plants of higher power: an input device, a compressor, a recuperator, a combustion chamber, a turbine, and an output device. However, it is possible to modify the thermal circuit to run on renewable fuel. Thanks to this feature, microturbine installations can be widely used in alternative energy [3]. The authors study the installation that works by burning household waste in specialized waste disposal boilers. This approach will

M. Laptev · V. Barskov (✉) · V. Rassokhin · A. Kurnukhin · G. Boven
Higher School of Power Engineering, Institute of Power Engineering, Peter the Great St.
Petersburg Polytechnic University, Polytechnicheskaya, 29, 195251 St. Petersburg, Russia

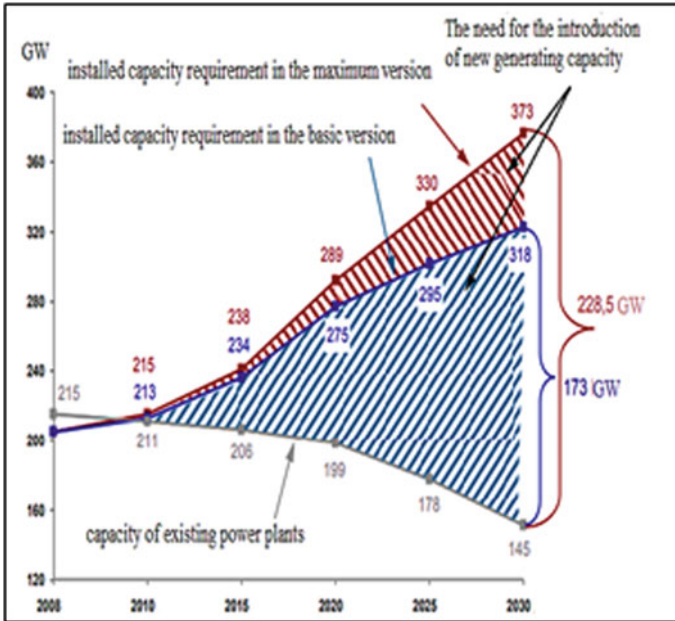


Fig. 1 The need for the introduction of new generating capacity

reduce CO_x and NO_x emissions into the atmosphere due to optimal fuel combustion. Working on this type of fuel allows us to solve two major environmental problems in the world:

- save the ozone layer from destruction;
- reduce the concentration of greenhouse gases in the lower atmosphere.

Thus, microturbine installations are:

- energy-and cost-effective turbine installations;
- allow for a smooth transition from a centralized power supply system to a distributed one;
- they solve two major environmental problems of our time.

2 Literature Review

Power plants with external heat supply are currently not widely used and are mostly experimental with great potential for further development of the power engineering industry. However, over the past ten years, there has been an increased interest in such installations, due to the current problems in the power engineering industry:

- The problem of centralized heat and electricity production;

- Backlog of modernization of the generating capacity from the increased consumption;
- Use of outdated electrical and heat generating equipment;
- Low efficiency of turbines running on alternative energy sources;
- Small interaction of electric power industry enterprises and development institutes;
- High cost of manufacturing and maintenance of installations running on alternative energy sources.

Largely due to these problems, the active development of low-power power plants began. The study and manufacture of such installations are engaged in many countries: the United States, China, South Korea, and Russia. Each country has its own unique approach to the study of these installations, aimed at solving specific problems [4].

USA. Capstone has chosen a unique path aimed at validating the thermodynamic model of the Capstone C30 micro-gas turbine. The methodology is based on a genetic optimization algorithm, where decision variables and goals are set depending on the available experimental data. The results of the studied case emphasize the ability of the method to identify some inconsistencies in the experimental data and lead to a consistent thermodynamic reconstruction of the behavior of the microturbine [5].

As a result, the micro-gas turbine plant revealed the absence of structures that allow achieving the declared values of the overall efficiency and useful power. To do this, a methodology was adopted that determined the optimal set of thermodynamic inputs, using the Euclidean norm to estimate the preferred solution.

Another area that was actively developing was the development of an operational identification method for obtaining simplified dynamic models that were tested on the CapstoneC30 microturbine [6]. For this purpose, a second-order model was identified by adopting a sensitivity theory involving the Lyapunov function, which gives stable solutions in an online environment, updating the model parameters with each change in the physical system. This characteristic can be fruitfully adopted to implement real models in simulators in the time domain, giving accurate results even if some internal parameters change. To investigate the effectiveness of the proposed methodology in obtaining a simplified dynamic model, several simulations and experimental tests were conducted. A good agreement between the simulation and laboratory tests confirms the correctness and applicability of the proposed methodology.

The developed methodology was tested using several simulations and experimental tests conducted on the Capstone C30 microturbine. The results showed that the proposed methodology is characterized by reliability, self-adaptability, high accuracy, stability, and good convergence rate.

China. At the Institute of Engineering Thermophysics, a computational model of heat transfer and pressure drop was established to optimize the design of an annular heat exchanger in a microturbine with a transversely undulating primary surface [7, 8]. The genetic algorithm method is used to solve the optimization problem of a ring heat exchanger with several design variables. Thus, the optimal approach to the design of such a recuperator is formulated. The reliability of the calculated model is verified

by comparing the calculation results with the experimental data of experimental prototype recuperators. Compared to the original design, the optimal design results in a significant reduction in pressure loss if all the constraints are met, indicating that the formulated optimal design approach is effective for a ring heat exchanger. Replacing the optimization goal, the approach to optimal design presented in this paper can be applied to single-purpose optimization for other purposes (compactness, heat transfer area, mass, volume, efficiency, etc.) and even multi-criteria optimization in accordance with the specific requirements of various microturbines [9, 10].

South Korea. Scientists from Korea's Inha University conducted a study to identify the most preferred cycle for a heat recovery system. In their experiment, the Rankine cycle (ORC) and the transcritical CO₂ cycle (tCO₂) were taken, which were applied to a micro-gas turbine plant (MSTU), and subsequently, a comparative performance analysis was performed.

Nonconstructive characteristics of two DND cycles with a change in the load of the MSTU were also analyzed. The performance curve, the efficiency method, and the Stodola equation were used to model the non-constructive operations of all components of the bottom cycle, such as pump, turbine, and heat exchangers [11]. According to the calculations, the output power of the ORC was higher than in the tCO₂ cycle, when the MSTU was operating at full load. On the other hand, since the change in output power when the MSTU load changes are greater in the ORC, the tCO₂ output power becomes greater when the MSTU operates at a partial load below 75%. Therefore, tCO₂ is suitable for a heat recovery system that uses exhaust gas in places where the MSTU must operate at low loads for many hours of its operation. On the other hand, ORC is more suitable in applications where MSTU can operate at almost full load [12, 13].

Russia. Specialists from SPbPU conducted an analysis, the main purpose of which was to find ways to increase the efficiency of the cycle of a simple thermal circuit. To do this, an analysis of four schemes suitable for this type of installation was carried out, because of which the corresponding pros and cons of each of them were identified.

According to the results of the study, the thermal scheme of a two-shaft small-sized gas turbine unit with a compressor driven by a separate electric motor was chosen, as it impresses with its simplicity of design and high reliability. Also, very important advantages of this scheme are the drive of the compressor from a separate electric motor, due to which there is an increase in the efficiency of the MSTU without the use of a regenerative air heater (RV) and the absence of "surge" zones due to the variable speed of the compressor impeller.

Also, specialists from SPbPU participated in the development of a steam turbine unit for TGC-1, operating on the ORC cycle. The main task was to create a new steam turbine plant based on existing prototypes. In addition, there was also an emphasis on improving efficiency. During the design of the installation, several variants of thermal schemes were considered, where the advantages and disadvantages of each of the schemes were identified.

Based on the results of the preliminary calculation, the scheme of a three-circuit power source based on the MTU-500 ORC was selected, which is currently the most

promising both in terms of increasing efficiency through the use of residual heat for thermal needs, and in terms of safety and ease of operation [14].

3 Materials and Methods

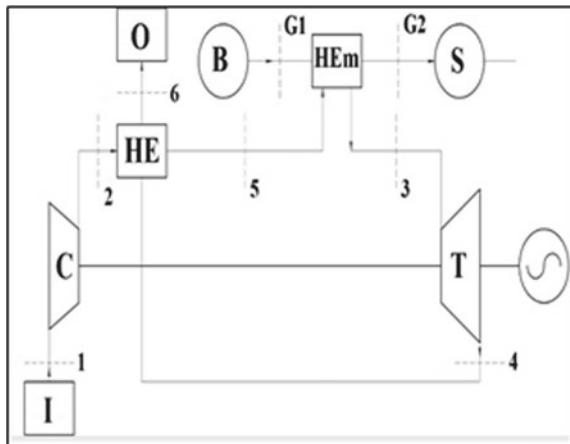
The authors propose a variant of a microturbine installation with an external heat supply (Fig. 2) by replacing the combustion chamber in the thermal scheme with a heat exchanger-mixer.

The description of the scheme is based on the characteristic sections:

- 1–2 Compression of air by the compressor and its displacement into the heat exchanger;
- 2–5 Heating of the working fluid supplied from the compressor;
- 5–3 the Supply of heat to the working fluid;
- G1–G2 Gas supply from the heat recovery boiler to the heat exchanger-mixer;
- 3–4 Expansion of the working fluid in the turbine;
- 4–6 Preheating the air in front of the heat exchanger-mixer;

As can be seen from the figure, the presented thermal scheme of the regenerative type. Based on this installation, a variant calculation of the thermal scheme was performed for three degrees of regeneration: 0.5; 0.7; 0.95—in order to identify the optimal variation. During the calculation of the gas temperature before and after the heat exchanger—mixer, the formulas of water equivalents for air and gas (1), (2) were used for three different values: 0.2; 0.5; 1.0—which also influenced the choice of the optimal strategy.

Fig. 2 Thermal diagram of a microturbine installation:
 I-input device;
 C-compressor; HE-heat exchanger; HEm-heat exchanger-mixer; T-turbine;
 B-heat recovery boiler; S-sparger; O-output device



$$\eta_p^a = \frac{c_p^a \cdot G_a \cdot (T_3^* - T_2^*)}{(c_p \cdot G)_{\min} \cdot (T_{G1}^* \cdot T_{G2}^*)} \tag{1}$$

$$\eta_p^g = \frac{c_p^g \cdot G_g \cdot (T_{G1}^* - T_{G2}^*)}{(c_p \cdot G)_{\min} \cdot (T_{G1}^* \cdot T_2^*)} \tag{2}$$

Based on the calculation, a graph of the dependence of the effective efficiency of the η_e installation on the degree of pressure increase π_k at different degrees of regeneration was drawn up (Fig. 3). It was this graph that played a decisive role in choosing the optimal variant of the thermal scheme.

In the calculations, it was found that the optimal variation of the installation is the scheme with the degree of regeneration equal $\eta_M = 0.7$ and the value of water equivalents equal to 1.0. It was under these parameters was achieved optimal parameters: temperature upstream of the turbine T_3 , the temperature of the exchanger-mixer T_{G2} , efficient work GTU H_E , airflow through the compressor G_A .

Having selected the optimal parameters of the thermal scheme, a variant thermal calculation of the heat exchanger—mixer and the heat exchanger-recuperator was performed. The main goal was to determine the optimal type of heat exchanger. For this purpose, three main types of heat exchangers were calculated: tubular, plate/plate finned. All types differ not only in weight and size and operational characteristics, but the description of heat exchangers is also summarized in Table 1. The thermal calculation was carried out based on the methodology developed at St. Petersburg Polytechnic University. The main initial parameters of the heat exchangers—recuperator and the heat exchanger—mixer were summarized in Tables 2 and 3, respectively.

Fig. 3 Graph of the dependence of the effective efficiency of the η_e installation on the degree of pressure increase π_k at different degrees of regeneration

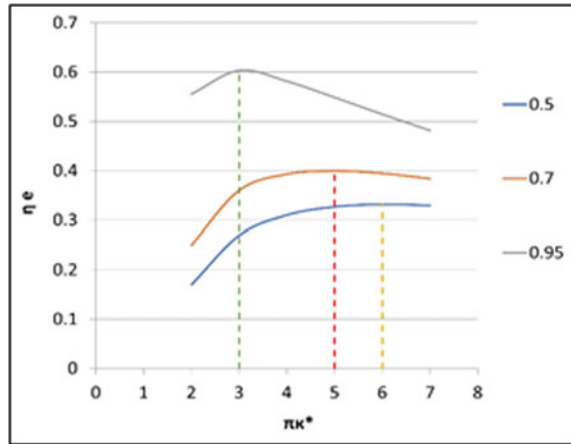


Table 1 Comparative characteristics of heat exchangers

Parameter	Tubular	Plate/plate finned
Surface type	Pipes with cross-sections of various shapes	Thin plate
Weight and size characteristics (conventional units)	5–6	1
Price (conventional units)	0.75	1
Heat transfer (conventional units)	1	3–5
Temperature difference between the heat carrier and the heated medium (°C)	5–10	1–2
Estimated service life (years)	5–10	15–20
Sensitivity to vibration	Sensitive	Insensitive

4 Results and Discussion

Based on the initial data, an optimized thermal calculation of heat exchangers with different combinations of regeneration degrees was performed. During the calculation, it was found that the optimal option for each type of heat exchanger is a combination with $\eta_m = 0.7$ and $\eta = 0.7$. It is with these parameters that the optimal mass and size characteristics of the recuperator are obtained. The data were summarized in comparative Table 4.

Based on the obtained weight and size characteristics, models of the heat exchanger-recuperator were designed, and channels were formed through which the main working fluid and gas flow. The model data for each type is shown in Figs. 4, 5, and 6.

Summarizing all the data obtained, it was found that the tubular heat exchanger has the minimum overall characteristics, but has the highest mass index, so the plate heat exchanger, which is lighter and has the best performance characteristics, was chosen as the optimal one.

Summing up the entire microturbine, it can be stated that installations with an external heat supply have excellent performance. In particular, there was an efficiency value of 33.1%, which is a good result for low-power power plants. The temperature of the working fluid in front of the turbine $T_3 = 873$ K. Among the main advantages of the installation can be noted: multi-fuel, as well as environmental friendliness. The disadvantages of this power plant can be attributed to the high cost, in comparison with powerful gas turbine installations.

Table 2 Initial parameters for the thermal calculation of the heat exchanger-recuperator

№	Parameter	Meaning												Unit of measurement	
		Tubular						Plate							
		0.5	0.7	0.95	0.5	0.7	0.95	0.5	0.7	0.95	0.5	0.7	0.95		
1	Air consumption, G_{a1}	0.81	0.77	0.87	0.8	0.77	0.87	0.8	0.77	0.87	0.87	0.8	0.77	0.87	kg/c
2	Air consumption, G_{a2}	0.81	0.69	0.87	0.72	0.69	0.87	0.72	0.69	0.87	0.78	0.72	0.69	0.78	kg/c
3	The outlet pressure from the compressor, P_2	680,736	486,240	291,744	583,488	486,240	291,744	583,488	486,240	291,744	583,488	486,240	291,744	583,488	Pa
4	The outlet pressure from the turbine, P_4	108,784.4	108,784.3	108,784.4	108,784.4	108,784.3	108,784.3	108,784.4	108,784.3	108,784.3	108,784.3	108,784.3	108,784.3	108,784.3	Pa
5	The outlet temperature from the compressor, T_2	462	425.73	376.1	445.01	425.73	376.1	445.01	425.73	376.06	445.01	445.01	883.08	376.06	K
6	The outlet temperature from the turbine, T_4	745.8	823.83	976.6	771	823.83	976.6	771	823.83	979.54	771	771	823.83	979.54	K
9	Diameter, d	0.006	0.006	0.006	0.006	0.006	0.006	0.006	0.006	0.006	0.006	0.00615	0.00615	0.00615	m
10	Hydraulic diameter, d_H	0.004	0.004	0.004	0.004	0.004	0.004	0.004	0.004	0.004	0.004	0.00384	0.00384	0.00384	m
11	Cross step, S_1	0.0075	0.0075	0.0075	0.012	0.012	0.0075	0.012	0.012	0.012	0.012	0.10	0.10	0.10	m
12	Longitudinal pitch, S_2	0.0065	0.0065	0.0065	0.056	0.056	0.0065	0.056	0.056	0.056	0.056	0.048	0.048	0.048	m

Table 3 Initial parameters for the thermal calculation of the heat exchanger-mixer

№	Parameter	Meaning												Unit of measurement
		Tubular						Plate						
		0.5	0.7	0.95	0.5	0.7	0.95	0.5	0.7	0.95	0.5	0.7	0.95	
1	Air consumption, G_A	0.81	0.77	0.87	0.8	0.77	0.87	0.8	0.77	0.87	0.8	0.77	0.87	kg/c
2	Gas consumption, G_G	0.72	0.7	0.78	0.72	0.69	0.78	0.72	0.69	0.78	0.72	0.69	0.78	kg/c
3	Pressure at the heat outlet of the exchanger of the recuperator, P_5	660,314	471,653	282,992	565,983.36	471,652.8	2,822,991.68	565,983.36	471,652.8	2,822,991.68	565,983.36	471,652.8	2,822,991.68	Pa
4	Pressure at the outlet of the heat recovery boiler, P_{G1}	110,000	110,000	110,000	110,000	110,000	110,000	110,000	110,000	110,000	110,000	110,000	110,000	Pa
5	Temperature at the outlet of the heat exchanger of the recuperator, T_5	604	704.41	949.37	608.45	704.41	949.37	608.45	704.41	949.37	608.45	704.41	949.37	K
6	Temperature at the outlet of the heat recovery boiler, T_{G1}	1300	1300	1300	1300	1300	1300	1300	1300	1300	1300	1300	1300	K
9	Diameter, d	0.006	0.006	0.006	0.006	0.006	0.006	0.006	0.006	0.006	0.006	0.006	0.006	m

(continued)

Table 3 (continued)

№	Parameter	Meaning										Unit of measurement			
		Tubular					Plate								
		0.5	0.7	0.95	0.5	0.7	0.95	0.5	0.7	0.95	0.5		0.7	0.95	
10	Hydraulic diameter, d_H	0.004	0.004	0.004	0.004	0.004	0.004	0.004	0.004	0.004	0.004	0.00384	0.00384	0.00384	m
11	Cross step, S_1	0.0075	0.0075	0.0075	0.012	0.012	0.012	0.012	0.012	0.012	0.012	0.10	0.10	0.10	m
12	Longitudinal pitch, S_2	0.0065	0.0065	0.0065	0.056	0.056	0.056	0.056	0.056	0.056	0.056	0.048	0.048	0.048	m

Table 4 Mass and size characteristics of the recuperator

Parameter	Type of heat exchanger			Unit of measurement
	Tubular	Plate	Plate finned	
Volume	0.016	0.042	0.118	m ³
Mass	197	27.13	32.25	kg
Compact size	252.2	285.71	282.55	l/m
Heat transfer surface area	4.03	12.19	33.34	m ²

Fig. 4 Model of a tubular heat exchanger

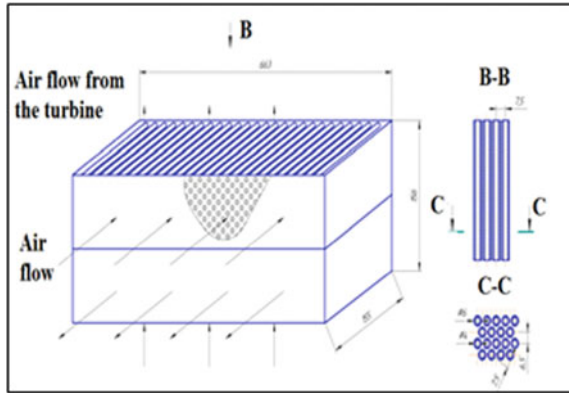
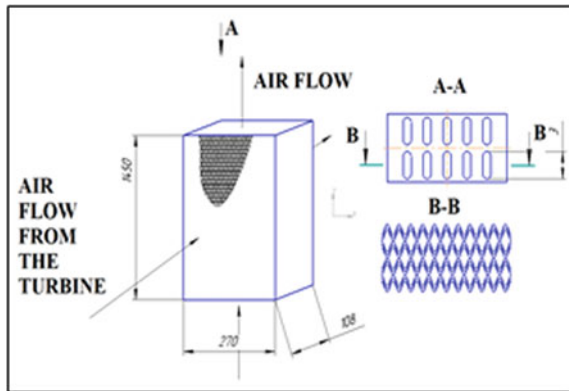


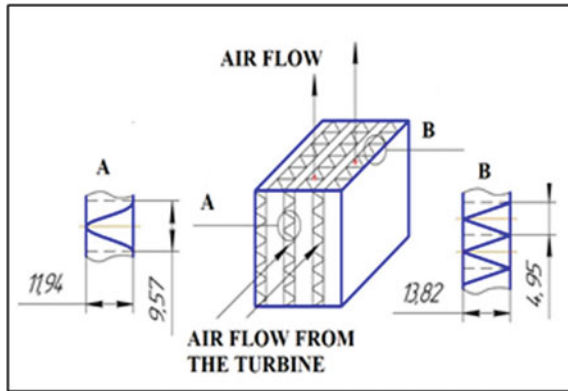
Fig. 5 Plate heat exchanger model



5 Conclusions

Summing up all the above, we can conclude that microturbine installations with external heat supply will help solve a number of problems, as well as create a foundation for future research. In particular, the foundation for the safe and efficient utilization of biomass, with the production of both heat and electricity. If we touch

Fig. 6 Model of a plate-fin heat exchanger



on the economic component, the use of such GTU will help to smoothly make the transition from a centralized power supply system to a distributed one.

References

1. Scenarnye usloviya razvitiya elektroenergetiki na period 2030 goda. Ministerstvo energetiki Rossijskoj Federacii Agentstvo po prognozirovaniyu balansov v elektroenergetike (2010)
2. Barskov, V.V.: Strategiya razvitiya energomashinostroeniya Rossijskoj Federacii (2010) Modern low-power class turbo generators in the gas transmission system. Special Issue **10**, 384–392 (2018)
3. Myakishev, N. et al.: Review of the current state of research of microturbine units. In: IOP Conference Series: Materials Science and Engineering, vol. 986, no. 1 (December 2020). <https://doi.org/10.1088/1757-899X/986/1/012061>
4. Gimelli, A., Sannino, R.: Thermodynamic model validation of Capstone C30 micro gas turbine. Energy Procedia **126**, 955–962 (September 2017). <https://doi.org/10.1016/j.egypro.2017.08.184>
5. do Nascimento, M.A.R., et al.: Micro gas turbine engine: a review. Progress in Gas Turbine Performance, InTech (2013)
6. Cai, J., Huai, X., Xi, W.: An optimal design approach for the annular involute-profile cross wavy primary surface recuperator in microturbine and an application case study. Energy **153**, 80–89 (2018). <https://doi.org/10.1016/j.energy.2018.04.016>
7. Liu, A., Yiwu, W.: Effects of lower heat value fuel on the operations of micro-gas turbine. Energy Power Eng. **01**(01), 28–37 (2009). <https://doi.org/10.4236/epe.2009.11005>
8. Kim, M.J., Kim, J.H., Kim, T.S.: The effects of internal leakage on the performance of a micro gas turbine **212**, 175–184 (2018)
9. Wang, X., Dai, Y.: Exergoeconomic analysis of utilizing the transcritical CO₂ cycle and the ORC for a recompression supercritical CO₂ cycle waste heat recovery: A comparative study **170**, 193–207 (April 2016)
10. Roy, P., Dias, G.: Prospects for pyrolysis technologies in the bioenergy sector: A review. Renew. Sustain. Energy Rev. **77**, 59–69 (1 September 2017). <https://doi.org/10.1016/j.rser.2017.03.136>
11. Bakalis, D.P., Stamatis, A.G.: Incorporating available micro gas turbines and fuel cell: matching considerations and performance evaluation. Appl. Energy **103**, 607–617 (2013). <https://doi.org/10.1016/j.apenergy.2012.10.026>

12. Thattai, T., Oldenbroek, V., Schoenmakers, L., Woudstra, T., Aravind, P.V.: Experimental model validation and thermodynamic assessment on high percentage (up to 70%) biomass co-gasification at the 253MWe integrated gasification combined cycle power plant in Buggenum. The Netherlands. **168**, 381–393 (2016)
13. Fokin, G.A.: Methodology of creation of the Autonomous sources of electric energy using energy of the compressed natural gas for own needs of gas transportation system of Russia (2015)
14. Zabelin, N., Lykov, A.V., Rassokhin, V.A., Sivokon, N.V., Fokin, G.A.: Steam-gas plant compressor station “Severnaya”. Science and Technology in the Gas Industry (2013)

Information-Measuring System for Monitoring Process Water in Power System Heat Supply Structures



Rimma Zaripova, Ilgizar Gaisin, Marina Tyurina, Olga Rocheva, and Elena Kubyshkina

1 Introduction

It is known that the hardness of the service water, together with the free oxygen content, is one of the two most important factors that affect the efficiency of the heat transfer process of the heat transfer medium and the service life of the equipment in the heat supply structures of various types (thermal power plants, combined heat and power plants, local heating systems). An increase in hardness levels associated with an increase in the concentration of metal ions in the aqueous medium will promote scale formation in the closed-loop heat exchanger pipe system and thereby reduce the efficiency of the heat transfer process [1–3]. This can lead to significant energy losses in water heating systems, just as it can in the case of a disturbance in the velocity regime of the water heat transfer medium. In order to avoid these problems, it is necessary to develop effective methods and devices for continuous monitoring of the water-chemical balance and the water velocity regime. In this context, the proposed project is relevant and aims at solving specific energy saving problems.

Among the great variety of analytical methods, increasing attention in our country and abroad is being paid to one of the most promising areas of electroanalysis—the method using membrane sensors based on ion-selective electrodes [1].

The main sources of highly concentrated multicomponent technological solutions at thermal power plants (TPPs) are water treatment plants. Analysis of operation of

R. Zaripova (✉)
Kazan State Power Engineering University, Kazan, Russia

I. Gaisin · E. Kubyshkina
Kazan (Volga region) Federal University, Kazan, Russia

M. Tyurina
Kazan National Research Technical University Named After A.N. Tupolev, Kazan, Russia

O. Rocheva
Kazan Innovative University named after V.G. Timiryasov (IEMML), Kazan, Russia

the ion exchange water treatment plant at the Nizhnekamsk Thermal Power Plant-1 showed that half of the alkali supplied to the regeneration of the anion-exchange alkali filters is not used, but is discharged for neutralization and then to wastewater. Due to the fact that the cost of alkali used in technological processes is quite high, it is economically feasible to process the alkaline waste with the alkali extraction and its reuse in the production cycle [4].

The main source of high drains on TPP are water treatment plants (WTP), mainly ion exchange baromembrane desalting plants. Currently, at most TPPs, acidic highly mineralized effluents from cation exchange filters and alkaline highly mineralized effluents from anion exchange filters are mutually neutralized, and the final highly mineralized discharge is discharged. In some countries, the method of utilization of highly mineralized effluent by evaporation with the disposal of solid salts is used, which cannot be called successful. In this case, all valuable chemical components of the effluent are irretrievably lost. In solving the problem, it is of interest to use electro dialysis concentration of liquid wastes prior to neutralization to a level suitable for reuse in the cycle of TPP. In this soft liquid wastes containing mainly sodium salts and alkaline liquidwastes of ion exchange, WTP are of great interest, since they do not contain hardness ions, and sodium salts and alkalis are valuable reagents themselves [5].

2 Materials and Methods

The innovative component of the project is to create inexpensive and competitive devices for continuous monitoring of the water-chemical balance and velocity regime of the heat carrier water in heat supply systems so that the costs of building, operating and maintaining these monitoring devices would be significantly lower than the economic losses caused by energy overconsumption [6].

1. Design and approach for hardness control of process water based on aqueous electrolyte conductivity method. The main tasks of the research are selection of design parameters of the device, selection of power supply network, detection of dependence of output signal on concentration (hardness) of water. The selection of design electrical parameters of the device is carried out in order to obtain an acceptable sensitivity of the device. For this purpose, experimental testing of device sensitivity at various design parameters (number of turns, diameter of liquid circuit tube, etc.) was carried out. It is difficult to reveal analytically the dependence of device sensitivity on mains supply frequency, so it was decided to conduct experimental research [7]. The program of experimental researches foresaw the conducting of measurements of output signal at varying frequency of 3–20 kHz with different stiffness of tested solution.
2. A device for measuring flow rate of electrically conductive fluid consists of a microcontroller acting as a programmable rectangular pulse generator (pulse duration varies in the range from 0.1 to 10 s) and recording the amplitude of the

current at strictly defined moments of time; two operational amplifiers required to generate and invert rectangular pulses generated by the microcontroller; one transistor amplifier for scaling the current signal received from the system of electrodiffusion electrodes; a macroelectrode serving to saturate the electrically conducting liquid with charged ions, and a platinum microelectrode which is a measuring element of the system. The experimental setup is used to write and debug the software for the information-measurement system and to implement the system on a microprocessor basis [8–10].

3. Continuous monitoring of process water hardness by measuring the concentration of metal ions using a membrane sensor. Membrane sensors based on ion-selective electrodes with interchangeable membranes are widely used to determine the ionic composition of aqueous solution, which allow the concentration of ions of different types to be determined with a high degree of accuracy. It is known that the membrane sensor is a measuring system of the first order with a transient mode, whose operation is described by an equivalent RC-chain circuit.

Consequently, the mathematical equation that is valid for the operation of a membrane sensor measuring the concentration of metal ions is described by the following differential equation [11]:

$$\frac{dE}{dt} + \frac{1}{\tau} E = \frac{1}{\tau} E_y(t), \tag{1}$$

provided that $E(0) = 0$. In Eq. (1) $E(t)$ is the current potential difference of the membrane sensor, $E_y(t)$ is the so-called steady-state potential difference of the membrane sensor, which is determined by the concentration of ions in the solution, τ —the time constant of the sensor. The term steady-state potential difference comes from a measuring process in which the concentration of ions in the solution is a constant value ($E_y(t) = \text{const}$).

The general solution to Eq. (1) is given by the expression

$$E(t) = e^{-\frac{t}{\tau}} \int_0^t dt' \frac{1}{\tau} E_y(t') e^{\frac{t'}{\tau}} \tag{2}$$

The proposed new method for measuring the variable concentration of ions in a solution is based on a fast-acting method. According to this approach, the membrane potential difference is measured at the times t_1 and $t_2 = t_1 + \Delta t$:

$$E(t_1) = e^{-\frac{t_1}{\tau}} \int_0^{t_1} \frac{dt'}{\tau} E_y(t') e^{\frac{t'}{\tau}}, \tag{3}$$

$$E(t_2) = e^{-\frac{t_2}{\tau}} \int_0^{t_2} \frac{dt'}{\tau} E_y(t') e^{\frac{t'}{\tau}} \tag{4}$$

provided that $\frac{\Delta t}{\tau} \ll 1$.

$E_y(t)$ is determined by two parameters: flow rate and diffusion. In the diffusion process, the desired function is the concentration of diffusing substance, usually denoted by $c = c(x, y, z, t)$.

Modeling is carried out by set functions $E_u(t)$ on the basis of expression (2) obtained earlier. As a law of variation $E_y(t)$, we will take the simplest cases: liquid flows through the pipe, liquid flow is laminar and the sensor is flush with the pipe wall. Then it can be assumed that diffusion process is dominant.

In the case where at the boundary of diffusing solution $x = 0$, constant concentration C_1 and initial concentration equals C_2 , then if diffusion coefficient $C(t)$ is invariant, this will be described by following equation:

$$C(x, t) = (C_2 - C_1) * \operatorname{erfc}\left(\frac{x}{2\sqrt{Dt}}\right) + C_1, \tag{5}$$

where t is time of diffusion, x is distance from origin to a plane of determined concentration.

3 Results

We use the mathematical program MatLAB to simulate the concentration measurement process. Various methods are implemented in MatLAB to solve systems of differential equations. Their implementations are called differential equation solvers. To solve them we use the function $[T,Y] = \operatorname{solver}(@F,tspan,y0)$, where instead of *solver* we substitute the name of a particular *solver*—integrating a system of differential equations of the form $y' = F(t, y)$ on the interval *tspan* with initial conditions $y0$.

At different ratios $C1$ and $C2$ and constant x we obtain graphs shown in Fig. 1, and at constant $C1$ and $C2$ and variable x we obtain graphs in Fig. 2.

Fig. 1 Plots of the dependence of $E(t)$ at different concentration ratios of $C1$ and $C2$

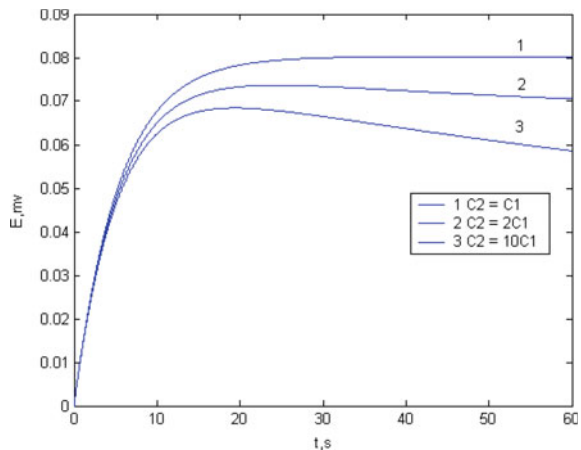
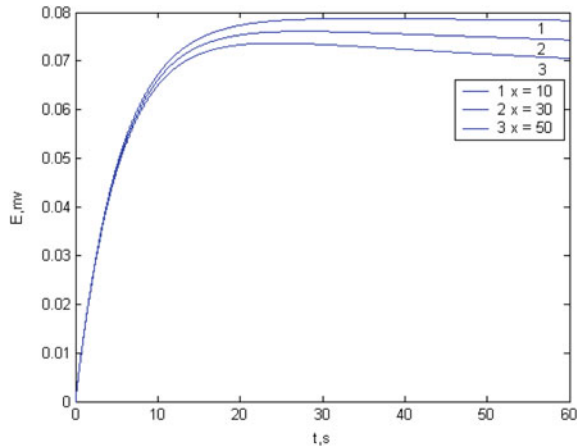


Fig. 2 Plots of the dependence of $E(t)$ at different x



As a result of the study it was determined that the concentration is influenced by two main parameters—diffusion and flow velocity. Some laws of concentration changes under different initial and boundary conditions in the case when concentration is only affected by diffusion (sensor is located at the pipe wall) were determined. The effective modes of operation of the membrane sensor for the known laws of concentration changes of ions in the solution have been analyzed.

Consequently, a standard measurement method under laboratory conditions would include taking water samples from the pipeline at a certain interval, possible sample pretreatment and the measurement itself after the sensor reaches a steady-state operating mode in a one-minute time interval. This method is well-proven and will be very effective when the ionic composition of the water coolant flowing in the pipeline deviates markedly from the tolerance at spatial scales determined by the water flow rate and the total time including the period of the measurement process and the duration of the individual measurement [12–14]. If the scale of deviations is much smaller than this, there is always a risk that a noticeable disturbance in the water-chemical regime may not be ‘seen’ between successive measurements. In order to avoid such a situation, it is necessary to make the measuring process continuous. For this purpose, the membrane sensor should be placed in a flow-through system with possible preconditioning of the water stream (filtering of solids, setting the required pH-factor and ionic strength of the solution, masking of interfering ions) and then transmit the digitized signal for remote processing in an appropriate information and measurement environment [15]. This approach will monitor the ionic concentration of the aqueous stream on a time scale determined by the signal-to-noise ratio of the analog signal of the membrane sensor and the sampling rate of an analog-to-digital converter, such as a microcontroller. If the change in the ionic composition of the aqueous medium occurs at times considerably longer than the time constant of the sensor, which is a few seconds, then the sensor has time to switch to steady-state operation. Otherwise, the transient behavior of the membrane sensor must be taken into account during the measuring process. A fast method of determining the

ionic concentration in an aqueous medium based on ion-selective electrodes makes continuous monitoring of its chemical composition possible [16].

When determining the variable concentration of metal ions in the liquid that washes the sensor, the measuring process will be affected by various lag effects, which depend on the thickness of the fixed diffusion layer near the surface of the membrane sensor (Nernst layer), which is determined by the flow regime of the water flow in the flow system [17]. Thus, in continuous electrochemical analysis of aqueous flow there are a number of features of the measurement process that require preliminary consideration in order to determine the optimum measurement modes and to develop an optimal appropriate information and measurement system.

The application of an information system using membrane sensors in the field of production control enables automatic, continuous monitoring of the ionic composition of solutions. Membrane sensors can be placed directly in the process solution, where they acquire a particular electrical potential depending on the composition of the solution. Because the data comes in quickly, it can be used to control the regulator or fed into a computer [18].

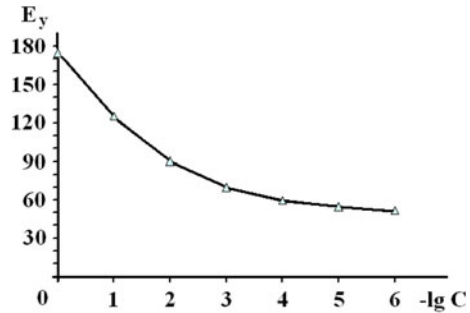
An information system for measuring metal ion concentrations has been developed. Different membrane sensors which are selective to metal ions are placed in the process solution. In each sensor, a voltage corresponding to a given concentration is generated, which is fed to an amplifier. The amplified signal is then fed to the appropriate analog-to-digital converter channel, where it is converted from analog form to digital code. The ionic composition of the solution is then digitally stored in the data bus system. A power supply unit is required to power all amplifiers and the analog-to-digital converter.

The following requirements are made to the equipment of interfacing of the membrane sensor with the computer: interfacing of the sensor according to the input resistances, providing the necessary accuracy of measurements, automation and increasing the speed of measurement.

To interface a membrane sensor with a computer, it is necessary to amplify the voltage received from the sensor. It is known that it is a high impedance sensor and its output resistance is about 1 M Ω . Hence, a voltage repeater must be supplied at its output, which is used as a matching stage. This ensures that the output resistance is as low as possible and the input resistance is as high as possible [19]. After the repeater a voltage amplifier must be included in the circuit. As output signal drift is possible, a voltage amplifier is used to amplify the voltage. The disadvantages of an amplifier are the small voltage gain and the small output voltage. These can be eliminated by using an additional voltage amplifier. The voltage after the amplifier goes to an analog-to-digital converter, which converts the analog voltage into a digital code. A bipolar power supply is required to power the analog-to-digital converter.

By making continuous measurements of the current sensitivity values and the electrochemical cell electromotive force at intervals, it is possible to monitor changes in the concentration of the ion under study in the aqueous medium, regardless of the operating mode of the membrane sensor. This is the basic concept of the proposed approach. Studies showed that continuous monitoring of ion concentration in aqueous medium by means of an information-measuring system based on a membrane sensor

Fig. 3 Dependence of electromotive force E_y on metal concentration



is in principle feasible. However, the accuracy of the obtained result will depend on the static and dynamic error of the real measuring process. The first one is determined by the methodical and instrumental errors of the analog membrane sensor, as well as by the error of the signal quantization scheme and the instrumental error of the analog-to-digital converter. The second is related to the finite time of a single act of signal conversion (dating error), which can be significantly reduced by increasing the maximum conversion frequency or by using an analog sampling and storage device [20]. The dynamic error due to the inertia of the membrane sensor in the transient mode is eliminated by simultaneously determining the current values of both the sensitivity and the electromotive force of the electrochemical cell. When the concentration of the ion under study in the coolant coincides with the permissible concentration, the membrane sensor operates in steady-state mode, in which the current value of sensitivity is zero and the error of the measurement process is the error in determining the current value of the electromotive force of the ion-selective electrode.

The advantage of the information system with a membrane sensor is the wide range of detectable concentrations. It was found experimentally that the sensor can be used for determination of metal ion concentrations in the range from 1 to 10^{-6} mol/l. The plot of the electromotive force dependence on concentration is shown in Fig. 3. The slope of this function shows the sensitivity of the membrane to a given ion. The higher the slope, the more sensitive the membrane is. As can be seen, the sensor is most sensitive at concentrations from 1 to 10^{-4} mol/L. Then the slope decreases. At concentrations below 10^{-6} mol/l the sensor loses its ability to detect ions.

4 Conclusion

In thermal power plants, the use of membrane sensors makes it possible to automate water-chemistry processes and automatically monitor the ionic composition of raw water at different stages of its treatment. Such wide application of sensors is due to their ability to determine concentration of relevant components without disturbing

the integrity of the object. The more selective the electrode is to a particular ion, the wider the range of applications for various media.

The advantages of membrane sensors are relative simplicity, compact hardware design, low cost, speed, high sensitivity, selectivity, environmental friendliness, continuity of the measurement process, and the possibility of its automation.

The accuracy of continuous measurements is comparable to traditional discrete measurements, which are made in the steady-state mode of the membrane sensor. This makes the resulting information on the ionic composition of the water reliable and allows its correct changes to be monitored in real time. A suitable information and measurement system is sufficiently simple in its design and does not require a lot of money for implementation.

The continuous monitoring of process water hardness is, therefore, carried out by measuring the concentration of metal ions with a membrane sensor based information and measuring system. Membrane sensors based on ion-selective electrodes with interchangeable membranes are widely used to determine the ionic composition of aqueous solutions, which allow the concentration of ions of different types to be determined with a high degree of accuracy.

References

1. Zariipova, R.S., Saltanaeva, E.A., Bikeeva, N.G., Priimak, E.V.: IOP Conf. Ser.: Earth Env. Sci. **288**, 012129 (2019)
2. Barmatov, E.B., Pebalk, D.A., Barmatova, M.V., Shibaev, V.P., Prosvirin, A.V., Galyametdinov, Yu.G.: Polymer Sci. Ser. A. **43**(2), 134–140 (2001)
3. Plotnikova, L.V., Giniyatov, R.R., Sitnikov, S.Y., Fedorov, M.A., Zariipova, R.S.: IOP Conf. Ser.: Earth Env. Sci. **288**, 012069 (2019)
4. Filimonova, A.A., Chichirova, N.D., Chichirov, A.A., Minibaev, A.I.: E3S Web Conf. **124**, 01029 (2019)
5. Chichirov, A.A., Chichirova, N.D., Filimonova, A.A., Minibaev, A.I., Tolmachev, L.I.: IOP Conf. Ser.: Earth Env. Sci. **288**, 012006 (2019)
6. Soloveva, O.V., Solovev, S.A., Khusainov, R.R.: J. Phys.: Conf. Ser. **1399**(2), 022059 (2019)
7. Chupaev, A.V., Zariipova, R.S., Galyamov, R.R., Sharifullina, A.Y.: E3S Web Conf. **124**, 03013 (2019)
8. Zariipova, R., Tyurina, M., Rocheva, O., Chupaev, A., Sharifullina, A.: Adv. Econ. Bus. Manag. Res. **131**, 271 (2019)
9. Rocheva, O., Khadiullina, L., Zariipova, R., Hamatgaleeva, G., Kosulin, V.: Adv. Econ. Bus. Manag. Res. **131**, 640 (2019)
10. Pilat, B.V.: Basics of electro dialysis. Avvalon, Moscow (2004)
11. Solovev, S.A., Soloveva, O.V., Gilmurahmanov, B.S., Lamberov, A.A.: J. Phys. Conf. Ser. **1399**(5), 055022 (2019)
12. Zariipova, R., Porunov, A., Zinurova, R., Galyamov, R., Stepanova, G.: Adv. Econ. Bus. Manag. Res. **131**, 663 (2019)
13. Soloveva, O.V., Solovev, S.A., Yafizov, R.R.: IOP Conf. Ser.: Mater. Sci. Eng. **709**(3), 033064 (2020)
14. Soloveva, O.V.: IOP Conf. Ser.: Earth Env. Sci. **421**(6), 062038 (2020)
15. Tyurina, M., Porunov, A., Zariipova, R., Gaynetdinova, A., Kosulin, V.: Adv. Econ. Bus. Manag. Res. **131**, 648 (2019)

16. Soloveva, O., Solovev, S., Khusainov, R., Yafizov, R.: *Adv. Int. Sys. Comp.* 1259 AISC, 371 (2021)
17. Soloveva, O.V., Solovev, S.A., Yafizov, R.R.: *Ecol. Ind. Rus.* **24**(9), 39 (2020)
18. Kuznetsov, A.P., Kalyashina, A.V., Koriath, H.-J.: *Langer Proc. Manuf.* **21**, 525–532 (2018)
19. Ivanova, V., Denisova, A., Ivanov, I.: *International Conf. on Electrotechnical Complexes and Systems (ICOECS): The international scientific and practical conference materials.* USATU, pp. 190–195 (2020)
20. Morozova, I.G., Abdullin, I.I., Khayaleeva, A.D., Rocheva, O.A.: *Adv. Econ. Bus. Manag. Res.* **145** (2020)

Development of a Method and Means for Saving Natural Non-Renewable Resources in the Operation of Electric Drives of Borehole Pumps of Water Supply Systems Operating in Hard Natural Conditions



George Palkin, Ivan Suvorov, Sergei Kakaurov, Roman Gorbunov, and Roman Dolgih

1 Relevance and Setting Tasks

Currently, the conservation of natural non-renewable resources is an important direction of improving environmental well-being in the sphere of human life.

Reducing the volume of electricity generated by traditional methods indirectly reduces the extraction of minerals and the negative impact of man-made processes on the environment.

A large share of the generated electricity is spent on providing housing and communal services and technical needs of the population and industrial enterprises. One of the main areas of electricity consumption is the process of organizing centralized water supply.

The number of centralized drinking water supply facilities on the territory of the Russian Federation (RF) for the last fully accounted period (2011 year) is 102,240 pieces of which 98% are underground, often artesian, water sources [1].

About 20% of centralized water supply sources operate seasonally at low ambient temperatures, while 13% of such water supply systems are concentrated in Siberia and the Far East.

G. Palkin (✉) · R. Dolgih

ICT and AM Department, FSBEI HE “Transbaikal State University”, 672039 Chita, Russia

I. Suvorov · S. Kakaurov · R. Gorbunov

Department of Energy, FSBEI HE “Transbaikal State University”, 672039 Chita, Russia

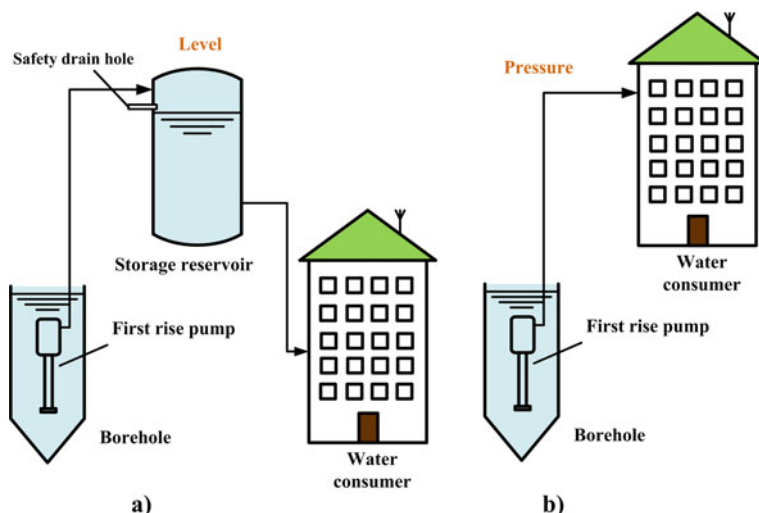


Fig. 1 Schemes of water supply systems: **a** with a reservoir; **b** with a direct parsing

On the territory of Zabaikalsky Krai, there are 331 sources of centralized drinking water supply, 323 of which are boreholes for raising underground water. The operation of such systems is often associated with additional energy costs to ensure the necessary conditions for the operation of water supply facilities.

To organize water intake from boreholes, a water supply scheme with a storage reservoir is often used, which allows to stabilize the water supply process [2]. In some cases, a direct water supply to the end user is used. The principle of organizing these water supply schemes is shown in Fig. 1.

In systems with storage reservoir, the key parameter is the water level in the reservoir, and in systems with direct water consumption, the pressure in the pipeline.

The section from the borehole to the reservoir or the first additional rise pump is called the first rise section. There can often be several boreholes on the first rise section, and several pumps for each borehole.

Regardless of the type of organization of the water supply system, there are problems that can negatively affect the technical and economic parameters of the system and, as a result, increase the irrational cost of resources. The main ones include [3]:

- exceeding productivity of borehole pumps over the required water consumption;
- accident rate and high wear of water supply system elements.

The first problem is the main source of operating costs of natural and energy resources [2], since it entails the leakage of artesian water and proportional energy consumption for pump excessive productivity. The leakage can be an overflow of water from a reservoir, a discharge of water from a pipeline system, or other unaccounted for losses. The total volume of water leak in the Russian Federation for the year 2019 amounted to 710,913.12 thousand cubic meters [4].

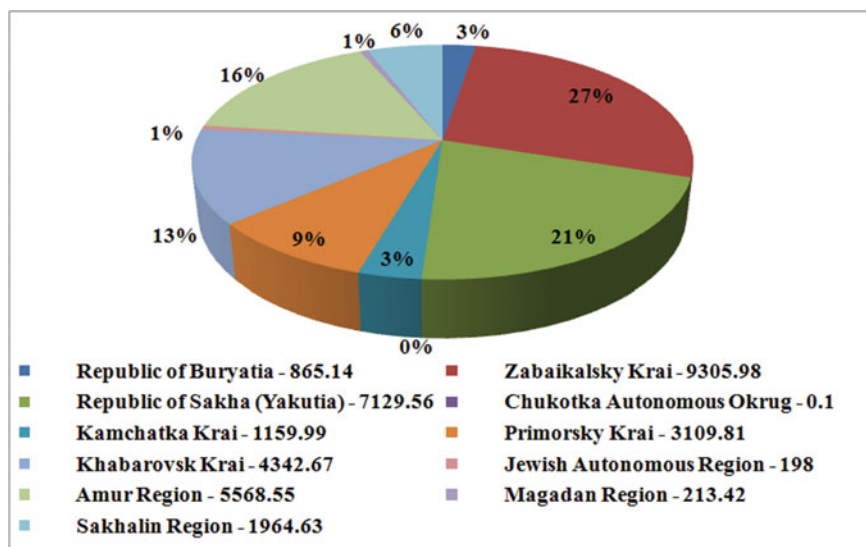


Fig. 2 The volume of water leakage (thousand cubic meters) by the regions of the Far Eastern District

The statistics of water leaks by regions of the Far Eastern Federal District of RF are shown in Fig. 2.

As can be seen from the figure, the Zabaikalsky Krai is the leader of the negative statistics of water leaks in the Far Eastern District. It is known that in some communal enterprises of this region, the amount of leaks in relation to the total volume of extracted water resources can reach more than 50% [3]. These costs are associated with drastic changes in the operating modes of water supply facilities in comparison with the conditions laid down at the design stage [2]. The main reason is the closure of large mining enterprises powered by the water supply systems of settlements. In this case, the planned design productivity of the equipment turns out to be excessive and processing and loss of natural resources and electricity inevitably occur. Sometimes exceeding the pump productivity is necessary to maintain the required values of certain parameters of the water supply system, ensuring trouble-free operation of the object.

One of the obvious ways to solve this problem is the global replacement and modernization of elements of water supply systems, including pumping equipment, pipelines, shut-off and control valves, and elements of the electrical complex. Serious reconstruction of water supply facilities is often not carried out on time due to high economic costs. At the same time, negative performance characteristics are reduced by less expensive methods, for example, by controlling the productivity of pumps, according to the current requests of the water consumer.

Changes in pump productivity affect the hydraulic and thermal parameters of the pipeline. Accordingly, it is very important to maintain these parameters within

acceptable limits, ensuring trouble-free operation of the system, especially in hard natural operating conditions. The most dangerous pipeline accident is water freezing. The situation is aggravated by the fact that many pipelines are laid above the ground due to the impossibility of their deepening below the level of soil freezing.

The total number of pipeline infrastructure facilities in the Russian Federation is 69,024 pieces [1, 5, 6]. The number of pipeline facilities that can be operated in conditions of prolonged negative temperatures is about 20%. In the Zabaikalsky Krai, the number of pipeline infrastructure facilities is 234 pieces.

A significant part of the above exploited water pipes does not comply with sanitary norms and rules. The total percentage of such objects in the Russian Federation is 19%. Most of these water pipes are concentrated in areas with hard natural conditions. In the Zabaikalsky Krai, the number of such objects is 5.6%.

The information provided determines the prerequisites for emergencies on pipelines. In 2019, 14,629 accidents occurred on the territory of the Russian Federation [7]. About 28% of accidents occurred in areas with severe natural operating conditions. The distribution of the number of accidents in the most unfavorable regions of the Far Eastern Federal District is shown in Fig. 3.

By analyzing the data in the figure, it can be concluded that the largest number of accidents was recorded in the southern territory of the District. This is due to both the largest number of settlements and water supply facilities in a given territory, and with changeable natural conditions, when water supply systems can operate simultaneously in conditions of low negative and high positive ambient temperatures, which can lead to ambiguous requirements for the design and operation of water supply systems. A sufficiently large number of accidents of water supply systems requires

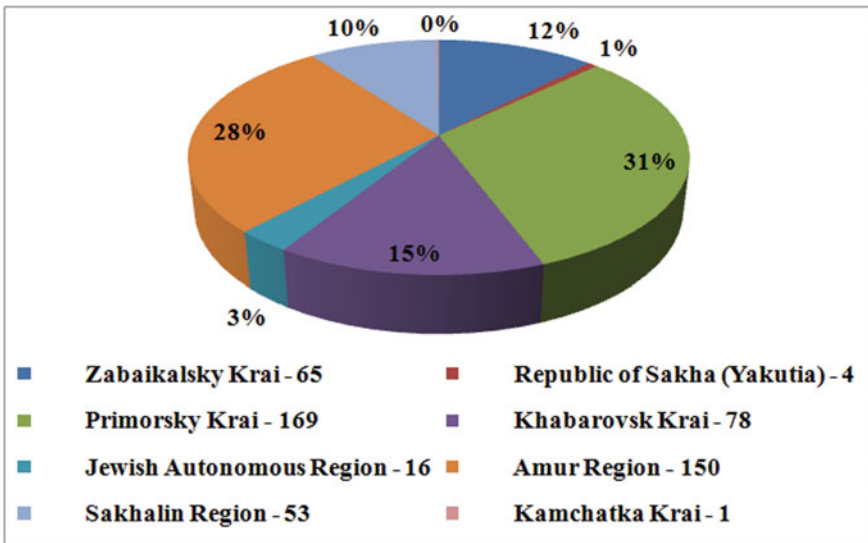


Fig. 3 Distribution of the number of accidents on water pipes in the Far Eastern District

taking into account their condition and parameters when implementing measures to reduce operating costs in water supply systems.

In addition to pipeline accidents, the pump can be disabled, which also entails serious consequences. In order to prevent the pump from failing, it is necessary to ensure the most rational and gentle operation of it, as well as provide all pumps with protection and diagnostic equipment.

Thus, while minimizing the cost of natural resources for organizing the process of centralized water supply, it is necessary to find an optimal solution that will also ensure the safety of the facility, especially in hard natural operating conditions. Without serious reconstruction of water supply facilities, this problem can be solved only by creating a specialized automatic control system, which is described in this paper.

2 Methods and Materials

In accordance with this goal, it is necessary to develop a methodology and technical means that will minimize the unjustified costs of natural resources and ensure a trouble-free operation of the borehole pump and the rise section of the water supply system in hard natural operating conditions.

To minimize costs, there is a need to control the productivity of the borehole pump. This problem is most effectively solved by frequency control of the pump electric drive [8–16]. In this case, the frequency of the supply voltage changes, which proportionally affects the hydraulic parameters of the pump [17–25].

Three-phase asynchronous motors with a squirrel cage rotor are used in the electric drive of pumps with a rated power of less than 250 kW. The frequency control of these machines changes the motor shaft speed and torque, which affects the hydraulic parameters of the pump such as head and feed (flow).

In addition to saving water, frequency control can significantly reduce the cost of electricity supplying the pump electric motor, in contrast to the methods of changing the hydraulic resistance of the pipeline by using control gate valve. The scalar frequency control method is often used to control the pump, since it is simpler and cheaper to implement [26–28].

When controlling the pump by the frequency method, it is assumed that the flow value is calculated, which will then be maintained by the frequency controller. The flow rate should be calculated taking into account the needs of the consumer and ensuring the safety of the system. As a need of the consumer, it is advisable to use the value of the water level in the reservoir, and to ensure the protection of the pipeline from accidents associated with water freezing, to analyze the temperature at the end of the pipeline [3]. To implement this task, a control system scheme was developed based on a two-channel PID controller. The first channel of the controller receives the signal of the water level in the reservoir, and the second—the water temperature in the pipeline. The controller is implemented on digital elements and is discrete.

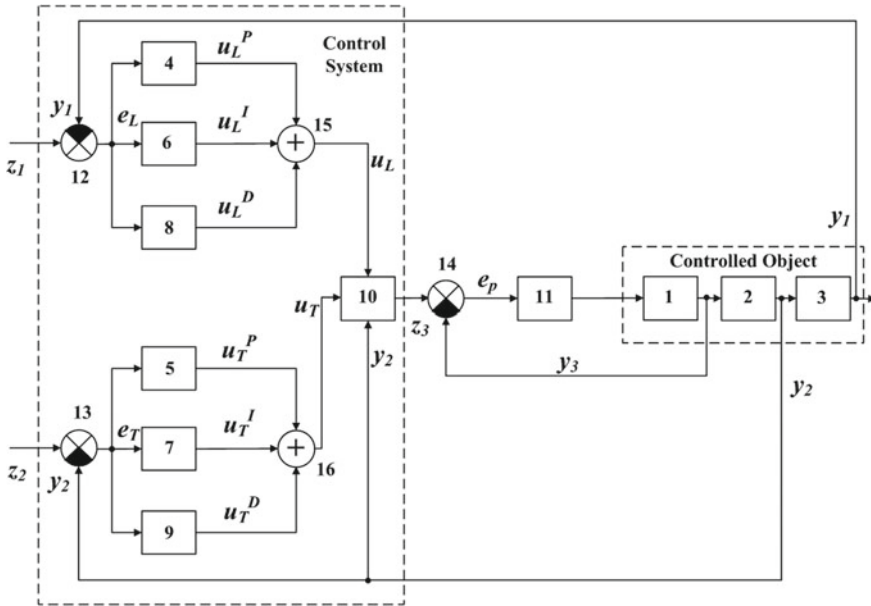


Fig. 4 The diagram of the control system

The block diagram of the proposed controller and the controlled object is shown in Fig. 4.

According to the figure, the system includes: flow meter 1; water temperature sensor in the pipeline 2; water level sensor in the storage reservoir 3; proportional regulators for level 4 and temperature 5; integrated regulators for level 6 and temperature 7; differential regulators for level 8 and temperature 9; flow calculation unit 10; flow controller (frequency controller and pump unit) 11; elements of comparison (subtraction) 12, 13, 14; adders 15, 16. Elements 4, 5, 6, 7, 8, 9, 10, 12, 13, 15, 16 are included in the control system (CS), which can be implemented both on basic digital elements using a programmable controller. Elements 1, 2, 3 are part of the controlled object.

In addition, the following symbols are used in Fig. 4: y_1 —the current value of the water level in the storage reservoir (m); y_2 —current temperature in the end part of the pipeline ($^{\circ}\text{C}$); y_3 —current flow rate in the pipeline (m^3/h); z_1 —setpoint of the water level in the storage reservoir (m); z_2 —setpoint of the temperature value in the end part of the pipeline ($^{\circ}\text{C}$); z_3 —calculated flow rate in the pipeline (m^3/h); e_L —the amount of misalignment (difference) by level; e_T —the amount of misalignment (difference) by temperature; e_p —the amount of misalignment (difference) by flow rate; u_L^P —proportional level control signal; u_L^I —integrated level control signal; u_L^D —differential level control signal; u_L —full level control signal; u_T^P —proportional temperature control signal; u_T^I —integral temperature control signal; u_T^D —differential temperature control signal; u_T —full temperature control signal.

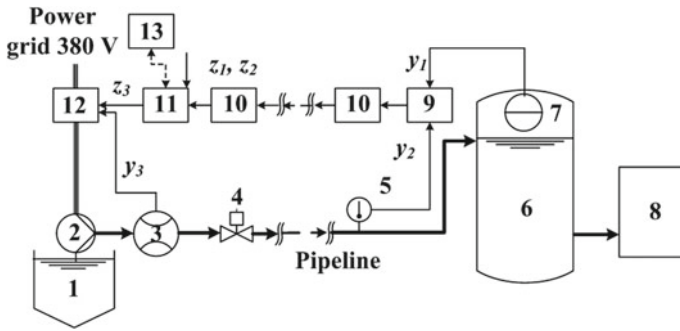


Fig. 5 The diagram of the controlled first rise section

The proposed scheme is implemented in the form of a hardware structure of the first rise section, shown in Fig. 5.

In accordance with the figure, the first rise section includes: water source 1; pump 2; flow meter 3; valves 4; water temperature sensor 5; storage reservoir 6; level sensor 7; water consumer 8; data collection device—interface converter 9; data transmission devices 10; control device 11; personal computer 13; frequency controller 12. Data collection and transmission devices are necessary for transmitting information over long distances, since the sensors are located at the end of the pipeline, and the control device near the borehole. The control device is the central element of the system. It collects information from all sensors, calculates the flow setpoint, and supports it with a frequency controller.

The calculation of the flow setpoint that must be maintained is proposed to be carried out according to the formula [3]:

$$\begin{cases} z_3 = \int \max\left(\frac{Q_m \cdot u_L}{h}, \frac{Q_m \cdot u_T}{\max(t_o, t_n)}\right) dt, & y_2 \geq z_k, \\ z_3 = Q_m, & y_2 < z_k \end{cases} \quad (1)$$

where Q_m —the maximum possible value of pump flow (m³/h); h —reservoir height (m); t_o —ambient temperature (°C); t_n —water temperature at the beginning of the pipeline (°C) z_k —critical temperature (°C), calculated by formula 2:

$$z_k = z_2 - d, \quad (2)$$

where d —the value of the permissible deviation of the setpoint temperature z_2 .

For implementation in a digital discrete control system, this dependence can be represented by the following expression:

$$\begin{cases} z_3(i) = z_3(i - 1) \\ + \max\left(\frac{Q_m \cdot u_L(i)}{h}, \frac{Q_m \cdot u_T(i)}{\max(t_o(i), t_n(i))}\right), y_2(i) \geq z_k, \\ z_3(i) = Q_m, y_2(i) < z_k \end{cases} \quad (3)$$

where i —the number quantization tact.

The value of the flow setpoint $z_3(i)$ is fed to the comparison element 14 of the controller, then the misalignment value is calculated for the feed $e_p(i)$, which is fed to the frequency converter to maintain the required amount of water supply in the pipeline.

Selecting the largest impact to change the flow setpoint minimizes tank overflow while still providing sufficient facility accident-free. For additional protection of the pipeline from freezing, in case of failures in the control system, when the critical water temperature is reached, the flow setpoint is taken as high as possible.

In addition to protecting the pipeline from freezing, it is necessary to ensure accident-free operation of borehole pumps. For this, it is necessary to perform preventive diagnostics of pump units, calculate their wear, and perform the required anti-accident actions. It is proposed to diagnose the condition of the pump motor windings and its bearings in the operating mode [29]. For this, the diagram of the first rise section is supplemented with pump diagnostic elements, as shown in Fig. 6.

According to the figure, the object in question includes: water source 1; pumps 2, 3, 4, one of which is the main one and the others are standby; flow meter 5; controlled valves 6; water temperature sensor 7; level sensor 8; storage reservoir 9; water consumer 10; data collection and transmission device 11; control device 12; frequency controller 13; switching unit 14; sensors of parameters of the state of the pumps electric motors 15.

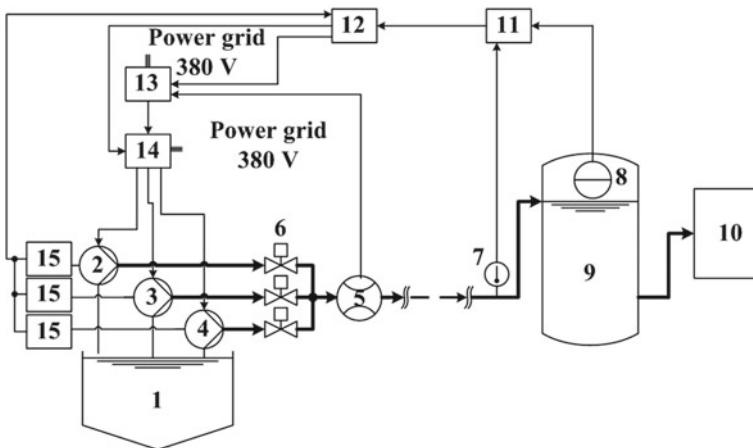


Fig. 6 The diagram of a system with pumps diagnostics

The proposed scheme makes it possible to continuously monitor the state of the main pump in operating mode, as well as to periodically monitor the standby pumps by connecting the studied pump to the main supply by unit 14. In this case, the wear coefficient is calculated for each pump. To do this, it is necessary to monitor the temperature of the bearings, as well as the values of the consumed voltages and currents for each phase of the pump motor. To calculate the pump wear coefficient K_w (%), the following dependence is proposed:

$$K_w = 100 - \frac{\sum_{i=1}^3 \left(\frac{100 \cdot K_c \cdot R(i)}{R_n} \right)}{3} + \frac{K_T \cdot T}{T_n}, \quad (4)$$

where $R(i)$ —the current value of the impedance of the i -th phase stator windings of the pump motor (Ω), calculated by known methods in the values of current and voltage on the phase windings measured by the feedback sensors; K_c —coefficient of influence of the state of the motor winding on the overall level of pump unit wear; R_n —nominal value of the impedance of the stator windings of the pump motor (Ω); T —the current value of the temperature of the bearings of the pump ($^{\circ}\text{C}$), measured by the feedback sensor; K_T —coefficient of bearings temperature influence on the overall level of pump unit wear; T_n —nominal value of the pump bearing temperature ($^{\circ}\text{C}$). The negative value of the wear is regarded as a pre-emergency situation (winding breakage).

The wear coefficient allows to determine the current state of the main pump and, if necessary, connect a backup pump with the least wear, as well as notify the maintenance personnel about an emergency.

The presented solutions are implemented in the hardware control system for borehole pumps [3].

3 Results and Discussion

To analyze the effectiveness of the proposed solutions, a computer simulation model of the rise section of the water supply system has been developed, including a frequency-controlled asynchronous electric drive, a borehole pump, a pipeline, and a storage reservoir [30].

The model was implemented in the Matlab Simulink computer simulation environment and was tested on a laboratory bench that simulates the first rise section [2, 30]. The block diagram of the computer simulation model is shown in Fig. 7.

The main internal parameters of the model are: voltage V , frequency f and current A of power grid 0.4 kV; frequency at the output of the frequency converter f_1 ; mechanical speed of the pump motor rotor n ; power consumption of the pump P ; moment of resistance on the pump motor shaft M_c ; pump feed Q_1 ; required pressure of the water supply system S_p ; the amount of water consumption Q_2 ; overflow of water from the tank Q_3 ; frequency setpoint f_u .

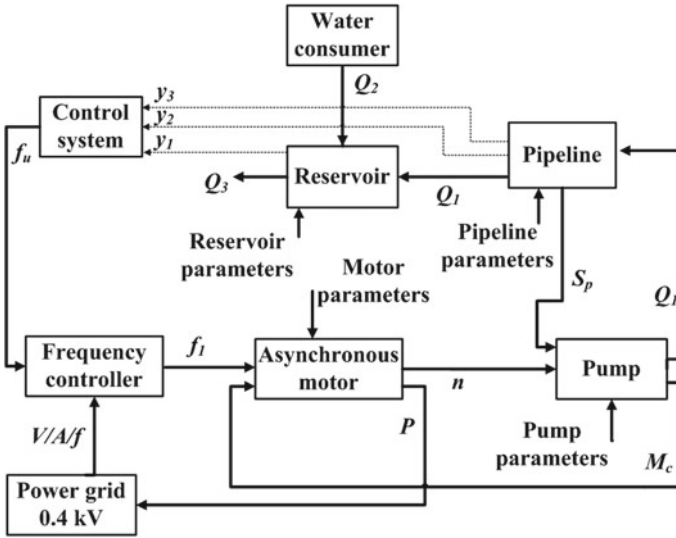


Fig. 7 The diagram of the simulation model

The model was used to calculate the transient and steady-state modes of the water supply system when external disturbances change, such as water flow from the reservoir and the ambient temperature. The dependence of the process of changing the ambient temperature and water consumption on time is shown in Fig. 8.

The simulation was performed at a time interval of 1 h. The value of setpoint by level was 0.8 m, by temperature—plus 4.7 °C. Reservoir volume 0.4 m³ (height—1 m); electric motor power 1.5 kW; maximum feed in the system 2 m³/h; begin water temperature +5 °C; pipe length 22.5 m; pipe material is polypropylene.

The results of calculations of the flow rate, overflow from the reservoir, water temperature at the end of the pipeline, level in reservoir, and power consumption are shown in Fig. 9.

As can be seen from the simulation results, the proposed control method allows minimizing the overflow of water from the reservoir and ensuring a significant reduction in electrical power consumption while ensuring a sufficient level of accident-free facility. It was found that, depending on the parameters of the object and the conditions of its operation, unjustified resource costs are reduced to 55%. Nevertheless, the figure shows frequent fluctuations in the value of the calculated flow setpoint, this is due to the different scale and speed of change of control actions in terms of level and temperature. Additionally, it is advisable to change the controller coefficients in accordance with external conditions. For this, adaptive elements of the control system can be used [31, 32].

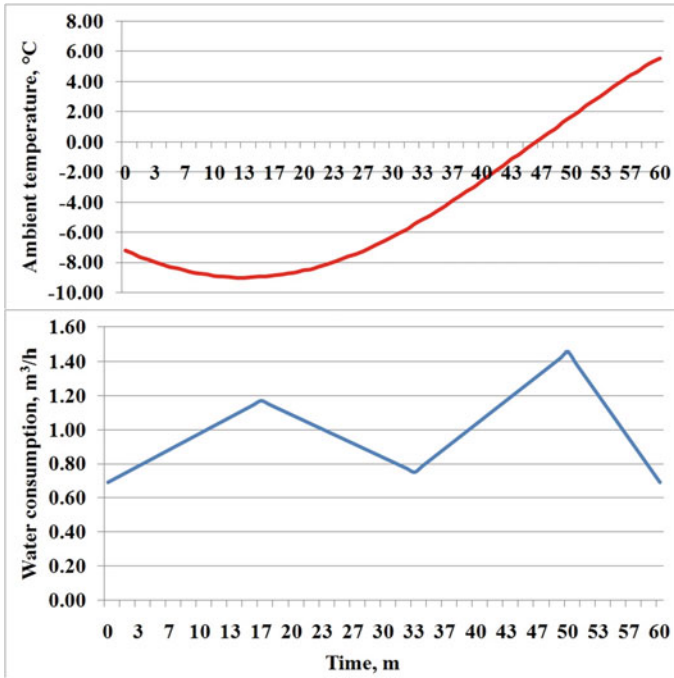


Fig. 8 Schedule of changing external disturbances

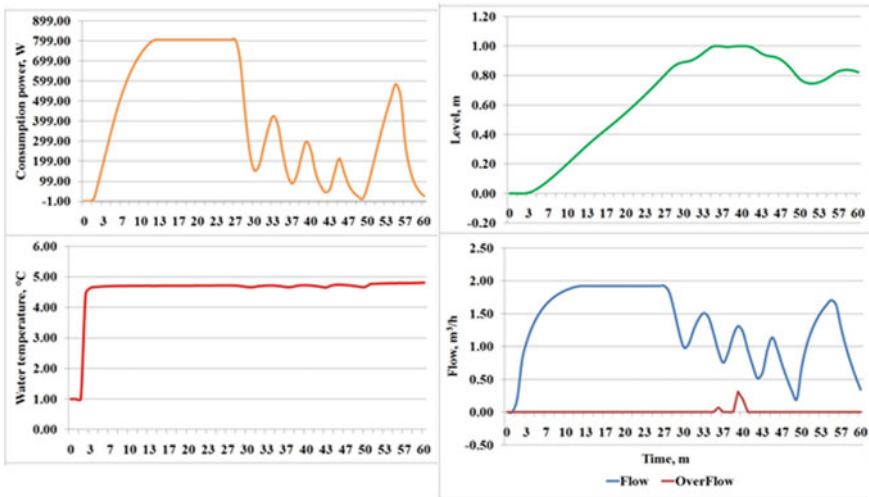


Fig. 9 Results of simulation

4 Conclusion

The developed methods and means for controlling the asynchronous electric motors of water rising pumps of water supply systems can significantly reduce the unjustified consumption of water resources and electrical energy while ensuring a sufficient level of accident-free facilities operated in hard natural conditions.

The results obtained can be applied at municipal facilities of small and medium-sized settlements, as well as industrial enterprises with autonomous water supply systems.

The prospects for the development of the project are the improvement of the control algorithm to increase stability and reduce overshoot under sharply changing external conditions by adding adaptive elements to the system. It is also advisable to integrate an electric water heater at the beginning of the pipeline to implement an extreme regulator that minimizes the economic costs of maintaining the permissible temperature by regulating feed or heat.

References

1. Number of objects of household and drinking centralized water supply, <https://www.fedstat.ru/indicator/37335>. Last accessed 2021/02/09
2. Palkin, G., Suvorov, I., Gorbunov, R.: Evaluation of ways to improve the energy efficiency of sites of first rise supply water systems with storage tank by laboratory modeling. In: UralCon, Chelyabinsk, pp. 227–234 (2018). <https://doi.org/10.1109/URALCON.2018.8544369>
3. Palkin, G.A., Suvorov, I.F.: Control of the first lifting pumping units on water supply system with storage reservoir. *Mod. High Technol* 7, 55–60 (2017)
4. Leakage and unrecorded water consumption (thousand cubic meters, the value of the indicator for the year), <https://www.fedstat.ru/indicator/34034>. Last accessed 2021/02/09
5. Commissioning of public utilities in the Russian Federation, <https://rosstat.gov.ru/folder/14458>. Last accessed 2021/02/09
6. Length of water supply networks, <https://www.fedstat.ru/indicator/33953>. Last accessed 2021/02/09
7. Number of accidents in the water supply system, <https://www.fedstat.ru/indicator/34186>. Last accessed 2021/02/09
8. Ahmed, A., Moharam, B., Rashad, E.: Power saving of multi pump-motor systems using variable speed drives. In: MEPCON, Cairo, Egypt, pp. 839–844 (2018). <https://doi.org/10.1109/MEPCON.2018.8635157>
9. Zheng, G., Huang, Q.: Energy optimization study of rural deep well two-stage water supply pumping station. In: *IEEE Transactions on Control Systems Technology*, vol. 24, no 4, pp. 1308–1316 (2016). <https://doi.org/10.1109/TCST.2015.2498140>
10. Fulai, Y., Hexu, S.: Optimal control in variable-speed pumping stations. In: *IEEE International Conference on Mechatronics and Automation*, Beijing, pp. 2397–2401 (2011). <https://doi.org/10.1109/ICMA.2011.5985981>
11. Meshcheryakov, V.N., Sibirtsev, D.S., Gracheva, E.G.: Frequency control system for a synchronized asynchronous electric drive. In: *E3S Web Conference*, vol. 220 (2020). <https://doi.org/10.1051/e3sconf/202022001054>
12. Ibraev, K.A., Sarsembieva, E.K.: Energy saving in electric drives and control of these processes in the sphere of housing and communal services. In: *Astana, SIBCON*, pp. 1–3 (2017). <https://doi.org/10.1109/SIBCON.2017.7998492>

13. Hruntovich, N.V., Kapanski, A.A., Baczynski, D., Vagapov, G.V., Fedorov, O.V.: Optimization of a variable frequency drive pump working on a water tower. In: E3S Web Conference, vol. 124, p. 05060 (2019). <https://doi.org/10.1051/e3sconf/201912405060>
14. Sapaev, K., Umarov, S., Abdullabekov, I.: Research energy and resource saving operating modes of the pump unit. In: E3S Web of Conference, vol. 216, p. 01150 (2020). <https://doi.org/10.1051/e3sconf/202021601150>
15. Gevorkov, L., Rassölkin, A., Kallaste, A., Vaimann, T.: Simulation study of a centrifugal pumping plant's power consumption at throttling and speed control. In: RTUCon, Riga, pp. 1–5 (2017). <https://doi.org/10.1109/RTUCon.2017.8124823>
16. Sperlich, A., Pfeiffer, D., Burgschweiger, J., Campbell, E., Beck, M., Gnirss, R., Ernst, M.: Energy efficient operation of variable speed submersible pumps: simulation of a ground water well field. *Water* **10**(9), 1255 (2018)
17. Tamminen, J., Ahonen, T., Kosonen, A., Ahola, J., Tolvanen, J.: Variable speed drive-based pressure optimization of a pumping system comprising individual branch flow control elements. In: 16th European Conference on Power Electronics and Applications, Lappeenranta, pp. 1–11 (2014). <https://doi.org/10.1109/EPE.2014.6910988>
18. Khasanov, A.R., Starodubtseva, V.A.: Analysis of technological solutions for the use of frequency converters. In: A Collection of Materials of the IV All-Russian Scientific and Technical Conference of Graduate Students, Undergraduates and Young Scientists with International Participation, Young Scientists—Accelerating Scientific and Technical Progress in the XXI Century, pp. 956–963. Izhevsk (2016)
19. Abidov, K., Zaripov, O., Zaripova, S.: Automatic drive-support method for constant pressure maintenance at pump units of the hydraulic power stations. In: E3S Web of Conference, vol. 216, p. 01110 (2020). <https://doi.org/10.1051/e3sconf/202021601110>
20. Muravleva, O.O., Tyuteva, P.V.: Operation features of the improved induction motors in the variable speed drive of pump units. In: IEEE EUROCON, St.-Petersburg, pp. 703–708 (2009). <https://doi.org/10.1109/EURCON.2009.5167710>
21. Gumerova, R.Kh., Chernyakhovsky, V.A.: Modeling of electric power consumption by pump drives under throttling and frequency regulation of productivity, news of higher educational institutions. *Kazan. Energy Prob.* **19**, 96–106 (2017)
22. Kan, E., Ikramov, N., Mukhammadiev, M.: The change in the efficiency factor of the pumping unit with a frequency converter. In: E3S Web Conference, vol. 97, p. 05010 (2019). <https://doi.org/10.1051/e3sconf/20199705010>
23. Pöyhönen, S., Simola, A., Ahola, J.: Variable-speed-drive-based sensorless estimation of pump system reservoir fluid level. In: EPE'20 ECCE Europe, Lyon, France, 1–10 (2020). <https://doi.org/10.23919/EPE20ECCEEurope43536.2020.9215786>
24. Kolesnikov, E.B., Shprekher, D.M., Malkov, S.B.: Automated System Ensuring Uninterrupted Water Supply for Small Settlements, UralCon, pp. 13–17, Chelyabinsk, Russia, 2019. <https://doi.org/10.1109/URALCON.2019.8877676>
25. Lysenko, A., Simakov, A.V.: The pump hydraulic load effect determination on the parameters of an frequency-controlled asynchronous electric drive. In: Dynamics of Systems, Mechanisms and Machines (Dynamics), Omsk, Russia, pp. 1–6 (2019). <https://doi.org/10.1109/Dynamics47113.2019.8944719>
26. Kukishev, D., Meshcheryakov, V., Boikov, A., Evseev, A. et al.: Energy saving in the scalar control system of an asynchronous electric drive. In: Novocherkassk, ICEPDS, pp. 30–31 (2018). <https://doi.org/10.1109/ICEPDS.2018.8571784>
27. Arribas, R.J., Gonzalez, V.C.M.: Optimal vector control of pumping and ventilation induction motor drives. In: IEEE Transactions on Industrial Electronics, vol. 49, no 4, pp. 889–895 (2002). <https://doi.org/10.1109/TIE.2002.801240>
28. Vladimir, P., Dmitry, S.: To issue of designing scalar closed-loop controllers for frequency controlled induction motor drives. In: Ekaterinburg, ACED, pp. 1–4 (2018). <https://doi.org/10.1109/ACED.2018.8341708>

29. Palkin, G.A., Suvorov, I.F.: Improving the fault tolerance of the water supply system by controlling the pumping units. Collection of scientific articles of the I All-Russian Scientific Conference: Information technologies in modeling and management: approaches, methods, solutions, Tolyatti, 656 (2017)
30. Palkin, G., Suvorov, I.: Development of a simulation model of the first rise area of a water supply system with a storage reservoir. In: RusAutoCon, Sochi, Russia, pp. 804–809 (2020). <https://doi.org/10.1109/RusAutoCon49822.2020.9208073>
31. Jahmeerbacus, M.I.: Flow rate regulation of a variable speed driven pumping system using fuzzy logic. In: EPECS, Sharjah, pp. 1–6 (2015). <https://doi.org/10.1109/EPECS.2015.7368520>
32. He, L., Song, L.: The pump house constant pressure fuzzy self-tuning PID control system simulation. In: Wuhan, International Conference on Electric Information and Control Engineering, pp. 5525–5527 (2011). <https://doi.org/10.1109/ICEICE.2011.5777320>

Verification of Computer Flow Simulation in Confuser and Diffuser Channels



Ivan Komarov, Sergey Osipov, Andrey Vegera, Darya Kharlamova, and Aleksey Zonov

1 Introduction

Nowadays, many methods for computer simulation of viscous liquor flows are known. The main difference between the methods is the approach to solution of the Navier–Stokes equations that are 4 equations with 4 unknown variables [1, 2] at given boundary conditions. This system of differential equations together with the boundary and initial conditions is principally nonlinear, so it is impossible to build its analytical solution. The only available method is the Direct Numerical Simulation (DNS). This method consists of numerical solution of the nonstationary Navier–Stokes equations by application of space grids and time steps sufficient for the presentation of the flow structures. The DNS method requires grids with very small cells so it needs large computer resources. Nowadays, this factor limits its application by simple laminar flows at low values of $Re < 103$ [3–5]. In visible prospects, introduction of the DNS method into applied technical problems does not seem realistic.

In practice, the applied technical problems are solved with the widely spread method known as Reynolds-averaged Navier–Stokes, or RANS, and the problem closure with semi-empirical turbulence models. The known turbulence models are numerous. The most common are the two-parameter turbulence equations classified to low Reynolds $k - \omega$ and SST and high Reynolds $k - \varepsilon$ models group.

The turbulence model together with the grid parameters influences the correspondence of calculation results and physical experiments. The turbulence model mostly determines the dimensionless distance y^+ between the wall and the first calculation cell. The y^+ parameter recommended values are known for different turbulence models. The high Reynolds $k - \varepsilon$ models require the first cell to correspond with the y^+ in the range of $30 \leq y^+ \leq 100$ [6, 7]. In the low Reynolds SST/ $k - \omega$ models, the first cell distance to the wall must be within $y^+ \leq 5$ [8].

I. Komarov · S. Osipov (✉) · A. Vegera · D. Kharlamova · A. Zonov
National Research University “Moscow Power Engineering Institute”, 111250 Moscow, Russia

Table 1 Review of papers devoted to the verification

Investigation object	y^+	Turbulence model	Paper
Pump	40	$k - \varepsilon$	[9]
Scrolled tube	1	SST	[10]
Radial turbine scroll channel	1	SST	[11]
Compressor duct	0.18–0.25	SST	[12]
Flat diffuser	1–15	SST	[13]
Combustor	1–5	RNG $k - \varepsilon$	[14]

The numerical experiment parameters that provide its minimal error are determined by experimental verification. Many published papers compare results of computer and physical experiments, but these papers do not always describe the complete set of the experiment parameters. Usually, attention is paid to the turbulence model and the y^+ parameter. Table 1 summarizes the results of the research literature review, turbulence models, and the y^+ parameter values that provide minimal computer experiment errors.

Usually, the tools for computer simulation of physical processes involve complicated models that suit the design of actual technical objects. At these conditions, the simulation result may be applied only to specific areas of the investigated object, but a transition to another design area may increase the simulation error which is caused by the large number of factors influencing the physical process. The computer tools application limits may be found in the simplified flow path of the technical object. The equipment flow path is decomposed into typical channels and the application limits of turbulence models and grid parameters are found in these simplified problems and flow parameters. The equipment elements simplification is not aimed at simulation of power industry problems by primary cases. The goal is to determine a similarity degree for problems and further verify the general approach to computer simulation. The simulation results' verification with the physical experiments in the simplified elements allows the development of general recommendations for simulation of similar problems, flow analysis in various diffuser and confuser channels, sudden expansion or throttling, etc. After the limits of computer experiment, are determined, that in complex channels the verification objects may be improved by combination of typical channels and the recommendations accuracy should be checked by the physical process simulation.

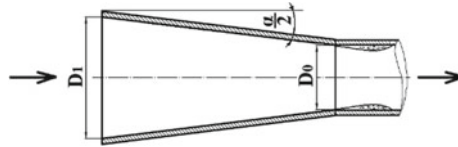


Fig. 1 Confuser scheme and its main geometry parameters, D_1 , D_0 —inlet and exit diameters, α —constriction angle

Table 2 Confuser geometry parameters for verification

No.	Geometry parameters			Flow parameters		
	α (°)	n_0	D_0 (mm)	Re		
1	3	0.64	50	100,000	200,000	400,000
2	3	0.39	50			
3	10	0.39	50			

2 Verification Results of the Computer Simulation for Flow Analysis in Confuser Channels

2.1 Investigation Object

Confuser or converging channels are widely used in various devices, centrifugal and axial compressors, jet pumps, cooling towers, fans, flow meters, etc. The confuser function is to produce a uniform flow velocity distribution in the equipment flow path. The confuser resistance coefficient at turbulent flow depends upon design and condition parameters. The geometry parameters are the constriction angle α (Fig. 1) and the constriction degree $n_0 = F_0/F_1$. The flow condition parameter is the Reynolds number Re.

An important stage of the recommendations issue for the flow analysis parameters is the selection of adequate physical experiment results with detailed descriptions of the test boundary conditions and the results analysis method. The computer experiment parameters with minimal simulation error were verified with the physical test results of the book [15]. The geometry and flow parameters taken from this book are summarized in Table 2.

2.2 Solver and Grid Parameters

The channel flow analysis involved the RANS averaging method and the turbulence models SST, $k - \omega$, and $k - \varepsilon$ Standard. The main grid and solver tuning verified parameters are the turbulence model, the y^+ parameter, the number of prismatic layers,

Table 3 Grid parameters

Parameter	Value
Grid type	Not structured
Global cell size (mm)	5
Prismatic grid growth law	Exponential
y^+ parameter	0.25 ... 90
Prismatic layers height ratio	1 ($k - \epsilon$), 1.3 ($k - \omega$, SST)
Number of layers	1 ($k - \epsilon$), 10–15 ($k - \omega$, SST)

Table 4 Flow simulation boundary conditions

Confuzer No.	G_0 , G/s		
	Re = 100,000	Re = 200,000	Re = 400,000
1	89.08	178.279	114.101
2	113.920	229.166	228.202
3	114.101	458.333	456.405

and the growth coefficient. The fixed parameters are the global cell size, the prismatic grid growth, and the wall function. The wall area cell parameters depend upon the preliminary assumed turbulence model. The verified and fixed grid parameters and the solver tuning are summarized in Table 3.

In the physical experiment [2], the working fluid was air as an ideal gas. The channel inlet boundary conditions are the working fluid mass flow G_0 determined in relation with the experiment value of Re criteria and D_0 (Table 4). The inlet flow temperature is $T = 20$ °C and the exit static pressure is $P = 1$ bar.

2.3 Verification of Flow Computer Simulation in Confuser Channels

The computer simulation results are compared with the physical experiment taken for reference by the energy loss coefficient ξ . Figure 2 shows the confuser #1 ($\alpha = 3^\circ$, $n_0 = 0.64$) simulation errors in relation to y^+ for the $k - \epsilon$ turbulence model.

All dependencies above are similar, the larger values of y^+ correspond to larger errors of the flow computer simulation. The area of acceptable errors of 10% for the whole range of Reynolds numbers contains the simulation results at $y^+ = 10 - 30$.

Figure 3 presents relations of the diffuser #1 computer simulation errors with the y^+ values at the same range of Re and the SST turbulence model.

The relations between gradual error and y^+ are logarithmic with the gradual error growth at y^+ increase and the rapid decrease into the large negative values at y^+ approach

Fig. 2 Confuser No. 1 with $\alpha = 3^\circ$, $n_0 = 0.64$, simulation error at $k - \epsilon$ turbulence model versus the y^+ parameter

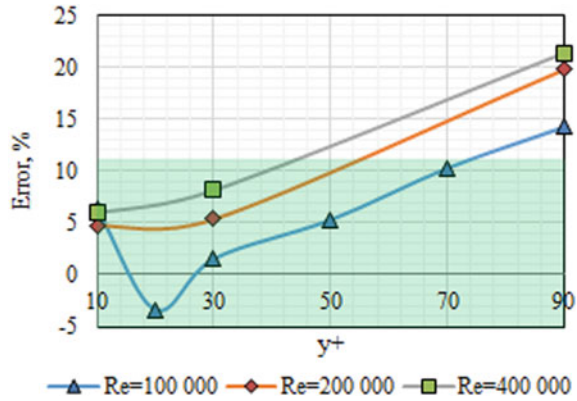
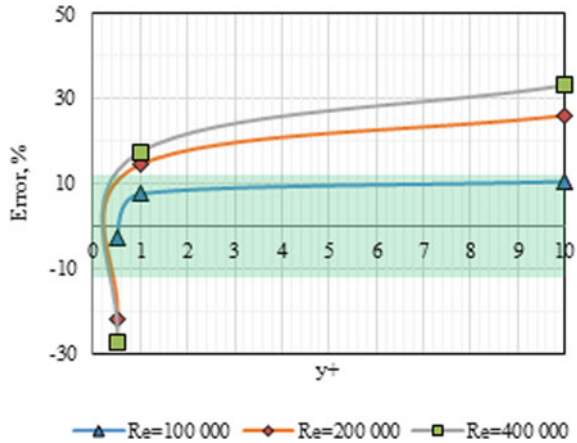


Fig. 3 Confuser No. 1 with $\alpha = 3^\circ$, $n_0 = 0.64$, simulation error at SST turbulence model versus the y^+ parameter



to zero. Also, at large values of Re, the error grows faster with the y^+ increase. Comparison of the results of simulation with SST turbulence model with the reference data shows that the simulation error stays acceptable only at $Re = 100,000$ and $y^+ = 0.5$ and $y^+ = 1$. Thus, the SST turbulence model may be applied only in a limited range of the channel flow regimes.

Figure 4 presents dependencies of the confuser #1 flow simulation errors from the y^+ parameter in the same range of Re values at the $k - \omega$ turbulence model. The dependencies logarithmic configuration is similar to the described above one obtained with the SST turbulence model. The area of acceptable error of 10% contains the $y^+ = 1$ for the whole range of the values $Re = 100,000 - 400,000$.

The number of prismatic layers is an important parameter for the flow computer simulation with low Reynolds models. The influence of this parameter upon the analysis error is evaluated by flow simulation in confuser #1 at $Re = 100,000$, $k - \omega$ turbulence model, $y^+ = 1$, and verified number prismatic layers (Fig. 5).

Fig. 4 Confuser No. 1 with $\alpha = 3^\circ$, $n_0 = 0.64$, simulation error at $k - \omega$ turbulence model versus the y^+ parameter

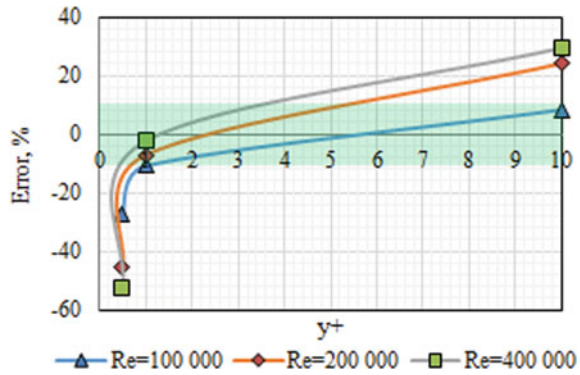
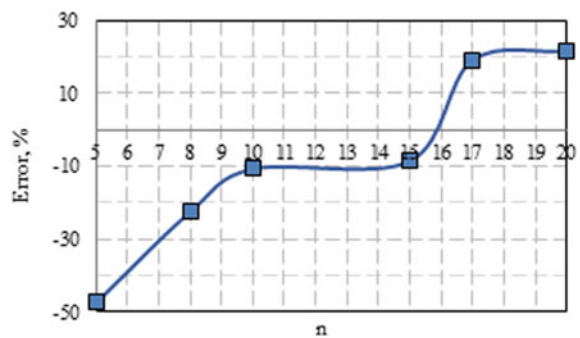


Fig. 5 Confuser No. 1 with $\alpha = 3^\circ$, $n_0 = 0.64$, simulation error at SST turbulence model, $y^+ = 1$ versus the number of prismatic layers n



The simulation error dependence upon the number of prismatic layers has four specific bands. In the first band, the layers number increase from 5 to 10 is followed by the error reduction from 50 to 10%. In the second band, the layers number increase from 10 to 15 is followed by the absence of error sensitivity upon the number of layers. The further increase of the layers number from 15 to 17 increased the error from -10 to 19% and the further number increase up to 20 does not show any changes of error. So the optimal prismatic layers number in terms of the acceptable analysis error below 10% and minimal time needed for the grid buildup is 10.

Based on the analysis results for confuser #1 with $\alpha = 3^\circ$, $n_0 = 0.64$, $D_0 = 50$ mm the analysis of confuser #2 with $\alpha = 3^\circ$, $n_0 = 0.39$, $D_0 = 50$ mm was carried out with $k - \varepsilon$ and $k - \omega$ turbulence models. The verification shows that the $k - \varepsilon$ model gives the error above 20% at $y^+ = 10 \dots 30$. For the confuser #2, the minimal error in the range of $Re = 10,000 - 400,000$ is obtained at $y^+ = 0.75$. On the other side the confuser #3 simulation with $k - \omega$ turbulence model shows, that the necessary error was obtained with the y^+ parameter reduced down to 0.25. Thus, the $k - \omega$ model shows the widest application range for the confuser channel flow analysis. These results make the base for the further described verification of flow analysis in diffuser channels.

Fig. 6 Diffuser main dimensions, D_0 , D_1 —inlet and exit diameters, α —expansion angle

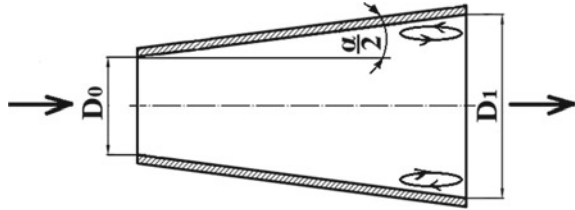


Table 5 Diffuser dimensions and flow parameters

No.	Dimensions			Flow parameters		
	α (°)	n_0	D_0 , (mm)	Re		
1	14	4	80	100,000	200,000	400,000
2	29	6	80			

3 Verification of Flow Computer Simulation in Diffuser Channels

3.1 Investigation Object

A diffuser is a smoothly divergent channel or tube that provides a transition from a smaller cross-section station to a larger one (Fig. 6). Diffuser flow path elements are quite usual, so the problem of computer simulation in terms of minimal calculation error is of importance.

Diffuser dimensions and flow parameters for verification are taken equal to experimental models for the hydraulic resistance tests [12]. Table 5 summarizes dimensions and flow parameters taken for the analysis results verification, the flow has separation on the channel inner wall.

3.2 Solver and Grid Parameters

The diffuser flow simulation involves the method of Reynolds averaging Navier–Stocks (RANS) like the confuser flow. The turbulence simulation model is the $k - \omega$ that shows a wider application range in confusers. The model grid parameters are presented in Table 6.

The physical experiment [2] is carried out with air as the ideal gas working fluid. The channel inlet boundary conditions working fluid G_0 mass flow and temperature $T = 20$ °C depend upon the experiment Reynolds number Re value and diameter D_0 (Table 7), the channel exit static pressure $P = 1$ bar.

Table 6 Diffuser model grid parameters

Parameter	Value
Grid type	Not structured
Global cell dimension, mm	8
Prismatic grid growth law	Exponential
y^+ parameter	0.005 ... 0.5
Prismatic layers ratio	1.3
Number of layers	10

Table 7 Flow simulation boundary conditions

Diffuser No.	$G_0, G/s$		
	Re = 100,000	Re = 200,000	Re = 400,000
1	113.965	227.930	455.860
2	113.965	227.930	455.860

3.3 Verification of the Flow Computer Simulation Results

Like in confusers (see above) the flow computer simulation results are compared against the reference ones by the hydraulic resistance coefficient ζ . Figure 7 presents dependencies of the resistance calculation errors upon the y^+ parameter at different Re values and $k - \omega$ turbulence model for the diffuser #1 with $\alpha = 14^\circ$ and $n_0 = 4$. Verification results for diffuser #2 with $\alpha = 20^\circ$ and $n_0 = 6$ are presented in Fig. 8.

The dependencies show the same tendency for the simulation error increase following the y^+ growth. On the other side, the y^+ values that provide acceptable error are 25–200 times smaller than the similar condition values in confusers. In the diffuser #1, with $\alpha = 14^\circ$ and $n_0 = 4$ at Re = 100,000–400,000, the simulation error below 10% is possible at $y^+ = 0.03$ –0.04. At the increase of the extension angle up to 20° and the expansion rate up to 6 in diffuser #2, the same simulation error of 10% is possible at $y^+ = 0.005$ –0.01.

Fig. 7 Diffuser No. 1 simulation error at $k - \omega$ turbulence model versus the y^+ parameter

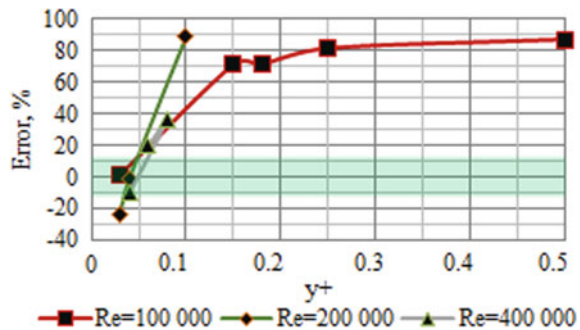
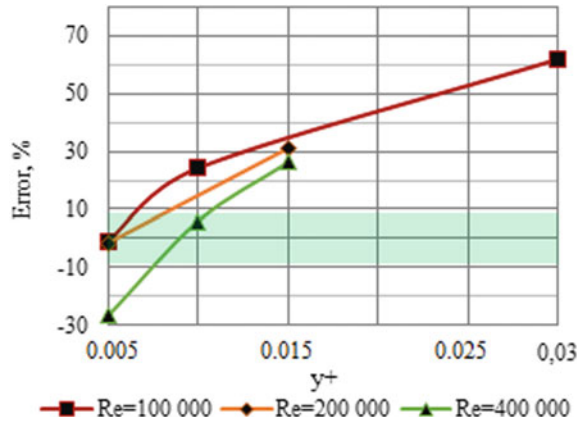


Fig. 8 Diffuser No. 2 simulation error at $k - \omega$ turbulence model versus the y^+ parameter



4 Conclusions

In flow computer simulation of confuser and diffuser channels the dimensionless parameter y^+ influences on the simulation error together with different turbulence models. The increasing of the y^+ parameter causes increasing of the calculation results errors at SST/ $k - \omega$ and $k - \varepsilon$ Standard turbulence models. The optimal number of prismatic layers for low Reynolds $k - \omega$ turbulence model with the simulation error below 10% and minimal model grid time spending is 10. In two ranges of layers number between 10 and 15 and between 17 and 20, the layers number does not influences the error. The $k - \omega$ turbulence model is applicable to the confuser and diffuser flow simulation with the simulation error below 10%. To keep the error below 10% at Reynolds number values $Re = 100,000 - 40,000$ in confuser channels, it is recommended to use the value $y^+ = 1$. In the flow simulation of diffusers with expansion angle $14 - 20^\circ$ at $Re = 100,000 - 40,000$ the error of 10% may be obtained at $y^+ = 0.005 - 0.04$ and the larger is the expansion angle the smaller y^+ values must be used.

This study conducted by Moscow Power Engineering Institute was financially supported by the Ministry of Science and Higher Education of the Russian Federation (project No. FSWF-2020-0020).

References

1. Pozrikidis, C.: Fluid Dynamics: Theory, Computation, and Numerical Simulation. Springer, New York (2016)
2. Versteeg, H.K., Weeratunge, M.: An Introduction to Computational Fluid Dynamics: The Finite Method. Pearson education, London (2007)
3. Elghobashi, S.: Annu. Rev. Fluid Mech. **51**, 217 (2019)
4. Zhang, C., Duan, L., Choudhari, M.M.: AIAA J. **56**, 4297 (2018)
5. Anantharamu, S., Mahesh, K.: J. Fluid Mech. **898** (2020)

6. Ahsan, M.: Beni-Seuf Univ. J. Appl. Sci. **4**, 269 (2014)
7. Salim, S.M., Cheah, S.: Proceedings of the international multiconference of engineers and computer scientists, vol. 2, p. 2165 (2009)
8. Catalano, P., Amato, M.: *Aerosp. Sci. Technol.* **7**, 493 (2003)
9. Yang, S.S., Derakhshan, S., Kong, F.Y.: *Renew. Energy* **48**, 507 (2012)
10. Tang, X., Dai, X., Zhu, D.: *Int. J. Heat Mass Transf.* **90**, 523 (2015)
11. Hamel, M., Hamidou, M.K., Cherif, H.T., Abidat, M., Litim, S.A.: In: Proceedings of Turbo Expo: Power for Land, Sea, and Air, vol. 43161, p. 2329 (2008)
12. Gileva, L.V., Aksenov, A.A., Kozhukhov, Y.V., Petrov, A.Y.: In: AIP Conference Proceedings, vol. 1, p. 030038 (2020)
13. DalBello, T., Dippold III, V., Georgiadis, N.J.: NASA TM 2005-213894 (2005)
14. Patil, S., Abraham, S., Tafti, D., Ekkad, S., Kim, Y., Dutta, P., Srinivasan, R.: *J. Turbomach* **1** (2011)
15. Idelchik, I.E.: *Handbook of Hydraulic Resistance*. Washington (1986)

Efficiency of Peat Combustion in a Low Capacity Boiler: Analysis of Peat Reserves in the Arkhangelsk Region and Efficiency of Its Energy Use



Victor Lyubov, Anatoly Popov, Evgeniya Popova, and Alexander Chernov

1 Introduction

One of the prospective directions of power engineering development is the use of renewable energy sources. Russia has almost all types of renewable energy sources. Their economical proved potential which is intended for priority exploration has 275 million tons of equivalent fuel in total which is equal to 25% of energy sources annual consumption in the country including the energy of biomass (35 million tons of equivalent fuel).

The Arkhangelsk region has the largest peat reserves among the regions located in the European part of Russia. The explored and previously estimated reserves of peat are about 4 billion tons, the predicted resources are determined at about 8 billion tons. Peat deposits are unevenly distributed across the districts of the region [1, 2] (Table 1), while the 17 largest deposits account for 28% of all peat reserves.

Peat is a geologically young, poorly decomposed fuel with a high content of volatile substances (Table 2), which simplifies its combustion. However, high and widely varying peat moisture creates significant difficulties in the combustion. Peat reserves in the Arkhangelsk region are terrestrial, mixed, transitional, and lowland types of deposits, and two thirds of them are concentrated in high bogs [1, 2].

The ash content of peat varies over wide limits for individual bogs and sometimes reaches significant values: the Bludnoe bog (Table 2) and the Charus bog of the

V. Lyubov · A. Popov (✉) · E. Popova
Higher School of Power Engineering, Oil and Gas, Northern (Arctic), Federal University named after M.V. Lomonosov, Northern Dvina Embankment, 17, 163002 Arkhangelsk, Russia
e-mail: a.n.popov@narfu.ru

A. Chernov
Arkhangelsk Plywood Factory, Frontovih Brigad 14, 164900 Arkhangelsk, Russia

© The Author(s), under exclusive license to Springer Nature Singapore Pte Ltd. 2022
A. Irina and P. Zunino (eds.), *Proceedings of the International Symposium on Sustainable Energy and Power Engineering 2021*, Lecture Notes in Mechanical Engineering,
https://doi.org/10.1007/978-981-16-9376-2_34

353

Table 1 Peat reserves in the fields of the Arkhangelsk region

Districts	Number of fields	The area in the border of the industrial depth of peat deposits, ha	Peat reserve at 40% moisture, thousand tons
Velsky	92	19.581	58.314
Verhnetoemsky	45	55.448	175.325
Vilegodsky	32	10.281	27.056
Vinogradovsky	68	47.806	172.927
Kargopolsky	151	139.878	533.340
Konoshsky	119	35.995	161.073
Kotlasky	55	18.174	56.750
Krasnoborsky	79	19.323	47.871
Lensky	11	10.164	27.193
Leshukonsky	66	32.807	63.413
Mezensky	121	211.469	500.333
Nyandomsky	22	33.428	152.651
Onezhsky	94	86.998	353.528
Pinezhsky	87	50.328	173.018
Plesecky	109	97.295	349.391
Primorsky	112	117.838	420.604
Ustyansky	124	10.811	30.711
Kholmogorsky	464	70.276	239.944
Shenkursky	57	47.406	189.590
Nenets Autonomous	18	2.974	6.851
Total	1.926	1.118.280	3.739.883

Table 2 Thermotechnical characteristics of peat from the Shenkursky deposit

Sample number	Moisture as received basis, W^r (%)	Ash content on dry weight basis/as received basis, A^d/A^r (%)	Volatiles on dry ash free basis, V^{daf} (%)	Lower calorific value as received/dry ash free basis, Q_r^r/Q_l^{daf} (MJ/kg)
Waimagan bog				
1	85	6.1/0.92	69.99	0.96/22.02
2	85	5.8/0.87	70.05	0.97/22.00
3	85	6.7/1.01	70.79	0.93/21.93
4	84	4.1/0.66	71.64	1.25/21.90
5	82	6.9/1.24	69.87	1.62/21.98

(continued)

Table 2 (continued)

Sample number	Moisture as received basis, W^r (%)	Ash content on dry weight basis/as received basis, A^d/A^r (%)	Volatiles on dry ash free basis, V^{daf} (%)	Lower calorific value as received/dry ash free basis, Q_i^r/Q_i^{daf} (MJ/kg)
6	86	8.8/1.23	70.17	0.63/21.89
7	82	11.4/2.05	68.32	1.45/21.99
8	78	8.2/1.80	69.56	2.48/21.97
9	86	5.7/0.80	70.22	0.75/22.03
Bludnoe bog				
1	82	20.7/3.73	68.59	0.94/21.05
2	82	26.8/4.82	71.25	0.73/21.20
3	84	18.7/2.99	70.90	0.63/21.06
4	85	17.4/2.61	69.33	0.49/21.23
Chistoe bog				
1	86	9.2/1.29	70.11	0.78/23.10
2	86	2.6/0.36	71.19	0.98/23.06
3	86	2.2/0.31	69.46	1.01/23.16
Zabegalka bog				
1	87	8.2/1.07	71.82	0.18/19.82
2	89	6.0/0.66	72.36	0.1/19.97
3	86	5.4/0.76	68.57	0.50/20.12
4	83	4.9/0.83	69.89	1.20/20.35
5	88	10.6/1.27	71.55	0.1/20.54

Kholmogorsky district. The not-go limit of ash content on dry weight is considered to be equal to 23% [3].

An extremely important characteristic of peat as a fuel is the degree of its decomposition. The entry of poorly decomposed peat into the boiler-house causes not only a sharp change in the combustion process, but also significantly complicates the operation of the transporting devices and feeders. This property, along with moisture and ash, characterizes sod and milled peat as fuel. The quality of peat is also largely dependent on its origin and nature of formation.

2 A Brief Overview of the Experimental Approaches

The number of production and operational testing of the boiler was determined by the necessity of obtaining the following basic dependences on heat output: flue gas heat loss, incomplete combustion heat loss and carbon loss, external heat loss, and

sensible heat of slag. Testing was performed to draw the air and gas balances, to determine boiler's actual efficiency, gaseous and particulate emissions of harmful substances, air leakage, aerodynamic resistance of air and gas paths, gas and air temperatures in controlled section areas of paths, etc.

Basic boiler's indicator measurements were carried out using regular measuring-and-recording apparatus including electronic sensors data received in the automated control system with the integrated BioControl 3000 microprocessor, and portable measuring instruments and research plants of the Research Center of Power Engineering Innovations of the Northern (Arctic) Federal University and the Shared Use of Equipment Center "Arktika".

Methods of production and operational testing of the boiler-furnace and auxiliary equipment are electrochemical method applied to flue gas analyzers, pressure and optical methods for determination of the volume of gas and airflow, ultrasonic fluid flow method, aspiration gas sampling method, thermal, pyrometric and contact methods for determination of the temperatures, combined relative and calorimetric methods supplemented by thermal imaging, weight and chemical methods for determination of the elemental composition of fuel, combustion residues, etc. [1, 3, 4].

Moisture, ash content, volatiles, low calorific value as received were determined in each of the main experiments for the sampled fuel. Experimental data analysis was performed using multiblock program-methodological complex [1, 5].

The analysis of fuels was carried out with the equipment of thermal analysis laboratory and IKA C2000 basic Version 2 calorimeter with LOIP FT-216-25 liquid cryothermostat. A study of the grain-size distribution of fuel composition and combustion residues was carried out with AS200 and Microtrac S3500 sieve shakers. The determination of velocity fields and flue gas flows was performed with a Pitot tube and a micromanometer of Testo-435 precision instrument. The results of the velocity fields study were used to determine the particulate matter concentrations at the flue gas after the boiler. In order to achieve that, an external filtration method was used, which is applied via an OP-442 TC impactor, a dust sampling probe, a filter holder, etc. [6]. A Testo 350XL gas analyzer was used to determine the content of combustion products. Fuel consumption was determined by the equation of the indirect heating balance.

Numerical modeling using ANSYS FLUENT Software is accomplished to elaborate the proved measures of further comprehensive increase of boiler operational performance.

All the burning processes (aerodynamics, ignition, burning out, heat and mass transfer, chemical reactions) are analyzed tied together. The gaseous medium consists of carbon dioxide, molecular nitrogen, moisture vapor, oxygen volatiles. Calculation of the biofuel particles trajectories was carried out using the Lagrangian approach. Heat and mass transfer are described for disperse phase. A two-parameter Realizable $k - \varepsilon$ model has been chosen to take turbulence of stream on particles movement into account.

3 Numerical Modeling of Burning Processes

3.1 Geometry

The boiler has a fuel storage with a screw system feeding biofuel into a holding bin and reverse ignition protection device. Fuel is fed by a screw feeder from a holding bin in the lower part of a stoker burner. The burner has an advanced contour, in the lower part of which a grate is mounted and it consists of two parts. It is possible to clean the grate by turning it down on 90°. Fuel is fed at a “cycle-pause” regime. An automated ignition of fuel occurs by an electrical hot-air gun. Primary and secondary air enters a furnace due to an exhaust fan vacuum. The main part of secondary air is fed through eight tangential nozzles and provides burning out of combustible components of fuel.

The operating pressure of a heat carrier on the output of the boiler does not exceed 0.3 MPa and the temperature does not exceed 95 °C. The boiler has two circulation contours. In the first one, equipped with a buffer tank, chemically pretreated and degassed water circulates. The estimated temperature regime for the processing medium of the first contour is 95/60 °C. Warming of heating system water of the second contour proceeds into a plate heat exchanger.

Combustion products from a stoker burner enter an afterburner where they give a part of the heat and go out it through the furnace throat placed at the back wall. Flue gas provides warming of the first contour boiler water flowing in two paths of fire tubes, then it is steered to the chimney by an exhaust fan. The turbolizer-cleaners are mounted into fire tubes to increase heat-exchange efficiency. After the first path in fire tubes, combustion products reverse, wherein larger fractions of soot are separated into an ash pit and collected in a bin. Ash and slag are removed from the combustion chamber by an individual screw into a collection bin too.

An exhaust fan motor has frequency control to provide smooth shift boiler performance. The boiler has required protection devices [7, 8]. An automated control system with an integrated BioControl 3000 microprocessor equipped with exhaust gas oxygen sensor, afterburner outlet temperature sensor, and outlet boiler temperature sensor as well as inlet and outlet water temperature sensor, etc. It provides ambient temperature-dependent control of heating contours and operates other significant boiler performances.

3.2 Mesh

A 3D model of boiler combustion chamber using builtin module ANSYS ICEM CFD [9] was developed on the preliminary stage of numerical modeling. Taking into account the unique geometry of a stoker burner and combustion chamber, it was decided to build an unstructured tetrahedral mesh with 1670 cells. Analysis of developed mesh has shown that it is acceptable for the objectives of this level of

complexity. Actual design and primary airflow rate through 16 gaps of grates were considered in numerical modeling. It was decided not to simulate undergrate part of the burner to simplify the computation.

3.3 *Boundary Conditions*

Calculation of the biofuel particles trajectories was carried out with the Discrete Phase Model and grain-size distribution of fuel was accounted using the Rosin–Rammner equation. Defined coefficients for this equation were determined by the sieve method [1]. It was resolved that fuel particles are spherical and consisted of coke and ash residue. There are the following stages of thermal treatment and burning of fuel particles calculation: warming, evaporation, ignition, burning of volatiles, coke residue burning out. Fuel particles in the furnace are thermally treated by radiative-convective heat transfer.

Heat transfer by radiation in the furnace was calculated using the P1-approximation. Primary and secondary air flow rates are given in boundary conditions [10].

The problem was solved by the method of successive approximations. At the initial stage, a coarser unstructured tetrahedral mesh with 672 thousand cells was used for the calculation. Then an increase in the number of calculated elements was made in order to eliminate the influence of the number of cells on the results of the solution. As a result, it was found that an increase in the number of design elements over 1.670 thousand does not have a significant impact on the outcome of the solution.

3.4 *Model Validation*

Also, to increase the accuracy of the solution results, the discretization scheme of convective terms of the basic equations was changed. At the first stage, a first-order discretization scheme (First Order Upwind) was chosen, which ensured fast convergence of the iterative process, but insufficient accuracy. At the second stage, a second-order discretization scheme (Second Order Upwind) was chosen using the algorithm for linking the speed and pressure fields SIMPLE [11–16].

Another factor affecting the accuracy of the solution is the convergence criterion. To ensure sufficient accuracy in solving this problem, an absolute criterion was established for all equations with a value of 0.001 (except for the energy and radiative heat-exchange equations 10^{-6}). The solution was launched on 1000 iterations. After reaching the value of the residuals for each equation, the program was reported “solution is converged (853 iteration)”. It means that the program has reached the required level of convergence.

3.5 Results of Numerical Modeling

Modeling results have shown that the working medium ensures reliable cooling of afterburner walls, where the temperature is 30–40 °C higher than the temperature of the boiler water (Fig. 1). Gas temperature in the furnace throat of the afterburner is 750–760 °C (Fig. 1), which is valid and much in line with the experimental data obtained from efficiency tests of the boiler. The main burn out area of peat combustibles is in the boiler’s afterburner where outlet gas and fuel flow velocity decrease quickly. The temperature range in this area has maximum value (~1.200 °C). The area of maximum carbon oxide and hydrogen concentrations is located slightly below (Fig. 2). A less bright area of active burning appears in the burner under secondary air tangential nozzles where the maximum temperature is about 1.080 °C. In this area, volatiles that are released during the thermal decomposition of small and large peat particles are burned out.

A huge concentration of fine particles in the sod peat makes a large part of them burn out in the gas flow. Uneven fuel distribution along the grate leads to the formation of craterlike combustion areas. However, gas flow swirling in the burner space formed by tangential secondary air nozzles allows to balance the concentrations of the gaseous components. Flow swirling intensity reduces, and its diameter increases when combustion products go to the afterburner. Gaseous combustible components are burnt out, providing minimum values of incomplete combustion heat loss, which is proved with experimental studies (Table 4) and numerical modeling. A huge concentration of fuel particles with the dimension of 125 μm and larger, which is not completely burnt out at the space of the combustion chamber and the after-

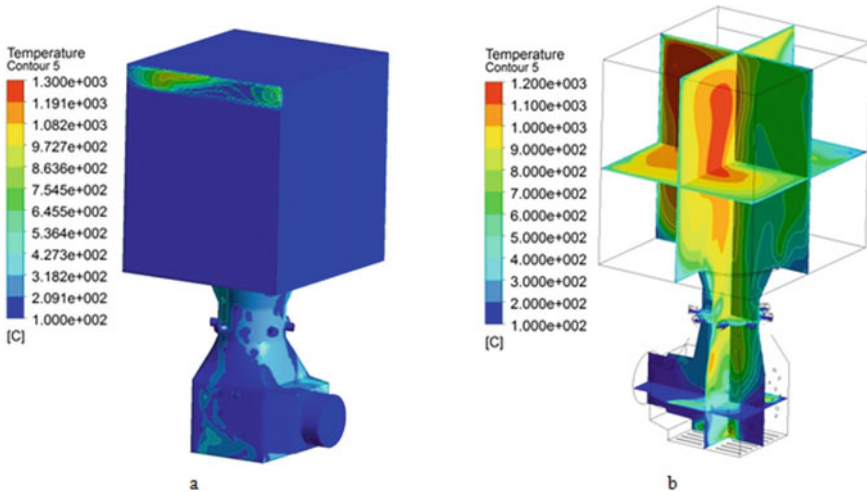


Fig. 1 Temperature distribution: **a** on the surface of the burner, the afterburner, and its furnace throat; **b** in the cross section of the burner and the afterburner

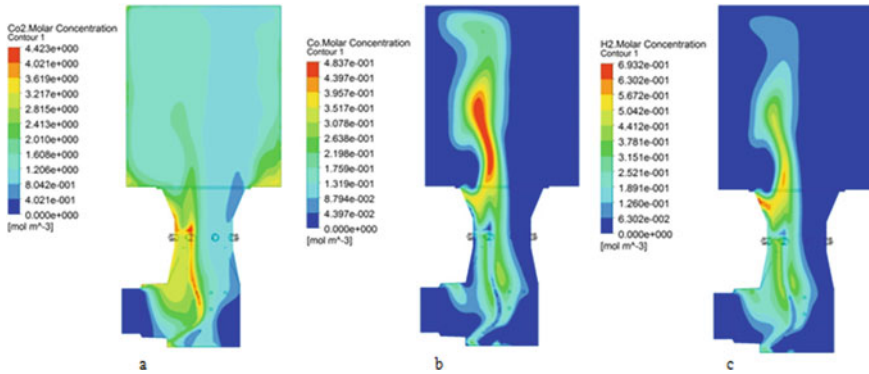


Fig. 2 The concentrations (Mol/m^3): **a** CO_2 ; **b** CO ; **c** H_2

burner, leads to a sharp increase in carbon loss up to 13% (Table 4). The separation of unburned fuel particles after the first path in fire tubes creates a risk of their ignition in the ash pit and the collection bin.

4 Full-Scale Experiments

Peat is in the intermediate position between renewable and fossil fuels. It is slowly renewing fuel because the recovery period on the mining area excess 200 years. However, peat consumption in the Russian Federation is significantly lower than the annual natural increase that allows considering peat as a renewable energy source in this condition. Terrestrial, transitional, and lowland peat deposits can be used as a fuel. Gas appearing while burning this kind of fuel is the greenhouse gas. However, its quantity and degree of danger directly depend on the combustion technology and the field where this resource is extracted.

According to the “Concept for the Protection and Rational Use of Peat Bogs of Russia”, the largest amount of peat reserves of categories A + B + C1—6.9 billion tons (36.2% of the reserves of the Russian Federation) was explored in the Northwest Federal District, with the current level of 5–10% peat formation. At the same time, the total number of deposits in this region is 18.912, and the projected peat resources are 16.2 billion tons [17, 18]. These data allow us to conclude about the potential use of reserves of this energy resource to ensure the generation of heat and electricity. It is important to note that not all deposits can be used at this stage of economic development. Therefore, the problem of choosing the best and most efficient peat resources is very serious. Evaluation is made in many ways, among which are thermal, grain size, morphological and other characteristics of fuels. The economic component of the issue is also of great importance, since some of the resources are located in hard-to-reach areas or in sparsely populated areas, where there is no need for large amounts of heat and electrical energy [1, 3, 4, 19]. Peat

extraction and use are possible only with the implementation of subsidy policies and state support in such regions.

The adoption of modern and highly efficient technologies and equipment for mining, agglomeration, and burning peat will allow increasing their range level in fuel balance of peat mining regions from 1–2% to 8–10% by 2030, which will increase their energy independence.

The basis of peat is made up of plant residues of solid polymers of cellulose nature and their decomposition products, which are in balance with an aqueous solution of low and high molecular weight substances. The inorganic part is represented in peat by insoluble minerals of different nature, adsorption formations of minerals with humic substances, inorganic components of peat water, ion-exchange heteropolar organo-mineral complexes, and complex-heteropolar derivatives [19].

4.1 Analysis of Peat Reserves in the Arkhangelsk Region and Its Thermotechnical Characteristics

Analysis of thermotechnical characteristics of peat from the Shenkursky and Kholmogorsky deposits allowed us to draw the following conclusions:

- the investigated samples of the original peat have a high content of external moisture, which reduces its calorific value as received basis to $Q_i^r = 0.1\text{--}2.48$ MJ/kg; therefore, the use of peat as an energy fuel without preliminary partial separation of external moisture is impractical. Partial separation of external moisture significantly increases its calorific value (Table 3);

Table 3 Thermotechnical characteristics of peat from the Rikasikha deposit of Primorsky district, the Charus deposit of Kholmogorsky district, and the Okulovo deposit of Mezensky district

Place of sampling	W_r (%)	A^d/A^r (%)	V^{daf} (%)	S^r (%)	Q_i^r/Q_i^{daf} (MJ/kg)	Note
Rikasikha, №1 site	34.42	3.92/2.57	76.39	0.14	13.87/23.39	Briquettes after drying in ambient conditions
Rikasikha, №2 site	61.53	5.67/2.18	79.34	0.08	6.96/23.46	Briquettes
Rikasikha, №3 site	46.79	6.43/3.42	71.22	0.12	10.46/23.36	Briquettes after drying in ambient conditions
Charus bog	12.4	33.6/29.4	70.4	0.17	11.07/19.58	Briquettes after drying in storage shed
Okulovo	90.3	4.1/0.4	77.51	0.02	2.27/23.43	Peat deposit

- using of peat-briquetting equipment during peat extraction improves the conditions for its transportation and storage, and also allows to partially separate of external moisture (Table 3);
- the Bludnoe bog is characterized by high ash content ($A^d = 17.4\text{--}26.8\%$) of peat, which will have even larger values in commercial production, therefore, it is not recommended to extract peat from this bog. This conclusion applies to the Charus bog of Kholmogorsky district ($A^d \geq 25.6\%$);
- taking into account the vulnerability of the northern nature, as well as increasing the fire danger of forests during preparing peat bogs for industrial extraction of peat, its energy use is advisable only in those areas of the region where there is no forest cutting waste, sawmill and wood processing waste, overripe or shrinking stand of trees, as well as deposits of high calorific fossil fuels.

Such a district on the territory of the Arkhangelsk region is Mezensky. This area has very large reserves of peat and is slightly inferior only to the Kargopolsky district (Table 1). The greatest effect from the extraction and processing of peat can be obtained with its integrated use as a fuel, organic fertilizer, the raw material for the production of fodder yeast, sugar, molasses, and other products.

The analysis showed that the Mezensky district of the Arkhangelsk region has very large reserves of peat (more than 500 million tons), however, in its fuel and energy balance, nowadays, expensive imported coal, whose share is more than 96%, dominates. Energy use of local fuels (peat and wood) will allow: to produce cheaper energy, decrease environmental pollution, increase the energy independence of the region, ensure the creation of new jobs, etc. For the widespread introduction of local fuels into the energy sector of the region, it is necessary to carry out research of determining the efficiency of use of existing domestic and imported equipment, including low-scale power.

4.2 Heat-Generating Plant for the Study of the Efficiency of Burning Local Fuels

Experiments were carried out at the building of Research Center of Power Engineering Innovations of NArFU named after M. V. Lomonosov which is connected to the district heat supply system. The Reserve heat supply source is the Austrian “Firematic 60” boiler of Herz Energietechnik GmbH which is also used to provide laboratory sessions and research. The boiler is designed to operate on wood pellets and chips [7, 8]. According to the manufacturer, the boiler nominal capacity (60 KW) is achieved while burning biofuel with specific moisture of $W_t^r < 25\%$.

4.3 Experimental Part

In the course of the boiler, efficiency tests were carried out while a combustion chamber was fed by peat pellets with a diameter of 10 mm and sufficient homogeneity composition (Table 4, tests No. 1, 2) and by sod peat (tests No. 3, 4). Sod peat had a high level of heterogeneity of grain-size distribution (an average coefficient of polydispersity was $n = 0.772$ and a coefficient characterized particle size was $b = 0.661 \times 10^{-3}$). The results of only two tests for each type of fuel are presented in accordance with requirements [20] and show the energy and environmental performance of the boiler.

After an automatic start-up of the boiler, the period it takes to reach the rated load does not exceed 20 min. After 33–38 min an automated control system provides inlet boiler water temperature close to the optimum value (60 °C).

Table 4 The main performance of the boiler burning peat pellets and sod peat

Value	Symbol, dimension	No			
		No. 1	No. 2	No. 3	No. 4
Heat capacity	Q , KW	79.7	79.7	74.8	74.8
Outlet operating pressure of the water	$P_{o,p}$, MPa	0.15	0.20	0.27	0.27
Outlet water temperature	$t_{o,w}$, °C	74.0	75.0	78.0	78.0
Moisture of fuel	W_t^r , %	16.50	8.20		
Ash content of fuel	A^r , %	9.95	11.76		
Sulfur content	S_t^r , %	0.22	0.19		
Volatile yield	V^{daf} , %	74.56	67.88		
Lower calorific value	Q_i^r , MJ/kg	14.875	15.469		
Flue gas temperature	$\vartheta_{f,g}$, °C	137.2	137.5	135.2	133.0
Excess air in flue gas	$\alpha_{f,g}$	1.38	1.41	1.27	1.24
Heat loss: Flue gas	q_2 , %	5.77	5.88	5.29	5.07
Incomplete combustion	q_3 , %	0.01	0.02	0.00	0.01
Carbon	q_4 , %	2.17	2.17	13.00	13.00
External	q_5 , %	0.38	0.38	0.40	0.40
Gross efficiency of the boiler	η_{gross} , %	91.37	91.24	81.01	81.22
Total fuel consumption	B , kg/h	21	21	21	21
Emission of NO _x	NO _x , mg/MJ	169	177	156	136
Emission of CO	CO, mg/MJ	7	23	4	11
Emission of SO ₂	SO ₂ , mg/MJ	338	331	272	278
Particulate matter emission	PM, mg/MJ	12.6	12.8	32.4	32.5

4.4 Results of Production and Operational Testing

The analysis of thermal conditions has shown that heat loss with flue gas is $q_2 = 5.00\text{--}6.00\%$, but it rises when load and inlet boiler water temperature increases.

A stage fuel combustion scheme and efficient mixing of secondary air with combustible components of fuel while keeping the excess air coefficient in the furnace within the range 1.21–1.41 allows reaching low values of heat loss due to incomplete fuel combustion (Table 4). Values of carbon oxide concentrations corrected to excess air coefficient of 1.4 are 9–58 mg/Nm³.

Carbon loss when the boiler operates on peat pellets is $q_4 = 2.17\%$ (content of combustibles in fly ash $C_c^{\text{ash}} = 19.50\%$). Conversion to burning the sod peat with high content of fine particles lead to a sharp increase of carbon loss to $q_4 = 13.00\%$ (content of combustibles in slag $C_c^{\text{slag}} = 20.70\%$, $C_c^{\text{ash}} = 53.17\%$). The gross efficiency of the boiler decreases by about an order of 10% (Table 4). When the combustion products reverse after the first path in fire tubes particulate matter with predominant dimensions of 125 μm and larger are separated into ash pit from where removed in a collection bin. Fractional fly ash analysis has shown that the greatest amount of combustible components is contained in particles of 0.5 mm or larger (Fig. 3a). Analysis of the experimental data, taking into account the mass content of different fractions, has shown that removal of unburned peat particles with the size of $0.25 < \delta < 2 \text{ mm}$ (Fig. 3b) has a significant role in the carbon loss.

External heat loss is determined according to the reference curves [21] for Russian heating installations during the engineering calculation as well as standard tests. Validity of appliance of master curves for the foreign devices should be proved experimentally. The amended approach was elaborated for the determination of external heat loss. This approach is based on the combined use of the relative and calorimetric methods supplemented with thermal imaging [7].

Experimental studies have shown that external heat loss for the rated load (60 KW) of the boiler does not exceed 0.5% that is significantly lower in comparison with Russian standards [21]. Low values of this loss are explained by moderate

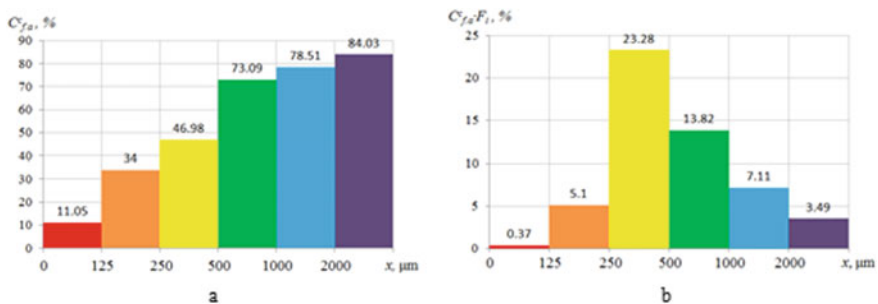


Fig. 3 Concentration of combustible substances in particles separated into collection bin while burning sod peat: **a** fractionating concentration of combustible substances; **b** concentration of combustibles taking into account weight percentage of different fractions

overall dimensions of the boiler and high quality of lining and thermo insulation materials. Losses due to the temperature of bottom ash while the boiler operates on peat are 0.30–0.31%.

Moderate emission of NO_x (Table 4) is explained by the low level of maximum temperatures and excess air in burner and afterburner as well as a two-stage combustion scheme. Sulfur dioxide concentration does not exceed 853 mg/Nm^3 (for $\text{O}_2 = 6\%$).

4.5 Results of Particulate Matter Investigation

The results of research of soot particles emission with the use of external filtration method under isokinetic conditions of gas extraction have shown that soot emission factor is 2.447 g/GJ , and emission factor $\text{PM}_{2.5}$ is 0.347 g/GJ while burning peat pellets. When the boiler operates on sod peat the soot emission factor increases fast up to 17.254 g/GJ and emission factor $\text{PM}_{2.5}$ —up to 2.416 g/GJ accordingly.

The captured particles were studied by the electronic scanning Zeiss SIGMA VP (Carl Zeiss) microscope. Three main types of particles in selected samples have been identified: spherical shape and solid crystal particles and particles with an amorphous structure.

Elemental composition, dimension and shapes of carried away particles have been studied [8, 22]. The obtained results have shown that solid particles with dimension less than $13 \mu\text{m}$ are predominantly carried away to the atmosphere.

5 Conclusions

Results from calculations and comparison of numerical studies with experimental data have shown that chosen model of burning can be used to study the boiler's operational performance with grate firing of solid fuels which contain a significant number of fine particles burning in a suspension state.

Numerical modeling and the boiler's efficiency tests have shown that stage combustion scheme and intensive mixing of secondary air with combustible components of fuel allow providing highly efficient operation of the boiler in the condition of low oxygen concentration of 4.0–6.0%. As oxygen concentration increases by more than 6%, the emission of harmful substances to the atmosphere also rises. To that end, the threshold value of oxygen concentration should be reduced to 4% in the automated control system.

Obtained experimental and estimated studies have shown that higher ash content (in 20 times approximately) and high heterogeneity of sod peat grain-size distribution in comparison with biofuels projected for this boiler do not allow to recommend this boiler to operate on sod peat with no significant changes in the collection and removal of the combustion residues as well as protection system for spontaneous ignition.

In addition, the transition from burning peat pellets to sod peat caused an almost threefold increase in solid particles concentrations in the flue gases removed (Table 4) which indicates the feasibility of installing an ash collector.

An analysis of peat reserves in the fields of the Arkhangelsk region has been carried out and the thermotechnical performance of some of them has been investigated. The factors that determine the prospects for the use of peat in the regional economy are found. It is shown that the Mezensky district of the Arkhangelsk region has peat reserves in the amount of more than 500 million tons, but in the fuel and energy balance of which dominated expensive imported coal, which accounts for more than 96%. The absence of deposits of high calorific fossil fuels, as well as overripe or shrinking stand trees and waste of logging and wood processing, makes it possible to consider the Mezensky District as a priority site for wide integrated use of peat.

A comprehensive energy survey has shown that the Firematic 60 boiler provides high technical and economic performance and minimum emissions of harmful substances to the atmosphere while combusting biofuels and peat pellets. It should be used for low-rise buildings heat supply in weather conditions of the Arctic region especially.

Effective combustion of sod peat with high heterogeneity of grain-size distribution cannot be organized in the furnace of this boiler with no significant changes in the collection and removal of the combustion residues system as well as protection system for spontaneous ignition and mounting of the ash collector.

References

1. Lyubov, V.K., Lyubova, S.V.: Increasing of Biofuels Usage Efficiency. NArFU, Arkhangelsk (2017)
2. Malygin, P.V., Lyubov, V.K.: The study of the structure, composition and characteristics of peat. *Bull. CHSU* **5**, 12 (2014)
3. Varankin, Yu.V.: Combustion of Sod and Milled Peat in Industrial Furnaces. Akademia nauk, Minsk (1952)
4. Solopov, S.G., Gorcakalyan, L.O., Samsonov, L.N.: Peat Machines and Complexes. Nedra, Moscow (1973)
5. Lyubov, V.K., Dyachkov, V.A.: In: Proceedings of 2nd Russian National Conference on Heat Exchange, Moscow, MEI 225 (1998)
6. Collection of Methods of determination of harmful substances concentrations in industrial emissions. *Gidrometeoizdat*, Leningrad (1987)
7. Lyubov, V.K., Malygin, P.V., Popov, A.N., Popova, E.I.: *Therm. Eng.* **572** (2015)
8. Popova, E.I., Popov, A.N., Lyubov, V.K., Varakin, E.A.: *Nat. Arctic* **464** (2015)
9. Gil', A.V., Starchenko, A.V., Zavorin, A.S.: The use of numerical modeling of combustion processes for the practice of converting boilers to non-project fuel. STT, Tomsk (2011)
10. Collazo, J., Porteiro, J., Míguez, J.L., Granada, E., Gomez, M.A.: *Energy Convers. Manag.* **87** (2012)
11. Gera, D., Mathur, M.P., Freeman, M.C.: *A. Robinson, Energy Fuels* **1523** (2002)
12. Mehrabian, R., Shiehnejadhesar, A., Scharler, R., Obernberger, I.: Numerical modelling of biomass grate furnaces with a particle-based model. In: 10th European Conference on Industrial Furnaces and Boilers (2015)

13. Scharler, R., Obernberger, I.: Numerical modelling of biomass grate furnaces. In: 5th European Conference on Industrial Furnaces and Boilers (2000)
14. Kruggel-Emden, H., Wirtz, S., Scherer, V.: Powder Technol. **261** (2013)
15. Simsek, E., Brosch, B., Wirtz, S., Scherer, V., Krüll, F.: Powder Technol. **266** (2009)
16. Kurz, D., Schnell, U., Scheffknecht, G.: Combust. Theory Modell. **251** (2012)
17. Inisheva, L.I.: Concept for the Protection and Rational Use of Peat Bogs of Russia. CNTI, Tomsk (2005)
18. Shtin, S.M.: Hydromechanized Peat Extraction and Peat Production for Energy Purposes. Gornaya kniga, Moscow (2012)
19. Lishtvan, I.I., Bazin, E.T., Gamayunov, N.I., Terent'e, A.A.: Physics and Chemistry of Peat. Nedra, Moscow (1989)
20. Trembovlya, V.I., Finger, E.D., Avdeeva, A.A.: Thermotechnical Tests of Boilers. Energoatomizdat, Moscow (1991)
21. Thermal design of boilers (Standard method). NPO CKTI, Saint-Petersburg (1998)
22. Lyubov, V.K., Popova, E.I., Popov, A.N.: In: Conference Proceedings 2nd International Conference on Atmospheric Dust, vol. 72 (2016)

General Methods for Loss Prediction in Axial Turbine Blade Cascades



A. A. Ukhlin, V. I. Brezgin, M. Yu. Stepanov, and G. R. Lotnik

1 Introduction

The modern world has ecological problems, which grows dramatically. Humanity recognizes the natural fossil fuels depletion and the rapid energy consumption increase in all countries. That's why power-engineering manufacturers exert all their efforts to increase efficiency of the new power-generating equipment. Despite the fact that modern turbine construction dates back to the end of the nineteenth century and has now reached a fairly high level of perfection, there is still a quite wide number of unexplored matters in terms of hydro-gas-dynamic and thermodynamic processes occurring in turbine blade cascades. One of these issues is to understand the losses physical nature arising in them, the ability to predict losses value with high accuracy, and also to minimize them as much as possible for the designed (calculated) mode of new equipment.

Historically, the most systematic and regular researches in this field were carried out in Sweden, Germany, USA, and Great Britain. The results of such investigations were made public to the international research community only after the expiration of the “statute of limitations”. The Second World War, as well as the post-war period, greatly accelerated the spread and development of turbine construction technologies, primarily to meet the needs of the military industry. However, the Cold War, as well as the fight against industrial espionage, led to an even greater split in the scientific community, and as a result, the creation of separate regional schools of turbine engineering—American, Soviet, and European. Despite the fact that the USSR was able

A. A. Ukhlin (✉) · M. Yu. Stepanov · G. R. Lotnik
AO «Ural Turbine Works», 18th Frontovyykh brigad, Ekaterinburg 620017, Russia
e-mail: apl@inbox.ru

A. A. Ukhlin · V. I. Brezgin · G. R. Lotnik
Federal State Autonomous Educational Institution of Higher Education «Ural Federal University named after the first President of Russia B.N. Yeltsin», 19 Mira street, Ekaterinburg 620002, Russia

to take an indisputable technological leadership in the aviation industry, the Soviet school of power turbine construction mainly tried to catch up with the advanced foreign developments of the capitalist camp, as evidenced by the records in [1]. However, taking into account the fact that the full texts of works by C. G. Laval and other pioneers of axial turbine technologies was not fully publicized, all researches were carried out completely independently, with a periodic focus on the new foreign scientific publications, which were monitored, translated and published in USSR by ROSENERGOIZDAT.

Thus, by the time of the beginning of systematic researches in the field of losses phenomena in the turbine blade cascades, large-scale studies had already been carried out in a number of foreign countries, and methods for predicting losses had already been developed. Then all new inventions and correlations were immediately applied at machine-building enterprises. Such works include studies of Ainley and Mathieson [2], Craig and Cox [3], Dunham and Came [4], Traupel [5], Kacker and Okapuu [6], and others.

In Russia, M. E. Deich, I. I. Kirillov, A. V. Shcheglyayev, and others researched this area of knowledge. One of the obvious examples of the differences between the Soviet school of turbine construction and the foreign one is the smaller discretization of the losses existing in the turbine stages. In this case, we are talking about the so-called “endwall losses”—losses which occur due to the phenomenon of the boundary layer on end walls of blade channels. In Russian turbine construction school, endwall losses are considered as a part of the profile losses.

It cannot be denied that this approach has several advantages. In particular, the simplification of the estimation of the total losses in the cascades of the blade channel, which, especially for turbines with an active type of blading, provides a sufficiently high level of losses prediction. Nevertheless, foreign scientists still research endwall losses as a separate phenomenon, Coull [7]. This losses separation approach allows to carry out deeper researches of the occurring physical phenomena. Hence it brings researchers to determine the key influencing parameters and factors that contribute to losses reduction. And as a result, on the basis of this kind of approach, there is a further increase in the efficiency of the flow path of axial turbines, an increase in the level of design quality, and accuracy of estimating the losses value in the turbine flow path.

2 Materials and Methods

This article is aimed to provide a brief overview of losses prediction methods, their accuracy, and to draw a conclusion about the feasibility of their application today.

The sources selected were publications in authoritative journals that were recognized by the scientific community and time.

It also should be noted, that it is much cheaper and easier to carry out experiments on gas turbines and test rigs with air as a workflow, than with steam. That’s why almost all researches were made with air and derived correlations primarily intended

for gas turbines. However, taking into account the theory of “ideal steam” (described by Traupel), described in this article methods are sure to be used for steam turbines (especially for high and intermediate pressure cylinders).

3 Loss Prediction Methods

The turbine design is a complex iterative process with a number of steps. To obtain a highly efficient design of the turbine flow path in accordance with the specifics of the customer’s requirements, which is currently the key criterion for competitiveness in the market [8], it is necessary to analyze the thermodynamic cycles for different turbine operation modes, taking into account the previously adopted flow path geometry. Based on the results of the analysis, losses prediction in the main modes is performed and a decision on further optimization of the aerodynamic characteristics of each blade row is made. These tasks are usually performed at the stages of preliminary design and mean line throughflow calculation. However, losses prediction methods also should be used at the stage of detailed design in order to prove the efficiency of the new turbine design.

Most loss models are empirical, derived from a large number of systematic experiments. Other methods, which are more modern, are a combination of empirical formulas, supplemented by analytical correlations based on the analysis of the dependence of physical parameters. Such methods are called semi-empirical ones. For such models, an extremely limited number of highly targeted experiments are carried out, as was done in the work of Matsunuma [9] in the study of the effects of Reynolds number and freestream turbulence on turbine tip clearance flow.

The first and probably the most widely used method for predicting the losses occurring in the flow path of axial turbines is the method developed by Ainley and Matheison [2]. In 1951, Ainley and Matheison presented a set of correlations to determine all types of losses for both design and non-design conditions. The proposed correlations were obtained on the basis of experimental data for traditional blades with a cylindrical profile. In addition, a number of significant assumptions were made, in particular, that the pressure loss coefficients do not depend on the value of the Mach number of the flow, or that the incidence (flow attack angle) does not affect the flow exit angle from the blade channel. Nevertheless, Ainley and Matheison experimentally determined that the error of the proposed method is within $\pm 3\%$ of the mass flow rate and $\pm 2\%$ of the total turbine efficiency.

To predict the total losses, the principle of linear distribution of losses with a correction factor was used. It should be noted that to date, the issue of distribution of losses has not been completely investigated [2, 4, 7, 10, 11]. However, it is known that this distribution is influenced by the type of turbine (HPC or LPC), design of seals, blade profiles, type of blading, turbine operating mode, etc. [12].

The Ainley and Matheison loss prediction method is suitable for axial turbines in which the following conditions are met:

- value of trailing edge thickness to pitch ratio is less than 0.02;
- value of Reynolds number is $Re < 2 \times 10^5$;
- value of Mach number is $M < 0.6$;
- traditional blades with a cylindrical profile are chosen.

When using these correlations, it should also be taken into account that for turbines with active type of blading, there is a significant overestimation of losses [12].

Since the publication of the Ainley and Matheison methodology in 1951, various scientists have continually conducted additional researches and proposed their own versions of the improved method. The most successful improvements were proposed by Dunham and Came [4] and Kacker and Okapuu [6].

During Ainley and Matheison method usage, a significant error was found for low power gas turbines, as well as for determining losses with high values of aspect ratio (relative height of the blades). Dunham and Came offered a number of improvements [4], namely:

- added consideration of the Reynolds number influence for the total losses prediction method (Additionally, it should be noted that the influence of Re on the distribution of total losses was experimentally proved by Matsunuma [9]);
- for profile losses prediction, the influence of the Mach number was added;
- for the secondary losses correlation, the influence of the relative blade height was added, and the flow acceleration coefficient in the channel was added;
- for the tip leakage losses, the influence of the number of the labyrinth seals and the size of the gap in the seals were added.

According to the results of experimental verification of the improved method, the accuracy of the total losses for turbines of any power with cylindrical blades was $\pm 3\%$ of the mass flow rate, and $\pm 2\%$ of the total efficiency of the turbine. In addition, the restriction on using the method depending on the value of Re was removed. Subsequently, this loss prediction method was called as “AMDC”.

Further improvements to the AMDC method were carried out by Kacker and Okapuu. The aim of their research was to improve the accuracy of existing correlations. The AMDC method was improved by adding special correction factors. These factors take into account influence of following parameters: effects of flow compressibility, occurrence of shock waves, analytical refinement of the influence of the Reynolds and Mach numbers on profile losses, influence of aspect ratio on secondary losses, and addition of losses at the trailing edge (with the outlet velocity). The total error of the improved losses prediction method is $\pm 1.5\%$ relative to full turbine efficiency. This improved method is called as “KO”.

Despite the fairly high accuracy rate of the total loss prediction, this method has retained a number of disadvantages that are inherent in the Ainley and Matheison method, limit its use and increase inaccuracy, namely:

- the method is based on experimental data of traditional cylindrical blades, and for blades with complex 3D profiles can give an increased error;

- Despite the significant analytical refinement of the parameters in the correlation formulas, the correlations still remain mainly empirical, which calls into question the validity of using each of the correlations separately, outside the full KO method. This fact is confirmed by Matsunuma [9], who performed an experimental comparison of methods for determining tip leakage losses with their own experimental work at the special test rig. The AMDC loss values 3 times exceeded the actually measured values, while the KO correlation error was 15%. The highest accuracy 7% was shown by the correlation proposed by Denton [13].

Apart from the AMDC methodology, in 1970, also based on a number of experimental data, Craig and Cox proposed their method [3], which subsequently gained recognition among both turbine and compressor designers.

Considering the known disadvantages of the original Ainley and Matheison method proposed in 1951, Craig and Cox initially formed empirical relationships including such parameters as Reynolds and Mach numbers, aspect ratio, trailing edge thickness, angle of attack, and other parameters as basic data.

The key features of this method are the total losses separating approach and these losses estimation.

Hence, the total losses were in linear proportion to the sum of the profile losses, secondary losses, and losses in the annular channel.

To determine the profile losses, Craig and Cox introduced the concepts of the blade lift parameter and the channel contraction ratio, for which graphical dependencies were plotted. The lift parameter of the blade is a function of the flow angle in the channel and the blade solidity. And the contraction ratio of the channel is the ratio of the area of the inlet blade channel to the area of the throat.

The correlation obtained by Craig and Cox for determining the profile losses showed insensitivity to Re numbers greater than $2 \cdot 10^5$, which is fundamentally incorrect, and therefore a correction factor for the Reynolds number was added.

Annular channel losses characterize the flow dissipation between two turbine stages or two neighbor blade rows (i. e., nozzle and rotor blade rows). They are determined on the basis of a graphical dependence with knowledge of the exact geometric characteristics of the turbine flow path.

Despite the large number of graphically determined correction factors, the proposed method showed an error of only $\pm 1.25\%$ of the total turbine efficiency.

The main disadvantages of this method are as follows:

- dependences of the channel contraction ratio and the blade lift coefficient, as well as losses in the annular channel, are determined on the basis of the known geometric design of the turbine flow path, which leads to additional iterations during the new turbine design development;
- as well as in the AMDC method, data from traditional cylindrical blades were used, which also makes the formed correlations imperfect for modern 3D blading.

Another noteworthy method was proposed by Denton [13] in 1994. Unlike the methods previously described in this article, Denton used the approach that is based not only on experimental data, but on the principles of changing the entropy of the

workflow due to the effects of viscosity in the boundary layers, flow compressibility, shock waves, mixing of the flow and heat transfer. Accordingly, losses are determined mainly not only by empirical correlations, but also by formulas obtained from simplified equations of conservation of impulse, mass, energy and in accordance with the theory of the boundary layer. Nevertheless, in this methodology, some empirical coefficients remain. So, Denton offered a semi-empirical method.

The author by himself, in his conclusions about the proposed method, notes that taking into account the insufficient knowledge of physical processes and the nature of entropy, as well as the adopted number of simplifications, in some cases the losses prediction error can be up to 20%.

This primarily concerns the determination of such types of losses as endwall losses, losses with the outlet velocity at supersonic flows, as well as losses associated with mixing of the flow in downstream blade rows.

Nevertheless, from the point of view of physical science, this approach is eligible for being promising, which is evidently or indirectly confirmed by studies and experiments by scientists from other countries [7, 9, 12, 14, 15].

From the point of view of a different methodological approach, it is also worth noting the method for determining losses according to Traupel [5], published in 1970. Similar to the AMDC and KO method, this method is entirely based on a significant amount of experimental data. However, in contrast to them, a different approach was applied, which consisted not in deriving purely empirical correlations, but in identifying physical laws of parameters contraction based on the accumulated experimental data. Further, simplified conclusions about the most obvious relationships were made, and based on them, methods for determining losses were formed.

A similar approach and scope of scientific work in the history of the Soviet turbine construction school was carried out by A. V. Shcheglyaev. Traupel and Shcheglyaev's methods are both semi-empirical.

There are many other loss prediction methods with different methodological approaches, advantages, and disadvantages, which can be considered further.

4 Basic Approaches for Loss Prediction in the Modern World

Due to the complexity, heterogeneity, and a lot of the physical processes occurring during the steam expansion process in axial turbine blade cascades, practically throughout the entire twentieth century, scientists from different countries carried out field experiments using blades of different geometric characteristics. According to the test results, a statistical accumulation of experimental data array was collected. Based on that experimental data a news correlation dependences were formed for certain types of losses prediction. These dependencies often ended up with a number of limitations and correction factors, some of which were described in the previous section.

With the development of electronic computing technologies, digital data processing, and software computing systems, it has become possible with much lower costs to solve more complex problems and to use methods of numerical simulation more intensively.

Today the software market offers many CAE and CAD solutions to turbine designers. These are both interdisciplinary computing systems suitable for use in any industry (AnSys, OMNIS NUMECA, etc.), as well as highly specialized software developed by turbine manufacturers independently or by their order (software developed by AO Ural Turbine Works, Siemens PLM, Concepts NREC software, etc.).

Nevertheless, till the moment, no one of the existing software products cannot provide solutions for non-stationary phenomena of the blade boundary layer. Moreover, in the case of formulating the problem of identifying parametric dependences of the formation of secondary losses, it will be necessary to solve a system of equations with 13 variables [9]. Only quantum computers, the development of which is still underway, can deal with this task.

In addition, it should be noted that the majority of software systems that can potentially solve the problems of thermodynamic and hydro gas and thermodynamics calculations of blade cascades or turbine units, in turn, have simplified methods. In some cases, the developers do not provide information about the programmed calculation methods.

This raises the problem of the reliability of numerical simulation methods, the results of which must be verified by experiments.

The task of verifying the software with the actual data of the experiment is performed individually and requires additional attention from the design engineer. To meet this target, full-scale experiments are carried out in order to obtain results similar to those obtained with numerical simulation [9, 12, 16].

5 Conclusion

A review of a number of loss prediction methods for axial turbines has been performed. Based on the information presented in this article, the following conclusions can be drawn:

1. Despite the active development of numerical modeling technologies and an increase in the computing power of computers, the calculation of non-stationary processes occurring in the boundary layers of a turbine blade is still not carried out.
2. The physical processes occurring in the turbine blade cascades have not yet been fully researched. Therefore, field experiments are carried out by a number of researchers in Canada, Germany, Poland, Japan, Russia, Iran, and other countries.

3. Taking into account the large number of interrelated parameters that affect the value of secondary losses, profile losses, and endwall losses, the calculation will be possible only with the use of quantum computers. Therefore, today for the design of the flow path of the turbine, the use of empirical and semi-empirical methods for determining losses has been justified.
4. Most of the currently existing correlations for loss prediction, despite the improvements, continue to have a number of assumptions associated with both the blade profile used in research and in terms of the physical processes in the turbine flow path. In addition, there are correlation methods based on open and outdated data, the reliability of which requires additional verification.
5. There is no universal method for determining all types of losses with high accuracy for design and off-design modes. However, there are correlations and calculation methods that can provide accuracy within 3–1.25%, on the condition that turbine design meets the accepted assumptions. The question of the correct application of the loss prediction method is entirely assigned to designers for each individual turbine project, requiring in-depth knowledge and features of the methods.
6. Between the Soviet and Western turbine construction schools, despite the general principles, there are a number of differences, both in terms of the concepts used and in terms of methods for determining losses. The European school is characterized by stronger discreteness in the theoretical approach and an emphasis on carrying out natural experiments, while in the Soviet school the methods of the analytical approach based on a smaller amount of experimental data, with less detailed parameters, are prevailed. However, in the modern world, taking into account the rapid development of computer software systems, research approaches are becoming more uniform, and computer modeling methods are increasingly becoming a key tool in this. At the same time, there is an acute problem of the reliability of computer modeling with real physical processes, which is currently the reason for further full-scale experiments.

References

1. Kirillov, I.I.: Aerodynamics of the flow path of steam turbines. Book 1. Bezhitsy Institute of Transport Engineering, MASHGIZ, Moscow (1955)
2. Ainley, D.G., Mathieson, G.C.R.: A method of performance estimation for axial flow turbines. In: British ARC, R&M, vol. 2974 (1951)
3. Craig, H., Cox, H.: Performance estimation of axial flow turbines. In: Proceedings of the Institution of Mechanical Engineers, vol. 185(1), pp. 407–424 (1970)
4. Dunham, J., Came, P.M.: Improvements to the Ainley-Mathieson method of turbine performance prediction. ASME 70-GT-2 (1970)
5. Traupel, W.: Thermische Turbomaschinen. Springer-Verlag, Berlin (1977)
6. Kacker, S.C., Okapuu, U.: A mean line prediction method for axial flow turbine efficiency. ASME 81-GT-58 (1982)

7. Coull, J.D.: Endwall Loss in Turbine Cascades. TURBO-16-1821 (2016)
8. Ukhlin, A.A., Stepanov, M.Yu., Shibaev, T.L.: Unique projects of steam turbines at AO ural turbine works for industrial power generation. *Thermal Eng.* **67**(12), 909–915 (2020)
9. Matsunuma, T.: Effects of Reynolds number and freestream turbulence on turbine tip clearance flow. *J. Turbomach.* **128** (January 2006). <https://doi.org/10.1115/1.2103091>
10. Hodson, H.P., Dominy, R.G.: Three-dimensional flow in a low-pressure turbine cascade at its design condition. *ASME J. Turbomach.* **109**, 177–185 (1987)
11. Hodson, H.P., Dominy, R.G.: The Off-Design Performance in a Low-Pressure Turbine Cascade. *ASME J. Turbomach.* **109**, 201–210 (1987)
12. Wei, N.: Significance of loss models in aerothermodynamic simulation for axial turbines. Doctorial Thesis (2000). ISBN: 91-7170-540-6. ISSN: 110-7990
13. Denton, J.D.: Loss mechanisms in turbomachines. *ASME, J. Turbomach.* **115**, 621–656 (1993)
14. Benner, M.W., Sjolander, S.A., Moustapha, S.H.: The influence of leading-edge geometry on secondary losses in a turbine cascade at the design incidence. *ASME J. Turbomach.* **126**, 277–287 (2004)
15. Benner, M.W., Sjolander, S.A., Moustapha, S.H.: An empirical prediction method for secondary losses in turbines—Part II: a new secondary loss correlation. *ASME J. Turbomach.* **128**, 281–291 (2006)
16. Feng, Z.-M., Guo, C., Wei, B., Cui, W., Gu, H., Zhang, J.: Axial-swept influence on inner flow performance of HP steam turbine based on CFD. *Hindawi, Mathematical Problems in Engineering* (2019). <https://doi.org/10.1155/2019/5363496>

The Technique for Estimation of Thermal Power Equipment Remaining Life Based on Service Life Index



Makhsud Sultanov, Iliia Boldyrev, Valentina Lunenko, Pavel Menshikov, and Kirill Evseev

1 Introduction

Thermal power plant is a high-risk facility, wherein the equipment fault leads to detrimental consequences for both the plant personnel and electrical power consumers, which outage can cause the technological process disturbances and business loss. The importance of estimation of thermal power plant equipment actual life and condition is noted in many researches, for instance, [1–4] consider techniques for estimation of coal and oil/gas 300-MW power unit equipment reliability and life working at super-critical service. In [5], the authors note that power unit efficiency and safety directly depend on the power equipment technical conditions. The operational parameter early warning systems can assist the operators in recognizing the faults in early stage and prevent its escalation.

The power generating equipment component life decreasing and depreciation are natural processes, nevertheless the faults occurred due to depreciation can lead to standstills and high economic expenditures of both repair and compensatory relief. Therefore, there is the problem of designing the systems for actual technological parameter values estimation in terms of their impact on the equipment life decrease rate. Implementation of the expert system, which provides an operator the information on how the technological parameters effect the output values and life to allow optimizing the power equipment operation mode.

The critical objective is design of techniques for monitoring the equipment condition and operation mode, estimating its decrease rate in real-time scale, and notifying an operator of the process parameters, which impact the equipment life most, reaching critical values.

M. Sultanov · I. Boldyrev (✉) · V. Lunenko · P. Menshikov · K. Evseev
Branch of National Research University “MPEI”, Volzhsky, Russian Federation
e-mail: boldyrev@vfmei.ru

2 Literature Review

The thermal power plant equipment critical state recognition is main and important procedure to determine the maintenance and decision-making strategy.

There are fairly large number of approaches to estimate the equipment technical state and make decisions on its maintenance. One of the techniques for power equipment maintenance strategy development is multicriteria decision-making. The authors of [5] note that multicriteria decision-making methods provide better results on decisions by considering multiple optimization factors and criteria.

The [6–13] present the aspects of applying the multicriterial decision-making techniques for thermal power plants for preventive, direct condition-based and probabilistic-based maintenance. According to the large variety of equipment types, possible failure causes and their aftermath many authors present the multicriterial techniques using fuzzy descriptions for estimation of fault criticality taking into account the criterion, which considers the aspects of safety, reliability, efficiency, operation conditions, and environmental stress. In [14], the authors used the fuzzy logic method to design the fuzzy early warning expert system for engineer constructions. The feature of the method is using the knowledgebase, based on fuzzy logic accuracy characteristics.

In [2], the authors propose the technique for power equipment early warning based on actual values analysis. The multidimensional state estimation technique with improved process memory matrices is used to build a non-parametric model, describing equipment normal condition. As the early warning estimation criteria the sliding window state similarity is used, which allows better estimation of belonging of multiple failure variables to the normal condition.

It is known that thermal power equipment life is mostly defined by actual operation conditions, for example, [15–17] present the relation of steam boiler set metal working service from steam temperature. In [18], the necessity of metal temperature state regulation is noted and the main and resuperheat steam temperature deviations are normalized by the tolerable nominal values of turbine set continuous operation. According to the [19], the equipment metal temperature mode should be recorded. For each steam line with 450 °C and over steam, the steam temperature overriding at each extra 5 °C over the nominal values and the duration should be recorded.

Thus, it is necessary to estimate the equipment life and condition for optimal maintenance strategy development, wherein it is possible to estimate the equipment life by the actual process values, which characterize the operation conditions. Using different estimations by the actual process values for defining the equipment state is a convenient mechanisms, including the possibility of using relatively simple calculation algorithms, which allows analyzing large amount of parameters at interval under the constraints of computational resources.

3 Problem Statement

The objective of the research is defining the criteria for estimation of the thermal power equipment life decrease rate and determine the most influencing technological parameters by their actual values.

One of the computational tasks of thermal power plant automated control system (ACS) is critical parameters overriding monitoring at both stationary and transient processes. The examples are steam boiler set surface and superheated steam temperature, power equipment metal temperature field non-uniformity, temperature change rate, working medium chemical composition, vibrations, etc. The deviation of the parameters leads to faster power equipment component life decrease rate. The significance of the process values deviation at life decrease is defined by both deviation range and duration. At stationary power equipment operation condition, the subject matter can be the normalized parameters deviation, wherein its duration is significant. At transient processes, including the significant power change, unit starts, and stops, deviation duration usually effects less, the parameter values and their change rate are more significant.

4 The Technique for Estimation of Life Decrease Rate

To estimate the life decrease rate and provide early warning of a possible power equipment malfunction, the algorithm based on the analysis of the technological parameter that directly affect the life is proposed. The basis of the proposed algorithm is to determine the interval within which the parameter deviates in different ranges from the nominal value.

The algorithm output parameters are actual parameter values at the observed time interval, parameter nominal value, number of intervals of estimation n , and the range of each interval.

The algorithm returns the duration of values being within the intervals, which can be represented as $n + 1$ -dimensional column-vector

$$\vec{\tau} = \begin{pmatrix} \tau_0 \\ \tau_1 \\ \vdots \\ \tau_n \end{pmatrix}, \min \tag{1}$$

Let us consider the weight coefficients ξ identified as

$$\xi_i = 1 - e^{-i/n}. \tag{2}$$

The physics of the weight coefficients are in regulating the parameter contribution into equipment component life decrease when the values are above the nominal over the certain degree.

In this case for the observed n number of estimation intervals, we shall obtain the $n + 1$ -dimensional vector of weight coefficients

$$\hat{\Xi} = \begin{pmatrix} 0 \\ \xi_1 \\ \vdots \\ \xi_n \end{pmatrix} \quad (3)$$

Based on (1) and (3), it is possible to obtain T_{ad} value, expressed in time unit,

$$T_{ad} = \hat{T}^T \cdot \hat{\Xi} = \begin{pmatrix} \tau_0 \\ \tau_1 \\ \vdots \\ \tau_n \end{pmatrix}^T \cdot \begin{pmatrix} 0 \\ \xi_1 \\ \vdots \\ \xi_n \end{pmatrix} \quad (4)$$

Parameter T_{ad} defines the additional contribution into faster equipment component life decrease rate.

It is proposed to define the equipment component service life index (SLI) θ

$$\theta = (T - T_{ad})/T, \quad (5)$$

where T —expected thermal power equipment component life before repair.

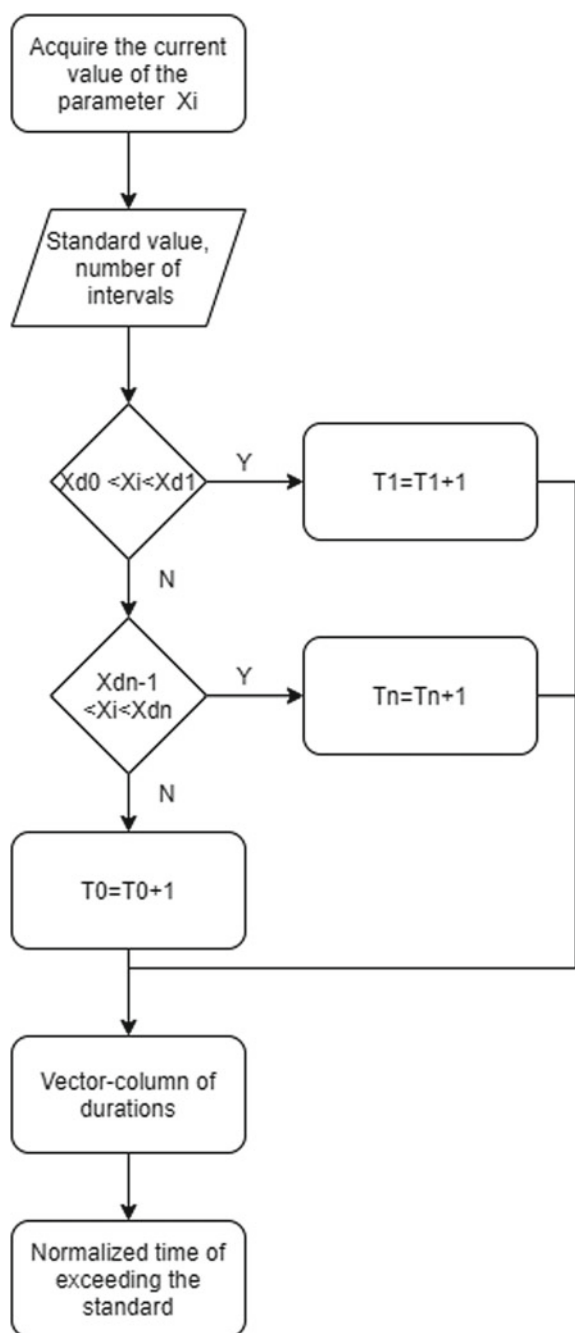
SLI is a universal complex index of equipment operation condition and directly effects the power equipment repair scheduling and extending operational life.

The SLI estimation algorithm is presented in Fig. 1.

The main phases of the algorithm are input data preprocessing and calculations at the observed interval.

The data preprocessing is executed by programmable logical computers (PLC) and includes actual analog signal values validation and technological state indicators. The actual values validation of the original analog signals is performed to assess the possibility of their use in the algorithm and is implemented by evaluating whether the values belong to a given range. If the values are rejected beyond the verification range, the parameter is considered invalid and no further calculation is performed. Signs of the technological situation are used to determine the possibility of carrying out the calculation, taking into account the operating mode of the power equipment. Signs are formed on the basis of the original discrete and analog signals by means of logical operations. The example of the indicators are “unit is in nominal operation mode,” “unit in single casing mode,” etc.

The second phase of the estimation is calculation at a given interval can be performed both at the PLC level, and at the level of server applications or SCADA

Fig. 1 SLI estimation diagram

systems. The source of information for this stage of calculation is a database of archived values of technological parameters. All the necessary source information is loaded from the database for a given time interval, after which the actual calculations are performed.

The proposed method is relatively simple to implement on the existing technical means of the automated process control system, since it does not require complex calculations. Currently, the number of technological parameters to be evaluated using the proposed approach is on average about 80 for a power unit, these are the metal temperatures of the heating surfaces of the boiler, turbine, superheated steam temperature, and indicators of the chemical composition of the working fluid. However, the scalability of the algorithm allows you to increase the number of parameters considered indefinitely.

5 Application of the Technique

Let us consider the example of application of the proposed technique for 300-MW fuel oil thermal power unit with non-circulation boiler. The values of the boiler set intermediate radiation section (IRS) rear wall temperature over a period of 120 h is presented in Fig. 2. The regulatory value of IRS rear wall temperature is 405 °C; by the figure, it can be observed the temperature override over a continuous-time intervals.

Let us split the upper range into nine sub-ranges with 10 °C bandwidth. In this case, the weight coefficient vector is

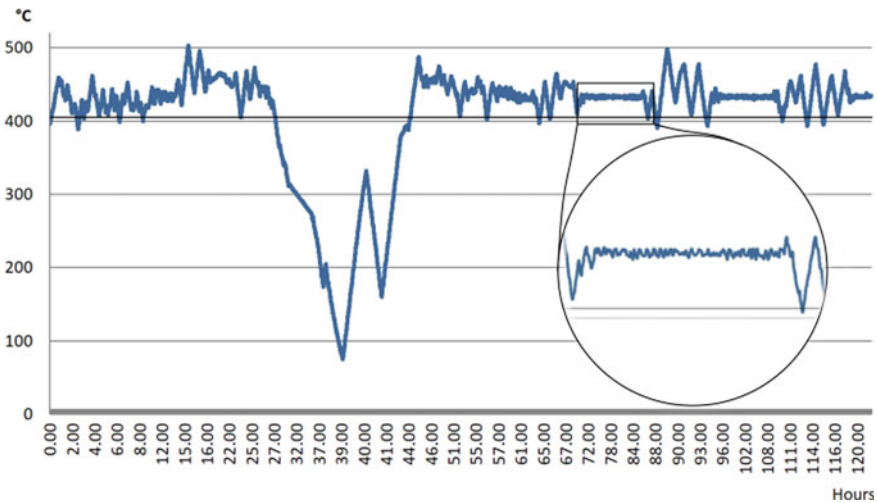


Fig. 2 IRS rear wall temperature trend

$$\hat{\xi} = \begin{pmatrix} 0 \\ 0.118 \\ 0.221 \\ 0.313 \\ 0.393 \\ 0.465 \\ 0.528 \\ 0.583 \\ 0.632 \end{pmatrix}$$

For the interval under observation, the vector of IRS rear wall temperature override duration is the following (in minutes):

$$\hat{\tau}_T = \begin{pmatrix} 990 \\ 180 \\ 60 \\ 3960 \\ 1710 \\ 210 \\ 100 \\ 60 \\ 20 \end{pmatrix}$$

In this case, according to (4), IRS rear wall temperature override speeds up the equipment life decrease rate for 2144 min at the observed interval.

Also, in the paper, the high-pressure cylinder cutout valve temperature change is consider at a period of 141 h. The maximum regulatory cutout valve temperature is 450 °C and during the values analysis the temperature above limit values was over 100 °C at the continuous time interval. The similar calculations show that the additional contribution into increasing equipment life decrease rate due to the regulatory temperature override of high-pressure cylinder cutout valve is 4050 min at the observed interval.

The application of the proposed approach to the analysis of resource changes will allow you to quickly monitor the technological situation in a visual form and take measures to eliminate deviations or plan equipment repairs. An additional step to improve the effectiveness of the proposed approach is the automated determination of the parameters that most affect the monitored indicators at the current time.

6 Estimation of the Technological Parameter Influencing on Control Values

The above-mentioned control values, which impact the equipment life, depend on a fairly large number of other actual process values. For instance, the turbo set metal temperature difference is commonly defined by load increase rate, current steam flow, and temperature at turbine, etc. Herewith, not all the input parameters effect the result equally and some of them can not be regulated online. Therefore, the task of automated prioritizing process parameters by their impact on the control values for building an expert system, which can assist an operator in power equipment monitoring, is crucial.

To analyze the technological parameter influence on the control values random forest is proposed, which is one of machine learning algorithm, often applied to estimate predictor importance. Applying such an approach requires splitting the obtained data into training and test sets and fitting the model with the former one and estimating its efficiency to predict the value with R^2 score for given input features using the last one. If the model accuracy is sufficient, then that model is used to estimate the technological parameter influence.

In the research, the comparison of results obtained by applying the above-mentioned method to analyze the turbine of 300-MW steam-power unit with non-circulation two furnace boiler and steam turbine of 310-MW steam-gas unit is presented. The predictors are superheated steam temperature on exit from the boiler, steam pressure before the cutout valve and turbine steam flow. The regressors are temperature and turbine metal temperature change rates taken at different parts of the turbine. The dataset contains values at a period of 140 h, including transient process. The data were retrieved from the unit ACS historical database and their size vary from 1500 to 12,000 values per parameter.

For each regressor a model was built, therewith each model accuracy is at least 99%. The feature importance was calculated for the full dataset without splitting using permutation feature importance, which means consequent shuffling each of the predictor values when the other ones are in original order. The results of parameter influence estimation of main steam temperature (T_s), steam pressure before the cutout valve (P_s), and turbine steam flow (F_s) on turbine metal temperature and turbine pin stud temperature are illustrated in Figs. 3 and 4, respectively.

The result repeatability shows the possibility of applying the machine learning methods for carrying out the analytical assessment of technological process behavior, including defining the most significant parameters. The mentioned method allows forming an approach to develop the algorithm, which assists an operator in monitoring power equipment at both nominal operation and transient and start processes.

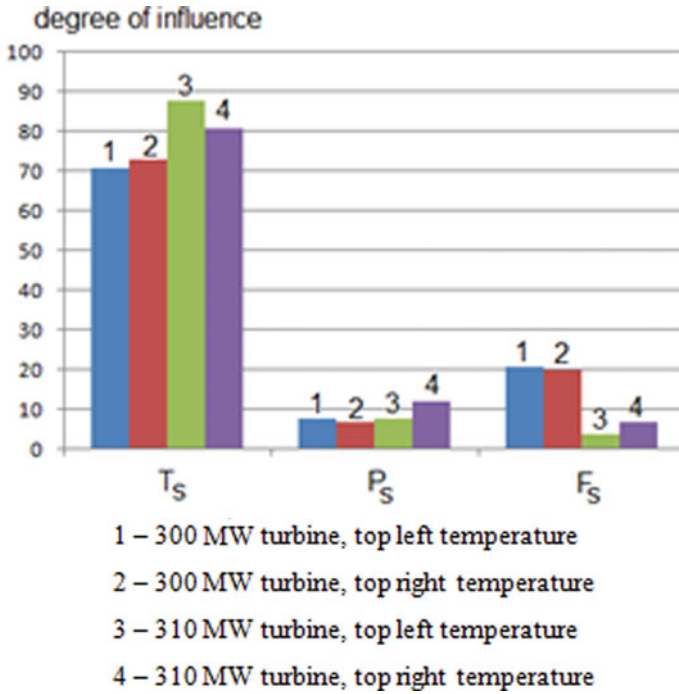


Fig. 3 Input parameter influence on turbine metal temperature

7 Results and Discussion

Checking the functioning of the proposed method for determining the technical resource index on real data from the archive of the automated process control system of a thermal power plant shows the possibility of using the proposed method for analyzing the power equipment operating mode. The relative simplicity to implement the approach allows getting an intuitive universal indicator of power equipment life decrease rate for scheduling its diagnostic and repair.

Applying the machine learning methods to analyze the technological parameters allows determining the process-specific features in real-time scale, which provides an approach for designing an operator assistance systems.

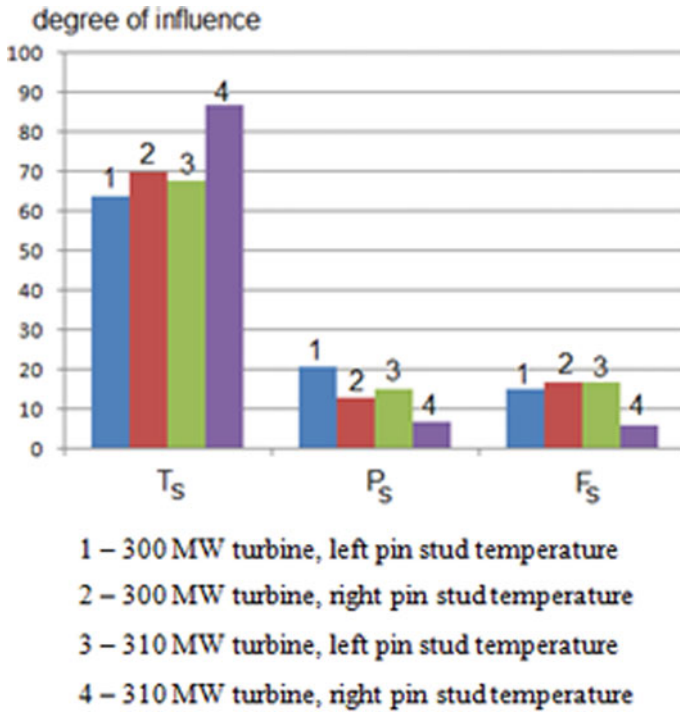


Fig. 4 Input parameter influence on turbine pin stud temperature

Acknowledgements The research is funded by Russian Federation public contract No FSWF-2020-0025 “Technique development and method analysis for ensuring power system object security and competitiveness based on the digital technologies.”

References

1. Jagtap, H., Bewoor, A.: Use of analytic hierarchy process methodology for criticality analysis of thermal power plant equipments. *Proceedings* **4**, 1927–1936 (2017)
2. Zhang, W., Liu, J., Gao, M., Pan, C., Huusom, J.K.: A fault early warning method for auxiliary equipment based on multivariate state estimation technique and sliding window similarity. *Comput. Ind.* **107**, 67–80 (2019)
3. Farhadzade, E., Muradaliev, A.Z., Farzaliev, Y.: Internal benchmarking of thermal power plants of electric power systems. *Energy* **63**(6), 541–553 (2020)
4. Savostyanova, L., Litvak, V.: Resource analysis of steam turbines based on production cycles. *321*(4), 11–15 (2012)
5. Widarsson, B., Dotzauer, E.: Bayesian network-based early-warning for leakage in recovery boilers. *Appl. Therm. Eng.* **28**(7), 754–760 (2008)
6. Wang, L., Chua, J., Wub, J.: Selection of optimum maintenance strategies based on a fuzzy analytic hierarchy process. *Int. J. Prod. Econ.* **107**, 151–163 (2007)

7. Bevilacqua, M., Bragliab, M.: The analytic hierarchy process applied to maintenance strategy selection. *Reliab. Eng. Syst. Safe.* **70**, 71–83 (2000)
8. Sergaki, A., Kalaitzakis, K.: A fuzzy knowledge based method for maintenance planning in power system. *Reliab. Eng. Syst. Safe.* **77**, 19–30 (2002)
9. Bertolini, M.: Fuzzy VIKOR criticality analysis approach for FMECA technique. *Safe. Reliab. Manag. Risk* **5**, 101–107 (2006)
10. Singh, R.K., Kulkarni, M.S.: *Int. J. Ind. Eng. Technol.* **3**, 1–14 (2013)
11. Adhikary, D., Bose, G.: Multi criteria FMECA for coal-fired thermal power plants using COPRAS-G. *Int. J. Q. Reliab. Manage.* **31**, 601–614 (2014)
12. Suebsomran, A.: Critical maintenance of thermal power plant using the combination of failure mode effect analysis and AHP approaches *Asian. Int. J. Sci. Technol. Prod. Manuf. Eng.* **3**, 1–6 (2010)
13. Sultanov, M., Trukhanov, V., Gorban, Y.: High value heat-power equipment component test planning with time-series technique at single reliability level. *Electr. Power Eng.* 9059231 (2020)
14. Dokas, I., Karras, D., Panagiotakopoulos, D.: Fault tree analysis and fuzzy expert systems: early warning and emergency response of landfill operations. *Environ. Modell. Softw.* **24**(1), 8–25 (2009)
15. Yasniy, O., Pyndus, Yu., Iasnii, V., Lapusta, Y.: Residual lifetime assessment of thermal power plant superheater header. *Eng. Fail. Anal.* (2017)
16. Li, M., Benaarbia, A., Morris, A., Sun, W.: Assessment of potential service-life performance for MarBN steel power plant header under flexible thermomechanical operations. *Int. J. Fatigue* (2020)
17. Yasniy, O., Pyndus, Yu., Brevus, V., Iasnii, V., Lapusta, Y.: Lifetime estimation of superheater header. *Procedia Struct. Integrity* **2** (2016)
18. GOST 24278-2016, Stationary steam turbine units for driving electric generators of thermal power plants. *General Technical Requirements* (2016)
19. RD 10-577-03, Standard instructions for metal control and service life extension of the main elements of boilers, turbines and pipelines of thermal power plants

Multichannel Majority System for Detection and Prevention of Emergency Modes of Gas Pumping Unit Filters



Marina Tyurina, Alexander Porunov, Alexander Nikitin, Rimma Zaripova, and Gulia Khamatgaleeva

1 Introduction

Safe and uninterrupted pumping of natural gas is impossible without an efficient operation of gas pumping units (GPU). Among the main functions of automatic control systems (ACS) of a GPU, high-precision implementation of such important functions as stabilization of operating parameters, direct fuel control of gas turbine engines, anti-surge control of a compressor (blowers), distribution of loads between jointly and in parallel operating GPUs, etc.

At present, OJSC «Gazprom» has developed a concept according to which the newly created ACS by technological objects of pumping stations (PS) and the GPUs that are part of them should be developed as an exclusively multilevel, hierarchically integrated system built based on a single software and algorithmic base. The use of the latest algorithms for the implementation of the listed functions should allow achieving significant economic results [1, 2]: reducing the consumption of fuel gas and electricity, increasing the resource of technological equipment, reducing the number of emergency shutdowns of GPUs, etc. [2, 3].

The inlet air path of the GPU includes the following main elements: an air-cleaning device (ACD) with a combined filtration system (CFS), a suction noise dampening unit, a suction unit, a cyclic air heating system, and a cyclone unit heating system [4, 5]. Reliable operation of GPU driven by a converted aircraft gas turbine engine

M. Tyurina (✉) · A. Porunov · A. Nikitin
Kazan National Research Technical University named after A.N. Tupolev-KAI, 420111 Kazan, Russia
e-mail: MMTyurina@kai.ru

R. Zaripova
Kazan State Power Engineering University, 420034 Kazan, Russia

G. Khamatgaleeva
Kazan Cooperative Institute, 420081 Kazan, Russia

(GTE) is largely determined by the quality of cleaning and preparation of cycle air [3–5], which is provided by air-cleaning devices in the inlet air duct (IAD) [1–6].

Thus, two aspects affect the effectiveness of the use of automated GPU. The first aspect is inextricably linked with the solution of the problem of information support of channels for the formation of informative signals and control actions when solving the problem of detecting and countering the deviation of the GPU operating parameters from the specified values. The second aspect is the timely determination of the need to replace filters in the air-cleaning devices of the GPU.

2 Materials and Methods

Solving problems of identifying and predicting emergencies in the work of GPU, the following methods are known: the theory of fuzzy sets [7], neural network technologies [8], a hierarchical model method [9], and methods for identifying GPU malfunctions by functional characteristics [10]. The use of these methods in assessing the technical condition (TS) of GPUs will require the development and application of rather complex software implemented using modern computing facilities. This will ultimately reduce the efficiency and validity of the decisions made when countering the development of emergencies in the work of the GPU.

The paper proposes the use of the method of parametric analysis of the dynamic characteristics of the GPU ACD, obtained from the results of current measurements of the GPU operating parameters [11]. At the same time, in real operating conditions of the GPU, as shown in the works of Antipov et al. [12], Grinchuk [4], Gavrilyuk et al. [7], Ulybin [13], Konovalov and Agafonov [14], and other researchers [1, 5–7, 15], the most important in identifying and countering the proximity of the ACD operating parameters to the critical values are [6, 7, 14]:

- icing of the elements of the ACD air inlet;
- clogging of elements of the ACD inlet air path by dust and other particles;
- increase in relative humidity (over 60%);
- lowering the air temperature (below +5 °C).
- dynamics of changes in the air pressure drop across the ACD filters and the pressure behind the cyclone unit.

When assessing the technical condition of the GPU, preference is given to the parametric method [10, 12, 16], and in this work it is proposed to assess the technical condition of the GPU based on the following parameters of the ACD GPU:

- vacuum p_{suc} in the suction chamber (less than –1.6 kPa);
- compressor rotation frequency n (5000–7000 rev. per min);
- pressure p_{CU} of air behind the cyclone unit (below –680 Pa);
- pressure p_{ACD} of air in ACD (below –680 Pa);

- differential pressure Δp_f across the filter elements (calculated parameter, the difference between the air discharge behind the cyclone unit and the air rarefaction in the ACD) (above 320 Pa);
- temperature T_{amb} of ambient air (entering the ACD) (below +5 °C);
- humidity Ψ_{amb} of ambient air (included in ACD) (over 80%);
- position of bypass valves, entrance doors (open, closed);
- position of the damper of the anti-icing system (AIS) ACD (open, closed);
- position of the damper of the AIS inlet guide vane (IGV) (open, closed);
- status of dust extraction fans (on, off).

Determination of the technical state of the inlet air-cleaning tract and the gas tract of the compressor unit supercharger (as well as an axial compressor when using a gas turbine drive) is carried out by the methods of functional diagnostics [1, 17], based on the analysis of measurement results of deviations of the main measured operating parameters (features), and the parametric method analysis.

A comprehensive assessment of the technical state of potentially dangerous elements of a technical system during operation is mainly based on the structural model of the functioning processes, which includes thermogasdynamic parameters and characteristics. The success of diagnostics is largely due to the correct choice of informative components for the construction of fundamental diagnostic models of the object and models of recognition and identification of signals from measuring systems.

To implement the process of recognizing and assessing the current state of the GPU as a system during operation, it is first of all necessary to solve the problem of classifying and describing their features. The number of classes in the assessment depends on how reliably and fully all the states of the GPU that are close to emergencies are described, which have clearly expressed signs in the form of a characteristic change in the parameters of the working process of both ACD and the parameters of the supercharger drive motor. To formulate and solve the recognition problem, the assumption is made that all faults can be combined into a finite number of classes, each of which is characterized by a finite number of features [10]. Deviations of operating parameters from nominal ones belong to a certain class. For example, detection of loss of stability and surge, in the gas-air path of the turbocharger, manifested by an increase in the temperature at the inlet of the engine VNA, a decrease in speed n , etc. Revealing the limiting values of parameters close to emergency ones, especially the parameters of the ACD and IGV flow paths, makes up about 60% of reliable information on the state of the gas-air duct of the GPU.

Therefore, to timely obtain information about the state of the flow path and the nature of the gas flow, it is necessary to assess the current parameters of the working elements that form the gas flow, the deviation of which from the permissible standards can lead to the failure of ACD units and assemblies and the compressor drive motor. Among these methods, the method of parametric analysis of the structural model of the GPU operation process (ACD and the gas-air path of the turbocharger) is used in this work.

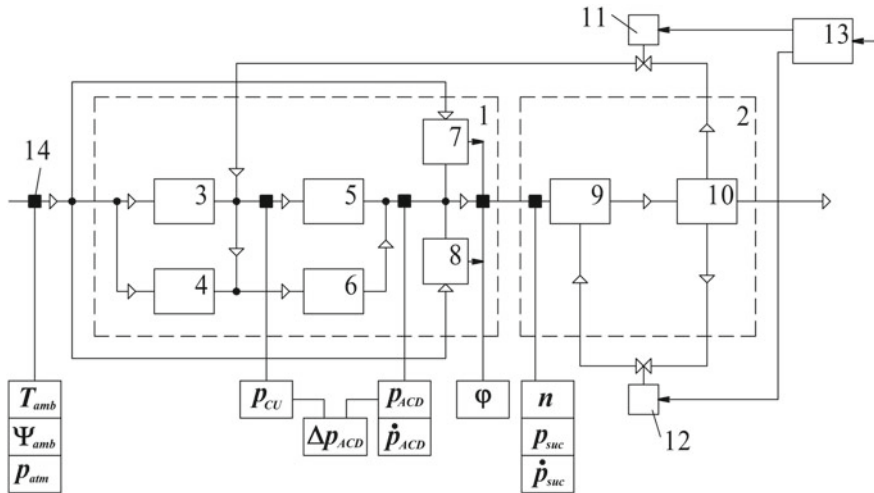


Fig. 1 The structural model of the process of functioning of the GPU inlet air duct: 1—air cleaning device (ACD); 2—engine; 3, 4—blocks of cyclones; 5, 6—fine cleaning filters; 7, 8—bypass valves; 9—engine suction chamber; 10—inlet guide vane (IGV) of the engine; 11—damper control unit AIS ACD; 12—damper control unit AIS IGV; 13—ACS AIS; 14—points of measurement of the operating parameters of the GPU

Figure 1 shows a structural model of the GPU air intake process, illustrating the location of the control points of parameters and actuating mechanisms of the GPU air intake duct.

The inlet air duct is equipped with control and measuring devices, which provide signals to the automatic control system (ACS) of the gas pumping unit and ensure control of the above parameters.

As a result of the above factors, at an ambient temperature below $+5\text{ }^{\circ}\text{C}$ and in conditions of high humidity, the likelihood of icing, clogging increases, which leads to an increase in the air pressure drop across the combined filter systems. At the same time, there is a significant decrease in pressure at the inlet of the IGV of the aircraft engine, which can lead to dangerous and emergencies in the operation of the GPU. To prevent damage to the drive motor, it is necessary to generate an alarm (optical and acoustic), according to which the operator can perform a forced shutdown of the GPU engine. If an emergency is missed for 1000 s, the ACS of the GPU generates a forced engine shutdown signal. Besides, to counter the icing process of the combined filter system and the inlet of the cyclone unit in case of significant changes in the climatic parameters of the atmosphere, as well as in the transitional modes of the GPU operation (with fluctuations in the pressure p_{atm} , temperature T_{amb} , the humidity Ψ_{amb} of atmospheric air, and the speed of the GPU drive n), it is necessary to determine not only the current values of climatic parameters but also the rate of their change.

Thus, the law of the formation of the informative signal $\Phi(\theta)$ should include components that reflect not only the statics but also the dynamics of these parameters change according to the model of the operation process of the inlet air duct of the GPU (Fig. 1). In the last decade, the issues of predicting the technical state of GPUs have been intensively studied, which are implemented in the framework of fundamental research and the works of specialized organizations [7, 8, 10].

The implementation of informative signals on the pressure drop and the rate of its change in the gas-air ducts of the ACD and IGV GPU will make it possible to predict and quantify the time interval

$$t_{pr} = \frac{\Delta p_{ACD}}{\Delta \dot{p}_{ACD}} \text{ or } t_{pr} = \frac{p_{suc}}{\dot{p}_{suc}}, \tag{1}$$

necessary to take measures to counter the dangerous development of an emergency in the operation of the GPU.

In this work, for the formation of informative signals $\Phi(\theta)$ when deciding to stop an aircraft engine $\Phi_{stop}(\theta)$ or form a control signal of the AIS $\Phi_{AIS}(\theta)$, it is we propose to use quorum elements [18] for the processing of measurement signals for each factor that affects the GPU operation mode. It is proposed to be implemented within the framework of structural diagrams (Figs. 2 and 3) [10] in the form of the following laws of formation of the informative signal:

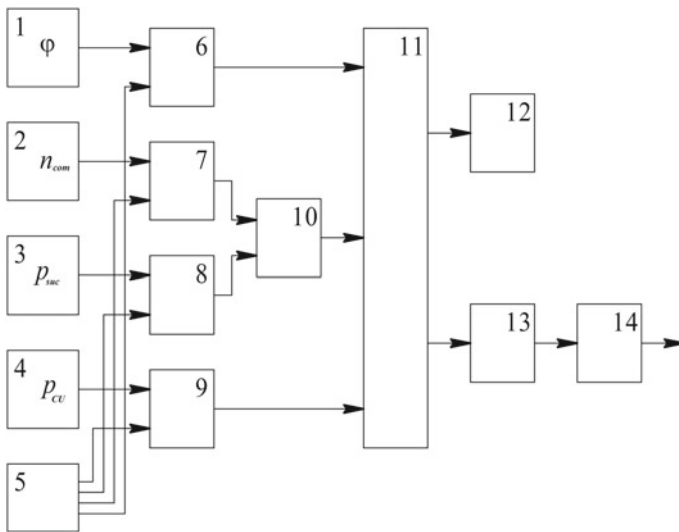


Fig. 2 Structural scheme of the control signal generation for the forced engine stop: 1—bypass valve position sensor; 2—engine compressor speed sensor; 3—pressure sensor in the suction chamber; 4—pressure sensor in the cyclone unit; 5—critical operating parameters setting block; 6–9—comparison elements; 10—logical element OR; 11—quorum-element; 12—alarm block; 13—block of time delay; 14—ACS GPU of forced engine shutdown

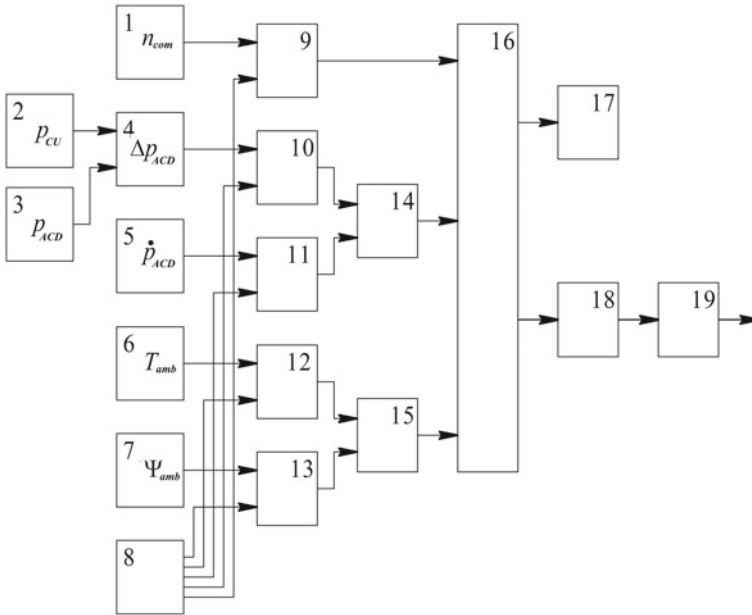


Fig. 3 Structural scheme of the AIS control signal generation during icing or clogging of ACD filters: 1—engine compressor speed sensor; 2—pressure sensor in the cyclone unit; 3—pressure sensor at the ACD outlet; 4—calculator of pressure drop at the ACD outlet; 5—sensor for the rate of pressure change at the ACD outlet; 6—ambient temperature sensor; 7—ambient humidity sensor; 8—block-setter of critical values of operating parameters; 9–13—comparison elements; 14, 15—logical element AND; 16—quorum-element; 17—alarm block; 18—block of time delay; 19—ACS AIS

$$\begin{aligned} \Phi_{stop}(\theta) &= K_{\Delta\phi} \Delta\phi + K_{p_{suc}} \Delta p_{suc} + K_{\Delta n} \Delta n + K_{\Delta p_{CU}} \Delta p_{CU}; \\ \Phi_{AIS}(\theta) &= K_{\Delta n} \Delta n + K_{\Delta p_f} \Delta p_f + K_{\Delta \dot{p}_f} \Delta \dot{p}_f \\ &\quad + K_{\Delta T_{amb}} \Delta T_{amb} + K_{\Delta \Psi_{amb}} \Delta \Psi_{amb} + K_{\Delta \phi} \Delta \phi, \end{aligned} \tag{2}$$

where $K_{\Delta\phi}$, $K_{p_{suc}}$, $K_{\Delta n}$, $K_{\Delta p_{CU}}$, $K_{\Delta p_f}$, $K_{\Delta \dot{p}_f}$, $K_{\Delta T_{amb}}$, $K_{\Delta \Psi_{amb}}$ —coefficients of influence of factors that determine the proximity of operating parameters to critical values. Influence factors can be determined based on the test results by the methodology [13].

In most of the well-known works [6, 7, 14, 19], there are no studies on the information support of the law of formation of the control and alarm signals for forecasting and warning of the approach of an emergency in the operation of the GPU.

3 Results and Discussions

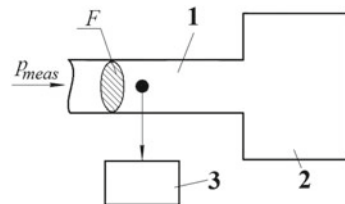
The presented work solves the issues of comparative analysis of methods and schemes for the forming of basic signals by the pressure drop across the ACD filters and the rate of its change basis on the research of the authors [20, 21] and generalization of the works of other researchers [22].

Analysis of publications [22, 23] devoted to the development and research of methods and means for measuring pressure and the rate of its change in closed (airtight) objects shows that their spectrum is quite wide and varied. In each of these devices, which are used to measure the rate of change of pressure, in the chain of transformation of the informative parameter, the operation of differentiating the signal by pressure is carried out. Pressure rate converters, in which the signal is continuously differentiated, can be divided into two subgroups according to the sequence of conversion of the original signal. The first subgroup includes devices in which pneumatic differentiation of a signal is carried out with its subsequent transformation into an informative signal of another type of energy. The second subgroup includes devices in which the primary (pneumatic) signal is first converted into an electrical signal, which is then differentiated. In the second case, the conversion of the pneumatic signal by pressure is carried out by mechanical, electromechanical, or thermoelectric converters. Mechanical and electromechanical transducers contain an aneroid box with a kinematic, potentiometric, inductive, or other transducers of the membrane deflection value into a movement or an electrical signal. Pneumatic differentiation is carried out, as a rule, on the elements «throttle—capacitance», and as a pneumatic container, a blind or flow-through chamber can be used. The output signal of the differentiator is either differential pressure or gas flow.

The analysis of the features of the implementation of the hot-wire method of measurement in the sensor for measuring pressure and the rate of its change will be carried out for the variant shown in Fig. 4. The sensor contains a blind cavity 1 connected to a variable pressure through channel 2. A change in the measured pressure entails a change in pressure in cavity 1. For in the case of a constant amount of air when it is compressed due to a volume change, the relationship between the parameters can be written using the Clapeyron equation:

$$V = \frac{m}{\mu} RT \frac{1}{p}, \tag{3}$$

Fig. 4 Schematic diagram of the pressure rate meter



where p, V, m —pressure, volume, and mass of air in the cavity; μ —molecular weight; R —gas constant, T —air temperature.

When the pressure changes, the volume occupied by a constant amount of air changes. Air flows through a channel of constant cross-section F , therefore, a change in the volume occupied by a constant amount of air can be considered as a movement along the channel of cross-section F , the air mass m in the cavity, at a distance Δl . The change in volume ΔV over the time interval Δt corresponds to the movement of this air mass of volume ΔV along the pipeline at a speed: $W = \frac{\Delta l}{\Delta t}$.

Let us differentiate expression (3) in time at $m = \text{const}$:

$$\frac{dV}{dt} = -\frac{W}{p} \frac{dp}{dt}. \quad (4)$$

A minus sign means that a positive increment in pressure corresponds to a negative increment in volume. Expressing the volume increment dV through the section of the channel F and the displacement of the section dl and denoting it $\frac{dp}{dt}$ through \dot{p} , we get

$$F \frac{dl}{dt} = -\frac{W}{p} \dot{p}. \quad (5)$$

Then the air flow rate in the pipeline:

$$W = -\frac{V \dot{p}}{F p}. \quad (6)$$

Taking into account that the air density $\rho = p/RT$ [22] and the mass air flow rate $G = WF\rho$, from (6) we can get

$$G = \frac{V}{RT} \dot{p}. \quad (7)$$

From expression (7), it follows that the mass flow rate of air in the pipeline connecting the blind chamber with a source of varying pressure is proportional to the rate of change of the measured pressure. By measuring the air flow rate in the pipeline, one can judge the rate of pressure change.

Thus, in a device consisting of a blind cavity connected by a channel with variable pressure, the values proportional to the rate of pressure change can be the pressure drop and the mass air flow through the channel, which communicates the blind chamber with pressure in the cyclone unit and ACD. If you choose a pressure drop as an informative signal, then such a device is made based on a combination of a variometric measurement method with the subsequent conversion of the pressure drop into a mass air flow through the communicating channel, which is measured using a hot-wire anemometer.

The hot-wire pressure-rate transducer is characterized by a temperature error, which occurs as a result of the fact that the power dissipated by the thermistor depends on the temperature difference between the air and the thermistor. However, it is not large, since the thermistors operate in constant temperature mode at $t = 150\text{ }^{\circ}\text{C}$. Besides, various schemes for compensating the temperature error are possible, for example, by introducing a signal proportional to the temperature into the measuring circuit, obtained using an additional thermistor. An error caused by a change in the air temperature in a dead chamber due to heat exchange through its walls can be eliminated by improving the thermal insulation of the chamber walls or by using an active thermostatic system.

The most convenient for measuring the mass flow rate in the channel connecting the non-flowing chamber with changing pressure are jet-convective converters (JCC) [23], which convert the mass flow rate of the gas into an electrical signal. The JCC is structurally made in the form of a module containing a nozzle that forms a jet that washes the anemosensitive element (ASE).

This design, in comparison with the placement of the ASE directly in the flow channel of the system sensor, not only provides a reliable measurement but also significantly reduces the dependence of the measurement result on the hydrodynamic error, which is inherent to a large extent to the hot-wire method of measurement [23].

The paper presents the results of the development of a jet-convective system for measuring pressure and the rate of its change based on jet-convective converters with a measurement range of $\pm 266\text{ Pa/s}$ (2 mmHg/s). The structural scheme of such a system is shown in Fig. 5 [24]. The study of the prototype of the system showed that it has several advantages over variometric and pulse converters, despite their simplicity of the circuit diagram and design. They have five times better response

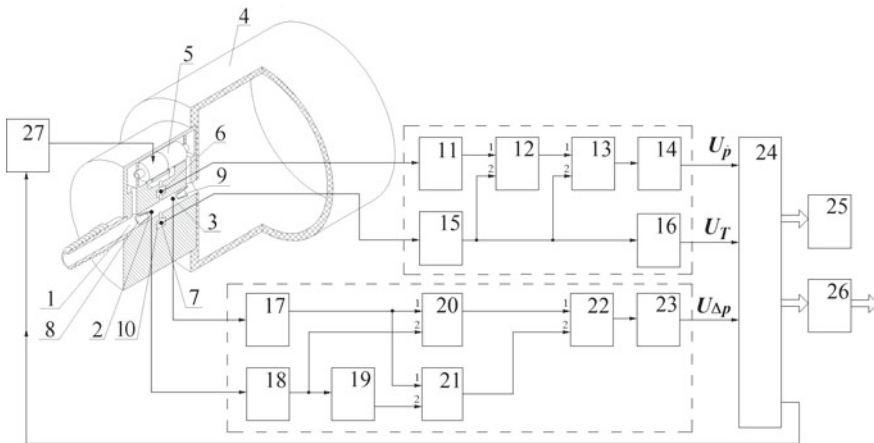


Fig. 5 Structural scheme of the sensor for measuring pressure and the rate of its change (denoted: 1–10—structural elements of the sensor for measuring pressure and rate of change; 11, 15, 17, 18—measuring circuits; 12, 20, 21—adder; 19—inverter; 14, 16, 23—low-pass filter; 13, 22—dividing devices; 24—microcontroller; 25—alarm unit; 26—ACS; 27—micro-blower drive control unit)

speed ($\tau = 0.1$ s) and almost an order of magnitude better response threshold ($\dot{p}_{\min} = 0.02$ Pa/s). The advantages also include an electrical signal based on the rate of pressure change.

An increase in the metrological characteristics of the jet-convective system for measuring pressure and the rate of its change is achieved due to the arrangement of pneumatic channels with ASE near the pneumatic outputs of the micro-blower 5. This, on the one hand, improves the dynamic characteristics of the system by reducing the length of the pneumatic channel communicating the control object (pressure source) with the blind chamber 4 of the pressure measurement system and the rate of its change, as well as reducing the response threshold (increasing sensitivity) by introducing a micro-blower 5, providing a displacement of the operating point of the ASE to the section of its characteristics with a high steepness.

The presented construction of the system for measuring pressure and the rate of its change also makes it possible to reduce the errors associated with the technological scatter of the ASE parameters. This is achieved by introducing two ASEs 6 and 7, the first of which is measuring and is placed in the channel that combines the positive outputs of the overpressure of the micro-blower 5 with a flow channel that communicates the dead chamber 4 with the gas-dynamic object and in which the first 2 and the second 3 ASE are located measuring the rate of change in pressure, and the second—compensating ASE 7 is placed in a non-flowing cavity 10. The voltage at the output of the measuring U_{meas} and compensating U_{com} pressure-dependent ASE is determined by the expressions, respectively:

$$U_{\text{meas}} = U_{0\text{meas}} + \gamma_{0\text{meas}}\rho V_H, \quad (8)$$

$$U_{\text{com}} = U_{0\text{com}}, \quad (9)$$

where $U_{0\text{meas}}$, $U_{0\text{com}}$ is the initial voltage at the output of the measuring U_{meas} and compensating U_{com} ASE, respectively; $\gamma_{0\text{meas}}$ —proportionality coefficient; ρV_H —mass velocity of the flow that washes over the measuring ASE, which operates on pressure.

The pressure (density) output signal is determined by the relationship

$$\Delta U = U_{\text{meas}} - U_{\text{com}} = \gamma\rho V_H, \quad (10)$$

where the density ρ under the condition of the passive or active thermostat of the blind chamber is proportional to the pressure in the gas-dynamic object, i.e., is determined by the expression $\rho = p/gRT$ (denoted by pressure p in a gas-dynamic object; gravitational acceleration g ; gas constant R ; temperature T).

When the pressure changes at a certain rate in the gas-dynamic object communicated with the flow channel 1, a pressure drop arises between blind chamber 4, and the controlled gas-dynamic object. As a result, air flows, the direction of which is determined by the sign of the rate of pressure change in the controlled gas-dynamic

object. For example, with a positive rate of change of the controlled pressure, the direction of the airflow is such that the first ASE 2 is washed first, and then the second ASE 3. In this case, the first ASE 2 is washed by a directed jet formed by the shaping nozzle 8 and thus having a higher blowing speed than the second ASE 3. At the output of the measuring circuits for switching on these ASEs, voltages U_1 and U_2 are formed, respectively. After processing the voltages U_1 and U_2 by the algorithm determined by the structural diagram (Fig. 5), digital signals about the pressure, as well as about the sign and rate of pressure change in the gas-dynamic object, are generated at the system output.

4 Conclusion

The paper shows the importance of developing new methods to recognize the current technical state of GPU based on the analysis of a set of parameters by all heterogeneous gas-thermodynamic parameters, characterizing both static and dynamic processes. A new set of monitored parameters is substantiated and presented by the structural diagram of the GPU, which shows the selection points of the mode parameters. This set includes new gas-dynamic parameters that control pressure, pressure drops, and their rate of change both in the channels of the combined filter system and in the channels of the engine inlet guide vanes. In this case, based on the proposed structural schemes of formation of control signals, the task of current control of GPU parameters and prediction of the moment of approaching the current value of monitored parameters to their maximum permissible values was solved. This allows the GPU operator to decide on the need to take measures to counter the development of an emergency. The results of the structural and circuit design of the module for measuring gas-thermodynamic parameters (p_{suc} , Δp , T , $\Delta \dot{p}$), built on ASEs, are presented. Measurements of integral and dynamic operating parameters will allow determining and predicting the “time to failure” interval t_{pr} , which can be used as a justification for the need to replace ACD filters. Carrying out these works will improve the efficiency of the GPU.

References

1. Belavin, M.A., Lazarevich, C.B., Shaikhutdinov, A.Z., Prodovikov, S.P., Nakhshin, G.S.: Experience in creating and implementing automatic control systems. *Gas. Ind* **8**, 58–61 (2006)
2. Shyrmovska, N.G., Levitska, G.I., Zayachuk, Y.I., Mykhajluk, I.R.: Building a knowledge base and its internal rules for an expert gas pumping unit diagnostic system. *Methods. Devices. Qual. Control.* **2**(41), 5–17 (2018). [https://doi.org/10.31471/1993-9981-2018-2\(41\)-5-17](https://doi.org/10.31471/1993-9981-2018-2(41)-5-17)
3. Semushkin, A.V., Podlozny, A.O., Chernikova, E.A., Shchurovsky, V.A.: Methodical grounds for parametric diagnostics of turbine gas-compressor units. *Vesti gazovoy nauki* **1**, 29 (2017)
4. Grinchuk, A.S.: Influence of cycle air parameters and flue gas path aerodynamics on the efficiency of gas turbine and steam gas plants. *Energetika*. In: Proceedings of Higher Educational

- Institutions and Energy Associations of the CIS, vol. 6, pp. 74–81 (2009)
5. Gritsenko, E.A., Klimnyuk, Yu.I., Stepanenko, O.A.: HEU GPA-Ts-16R NK-38 anti-icing system at the Togliattinskaya compressor station. Test results. *Gas. Turbo. Technol.* **4**, 26–29 (2002)
 6. Budusov, V., Kobelev, A., Tokranov, A.: Cycle air heating system for GPU series “Ural”. *Gas. Turbo. Technol.* **3**(13) (2001)
 7. Gavrilyuk, E.A., Mantserov, S.A., Ilichev, K.V., Turikov, M.I.: Support system based on the method of diagnostics and control of the technical state of industrial equipment. In: *IEEE Xplore Digital Library*, 1–7 (2018)
 8. Maksimenko, A.V.: Application of multilayer neural network structures for predicting the technical condition of gas pumping units. In: *IX International Scientific-Practical Conference: Actual Problems of Science*, pp. 71–75 (2013)
 9. Antonova, E.O., Ivanov, I.A.: Application of multilayer neural network structures for predicting the technical condition of gas pumping units of compressor stations. In: *Collection. Report Conf.: Problems of the oil and gas complex of Russia*, pp. 114–115 (1995)
 10. Semenov, A.S., Ivanov, V.A., Kuzmin, S.V., Gimadutdinov, A.R.: identification of malfunctions of gas compressor units by functional features. In: *Coll. Scien. tr. «Oil and gas. New technologies in transport systems»*, pp. 69–74 (2004)
 11. Antonova, E.O., Ivanov, I.A., Stepanov, O.A., Chekardovsky, M.N.: *Monitoring of power units at compressor stations*, (1998)
 12. Antipov, B.N., Egorov, I.F., Bandaletov, V.F., Nogin, E.M.: Operational reliability of the fleet of gas pumping units is the basis for the stable operation of the gas transmission system «Gazprom». *Gas. Turbo. Technol.* **1**, 4–7 (2009)
 13. Ulybin, S.V.: Creation of system structure and control instructions for the information control state monitoring system of the aviation engine air tract at a gas-pumping aggregate. *Vestnik KGTU* **2**, 62–70 (2016)
 14. Kononov, R.N., Agafonov, A.V.: Features of gas turbine air purification systems based on test results and operating experience. *Gas. Turbo. Technol.* **4**, 40–42 (2008)
 15. Muscroft, F.: Impact of the gas turbine cycle air filtration system on operating costs. *Gas Turb. Technol.* **8**, 18–22 (2004)
 16. Kudashev, E.R., Gimadutdinov, A.R.: Features of diagnosing a gas compressor unit. *Sb. “Megapascal Issue 1”*. TSOGU, Tyumen (2005)
 17. Chekardovsky, M.N., Razboynikov, A.A., Ivanov, H.A.: Methodology for diagnosing power equipment. *Sb. «New high technologies for the oil and gas industry and energy of the future»*, 143 (1996)
 18. Braslavsky, D.A., Yakubovich, A.M., Chesnokov, G.I.: Variable structure systems and their application in flight automation problems. *Instrum. Control. Syst.* **3**, 25–28 (1968)
 19. Sammak, M.: Master thesis. Lund University, Sweden, 117 (2006)
 20. Tyurina, M., Porunov, A., Zaripova, R., Gaynetdinova, A., Kosulin, V.: In: *NSRBCPED 2019, Advances in Economics, Business and Management Research*, vol. 131, p. 648 (2019)
 21. Tyurina, M.M., Porunov, A.A.: Device for measuring pressure and its rate of change. *Pat. RF №2518851*, 4 (2014)
 22. Voronin, G.I., Safonov, O.A.: Measuring converters of the speed of pressure change. **89** (1974)
 23. Gainullina, E.Y., Kashin, A.V., Kornev, N.S., Nazarov, A.V.: *Prib. & Tech. Eksp.* <https://doi.org/10.1134/S0032816219030170>
 24. Tyurina, M.M., Porunov, A.A.: Development and research of a jet-convective module based on an anemosensitive element. *Vestnik Bul. KSTU* **4**, 113–119 (2013)

Study of the Properties of Fuel Gas in Gas Turbine Plants Depending on Its Composition



George Marin, Boris Osipov, and Dima Mendeleev

1 Introduction

The program for the development of traditional energy in the Russian Federation provides for an increase in the number of construction of combined cycle power units. According to the energy strategy of Russia until 2035, the priority will be to use gas turbine technologies. The total commissioning of new generating capacities will be 15–18 GW. This includes efficient gas turbines of large unit capacity (160, 400, 500 MW) and combined cycle gas turbines based on them (250–850 MW) with an effective efficiency of up to 63%, as well as mini-CHP plants based on gas turbines (5–15 MW) [1, 2].

The combustion systems in these plants allow gas turbines to operate with a wide range of fuel gases, while maintaining environmental policies and keeping emissions to a minimum. Therefore, fuel combustion systems require special attention to the quality of the fuel and its component composition.

Modern gas turbines are characterized by the combination of quantitative and qualitative control over the entire load range. The first gas turbine engines began to be used in the power industry thanks to aviation. The main function of the control system for adjusting the fuel consumption was reduced to the correct dosage of fuel for the basic and afterburner modes of operation, since the composition of the fuel did not change during the flight of the aircraft, and the emissions depended on the perfection of the combustion chamber. Power gas turbine plants operate in different load ranges and with changes in fuel composition. Therefore, the engine management system plays an important role. Hence, the importance of fuel preparation and fuel

G. Marin (✉) · B. Osipov
Kazan State Power Engineering University, Krasnoselskaya St., 51, 420034 Kazan, Russian Federation

G. Marin · D. Mendeleev
JSC “Tatenergo” Branch “Kazan CHP-2”, Tatsevsкая St., 11, 420036 Kazan, Russian Federation

combustion, which will reduce emergency engine operation and minimize emissions of harmful substances [3–5].

2 Materials and Methods

At the moment, the main type of fuel gas is natural gas of various compositions. Nevertheless, gradually other gaseous fuels and their mixtures are starting to be used. The composition of the fuel gas can vary widely. From gas, consisting mainly of methane, to gases with heavy hydrocarbons (butane and heavier), or gases with a large amount of non-combustible gases. Modern gas turbines are focused on burning natural gas consisting of methane. However, the development of hydrogen energy, the production of gas from biomass, the release of various process gases pose the problem of adapting the gas turbine fuel system for each type of fuel separately, and ideally for the joint or sequential combustion of multicomponent fuel gases [6–8].

Fuel gas is a mixture of combustible and inert fuel gases covering a wide range of heating values. The quality and composition of the fuel burned in a gas turbine affect not only the quality of combustion but also the service life of the hot section of the turbine. In addition, the composition of the gas affects the generated power and the efficiency of the gas turbine.

This study considers the issue of changing the energy characteristics of a gas turbine depending on the component composition of the fuel. Alternative fuels are very different in composition compared to natural gas, and therefore affect the efficiency of equipment. The use of alternative fuels will also affect the final price of the product—electricity, since the main costs of its production are fuel costs.

Fuel conversion and combustion are complex processes. Nevertheless, during operation, as well as design, it is necessary to determine the thermodynamic properties. During combustion, combustion products are formed, which are a multicomponent gaseous mixture. To determine the composition of a given mixture, it is necessary to determine the individual substances included in this mixture. Fuel can be one-component, two-component, and multicomponent. The elemental composition, which describes the content of chemical elements in the fuel gas, must be specified in the form of a conditional formula.

During long-term operation, it is possible to change the component composition of gas coming from a certain field. In this regard, in this work, natural gas of the same field is considered, but taking into account the change in its component composition. The use of hydrogen is considered as an alternative gas. With the development of alternative fuels, the issue of interchangeability of fuel gases with minimal changes in the fuel system becomes very acute. Depending on the ratio of combustible gases, the fuel gas has a different heating value. And subsequently, during combustion, the density and temperature of the fuel also differ, which also affect the service life of the gas turbine unit. In this article, hydrogen is considered as an alternative fuel. Gas No. 1, No. 2, and No. 3 is gas from the same field with a difference of 10 and 15 years (Tables 1 and 2).

Table 1 Change in gas composition with time

No.	Component	Formula	Gas No. 1, %	Gas No. 2, %	Gas No. 3, %
1	Methane	CH ₄	95.16	93.22	90.750
2	Ethane	C ₂ H ₆	0.24	2.861	3.8616
3	Propane	C ₃ H ₈	0.01	0.992	1.3484
4	Isobutene	C ₄ H ₁₀	0	0.336	0.7109
5	Oxygen	O ₂	0.0471	0.0489	0.0489
6	Nitrogen	N ₂	4.27	2.2059	2.741
7	Carbon dioxide	CO ₂	0.268	0.335	0.538

Table 2 Approximation of the thermodynamic properties of fuels of various compositions

No.	Fuel	C	H	N	O	Enthalpy, kJ/kg
1	Gas No. 1	5.978517	23.53828	0.30283	0.056426	-4489.23
2	Gas No. 2	6.032803	22.77181	0.239385	0.056426	-4435.34
3	Gas No. 3	6.080788	23.52725	0.19374	0.056426	-4462.819
4	Hydrogen	-	99.21619	-	-	-3965.1

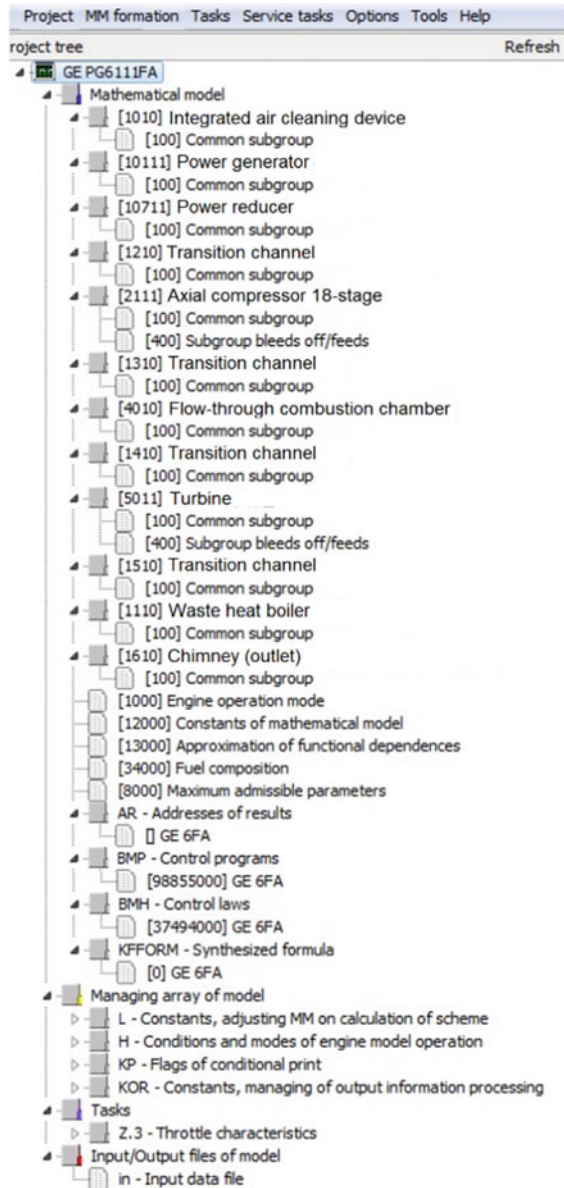
Another important parameter for continuous gas turbine operation is the Wobbe index. The Wobbe index is calculated for a specific gas and its supply pressure to the combustion chamber. If this index of two different gases coincides, then the operation of the fuel preparation system and the setting of the gas supply system remains unchanged. If the deviation is more than 5%, then it is necessary to stop the equipment and adjust the turbine combustion system. This condition is true when the turbine is running on two types of fuel, the main and reserve. Therefore, research on the composition of biogas of various compositions is promising. Thus, it is possible to add hydrogen to biogas, thereby increasing the energy characteristics of the fuel. Gasification technologies also make it possible to process hydrocarbons into synthesis gases, and later be used in power plants.

A 110-MW gas turbine GEPG1116FA was selected for research. The gas turbine unit is a single-shaft axial-flow turbine unit equipped with an 18-stage compressor with one row of rotary guide vanes at the compressor inlet, six combustion chambers, and a 3-stage air-cooled turbine in all three-nozzle stages. The generator is driven through a reduction gear at the front end of the compressor shaft.

The PG6111FA gas turbine is specially designed for operation in a combined cycle. The heat of hot exhaust gases from the GTU is used in the waste heat boiler to produce superheated steam.

To study the effect of different compositions of fuels, a mathematical model of the GTU was created (Figs. 1 and 2) using the AS GRET software package [9], developed by a team of authors at KSPEU, in addition, this complex can take into account changes in the load in the power system [10].

Fig. 1 Menu of the software package for calculating the PG1116FA gas turbine unit in the AS “GRET” nuclear power plant



Because most often powerful gas turbines are included in the scheme of combined cycle plants, the operating mode at constant load is considered. This mode of operation is necessary for more economical operation. Basic operation assumes a constant temperature at the outlet and in the combustion chamber of the gas turbine [10–14].

Initial data:

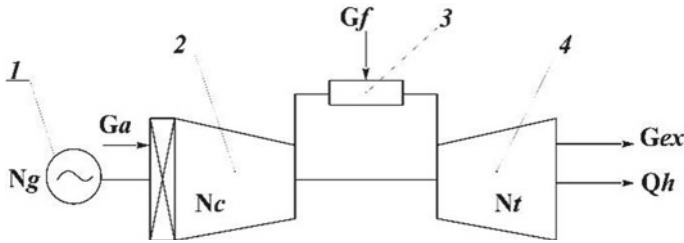


Fig. 2 Gas turbine plant simulation scheme in the software package of the AS “GRET”. 1—an electric generator; 2—a compressor; 3—a combustion chamber; 4—a gas turbine. N_g —a generated power, MW, N_c —a power consumed for air compression, MW, N_t —power a generated by a gas turbine, MW, G_a —an air entering the gas turbine compressor, G_f —a fuel gas entering the combustion chamber, G_{ex} —a GTU exhaust gases, Q_h —the heat of GTU exhaust gases

Atmospheric pressure at the compressor inlet:

$$P_{in} = 0.101325 \text{ MPa};$$

Air temperature at the compressor inlet:

$$T_{in} = 288 \text{ K};$$

Compressor inlet relative humidity 60%;

Flue gas temperature: $T_{out} = 874 \text{ K}$.

The efficiency can be determined using the following formula:

$$\eta = \frac{N_t}{G_f \cdot H_n} \cdot 3600$$

where

η_t —Efficiency;

N_t —Power developed by a gas turbine.

G_f —Instant fuel consumption.

H_n —Net calorific value of fuel.

3 Results and Discussion

Figure 3 shows the change in air consumption with a deterioration in the composition of the fuel gas, an increase in the amount of air required for complete combustion of the fuel occurs.

In turn, the increased air flow leads to a decrease in the effective efficiency, Fig. 4.

The appearance of impurities and inert gases in the initial gases (Gas No. 2 and No. 3) leads to an increase in fuel consumption (Fig. 5).

Figure 5 shows that the change in gas composition led to an increase in fuel consumption by 11% at the same generated power. One of the most important changes

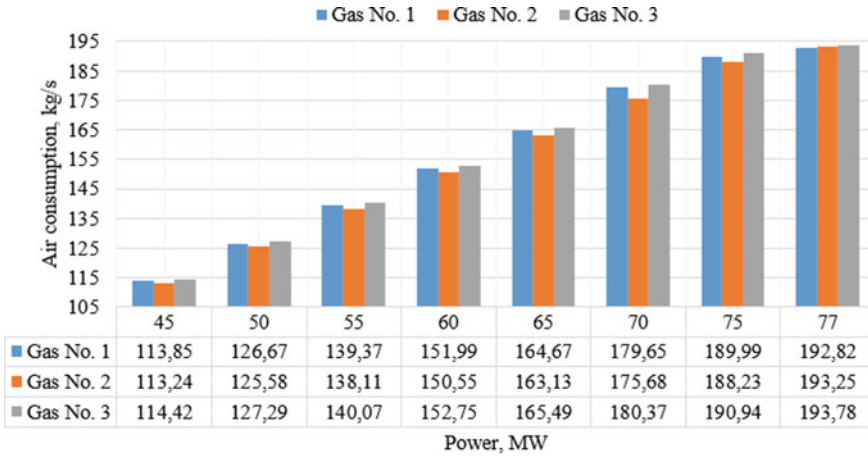


Fig. 3 The change in the air consumption of a gas turbine depending on the instantaneous power and gas composition

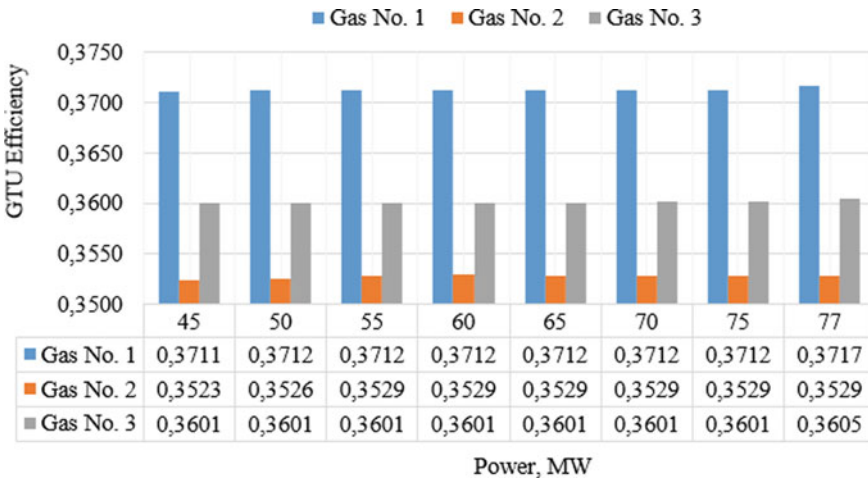


Fig. 4 The change in effective efficiency of a gas turbine depending on the instantaneous power and gas composition

in gas turbine fuel changes is the change in the composition of the exhaust gases. An increase in fuel gas consumption leads to an increase in emissions (Table 3).

With a further change in the composition of the fuel gas, an increase in fuel consumption will occur. A feature of gas turbines is that they carry maximum loads during the period of negative temperatures, which leads to an increase in instantaneous fuel consumption. The increase in fuel consumption is permissible within certain limits, since the auxiliary equipment and gas supply pipelines are designed for certain operating parameters. In this regard, reaching the maximum generated power

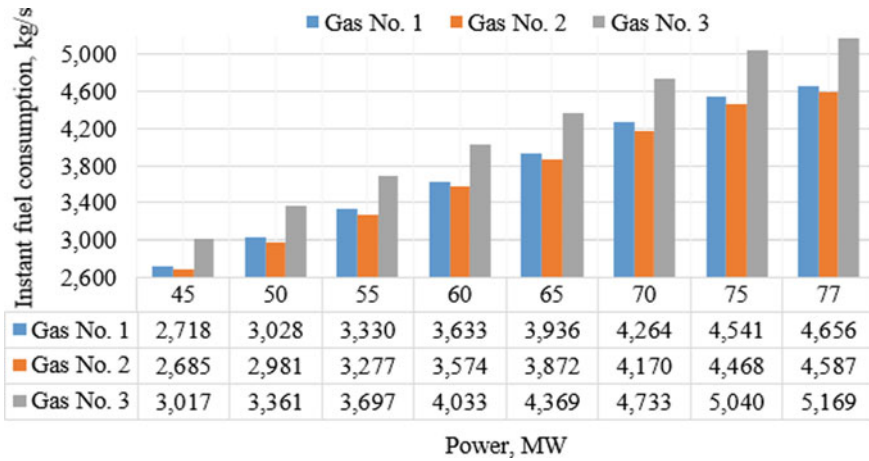


Fig. 5 The change in instantaneous fuel consumption depending on instantaneous power and gas composition

is impossible. The gas distribution and gas consumption system has an established scheme of natural gas supply, and the laying of new communications, in addition to the high cost, requires long approvals [15–18].

One of the ways to improve the efficiency of fuel use can be the addition of alternative fuels to the natural gas feed. In this case, it is shown what happens when hydrogen is added with the conditional formula $H_{99.21619}$, Fig. 6.

Now, hydrogen as a fuel for gas turbines is very expensive. Therefore, a variant of mixing hydrogen with natural gas is considered [19, 20]. Because the capacity of the fuel gas booster compressor is taken with a margin of not more than 10%, then upon reaching the maximum capacity, the power of the gas turbine unit will depend on the operation of the booster compressor (the power of the gas turbine unit will be limited).

As a result of research, the consumption of hydrogen admixture was determined. It is 4.5%. Figure 6 shows the dependence of the gas turbine power on the consumption of fuel gas with hydrogen. Figure 7 shows the hourly fuel consumption at different power of the GTU.

Figure 7 shows that at a constant gas flow rate of 5.04 kg/s, the addition of hydrogen leads to an increase in the power of the gas turbine.

4 Conclusion

The article shows that over time there is a change in the component composition of the gas of one field. With the deterioration of the energy characteristics of the fuel, the fuel consumption increases by 11%. Such an increase in fuel consumption does

Table 3 Emissions consumption for different gas turbine power and fuel composition changes

Emission parameter	Fuel	Power									
		45	50	55	60	65	70	75	77		
CO ₂	Gas No. 1	0.102154	0.113918301	0.1252785	0.1366996	0.1480923	0.1604226	0.1708573	0.17693731		
	Gas No. 2	0.1032519	0.114776303	0.1260938	0.1375958	0.149091	0.1605493	0.1720079	0.1765946		
	Gas No. 3	0.1254002	0.140358739	0.1543557	0.1684276	0.1824645	0.1976648	0.2105132	0.21800446		
NO	Gas No. 1	0.000011610	0.000013202	0.000014494	0.000015840	0.000017161	0.000018579	0.000019788	0.00001995		
	Gas No. 2	0.000011181	0.000012462	0.000013599	0.000014871	0.000016128	0.000017362	0.000018596	0.00001909		
	Gas No. 3	0.000001186	0.000001504	0.000001816	0.000002165	0.000002541	0.000002981	0.000003381	0.00000353		
NO ₂	Gas No. 1	0.000001342	0.00000132	0.000001659	0.00000181	0.000001961	0.000002124	0.000002263	0.00000226		
	Gas No. 2	0.000001312	0.000001457	0.000001597	0.000001742	0.000001889	0.000002034	0.000002179	0.00000223		
	Gas No. 3	0.000004050	0.000004436	0.000006133	0.000007302	0.000008571	0.000010056	0.000011406	0.00001171		
O ₂	Gas No. 1	0.279715392	0.311574994	0.342817382	0.373890195	0.40505057	0.43877165	0.467347779	0.4754667		
	Gas No. 2	0.274898856	0.304932173	0.335313973	0.365580975	0.39612396	0.426587199	0.45705163	0.46923918		
	Gas No. 3	0.843881082	1.047065163	1.267293301	1.507760817	1.769549826	2.076814855	2.355656744	2.45750791		

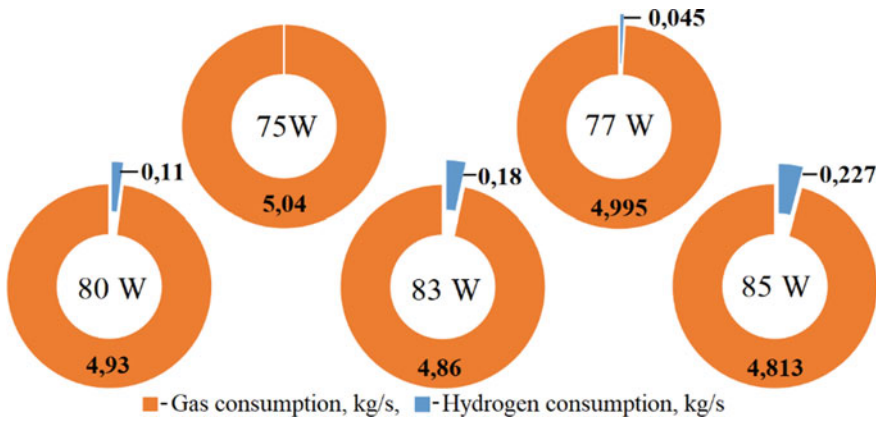


Fig. 6 Dependence of gas turbine power on fuel gas consumption with hydrogen

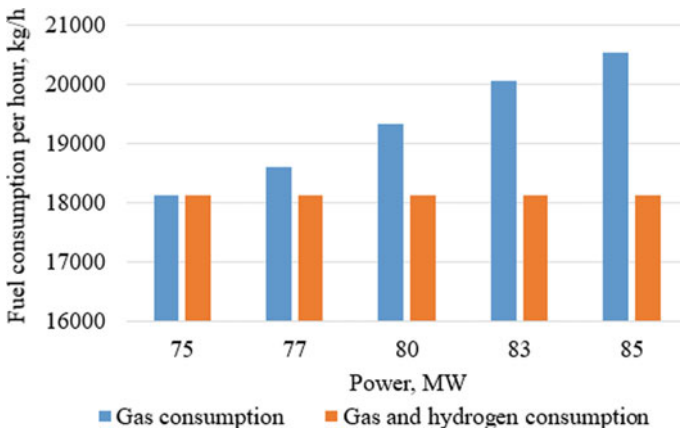


Fig. 7 Dependence of the hourly fuel consumption at different power of the GTU

not allow the fuel preparation system to operate in the optimal range. The solution to this problem is to add hydrogen to the feed gas to improve energy performance. For research, a mathematical model of a gas turbine was created and an approximation of the fuel gas was carried out. The result of the study is to find the optimal ratio of natural gas and hydrogen. Adding 4.5% hydrogen to the fuel gas allows the gas turbine to operate without any power generation constraints.

References

1. Akhmetshin, A., Marin, G., Mendeleev, D.: E3S Web Conf. **178**, p. 01015 (2020)
2. Alcaráz-Calderon, A.M., González-Díaz, M.O., Mendez, Á., González-Santaló, J.M., González-Díaz, A.: J. Energy Inst. **92**, 370 (2019)
3. Bakirov, F., Ibragimov, E.: In: 2020 International Multi-conference on Industrial Engineering and Modern Technologies, FarEastCon 2020, p. 9271294 (2020)
4. Basha, M., Shaahid, S.M., Al-Hadhrami, L.: Energy Procedia **14**, 558–565 (2012)
5. Benato, A., Stoppato, A., Bracco, S.: Energy Convers. Manag. **87**, 1269–1280 (2014)
6. Blakey, S., Rye, L., Wilson, C.W.: Proc. Combust. Inst. **33**, 2863–2885 (2011)
7. Chiesa, P., Lozza, G., Mazzocchi, L.: J. Eng. Gas Turbines Power **127**, 73–80 (2005)
8. Dodds, P.E., Staffell, I., Hawkes, A.D., Li, F., Grünewald, P., McDowall, W., Ekins, P.: Int. J. Hydrogen Energy **40**, 2065–2083 (2015)
9. Marin, G.E., Osipov, B.M., Mendeleev, D.I.: E3S Web Conf. **124**, 05063 (2019)
10. Henke, M., Kallo, J., Friedrich, K.A., Bessler, W.G.: Fuel Cells **11**(4), 581–591 (2011)
11. Soluyanov, Y.I., Fedotov, A.I., Soluyanov, D.Y., Akhmetshin, A.R.: IOP Conf. Ser.: Mater. Sci. Eng., **860**, p. 012026
12. Akhmetshin, A., Mendeleev, D., Marin, G.: In: 2020 International Russian Automation Conference, RusAutoCon 2020, p. 9208158 (2020)
13. Islamova, S.I., Timofeeva, S.S., Khamatgalimov, A.R., Ermolaev, D.V.: Solid Fuel Chem. **54**, 251 (2020)
14. Kayfeci, M., Keçebaş, A., Bayat, M.: Sol. Hydrog. Prod. Process. Syst. Technol. **45** (2019)
15. Kiernan, J.G., Foster, A.D., Harden, D.T.: Power Eng. Barrington, Illinois (1978)
16. Esclapez, L., Ma, P.C., Mayhew, E., Xu, R., Stouffer, S., Lee, T., Wang, H., Ihme, M.: Combust. Flame **181**, 82–99 (2017)
17. Marin, G.E., Mendeleev, D.I., Akhmetshin, A.R.: In: 2019 International Multi-conference on Industrial Engineering and Modern Technology, FarEastCon 2019, p. 8934021 (2019)
18. Marin, G., Mendeleev, D., Osipov, B., Akhmetshin, A.: E3S Web Conf. **178**, 01033 (2020)
19. Rochelle, D., Najafi, H.: Renew. Sustain. Energy Rev. **105**, 129–137 (2019)
20. Swamy, M., Singh, K., Pavan, A.H.V., Harison, M.C.A., Jayaraman, G.: Trans. Indian Inst. Metals **69**, 647–651 (2016)